# Electron and Scanning Probe Microscopies

## *2016 Principal Investigators' Meeting*

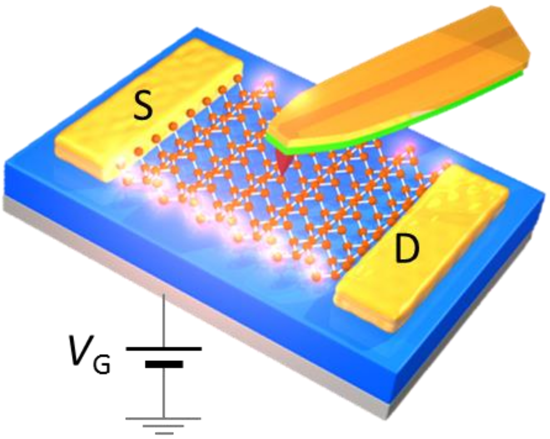

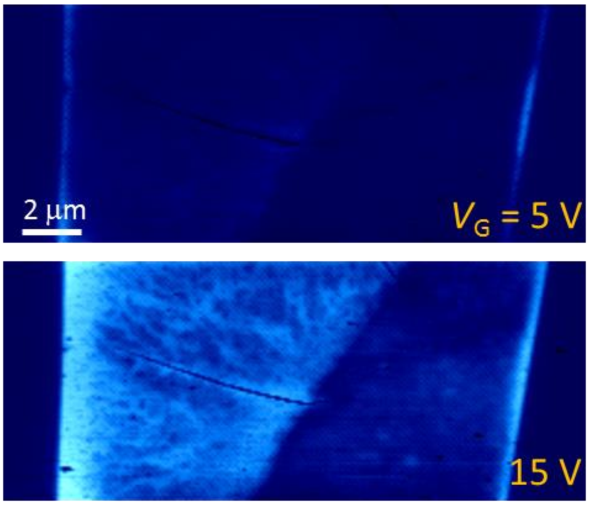

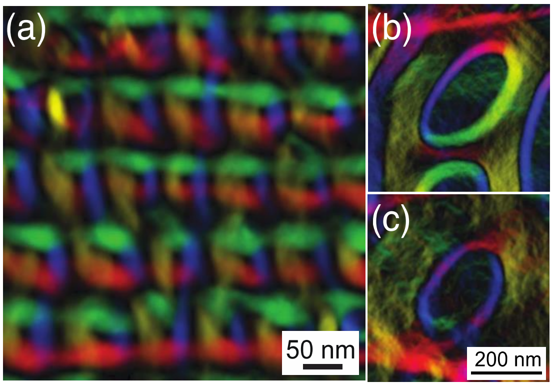

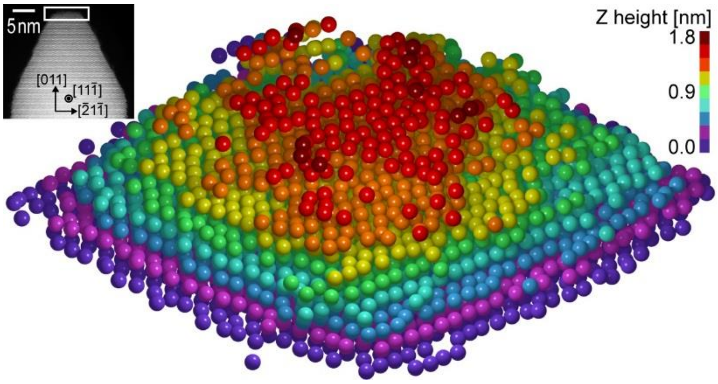

Hilton Washington DC North/Gaithersburg
Gaithersburg, Maryland
October 24-26, 2016

U.S. DEPARTMENT OF ENERGY | Office of Science

**Office of Basic Energy Sciences**
**Materials Sciences and Engineering Division**

# On the Cover

Top: *Inner Workings of Atomically Thin Transistors Revealed by Scanning Microwave Impedance Microscopy*. (Left) Artistic rendering of the conductivity imaging experiment on a back-gated transistor made from two-dimensional atomic sheets of molybdenum disulfide ($MoS_2$). (Upper right) $MoS_2$ device with a low gate bias of 5 V, where the conductive channels appear first at the two physical edges of the flake. (Lower right) The same $MoS_2$ device under a higher gate bias of 15 V. The left part of the device (3 nanometers in thickness) was turned on, with thread-like defects observed in the scanning microwave image. The right part of the sample remained off under this condition. Work published in *Proc. Nat. Acad. Sci.***113**, 8583 (2016).
***Courtesy**: Keji Lai, University of Texas at Austin*

Bottom Left: *Nanoscale Skyrmions in a Nonchiral Metallic Multiferroic:* $Ni_2MnGa$ *Investigated by using Lorentz Transmission Electron Microscopy*. (a) Color magnetic induction map showing the formation of skyrmion lattice in a narrow twinned region of $Ni_2MnGa$ with individual skyrmions of the order of 30 nm. Color magnetic induction map showing the change in topology of an individual skyrmion from (b) non-trivial to (c) trivial. Work published in *Nano Letters* **16**, 4141 (2016).
***Courtesy**: Amanda Petford-Long, Argonne National Laboratory*

Bottom Right: *Three-Dimensional (3D) Coordinates of Individual Atoms in Materials Revealed by Electron Tomography with 19 Picometers Precision*. The 3D atomic model of the sample consists of 9 atomic layers along the [011] direction, labelled with crimson (dark red), red, orange, yellow, green, cyan, blue, magenta and purple from layers 1 to 9, respectively. Work published in *Nature Materials* **14**, 1099 (2015).
***Courtesy**: Jianwei (John) Miao, University of California, Los Angeles*

This document was produced under contract number DE-AC05-06OR23100 between the U.S. Department of Energy and Oak Ridge Associated Universities.

The research grants and contracts described in this document are supported by the U.S. DOE Office of Science, Office of Basic Energy Sciences, Materials Sciences and Engineering Division.

# Foreword

This volume comprises the scientific content of the 2016 Electron and Scanning Probe Microscopies Principal Investigators' Meeting sponsored by the Materials Sciences and Engineering Division (MSED) in the Office of Basic Energy Sciences (BES) of the U.S. Department of Energy (DOE). The meeting, held on October 24–26, 2016, in Gaithersburg, Maryland, is the sixth biennial meeting in the Electron and Scanning Probe Microscopies area organized by BES. The purpose of the meeting is to bring together researchers funded in this core research area to facilitate the exchange of new results and research highlights, to foster new ideas and collaborations among the participants, and to discuss how to advance electron and scanning probe microscopy and spectroscopy, as well as the associated theoretical tools, in order to address forefront scientific challenges. In addition, the meeting affords BES program managers an opportunity to assess the state of the entire program collectively on a periodic basis, in order to chart future directions and identify new programmatic needs.

A recent report from the Basic Energy Sciences Advisory Committee has identified "Exploiting Transformative Advances in Imaging Capabilities across Multiple Scales" as a transformative opportunity for discovery science. To address the materials science challenges, the Electron and Scanning Probe Microscopies Core Research Activity supports basic research using advanced electron and scanning probe microscopy and spectroscopy techniques to understand the atomic, electronic, and magnetic structures and properties of materials. This activity also supports the development of new instrumentation and techniques to advance basic science and materials characterizations for energy applications. Topical areas highlighted in this year's meeting include two-dimensional materials, quantum and ferroic materials, material dynamics, complex and correlated electron materials, and multimodel and ultrafast imaging. Special at this year's meeting are two panel discussions on topical areas that appeal broadly to the PIs in the program: (i) multimodal imaging and (ii) computational and model-driven imaging.

I look forward to the active participation of the attendees at this meeting during the presentations, panel discussions, poster sessions, and other opportunities for discussions. I hope that the collective sharing of ideas and new research results will bring fresh perspective and insights for the continued advancement of this field and its value to DOE's mission. I would like to thank the Meeting Chairs, Markus Raschke and Amanda Petford-Long, for their dedicated efforts and invaluable assistance towards organizing this meeting. My sincere thanks also go to Teresa Crockett in MSED and Linda Severs and her colleagues at the Oak Ridge Institute for Science and Education for their excellent work providing all the logistic support for the meeting.

Jane G. Zhu
Program Manager, Electron and Scanning Probe Microscopies
Division of Materials Sciences and Engineering, Basic Energy Sciences
Office of Science
U.S. Department of Energy

# Table of Contents

## Laboratory Projects

**University Grant Projects**

**Invited Talk**

# AGENDA

## 2016 Electron and Scanning Probe Microscopies
## Principal Investigators' Meeting
## Materials Sciences and Engineering Division, Office of Basic Energy Sciences
## U. S. Department of Energy

## MONDAY, OCTOBER 24, 2016

| | |
|---|---|
| 7:00 – 8:30 am | *****Breakfast***** |
| 8:30 – 9:00 am | *Division and Program Updates*<br>Linda Horton<br>Director, Materials Sciences and Engineering Division, Basic Energy Sciences |
| 9:00 – 9:20 am | Jane Zhu<br>Program Manager, Electron and Scanning Probe Microscopies |
| | Meeting Chairs: Amanda Petford-Long and Markus Raschke<br>Argonne National Laboratory/University of Colorado |
| **Session I** | **2D Materials**<br>Chair: Amir Yacoby, Harvard University |
| 9:20 – 9:45 am | Matthew Chisholm, Oak Ridge National Laboratory<br>*Scanning Transmission Electron Microscopy: Atomic Structure and Properties of Materials – Functional Structures in 2D Materials* |
| 9:45 – 10:10 am | Lian Li, West Virginia University<br>*Heterostructures of Dirac Materials* |
| 10:10 – 10:30 am | *****Break***** |
| **Session II** | **Quantum Materials**<br>Chair: Markus Raschke, University of Colorado |
| 10:30 – 11:05 am | Dmitri Basov (invited), Columbia University<br>*Quantum Materials: Insights from Infrared Nano-Optics* |
| 11:05 – 11:30 am | Keji Lai, University of Texas Austin<br>*Spatial Evolution of Electric-Field-Driven Metal-Insulator Transitions* |
| 11:30-11:55 am | Joe Orenstein, Lawrence Berkeley National Laboratory<br>*Spin Physics and Nanoscale Probes of Quantum Materials* |

| | |
|---|---|
| 11:55 – 12:00 pm | Chair-led introduction for the concept of the Panel Sessions |
| 12:00 – 1:10 pm | *****Working Lunch***** |
| **Panel Discussion I**<br>1:10 – 3:10 pm | ***Multimodal Imaging: Combining Different Techniques to Image across Length-Scales***<br>Chair: Markus Raschke<br>Panel members: Yimei Zhu, Pramod Reddy, Joe Orenstein |
| 3:10 – 5:10 pm | **Poster Session I (with refreshments)** |
| **Session III** | **Multimodal Imaging**<br>Chair: Amanda Petford-Long, Argonne National Laboratory |
| 5:20 – 5:45 pm | Shen Dillon**,** University of Illinois<br>*Development of Flexible In Situ Electrochemical Cell for Surface Sensitive Techniques; XPS, AES, SEM, and AFM* |
| 5:45 – 6:10 pm | David Ginger, University of Washington<br>*Multimodal In Situ Scanning Probes for Understanding Hybrid Perovskite Solar Cells* |
| 6:20 – 7:40 pm | *****Working Dinner***** |
| 7:40 – 8:30 pm | **Panel Session I Report Back from the breakout sessions** |

## TUESDAY, OCTOBER 25, 2016

| | |
|---|---|
| 7:00 – 8:00 am | *****Breakfast***** |
| **Session IV** | **Energy Materials**<br>Chair: Shirley Meng, University of California San Diego |
| 8:00 – 8:25 am | Dongheng Li, Pacific Northwest National Laboratory<br>*In Situ TEM Study of Branched Nanocrystal Growth Mechanisms: Understanding Non-classical Processes Controlling Formation of Hierarchical Nanostructures* |

| | |
|---|---|
| 8:25 – 8:50 am | Philip Batson, Rutgers University<br>*Mapping Bulk Phonon and Surface Phonon Polariton Modes in MgO* |
| 8:50 – 9:15 am | Jon Camden**,** University of Notre Dame<br>*Nanoscale Imaging of Optical-Frequency Plasmonic Energy Transfer in Hybrid Metal-Semiconductor Systems and Magnetic Metamolecule Assemblies* |
| 9:15 – 9:40 am | Pramod Reddy, University of Michigan<br>*Radiative Heat Transfer at the Nanoscale* |
| 9:40 – 10:05 am | Nitash Balsara**,** Lawrence Berkeley National Laboratory<br>*Toward Atomic Resolution Electron Microscopy of Soft Matter* |
| 10:05 – 10:25 am | *****Break***** |
| **Session V** | **Ferroic Materials**<br>Chair: Chris Hammel, Ohio State University |
| 10:25 – 10:50 am | Sergei Kalinin, Oak Ridge National Laboratory<br>*Probing Coupled Metal-Insulator and Ferroic Transitions from the Atomistic to Mesoscopic Scales* |
| 10:50 – 11:15 am | Xiaoqing Pan**,** University of California Irvine<br>*Structure and Dynamics of Domains in Ferroelectric Nanostructures – In-situ TEM Studies* |
| 11:15 – 11:40 am | Jim Zuo**,** University of Illinois<br>*Fundamental Symmetry of Ferroelectric Crystals* |
| 11:40 – 12:05 pm | Gregory Fuchs**,** Cornell University<br>*Chiral Magnetic Excitations in FeGe Thin Films* |
| 12:10 – 1:10 pm | *****Working Lunch***** |
| **Panel Discussion II**<br>1:10 – 3:10 pm | **Computational and Model-Driven Imaging**<br>Chair: Amanda Petford-Long<br>Panel Members: Lawrence Marks, Andrew Lupini, Weida Wu |
| 3:10 – 5:10 pm | **Poster Session II (with refreshments)** |

| | |
|---|---|
| **Session VI** | **Complex Materials**<br>Chair: David Muller, Cornell University |
| 5:20 – 5:45 pm | Ali Yazdani, Princeton University<br>*Probing Correlated Superconductors and Their Phase Transitions on the Nanometer Scale* |
| 5:45 – 6:10 pm | Paul Voyles, University of Wisconsin<br>*High Precision STEM Imaging: Improved Data Quality, Imaging Vacancies* |
| 6:10 – 7:30 pm | *****Working Dinner***** |
| 7:30 – 8:30 pm | **Panel Session II report and Wrap-up Discussions** |

## WEDESDAY, OCTOBER 26, 2016

| | |
|---|---|
| 7:00 – 8:00 am | *****Breakfast***** |
| **Session VII** | **Ultrafast Dynamics**<br>Chair: Jing Tao, Brookhaven National Laboratory |
| 8:00 – 8:25 am | Geoff Campbell, Lawrence Livermore National Laboratory<br>*Complex Fundamental Mechanisms of Transient States in Materials Quantified by DTEM* |
| 8:25 – 8:55 am | Yimei Zhu, Brookhaven National Laboratory<br>*Probing Charge and Lattice Correlation Using Ultrafast Electron Pulses* |
| 8:55 – 9:20 am | Markus Raschke, University of Colorado<br>*Nano-imaging and -spectroscopy of Complex and Correlated Materials* |
| 9:20 – 9:45 am | Chong-Yu Ruan, Michigan State University<br>*Femtosecond Imaging of Dynamical Texture (Re)formation in Charge-Density Wave Systems with Coherent Electron Beams* |
| 9:45 – 10:05 am | *****Break***** |

| | |
|---|---|
| **Session VIII** | **Correlated Electron Materials**<br>Chair: David Cobden, University of Washington |
| 10:05 – 10:30 am | Ward Plummer, Louisiana State University<br>*Emerging Functionality in Transition-Metal Compounds Driven by Spatial Confinement* |
| 10:30 – 10:55 am | Maria Iavarone, Temple University<br>*Vortex Matter in Superconductor/Ferromagnet Heterostructures* |
| 10:55 – 11:20 am | Susanne Stemmer, University of California Santa Barbara<br>*Probing Correlated Phenomena in Oxide Structures with Quantitative STEM* |
| 11:20 – 12:00 pm | ***Open Discussion on Future Program Topics & Science-Driven Tools Development, Concluding Comments***<br>Markus Raschke and Amanda Petford-Long, Meeting Chairs<br>Jane Zhu, Program Manager, Electron and Scanning Probe Microscopies |

**ESPM PI Meeting**

# Poster session I

Monday, October 24th, 3:10 – 5:10 PM

I.1 **Xia Hong**, University of Nebraska-Lincoln
*Transport and Optoelectronic Studies of van der Waals Material-Based Homojunctions and Heterojunctions*

I.2 **Mark P. Oxley, Wu Zhou, Andy R. Lupini, Matthew F. Chisholm**, Oak Ridge National Laboratory
*Scanning Transmission Electron Microscopy: Atomic Structure and Properties of Materials – Quantification of Low Voltage Images of 2D Materials*

I.3 **Amir Yacoby, Pablo Jarillo-Herrero**, Harvard University & MIT
*Transport and Imaging of Mesoscopic Phenomena in Novel Low-Dimensional Materials*

I.4 **Weida Wu**, Rutgers University
*Visualizing Emergent Phenomena in Topological and Quantum Materials*

I.5 **Jay A. Gupta, Michael Flatté**, Ohio State University and University of Iowa
*Atomistic Studies of Individual Impurities and Impurity Complexes in III–V Semiconductors*

I.6 **Daniel B. Dougherty**, North Carolina State University
*Spin Polarized STM and STS of Hybrid Interface States at Organic Semiconductor Interfaces*

I.7 **Andrew R. Lupini, Mark P. Oxley, Matthew F. Chisholm**, Oak Ridge National Laboratory
*Scanning Transmission Electron Microscopy: Atomic Structure and Properties of Materials – Physics of Electron Microscopy*

I.8 **Jianwei (John) Miao**, University of California, Los Angeles
*Atomic Electron Tomography: 3D Structure without Crystals*

I.9 **Sokrates T. Pantelides**, Vanderbilt University
*Physics of Complex Materials Systems through Theory and Microscopy/EELS*

I.10 **Peter A. Crozier**, Arizona State University
*Probing Vibrational and Electronic Excitations on Photocatalytic Nanoparticles for Solar Fuel Generation*

I.11 **Ying Shirley Meng**, University of California, San Diego
*Advancing In situ Analytical Electron Microscopy for Probing Dynamic Nano-Scale Solid State Electrochemistry*

I.12 **Santiago D. Solares**, The George Washington University
*Characterization of Energy-Relevant Materials with Multifrequency and Conductive Atomic Force Microscopy, and Kelvin Probe Force Microscopy*

I.13 **Peter Sutter**, University of Nebraska–Lincoln
*Exploring and Embracing Heterogeneity in Atomically Thin Energy Materials*

I.14 **Lijun Wu, Jing Tao, Yimei Zhu**, Brookhaven National Laboratory
*Electron-Spin-Lattice Interplay and Charge Transfer in Quantum and Energy Materials*

I.15 **David A. Muller, Craig J. Fennie, Darrell G. Schlom**, Cornell University
*Atomically Engineered Ferroic Layers Yield a Room-Temperature Magnetoelectric Multiferroic: Design, Realization, and Picometer-Precision Imaging of Polarization Switching*

I.16 **P. Chris Hammel**, Ohio State University
*Understanding and Control of Spin Currents in Diverse Materials and Settings*

I.17 **Haimei Zheng**, Lawrence Berkeley National Laboratory
*Real Time Imaging of Materials Transformations in Liquids*

## Poster session II

Tuesday, October 25th, 3:10 – 5:10 PM

II.1 **Jesse Berezovsky**, Case Western Reserve University
*Mapping Interactions between Individual Coherent Spins and Dynamically Driven Ferromagnetic Vortices*

II.2 **Benjamin J. McMorran**, University of Oregon
*Structured Electron Beams for Electron Microscopy*

II.3 **Amanda K. Petford-Long, Seungbum Hong, Charudatta Phatak**, Argonne National Laboratory
*3D Visualization of Emergent Behavior in Nanoscale Functional Heterostructures*

II.4 **Udo Schwarz**, Yale University
*Atomic-scale Surface Studies of Bulk Metallic Glasses*

II.5 **Albina Y. Borisevich, Valentino Cooper**, Oak Ridge National Laboratory
*Probing Phase Transitions, Chemical Reactions, and Energy Transfer at the Atomic Scale*

II.6 **J. C. Séamus Davis, Kazuhiro Fujita**, Brookhaven National Laboratory
*Spectroscopic Imaging STM and Complex Electronic Matter*

II.7 **Laurence D. Marks**, Northwestern University
*Oxides Surfaces and Novel Electromechanical Phenomena*

II.8 **David H. Cobden**, University of Washington
*Combined Microscopy Studies of Complex Electronic Materials*

II.9 **Long-Qing Chen**, The Pennsylvania State University
*Domain Wall Stability and Domain Switching: Role of Oxygen Octahedral Tilt*

II.10 **Benjamin Lev**, Stanford University
*The SQCRAMscope: A Scanning Quantum Cryogenic Atom Microscope*

II.11 **Jing Tao**, Brookhaven National Laboratory
*Tracing Non-equilibrium Phenomena in Correlated Materials by using Ultrafast Electron Probes*

II.12 **Vidya Madhavan**, University of Illinois, Urbana-Champaign
*Quasiparticle Interference and Strong Electron-Mode Coupling in the Quasi-One-Dimensional Bands of* $Sr_2RuO_4$

II.13 **Myung-Geun Han and Yimei Zhu**, Brookhaven National Laboratory
*Dynamics of Topological Ferroelectric and Ferromagnetic Nanostructures*

II.14 **Venkat Chandrasekhar**, Northwestern University
*Tunable Anisotropy at the (111)* $LaAlO_3/SrTiO_3$ *Interface*

II.15 **Ian M. Robertson**, University of Wisconsin–Madison
*Deformation Process in Multi-layered Ag-Cu System*

II.16 **Katja Nowack**, Cornell University
*Magnetic Imaging of Topological Phases of Matter*

II.17 **David J. Masiello, Jon P. Camden**, University of Washington & University of Notre Dame
*Theoretical Insights into Plasmonic Energy Transfer in Individual Nanoparticles and Their Assemblies*

II.18 **S. V. Kalinin, M. Ziatdinov, R. K. Vasudevan, P. Maksymovych**, Oak Ridge National Laboratory
*Local Physics from Machine Learning of Atomically Resolved Images*

# LABORATORY PROJECTS

## Toward Atomic Resolution Electron Microscopy of Soft Matter

**Principal Investigators: Nitash Balsara*,** Kenneth Downing, Andrew Minor, Ronald Zuckermann, David Prendergast

*Materials Sciences Division, Lawrence Berkeley National Laboratory, Berkeley, CA 94709. email: nbalsara@lbl.gov

### Research Scope

We aim to produce images of soft materials with atomic resolution using electron microscopy (EM). This is inherently challenging because soft materials are unstable under the electron beam. Sophisticated averaging algorithms are being developed to extract high resolution information from low exposure images, where Fourier transforms along orthogonal directions will be used to align individual images. To demonstrate these imaging concepts, we will use crystalline nanostructures formed by self-assembly of amphiphilic peptoid molecules in water. Of particular interest are structures formed by diblock copolypeptoids wherein conventional wisdom suggests that these molecules should form micellar aggregates with collapsed hydrophobic cores. In contrast, we obtain crystalline hollow tubes and sheets with hydrophobic groups exposed to water. Confirming this by atomic-scale imaging is important for a general understanding of molecular self-assembly. A series of peptoids with sequences of monomers specifically designed to enable high resolution electron microscopy will be synthesized by solid phase synthesis. In the future, we will use molecular dynamics to characterize thermal fluctuations and disorder, and this information will be convoluted with the contrast transfer function of the microscope used in experiments to obtain theoretical images. This new framework for atomic resolution imaging on model peptoids will be applied to improve the resolution of electron microscopy of more conventional soft polymeric materials.

### Recent Progress

We synthesized and characterized block copolypeptoids comprising a hydrophobic block of poly-N-decylglycine (pNdc), and a hydrophilic block of poly-N-2-(2-(2-methoxyethoxy)ethoxy)ethylglycine (pNte) [1]. The pNdc-pNte symmetric diblock copolymers with 36 monomer units total self-assembled into curved molecular tile units to give hollow nanotubes in water as demonstrated by cryo-EM (Fig 1). We reasoned that each polymer unit can assemble into a brick-like lattice and form either sheets or tubes. We demonstrated by calorimetry and X-ray scattering that in the nanotubes and the nanosheets, both the hydrophilic and hydrophobic domains are crystalline. Unstained Cryo-EM revealed that the nanotubes have very distinct latitudinal stripes representing the backbone-backbone distance. Tubes when stained with an agent that is specific for the hydrophilic moieties reveal longitudinal stripes. Cryo-EM is able to see domains in these structures, but atomic data is not yet available.

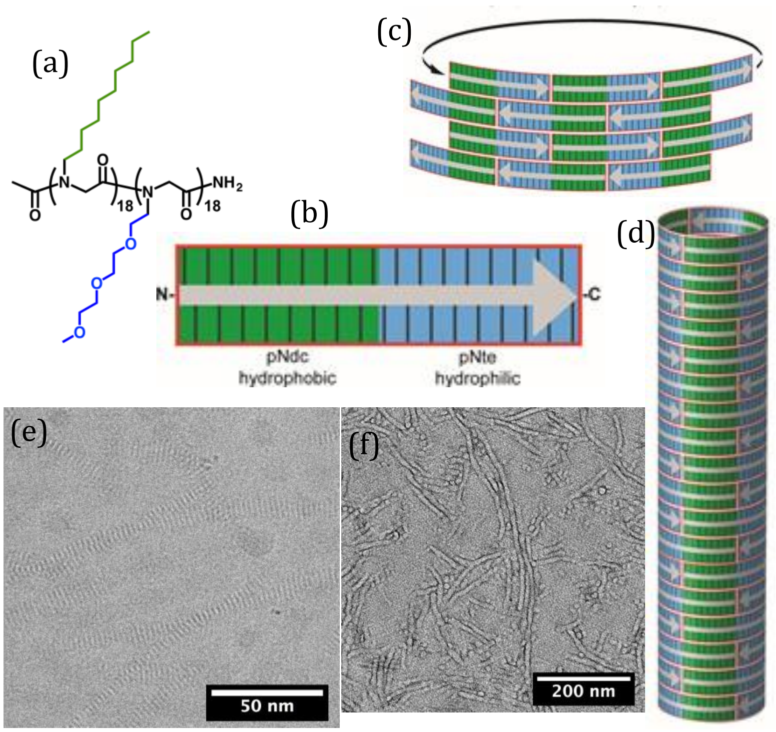

Fig 1 (a) Molecular structure of 36-mer pNdc-pNte peptoid block copolymer. (b) Schematic of molecule. (c) Schematic of assembly mechanism. (d) Structure of nanotube. (e) Unstained cryo-EM showing end view of nanotubes and side view that reveals backbone spacing (2.4 nm). (f) Stained tubes deposited on a surface showing vertically arranged hydrophilic and hydrophobic domains.

The pNdc-pNte diblock copolymers with 18 monomer units self-assembled into molecular tile units to give flat nanosheets (Fig 2, next page). The planar structure facilitates obtaining high resolution information. The Fast Fourier Transforms (FFTs) of the low resolution images show many higher-order reflections even in the off-axis side chain packing indicating information on the side chain packing in the off-axis diffraction spots at around 4 Å resolution (Fig 2b). This image was obtained with an exposure of 26 e/Å$^2$. In Fig 2b, the resolution at 3 Å can be achieved. We scanned the images of single sheets and collected sections that had identical FFTs. After corrections for contrast transfer function, beam-induced movement, and lattice distortion, five corrected images were superimposed. The projection map of these five images is displayed in Fig 2c which shows both the backbone (bright vertical feature) and sidechain packing within a unit cell at near-atomic resolution. To our knowledge, this unpublished image represents the first step toward atomic resolution of synthetic soft materials, i.e. materials that are not proteins (which are identical by design) nor hard materials like metals, semi-conductors, etc.

The projection map in Fig, 2c is evidence that atomic-scale imaging of soft matter is a challenging but achievable goal. We are working toward the goal of true atomic-scale imaging by using custom synthesis, leveraging EM instrument progress, and developing advanced data processing algorithms.

## Future Plans

Our ability to determine the structure of supramolecular peptoid assemblies on the atomic scale by electron microscopy rests, not only in our ability to use state-of-the-art instrumentation and data analysis, but also on our ability to design and execute atomic changes to the chemical structure of the peptoids. We plan to introduce heavy atoms to the peptoid chains at specific locations. We will then use EM to observe the spatial relationships of these heavy-atom labels to one another in the assembled structures.

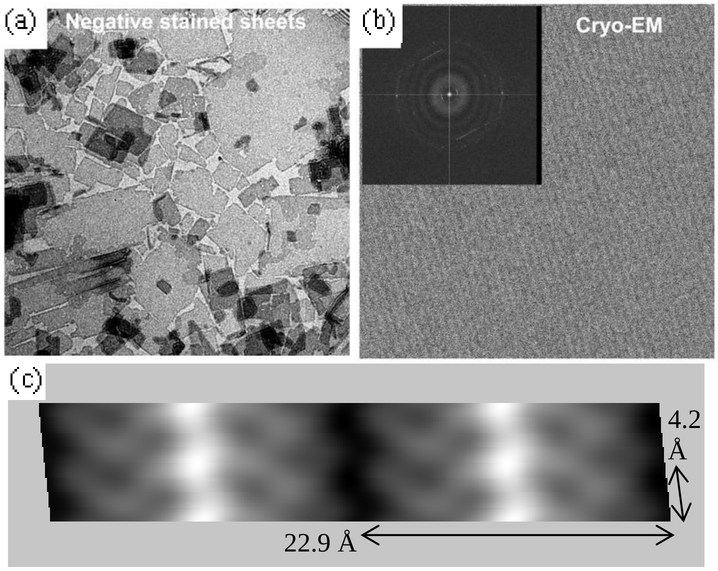

Fig 2 (a) Dry stained EM of 18-mer nanosheets. (b) Unstained cryo-EM showing backbone striping of nanosheet. Inset shows FFT. (c) Projection map showing four unit cells reconstructed from five averaged cryo-EM images.

With an exposure limit on the order of 10-50 e/Å$^2$, the signal-to-noise ratio in images is simply not high enough to directly see details at near-atomic resolution. However, with averaging techniques that have been developed over the last four decades, data from many images – thousands to millions – can be combined to reveal fine structure. These techniques, still in development, have been applied to achieve 3 Å resolution of planar peptoids. The techniques will be expanded for higher resolution and use in other systems, such as tubes. We will also make use of molecular dynamics simulations in order to draw direct connections between EM measurements and atomistic models of soft materials. Current evidence for peptoid nanotube formation in water rests on the EM observation of extended structures with lateral bands separated by 2.4 nm and cross-sectional circular diameters of 12 nm. We will determine the atomic structure and dynamics of these nanotubes [2] and establish the self-assembly pathway that drives spontaneous tube formation from dispersed oligomers in aqueous solution.

## References

1. J. Sun, X. Jiang, R. Lund, K.H. Downing, N.P. Balsara, and R.N. Zuckermann, Self-assembly of crystalline nanotubes from monodisperse amphiphilic diblock copolypeptoid tiles, Proceedings of the National Academy of Sciences, on the web, **2016**.

2. D. T. Mirijanian, R. V. Mannige, R. N. Zuckermann, and S. Whitelam, Development and use of an atomistic CHARMM-based forcefield for peptoid simulation, Journal of computational chemistry **35**, 5, 360 (2014).

**Publications from Program**

1. “Self-assembly of crystalline nanotubes from monodisperse amphiphilic diblock copolypeptoid tiles”, J. Sun, X. Jiang, R. Lund, K.H. Downing, N.P. Balsara, and R.N. Zuckermann, *Proceedings of the National Academy of Sciences*, vol. 113(1), pg. 52–57, **2016**. DOI: 10.1073/pnas.1520394112

2. **“**Morphology and Proton Transport in Humidified Phosphonated Peptoid Block Copolymers”, J. Sun, X. Jiang, A. Siegmund, M. D. Connolly, K.H. Downing, N.P. Balsara, R.N. Zuckermann, *Macromolecules*, vol. 49(8), pg. 3083–3090, **2016**. DOI: 10.1021/acs.macromol.6b00353

3. "Electrochemical Deposition and Stripping Behavior of Lithium Metal across a Rigid Block Copolymer Electrolyte Membrane", K. J. Harry, X. Liao, D.Y. Parkinson, A.M. Minor, N.P. Balsara, *Journal of the Electrochemical Society*, vol. 162(3), p. A389-A405, **2015**. DOI: 10.1149/2.0511503jes

4. "Water Uptake and Proton Conductivity in Porous Block Copolymer Electrolyte Membranes", X.C. Chen, J.B. Kortright, N.P. Balsara, *Macromolecules*, vol. 48, p. 5648-5655, **2015**. DOI: 10.1021/acs.macromol.5b00950.

5. "Failure Analysis of Batteries using Synchrotron-based Hard X-ray Microtomography", K.J. Harry, D.Y. Parkinson, N.P. Balsara, *Journal of Visualized Experiments*, issue: 102, article: 53021, **2015**. DOI: 10.3791/53021

6. "Conductivity of Block Copolymer Electrolytes Containing Lithium Polysulfides", D.R. Wang, K.H. Wujcik, A.A. Teran, N.P. Balsara, *Macromolecules*, vol. 48, p. 4863-4873, **2015**. DOI: 10.1021/acs.macromol.5b00928.

7. "Lithium Dendrite Growth in Glassy and Rubbery Nanostructured Block Copolymer Electrolytes", N.S. Schauser, K.J. Harry, D.Y. Parkinson, H. Watanabe and N.P. Balsara, *Journal of the Electrochemical Society*, vol. 162(3), p. A389-A405, **2015**. DOI: 10.1149/2.0511503jes.

8. "Morphology-Conductivity Relationships in Crystalline and Amorphous Sequence-Defined Peptoid Block Copolymer Electrolytes", J. Sun, X. Liao, A. Minor, N.P. Balsara, R.N. Zuckermann, *Journal of the American Chemical Society*, vol. 136, pg. 14990-14997, **2014**. DOI: 10.1021/ja5080689.

9. "Effect of Crystallization on Proton Transport in Model Polymer Electrolyte Membranes", K.M. Beers, D.T. Wong, A. Jackson, X. Wang, J.A. Pople, A. Hexemer, N.P. Balsara, *Macromolecules*, vol. 47(13), p. 4330-4336, **2014**. DOI: 10.1021/ma500298w.

10. "Effect of Morphology of Nanoscale Hydrated Channels on Proton Conductivity in Block Copolymer Electrolyte Membranes", X.C. Chen, D.T. Wong, S. Yakovlev, K.M. Beers, K.H. Downing, N.P. Balsara, *Nano Letters*, vol. 14(7), p. 4058-4064, **2014**. DOI: 10.1021/nl501537p.

11. "Absence of Schroeder's Paradox in a Nanostructured Block Copolymer Electrolyte Membrane", K.M. Beers, S. Yakovlev, A. Jackson, X. Wang, A. Hexemer, K.H. Downing, N.P. Balsara, *Journal of Physical Chemistry, B: Biomaterials, Surfactants, and Membranes,* vol. 118 (24), p. 6785–6791, **2014**. DOI: 10.1021/jp50137r.

12. "Crystallization in Sequence-Defined Peptoid Diblock Copolymers Induced by Microphase Separation", J. Sun, A.A. Teran, X. Liao, N.P. Balsara, R.N. Zuckermann, *Journal of the American Chemical Society*, vol. 136, p. 2070-2077, **2014**. DOI: 10.1021/ja412123y.

## Probing Phase Transitions, Chemical Reactions, and Energy Transfer at the Atomic Scale

PI: Albina Y. Borisevich[1] Co-PI: Valentino Cooper[1]
Postdocs: Qian He,[1] Rohan Mishra[2], Yael Birenbaum[1]
[1]Materials Science and Technology Division, Oak Ridge National Laboratory
[2]Department of Physics and Astronomy, Vanderbilt University, Nashville, TN 37235

### Research Scope

The overarching goal of this proposal is to provide a new level of understanding to bias-induced transitions in functional oxides by probing their mechanisms across a hierarchy of length scales. We will use a combination of scanning transmission electron microscopy, local-field confinement in *ex-situ* and *in-situ* active device configurations, and advanced theoretical methods to unravel the complex interplay between order parameter dynamics, ionic flows, electrochemical reactions, and mechanical phenomena driven by electrical bias. This research is only now possible due to emerging experimental and computational capabilities and will specifically exploit advanced scanning transmission electron microscopy, local-field confinement in *ex-situ* and *in-situ* active device configurations, and advanced theoretical methods. To achieve our overarching goal, our scientific aims are to: (1) understand the atomistic configurations that underpin order parameters and chemical states and explore their coupling in static and ex situ configurations at the atomic scale; (2) control the response of the materials to the applied bias and in dynamic conditions: separating electronic and ionic degree of freedom, and (3) elucidate dynamic atomic scale pathways that connect local changes to mesoscopic/global property modifications. Ultimately, we seek a predictive knowledge of the dynamic behavior of bias-induced functional oxide phase transitions including an understanding of the optimal defect distribution that will produce a desired dynamic response. This work will enable optimization of a broad range of energy and information technologies from fuel cells, supercapacitors and batteries, to memristive data storage and logic devices.

### Recent Progress

***1. Determination of 3D symmetry information from ABF STEM images***. The rich functionalities in the $ABO_3$ perovskite oxides originate, at least in part, from the ability of the corner-connected $BO_6$ octahedral network to host a large variety of cations through distortions and rotations. Transitions between rotational states with different symmetries accompany many dynamic processes in oxides. Characterizing these rotations *locally* remains a major challenge. Recently [8] we were able to demonstrate that 3D symmetry information can be extracted from the Annular Bright Field (ABF) Scanning Transmission Electron Microscopy (STEM) images of oxide interfaces and heterostructures. While previously only projected tilt information was considered to be analyzable, we were able to demonstrate that 3D symmetry information is also present in the projected images in the shapes of oxygen atomic columns, which are not circular in tilted structures due to imperfect overlap of oxygen atoms at different heights.

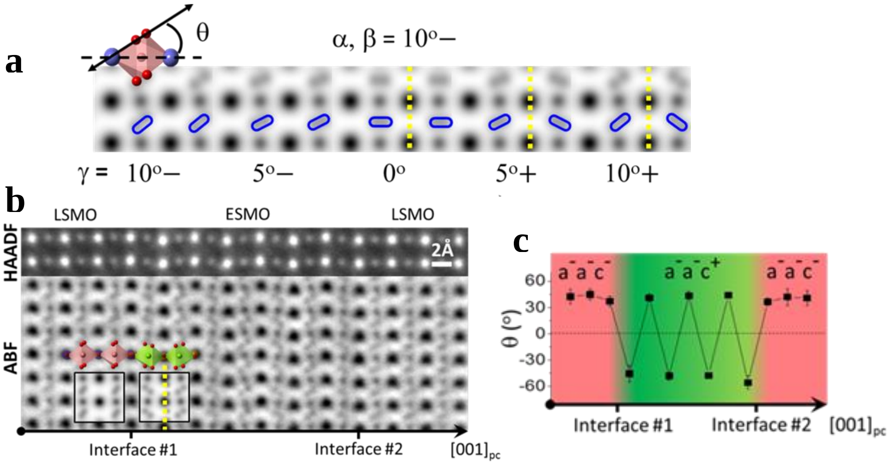

Fig.1. Quantitative determination of 3D structure evolution at perovskite oxide interfaces: (a) simulated ABF images of a series of tilted structures from $a^-a^-c^-$ to $a^-a^-c^+$, (b) HAADF and ABF images of the LSMO/ESMO superlattice showing clear transitions from $a^-a^-c^-$ to $a^-a^-c^+$ symmetry at interfaces; (c) plot of the tilt angle $\theta$ of the oxygen column ellipse computed from the ABF image in (b) (adapted from [8]).

Using the complete set of crystallographically allowed tilted perovskite unit cells,[1,2] we were able to demonstrate that any of the possible symmetries can be identified with this approach. For a subset of structures, it was also possible to discern the parameters of the 3D unit cell quantitatively. Fig.1(a) shows such an example in the progression of simulated images of structures from $a^-a^-c^-$ to $a^-a^-c^+$ with α, β = -10°, and γ varying from -10° to 10°. O column in the image (outlined in blue) has an eliptical shape. The change in symmetry ($c^-$ to $c^+$) can be clearly identified by the appearance of the mirror planes on the right hand side (denoted by yellow dashed lines). Moreover, the rotation of the main axis of the ellipse with respect to the 100 direction of the unit cell is clearly proportional to the value of γ. The same type of determination can be accomplished using experimental images; Fig. 2(b) shows HAADF and ABF images of the $(La,Sr)MnO_3/(Eu,Sr)MnO_3$(LSMO/ESMO); in the bulk, LSMO and ESMO adopt $a^-a^-c^-$ and $a^-a^-c^+$ tilt systems, respectively. Fig.1(c) shows the plot of ellipse rotation angles computed from the ABF image, demonstrating that the symmetry transition at the heterostructure interface is abrupt and that the value of γ is constant across the interface, with only the sign changing. In contrast, $CaTiO_3/(La,Sr)(Al,Ta)O_3$ interfaces (not shown) have demonstrated gradual transition between symmetries and changes in the value of the tilt angles at nm scale distances from the interface [8].

We believe that this new method will greatly enhance our capability to characterize the heterointerface structure before, after, and during phase transitions, allowing us to test the existing theories and ultimately enabling the design new materials with tailored interface properties.

***2. Atomic level sculpting of crystalline oxides***. Progress in nanoscience and technology necessitates continuous advancement in the techniques for manipulation and control of matter at the nanometer and ultimately atom by atom. The demonstration of atomic manipulation of xenon atoms by Scanning Tunneling Microscopy (STM) at IBM Almaden[3] was one of the seminal achievements of nanotechnology and nanoscience; however, this approach is limited to surface structures and is extremely slow. Aberration-corrected microscopy with its sub-Angstrom focused probe is an interesting prospect, especially given multiple reports of beam

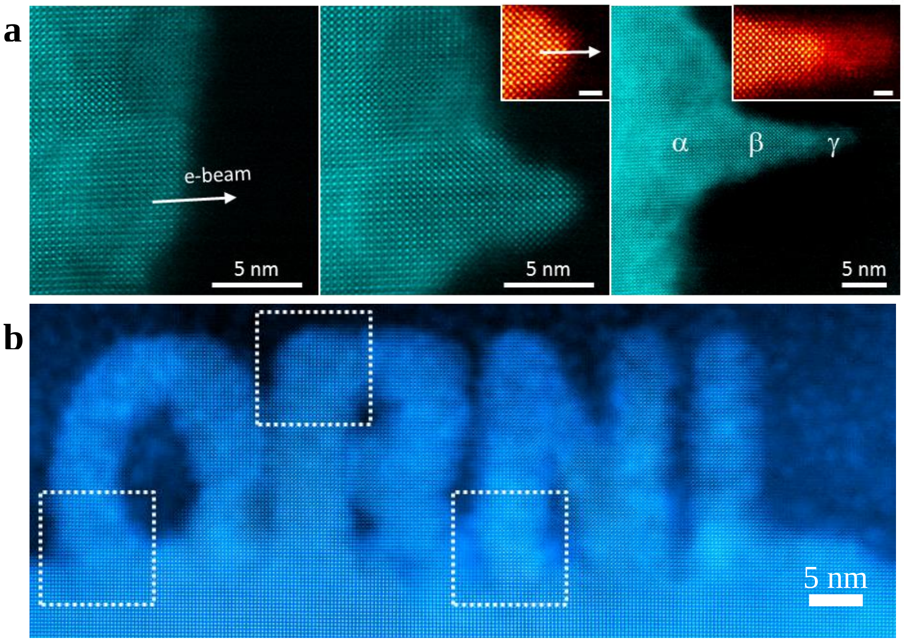

Fig.2. Atomic-level sculpting of $SrTiO_3$ with electron beam: (a) snapshots showing stages of directional growth during a linescan; (b) example of a patterned epitaxial structure (shaped as text "ORNL") demonstrating high level of precision in sculpting (adapted from [6]).

induced changes in 2D materials,[4] amorphous oxides,[5] and others. However, to make a feasible fabrication tool, one should be able to also demonstrate precise control of the process. Recently [6] we were able to show that a scanning transmission electron microscope (STEM) can create crystalline epitaxial oxide structures from metastable amorphous precursors with atomic plane precision. Fig. 2(a) shows a proof-of-concept experiment, where a slow line scan across crystalline-amorphous interface in $SrTiO_3$ results in local crystallization. Implementing flexible beam control (common for electron lithography SEM-based systems but unavailable for high resolution STEM systems) uncovers full potential of the method. Fig. 2(b) shows an artificially patterned structure spelling "ORNL" that was created from amorphous $SrTiO_3$ with 200kV electron beam. Note that the epitaxial registry with the substrate is preserved across the entire structure, and the letter shapes are instantly recognizable. Preliminary results show that this approach can also be used to create heterointerfaces. This type of experiment creates a versatile platform for the studies of diffusion and enables us to create e.g. series of structures with continuously varying length for studies of thickness-related structural transitions. Understanding and control of beam induced properties has the potential to contribute to the interpretation of many *in situ* studies conducted inside an electron microscope

***3. Investigating the electronic structure of surfaces and predicting promising routes for surface modification.*** Surfaces play an outsize role in many phase transitions and dynamic phenomena, such as oxygen reduction reactions in fuel cells or screening effects in ferroelectric materials. Ideally, one should be able to not only know the surface structure and properties in detail, but also know how these properties can be modified to potentially change the outcome of the dynamic process. Control over the functionalities of oxide surfaces, however, requires extensive quantitative information about their structure and behavior at the atomic scale to enable the construction of a comprehensive, predictive theoretical model. Recently [1] we were able to show the feasibility of this approach using $LaFeO_3/SrFeO_3$ (LFO/SFO) superlattices. Fig. 1(a) shows a HAADF STEM image of a $LFO_8/SFO$ superlattice grown by

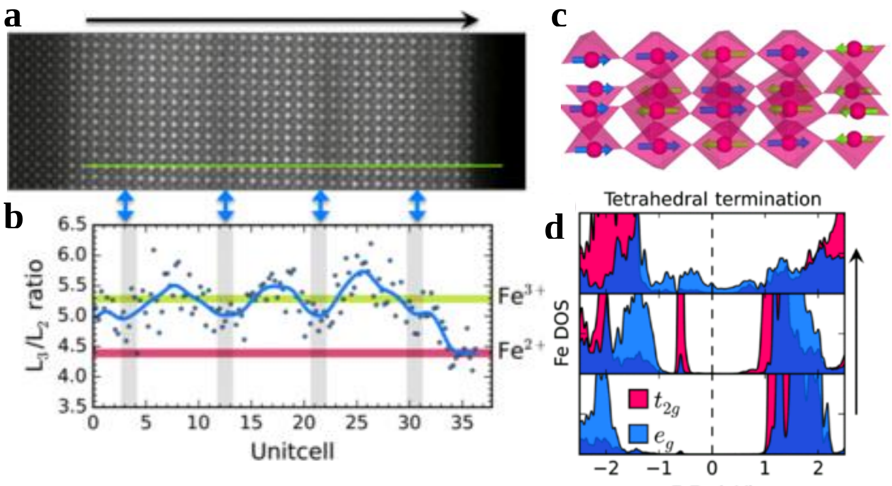

Fig.3. Electronic structure of oxide surfaces and prospects for its engineering: (a) HAADF image of the $(LaFeO_3)_8(SrFeO_3)_1$ superlattice; (b) profile of the Fe $L_3/L_2$ ratio in the superlattice; note decrease of the Fe valence at the surface; (c) lowest energy magnetic configuration and (d) Fe 3d DOS for the three top layers for highly reduced $LaFeO_3$ surface, indicating that metallic and ferromagnetic state confined to the surface can become stable at higher vacancy concentration (adapted from [1]).

Molecular Beam Epitaxy; green line denotes the direction of an EELS line scan. Fig. 2(b) shows a plot of the Fe $L_3/L_2$ ratio (indicative of Fe oxidation state) computed from the EELS data as a function of the position within the image. Within the superlattice, Fe oxidation state oscillates around +3, commensurate with superlattice periodicity. However, with 2-3 surface layers oxidation state sharply decreases to +2, indicating presence of oxygen vacancies. Investigations of the shapes of Fe L edges also show decreased coordination at the surface (octahedral and tetrahedral). Density functional calculation using a slab of $LaFeO_3$ with the surface layer was able to reproduce the experimentally observed structure of the superlattice, including polyhedral tilts. In the theoretical study it was possible to investigate surface structure as a function of vacancy content. Interestingly, for vacancy content just under fully tetrahedral Fe surface coordination, the surface is predicted to undergo an insulator to metal transition, with the bulk remaining in insulating state. Moreover, the corresponding lowest energy magnetic structure is ferromagnetic at the surface and antiferromagnetic in the bulk, a state akin to a topological insulator. This finding underscores the importance of combining high quality structural characterization with theoretical studies, and suggests a promising experimental direction using *in situ* surface reduction on this superlattice.

## Future Plans

Utilizing the methods for comprehensive structural characterization developed for the interfaces, we plan to conduct studies of oxide surfaces, specifically those of mixed ionic-electronic conductors, ex situ and in situ under applied bias. The sculpting approach that we developed will enable us to analyze the impact of the surface texture and compositional gradients in ways not achievable with conventional growth. We plan to explore whether we can control surface oxidation states via application of electrical bias. We will use our data on structure and electronic properties to develop advanced theoretical models, directing further studies. These studies will reveal the interplay between structural order parameters, strain, and oxygen chemical potential in oxides, and will enable optimization of a broad range of energy and information technologies from fuel cells to memristive data storage and logic devices.

## References

[1] A. M. Glazer, Acta Crystallographica Section B-Structural Science **B 28** (NOV15), 3384-& (1972).

[2] P. M. Woodward, Acta Cryst. Sec. B-Structural Science **53**, 44 (1997).

[3] D. M. Eigler and E. K. Schweizer, Nature **344** (6266), 524-526 (1990).

[4] Junhao Lin, Ovidiu Cretu, Wu Zhou, Kazu Suenaga, Dhiraj Prasai, Kirill I. Bolotin, Nguyen Thanh Cuong, Minoru Otani, Susumu Okada, Andrew R. Lupini, Juan-Carlos Idrobo, Dave Caudel, Arnold Burger, Nirmal J. Ghimire, Jiaqiang Yan, David G. Mandrus, Stephen J. Pennycook, and Sokrates T. Pantelides, Nat Nano **9** (6), 436-442 (2014).

[5] Kun Zheng, Chengcai Wang, Yong-Qiang Cheng, Yonghai Yue, Xiaodong Han, Ze Zhang, Zhiwei Shan, Scott X. Mao, Miaomiao Ye, Yadong Yin, and Evan Ma, Nat Commun **1**, 24 (2010).

## Publications

[1]. R. Mishra, Y.-M. Kim, Q. He, X. Huang, S. K. Kim, M. A. Susner, A. Bhattacharya, D. D. Fong, S. T. Pantelides, A. Y. Borisevich, Towards spin-polarized two-dimensional electron gas at a surface of an antiferromagnetic insulating oxide, Physical Review **B 94**, 045123 (2016)

[2]. X. Sang, A. R. Lupini, R. R. Unocic, M. Chi, A. Y. Borisevich, S. V. Kalinin, E. Endeve, R. K. Archibald and S. Jesse, Dynamic scan control in STEM: spiral scans, Advanced Structural and Chemical Imaging 2 (1), 1-8 (2016)

[3]. S. J Freakley, Q. He, J. H. Harrhy, Li Lu, D. A. Crole, D. J. Morgan, E. N. Ntainjua, J. K. Edwards, A. F. Carley, A. Y. Borisevich, C. J. Kiely, G. J. Hutchings, Palladium-tin catalysts for the direct synthesis of $H_2O_2$ with high selectivity, Science **351** (6276), 965-968 (2016)

[4]. Wu Zhou, K. Yin, C. Wang, Y. Zhang, T. Xu, A. Borisevich, L. Sun, J. C. Idrobo, M. F. Chisholm, S. T. Pantelides, R. F. Klie, A. R. Lupini, The observation of square ice in graphene questioned, Nature **528** E1 (2015)

[5]. Y. Y. Zhang, R. Mishra, T. J. Pennycook, A. Y. Borisevich, S. J. Pennycook and S. T. Pantelides, Oxygen Disorder, a Way to Accommodate Large Epitaxial Strains in Oxides, Adv. Mater. Interfaces, **2** 00344 (2015)

[6]. S. Jesse, Q. He, A. R. Lupini, D. N. Leonard, M. P. Oxley, O. Ovchinnikov, R. R. Unocic, A. Tselev, M. Fuentes-Cabrera, B. G. Sumpter, S. J. Pennycook, S. V. Kalinin, A. Y. Borisevich, Atomic-Level Sculpting of Crystalline Oxides: Toward Bulk Nanofabrication with Single Atomic Plane Precision, Small, **11** 5895 (2015)

[7]. A. Belianinov, Q. He, M. Kravchenko, S. Jesse, A. Borisevich & S. V. Kalinin, Identification of phases, symmetries and defects through local crystallography, Nature Commun., **6** 7801 (2015)

[8]. Q. He, R. Ishikawa, A. R. Lupini, L. Qiao, E. J. Moon, O. Ovchinnikov, S. J. May, M. D. Biegalski, A. Y Borisevich, Towards 3D Mapping of $BO_6$ Octahedron Rotations at Perovskite Heterointerfaces, Unit Cell by Unit Cell, ACS Nano, **9** 8412 (2015)

[9]. Q. He, J. Woo, A. Belianinov, V. V. Guliants and A. Y. Borisevich, Better Catalysts through Microscopy: Nanometer Scale M1/M2 Intergrown Heterostructure in Mo-VM Complex Oxides, *ACS Nano*, **9** 3470–3478 (2015)

[10]. M. D. Biegalski, L. Qiao, Y. Gu, A. Mehta, Q. He, Y. Takamura, A. Borisevich, L.-Q. Chen, Impact of symmetry on the ferroelectric properties of $CaTiO_3$ thin films, Appl. Phys. Lett., **106** 162904 (2015)

[11]. YL Tang, YL Zhu, XL Ma, AY Borisevich, AN Morozovska, EA Eliseev, WY Wang, YJ Wang, YB Xu, ZD Zhang, SJ Pennycook, Observation of a periodic array of flux-closure quadrants in strained ferroelectric PbTiO3 films, *Science,* **348** 547-551 (2015)

[12]. A. Belianinov, Q. He, A. Dziaugys, P. Maksymovych, E. A. Eliseev, A. Borisevich, A. Morozovska, J. Banys, Y. Vysochanskii, S. V Kalinin, $CuInP_2S_6$-Room Temperature Layered Ferroelectric, *Nano Lett.*, **15** 3808–3814 (2015) (PTS # 56695)

[13]. YW Yin, M Raju, WJ Hu, JD Burton, Y-M Kim, AY Borisevich, SJ Pennycook, SM Yang, TW Noh, A Gruverman, XG Li, ZD Zhang, EY Tsymbal, Qi Li, Multiferroic tunnel junctions and ferroelectric control of magnetic state at interface, *J. Appl. Phys*., **117** 172601 (2015) A. Belianinov, R. Vasudevan, E. Strelcov, C. Steed, S. M. Yang, A. Tselev, S. Jesse, M. Biegalski, G. Shipman, C. Symons, A. Borisevich, R. Archibald, S. Kalinin, Big data and deep data in scanning and electron microscopies: deriving functionality from multidimensional data sets, *Advanced Structural and Chemical Imaging*, **1** 1-25 (2015)

[14]. L. Qiao, J. H. Jang, D. J. Singh, Z. Gai, H. Xiao, A. Mehta, R. K. Vasudevan, A. Tselev, Z. Feng, H. Zhou, S. Li, W. Prellier, X. Zu, Z. Liu, A. Borisevich, A. P. Baddorf, M. D. Biegalski, Dimensionality Controlled Octahedral Symmetry-Mismatch and Functionalities in Epitaxial $LaCoO_3/SrTiO_3$ Heterostructures, *Nano Lett.*, **15** 4677–4684 (2015)

[15]. E. Strelcov, J. Cothren, D. Leonard, A. Y. Borisevich and A. Kolmakov, In situ SEM study of lithium intercalation in individual $V_2O_5$ nanowires, Nanoscale 7 3022-27 (2015)

[16]. E. - M. Choi, T. Fix, A. Kursumovic, C. J. Kinane, D. Arena, S. - L. Sahonta, Z. Bi, J. Xiong, Li Yan, J. - S. Lee, H. Wang, S. Langridge, Y. - M. Kim, A. Y Borisevich, I. MacLaren, Q. M. Ramasse, M. G. Blamire, Q. Jia, J. L. MacManus - Driscoll, Room Temperature Ferrimagnetism and Ferroelectricity in Strained, Thin Films of $BiFe_{0.5}Mn_{0.5}O_3$, Adv. Func. Mater., 24(47), 7478-7487 (Dec. 2014)

[17]. Y.-M. Kim, A. Morozovska, E. Eliseev, M. P. Oxley, R. Mishra, S. M. Selbach, T. Grande, S.T. Pantelides, S. V. Kalinin, A. Y. Borisevich, Direct observation of ferroelectric field effect and vacancy-controlled screening at the $BiFeO_3/La_xSr_{1-x}MnO_3$ interface, Nature Mater., 13, 1019 (Nov 2014).

[18]. M. Biegalski, Y.i Takamura, A. Mehta, Z. Gai, S. V. Kalinin, H. Ambaye, V. Lauter, D. Fong, S. T. Pantelides, Y. M. Kim, J. He, A. Borisevich, W. Siemons, H. M. Christen, Interrelation between Structure – Magnetic Properties in $La_{0.5}Sr_{0.5}CoO_3$, Adv. Mater. Interfaces, 1(8) 1400203 (Nov 2014)

# Complex Fundamental Mechanisms of Transient States in Materials Quantified by DTEM

**Geoffrey H. Campbell (PI), Joseph T. McKeown, Robert E. Rudd, Tian T. Li, Garth C. Egan, and Tae Wook Heo**

**Materials Science Division, Physical and Life Sciences Directorate, Lawrence Livermore National Laboratory, PO Box 808, Livermore, CA 94550, Email: ghcampbell@llnl.gov**

## Program Scope

The thrust of this project is to measure rates of processes occurring during solid – solid phase transformations in materials, explore the variability of these rates as they depend on pre-existing structure of the materials, and compare with simulations of the phase transformations to reveal and quantify the fundamental controlling mechanisms. To make measurements of the dynamic event *in situ*, we use a time resolved transmission electron microscope (DTEM) that is still unique in the world because of its single shot imaging capability. Since it is a real space imaging capability, it allows us to identify and measure rates of individual processes, for example nucleation or growth, which other methods cannot deconvolve. We currently focus on the amorphous to crystalline transformation in semiconductors and investigate the effect of changes in the glass structure on transformation rates.

## Recent Progress

The structure-property relationships of amorphous group IV semiconductors such as germanium (a-Ge) have attracted wide research interest over the past decades. It has been shown that the crystallization behavior of amorphous semiconductors can vary significantly due to changes in the medium range order (MRO) of the material[1-3]. MRO extends beyond the nearest neighbor atom and has a typical length scale of 1 – 3 nm. MRO has been shown to be present in many amorphous materials including a-Ge[1-6], and can be altered by post-processing such as thermal annealing[1, 3, 6], ion and electron irradiation[1, 4, 6], and mechanical stress[1].

It has been reported that laser-induced rapid crystallization of a-Ge is facilitated by the formation and propagation of a thin, undercooled liquid layer[7-11]. We investigated the effect of MRO on liquid-mediated crystallization dynamics using the movie-mode DTEM. We prepared our a-Ge thin film by DC magnetron sputtering. 33 ± 1 nm of a-Ge was sputtered at room temperature onto commercially available TEM grids with a $SiN_x$ window of 20 nm thick, 0.25 x 0.25 mm in size. In order to alter the MRO of the a-Ge thin films, we irradiated them at liquid nitrogen temperature with 500 keV $^{40}Ar^+$ ions with a constant dose rate of $10^{12}$ ions $cm^{-2}s^{-1}$ using the 4 MV ion accelerator at LLNL. The total dose rate was 4 x $10^{14}$ ions $cm^{-2}$. For the given irradiation condition, >99.5% of $Ar^+$ ions penetrates completely through the a-Ge thin film, assuring that any observed differences will not be due to residual Ar remaining in the film as a result of ion bombardments.

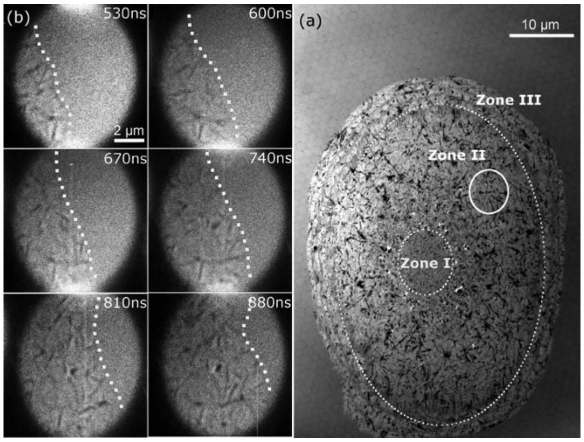

Figure 1: (a) Bright field TEM image of the 33 nm as-deposited a-Ge thin film after crystallized by a single 3.3 μJ laser shot. (b) Time resolved images over the circled region in (a) at the time step, relative to the specimen laser heating, indicated on each frame. The migration of Zone II crystallization front is marked by the dotted line.

For the movie-mode DTEM experiments, we use 3.3 ± 0.2 μJ laser pulses to induce the crystallization. Figure 1a shows a typical bright field image of the crystallized region, where we can see formation of all three zones defined in previous publications[9, 12, 13]. We observe here the evolution of the Zone II crystallization front. Each crystallization event was imaged using nine 20-ns electron pulses with 50 ns delay between each pulse. To account for the incubation time for nucleation and zone I growth, we introduced a delay of 340 ns between the specimen laser and the first electron pulse. We positioned our field of view (circled in Fig. 1a) to image Zone II formation, and could clearly track the position of the crystallization front at different time steps (Fig. 1b). In this "movie", the crystallization front appeared in the field of view at ~500 ns after the specimen laser pulse, and moved across a region of ~4μm over ~350 ns. We captured several movies of the crystallization process for both as-deposit and ion-bombarded materials.

We use fluctuation electron microscopy (FEM) to measure the MRO in the various a-Ge samples. FEM is based on statistical analysis of the scattering data and has the unique sensitivity to MRO in otherwise diffraction amorphous materials [2, 4, 5, 14]. We perform FEM experiments on the Zeiss Libra microscope at the National Center for Electron Microscopy (NCEM) at LBNL. The Libra operates at 200kV in STEM mode and we formed a minimally convergent 2.0± 0.1 nm (FWHM) electron probe and collected hundreds of localized diffraction patterns as the electron probe rasters over the sample. We then calculate the normalized variance of the diffraction intensity. A higher variance means an increase of MRO in the material[14, 15]. Figure 2 shows the FEM spectra of as-deposit and ion-bombarded material with the inset comparing the traditional, large-area diffraction intensities of the two samples. While the large-area diffraction intensity remains the same after ion bombardment, the reduction in variance peak magnitude clearly shows a reduction of MRO in the bombarded sample. We interpret the reduction of MRO in the bombarded film as $Ar^+$ ions displacing Ge atoms that form ordered clusters[16, 17].

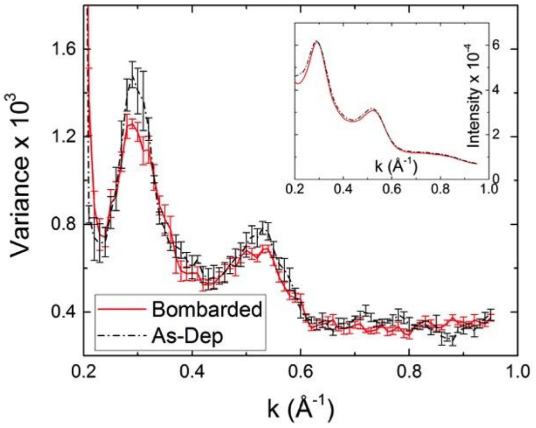

Figure 2: FEM variance spectra of the as-deposit versus ion-bombarded a-Ge thin films. The inset shows the intensity profiles of the two materials being virtually indistinguishable under traditional, large area diffraction. Both the FEM variance and diffraction intensity have broad peaks centered at k ≈ 0.29Å$^{-1}$ and k ≈ 0.52 Å$^{-1}$, matching the structural factor maxima.

Figure 3 shows the growth front position as a function of time for both as-deposited and bombarded samples. Each symbol and line fit corresponds to an individual crystallization event. Data from each crystallization event are shifted arbitrarily in the vertical direction for clarity. The observed velocities are within the range of previously reported values of 8 – 12 m/s[9, 13, 18, 19]. The weighted average shows that the crystalliza-

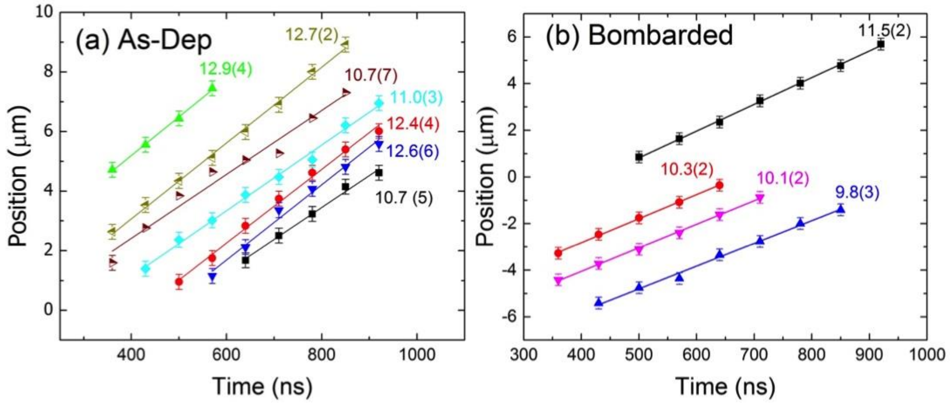

Figure 3: Position of the Zone II crystallization front as a function of time for (a) as-deposited a-Ge and (b) after bombarded by $Ar^+$. Time = 0 corresponds to when the laser hits the specimen. Each symbol corresponds to an individual crystallization event and is fitted to a straight line. The number is the crystallization front migration velocity (slope of the line) in m/s, with the number in the parentheses indicating the uncertainty on the last digit.

tion front velocity of the bombarded film is 10.5 ± 0.7 m/s, whereas the as-deposit film has velocity of 12.0 ± 0.9 m/s. The 95% confidence interval of the velocity difference is 1.5 ± 0.9 m/s, clearly suggesting a statistically significant reduction in crystallization velocity upon ion bombardment.

Our result clearly shows that the bombarded material, resulting in less MRO, exhibits the slower Zone II crystallization front migration. We hypothesize that the differences in MRO changed the formation a thin liquid layer during crystallization, and altered the energetic landscape of the system. To verify the possible mechanisms, we employ a phase-field model [20, 21] for simulating the crystallization process involving a thin liquid layer. Our simulation results in Figure 4 establish two mechanisms that support our proposed hypotheses. First, the liquid layer provides enhanced mobility and sensitivity of migration rates to the driving force for crystallization Δ*f*. These results indicate that the liquid layer is likely to lead to the observed variation of the rates of crystallization. According to our simulation results in Figure 4a, the larger driving force drives the faster interface migration, which suggests that our ion-bombarded material could have lower internal energy than the as-deposit material. Second, the liquid layer lateral thickness evolution is sensitive to the crystallization driving force Δ*f*. It indicates the possibility of further impacts to the liquid layer on the kinetic behavior of crystallization. In particular, as shown in Figure 4b, the thickness evolution exhibits highly nonlinear characteristics with time and Δ*f*. After the liquid layer is gone, we confirmed that crystallization is sluggish. Therefore, we may further consider the possible strategies to control the liquid phase behavior by changing the microscopic structures (or MRO) of the prepared amorphous phase, which

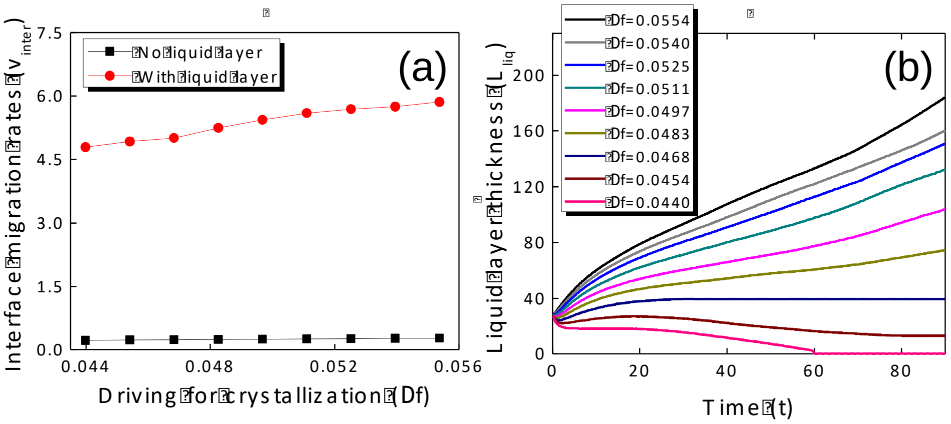

Figure 4: Phase-field simulations of interface evolution: **(a)** simulated interface migration rates as a function of the driving force for crystallization, Δ*f*, without and with a thin liquid layer at the interface (for Δ*f*=0.0440, the rate is obtained only when the liquid layer is retained), and **(b)** corresponding liquid layer lateral thickness evolution with time for different driving forces for crystallization.

determines the overall crystallization rates.

## Future Plans

It's not obvious what the ion bombardment did to the free energy of the amorphous phase. It may have increased it or decreased it. As such, we will be treating thin amorphous films of Ge under differing conditions, for example by annealing, in order to change the energetics of the amorphous phase in a well defined way (it should be lowered). These amorphous structures will be characterized and quantified with fluctuation electron microscopy (FEM) and then their crystallization kinetics measured in the DTEM. We will use phase field simulations to create model predictions of transformation rates to quantitatively compare to the experimental results. The trends found should further elucidate the effects of ion bombardment on the structure of the amorphous Ge.

## References

1. B. Haberl, S. N. Bogle, T. Li, I. McKerracher, S. Ruffell, P. Munroe, J. S. Williams, J. R. Abelson and J. E. Bradby, Journal of Applied Physics **110** (9), 096104 (2011).
2. K. Darmawikarta, S. Raoux, P. Tchoulfian, T. Li, J. R. Abelson and S. G. Bishop, Journal of Applied Physics **112** (12), 124907 (2012).
3. B.-S. Lee, G. W. Burr, R. M. Shelby, S. Raoux, C. T. Rettner, S. N. Bogle, K. Darmawikarta, S. G. Bishop and J. R. Abelson, Science **326** (5955), 980-984 (2009).
4. T. T. Li, T. H. Lee, S. R. Elliott and J. R. Abelson, Applied Physics Letters **103** (20) 201907 (2013).
5. M. M. J. Treacy and K. B. Borisenko, Science **335** (6071), 950-953 (2012).
6. J. Y. Cheng, J. M. Gibson and D. C. Jacobson, Journal of Materials Research **16** (11), 3030-3033 (2001).
7. F. Spaepen and D. Turnbull, AIP Conference Proceedings **50** (1), 73-83 (1979).
8. B. G. Bagley and H. S. Chen, presented at the Materials Research Society, Boston, 1979.
9. M. K. Santala, S. Raoux and G. H. Campbell, Applied Physics Letters **107** (25), 252106 (2015).
10. A. P. Chojnacka, Ph.D. Thesis, Cornel University, 2002.
11. C. Grigoropoulos, M. Rogers, S. H. Ko, A. A. Golovin and B. J. Matkowsky, Physical Review B **73** (18), 184125 (2006).
12. L. Nikolova, T. LaGrange, B. W. Reed, M. J. Stern, N. D. Browning, G. H. Campbell, J.-C. Kieffer, B. J. Siwick and F. Rosei, Applied Physics Letters **97** (20), 203102 (2010).
13. L. Nikolova, T. LaGrange, M. J. Stern, J. M. MacLeod, B. W. Reed, H. Ibrahim, G. H. Campbell, F. Rosei and B. J. Siwick, Physical Review B **87** (6), 064105 (2013).
14. M. M. J. Treacy, J. M. Gibson, L. Fan, D. J. Paterson and I. McNulty, Reports on Progress in Physics **68** (12), 2899 (2005).
15. T. T. Li, S. N. Bogle and J. R. Abelson, Microscopy and Microanalysis **20** (5), 1605-1618 (2014).
16. S. V. Khare, S. M. Nakhmanson, P. M. Voyles, P. Keblinski and J. R. Abelson, Applied Physics Letters **85** (5), 745-747 (2004).
17. N. B. Stephanie, M. V. Paul, V. K. Sanjay and R. A. John, Journal of Physics: Condensed Matter **19** (45), 455204 (2007).
18. L. Nikolova, M. J. Stern, J. M. MacLeod, B. W. Reed, H. Ibrahim, G. H. Campbell, F. Rosei, T. LaGrange and B. J. Siwick, Journal of Applied Physics **116** (9), 093512 (2014).
19. O. Bostanjoglo, R. P. Tornow and W. Tornow, Ultramicroscopy **21** (4), 367-372 (1987).
20. L.-Q. Chen, Annual Review of Materials Research **32** (1), 113-140 (2002).
21. I. Steinbach, Modelling and Simulation in Materials Science and Engineering **17** (7), 073001 (2009).

## Publications

L. Nikolova, M.J. Stern, J.M. MacLeod, B.W. Reed, H. Ibrahim, G.H. Campbell, F. Rosei, T. LaGrange, and B.J. Siwick, "*In situ* investigation of explosive crystallization in a–Ge: Experimental determination of the interface response function using dynamic transmission electron microscopy," *Journal of Applied Physics* **116** [9] 093512 (2014).

M.K. Santala, S. Raoux, T. Topuria, B.W. Reed, T. LaGrange, and G.H. Campbell, "Distinguishing mechanisms of morphological instabilities in phase change materials during switching," *Thin Solid Films*, **571** 39 – 44 (2014).

M.D. Grapes, T. LaGrange, K. Woll, B.W. Reed, G.H. Campbell, D.A. LaVan, and T.P. Weihs, "*In Situ* TEM investigation of the interfacial reaction between Ni and Al during rapid heating in a nanocalorimeter," *APL Materials* **2** [11] 116102 (2014).

G.H. Campbell, J.T. McKeown, and M.K. Santala, "Time resolved electron microscopy for *in situ* experiments," *Applied Physics Reviews* **1** [4] 041101 (2014).

J.T. McKeown, Y. Wu, J.D. Fowlkes, P.D. Rack, G.H. Campbell, "Simultaneous in-situ synthesis and characterization of Co@Cu core-shell nanoparticle arrays," *Advanced Materials* **27** [6] 1060 – 1065 (2015).

X. Zhang, T. Hu, J.F. Rufner, T. LaGrange, G.H. Campbell, E.J. Lavernia, J.M. Schoenung, K. van Benthem, "Metal/ceramic interface structures and segregation behavior in aluminum-based composites," *Acta Materialia* **95** 254 – 263 (2015).

M.K. Santala, S. Raoux, and G.H. Campbell, "Kinetics of liquid-mediated crystallization of amorphous Ge from multi-frame dynamic transmission electron microscopy," *Applied Physics Letters*, **107** [25] 252106 (2015).

Grapes, M.D., Zhang, Y., Santala, M.K., Voisin, T., Campbell, G.H. and Weihs, T.P., "In Situ High-Rate Mechanical Testing in the Dynamic Transmission Electron Microscope," in *MEMS and Nanotechnology, Volume 5* (pp. 25-30), Springer International Publishing (2016).

J.T. McKeown, K. Zweiacker, C. Liu, D.R. Coughlin, A.J. Clarke, J.K. Baldwin, J.W. Gibbs, J.D. Roehling, S.D. Imhoff, P.J. Gibbs, D. Tourret, J.M.K. Wiezorek, and G.H. Campbell, "Time-Resolved In Situ Measurements During Rapid Alloy Solidification: Experimental Insight for Additive Manufacturing," *JOM*, **68** [3] 985 – 999 (2016).

S. Hihath, M.K. Santala, X. Cen, G.H. Campbell, K. van Benthem, "High speed direct imaging of thin metal film ablation by movie-mode dynamic transmission electron microscopy," *Scientific Reports* **6**, 23046 (2016).

T.T. Li, L.B. Bayu Aji, M.K. Santala, S.O. Kucheyev, and G.H. Campbell, "The effect of medium range order on pulsed laser crystallization of amorphous germanium thin films," *Applied Physics Letters* **108** [22] 21906 (2016).

M.M. Winsek, H.Y. Cheng, G.H. Campbell, and M.K. Santala, "Crystallization kinetics of the phase change material GeSb6Te measured with dynamic transmission electron microscopy," *Dalton Transactions* **45** [45] 9988 – 9995 (2016).

K. Zweiacker, J.T. McKeown, C. Liu, T. LaGrange, B.W. Reed, G.H. Campbell, and J.M.K. Wiezorek, "Determination of crystal growth rates during rapid solidification of polycrystalline aluminum by nano-scale spatio-temporal resolution *in situ* transmission electron microscopy," *Journal of Applied Physics* **120** [5] 055106 (2016).

S. Hihath, M.K. Santala, G. H. Campbell, K. van Benthem, "High-speed nanoscale characterization of dewetting via dynamic transmission electron microscopy," *Journal of Applied Physics* **120** [8] 085301 (2016).

# Scanning Transmission Electron Microscopy: Atomic Structure and Properties of Materials

## Functional Structures in 2D Materials

**Principle Investigators: Matthew F. Chisholm, Wu Zhou, Andrew R. Lupini, Mark P. Oxley**

**Materials Science & Technology Division, Oak Ridge National Laboratory, TN 37831**

### Research Scope

The mission of this project is to transform our understanding of how interfaces, surfaces and other defects impact *functionality* and structures at the atomic level. With the installation of a new sharper emitter, the Nion UltraSTEM200 has achieved atomic resolution while operating at 40 keV. With this tool, the group can now probe the connections between a material's spin, charge, orbital and structural degrees of freedom with accelerating voltages ranging from 40 to 200 keV. The scientific advances from this work will provide new approaches to determine local functionalities at the atomic scale, enabling fundamental understanding of materials properties that is crucial for further development of energy materials. Here we focus on our recent studies of functional structures in 2D materials.

### Recent Progress

Two-dimensional materials have relatively simple structures for both electron microscopy and theoretical modeling and contain rich new physics and novel properties. They serve as an excellent platform to obtain the fundamental correlation of defect structure and local properties at the single atom level via low-voltage STEM imaging and spectroscopy and to further develop quantitative microscopy. Understanding the materials physics of these systems enables fundamental understanding of how local variations of properties interact with atomic structure and will ultimately lead to the design of improved energy materials.

#### 1. Functional Graphene

Pure graphene has limited practical applications due to its low carrier density, zero band gap, and chemical inertness. The controlled introduction of nanoscale pores in graphene will be necessary for applications that involve water purification, chemical separation, and DNA sequencing. However, graphene nanopores are unstable against filling by carbon adatoms.*(1)* Using aberration-corrected scanning transmission electron microscopy and density-functional calculations, we found that Si atoms stabilize graphene nanopores by bridging the dangling bonds around the perimeter of the hole as seen in Figure 1. Si-passivated pores remain intact even under intense electron beam irradiation, and they were observed several months after the sample fabrication, demonstrating that these

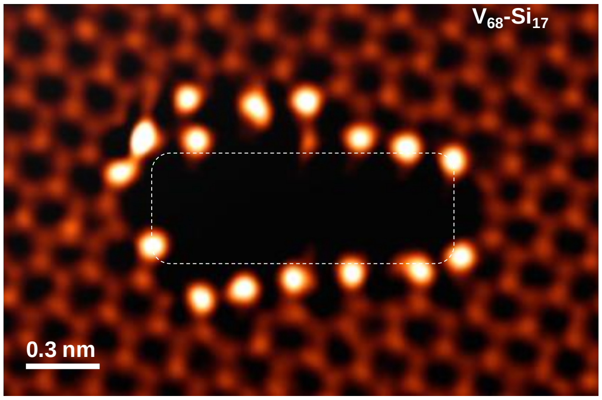

Figure 1 *Z*-contrast image of a graphene nanopore passivated with 17 Si atoms.

structures are intrinsically robust and stable against carbon filling. Theoretical calculations reveal the underlying mechanism for this stabilization effect: Si atoms bond strongly to the graphene edge, and their preference for tetrahedral coordination forces C adatoms to form dendrites sticking out of the graphene plane, instead of filling the nanopore. Our results provide a novel way to develop stable nanopores, which is a major step toward reliable graphene-based molecular translocation devices.*(2)*

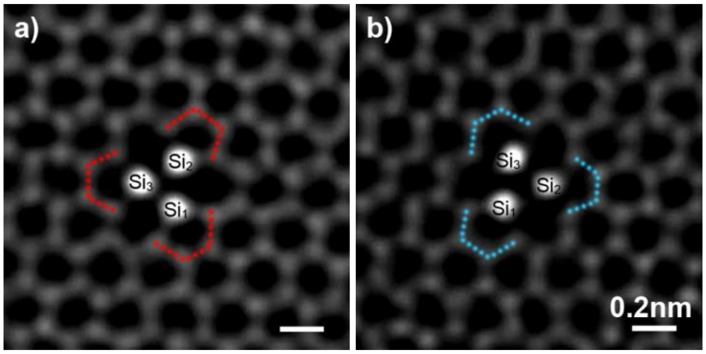

Figure 2. STEM image shows a silicon trimer in graphene nanopore (a) before and (b) after one stepwise rotation.

We observed three silicon atoms that replaced a single hexagonal ring of carbon atoms in a graphene layer (Fig. 2), under the electron beam, rotates as a single unit in stepwise jumps while the surrounding carbon atoms remain fixed. Theoretical calculations indicate that the energy barrier to rotate the trimer is about 2 eV, corresponding to a tangential force of only 4.3 nN parallel to the graphene layer. This small force, provided by an electron beam to any of the three silicon atoms, generates a torque on the trimer and results in a rotation of 60° in about 140 femtoseconds and demonstrates that the ultimate miniaturization of a mechanical device (switch, oscillator, stirrer) down to a triangular arrangement of three atoms is possible. *(3)*

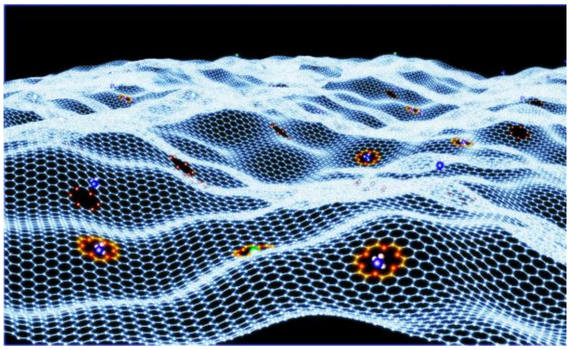

Figure 3. Schematic showing a graphene sheet containing an array of ideal crown ethers.

We found that residual oxygen atoms in oxidized graphene form highly stable crown ether configurations within the two-dimensional graphene layer. *(4)* Density functional calculations show that these oxygen atoms have binding energies of ~9 eV. The calculations indicate that the crown ether configurations in graphene should exhibit selectivity for different cations depending on the crown ether ring size, a key property of individual crown ether molecules, but have the added property of being rigid and planar, prized features sought in preorganized receptors for selective ion binding. The demonstration of ideal crown ethers in graphene with greatly increased binding energy is expected to open up new applications in a wide range of fields, including sensing, analytical separations, nuclear-waste cleanup, hydrometallurgy, biotechnology, catalysis, medicine and information storage. Additionally, crown ethers in graphene offer a simple environment that can be systematically tested and modeled. Thus, we expect that our finding will introduce a new wave of investigations and applications of chemically functionalized graphene.

## 2. Transition metal dichalcogenides

Transition metal dichalcogenides (TMDC) have exceptional optical and transport properties (*5*,*6*). An important step towards practical application of these materials is to realize large-scale growth of monolayers and to understand the intrinsic structural defects present in these CVD-grown monolayers. However, obtaining intrinsic structural information from the semiconducting TMDC monolayers with atomic resolution is challenging, as the material is prone to both knock-on damage at high electron beam energy and ionization damage at low voltage. In collaboration with Pulickel Ajayan and Jun Lou's groups at Rice University, who were among the first to demonstrate CVD growth of centimeter size $MoS_2$ monolayers (*7*,*8*), we used low-voltage STEM imaging to systematically study intrinsic structural defects, including point defects, defect complexes, dislocation cores, grain boundaries, and edges, in these CVD $MoS_2$ monolayers (*7*,*9*). We showed that both mono-vacancies of Mo and S as well as anti-site defects and vacancy complexes are naturally present during the CVD growth process (Fig. 4A). These point defects induce deep levels within the bandgap, and may contribute to the omnipresence of n-type conductivity in CVD $MoS_2$. With quantitative low-voltage STEM, the various theoretically predicted dislocation core structures were experimentally observed for the first time (Fig. 4B). We also identified two new types of 60˚ grain boundaries, consisting of 4-fold rings (Fig. 4C), which are shown to be metallic by DFT calculations, and can serve as conducting channels within the semiconducting matrix. This is the first comprehensive study of structural defects in monolayer TMDC materials, and serves as the foundation for continuing studies on these materials.

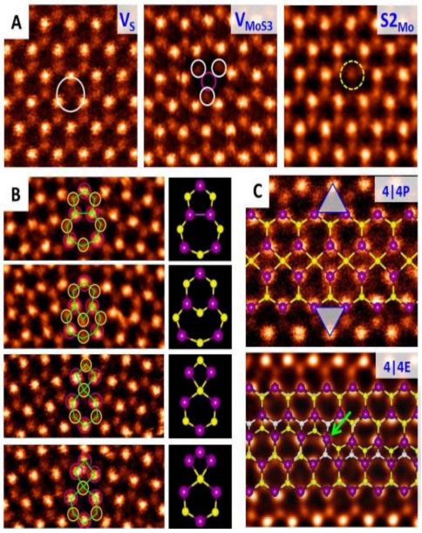

Figure 4. STEM annular dark field images of intrinsic defects in CVD-grown $MoS_2$ monolayer. (A) Point defects; (B) Dislocation cores; (C) 60˚ grain boundaries.

In the pursuit of ultrasmall electronic components, monolayer electronic devices have been fabricated using transition-metal dichalcogenides. However, the controlled connection of individual nanowires to monolayers, an important step in creating a two-dimensional integrated circuit, has so far remained elusive. In this work, by steering a focused electron beam, as shown in Figure 5, we produced MX nanowires that are less than a nanometer in width and Y junctions that connect designated points within a transition-metal dichalcogenide monolayer.*(10)* In situ electrical measurements demonstrate that these nanowires are metallic, so they can serve as interconnects in future flexible nanocircuits fabricated entirely from the same monolayer.

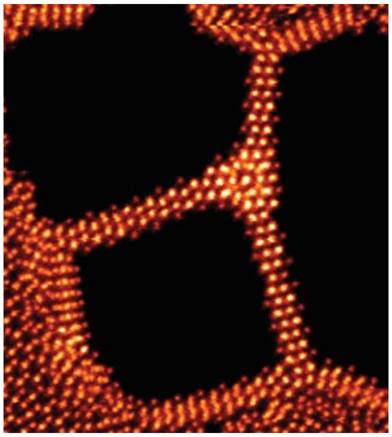

Figure 5. Fabrication of nanowires from $MoSe_2$ monolayers using a focused electron beam. STEM annular dark field image of Y junction of thee MoSe metal wires.

## Future Plans

For wide range of material systems, properties are controlled by local structure at atomic defects and interfaces. The aberration corrected STEM can reveal the density, distribution, atomic species and configurations at point defects, grain boundaries and edges. What is now needed is a means to obtain the vibrational, magnetic and optical properties of these local atomic arrangements. Thus, the goal of this project is to transform our understanding of how interfaces, surfaces and other defects impact functionality and structures at the atomic level. Specifically, we plan (1) to enable the measurement of local physical properties down to the level of single atom dopants, defect configurations and interfaces in 2D materials, (2) to realize true atomic resolution of both structure and functionality by incorporating dynamical scattering effects in data analysis and (3) to understand local transport in optically active materials through *in-situ* measurements of properties. Realizing all three of these goals will require novel applications of existing state-of-the-art microscopes, development of new techniques and close integration with theory.

As we develop new capabilities to measure atomic-scale properties, we will continue to focus on 2D layered materials, as these are both relevant and model energy materials. High-quality samples of new and cutting edge materials will be obtained through collaborations with groups at ORNL and others worldwide. Collaborations with theorists at ORNL and especially with Professor Sokrates T. Pantelides of Vanderbilt University study correlations between local atomic configurations and functionalities.

## References

[1] R. Zan, Q. M. Ramasse, U. Bangert, K. S. Novoselov, Graphene reknits its holes. *Nano Letters* **12**, 3936-3940 (2012).

[2] J. Lee, Z. Yang, W. Zhou, S. J. Pennycook, S. T. Pantelides, M. F. Chisholm, Stabilization of graphene nanopore. *Proceedings of the National Academy of Sciences* **111**, 7522-7526 (2014).

[3] Z. Yang, L. Yin, J. Lee, W. Ren, H.-M. Cheng, H. Ye, S. T. Pantelides, S. J. Pennycook, M. F. Chisholm, Direct Observation of Atomic Dynamics and Silicon Doping at a Topological Defect in Graphene. *Angewandte Chemie International Edition* **53**, 8908-8912 (2014).

[4] J. Guo, J. Lee, C. I. Contescu, N. C. Gallego, S. T. Pantelides, S. J. Pennycook, B. A. Moyer, M. F. Chisholm, Crown ethers in graphene. *Nature Communications* **5**, 5389 (2014).

[5] K. F. Mak, C. Lee, J. Hone, J. Shan, T. F. Heinz, Atomically thin $MoS_2$: A new direct-gap semiconductor. *Physical Review Letters* **105**, 136805 (2010).

[6] Q. H. Wang, K. Kalantar-Zadeh, A. Kis, J. N. Coleman, M. S. Strano, Electronics and optoelectronics of two-dimensional transition metal dichalcogenides. *Nature Nanotechnology* **7**, 699-712 (2012).

[7] S. Najmaei, Z. Liu, W. Zhou, X. Zou, G. Shi, S. Lei, B. I. Yakobson, J.-C. Idrobo, P. M. Ajayan, J. Lou, Vapour phase growth and grain boundary structure of molybdenum disulphide atomic layers. *Nature Materials* **12**, 754-759 (2013).

[8] A. M. van der Zande, P. Y. Huang, D. A. Chenet, T. C. Berkelbach, Y. You, G.-H. Lee, T. F. Heinz, D. R. Reichman, D. A. Muller, J. C. Hone, Grains and grain boundaries in highly crystalline monolayer molybdenum disulfide. *arXiv:1301.1985*, (2013).

[9] W. Zhou, X. Zou, S. Najmaei, Z. Liu, Y. Shi, J. Kong, J. Lou, P. M. Ajayan, B. I. Yakobson, J.-C. Idrobo, Intrinsic Structural Defects in Monolayer Molybdenum Disulfide. *Nano Letters* **13**, 2615-2622 (2013).

[10] J. Lin, O. Cretu, W. Zhou, K. Suenaga, D. Prasai, K. I. Bolotin, N. T. Cuong, M. Otani, S. Okada, A. R. Lupini, J.-C. Idrobo, D. Caudel, A. Burger, N. J. Ghimire, J. Yan, D. G. Mandrus, S. J. Pennycook, S. T. Pantelides, Flexible metallic nanowires with self-adaptive contacts to semiconducting transition-metal dichalcogenide monolayers. *Nature Nanotechnology* **9**, 436-442 (2014).

# Spectroscopic Imaging STM and Complex Electronic Matter

**Kazuhiro Fujita**
CMP&MS Department, Brookhaven National Laboratory, Upton, NY 11973, USA
Office: 631-344-3933 / Mobile: 607-351-5800 / Email: kfujita@bnl.gov

**J. C. Séamus Davis**
CMP&MS Department, Brookhaven National Laboratory, Upton, NY 11973, USA
LASSP, Physics Department, Cornell University, Ithaca, NY 14853, USA.
Office: 607-254-8965 / Mobile: 607-220-8685 / Email: jcseamusdavis@gmail.com

## Research Scope

We study advanced quantum materials with focus on superconductivity, gapped topological matter, spin liquids, nematic and density wave ordered states. We address these issues by direct atomic scale visualization of electronic structure using a suite of specialized SI-STM systems, or by advanced magnetic transport and imaging techniques.

## Recent Progress

### *1. Discovery of Pair Density Wave State in Cuprate HTS*

A central issue of copper-oxide high temperature superconductivity research is to understand the relationship between the hole-doped antiferromagnetic Mott insulator (MI) and both the superconducting and broken-symmetry states. Our technique for sub-lattice phase-resolved electronic structure visualization revealed the existence of the cuprate electronic nematic [1], that the cuprate charge density wave (CDW) has a predominant *d*-symmetry form factor [2,3], and that the disappearance of both these broken-symmetry states near the doping terminus of the pseudogap ($p$=19%) coincides with the *k*-space reconstruction [4]. The existence of this exotic d-symmetry CDW state then motivated widespread predictions that the pseudogap phase should also contain a spatially modulating Cooper-pair density wave (PDW) state. In theory, such a state is akin to the famous FFLO state of spatially modulated superconductivity, but generated by strong correlations instead of high magnetic fields. However, no FFLO or PDW state had ever been observed in any superconductor. To search for a cuprate PDW, we developed nanometer-resolution millikelvin scanned Josephson tunneling microscopy (SJTM) to image Cooper-pair tunneling from a d-wave superconducting STM tip to the Cooper-pair condensate of $p$=17% $Bi_2Sr_2CaCu_2O_8$. Imaging the Cooper-pair condensate then revealed clear pair density modulations oriented along the Cu-O bond directions, the first observation of a PDW in any material. This Cooper-pair density wave occurs at wavevectors $Q_{PDW}=(0.25,0)2\pi/a_0;(0,0.25)2\pi/a_0$, [5] with an amplitude ~ 5% of the background condensate density (***Nature*** 532, 343 (2016).

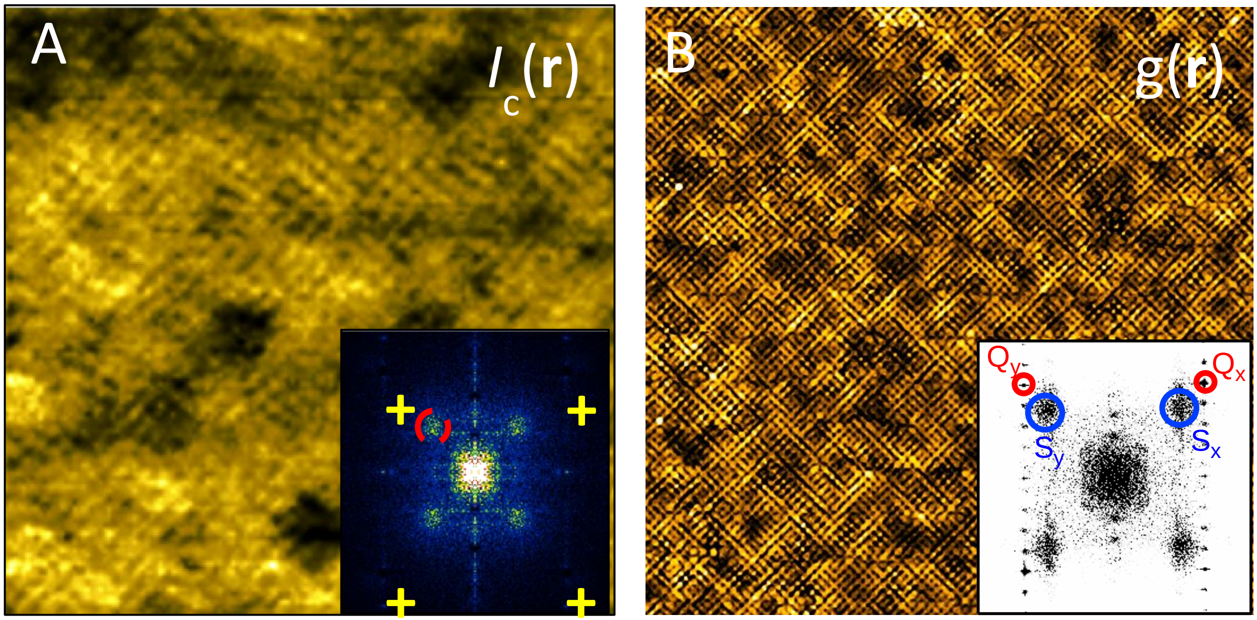

Figure 1A. Nanometer-resolution visualization of Cooper-pair (Josephson) current $I_c(\boldsymbol{r})$ reveals four-unit-cell periodic modulations – a Pair Density Wave. Inset: Fourier transform of Josephson current image $I_c(\boldsymbol{q})$ . Figure 1B. Conventional single particle conductance $g(\boldsymbol{r})$ imaging reveals coexisting d-symmetry charge density wave. Inset: d-symmetry Fourier transform of $g(\boldsymbol{r}) = g(\boldsymbol{q})$.

### 2. *Dirac Mass Imaging in Ferromagnetic TI*

The surface states of 3D topological insulators (TI) should exhibit many unusual and potentially valuable phenomena when a "Dirac-mass gap" opens in their spectrum. Magnetic dopant atoms are typically used to create a ferromagnetic state in order to generate the Dirac mass. Visualizing the magnetic (Cr) dopant atoms in the ferromagnetic TI $Cr_{0.08}(Bi_{0.1}Sb_{0.9})_{1.92}Te_3$ while simultaneously visualizing the Dirac-mass gap revealed its intense disorder. Fluctuations in the Cr density $n(r)$ were shown to be the source of this effect. The predicted relationship of Dirac mass to dopant density was confirmed to have an electron-dopant interaction energy $J^*$=145 meV·nm$^2$. These data demonstrate that to achieve the key fundamental physics expected of time-reversal-symmetry breaking TI materials, a technique for avoiding this extreme Dirac-mass disorder must first be identified (***Proc. Nat'l. Acad. Sci.*** 112, 1316 (2015).

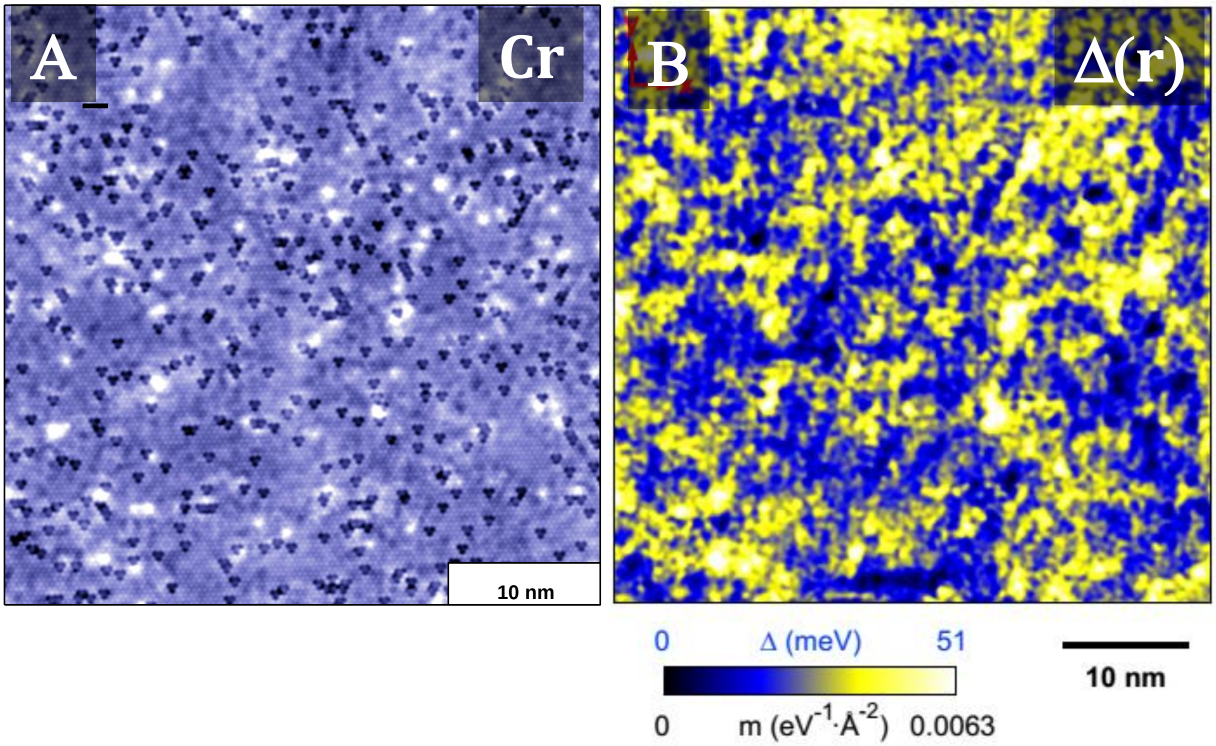

Figure 2A. Visualization of Cr magnetic dopant atom locations in CR-doped TI BiSbTe . Figure Simultaneous visualization of Dirac mass Δ of topological surface states; it is strongly disordered at nanoscale, with the Dirac-mass disorder is tightly correlated with Cr-dopant density

### 3. *Atomic-scale visualization of electronic structure and symmetry in underdoped Cuprates*

We prepared a comprehensive review of SISTM studies of cuprate electronic structure, describing how the Bogoliubov QPI signature of delocalized Cooper pairs (exhibiting a spatially homogenous pairing energy gap) exists upon the arc in k-space. The Bogoliubov QPI disappears near the lines connecting ***k***=(0,±π/a0) to ***k***=(±π/a0,0)—thus defining a ***k***-space arc which supports the delocalized Cooper pairing. This arc shrinks rapidly points with falling hole-density in a fashion which could satisfy Luttinger's theorem if it were actually a hole-pocket bounded from behind by the ***k***=± (π/a0, 0) − ***k*** ± (0,π/a0) lines. The pseudogap excitations exhibit a radically different r-space phenomenology locally breaking the expected C4 symmetry of electronic structure at least down to C2, by rendering the two oxygen sites electronically inequivalent within each CuO2 unit cell. These intra-unit-cell broken C4-symmetry states coexist with incommensurate modulations that break translational and rotational symmetry locally. Finally, site-specific measurements within each CuO2 unit-cell that are segregated into three separate electronic structure images (containing only the Cu sites (Cu(r)) and only the x/y-axis O sites (Ox (r) and Oy (r))) allows sublattice phase resolved Fourier analysis. By introducing this novel approach, we demonstrated by direct sublattice phase-resolved visualization that the cuprate density state is in fact a d-form factor density wave [***Strongly Correlated Systems - Experimental Techniques***, Springer (ISBN 978-3-662-44132-9 (2015)]

## Future Plans

### *1. Visualization of Dirac Mass Disorder*

We propose to expand our exploration of ferromagnetic topological insulators to high magnetic fields. The spontaneous magnetization of ferromagnetic topological insulator opens a 'mass-gap' in the spectrum of topological surface states. However, intense Dirac-mass disorder caused by heterogeneous magnetic dopant atoms actually suppress much of the novel physics expected of time-reversal-symmetry breaking TI materials. We will millikelvin high-field scanning tunneling microscopy for Landau-level spectroscopic imaging and understanding of 2D Dirac mass disorder.

### *2. Scanned Josephson Tunneling Microscopy*

We propose to expand usage of our recently developed millikelvin, nanometer resolution scanned Josephson tunneling microscopy system (***Nature*** 532, 343 (2016)) to visualize pair density waves in materials with coexisting charge density wave and superconductivity.

### *3. OASIS*

We propose to expand simultaneous SI-STM and ARPES studies to multiple cuprate families of compounds, including $La_{2-x}Sr_xCuO_4$, $La_{2-x}Ba_xCuO_4$, $YBa_2Cu_3O_{6+}$, n-type cuprates such as $Nd_{2-x}Ce_xCuO_4$ and $La_{0.2}Sr_{0.8}CuO_4$, and 'infinite-layer' compounds such as $CaCuO_2$, $SrCuO_2$, and $BaCuO_2$ by using a combined oxide MBE, ARPES and STM system dubbed ***OASIS***, now being commissioned at BNL.

## References

M. J. Lawler, K. Fujita, Jhinhwan Lee, A. R. Schmidt, Y. Kohsaka, Chung Koo Kim, H. Eisaki, S. Uchida, J. C. Davis, J. P. Sethna and Eun-Ah Kim, ***Nature 466***, 374 (2010).

K. Fujita, M. H. Hamidian, S. D. Edkins, Chung Koo Kim, Y. Kohsaka, M. Azuma, M. Takano, H. Takagi, H. Eisaki, S. Uchida, A. Allais, M. J. Lawler, E. -A. Kim, S. Sachdev, J. C. Séamus Davis, ***PNAS 111***, E3026 (2014).

M. H. Hamidian, S. D. Edkins, C.K. Kim, J. C. Séamus Davis, A. P. Mackenzie, H. Eisaki, S. Uchida, M. J. Lawler, E. -A. Kim, Subir Sachdev, K. Fujita, ***Nat. Phys.* 12,**150 (2016).

K. Fujita, C.K. Kim, Inhee Lee, Jinho Lee, M. H. Hamidian, I. A. Firmo, S. Mukhopadhyay, H. Eisaki, S. Uchida, M. J. Lawler, E. -A. Kim, and J. C. Davis, ***Science* 344**, 612 (2014).

M. H. Hamidian, S. D. Edkins, Sang Hyun Joo, A. Kostin, H. Eisaki, S. Uchida, M. J. Lawler, E. -A. Kim, A. P. Mackenzie, K. Fujita, Jinho Lee, J. C. Davis, ***Nature* 532**, 343 (2016).

**Publications**

Detection of a Cooper Pair Density Wave in Bi2Sr2CaCu2O8+x
M. H. Hamidian, S. D. Edkins, Sang Hyun Joo, A. Kostin, H. Eisaki, S. Uchida, M. J. Lawler, E. -A. Kim, A. P. MacKenzie, K. Fujita, Jinho Lee, J. C. Séamus Davis, ***Nature 532***, 343 ( 2016)

Imaging Dirac-mass disorder from magnetic dopant atoms in the ferromagnetic topological insulator Crx(Bi0.1Sb0.9)2-xTe3
Inhee Lee, Chung Koo Kim, Jinho Lee, Simon J. L. Billinge, Ruidan Zhong, John A. Schneeloch, Tiansheng Liu, Tonica Valla, John M. Tranquada, Genda Gu, and J. C. Séamus Davis ***Proc. Nat'l. Acad. Sci. 112,*** 1316 (2015)

Spectroscopic Imaging STM: Atomic-scale visualization of electronic structure and symmetry in underdoped cuprates K. Fujita, M. Hamidian, I. Firmo, S. Mukhopadhyay, C. K. Kim, H. Eisaki, S. Uchida, J. C. Davis ***Strongly Correlated Systems - Experimental Techniques*** Springer (ISBN 978-3-662-44132-9) (2014)

## Probing Coupled Metal-Insulator and Ferroic Transitions from the Atomistic to Mesoscopic Scales

S.V. Kalinin, P. Maksymovych, N. Balke, and R.K. Vasudevan
(sergei2, maksymovych, n2b, vasudevanrk)@ornl.gov

**Postdocs:** Y. Cao, M. Ziatdinov, and S. Somnath

Oak Ridge National Laboratory, Oak Ridge, TN 37831

### Research scope

The coupling between electronic and ferroic behaviors has emerged as one of the most intriguing aspects of condensed matter physics, with examples including phase separation in complex oxides, metal-insulator transitions in ferroelastic oxides, and complex electronic ordering patterns in superconducting and charge-density wave materials. The structural and electronic aspects of these behaviors are intrinsically intertwined. The overarching goal of this project is to explore, understand, and ultimately control the interplay between ferroic (ferro- and antiferroelectric and ferro- and antiferroelastic), ionic degrees of freedom, and electronic properties in systems lacking long-range periodicity, including single and interacting topological defects in ferroics and ultimately atomically-disordered materials. To achieve this goal, we will pursue three synergistic aims, including (a) uncoupling of order parameters and chemical phenomena at dynamic topological defects, (b) electrochemical tuning of oxides via charge injection and ionic gating and (c) directly probing structure-property relations on the level of a single unit cell. Unraveling and subsequently understanding the energy balance between competing interactions and establishing the atomic configurations responsible for desired materials functionalities will pave the way to deterministic design of novel electronic materials, and reveal the key structural and electronic mechanisms involved in energy storage, generation and dissipation processes. This will provide a fundamental, scientific basis for optimization and engineering of energy-related materials, with enormous potential benefits to fuel cells, batteries, data storage, energy transport, and other vital energy technologies, and lay down the foundation for experimental counterparts for materials genome projects.

### Recent Progress

In the present period (2014-2016), the research was focused on exploring the coupling between ferroic behavior, chemical degrees of freedom, and electronic phenomena on atomic and mesoscopic level. Here, we (a) demonstrate the preponderant role of surface (electro)chemistry on the phenomena suchas ferroelectric phase stability and (b) disorder and chemical effects on domain wall conductance in ferroelectric films, and demonstrate pathways to control the electrochemical degrees of freedom via (c) ionic liquid gating and (d) atomically resolved in-situ studies of model oxides. We also explore, but do not report here (e) development of ultrafast PFM methods to distinguish ferroelectric and electrochemical phenomena based on the rates and (f) the use of the machine learning and image analysis methods to extract physically relevant information from atomically resolved images of systems such as Kitaev $RuCl_3$, graphene, molecular ad-layers and superconducting pnictides, as models to oxides.

**Chemical control of ferroelectricity in ultrathin film:** From the early days of ferroelectricity, it has long been realized that polarization discontinuities at surfaces and interfaces necessitates screening mechanisms. Whereas at solid interfaces the electronic and lattice screening mechanisms have been extensively explored both on the mesoscopic and atomic level, ferroelectric surfaces remain ill-understood. Here we developed a self-consistent phase-field model for ferroelectrics with boundary conditions based on electrochemical equilibria, and systematically explore the domain structure evolution under electrochemical control. For the 1D case the model allows for an analytical solution.

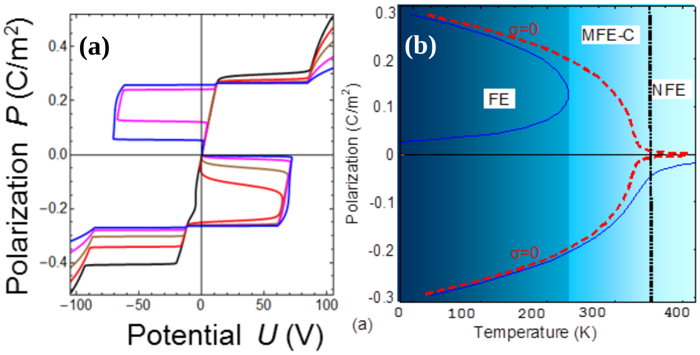

**Fig. 1. (a)** Intrinsic ferroelectric hysteresis loop in the region with strong polarization-surface chemistry coupling and **(b)** phase diagram of BaTiO$_3$ under classical (red) and electrochemical (blue) boundary conditions

Using it, we show that in nanoscale systems, the ferroelectric state is fundamentally inseparable from electrochemical state of the surface, leading to emergence of a mixed electrochemical-ferroelectric state (Fig. 1). We explore the nature, thermodynamics and thickness evolution of such states, and demonstrate the experimental pathway to establish its presence. This analysis reconciles multiple prior studies, establishes the guidelines for studies of ferroelectric material son the nanoscale, and establishes the design paradigm for new generations of ferroelectric devices with coupled order parameters.

**Domain wall conductivity in ferroic oxides:** We explored the conductivity of ferroelectric oxides, particularly at domain walls. Here, the problem of surface contact has so far limited progress in the understanding of virtually every aspect of conducting domain walls – from structure, to mechanisms, to control. To overcome the contact problem, we have shifted from direct current (DC) conductive measurements, to AC conductance at microwave frequencies of 3GHz, where the large surface resistance can be effectively shorted by now conductive surface capacitance. We have found that domain walls in ferroelectrics are ubiquitously conducting at microwave frequencies, with a surprisingly large conductance of ~5 S/m, comparable to doped silicon (Fig. 2). Even more importantly we have obtained the first direct evidence that conducting domain walls require finite, and quite large conductivity of the surrounding ferroelectric – pointing to new ways of deterministic control of the absolute domain wall conductance, and possibly increasing the carrier density to fundamentally interesting levels at the wall. Finally, we propose a new model for the structure of the conducting domain wall where disorder-induced morphological “roughening” is responsible for creating local pockets of accumulated charge along the wall.

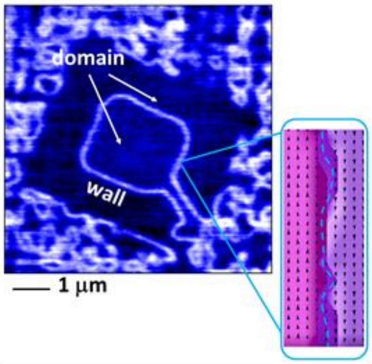

**Fig. 2**. Microscopic image of conducting ferroelectric domain walls (bright) in lead zirconate-titanate detected by microwave radiation. Inset shows phase-field model of “rough” ferroelectric domain characterized by irregular shape (blue dashed line).

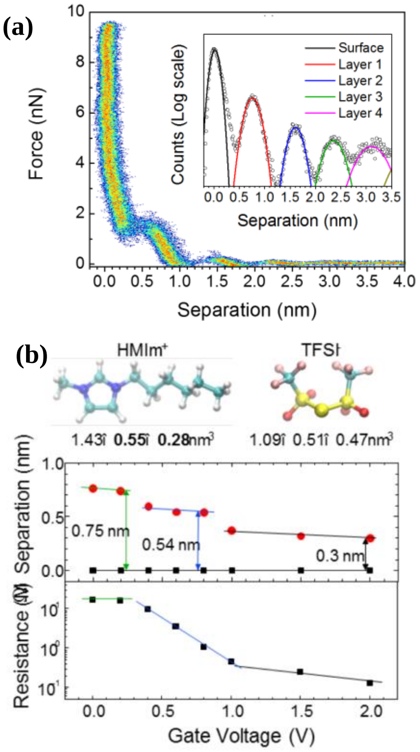

**Fig. 3. (a)** Statistical force-distance curves for [Hmim+][TFSI-] on oxide surface. **(b)** Position of cation layer at oxide surface as function of gate voltage and corresponding oxide resistance.

**Ionic Liquid control:** The fundamental studies of ferroelectric and conductive phenomena at surfaces and ultrathin films require control of electrochemical degrees of freedom. As one route to establish this control, we explore the feasibility of ionic liquid gating. As a model oxide, we investigate the structure of an ionic liquid at a semiconducting oxide interface during the operation of a thin film transistor where the electrical double layer gates the device. We show that the transition between the ON and OFF states of the amorphous indium gallium zinc oxide transistor is accompanied by a densification and preferential spatial orientation of counter-ions at the oxide channel surface. This process occurs in three distinct steps (Fig. 3), corresponding to ion orientation and regimes of different electrical conductivity. The electrical double layer thickness associated with the flat arrangement of cations at the surface is strongly correlated with the highest ON currents.

**Chemical control of oxide surfaces on mesoscopic and atomic level:** As a second strategy to enable electrochemical control over oxide surfaces, we pursue the studies of *in-situ* pulsed laser deposition grown oxides in ultra-high vacuum environment. As one example, we explored the coupling between the surface chemistry and the electronic properties of $LaMnO_3$ thin films, and attempted to modify the surface by applying pressure and voltage through a scanning probe microscopy tip. We find that merely scanning the surface with a small amount of pressure (~100MPa) is sufficient to modify the conductivity by an order of magnitude. We further determined the chemical changes occurring in this system, by site-correlated time-of-flight secondary ion mass spectrometry measurements (TOF-SIMS). The results can be seen in Figure 4, and clearly indicate that merely applying pressure can modify the first two layers of the film. These results are surprising and suggest that cation stoichiometry need not be fixed during SPM measurements.

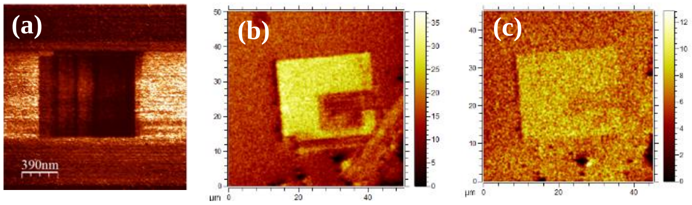

**Fig. 4: Pressure and bias-induced changes in $LaMnO_3$ ultra-thin films (a)** c-AFM of a square 'poled' by applying pressure by the tip, with varying setpoints. **(b,c)** TOF-SIMS mapping of **(b)** Mn ions, at the surface, and **(c)** LaO+ ions, 1.5nm deep into the film. Merely scanning increases Mn concentration at the surface. Applying -4V to the sample reverses this effect.

Precise electrochemical control requires a fundamental understanding of available atomic configurations and interaction energies e.g. of dopants and segregation at oxide surfaces, which we have explored through the model manganite system, pulsed laser deposition-grown $La_{5/8}Ca_{3/8}MnO_3$ (LCMO) films, imaged with *in-situ* STM. In conjunction with basic thermodynamic models and supplemented with density functional theory (DFT), we find a link between the intensity as measured on oxygen atoms in the STM image and the local environment, i.e., it can be used as a marker for the presence of Ca in the unit cell. The model parameters can then be adjusted to match the distributions of dopants found in the real-space atomic image, providing the insight to the surface (in-plane) segregation of the dopant and the strength of inter-atomic interactions (Fig. 5). These approaches can be combined with the out-of-plane segregation data, obtained by angle-resolved XPS in the same Nanotransport system *in-situ*, for full 3D reconstruction of the segregation profile, providing unparalleled atomic-scale insight and directly allowing determination of relevant thermodynamic parameters.

### Future plans:

Understanding of the fundamental physics of coupling between electronic properties and ferroic behaviors on strongly correlated oxide surfaces necessitates a synergistic view of (a) local *in-situ* studies of surfaces via high-resolution imaging, (b) development of data analytics tools that allow extraction of chemical, physical, and structural information from multidimensional data sets, and (c) theoretical framework that allows describing the coupling between structural degrees of freedom, at mesoscopic and atomic levels. Our research will pursue these directions, aimed at the following fundamental issues:

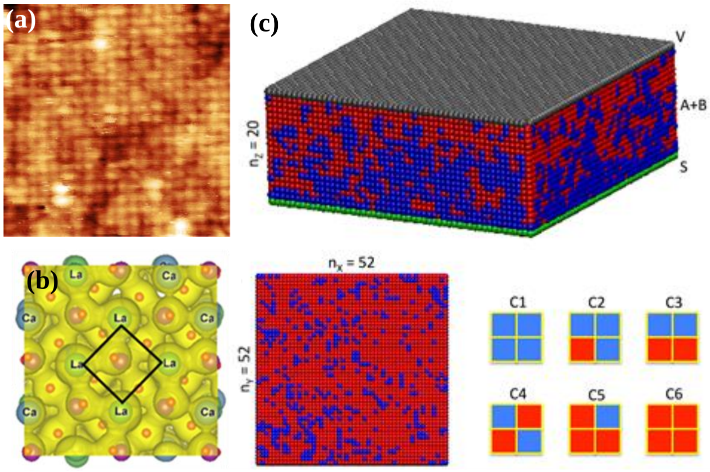

**Fig. 5: (a)** 10nm x 10nm STM Image of A-site terminated LCMO film. **(b)** Total electron density of A-site terminated LCMO, from DFT. **(c)** Thermodynamic model, with Top: Dimensions and composition of target systems. La (blue), Ca (red), substrate S particles (green), and interface with vacuum V (gray); Bottom left: View of the surface layer; Bottom right: Six types of local configurations identified in the surface layer.

- **Chemically induced mesoscopic oxide functionalities:** We aim to couple mesoscopic thermodynamic theory of oxide interfaces and bulk Ginzburg-Landau-Devonshire theory of ferroelectrics to explore new phenomena emerging from chemical control of polarization in uniaxial, multiaxial, and poly-domain materials. The theoretical studies will be combined with General-Mode enabled ultrafast SPMs to separate the chemical and physical phenomena based on response time scales.
- **AC-**conduction in complex oxide materials. Direct observation of large conductivity of ferroelectric domain walls at microwave frequencies is highly encouraging, but we also observe large conductivity the substrate. The origins of this effect are presently unknown, but it must be related to the defect structure of the materials. This is a comparably new field, ripe in opportunities for fundamental aspects of defect chemistry, electronic conduction, and lattice tunability in applied electric fields. We will study evolution of microwave conductance in perovskite ferroelectrics as a function of doping, different geometries, as well as in liquid-gated geometries. In all cases, the emphasis will be placed on determination of the feasibility of doping complex oxides, establishing the cross-over from electronic to electrochemical mechanisms and looking for electronic phase transitions in the bulk of the oxide or localized to the topological defects of its lattice or order parameters.
- **Coupling between physics and electrochemistry on molecular and atomic level.** We aim to explore the coupled ferroelectric and electrochemical phenomena via high resolution imaging under (a) ionic liquid gating and (b) in-situ grown films. In the former case, we aim to explore double layers on gated ferroelectric films as a function of gate and ferroelectric state. In the latter, we will utilize the atomically resolved information to describe structure-property relationships on atomic level, building bottom-up picture of ferroelectric surfaces and exploring fundamental coupling mechanisms on atomic level.

Research supported by the U.S. Department of Energy Office of Basic Energy Sciences Division of Materials Sciences and Engineering and performed at the Center for Nanophase Materials Sciences supported by Division of Scientific User Facilities.

**DOE-sponsored publications 2012-2014** [36 peer-reviewed papers including 1 *Nature Mat*., 5 *Nat.Comm.*, 3 *ACS Nano*, 2 *Nano Lett*., 1 *Adv.* (*Func, En.*) *Mat*.**]**

1. A. Tselev, P. Yu, Y. Cao, L. R. Dedon, L. W. Martin, S. V. Kalinin, Petro Maksymovych, "*Microwave ac conductivity of domain walls in ferroelectric thin films*", Nature Communications, 2016, 7, 11630.
2. R.K. Vasudevan, M. Ziatdinov, S. Jesse, and Sergei V. Kalinin*, Phases and Interfaces from Real Space Atomically Resolved Data: Physics-Based Deep Data Image Analysis Nano Lett, in print
3. R.K. VASUDEVAN, A. TSELEV, A.P. BADDORF, and S. V. KALININ, *Big-Data Reflection High Energy Electron Diffraction Analysis for Understanding Epitaxial Film Growth Processes*, ACS Nano **8**, 10899 (2014).
4. A. TSELEV, R.K. VASUDEVAN, A.G. GIANFRANCESCO, L. QIAO, P. GANESH, T.L. MEYER, H.N. LEE, M.D. BIEGALSKI, A.P. BADDORF, and S. V. KALININ, *Surface Control of Epitaxial Manganite Films via Oxygen Pressure*, ACS Nano **9,** 4316 (2015).
5. R.K. VASUDEVAN, A. TSELEV, A.G. GIANFRANCESCO, A.P. BADDORF, and S. V. KALININ, *Atomic-scale electrochemistry on the surface of a manganite by scanning tunneling microscopy*, Appl. Phys. Lett. **106**, 143107 (2015).

# In situ TEM study of branched nanocrystal growth mechanisms: understanding non-classical processes controlling formation of hierarchical nanostructures

**Dongsheng Li, Pacific Northwest National Laboratory**

## Research Scope

The long-term goal of this project is to reveal the unknown molecular mechanisms of mass transport and structural evolution during non-classical processes of nanocrystal synthesis to enable the design of nanostructures with controlled size and morphology, and tailored properties. Hierarchical nanostructures, such as highly branched nanowires, provide a clear example. These complex structures crystalize through non-classical pathways of nucleation and growth including assembly of nanoparticles and/or multi-phase pathways sometimes involving competition between these non-classical processes and classical monomer-by-monomer growth. However, no quantitative framework exists to describe these processes. Due to this lack of understanding, growth of nanostructures is empirical rather than predictive. However the emergent physical and chemical properties are inherently tied to size and geometry. For example branched nanowires can have large absorption cross-sections, short electron mean free paths, or complex patterns of optical interference. To fill this major gap in the science of synthesis and build quantitative kinetic models that make atom- and energy-efficient synthesis of these materials a reality, in situ data on the dynamics of these non-classical processes — rather than just the outcomes — are required.

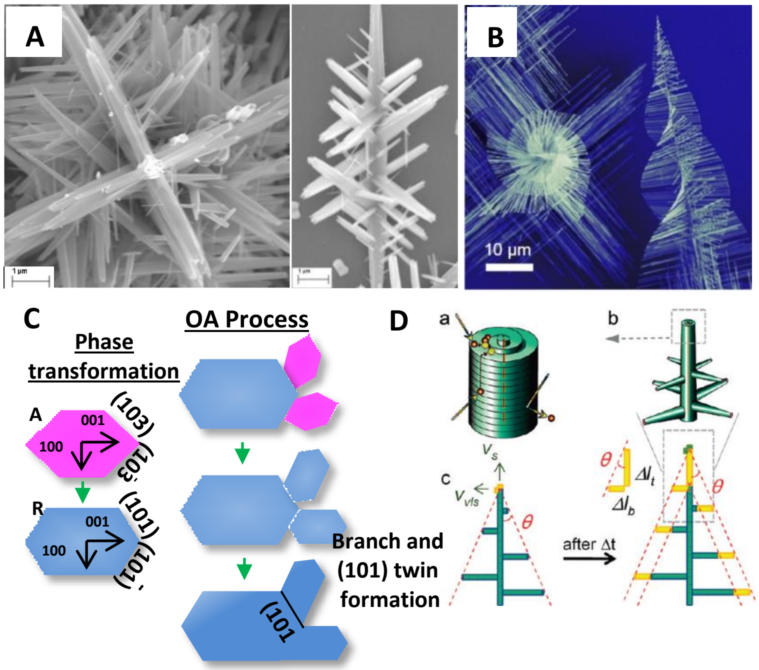

Figure 1. SEM images. A: top view and side view of branched $TiO_2$ nanostructures; B: PbS “pine-tree” nanowires; C: illustration of phase transformation from anatase into rutile and formation of the $TiO_2$ structures through OA of nanoparticles, which can either extend a wire or form a branch depending on which of two symmetrically related planes attachment occurs; D: a and b, the main trunk of PbS wires forms through growth on a central screw dislocation; c, the branches are believed to form via catalyzed VLS growth[13]. A: anatase; R: rutile

Here we develop a predictive understanding for two important categories of non-classical processes of branched nanowire formation: (1) particle-based growth, particularly oriented attachment (OA)(*1*) (Figure 1A and C), and (2) competition between classical and non-classical mechanisms(*2*), specifically screw dislocation-driven trunk growth and vapor-liquid-solid (DD-VLS) branch nucleation (Figure 1B and D).

My objectives are: (1) Establish the source of the driving force for OA, the barrier to OA, and the factors that control them; (2) Determine the origin of the screw dislocation and factors that control it; (3) Understand the source of hierarchical organization; (4) Use the knowledge gained from Objectives 1, 2, and 3 to direct hierarchical growth. I will employ *in situ* transmission electron microscopy (TEM) and atomic force microscopy (AFM) based dynamic force spectroscopy (DFS) techniques to relate solid/solution structure to inter-particle forces and attachment dynamics. I chose $TiO_2$ and Ag to investigate the OA process and PbS/PbSe to study DD-VLS growth, because these two systems provide clear examples of OA and DD-VLS branched nanowire growth.

## Recent Progress

Ex situ synthesis of $TiO_2$ and Ag nanowires

Due to the limited reaction conditions (temperature (T) < 100°C, 2 < pH < 12 in aqueous solution) for in situ experiments, ex situ experiments were carried out first in order to optimize the chemical reaction conditions for in situ studies. For the $TiO_2$ system, reaction conditions have not yet met the requirements for in situ transmission electron microscopy (TEM) studies. Rutile nanowires have been obtained (Figure 2 A and B) under the condition of 2 < pH <12; however, the temperature is over 100°C. Ag nanoplates (Figure 2C) and nanowires (Figure 2D) have been achieved under the conditions of T < 100°C and 2 < pH < 12.

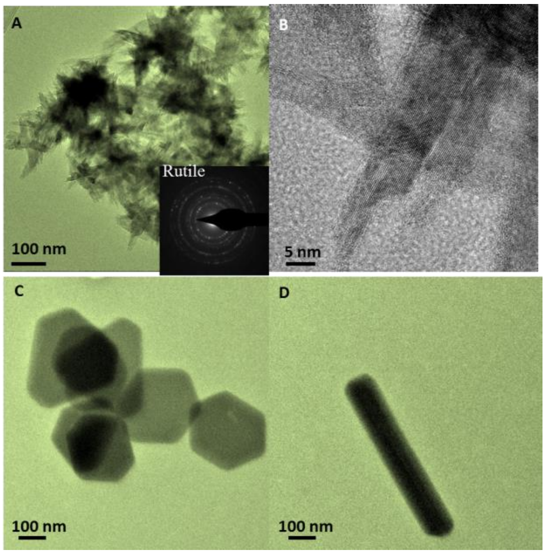

Figure 2. TEM images of synthesized $TiO_2$ (A and B) and Ag (C and D) nanoparticles

In situ TEM study of Ag nanowire growth via OA

Reaction solutions will be loaded into either a static or flow cell with temperature control. The crystal nucleation and growth will be initiated by temperature increase. We are not yet able to reproduce the Ag nanoplates or nanowires in an in situ TEM liquid cell. We suspect that this may be a result of the confined volume of the liquid cell or electron beam effects. Further ex situ and in situ experiments are under way in order to modify the reaction conditions to obtain Ag nanowires in a confined space and avoid/minimize the electron beam effect.

In situ TEM study of phase transformation of anatase into rutile

For the $TiO_2$ system, we hypothesized that after a primary rutile wire forms, subsequent branching occurs via oriented attachment (OA) in which (103) planes of anatase nanoparticles attach onto (101) planes of rutile, followed by phase transformation of anatase into rutile upon attachment, resulting in wire growth, branch formation, and formation of (101) twins with growth along [001] directions (Figure 1C). Therefore, we investigated the phase transformation of anatase into rutile. Different sizes and morphologies of $TiO_2$ (Figure 3) were chosen for investigation in order to view the phase transformation via various zone directions (i.e., [010] and [001]).

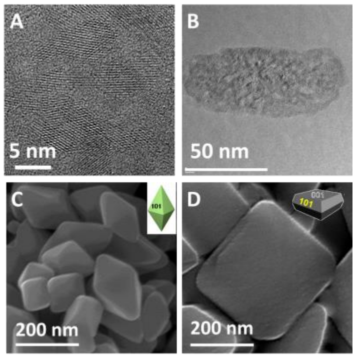

Figure 3. TEM and SEM images showing different anatase particles.

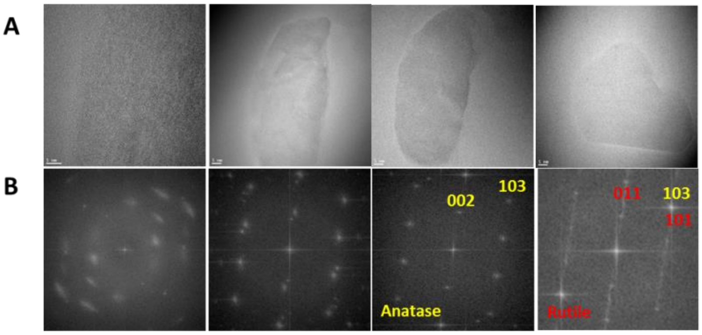

Figure 4. In situ TEM images of morphologies of anatase during phase transformation (A) and corresponding FFT diffraction patterns showing structure change from anatase into rutile.

In our preliminary in situ TEM experiments, we investigated the [010] direction and observed morphological changes (Figure 4A) and structure change (Figure 4B). Fast Fourier transform (FFT) diffraction patterns proved that (103) planes of anatase transformed into (101) planes of rutile after phase transformation. This confirmed our hypothesis of a branched $TiO_2$ nanowire twin-formation mechanism.

In situ investigation of crystal surface interaction via DFS/AFM

Observations showed that approaching particles rotate to achieve co-alignment while separated by nanometer-scale solvent layers. Little is known about the forces that drive co-alignment, particularly in this “solvent-separated” regime. To obtain a mechanistic understanding of this process, we used AFM based DFS with tips fabricated from oriented mica to measure the adhesion forces between

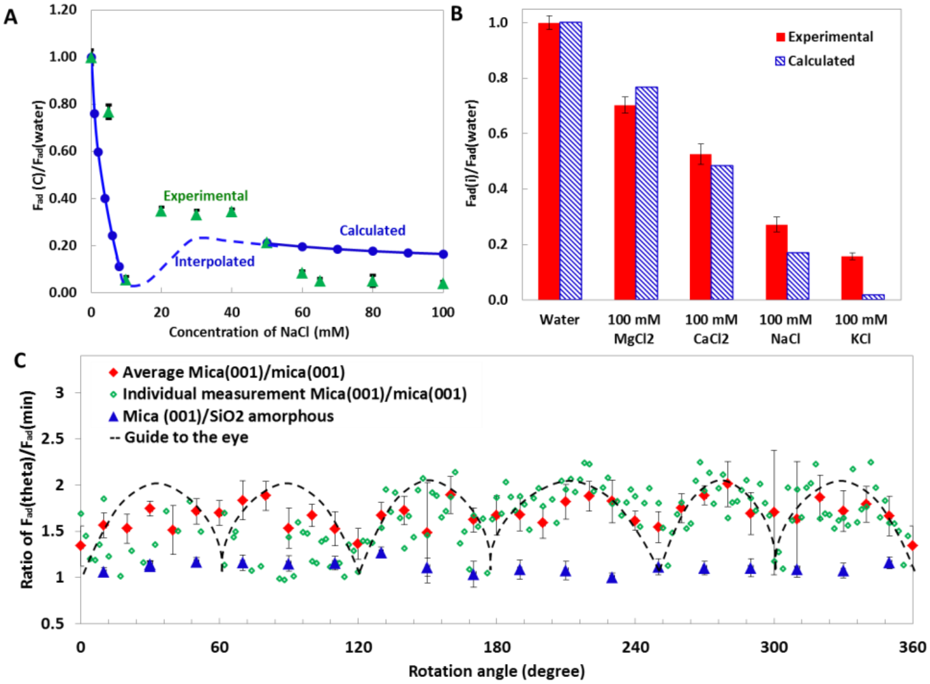

Figure 5. Dependence of adhesion force ($F_{ad}$) on (A) NaCl concentration, (B) electrolyte type, and (C) relative in-plane orientation. $F_{ad}$(C) is $F_{ad}$ at various concentration. Theta is rotation angle.

mica (001) surfaces in electrolyte solutions as a function of orientation, electrolyte concentration (Figure 5A), and electrolyte (Figure 5B). The results reveal a ~60° periodicity (Figure 5C) as well as a complex dependence on electrolyte concentration and temperature. A continuum model that accounts for molecular details of effective surface separation, water structure, ion hydration, charge regulation at mica-water interfaces, and mica lattice symmetry reproduces the observed trends. Most importantly, we found that dispersion-based forces are most likely responsible for establishing co-alignment in the solvent-separated state.

## Future Plans

We will work on the following investigations.

1. Further ex situ experiments of synthesis of $TiO_2$ and Ag nanowires to optimize the reaction conditions to meet the requirements for in situ TEM experiments.
2. In situ investigations of $TiO_2$ and Ag nanowire growth mechanisms.
3. Further in situ study of the phase transformation from anatase into rutile along [001] and [101] directions to confirm the structure change.
4. Modification of the flow system of the gas heating cell to precisely control the gas flow rate and pressure, which is needed for PbS/PbSe wire growth.
5. In situ investigation of the DD-VLS growth mechanism of PbS/PbSe.

## References

1. D. Li *et al.*, Growth Mechanism of Highly Branched Titanium Dioxide Nanowires via Oriented Attachment. *Crystal Growth & Design* **13**, 422-428 (2013).
2. M. J. Bierman, Y. K. A. Lau, S. Jin, Hyperbranched PbS and PbSe nanowires and the effect of hydrogen gas on their synthesis. *Nano Letters* **7**, 2907-2912 (2007).

## Publications

1. D. Li et al., Long-range dispersion forces drive nanocrystal aggregation and co-alignment, to be submitted to *Science.*
2. D. Xiao et al., Revealing the van der Waals induced directional adhesive forces between crystal surfaces, to be submitted to *Nano Letters.*
3. Z. Wu et al., Novel Methods for Attaching Thin Platelets for Colloid Probe Microscopy, to be submitted to *Nanotechnology.*
4. D. Li et al., ZnO nanowire growth mechanism of monomer addition via in situ TEM, to be submitted to *Crystal growth and design*.

# Scanning Transmission Electron Microscopy: Atomic Structure and Properties of Materials

## Physics of Electron Microscopy

Principal Investigators: Andrew R. Lupini, Mark P. Oxley, Matthew F. Chisholm

Materials Science & Technology Division, Oak Ridge National Laboratory, TN 37831

### Sub-Program Scope

This task aims to explore the frontiers of new techniques in the aberration-corrected scanning transmission electron microscope (STEM), aiming for the highest resolution and sensitivity. The overarching goal is to push the limits of electron microscopy towards new methods and new materials.

### Recent Progress

Universal Detector: The traditional imaging modes in STEM consist of integrating the scattered flux of electrons over a range of angles, with the canonical example being collection of the high-angle scattering to give "Z-contrast" images. However, novel detectors allow the whole two-dimensional (2D) scattering distribution to be detected as a function of 2D probe position. This 4D dataset contains a lot more information than a single image. For example, the images that would be seen on any specified detector can be reconstructed mathematically. Advantages are that multiple, overlapping detectors can be emulated simultaneously, the alignment can be adjusted numerically, and detectors that could not be physically realized can be employed (Fig. 1). A numerical phase plate with response varying with spatial frequency enables much more efficient use of the transmitted signal [1]. The extremely large datasets that result will require new processing and analysis methods, which will require extensive collaboration with the advanced computational facilities available at ORNL [2].

Imaging Magnetism at Atomic Resolution: One of the fundamental problems with analyzing magnetic materials is that ferromagnetism and related phenomena are intrinsically atomic-scale effects, arising from the alignment of individual spins, but existing techniques to study magnetism do not provide atomic resolution. Thus the demonstration by Schattsneider that an electron beam can be used to examine electron magnetic circular dichroism (EMCD) generated considerable interest. In collaboration with Dr. J.-C. Idrobo of the ORNL user facility, we have recently developed a method where we deliberately applying aberrations to the probe in order to obtain a dichroic signal at atomic resolution [3]. This method requires precise control of the phase of the electron beam incident on the sample, thus renewing interest in aberration measurement and more accurate control of all aspects of the electron beam.

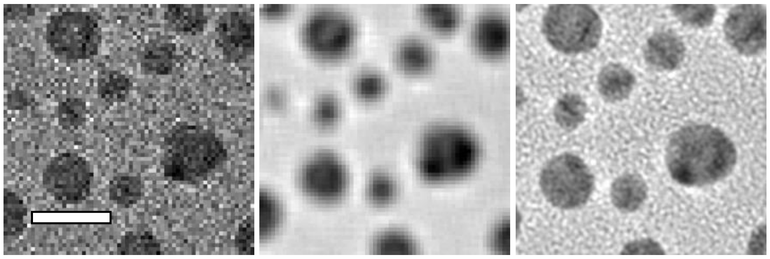

**Figure 1.** (Left) BF image generated from a single pixel in a Ronchigram series. Scale bar is nominally 20 nm. (Center) As more pixels are used to form a BF image, the noise improves but fine details are lost. (Right) The same dataset is used to generate an image with finer spatial sampling.

Aberration measurement: One of the key technological problems in aberration-corrected electron microscopy is the precise alignment of the aberration-corrector. Making use of the multi-dimensional dataset provides several routes to accurately measure the microscope. For example, by the theory of reciprocity, a set of STEM images acquired at different detector tilt angles is equivalent to a set of CTEM images acquired at different illumination tilt angles, which form a so-called Zemlin tableau. Thus by taking the 4D dataset, slicing it into bright field images, and determining the shift of each image, the gradient of the aberration function can be determined (Fig. 2) [4]. Since in a STEM with a pixelated detector, the images at different tilts are acquired simultaneously, the advantage is that this measurement can be performed extremely quickly and is less sensitive to drift.

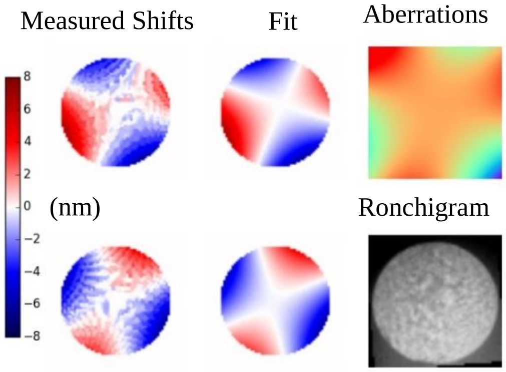

**Figure 2.** Example measurement of aberrations from a Nion UltraSTEM 200. Adapted from [4].

Precise Control of the Electron Beam: Continuing the theme of more precise control of the probe, in collaboration with the scanning probe group at ORNL, we have recently developed a customized scan unit, capable of employing non-traditional scan paths. One of the major problems in any scanned image is that the true probe position might deviate from the nominal position, causing image distortions and difficulties for precise interpretation. Some of these complications arise because of the ‘flyback’ delay at the end of each scanline. Similarly, the speed with which it is possible to move the probe limits the frame acquisition rate. Novel scan paths provide a solution to both of these problems. Spiral paths can be designed that do not have flyback between scanlines and so can be acquired more rapidly than conventional images (Fig. 3) [5].

Nanofabrication: The enhanced control of the electron probe has enabled the atomic level control of nanofabrication, allowing crystalline materials to be sculpted with single atomic plane precision [6,7].

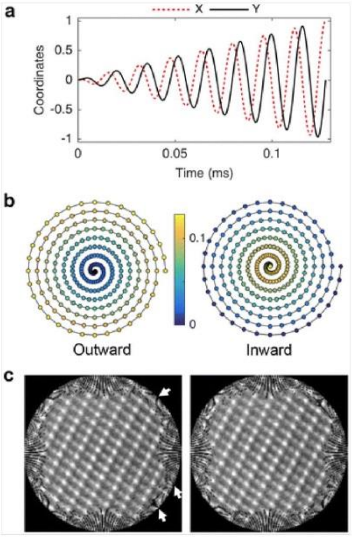

**Figure 3.** Schematic illustration of a spiral scan. (a) Voltages. (b) Scan paths. (c) Reconstructed images. Adapted from [5].

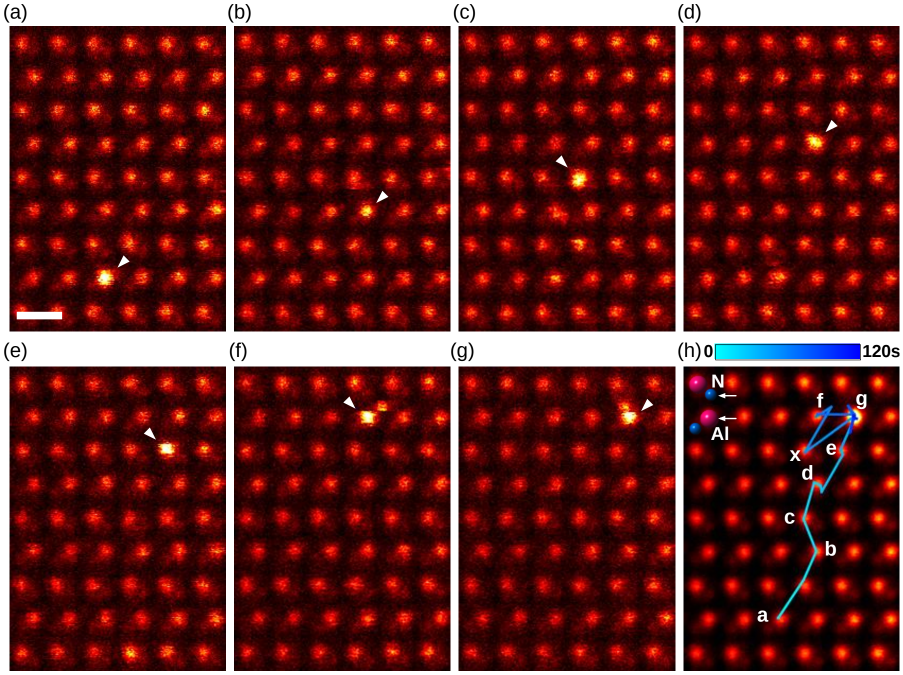

**Figure 4.** Selected frames from a sequence of STEM images show the diffusion pathway of a Ce dopant (the bright atom highlighted with a white arrow) as it moves inside a bulk AlN crystal. The final frame overlays the Ce pathway on the Z-contrast image obtained by averaging each frame. Adapted from [8].

<u>Direct Imaging of Single Dopant Diffusion:</u> One of the recent themes of this sub-task has been to use the electron beam as an *actor*, supplying energy to the sample. This has allowed us to obtain the first direct imaging of single tracer atoms diffusing inside a solid, providing a new method to study diffusion at the single-atom level [8]. Moreover, this technique has allowed us investigate how the size of dopant atoms affects their diffusivity in a solid. This work is relevant to both semiconductor and energy industries because migration of dopants is one of the most common methods of device failure.

## Future Plans

The Nion UltraSTEM microscope can be operated at a range of voltages, which provides a degree of freedom that has not yet been well explored. We have developed an interface allowing us to use conventional heating chips in the Nion microscopes. We will use these capabilities to investigate the effects of thermal excitation and to explore electrical properties. The new Monochromated Aberration-corrected (MAC)STEM arriving at ORNL will allow the vibrational properties of materials to be probed at unprecedented energy and spatial resolution.

## Selected Publications

**1.** T. Pennycook, A. Lupini, H. Yang, M. Murfitt, L. Jones, P. Nellist. (2015) *Efficient phase contrast imaging in STEM using a pixelated detector. Part 1: Experimental demonstration at atomic resolution*, ULTRAMICROSCOPY **151**, pages 160-167.
**2.** S. Jesse, M. Chi, A. Belianinov, C. Beekman, S. Kalinin, A. Borisevich, A. Lupini. (2016) *Big Data Analytics for Scanning Transmission Electron Microscopy Ptychography*, SCIENTIFIC REPORTS **6**, 26348.

**3.** J. Idrobo, J. Rusz, J. Spiegelberg, M. McGuire, C. Symons, R. Vatsavai, C. Cantoni, A. Lupini (2016) *Detecting magnetic ordering with atomic size electron probes*, ADV. STRUC. & CHEM. IMAGING

**4.** A. Lupini, M. Chi, S. Jesse. (2016) *Rapid aberration measurement with pixelated detectors*, JOURNAL OF MICROSCOPY **263**(1), pages 43-50.

**5.** X. Sang, A. Lupini, R. Unocic, M. Chi, A. Borisevich, S. Kalinin, E. Endeve, R. Archibald, S. Jesse (2016) *Dynamic scan control in STEM: spiral scans,* ADV. STRUC. & CHEM. IMAGING

**6.** S. Jesse, Q. He, A. Lupini, D. Leonard, M. Oxley, O. Ovchinnikov, R. Unocic, A. Tselev, M. Fuentes-Cabrera, B. Sumpter, S. Pennycook, S. Kalinin, A. Borisevich. (2015) *Atomic-Level Sculpting of Crystalline Oxides: Toward Bulk Nanofabrication with Single Atomic Plane Precision*, SMALL **11**(44), pages 5895-5900.

**7.** S. Jesse, A. Borisevich, J. Fowlkes, A. Lupini, P. Rack, R. Unocic, B. Sumpter, S. Kalinin, A. Belianinov, O. Ovchinnikova. (2016) *Directing Matter: Toward Atomic-Scale 3D Nanofabrication*, ACS NANO **10**(6), pages 5600-5618.

**8.** R. Ishikawa, R. Mishra, A. Lupini, S. Findlay, T. Taniguchi, S. Pantelides, S. Pennycook. (2014) *Direct Observation of Dopant Atom Diffusion in a Bulk Semiconductor Crystal Enhanced by a Large Size Mismatch*, PHYSICAL REVIEW LETTERS **113**(15), 155501.

**9.** R. Guzman, L. Maurel, E. Langenberg, A. Lupini, P. Algarabel, J. Pardo, C. Magen. (2016) *Polar-Graded Multiferroic SrMnO3 Thin Films*, NANO LETTERS **16**(4), pages 2221-2227.

**10.** C. Narula, X. Yang, C. Li, A. Lupini, S. Pennycook. (2015) *A Pathway for the Growth of Core-Shell Pt-Pd Nanoparticles*, Journal of Physical Chemistry C **119**(44), pages 25114-25121.

**11.** E. Rotunno, M. Longo, C. Wiemer, R. Fallica, D. Campi, M. Bernasconi, A. Lupini, S. Pennycook, L. Lazzarini. (2015) *A Novel Sb2Te3 Polymorph Stable at the Nanoscale*, CHEMISTRY OF MATERIALS **27**(12), pages 4368-4373.

**12.** R. Ishikawa, A. Lupini, Y. Hinuma, S. Pennycook. (2015) *Large-angle illumination STEM: Toward three-dimensional atom-by-atom imaging*, ULTRAMICROSCOPY **151**, pages 122-129.

**13.** M. Troparevsky, J. Morris, P. Kent, A. Lupini, G. Stocks. (2015) *Criteria for Predicting the Formation of Single-Phase High-Entropy Alloys*, PHYSICAL REVIEW X **5**(1), 011041.

**14.** M. Mahjouri-Samani, M. Lin, K. Wang, A. Lupini, J. Lee, L. Basile, A. Boulesbaa, C. Rouleau, A. Puretzky, I. Ivanov, K. Xiao, M. Yoon, D. Geohegan. (2015) *Patterned arrays of lateral heterojunctions within monolayer two-dimensional semiconductors*, NATURE COMMUNICATIONS **6**, 7749.

**15.** L. G. De, G. Ghiringhelli, C. Perroni, V. Cataudella, F. Chiarella, C. Cantoni, A. Lupini, N. Brookes, M. Huijben, G. Koster, G. Rijnders, M. Salluzzo. (2014) *Ubiquitous long-range antiferromagnetic coupling across the interface between superconducting and ferromagnetic oxides*, NATURE COMMUNICATIONS **5**, 5626.

**16.** T. Aytug, A. Lupini, G. Jellison, P. Joshi, I. Ivanov, T. Liu, P. Wang, R. Menon, R. Trejo, E. Lara-Curzio, S. Hunter, J. Simpson, M. Paranthaman, D. Christen. (2015) *Monolithic graded-refractive-index glass-based antireflective coatings: broadband/omnidirectional light harvesting and self-cleaning characteristics,* J. OF MATERIALS CHEMISTRY C **3**(21), 5440-5449.

# Scanning Transmission Electron Microscopy: Atomic Structure and properties of Materials

## Quantification of low voltage images of 2D materials

**Principle Investigators: Mark P. Oxley, Wu Zhou, Andy R. Lupini, Matthew F. Chisholm**

**Materials Science & Technology Division, Oak Ridge National Laboratory, TN 37831**

### Sub-Program Scope

The properties of 2D materials are often determined by the presence of impurities and other lattice defects and STEM is the ideal tool for probing these defects. Many 2D materials however are beam sensitive and can only be imaged at lower accelerating voltages where knock-on damage is reduced. At lower voltages, the chromatic aberrations of the imaging system result in the degradation of image resolution and contrast. This 'temporal incoherence', along with residual aberrations make true quantification of STEM images difficult. Images also tend to have a low signal to noise ratio (SNR), further complicating image quantification. We have developed techniques to remove both temporal incoherence and residual aberration from images of 2D materials. These methods are robust in the presence of noise and allow direct comparison with simulation, allowing for true quantification.

### Recent Progress

#### 1. The problem of temporal incoherence

Aberration correction of electron optics has allowed imaging of 2D materials at 60 KV with near Ångstrom resolution. The limiting factor on image resolution is now temporal incoherence, due to fluctuations in the incident electron energy and chromatic aberration of the microscope lenses. This results in an effective spread of defocus values for the probe, leading to intensity being shifted from the probe position to the tails of the probe. The effect of temporal incoherence on images of 2D materials has been discussed in detail elsewhere [1]. Residual coherent aberrations also lead to further redistribution of intensity as shown in figure 1 for 60 kV incident electrons. While the probe retains a similar width, aberrations and incoherence result in a halving of the probe peak intensity and a subsequent shifting of intensity into the probe tails. Non circular aberrations also lead to intensity being shifted in a non-uniform manner. The tails on such images have previously been dealt with in an ad hoc manner [2] which makes direct comparison with simulated images impossible. Here instead, we derive a correction factor from the calculated probe shapes, and apply it to STEM images of 2D materials. For probe intensities this correction factor is trivially defined by the relationship

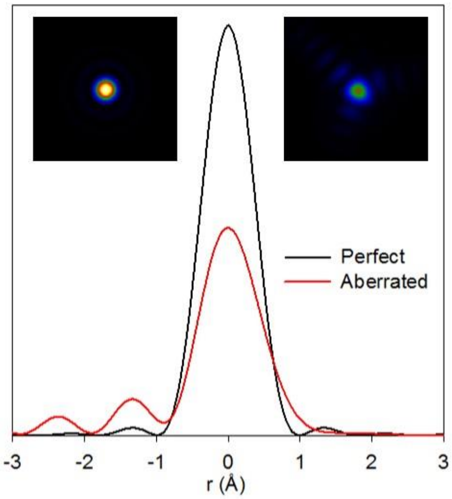

Figure 1. Comparison of probe intensities for a perfect probe and one with aberrations and temporal incoherence

$P_\Delta(\mathbf{r}) = F(\mathbf{r}) \otimes P_0(\mathbf{r})$ where $P_\Delta(\mathbf{r})$ is the aberrated incoherent probe, $F(\mathbf{r})$ the correction factor and $P_0(\mathbf{r})$ the perfect, aberration free probe. The symbol $\otimes$ represents a convolution. In order to obtain the correction factor, we simply deconvolve the intensity of the perfect probe from that of the aberrated incoherent probe.

## 2. Application to simulated images

In what follows the correction factor is deconvolved from the experimental image to obtain an image that can be compared directly with a simulated image. The mathematical proof that this is a reasonable approximation for the STEM imaging modes commonly used for 2D materials is both involved and lengthy and is presented elsewhere [3]. Instead we demonstrate the utility of this method using simulated images containing both temporal incoherence and residual aberrations. In figure 2 (a) we show a calculated image of $MoS_2$ assuming a perfect probe. In figure 2 (b) we have a simulated image including aberrations and incoherence. The result of the deconvolution process is shown in (c). As can be seen from the accompanying line profiles, the deconvolution process does an excellent job reproducing the intensities of the original image, albeit with some small residual aberrations. These residual aberrations are due to the approximations made in the treatment deconvolution of the inelastic signal described above.

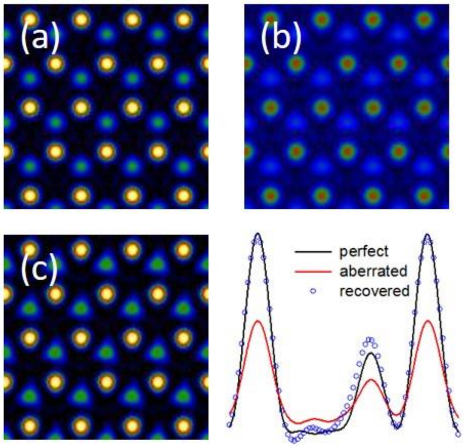

Figure 2. Calculated images of $MoS_2$ without (a) and with aberration and incoherence (b). The recovered image is shown in (c).

Deconvolutions are carried out using a Lucy-Richardson algorithm [reference] which is robust in the presence of noise and unlike methods such as Weiner deconvolution, there are no user input parameters. It is important to note that the Lucy-Richardson algorithm assumes both the input image and recovered image are positive at all points. For this reason, it is not practical to simply deconvolve the probe from the image. The result of such a deconvolution is in principle the inelastic scattering potential, however the potential is band width limited by the probe forming aperture and so oscillates about zero in a similar way to an Airy function. In addition, for 2D materials, there is significant intensity formed by the elastically scattered electrons reaching the detector. The image can then not simply be described as a convolution of the probe intensity and some inelastic scattering potential.

## 3: Application to experimental images

Mono-layer tungsten disulfide ($WS_2$) is an excellent specimen on which to test this algorithm. It contains both heavy and light atoms which are often not clearly separated in raw experimental data. In addition, the specimen examined here contains impurity atoms on the W sites which we suspected to be Mo, but this could not be confirmed by EELS. This work has been used to confirm the presence of Mo in these samples.

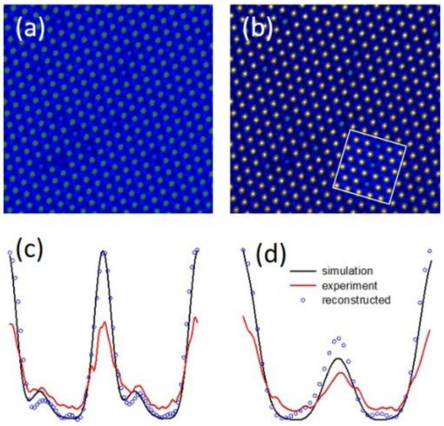

In figure 3 we demonstrate the reconstruction of an image of Mo doped $WS_2$. Shown in figure 3 (a) is the raw data while the reconstruction is shown in figure 3 (b). The inset in figure 3(b) is the calculated image assuming a perfect probe. The only processing of the simulation is to add a Gaussian blur to account for source size effects in order to match the overall image contrast to the reconstruction. In figure 3 (c) we show a line profile through adjacent Mo and S atoms. The S columns are clearly delineated in the reconstruction and their intensity is in good agreement with the simulated result. In figure 3 (d) we show a line scan through W and Mo atoms. Again the agreement between the simulation and reconstruction is good. A major issue with matching the contrast of experimental images of 2D materials is surface contamination. This makes a far greater contribution to the overall image contrast than it does in the bulk crystalline case. This leads to a significant spread of intensities from the W and Mo atomic sites and makes true quantification difficult. The result shown here comes from a relatively clean section of the sample and is sufficient for the identification of these heavy elements. However, for 2D materials with lighter component atoms, specimen preparation will play a vital role in true quantification.

Figure 3. (a) Raw experimental image of $WS_2$. (b) Reconstructed image with simulation inset. (c) Line profiles through W and S atoms. (d) Line profiles through W and Mo atoms.

## Future Plans

We intend to make these techniques available for use at the microscope so that images can be processed immediately after acquisition and their suitability for further analysis can be determined. We will also further develop imaging techniques designed to improve the SNR of images of 2D materials. In order optimize this technique, we need to determine the best detector collection angles to maximize the signals from atoms of varying atomic number.

## References

[1] Oxley et al., Reports on Progress in Physics, accepted for publication (2016).
[2] Krivanek et al., Nature **464**, 571, (2010).
[3] Oxley et al., in preparation.
[4] This work was done in collaboration with Gerd Duscher from the University of Tennessee, Knoxville and Les Allen from the University of Melbourne, Australia.

## Selected Publications on 2D Meterials

Junjie Guo, Jaekwang Lee, Cristian I Contescu, Nidia C Gallego, Sokrates T Pantelides, Stephen J Pennycook, Bruce A Moyer, Matthew F Chisholm, “Crown Ethers in Graphene,” *Nature Communications* **5**, 5389 (2014).

Xia, M.; Li, B.; Yin, K.; Capellini, G.; Niu, G.; Gong, Y.; Zhou, W.; Ajayan, P.M.; Xie, Y-H. Spectroscopic signatures of AA' and AB stacking of chemical vapor deposited bilayer $MoS_2$. *ACS Nano* **9**, 12246-12254 (2015).

Myron D. Kapetanakis, Wu Zhou, Mark P. Oxley, Jaekwang Lee, Micah P. Prange, Stephen J. Pennycook, Juan Carlos Idrobo, and Sokrates T. Pantelides, "Low-loss electron energy loss spectroscopy: An atomic-resolution complement to optical spectroscopies and application to graphene," *Physical Review B* **92**, 125147 (2015).

Gong, Y.; Lei, S.; Ye, G.; Li, B.; He, Y.; Keyshar, K.; Zhang, X.; Wang, Q.; Lou, J.; Liu, Z.; Vajtai, R.; Zhou, W.; Ajayan, P.M. Two-step growth of two-dimensional $WSe_2$/$MoSe_2$ heterostructures," *Nano Letters* 15, 6135-6141 (2015).

Gong, Y.; Ye, G.; Lei, S.; Shi, G.; He, Y.; Lin, J.; Zhang, X.; Vajtai, R.; Pantelides, S.T.; Zhou, W.; Li, B.; Ajayan, P.M. Synthesis of millimeter-scale transition metal dichalcogenides single crystals. *Advanced Functional Materials* **26**, 2009-2015 (2016).

Ye, G.; Gong, Y.; Lin, J.; Li, B.; He, Y.; Pantelides, S.T.; Zhou, W.; Vajtai, R.; Ajayan, P.M. Defects engineered monolayer $MoS_2$ for improved hydrogen evolution reaction. *Nano Letters* **16**, 1097-1103 (2016).

Li, X.; Lin, M.; Lin, J.; Huang, B.; Puretzky, A.A.; Ma, C.; Wang, K.; Zhou, W.; Pantelides, S.T.; Chi, M.; Kravchenko, I.; Fowlkes, J.; Rouleau, C.M.; Geohegan, D.B.; Xiao, K. Two-dimensional GaSe/$MoSe_2$ misfit bilayer heterojunctions by van der Waals epitaxy. *Science Advances* 2, e1501882 (2016).

# 3D Visualization of Emergent Behavior in Nanoscale Functional Heterostructures

**Amanda K. Petford-Long, Seungbum Hong, Charudatta Phatak**
**Materials Science Division, Argonne National Laboratory, 9700 S Cass Avenue, Argonne, IL 60439**
petford.long@anl.gov, hong@anl.gov, cd@anl.gov

## Research Scope

The properties of ferroic materials at the nanoscale are governed by their complex energy landscape, which must be understood if emergent behavior is to be controlled. We are focusing on nanoscale heterostructures whose building blocks show ferromagnetic, ferroelectric, and resistance switching behavior. We aim to obtain a fundamental understanding of domain behavior and charge transport properties in these nanostructures through control of parameters that contribute to their energy landscape, such as interlayer coupling, geometric effects, and interactions between adjacent nanostructures. Further degrees of freedom can be achieved in `designer' heterostructures, in which there is coupling between the order parameters in materials with different ferroic order. Our approach involves an interwoven combination of aberration-corrected Lorentz transmission electron microscopy (LTEM) and advanced scanning probe microscopy (SPM) and a particular focus is the use of three-dimensional (3D) analysis and imaging techniques that we have developed to visualize domain and transport behavior in nanostructures as a function of external stimuli such as applied fields, temperature and/or time.

## Recent Progress

### *Nanoscale Skyrmions in Non-Chiral Multiferroic*

Magnetic skyrmions belong to a set of topologically non-trivial spin textures at the nanoscale that have received increased attention due to their emergent behavior and novel potential spintronic applications. In this work, we have shown the formation of nanoscale skyrmions in a non-chiral multiferroic material that is ferromagnetic and ferroelastic, namely $Ni_2MnGa$, at room temperature, without the presence of an external magnetic field. Using aberration-corrected Lorentz transmission electron microscopy (LTEM), we were able to elucidate that skyrmion formation resulted from geometric confinement of the magnetic spin texture inside alternate microstructural nanoscale twins, as seen in Fig. 1(a). Using in-situ magnetizing experiments coupled with micromagnetic simulations, we observed the deformation of skyrmions with skyrmion number 1 (Fig. 1(b)) into trivial

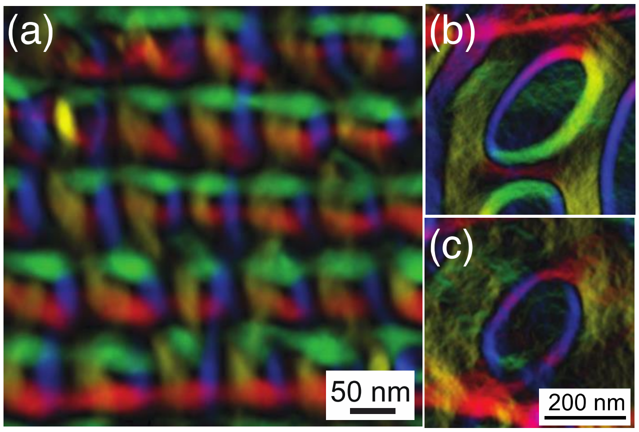

Figure 1 (a) Color magnetic induction map showing the formation of skyrmion lattice in a narrow twinned region of $Ni_2MnGa$ with individual skyrmions of the order of 30 nm. Color magnetic induction map showing the change in topology of an individual skyrmion from (b) non-trivial to (c) trivial. [15]

bubble domain with skyrmion number 0 (Fig. 1(c)). Our results show that chiral interactions are not necessary for a material to host a skyrmion phase.

### *Charge gradient microscopy (CGM) with semiconductor-metal tips*

Advanced SPM techniques open up the possibility of next-generation ferroic devices that utilize both domains and domain walls (DWs) as active elements. However, current SPMs lack the capability to dynamically monitor domain and DW motion in addition to transport of the screening charges that lower the total electrostatic energy. Charge gradient microscopy (CGM) maps domains and DWs at high speed and mechanically removes the screening charges, however the underlying signal generation mechanism is not fully understood due to the complexity of the electrostatic interactions. We developed a semiconductor−metal CGM tip and showed that by changing the scan direction of the tip we could separate and quantify the signals from the ferroelectric domain and the DW signals (Fig. 2). Our investigation showed that the DW signal is due to the spatial change of the polarization charges, while the domain signal is due to the continuous removal and supply of screening charges at the CGM tip. In addition, we observed asymmetric CGM signals from the up and down domains, which originate from the different debonding energies and the amount of the screening charges for positive and negative bound charges. We believe that our findings can help lead to breakthroughs in information storage and energy-harvesting devices.

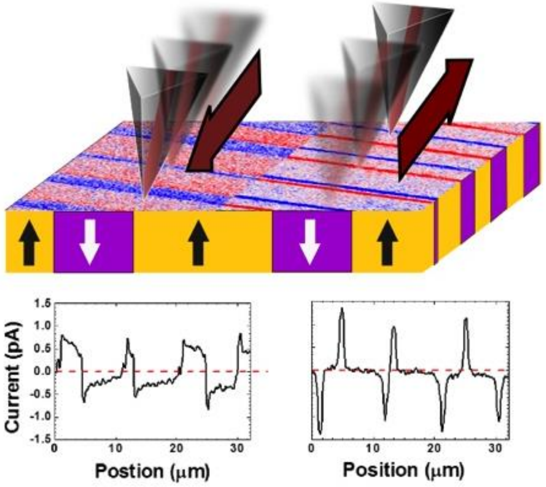

**Figure 2** Schematic of a semiconductor-metal CGM tip moving forwards and backwards. The graphs show the corresponding current from the surface of a $LiNbO_3$ sample with periodic domains (the blue and red stripes). The left graph corresponds to semiconductor edge leading and the right graph to the metal tip-edge leading. [13]

### *In-situ TEM of reversible and irreversible electroforming in Pt/NiO/Pt heterostructures*

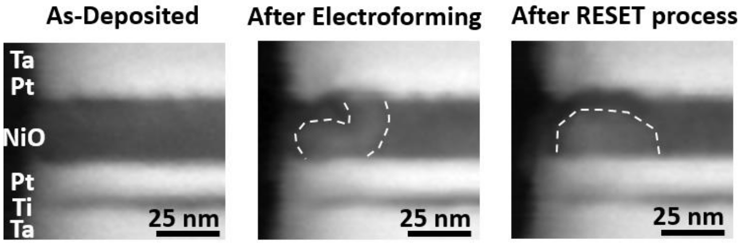

Fig. 3 In-situ TEM images of formation and partial redissolution of reduced $NiO_x$ pillar in Pt/NiO/Pt heterostructure. [3]

Numerous reports suggest that resistance switching in binary transition metal oxides is caused by local reduction of the oxide layer into conducting filaments, but few reports have shown experimental evidence correlating electroforming with site-specific changes in composition that can be interpreted as individual conducting filaments. We explored the mechanisms of reversible and irreversible electroforming in 250–500 nm wide pillars that we patterned from a single Ta/Ti/Pt/Ti-doped

NiO/Pt/Ta heterostructure, and showed that these can co-exist within a single sample. We performed in-situ TEM electroforming and switching on each pillar to correlate the local electron transport behavior with microstructure and composition in each pillar. DFT calculations fitted to electron energy loss spectroscopy data showed that the Ti-doped NiO layer is partially reduced after reversible electroforming (Fig. 3), with the formation of oxygen vacancies ordered into lines in the <110> direction. However, under the same probing conditions, adjacent pillars show irreversible electroforming caused by electromigration of metallic Ta to form a single bridge across the oxide layer. We propose that the different electroforming behaviors are related to microstructural variations across the sample and can lead to switching variability.

## Future Plans

### ***Exploring ferroic domain behavior at the nanoscale***

We seek to develop a systematic understanding of the contribution and relative scale of various energy terms governing the domain behavior in vertically and laterally confined ferromagnetic heterostructures, and ferroelectric nanostructures. We will then build upon this fundamental understanding to control the behavior at the mesoscale and enable emergent phenomena such as non-trivial spin or polarization textures, and magnetic excitations.

We are extending our previous work on artificially frustrated magnetic nanostructures to understand the magnetic excitations and frustration behavior in aperiodic spin ice arrays. We will explore the emergence of localized ground states, the effect of edge states and the reversal behavior in quasicrystal spin ice lattices. We will use a unique approach based on graph theory and Monte Carlo simulations to analyze and understand the correlations in such lattices. Based on our recent results on creation of artificial skyrmions and antiskyrmions, we will continue to explore the competing energy landscape of nanoscale heterostructures, by exploring the quasistatic domain behavior in response to applied electric current and magnetic fields for systems into which we now introduce the symmetry-breaking Dzyaloshinskii-Moriya interaction in conjunction with other interactions such as exchange bias or indirect exchange.

In ferroelectric nanostructures we seek to understand the main driving force that controls the behavior of domains, as well as the distribution of charged and uncharged domain boundaries, as a function of the size and shape of the nanostructures. Our newly-developed semiconductor-metal CGM tip is ideally suited to distinguish the roles of the underlying polarization and the screening ions. This will help us elucidate the role of screening charge on the resulting domain structure. We will then explore the domain behavior using in-situ environmental cell for AFM by controlling the environments (e.g. humidity, surface modification (hydrophobic vs. hydrophilic overcoating). We will also explore the domain switching in our patterned ferroelectric nanostructures to understand the local effects that hinder or facilitate domain motion. Our observations of domain nucleation and growth as well as DW conduction will allow us to understand the effects of shape and size on domain structure and its electrical properties in ferroelectric nanostructures.

### ***Resistive Switching oxides***

Our exploration of resistive-switching oxide (RSO) materials will focus on understanding how confinement and the motion of charged defects control the 3D distribution of conduction pathways. We are developing novel artificial resistive-switching network configurations using block copolymer self-assembly followed by the sequential infiltration synthesis (SIS) process using atomic layer deposition (ALD) in collaboration with colleagues in the Institute of Molecular Engineering. We will then use in-situ c-AFM and TEM to study the changes in conductivity, crystal structure and oxidation states to understand the 'random circuit-breaker model' for RSOs and to determine whether conducting filament formation is a self-limiting process. In order to understand the effects of defect distribution in RSO films, we will extend our 2D studies of conducting filament distribution to three dimensions using a novel method involving the use of an AFM tip to first map current distribution and then serial section down through the filaments. We will use our newly installed aberration-corrected off-axis electron holography capability on our Lorentz TEM to quantitatively image nanoscale electric fields and potentials in and around the nanostructures.

### Selected Publications (from FY15 and FY16)

1. "Vortex jump behavior in coupled nanomagnetic heterostructures", S. Zhang, A.K. Petford-Long, O. Heinonen, C. Phatak, *Appl. Phys. Lett.* **105**, 212409 (2014). DOI: 10.1063/1.4902922
2. "Tunable and rapid self-assembly of block copolymers using mixed solvent vapors", W.I. Park, S. Tong, Y. Liu, I. W. Jung, A. Roelofs, and S. Hong, *Nanoscale* **6**, 15216 (2014). DOI: 10.1039/c4nr04726e
3. "In-situ TEM study of reversible and irreversible electroforming in Pt/Ti:NiO/Pt heterostructures", K. D'Aquila, Y. Liu, H. Iddir and A.K. Petford-Long, *Phys. Status solidi RRL* **9(5)**, 301 (2015).
4. "Ferromagnetic domain behavior and phase transition in bilayer manganites investigated at the nanoscale", C. Phatak, A.K. Petford-Long, H. Zheng, J.F. Mitchell, S. Rosenkranz, M. Norman, *Phys. Rev B* **92**, 224418 (2015). DOI: 10.1103/PhysRevB.92.224418
5. "Iterative reconstruction of magnetic induction using Lorentz transmission electron tomography", C. Phatak and D. Gürsoy, *Ultramicroscopy* **150**, 54 (2015).
6. "Towards Multiresolution Phase Retrieval using Electron Ptychography", C. Phatak, Y. Nashed, and T. Peterka, *Microsc. Microanal.* **21 (Suppl 2)**, 2151 (2015).
7. "Mechanical removal and rescreening of local screening charges at ferroelectric surfaces," S. Tong, W. I. Park, Y.-Y. Choi, L. Stan, S. Hong and A. Roelofs, *Phys. Rev. Appl.* **3**, 014003 (2015). DOI: 10.1103/PhysRevApplied.3.014003
8. "Hierarchically Self-Assembled Block Copolymer Blends for Templating Hollow Phase-change Nanostructures with an Extremely Low Switching Current," W. I. Park, J. M. Kim, J. W. Jeong, Y. H. Hur, Y. J. Choi, S. Kwon, S. Hong, Y. Yin, Y. S. Jung, and K. H. Kim, *Chem. Mater.* **27**, 2673 (2015). DOI: 10.1021/acs.chemmater.5b00542
9. "Fabrication of highly-ordered and well-aligned $PbTiO_3$/TiN core-shell nanotube arrays," J. Yoon, S. Kim, D. Kim, I.-D. Kim, S. Hong and K. No, *Small* **11**, 3750 (2015). DOI: 10.1002/smll.201500087
10. "Quantitative 3D electromagnetic field determination of 1D nanostructures from single projection", C. Phatak, L. de Knoop, F. Houdellier, C. Gatel, M. J. Hÿtch, and A. Masseboeuf, *Ultramicroscopy* **164**, 24 (2016).
11. "Visualization of ion transport in Nafion using electrochemical strain microscopy," S. Kim, K. No and S. Hong, *Chem. Comm.* **52**, 831 (2016). DOI: 10.1039/c5cc07412f

12. “Atomic layer deposition of environmentally benign $SnTiO_x$ as a potential ferroelectric material,” S. Chang, S. K. Selvaraj, Y.-Y. Choi, S. Hong, S. Nakhmanson, and C. G. Takoudis, *J. Vac. Sci. Technol. A* **34**, 01A119 (2016). DOI: 10.1116/1.4935650
13. “Imaging Ferroelectric Domains and Domain Walls Using Charge Gradient Microscopy: Role of Screening Charges,” S. Tong, I. W. Jung, Y.-Y. Choi, S. Hong, and A. Roelofs, *ACS Nano* **10**, 2568 (2016). DOI: 10.1021/acsnano.5b07551
14. “Recent advances in Lorentz microscopy”, C. Phatak, A.K. Petford-Long and M. De Graef, *Current Opinion in Solid State and Materials Science* **20**, 107 (2016).
15. “Nanoscale skyrmions in a non-chiral metallic multiferroic: $Ni_2MnGa$”, C. Phatak, O. Heinonen, M. De Graef, A. Petford-Long, *Nano Lett.* **16**, 4141 (2016). doi: 10.1021/acs.nanolett.6b01011
16. “Screening Mechanisms at Polar Oxide Heterointerfaces,” S. Hong, S. M. Nakhmanson, and D. D. Fong, *Rep. Prog. Phys.* **79**, 076501 (2016). DOI: 10.1088/0034-4885/79/7/076501
17. “Visualization of magnetization in CoFe nanofibers by Lorentz TEM and electron holography” S. Zhang, Z. Zhou, G. Grocke, A. Petford-Long, Y. Liu, X. Chen, C. Phatak, *Microsc. Microanal.***22** (S3)**,** 1692 (2016). DOI: 10.1017/S1431927616009302
18. “Synthesis of Ferroelectric Lead Titanate Nanohoneycomb Arrays via Lead Supplement Process,” B. Kim, S. Hong, G. Ahn, and K. No, *J. Am. Ceram. Soc.* **99**, 2221-2225 (2016). DOI: 10.1111/jace.14307
19. “Creation of artificial skyrmions and antiskyrmions by anisotropy engineering”, S. Zhang, A. K. Petford-Long, C. Phatak, *Scientific Reports* **6**, 31248 (2016). DOI: 10.1038/srep31248

# Tracing non-equilibrium phenomena in correlated materials by using ultrafast electron probes

Jing Tao and Junjie Li
Department of Condensed Matter Physics and Materials Science
Brookhaven National Laboratory, Upton, NY 11973

## Research Scope

The Early-Career-Award (ECA) research task under the FWP Number 2015-BNL-PM046-Fund is to establish an understanding of the competing degrees of freedom in many emergent properties in strongly correlated materials by investigating non-equilibrium phenomena. The project will be carried out using an existing ultrafast electron diffraction (UED) instrument at Brookhaven National Laboratory (BNL). Utilizing pump-probe techniques with MeV electrons as the probe, the BNL-UED system has demonstrated the potential for extraordinary sensitivity and high temporal-resolution in detecting electronic structures far from the equilibrium. During the course of the project instrumentation modifications will be conducted to enhance the performance of the UED, including a double-tilt stage for precise positioning the sample materials and an optical parametric amplifier for continuous tuning of the pumping energy. Individual orders, such as charge order and orbital order, associated with optical excitations will be probed and analyzed separately in the ultrafast time-domain in order to distinguish their roles in structural relaxation.

## Recent Progress

*A new environmental room for BNL-UED* The UED instrument is now located in a new environmental room with accurate control of temperature (fluctuation within 0.1 K) and humidity (40 ± 1 %) to improve the stability of the instrument. An overview of the current situation of the UED and the environmental room is shown in the photos in Fig. 1. The klystron, which generates the radio-frequency accelerating field for the gun at the repetition rate of 5Hz, and the UED room entrance are highlighted in the insets of Fig. 1a). The majority part of the UED instrument is in the room behind the concrete wall in the picture and the setup is shown in Fig. 1b). After the beam commissioning in June of 2016, the first UED pattern was obtained from the testing sample $LaSr_2Mn_2O_7$ using a 5 fC electron bunch, shown as the inset of Fig 1b).

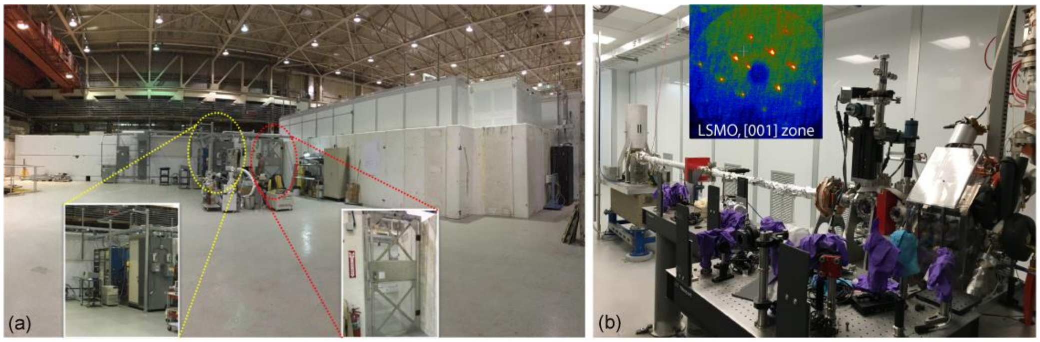

Fig. 1. (a) Front view of the environmental room. The klystron with the control panel and the UED room entrance are highlighted in the left and right insets, respectively. b) The UED setup in the room. The inset is an UED pattern obtained from the $LaSr_2Mn_2O_7$ (LSMO) sample after the beam commissioning on June 30.

*Double-tilt sample stage* Precise positioning and tilting of single-crystal samples in the UED experiments are critical to this ECA project. The data processing and interpretation will be rigorously dependent on the original data quality of all the reflections over two-dimensional UED patterns.

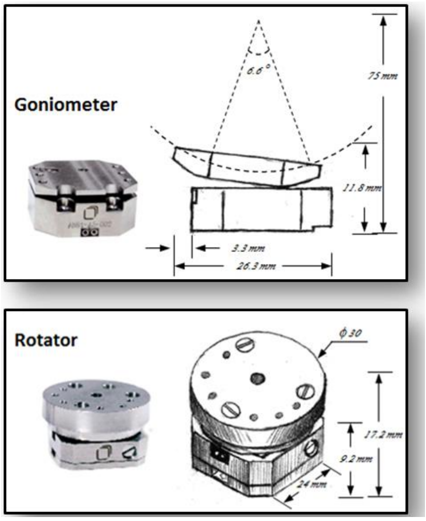

Fig. 2. A schematic drawing of the goniometer and the rotator in the double-tilt UED stage with dimensions.

Therefore, how well the crystals are aligned with the incident beam is a prominent factor. The former BNL-UED was equipped with a single-tilt sample stage, which cannot provide the accurate tilting in experiments. A double-tile stage was designed for the restricted sample space and an UHV (< 10-9 torr) environment with motorized drives connected to outside. Moreover, the double-tilt stage will be compatible for the low-temperature (< 20 K) experiments in the future, and the tilting/rotation steps have very little hysteresis. Based on the project's requirements and the capability of the manufacturer, the design of the stage is shown in Fig. 2. It has a goniometer (step size of 0.1 milli-degree at 300 K and 20 micro-degree at 4 K; repeatability of step sizes ~ 5 % over full ranges) and a rotator (travel range of 360° endless in both directions; step size of 1 milli-degree at 300 K and 0.5 milli-degree at 4 K; repeatability of step sizes ~ 5 % over full ranges) to fulfil the tilting along two independent angles. The additional thermal coupling (not shown in the figure) is specially designed for the temperature control. Together with the existing motion drives along x, y and z directions, the sample mounted on the new stage will have five degrees of freedom in precise positioning.

*Optical parametric amplifier (OPA)* The current BNL-UED laser wavelength is near-infrared 800 nm, i. e., the pump energy is fixed at a photon energy of 1.55 eV. While this energy is close to the Mott insulator gap and to the orbital-ordering (OO) excitation energy, and is well suited for studying the photon-induced metal-insulator transition and OO related phenomena in certain correlated materials, it is certainly insufficient for exploring complicated dynamics in a broad range of strongly correlated materials. For example, charge-ordering (CO) and charge-density-wave (CDW) excitation energies may vary from tens of meVs to the eV level. Typical phonon modes corresponding to emergent phenomena have excitation energies of tens of meVs. In addition, OO/CO states are often coupled to the spin-ordering in correlated materials, and the excitation of spin ordering or spin density wave are at the level of hundreds of meVs. Therefore, driving the material to excited states by tunable pumping energy is important to the understanding of the dynamic response of electronic structures. The purchase order of an OPA system has been placed and it will be installed at BNL-UED, which will enable us to continue tune the pumping energy from 110 meV per photon (corresponding to 11 µm in wavelength and 27 THz in frequency) to 6 eV per photon (corresponding to 200 nm and 1500 THz).

## Future Plans

*Understanding CDW in "3D" dichalcogenides* Stacking sequence of the repeating structural layers was considered not to have a significant impact on materials' properties especially when the geometry of the repeating layers is maintained. However, a previous work showed a surprising case that the superconductivity measurements in Te-doped $TaSe_2$ samples are very different with the 1T, 2H and 3R structures [1]. Conventional electron diffraction patterns further demonstrated distinct behaviors of the CDW electronic structure in 1T and 3R samples (Fig. 3a)). The reason of the drastic change in the properties with different structures is unknown. These samples are excellent candidates for the UED study because the CDW structures with well-defined symmetry give rise to superlattice reflections separated from fundamental reflections and make the intensity measurements straightforward (see the highlighted CDW reflections in an UED pattern in Fig. 3b)). With the collaboration of Prof. R. Cava's group at Princeton Univ., we plan to study the electron-phonon coupling by probing the structural dynamics of the CDW in those materials. Theoretical calculations will be integrated into this work to particular address the interaction between the stacking layers. We expect that the UED experiments and the analysis could answer the question that whether the distinct properties arise from the subtle difference between intralayer coupling in single layer systems vs interlayer coupling in 3D materials.

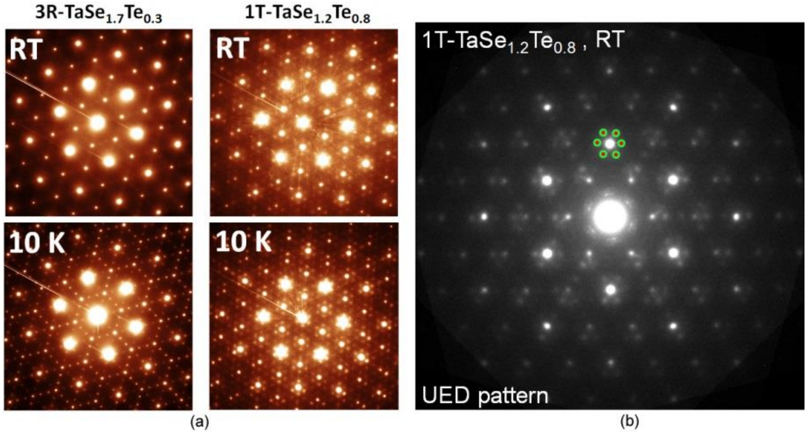

Fig. 3. (a) Conventional electron diffraction patterns were obtained from TaSeTe samples with different polytypism of 3R and 1T. Distinct CDW behaviors, in terms of the CDW peak positions, peak widths and their thermal evolution, can be clearly seen at both room temperature and the low temperature at 10 K. (b) An UED pattern was obtained from the 1T-$TaSe_{1.2}Te_{0.8}$ sample at room temperature in an ultrafast pump-probe experiment. Six CDW diffuse peaks are highlighted on the pattern.

*Probing strong charge-orbital-spin coupling in doped manganites*

After extensive studies in the past decades of perovskite manganites, fundamental questions, such as the nature of the CO/OO superstructures and the role of the dopants in forming various electronic structures, still remain open. With the collaboration of Prof. S-W. Cheong's group at Rutgers Univ., we propose an UED study on $La_{0.35}Pr_{0.275}Ca_{0.375}MnO_3$ and $La_{0.25}Pr_{0.375}Ca_{0.375}MnO_3$ single-crystals. These materials have short-range CO/OO existing at various temperatures and strongly coupled to the spin orders [2]. Previous work indicated that short-range OO can be more sensitive to the local electron-electron interaction than long-range ordering, thus short-range electronic structures are "electronically softer" [3]. We plan to perform the UED experiment at different temperatures and with various pump energies to probe the structural dynamics of the short-range CO/OO ordering. Using the developed method in the previous UED work [4] and with tunable pumping energy by integrating OPA into the UED optics, we expect to separate the coupling of CO and OO to the spin and the lattice degrees of freedom for a better understanding of the nature of the electronic states in doped manganites.

## References

1. Luo, H-X. et al., "Polytypism, polymorphism, and superconductivity in $TaSe_{2-x}Te_x$", *PNAS* **112**, E1174 (2015).
2. Uehara, M. et al., "Percolative phase separation underlies colossal magnetoresistance in mixed-valentmanganites", *Nature* **399**, 560 (1999).
3. Tao, J. et al., "Direct observation of electronic-liquid-crystal phase transitions and their microscopic origin in $La_{1/3}Ca_{2/3}MnO_3$", *Scientific Reports, in press*
4. Li, J-J. et al., "Dichotomy in ultrafast atomic dynamics as direct evidence of polaron formation in a manganite", *submitted.*

# Spin Physics and Nanoscale Probes of Quantum Materials

**Shoucheng Zhang[1], Hari C. Manoharan[1], David Goldhaber-Gordon[1], Joseph Orenstein[2]**

[1] ***Stanford Institute for Materials and Energy Sciences, SLAC National Accelerator Laboratory & Department of Physics, Stanford University;*** [2] ***Lawrence Berkeley National Laboratory & Department of Physics, University of California, Berkeley***

## Program Scope

The main goals of this FWP are to discover new states of quantum matter and novel physical effects associated with the electron spin, to observe and to manipulate quantum spin degrees-of-freedom at the microscopic scale, and to design and predict materials with tailored functionality. The spin physics program investigates novel phenomena arising from spin coupling in solids. Recently, it was realized that spin-orbit coupling can lead to a fundamentally new state of matter, the topological insulator. These materials have an energy gap in the bulk, and a conducting topological state on the surface. The spin program develops theoretical concepts and experimental tools to investigate these novel effects.

## Recent Progress

Pushing topological insulators to the spatial limit. Using materials growth expertise from MSD/SLAC (Yi Cui), Manoharan completed an STM/STS survey of topological insulator materials as they are scaled down to the spatial limit (down to single quintuple layers in thickness and nanometer scale in lateral extent). These studies have revealed several new phenomena including self-doping tied to layer-dependent epitaxial growth, and the emergence of a disordered stripe-like electronic phase separation possessing a characteristic length scale that decreases as the spatial limit is approached. Beyond the new observations, these results can also be used to tune the Dirac point and mobility in ultra-small topological insulator nanostructures (see Figure 1a).

Single magnetic and nonmagnetic dopants in ultrathin semiconductors. Manoharan and Orenstein tracked the spectral evolution of single dopants in TMDC monolayers. Behavior such as the presence and absence of spin splitting based on impurity incorporation, and the temperature dependence were studied. The results show that the electronic configuration of the individual dopants is extremely sensitive to the growth conditions of the monolayers, as well as to band-bending induced by the measurements themselves. In other related work, Manoharan performed STM/STS experiments on monolayer $MoS_2$ to help show the correlation between strain, single sulphur vacancies, and electronic structure in collaboration with Jens K. Nørskov (SLAC).

Searching for semimetals of exotic symmetry and topology. Zhang has proposed material platforms with broken symmetries and non-trivial topologies as potential hosts of exotic quasiparticle excitations, including gapless Dirac fermions, Weyl fermions, and Majorana fermions. Recently, Zhang has proposed a candidate platform, CuMnAs, for the surprising possibility of finding massless Dirac fermions in a magnetic material having broken time-reversal and inversion symmetry. Zhang has shown that HgTe and half-Heusler compounds, including LaPtBi, could be ideal Weyl semimetals, having all Weyl nodes lying exactly at the

Fermi level. Zhang has suggested experimental methods to detect chiral Majorana edge modes at interfaces of topological insulators and superconductors. Material hosts of Majorana states are sought after as their non-Abelian exchange statistics could underpin topological quantum computation.

Unraveling the macroscopic signatures of the quantum anomalous hall phase. Magnetic doping of thin topological insulators has led to the realization of the quantum anomalous hall effect, in which carriers flow in nearly dissipationless spin-polarized chiral edge modes in otherwise insulating materials. Goldhaber-Gordon has discovered thermally-activated bulk conduction in quantum anomalous hall insulators using Corbino-geometry devices, which points to the increase or greater homogeneity of the exchange gap as a primary means to decrease dissipation in these materials. Goldhaber-Gordon has found transport signatures of apparent domain motion in quantum anomalous hall insulators at low temperatures (see Figure 1b). Zhang has theoretically proposed and collaborated with Kang Wang (UCLA) to experimentally detect Majorana chiral edge modes in a region of topological superconductivity induced in a proximitized quantum anomalous hall host (see Figure 1c).

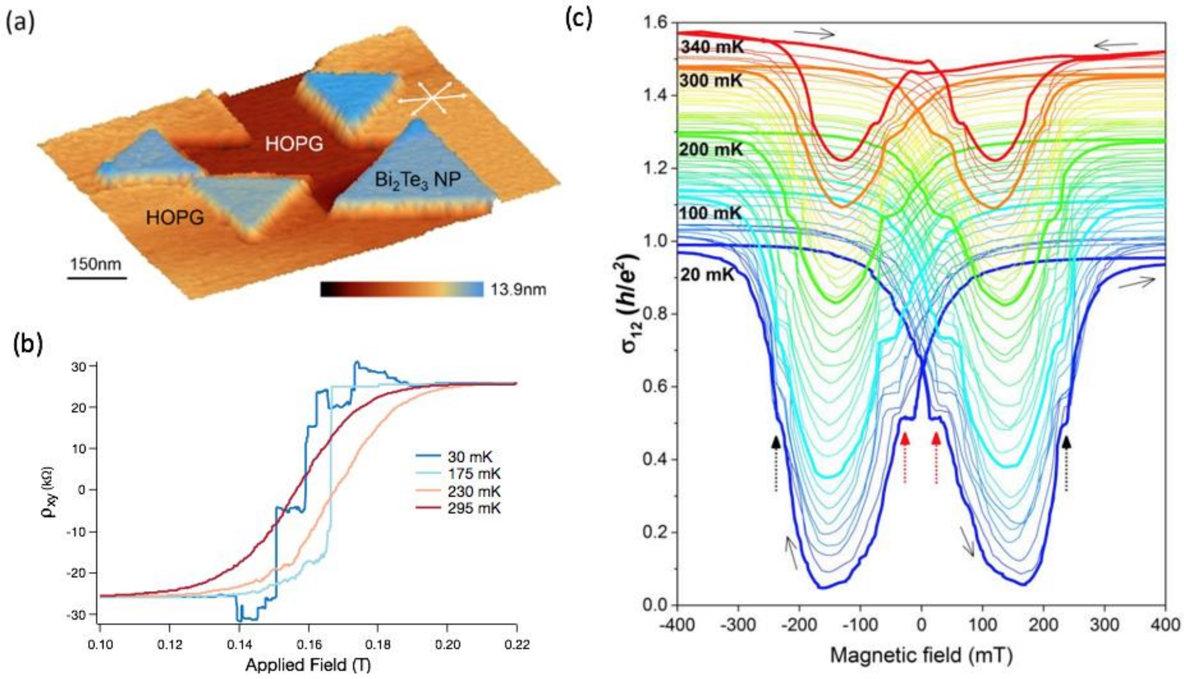

Figure 1 | (a) STM topograph of a group of $Bi_2Te_3$ nanoplatelets grown on HOPG. Topological insulator nanoplatelets (in blue) with uniform thicknesses are shown aligned to the same crystallographic directions (white arrows) set by the substrate, an unequivocal sign of epitaxial growth. (b) Transport measurement in the quantum anomalous hall state displaying jumps in Hall resistance indicative of the motion of magnetic domains in the topological insulator material. (c) Transport measurement of a magnetic topological insulator device with a proximitized region of topological superconductivity, displaying half-quantized conductance regions (black and red arrows) indicative of single chiral Majorana edge modes.

## Future Plans

Manoharan and Zhang are experimentally and theoretically investigating the vortex state of the proximity coupled system of superconductor with $NaCoO_2$, looking for signatures of expected Majorana bound states at zero energy and the presence of topological superconductivity. Together with Manoharan and Harold Hwang of MSD/SLAC, Orenstein is performing optical measurements on systems with strong spin-orbit coupling, and probing the interface of superconductors grown on small gap semiconductors. Goldhaber-Gordon, Orenstein, and Manoharan are using heterostructures of graphene and a ferromagnetic insulator to develop semiconducting devices featuring gate-tunable spin polarization. Orenstein is performing second harmonic generation experiments on ferroaxial crystals in collaboration with Sang-Wook Cheong at Rutgers and terahertz transmission measurements on materials showing proximate Kitaev spin liquid behavior.

Goldhaber-Gordon is performing transport measurements of $Cr\text{-}(BiSb)_2Te_3$ magnetically-doped topological insulator devices, examining the macroscopic signatures of the quantum anomalous hall phase of matter. Following theoretical proposals by Zhang, Goldhaber-Gordon is working to interface topological insulators and superconductors in order to observe Andreev reflection of proximitized chiral Majorana edge modes. Goldhaber-Gordon is working to artificially induce magnetic domains in quantum anomalous hall devices, allowing the controlled study of chiral transport at domain boundaries along with the development of transistor-like devices in highly spin-protected systems. Goldhaber-Gordon continues to use varied device geometries to probe how edge and bulk conduction generate dissipation in quantum anomalous hall transport. Further, Goldhaber-Gordon is utilizing magnetic impedance microscopy (collaboration with ZX Shen) and scanning SQUID microscopy (collaboration with Kathryn Moler) for their capacity to generate real-space images of the chiral conduction channels in quantum anomalous hall insulators. Zhang will continue proposing topological systems combined with interactions.

## Publications

1. Jason C. Randel, Francis C. Niestemski, Andrés R. Botello-Mendez, Warren Mar, Georges Ndabashimiye, Sorin Melinte, Jeremy E. P. Dahl, Robert M. K. Carlson, Ekaterina D. Butova, Andrey A. Fokin, Peter R. Schreiner, Jean-Christophe Charlier, and Hari C. Manoharan, *Unconventional molecule-resolved current rectification in diamondoid-fullerene hybrids.* Nature Communications **5**, 4877 (2014).
2. Wang, J., B. Lian, and S.-C. Zhang, *Universal scaling of the quantum anomalous Hall plateau transition.* Physical Review B, 2014. **89**(8): p. 085106.
3. Wang, J., H. Mabuchi, and X.-L. Qi, *Calculation of divergent photon absorption in ultrathin films of a topological insulator.* Physical Review B, 2013. **88**(19): p. 195127.
4. Wang, J., Y. Xu, and S.-C. Zhang, *Two-dimensional time-reversal-invariant topological superconductivity in a doped quantum spin-Hall insulator.* Physical Review B, 2014. **90**(5): p. 054503.
5. Wang, Z. and S.-C. Zhang, *Topological Invariants and Ground-State Wave functions of Topological Insulators on a Torus.* Physical Review X, 2014. **4**(1): p. 011006.
6. Yuan, H., et al., *Generation and electric control of spin-valley-coupled circular photogalvanic*

*current in $WSe_2$*. Nat Nano, 2014. advance online publication.

7. Yuan, H., et al., *Generation and electric control of spin–valley-coupled circular photogalvanic current in WSe2.* Nat Nano, 2014. **9**(10): p. 851-857.
8. Zhang, H., et al., *Topological States in Ferromagnetic CdO/EuO Superlattices and Quantum Wells.* Physical Review Letters, 2014. **112**(9): p. 096804.
9. Zhang, H., et al., *Quantum Spin Hall and Quantum Anomalous Hall States Realized in Junction Quantum Wells.* Physical Review Letters, 2014. **112**(21): p. 216803.
10. A.J. Bestwick, E.J. Fox, Xufeng Kou, Lei Pan, Kang L. Wang, D. Goldhaber-Gordon, *Precise Quantization of the Anomalous Hall Effect near Zero Magnetic Field.* Physical Review Letters **114**, 187201 (2015).
11. Eric Yue Ma, M. Reyes Calvo, Jing Wang, Biao Lian, Mathias Mühlbauer, Christoph Brüne, Yong-Tao Cui, Keji Lai, Worasom Kundhikanjana, Yongliang Yang, Matthias Baenninger, Markus König, Christopher Ames, Hartmut Buhmann, Philipp Leubner, Laurens W. Molenkamp, Shoucheng Zhang, David Goldhaber-Gordon, Michael K. Kelly, and Zhi-Xun Shen. To be published in Nature Communications. [Primary ownership is in another FWP, but Zhang and Goldhaber-Gordon, together with our group members supported on DOE, participated in key ways].
12. Shreyas Patankar, J. P. Hinton, Joel Griesmar, J. Orenstein, J. S. Dodge, Xufeng Kou, Lei Pan, Kang L. Wang, A. J. Bestwick, E. J. Fox, D. Goldhaber-Gordon, Jing Wang, Shoucheng Zhang, *Resonant magneto-optic Kerr effect in the magnetic topological insulator $Cr:(Sb_x,Bi_{1-x})_2Te_3$,* arXiv:1505.00728.
13. P. Giraldo-Gallo, Y. Zhang, C. Parra, H. C. Manoharan, M. R. Beasley, T. H. Geballe, M. J. Kramer, I. R. Fisher, *Stripe-like nanoscale structural phase separation in superconducting $BaPb_{1-x}Bi_xO_3$*, Nature Communications **6**, 8231 (2015).
14. Hong Li, Charlie Tsai, Ai Leen Koh, Lili Cai, Alex W. Contryman, Alex H. Fragapane, Jiheng Zhao, Hyun Soon Han, Hari C. Manoharan, Frank Abild-Pedersen, Jens K. Nørskov, Xiaolin Zheng, *Activating and Optimizing $MoS_2$ Basal Planes for Hydrogen Evolution through the Formation of Strained Sulphur Vacancies*, Nature Materials **15**, 48–53 (2016).
15. Biao Lian, Jing Wang, and Shoucheng Zhang, *Edge State Induced Andreev Oscillation in Quantum Anomalous Hall Insulator-Superconductor Junctions*, Phys. Rev. B **93**, 161401 (2016).
16. Jiawei Ruan, Shao-Kai Jian, Hong Yao, Haijun Zhang, Shoucheng Zhang, Dingyu Xing, *Symmetry-protected Ideal Weyl Semimetal in HgTe-class materials, Nature Comm. **7**, 11136 (2016).*
17. Peizhe Tang, Quan Zhou, Gang Xu, Shoucheng Zhang, *Dirac Fermions in an Antiferromagnetic Semimetal,* Nature Physics (2016) advance online publication.
18. Carolina. Parra, Thiago Henrique Rodrigues da Cunha, Alex W. Contryman, Desheng Kong, Francisco Montero-Silva, Pedro Henrique Rezende Gonçalves, Diogo Duarte Dos Reis, Paula Giraldo-Gallo, Rodrigo Segura, Fernanda Olivare, Francis Niestemski, Yi Cui, Rogerio Magalhaes-Paniago, Hari C. Manoharan, *Self-Organized Phase Separation of Dirac Electrons in Topological Insulators at the Spatial Limit*, submitted (2016).
19. Q. L. He, et al., *Chiral Majorana Edge State in a Quantum Anomalous Hall Insulator-Superconductor Structure*, submitted (2016).

# Real Time Imaging of Materials Transformations in Liquids

**Haimei Zheng (PI), Materials Sciences Division, Lawrence Berkeley National Laboratory**

## Research Scope

Understanding how materials grow, function, and transform dynamically in their working environment at nanometer or atomic level is crucial to the development of energy conversion and storage technologies. In this program, we study growth and transformation processes of materials in liquids (including gases) in situ using transmission electron microscopy (TEM). By real time imaging of materials transformations, such as nanocrystal growth in solution, structural dynamics in catalysis, mass transport in electrochemical processes, this project will result in the fundamental understanding of the dynamic processes of materials in energy applications.

## Recent Progress

Liquid cell TEM has proven to be an excellent tool for studying the dynamic processes of colloidal nanoparticles in solution. We study single nanoparticle growth trajectories using liquid cells TEM. Our recent work show that in addition to metal noble nanoparticles, we can also visualize the growth pathways of oxide and heterostructured nanoparticles in a liquid cell[2, 3].

Further more, we have developed electrochemical liquid cells for the study of electrochemical processes in situ[1, 4, 5]. By incorporating advanced TEM techniques into the liquid cell TEM platform, such as, 4D STEM (diffraction imaging) and electron dispersive spectroscopy (EDS) analysis, previously unreachable details of a reaction have been achieved. For example, structure changes of electrode materials, i.e., $MoS_2$, during charge and discharge has been captured in situ. With the assistance of advanced imaging in liquid cell TEM (Fig. 1), we found that $MoS_2$ broke into pieces after fast discharge[1], which is otherwise hard to distinguish.

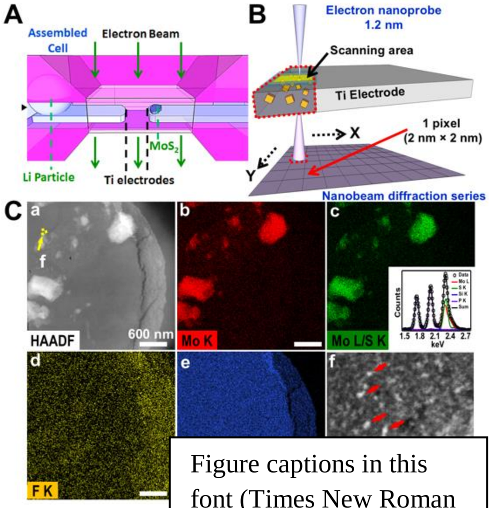

Figure captions in this font (Times New Roman 10 Pt).

**Figure 1.** *In* induced structu electrochemical liquid cell (E-LC)[1]. A. A home-made E-LC. B. 4D STEM was used. C. Ti electrode with $MoS_2$ after the discharge process. (b-e) EDS maps showing elemental distribution. Inset in (c) shows quantitative analysis of elements after deconvolution. (f) 4D STEM demonstrates that $MoS_2$ broke into small nanoparticles during fast discharge process.

## Future Plans

Liquid cell TEM has been a powerful approach for the exploration of new frontiers of materials synthesis, electrochemistry, catalysis, fluid physics, biological materials in aqueous environments and many other areas of research[6]. In situ liquid cell TEM imaging is a fast-growing and fascinating area of research, which has great potential to bring broad impact ranging from materials science to chemistry and biology[6-9]. Recently, in addition to advances in aberration-corrected electron microscopy, there have been revolutionary developments in electron beam detection and imaging, improved technology for liquid cell fabrication, which provides an unprecedented opportunity for the development and applications of the next generation liquid cell TEM with high spatial and temporal resolution for basic energy research. In the future, I plan to advance atomic resolution liquid cell TEM for a significant leap in the study of materials dynamic processes in situ. Especially nucleation and early stages of growth, which are mostly unreachable so far, will become available. The development of liquid cell TEM with high spatial and temporal resolution may also bring breakthroughs in other many areas of research that involves imaging through liquids.

## References

1. Zeng, Z.Y., et al., *In Situ Study of Lithiation and Delithiation of MoS2 Nanosheets Using Electrochemical Liquid Cell Transmission Electron Microscopy.* Nano Letters, 2015. 15(8): p. 5214-5220.
2. Liang, W.I., et al., *In Situ Study of Spinel Ferrite Nanocrystal Growth Using Liquid Cell Transmission Electron Microscopy.* Chemistry of Materials, 2015. 27(23): p. 8146-8152.
3. Liang, W.I., et al., *In Situ Study of Fe3Pt-Fe2O3 Core-Shell Nanoparticle Formation.* Journal of the American Chemical Society, 2015. 137(47): p. 14850-14853.
4. Zeng, Z.Y., et al., *In situ TEM study of the Li-Au reaction in an electrochemical liquid cell.* Faraday Discussions, 2014. 176: p. 95-107.
5. Zeng, Z.Y., et al., *Visualization of Electrode-Electrolyte Interfaces in LiPF6/EC/DEC Electrolyte for Lithium Ion Batteries via in Situ TEM.* Nano Letters, 2014. 14(4): p. 1745-1750.
6. Ross, F.M., *Opportunities and challenges in liquid cell electron microscopy.* Science (New York, N.Y.), 2015. 350(6267): p. aaa9886-aaa9886.
7. Zheng, H.M., Y.S. Meng, and Y.M. Zhu, *Frontiers of in situ electron microscopy.* Mrs Bulletin, 2015. 40(1): p. 12-18.
8. Liao, H.G. and H.M. Zheng, *Liquid Cell Transmission Electron Microscopy.* Annual Review of Physical Chemistry, 2016. 66.
9. de Jonge, N., M. Pfaff, and D.B. Peckys, *Practical Aspects of Transmission Electron Microscopy in Liquid*, in *Advances in Imaging and Electron Physics, Vol 186*, P.W. Hawkes, Editor. 2014, Elsevier Academic Press Inc: San Diego. p. 1-37.

## Publications

1. A. S. Powers, H. G. Liao, S. N. Raja, N. D. Bronstein, A. P. Alivisatos, H. Zheng*, “Tracking nanoparticle siffusion and interaction during self-assembly in a liquid cell” ***Nano Letters*** in review (2016).
2. K. Niu, F.Liang, R. Ye, F. Lin, D. Nordlund, M. M. Doeff, G. A. Somorjai, H. Zheng*, “Tailoring transition metal (hydr-)oxides by photon induced reactions” ***Angewandte Chemie International Ed.*** accepted (2016).
3. T. Zhou, Y. Du, S. Yin, X. Tian, H. Yang, X. Wang, B. Liu, H. Zheng, S. Qiao, R. Xu, “Nitrogen-doped cobalt phosphate@nanocarbon hybrids for efficient electrocatalytic oxygen reduction” ***Energy & Environmental Science*** DOI: 10.1039/C6EE01297C (2016).
4. K. Niu, M. Liu, K. A. Persson, Y. Han, H. Zheng* “Strain-mediated interfacial dynamics during Au–PbS core–shell nanostructure formation” ***ACS Nano*** 10, 6235 (2016).
5. C. Tan, W. Zhao, A. Chaturvedi, Z. Fei, Z. Zheng, J. Chen, Y. Huang, P. Ecius, Z. Luo, X. Qi, B. Chen, Z. Lai, B. Li, Z. Zhang, J. Yang, Y. Zong, C. Jin, H. Zheng, C. Kloc, H.

Zhang “Preparation of single-layer $MoS_{2x}Se_{2(1-x)}$ and $Mo_xW_{1-x}S_2$ nanosheets with high-concentration metallic 1T phase.” ***Small,*** 12, 1866 (2016).

6. H.G. Liao, H. Zheng*, “Liquid cell transmission electron microscopy.” ***Annu. Rev. Phys. Chem.*** 67, 719 (2016).
7. W. Liang, X. Zhang, Y. Zan, M. Pan, C. Czarnik, K. Bustillo, J. Xu, Y. Chu, H. Zheng*, “In situ study of $Fe_3Pt$-$Fe_2O_3$ core-shell nanoparticle formation.” ***J. Am. Chem. Soc.*** *137*, 14850 (2015).
8. W. Liang, X. Zhang, K. Bustillo, C. Chiu, W. Wu, J. Xu, Y. Chu, H. Zheng* “In situ study of spinel ferrite nanocrystal growth using liquid cell TEM.” ***Chemistry of Materials*** *27*, 8146 (2015).
9. K. Y. Niu, T. Frolov, H. L. Xin, J. Wang, M. Asta, H. Zheng*, “Bubble nucleation and migration in a lead-iron hydroxide core-shell nanoparticle.” ***PANS*** 112, 12928 (2015).
10. A Robertson, G. Lee, K. He, Y. Fan, C. Allen, S. Lee, H. Kim, E. Yoon, H. Zheng, A. Kirkland, J. Warner, “Partial Dislocations in Graphene and their Atomic Level Migration Dynamics" ***Nano Lett.*** 15, 5950 (2015).
11. K. Liu, C. Hsin, D. Fu, J. Suh, S. Tongay, M. Chen, Y. Sun, A. Yan, J. Park, K. M. Yu, W. Guo, A. Zettl, H. Zheng, D. C. Chrzan, J. Wu "Self-passivation of defects: effects of high-energy particle irradiation on elastic modulus of multilayer graphene" ***Advanced Materials*** 27, 6841 (2015).
12. Z. Zeng, X. Zhang, K. Bustillo, K. Niu, C. Gammer, J. Xu, H. Zheng* “In situ study of lithiation and delithiation of MoS2 nanosheets using electrochemical liquid cell TEM.” ***Nano Lett.*** 15, 5214 (2015).
13. K. Niu, S. Jung, F. Lin, F. Liang, D. Nordlund, C. C. L. McCrory, T. Weng, P. Ercius, M. Doeff, H. Zheng*, “A laser-chemical route for accessing complex hydroxides as efficient electrocatalysts for water oxidation.” ***Nano Lett.*** 15, 2498 (2015).
14. Q. Lu, G. S. Hutchings, W. Yu, Y. Zhou, R. V. Forest, R. Tao, J. Rosen, B. T. Yonemoto, Z. Cao, H. Zheng, J. Q. Xiao, F. Jiao, J. G. Chen, “Highly porous non-precious bimetallic electrocatalyst for efficient hydrogen evolution.” ***Nature Communications*** 6, 6567 (2015).
15. K. Niu, F. Lin, F. Liang, D. Nordlund, R. Tao, T. Weng, M. Doeff, H. Zheng*, “Structural and chemical evolution of amorphous nickel iron complex hydroxide upon lithiation/delithiation.” ***Chemistry of Materials*** 27, 1583 (2015).
16. H. Zheng*, S. Meng, Y. Zhu, “Frontiers of in situ Electron Microscopy” ***MRS Bulletin*** 40, 12 (2015).

## Dynamics of Topological Ferroelectric and Ferromagnetic Nanostructures

Myung-Geun Han, Javier F. Pulecio, Joe Garlow, and Yimei Zhu
Department of Condensed Matter Physics and Materials Science
Brookhaven National Laboratory, Upton, NY 11973

### Research Scope

The focus of this research task under the FWP Number MA-015-MACA is to study ferroelectric and ferromagnetic dynamics at relevant time and length scales in advanced materials and devices under external stimuli to unveil the underpinning physical principles that control emergent macroscopic functionalities. The research areas include (i) intriguing electronic or magnetic phenomena of nanostructure and at domain interfaces, and (ii) understanding topological dynamics and switching of ferroelectric and ferromagnetic texture. We take a correlative approach combining *in situ* electron microscopy with property measurements in order to establish direct structure-property relationships. We particularly emphasize elucidating nanostructure-induced emergent behaviors of exciting functional materials.

### Recent Progress

*Coupling between bias-induced defects and charged domain walls in ferroelectric films*

Ferroelectric domain walls often exhibit novel properties due to local broken symmetry to accommodate changes in polarization direction and charge compensation for bound charges due to polarization discontinuity[1]. Understanding necessary charge compensation phenomena at charged domain walls (CDWs) may lead to new avenues for nanoelectronic applications. Noticeably, charged defects associated with nonstoichiometry, such as oxygen vacancies, are believed to play an important role in providing compensation charges for polar interfaces[2]. One example is our recent work of CDWs in ferroelectric $PbZr_{0.2}Ti_{0.8}O_3$ (PZT) epitaxial thin films induced by *in situ* TEM biasing, showing strongly coupled to {*h0l*} polar interfaces by formation of ½<101>{*h0l*} type crystallographic shear planes (CSPs)[1] (Fig.1). By atomic imaging and spectroscopy we illustrate that CSPs consist of both conservative and nonconservative segments when coupled to CDWs. The CDW/CSP coupling yields an atomically narrow domain walls, consisting of a single layer of oxygen. Our results show that CDW/CSP coupling can be a fascinating venue to develop and control functional properties for nanoelectronic applications.

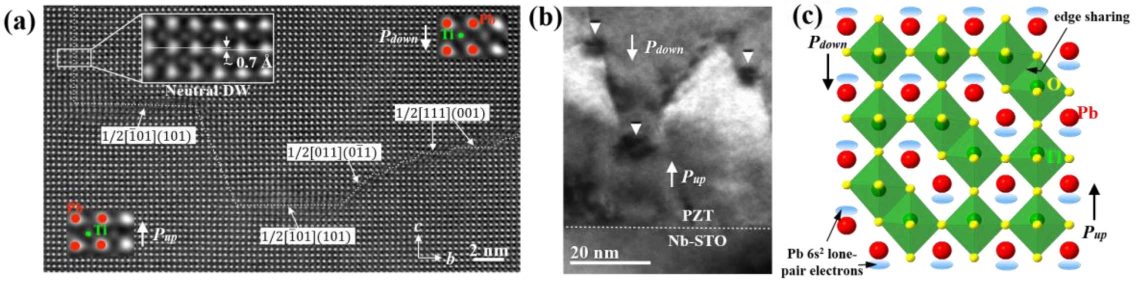

Fig. 1. STEM image (top) showing coupled CDW/CSPs in epitaxial $PbZr_{0.2}Ti_{0.8}O_3$ thin films grown on Nb-doped $SrTiO_3$ substrate. Dark-field TEM image (bottom left) shows coupled CDW/CSPs marked by arrow heads. Schematic of ½[101](101) CSP coupled to CDW (bottom right).

*Dynamics of topological ferromagnetic quasiparticles*

Dynamic control of topological magnetic quasiparticles, such as magnetic vortices and skyrmions, has received a great deal of attention due to their promising applications in spintronic applications[4,5]. A specific area of interest is the use of spin-transfer torque, the

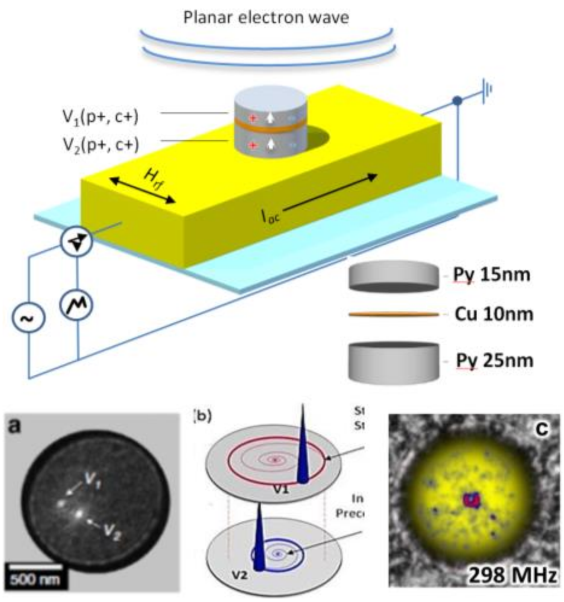

Fig. 2. A schematic of patterned heterostructure (top panel) containing two magnetic vortex cores on top of an Au waveguide and $Si_3Ni_4$ membrane. (a) Lorentz image of the two vortex cores (bottom left) labelled V1 and V2 corresponding to the top and bottom layers, respectively. (b) Dissimilar gyrotropic motion of the vortex cores at the respective eigenfrequencies (bottom center). (c) Lorentz image of singular orbit near resonance of the multilayer disc (bottom right) showing the spatial coherence of the two vortices gyrotropic motion under pulse frequency of 298MHz.

process by which an imbalance in spin populations of conduction electrons leads to a polarization of an electric current. To study this effect, as well as other high frequency spin procession, we have developed a unique capability on high frequency (MHz-GHz) electronic excitations in TEM allowing magnetic nanostructure be tuned to the resonance or off-resonance frequency for the in-plane gyrotropic mode of magnetic vortices[6,7]. These measurements enable us to direct observe models for vortex core motion and processing orbits. To further understand the dynamics of magnetic vortices, we coupled a vortex pair in a trilayer stack geometry via the RKKY interaction across the interface (Fig. 2). Resonant dynamics of these topological dipolar- or exchange-coupled vortices provide critical insights of the fundamental features of collective vortex-based microwave generators, such as their steady-state amplitudes, tunability and mode-coupled dynamic behavior.

## Future Plans

*Direct correlation between ferroelectric domain structures and dielectric modulation in multiferroic hexagonal manganites*

Electron microscopy has been indispensable in condensed matter research. However, great details of atomic structure obtained by electron microscopy may not be the property-dictating ones and thus often are insufficient to predict or understand emergent microscopic behaviors and properties. To directly probe the property-dictating structural motifs, we directly correlate electron microscopy data with local properties measured from TEM samples (Fig. 3) under external stimuli, such as electric/magnetic fields, photo excitation, temperature, mechanical

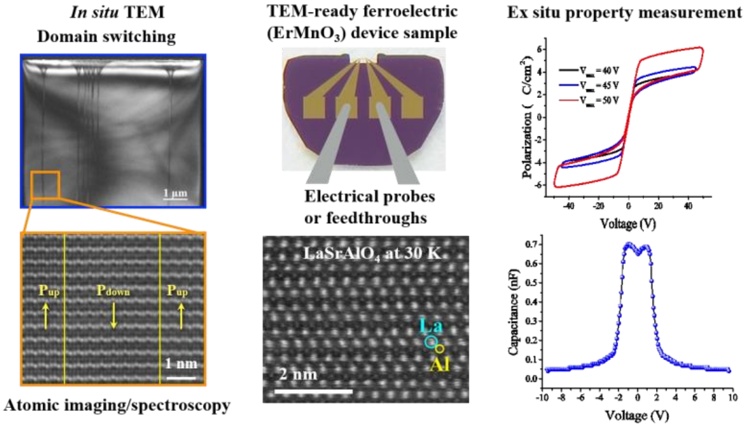

Fig. 3. TEM-ready ferroelectric device sample (upper center panel). Left panel shows *in situ* dark-field TEM (top) and STEM image (bottom). Right panel shows P-V (top) and C-V (bottom) loops measured from the same TEM sample. Atomic resolution STEM image taken at 30 K (bottom center).

strain. Electrical measurements have been performed on the TEM samples using typical electrical probe systems. For an example, we have studied stripe-domain hexagonal manganites (Fig. 3, top left) and atomic displacements (Fig. 3, bottom left) were correlated with polarization-voltage (P-V, top right) and capacitance-voltage (C-V, bottom right) loops measured *ex situ*. Surprisingly, both TEM domain switching experiment and electrical measurements show low-field (20 kV/cm) switching and strong back switching behaviors near the *ab* surface of hexagonal manganites, revealing capacitance modulation by 50 times in magnitude by external electric fields[8]. We have expanded this capability to low temperature regimes to study more complex correlated electron behavior including superconductivity, CDWs, and colossal magnetoresistance across phase transitions upon cooling and electrical biasing. We have demonstrated, for the first time, atomic resolution imaging in STEM mode using a biasing liquid helium stage (not by averaging noisy images), as shown in Fig. 3 (bottom center).

### Manipulation of multiferroic topological defects

We will continue to investigate roles played by defects in multiferroic domain structures. Especially, we will investigate a rational way to control topological domain structures such as 6-fold vortex domains in hexagonal manganites by intertwining other types of topological defects. For example, Mn-trimer connectivity in $YMnO_3$ can be altered by conventional edge dislocations (EDs) and thus can be used to structurally transform conventional 6-fold vortex to crystallographically forbidden 2, 4, and 8-fold vortices (Fig. 4). We have classified these unconventional 2, 4, and 8-fold vortices using Homotopy group theory and their interwined relationship has been understood by Landau-based numerical simulation. New route to unlock topological protection in technologically important multiferroics may provide new insights into topological defects.

### Dynamics of topological spin textures

Skyrmions are topologically protected spin textures that can be stabilized in chiral magnetic systems by the Dzyaloshinskii-Moriya interaction[9] and display intriguing properties for emergent technologies. While skyrmions have attracted significant interest since the identification of skyrmion lattices in non-centrosymmetric crystals such as $Fe_{0.5}Co_{0.5}Si$[10], understanding their full character requires direct observations from the controlled formation of skyrmions under applied stimulus. Lorentz phase microscopy[11] provides a unique role in skyrmion structural characterization by allowing the manipulation of applied electric and magnetic fields while monitoring local spin structure response and reorganization[12]. We seek to unveil the dynamic behavior of skymrions in confined geometries and patterned wires at multiple length scales relevant to applications in tuning skyrmion properties. The planned experiments entail the patterning of perpendicular magnetic anisotropy thin films into patterned shapes to pinpoint how physical constraints vary the energy landscape of skyrmion nucleation through magnetic reversal. Subsequent experiments will characterize the dynamic behavior of skyrmion motion induced by the application of *in-situ* current pulses. Understanding the dynamic behavior of skyrmion motion and nucleation will provide key insights into topological magnetism. Preliminary results from Co/Pd thin

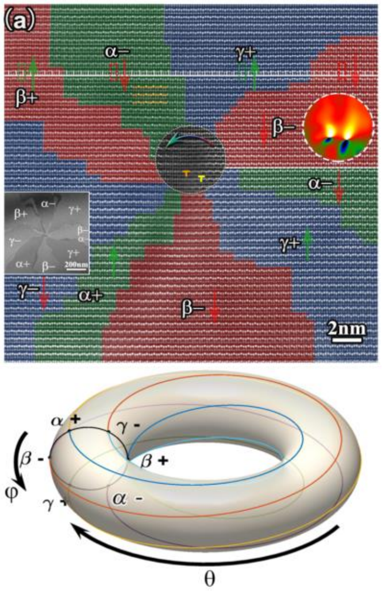

Fig. 4. An 8-fold vortex in hexagonal $YMnO_3$ observed by atomic resolution dipole mapping (top) and its torus-like order-parameter space (bottom) revealed by Landau-based numerical calculation.Insets show dark-field TEM image and strain map around dislocation and vortex core.

films have revealed the tilt-dependent phase contrast generated by Neel skyrmions through complimentary micromagnetics simulations.

## References

[1] Catalan, G., Seidel, J., Ramesh, R., and Scott, J. F., Rev. Modern Phys. 84, 119-156 (2012).
[2] Yu, L. and Zunger, A., 5, 5118 Nat. Commun. (2014).
[3] Han, M.-G., et al., Phys. Rev. B in press (2016).
[4] Jung, H. et al.m ACS nano 6, 3712–7 (2012).
[5] Parkin, S. S. P., Hayashi, M. and Thomas, L., Science, 320, 190–194 (2008).
[6] Pollard, S. D., Huang, L., Buchanan, K. S., Arena, D. A. & Zhu, Y., Nat. Commun. 3, 1028 (2012).
[7] Pulecio, J. F., Warnicke, P., Pollard, S. D., Arena, D. A. & Zhu, Y., Nat. Commun. 5, 3760 (2014).
[8] Han, M.-G., et al., in preparation.
[9] Nagaosa, N. and Tokura, Y., *Nature nanotechnology*, *8* 899 (2013).
[10] Yu, X.Z. et al. *Nature materials*, *10*(2), pp.106-109 (2013).
[11] Beleggia, M., Schofield, M.A., Volkov, V.V. and Zhu, Y., *Ultramicroscopy*, *102*37-49 (2004).
[12] Yu, X.Z., et al. *Nature*, *465* 901 (2010).

## Publications

1. Garlow, J.A., Barrett L.K., Wu. L., Kisslinger, K., Zhu, Y., Pulecio, J.F., “Large-Area Growth of Turbostratic Graphene on Ni(111) via Physical Vapor Deposition”, Scientific Reports, 6, 19804 (2016).
2. Brahlek, M.J., Koirala, N., Liu, J., Yusufaly, T.I., Salehi, M., Han, M.-G., Zhu, Y., Vanderbilt, D., and Oh, S., “Tunable inverse topological heterostructure utilizing $(Bi1\text{-}xInx)_2Se_3$ and multichannel weak-antilocalization effect”, Phys. Rev. B 93, 125416 (2016).
3. Koirala, N., Brahlek, M., Salehi, M., Wu, L., Dai, J., Waugh, J., Nummy, T., Han, M.-G., Moon, J., Zhu, Y., Dessau, D., Wu, W., Armitage, N.P., and Oh, S., “Record Surface State Mobility and Quantum Hall Effect in Topological Insulator Thin Films via Interface Engineering”, Nano Letters, 15, 8245-8249 (2015).
4. Zhang, B., Sun, C.-J., Lu, W., Venkatesan, T., Han, M.-G., Zhu, Y., Chen, J., and Chow, G. M., “Electric-field-induced strain effects on the magnetization of a $Pr_{0.6}Sr_{0.33}MnO_3$ film”, Phys. Rev. B 91, 174431 (2015).
5. Meng, Q., Han, M.-G., Tao, J., Xu, G., Welch, D.O., and Zhu, Y., “The velocity of domain-wall motion during polarization reversal in ferroelectric thin-films: Beyond Merz’s law”, Phys. Rev. B, 91, 054104 (2015).
6. Marshall, M.S.J., Malashevich, A., Disa, A.S., Han, M.-G., Chen, H., Zhu, Y., Ismail-Beigi, S., Walker, F.J., and Ahn, C.H., “Conduction at a ferroelectric interface”, Phys. Rev. Appl., 2, 061001 (2014).
7. Patete, J.M., Han, J., Tiano, A.L., Liu, H., Han, M.-G., Simonson, J.W., Li, Y., Santulli, A.C., Aronson, M.C., Frenkel, A.I., Zhu, Y., and Wong, S.S., “Observation of ferroelectricity and structure-dependent magnetic behavior in novel one-dimensional motifs of pure, crystalline yttrium manganese oxides”, J. of Phys. Chem. C, 118, 21695-21705 (2014).
8. Liu, S., Akbashev, A., Yang, X., Liu, X., Li, W., Zhao, L., Li, X., Couzis, A., Han, M.-G., Zhu, Y., Krusin-Elbaum, L., Li, J., Huang, L., Billinge, S., Spanier, J., and O’Brien, S., “Hollandites as a new class of multiferroics”, Scientific Reports, 4, 6203 (2014).
9. Han, M.-G., Marshall, M.S.J., Wu, L., Schofield, M.A., Aoki, T., Twesten, R., Hoffman, J., Walker, F.J., Ahn, C.H., and Zhu, Y., “Interface-induced nonswitchable domains in ferroelectric thin films”, Nat. Commun., 5:4693 (2014).
10. Pulecio, J.F., Pollard, S.D., Warnicke, P., Arena, D.A., and Zhu, Y., “Symmetry breaking of magnetic vortices before annihilation,” Appl. Phys. Lett. 105, 132403 (2014).
11. Pulecio, J.F., Warnicke, P., Pollard, S.D., Arena, D.A., and Zhu, Y., “Coherence and modality of driven interlayer-coupled magnetic vortices,” Nat. Comm., 5, 3760 (2014)
12. Wang, X., Mostovoy, M., Han, M.-G., Horibe, Y., Aoki, T., Zhu, Y., and Cheong, S.-W., “Unfolding of vortices into topological stripes in a multiferroic material”, Phys. Rev. Lett., 112, 247601 (2014).
13. Bansal, N., Koirala, N., Brahlek, M., Han, M.-G., Zhu, Y., Cao, Y., Waugh, J., Dessau, D.S., and Oh, S., “Robust topological surface states of $Bi_2Se_3$ thin films on amorphous $SiO_2$/Si Substrate and a large ambipolar gating effect”, Appl. Phys. Lett., 104, 241606 (2014).

# Electron-spin-lattice Interplay and Charge Transfer in Quantum and Energy Materials

Lijun Wu, Jing Tao and Yimei Zhu
Department of Condensed Matter Physics and Materials Science
Brookhaven National Laboratory, Upton, NY 11973

## Research Scope

The current focus of this research task under the FWP Number MA-015-MACA is to investigate electron, spin and lattice correction and their roles at surfaces, interfaces and defects that control the utility of functional materials. It covers a wide range of compounds, ranging from single crystal and thin films to nanostructured materials with low dimensionalities. Particular interests are the doping effect, topological proximity effect, and surface and interfacial phenomena that lead to emergent physical properties in oxides and quantum materials, and ionic transfer on electrochemical performance in energy storage materials. Various quantitative electron microscopy techniques are carried out to understand structure and property relationship. Theoretical calculations based on complex home-made computer codes are used to verify experimental observations.

## Recent Progress

*Van Vleck ferromagnetism in topological insulator* Topological insulator (TI) is a unique material with insulating bulk but exotic surface electrons. The breaking of time-reversal symmetry and the opening of a surface band gap of a TI is an essential step towards observing other quantum states. When the TI's chiral Dirac surface state is gapped, a number of promising novel phenomena could be realized, including the quantum anomalous Hall effect, which can potentially lead to low-power electrically controlled spintronic devices. Doping transition metal (TM, i.e. V, Cr, Mn) into TI can induce a perpendicular ferromagnetic anisotropy, providing a straightforward method to open up the band gap of the TI's chiral surface state and tune the corresponding transport properties. The first-principles calculations predicted that the insulating magnetic ground state can be obtained by a proper choice of TM dopants through van Vleck-type ferromagnetism (Fig. 1) in the absence of itinerant carriers. Using low-temperature electron energy loss spectroscopy (EELS, Fig. 1c), we observe, for the first time, the magnetization of partially filled vanadium (V) $2p_{3/2}$ and $2p_{1/2}$ ($L_3$ and $L_2$) core states of the V-doped $Sb_2Te_3$ film (Fig. 1a). Analysis of the fine structure of the EELS spectra reveals crucial information on the unoccupied local density of states, the angular momentum, spin, and chemical nature of the dopant. We find by comparing with the room temperature EELS, the Te $M_{54}$ edge at T = 10 K shows no chemical shift, while the V $L_3$ and $L_2$ peaks exhibits a redshift as large as 0.6 eV. In addition, there is a clear drop of the $L_3/L_2$ peak intensity ratio.

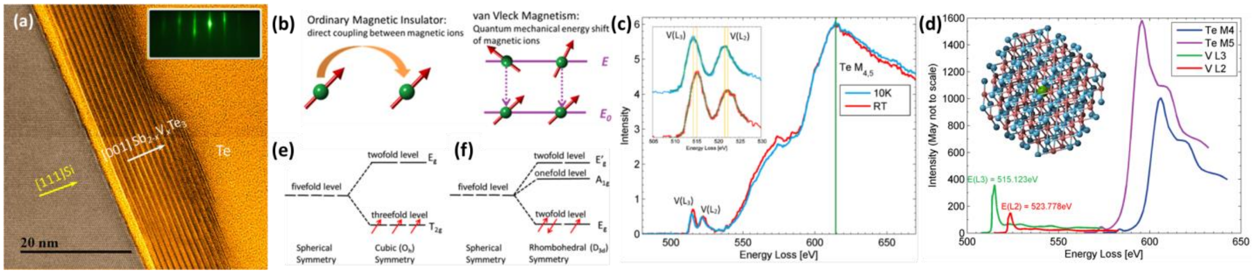

Fig. 1. (a) HRTEM image of the V-doped $Sb_2Te_3$. (b) Schematics of ordinary magnetic insulator and van Vleck magnetism. (c) EELS spectra of V $L_{32}$ and Te $M_{54}$ edges at RT and 10 K. The energy position of Te $M_{54}$ edge is invariant of temperature, while there is a clear redshift of V $L_3$ and $L_2$ positions and a drop of $L_3/L_2$ ratio. (d) EELS simulation based on FEFF codes of V-doped $Sb_2Te_3$, using a nanosphere (inset) with a scattering center in the middle. (e,f) Crystal field splitting in the cubic (e) and rhombohedral crystal field (f).

EELS simulations (Fig. 1d) suggest that such shift is a signature of onset of ferromagnetic order, which is further verified through magneto-transport measurements and crystal field theory (Fig. 1e and 1f). We therefore experimentally proven the long-sought new-type Ferromagnetism of the van Vleck nature in the V-doped three-dimensional topological insulator, paves the way to bring TI for low-dissipation spintronic and quantum computation applications [1].

*Ionic transport and the roles of defects in battery electrodes* Surface defects and oxygen vacancies are crucial for lithium-ion battery performance. For instance, we have found the excess amounts of oxygen vacancies and surface defects in low Ag-doped hollandite one-dimensional nanorods ($Li/Ag_xMn_8O_{16}$) which have a tunnel structure that is ideal for studying ionic transport during the lithiation and delithiation process. Combining local probes (atomic imaging, diffraction, spectroscopy and in-situ electric biasing) with bulk measurements (synchrotron x-ray diffraction and thermogravimetric and electrochemical analysis), we discover the origin of the seven-fold increase in delivered capacity for different Ag contents [2]. In Li-rich layered oxides, $Li[Li_{0.144}Ni_xCo_xMn_{4x}]O_2$ (x=0.136), our theoretical calculations and experimental characterizations demonstrate that oxygen vacancies in the surface regions facilitate Li diffusion by activating the Li ions occupying in the tetrahedral sites and suppress the release of gas from the surface. This subsequently leads to higher discharge capacity and a much improved rate capability of the battery electrodes [3].

*Smectic-nematic transition in correlated materials* We reveal microscopic characteristics of electronic-liquid-crystal (ELC) phase transitions in a doped manganite, $La_{1/3}Ca_{2/3}MnO_3$, by in situ TEM studies. For the first time, our observations experimentally confirm the role of electronic defects in the ELC phase transition, which was proposed in theory about two decades ago. We are able to distinguish anisotropy from electronic-nematicity, the two concepts often mixed in previous ELC research. A new model was proposed for the incommensurate orbital ordering that the combination of $d_{3z^2-r^2}$ and $d_{x^2-y^2}$ orbitals has the orbital mixing angle θ which changes continuously in real-space as a result of electron-electron coupling. Such a new model together with the observed electronic phase separation scenario resolved a long-standing controversy over the origin of the incommensurate superstructure in manganites.

## Future Plans

*Interfacial coupling-induced emergent state in manganite film* In manganites, the ferromagnetic insulator (FI) phase was observed in bulk for $La_{0.88}Sr_{0.12}MnO_3$. Theoretical work on bulk manganite at x~0.3 predicts a metal-polaronic insulator phase transition controlled by the strength of electron-phonon interaction (λ) and/or quenched disorder (Δ). The interfacial structural asymmetry in films significantly affects the local unit-cell dimension and the $MnO_6$ octahedral rotation/distortion, resulting in significant deviation of the bond length and angle, and magnetic ordering temperature from its bulk counterpart. For instance, the phase diagram of the 12 nm thick $Pr_{0.67}Sr_{0.33}MnO_3$ (PSMO) film on $SrTiO_3$ (STO) substrate remarkably differs from the 30nm film, with an unexpected interface-induced novel FI' phase (Fig. 2a).

To understand the origin of the FI' phase, atomically resolved STEM high-angle annular-dark-field (HAADF) and annular-bright-field (ABF) images are acquired to quantitatively measure depth-profiles of lattice and $MnO_6$ octahedral tilt. The oxygen-sensitive ABF images (Fig. 2b and 2c) suggest that the $MnO_6$ octahedra are distorted and their rotation is asymmetric. We further refine oxygen-atom positions with a Gaussian function (red line in the inset III of Fig.2g) and the depth-profiles are then calculated from the measurements. With the accurately measured depth-profiles of the $MnO_6$ octahedral tilt, we reveal a thickness dependent nonuniform interfacial environment that might enhance the site disorder strength (Δ) with contribution from random local $TiO_6$ rotation near the STO interface at the onset of STO phase transition. Increasing softening of the $\Gamma_{25}$ phonon mode with decreasing temperature may strengthen electron-phonon interaction (λ) of PSMO film through interfacial coupling by decreasing carrier relaxation time. Both enhanced λ and Δ could induce formation of theoretically predicted polaronic insulator FI' as shown in the 12 nm film [4].

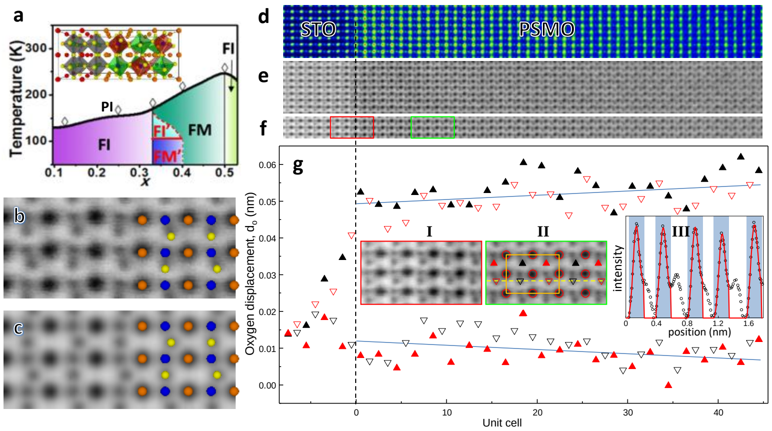

Fig. 2. (a) Phase diagram of the 12 nm thick PSMO film on STO substrate. (b,c) STEM-ABF image of the film (b) and simulation (c) based on asymmetric $MnO_6$ octahedral rotation. The atomic model is embedded in the image with Pr/Sr, Mn and O represented by orange, blue and yellow dots, respectively. (d-f) Simultaneously acquired (d) HAADF and (e) ABF images of the PSMO/STO film. (f) ABF image after averaging the ABF image vertically in (e) for accurate displacement measurement. (g) Displacement of oxygen ($d_O$). There are four sets of data for $d_O$, as indicated by the four kinds of triangles in the inset II. The inset III shows the intensity profile (open circles) from the horizontal scan line (yellow dash line in inset II). The red line is the fitting curve by fitting the individual O-peak with a Gaussian function within the shadow region.

*Magnetic-field effect on short-range electronic structures* Given the "electronically soft" behavior, correlated materials often exhibit gigantic secondary effects such as magnetoresistance, multiferroics and magnetocaloric effects, offering great opportunities as a testbed for manipulating materials' properties. Comparing to long-range phases, short-range electronic structures are more sensitive to electron-electron coupling and thus can be "electronically softer". Using Lorentz microscopy and phase imaging methods, we have observed a surprisingly pronounced difference in structural characteristics of SR orbital-ordering with and without applied magnetic field. Such a phenomenon can be correlated with the doping level and the change of spin structure. We will continue studying the magnetic-field effect in manganites to understand the interplay among spin, charge and orbital by tuning the valence and spin states of Mn ions.

Other future work includes, but is not limited to: 1) tunable magnetic anisotropy in superlattice films, e.g. $(La_{1-x}Sr_xMnO_3)_n/(SrTiO_3)n]$; 2) interface manipulation and control with incompatible in-plane symmetry between the film and substrate, e.g. hexagonal ZnO on cubic MgO substrate; and 3) in-situ and ex-situ measurement of Li-ion diffusion rate at different charged and discharged states in one-dimensional Ag-hollandite nanorods of battery electrodes.

## References

1. Li, M. et al., "Proximity-driven enhanced magnetic order at ferromagnetic-insulator-magnetic-topological-insulator interface", *Phys. Rev. Lett.* **114**, 146802 (2015).
2. Wu, L. et al., "Structural Defects of Silver Hollandite, AgxMn8Oy, Nanorods", *ACS Nano* **9**, 8430-8439 ( 2015).
3. Qiu, B.; Zhang, M.; Wu, L.et al., "Gas–solid interfacial modification of oxygen activity in layered oxide cathodes for lithium-ion batteries", *Nature Communications*, 7 12108 (2016).
4. Zhang, B. et al., "Interfacial coupling-induced ferromagnetic insulator phase in manganite film", *Nano Lett.* **16**, 4174 (2016).

## Publications

1. Das P. K. et al., "Layer-dependent quantum cooperation of electron and hole states in the anomalous semimetal $WTe_2$", *Nature Comms.* **7**, 10847, (2016), DOI: 10.1038/ncomms10847
2. Garlow, J. A. et al., "Large-Area Growth of Turbostratic Graphene on Ni(111) via Physical Vapor Deposition", *Scientific Report* **6**, 19804, DOI: 10.1038/srep19804 (2016).
3. Hu, J.; Wu, L. et al., "Increasing Stability and Activity of Core-shell Catalysts by Preferential Segregation of Oxide on Edges and Vertexes: Oxygen Reduction on Ti-Au@Pt/C", *J. Am. Chem. Soc.* 138 (29), pp 9294–9300 (2016).
4. Luo, H. X. et al., "Differences in Chemical Doping Matter: Superconductivity in $Ti_{1-x}Ta_xSe_2$ but Not in $Ti_{1-x}Nb_xSe_2$," *Chemistry of Materials* **28**, 1927, (2016)

5. Ling, X. et al., “Parallel Stitching of 2D Materials”, *Adv. Mater.* **28**, 2322–2329 (2016).
6. Liu, J.; Yin, L.; Wu, L. et al., "Quantification of honeycomb number-type stacking faults: application to $Na_3Ni_2BiO_6$ cathodes for Na-ion batteries", *Inorganic Chemistry*, (accept, 2016).
7. Ozaki, T.; Wu, L.; Zhang, C.; Jaroszynski, J.; Si, W.; Zhou, J.; zhu, Y.; Li, Q. "A route for a strong increase of critical current in nano strained iron-based superconductors", *Nature communications* (accepted, 2016).
8. Poyraz, A. et al. “Effective Recycling of Manganese Oxide Cathodes for Lithium Based Batteries”, *Green Chem.* **18**, 3414 (2016).
9. Qiu, B.; Zhang, M.; Wu, L. et al., “Gas–solid interfacial modification of oxygen activity in layered oxide cathodes for lithium-ion batteries”, *Nature Communications*, 7:12108, DOI: 10.1038/ncomms12108 (2016).
10. Tao, J. et al., “Direct observation of electronic-liquid-crystal phase transitions and their microscopic origin in $La_{1/3}Ca_{2/3}MnO_3$”, *Scientific Reports* (2016) in press
11. Xu, F. et al., “Scalable shear-exfoliation of high-quality phosphorene nanoflakes with reliable electrochemical cycleability in nano batteries”, *2D Mater.* **3**, 025005 (2016).
12. Zhang, B.; Wu, L. et al., “Interfacial Coupling-Induced Ferromagnetic Insulator Phase in Manganite Film”, *Nano Lett.* **16**, 4174 (2016).
13. Zhang, W. et al., “Two-Dimensional Layered Oxide Structures Tailored by Self-Assembled Layer Stacking via Interfacial Strain”, *ACS Appl. Mater. Interfaces* **8**, 16845-16851 (2016).
14. Zhang, W. et al., “Insights into Ionic Transport and Structural Changes in Magnetite during Multiple-Electron Transfer Reactions”, Adv. Energy Mater. **6**, 1502471 (2016).
15. Abeykoon, A. M. M.; Hu, H.; Wu, L.; Zhu Y. et al., “Calibration and data collection protocols for reliable lattice parameter values in electron pair distribution function studies,” *Journal of Applied Crystallography* **48**, 244-251 (2015).
16. Li, M. et al., “Proximity-driven enhanced magnetic order at ferromagnetic-insulator--magnetic-topological-insulator interface”, *Phys. Rev. Lett.* **115**, 087201 (2015).
17. Li, M. et al., “Experimental Verification of the Van Vleck Nature of Long-Range Ferromagnetic Order in the Vanadium-Doped Three-Dimensional Topological Insulator $Sb_2Te_3$”, *Phys. Rev. Lett.* **114**, 146802 (2015).
18. Li, M.; Cui, W.; Wu, L. et al., “Topological effect of surface plasmon excitation in gapped isotropic topological insulator nanowires”, Can. J. Phys. **93**: 591–598 (2015).
19. Luo, H. X. et al., "Cr-Doped $TiSe_2$ - A Layered Dichalcogenide Spin Glass", *Chemistry of Materials* **27**, 6810, (2015)
20. Luo, H. X. et al., “Polytypism, polymorphism, and superconductivity in $TaSe_{2-x}Te_x$,” *PNAS* 112, E1174-1180, (2015)
21. Ma, J.; Bo, S.; Wu, L.; Zhu, Y. et al., “Ordered and Disordered Polymorphs of $Na(Ni_{2/3}Sb_{1/3})O_2$: Honeycomb-Ordered Cathodes for Na-Ion Batteries”, *Chem. Mater.* **27** (7), 2387–2399 (2015).
22. Meng, Q.; Wu, L.; Welch, D. O.; and Zhu, Y. “Lattice vibrations in the Frenkel-Kontorova model. I. Phonon dispersion, number density, and energy”, *Phys. Rev. B* **91**, 224305 (2015).
23. Meng, Q.; Wu, L.; Welch, D. O.; and Zhu, Y. “Lattice vibrations in the Frenkel-Kontorova Model. II. Thermal conductivity”, *Phys. Rev. B* **91**, 224306 (2015).
24. Shi, X.; Yang, J.; Wu, L.; Salvador, J. R.; Villaire, W. L.; Haddad, D.; Yang, J.; Zhu, Y.; and Li, Q., "Band Structure Engineering and Thermoelectric Properties of Charge-Compensated Filled Skutterudites", *Scientific Report*, **5**, 14641 (2015).
25. Si, W.; Zhang, C.; Wu, L. et al., “Superconducting thin films of (100) and (111) oriented indium doped topological crystalline insulator SnTe”, *Appl. Phys. Lett.* **107**, 092601, DOI: 10.1063/1.4929815 (2015).
26. Ugur, A.; Katmis, F.; Li, M.; Wu, L. et al., “Low-Dimensional Conduction Mechanisms in Highly Conductive and Transparent Conjugated Polymers”, *Adv. Mater.* 27, 4604 (2015).
27. Wu, D. et al., “Superior thermoelectric performance in PbTe–PbS pseudo-binary: extremely low thermal conductivity and modulated carrier concentration”, *Energy Environ. Sci.* **8**, 2056 (2015).
28. Wu, L. et al., “Structural Defects of Silver Hollandite, AgxMn8Oy, Nanorods: Dramatic Impact on Electrochemistry”, *ACS Nano* **9**, 8430-8439 (2015).
29. Bo, S.H. et al., “Structures of Delithiated and Degraded $LiFeBO_3$, and Their Distinct Changes upon Electrochemical Cycling”, Inorg. Chem. 53, 6585−6595 (2014).
30. Dai, Y.; Cai, S.; Wu, L.; Yang, W.; Xie, J.; Wen, W.; Zheng J.; and Zhu, Y. “Surface modified CFx cathode material for ultrafast discharge and high energy density”, *J. Mater. Chem. A*, **2**, 20896–2090 (2014).
31. Das, S., Rastogi, A.; Wu, L.; Zheng, J-C., Hossain, Z.; Zhu, Y.; and Budhani, R. C.; “Kondo scattering in δ-doped $LaTiO_3/SrTiO_3$ interfaces: Renormalization by spin-orbit interactions”, *Phys. Rev. B* **90**, 081107(R) (2014).
32. Kuttiyiel, K.A.; Sasaki1, K.; Su, D.; Wu, L.; Zhu, Y.; Adzic, R.R. “Au–Promoted Structurally Ordered Intermetallic PdCo Nanoparticles for the Oxygen Reduction Reaction”, *Nature Communications*, | 5:5185 | DOI: 10.1038/ncomms6185 | (2014).
33. Li, M. et al., “Tunable THz surface plasmon polariton based on a topological insulator/layered superconductor hybrid structure”, *Phys. Rev. B* 89, 235432 (2014).
34. Ma, C.; Wu, L., et al., “Strong Coupling of the Iron-Quadrupole and Anion-Dipole Polarizations in $Ba(Fe_{1-x}Co_x)_2As_2$”, *Phys. Rev. Lett.* **112**, 077001 (2014).
35. Smith et al., “Intrinsic nanostructure in $Zr_{2-x}Fe_4Si_{16-y}$ ($x = 0.81$, $y = 6.06$)”, *J. Phys.: Condens. Matter*. **26,** 376002 (2014).
36. Sokolov, D. A; Aronson, M. C.; Wu, L. et al., “Neutron, electron, and x-ray scattering investigation of $Cr_{1-x}V_x$ near quantum criticality”, *Phys. Rev. B* **90**, 035139 (2014).
37. Yin, Y-W. et al., “Octonary Resistance States in $La_{0.7}Sr_{0.3}MnO_3/BaTiO_3/La_{0.7}Sr_{0.3}MnO_3$ Multiferroic Tunnel Junctions”, *Adv. Electronic Mater.* Nov. 1 1500183 (2015).

## Probing Charge and Lattice Correlation Using Ultrafast Electron Pulses

Yimei Zhu, Junjie Li, Lijun Wu, Jing Tao and Tatiana Konstantinova
Department of Condensed Matter Physics and Materials Science,
Brookhaven National Laboratory, Upton, NY 11973

### Program Scope

Ultrafast electron diffraction, imaging, and spectroscopy are the frontier of modern electron microscopy. They represent grand challenges in electron scattering instrumentation, whilst offering unique opportunities for understanding structural dynamics and behavior of matter under conditions far away from equilibrium. The ultrafast pump-probe approach affords us a new means to discover “hidden states” and emergent properties of materials by tuning photon excitation energy in matter. The focus of this research task under the FWP Number MA-015-MACA is to explore structure dynamics and electron-lattice interplay in strongly correlated electron systems using ultrafast electron pulses. We utilize the 3MeV electron ultrafast diffraction instrument developed at BNL to understand the dynamics of charge density wave, charge and orbital ordering and their completing degrees of freedom, and electron-lattice interactions in functional materials. Instrumentation and method development on ultrafast electron scattering is an important ingredient of the research.

### Recent Progress

The physics of strongly correlated electron systems is often driven by a complex interplay and competing energetics of spin, charge, lattice and orbital. Unfortunately, this same interplay makes the physical picture very complex and inhibits our understanding of these materials [1-4]. In large part, this is because of the difficulty in separating out the relative roles of the different interactions in a given problem. A classic example of this is the existence of charge and orbital order in doped manganites which exhibit strong electron-electron interactions and electron-phonon coupling. Due to their difference in response time under photoexcitation, the pump-probe ultrafast approach enables us to gain insight into the exotic electron and phonon behavior.

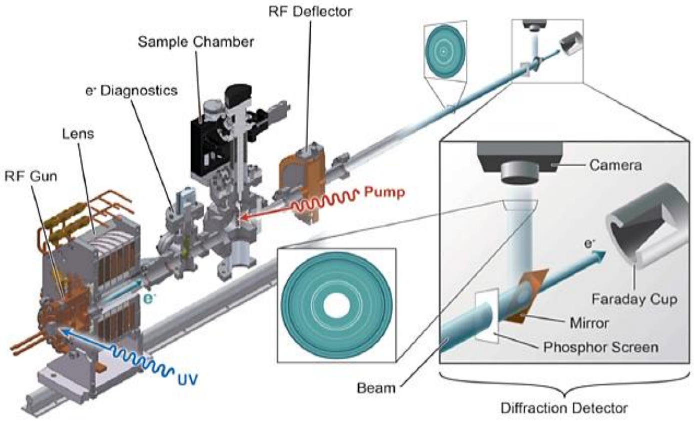

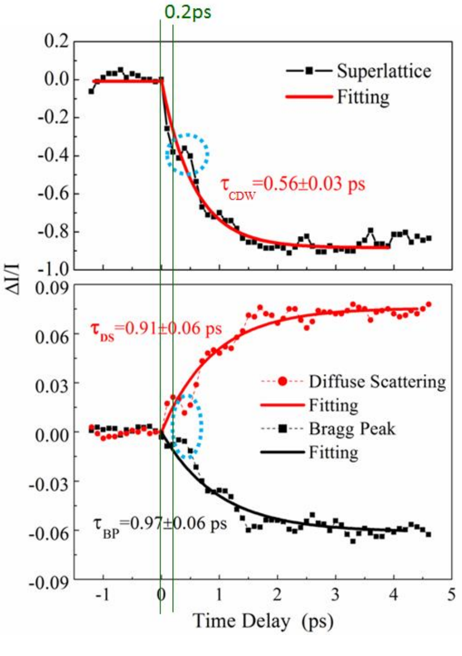

Fig. 1 (left) Schematic of the BNL MeV ultrafast electron diffraction apparatus. UV photons (blue) from a Ti-sapphire laser are used to generate electrons in the RF gun. Near-IR pulses (red) from the same laser are used to optically pump the sample [5]. (right) structure dynamics of $2H\text{-}TaSe_2$: temporal evolution of the CDW supplattice peaks (top) and Bragg peaks and diffuse scattering (bottom). For clarity, the change of diffuse scattering intensity is multiplied by 3 (795 nm optical pump at a fluence of 1.4 mJ/cm$^2$).

*Femtosecond time-resolved MeV electron diffraction instrument* With the initial laboratory directed R & D funding at BNL we have developed a ultrafast electron diffraction apparatus (MeV UED) [5] (Fig.1) that can achieve 5fC (~$3\times10^4$ electrons) per pulse with 130fs temporal resolution at 2.8MeV. The goal of this research is to exploit the exceptional opportunity of the ultrafast electron diffraction instrument to understand electron-lattice correlation and dynamics. The advantage of the electron probe in ultrafast experiments, comparing with its counterpart of x-ray photons, is its ~$10^5$ times larger scattering cross-section with matter. The challenge, however, due to the Coulomb repulsion between electrons, is the difficulty in confining a large number of electrons into a small volume. The transverse space charge effects scale as $1/\beta^2\gamma^3$ and longitudinal as $1/\beta^2\gamma^5$ where $\beta$ and $\gamma$ are the relativistic velocity and energy, respectively. Thus, the resolution power of an instrument, either for ultrafast diffraction or imaging, increases significantly by going to higher operation voltages, which was realized in our system by adopting the RF (radio frequency) gun originally developed for free-electron laser.

*Charge density wave & lattice dynamics in 2H-TaSe$_2$* The right panel of Fig.1 shows an example of our study on the charge-density wave (CDW) in 2H-TaSe$_2$. Our investigation has revealed a two-step photoexcitation process in the system. Upon impulsive optical pumping the CDW state is first suppressed promptly (~120fs) by the electronic excitation and scattering, and then subsequently by lattice thermalization through electron-phonon interaction on a much longer time scale (~2ps). The latter leads to the final, full melting of the CDW and thermal equilibrium between the electron subsystem and the lattice.

*Role of various phonon modes in charge and orbital ordered LaSr$_2$Mn$_2$O$_7$* Another example is our study on polaron transport, in which electron motion is strongly coupled to the underlying lattice deformation or phonons. This is crucial to the understanding of electrical and optical conductivities in many solids, nevertheless, currently little is known experimentally about the dynamics of individual phonon modes during polaron motion. Using MeV UED we quantify the dynamics of both electronic and atomic motion in the correlated LaSr$_2$Mn$_2$O$_7$. Using photoexcition to set the electronic system in motion, we find that Jahn-Teller-like O, La/Sr, and Mn$^{4+}$ displacements dominate the lattice response and exhibit a dichotomy in behavior - overshoot-and-recovery for one sublattice versus normal behavior for the other. This dichotomy, attributed to slow electronic relaxation, proves that polaron transport is a key process in doped manganites.

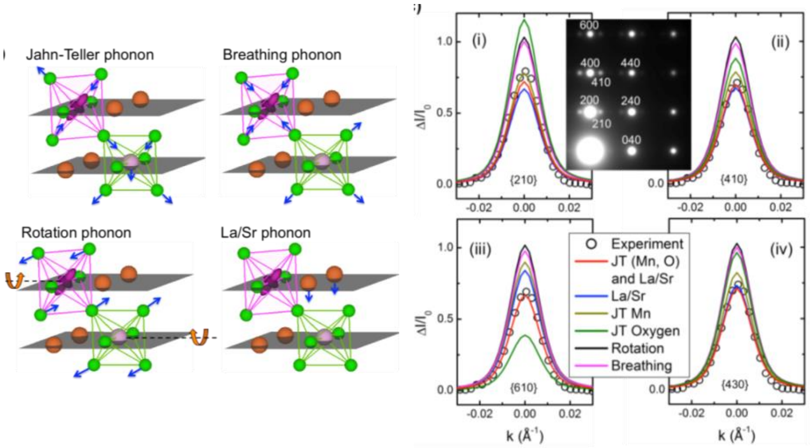

Fig. 2 (far left) Four typical phonon modes LaSr$_2$Mn$_2$O$_7$. (left) Separating the roles of various phonon modes by quantitative analysis of the intensity reduction of orbital order superlattice peaks (inset) (i) {210}, (ii) {410}, (iii) {610} and (iv) {430} at quasi-equilibrium (14ps after photo-excitation). A combined phonon mode of Jahn-Teller distortion (O, Mn$^{4+}$) and La/Sr (A-site cations) displacement shows the best agreement with experiment with $\chi^2$=0.003.

To quantify time resolved correlations of the atomic and electronic systems in complex functional materials we have developed an unprecedented dynamic diffraction method via quantitative electron crystallography and structural refinement, which allows us to reveal orbital and charge order dynamics and disentangle various phonon modes in the systems. Automated refinement computer codes for quantitatively measuring atomic displacement and vibration related to Wyckoff positions have been developed based on Bloch-wave diffraction theories. Millions iterations are carried out using homemade parallel computer programs to achieve the best fit, or the global minimum ($\chi_{min}^2$), at different time delays. One unique strength of our approach, in comparison to x-ray, is that it can simultaneously measure a large number of reflections that are very sensitive to atomic motion, thus provide time-dependent quantitative analysis of the atom-specific lattice dynamics on pico- and sub-picosecond time scale.

## Future Plans

*Electron-lattice interaction in cuprate superconductors* High temperature superconductivity is one of the most fascinating and promising phenomena that had been discovered in physics for the last decades. $Bi_2Sr_2CaCu_2O_{8+\delta}$ (Bi 2212), for example, belongs to the family of layered high temperature superconducting cuprates and has a critical temperature of 91K at optimal doping. This material exhibits incommensurate modulation in crystal structure along the b-axis due to CuO and BiO bonds mismatch. Electronic properties of high-Tc cuprates are widely studied in the search of Cooper-pair gluing mechanism. Strong coupling with selective "hot" phonon modes is suggested, but is lacking confirmation from direct lattice-sensitive experiments. Using the ultrafast pump-probe approach, we propose to investigate in-plane phonon dynamics under polarized laser excitation to test "hot phonon" model and determine the time scale of electron-lattice interactions in bulk for superconducting and normal states. Besides, we will determine whether charge ordering is involved in the formation of incommensurate structural modulation.

*Explore phonon-scattering and heat-transport mechanisms* Harvesting sunlight and miniaturizing nanoscale electronic devices require knowledge of heat transport and precise control of its efficiency. The phonon scattering and heat transport at nanometer scale differ significantly from their bulk counterparts. However, the required information is inaccessible with conventional optical and electron microscopy techniques. We target to investigate electron-phonon interaction, phonon population, phonon-phonon scattering and thermal transport in nanostructure architectures (Fig.3 right panel) using MeV-UED. We will be able to test physical models and mechanisms, which are critical to thermal transport, such as phonon ballistic transport, electron ballistic transport, size and temperature dependence of phonon scattering in various thermoelectric films and nanostructured materials, including $Bi_2Te_3$. We will quantitatively measure intensity change of Bragg reflections and diffuse scattering as a function of time delay using the Debye-Waller model (see the formula in Fig.3, where $\Delta\langle u_\perp^2\rangle$ is the atomic displacement and can be used to describe phonon population) to understand how phonon scatter at, the heat transfer across, the interfaces of dissimilar materials.

*Development of a novel electron pulser device for ultrafast electron microscopy* A novel time-resolved GHz stroboscopic concept for an ultrafast pulser device has been recently developed [6], as shown in the left panel of Fig. 3. It is laser-free and aimed at resolving sub-nanosecond dynamic processes of advanced magnetic, electronic, ionic and photonic materials under actual operation conditions in conventional transmission electron microscopes (TEMs). The device is based on an electromagnetic-mechanical pulser that consists of a series of transverse deflecting cavities and magnetic quadrupoles. It modulates and chops the incoming dc electron beam and converts it into pico- and sub-picosecond electron pulse sequences, or pulse trains, at a GHz repetition rate. The temporal pulse length and repetition rate for the device can be continuously tuned over a wide range. Without laser excitation on the sample, the problem of pump laser induced residual heating and damage on the sample, which is often an issue in ultrafast pump-probe experiments, can be eliminated. The device can be retrofit into a commercial TEM and convert its standard dc beam into pulse trains being driven by the same radiofrequency source for ultrafast electron diffraction, imaging and spectroscopy. The development is in part supported by the Federal Small Business Innovation and Research grants with a collaborative effort from several institutions including Euclid TechLabs, IDES, NIST and BNL. The device will be built at Euclid and tested on the dedicated Lorentz microscope (JEM2100F-LM) at BNL.

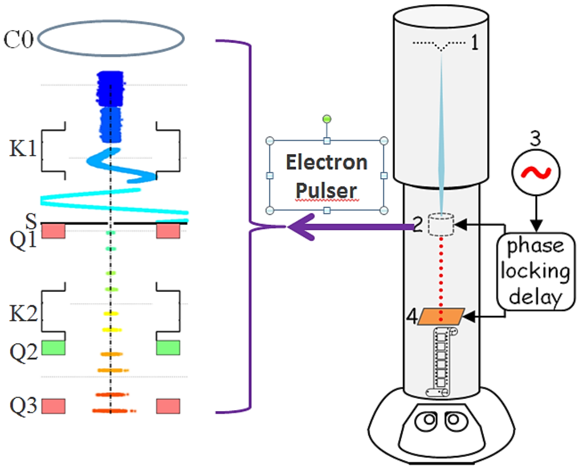

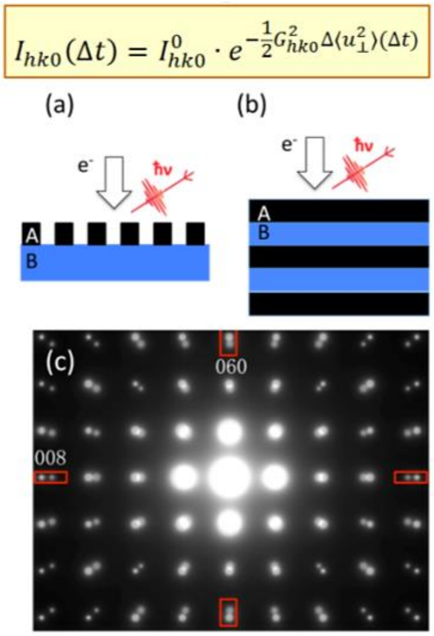

Fig. 3 (top) Schematic of the novel laser-free pulser device that produces ultrashort electron pulse trains with GHz repetition rates to convert a conventional transmission electron microscope to a time resolved microscope [6]. (right) The pump-probe geometry to explore phonon scattering and heat transport mechanisms. Laser pulses excite on (a) nano heater antennas, (b) supperlattice, and (c) simulated diffraction pattern.

## References

[1] Lim, D. et al. Phys. Rev. B 71134403 (2005).
[2] Polli, D. et al. Nat. Mater. 6, 643-647(2007); Rini, M. et al. Nature 449, 72-74(2007).
[3] Beaud, P., et al Nat. Mat. 13 923 (2014).
[4] Tobey, R. I., Prabhakaran, D., Boothroyd, A. T. & Cavalleri, A. Phys. Rev. Lett. 101, 197404 (2008).
[5] Zhu, P., et al New J. of Physics, 17 063004 (2015).
[6] Qiu, J., et al, Ultramicroscopy 161, 130-136 (2016).

## Publications

US patent (Provisional): “Gigahertz Rate High Duty Cycle Device to Pulse and Manipulate Direct Current Electron Beams of Low and Medium Energies (No. 62/143,667), S. Baryshev, J. Qiu, C. Jing, S. Antipov, J. Lau, and Y. Zhu.

US patent (Provisional): “A Stroboscopic Transmission Electron Microscope for Imaging at MHz and GHz Rates”, (No. 62/236,567), S. Baryshev, J. Qiu, J. Lau, and Y. Zhu.

Egerton, R.F.; Konstantinova, T.; Zhu, Y.; “Analysis of Beam-Sensitive Materials by Electrons and X-rays”, in: M. Berz, P.M. Duxbury, K. Makino, C.-Y. Ruan (Eds.), Femtosecond Electron Imaging and Spectroscopy 2013, Advances in Imaging and Electron Physics 191, pp. 70–80, Elsevier, 2015.

Li, J., Yin, W.-G., Wu, L., Zhu, P., Konstantinova, T., Tao, J., Yang, JJ., Cheong, SW., Carbone, F., Misewich, J., Hill, JP., Wang, XJ., Cava, RJ., and Zhu, Y., “Dichotomy in ultrafast atomic dynamics as direct evidence of polaron formation in manganites”, under review.

Piazza, L., Mann, A., Ma, C., Yang, H., Zhu, Y., Li, L., and Carbone, F., "Ultrafast structural and electronic dynamics of the metallic phase in a layered manganite", Structure Dynamics, 1 014501 (2014).

Qiu, J., Ha, G., Jing, C., Baryshev, S.V., Reed, B.W., Lau, L.W., Zhu, Y., “GHz Laser-free Time-resolved Transmission Electron Microscopy: a Stroboscopic High-duty-cycle Method”, Ultramicroscopy 161, 130-136 (2016).

Zhu, P., J. Cao, Y. Zhu, J. Geck, Y. Hidaka, S. Pjerov, T. Ritschel, H. Berger, Y. Shen, R. Tobey, J.P. Hill and X.J. Wang, "Dynamic separation of electron excitation and lattice heating during the photoinduced melting of the periodic lattice distortion in 2H-TaSe2", Appl. Phys. Lett., 103 071914 (2013).

Zhu, P.; Y. Zhu, Y. Hidaka, L. Wu, J. Cao, H. Berger, J. Geck, R. Kraus, S. Pjerov, Y. Shen, R. Tobey, J.P. Hill, and X.J. Wang, “Femtosecond time-resolved MeV electron diffraction”, New J. of Physics, 17 063004 (2015).

Zhu, Y. and H. Durr, “The future of electron microscopy”, Physics Today, 68 32-38 (2015).

# UNIVERSITY GRANT PROJECTS

# Mapping Bulk Phonon and Surface Phonon Polariton Modes in MgO

**P.E. Batson and M.J. Lagos**

**Institute for Advanced Materials, Devices and Nanotechnology**
**Departments of Physics, and Materials Science**
**Rutgers, the State University of New Jersey**
**607 Taylor Road, Piscataway, NJ 08854-8019**
**batson@physics.rutgers.edu**

## Research Scope

This project seeks to explore the dynamic dielectric response of nano-scale structures in *time and space*, using inelastic scattering of an Angstrom-sized swift electron beam. Whenever finite materials systems are subjected to localized EM fields or charges, the local system response propagates within the structure with velocities governed by the materials system – at the Fermi velocity for metals, or the velocity of sound for phonons, for instance. We describe this using a density-density correlation function, $\chi(\vec{r_1}, \vec{r_2}, t_1, t_2)$, which gives the excitation response density at a position and time ($r_2$, $t_2$), due to a disturbance at ($r_1$, $t_1$).

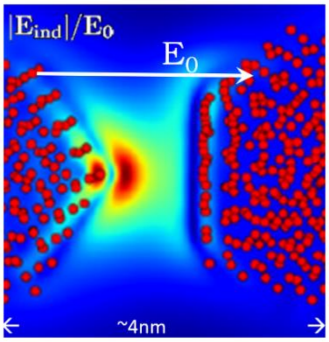

Fig. 1. Na Dimer, excited by an external field $E_0$ resulting in a response field $E_{ind}$. [1]

In the Fig. 1, we show a DFT calculation of the response field $E_{ind}$ generated by a steady state applied electric field $E_0$ [1]. The calculation is useful down to atomic coordinates, and provides insight into how the absorption of a photon by the Na dimer system drives a very strong field near a single atom of one of the two Na particles. Further, the field distribution suggests an overlap of photon-driven response with the regions of the particle occupied by atomic bonds, and presumably, associated unoccupied anti-bonding states. If $E_0$ were described by a fast pulsed light source, then $E_{ind}$ would require some finite time delay to increase to a maximum and then decay. We could then describe an energy flow, from the pump to the induced response during a finite time.

The passage of a swift electron nearby or through a nanostructure such as that shown in Fig. 1 generates disturbances similar to those shown in the figure. Associated information is encoded in the electron energy loss function – spectral peaks provide energy or frequency information, while the phases of the spectral peaks provide information about the *timing* of the various excitations. In electron diffraction, phases are not measured and need to be estimated in order to recover real space structure. In EELS, causality provides a phase measurement method, Kramers-Kronig analysis, to retrieve the phase from spectroscopy data, allowing the recovery of the timing of excitations within the specimen, relative to the impact of the swift electron.

Electrons, of course, produce highly divergent fields, quite unlike the dipole applied field of this example. Thus, in order to assemble information that might be comparable to the calculation of Fig. 1, we expect to need many mapped EELS spectra. We think this possibility is enabled by the reversibility of the processes described in Fig. 1. Thus, the presence of a response disturbance at a particular position in the image, caused by the presence of an external dipolar field, implies that the introduction of a test charge at that position will cause a similar external dipolar response field to be established with a similar probability. A caveat here is that in the initial work, at least, a 2-d projection must be assumed, unless tomographic techniques are used. Therefore, we believe that Spatially Resolved EELS maps can be processed through Kramers-Kronig methods to produce time resolved maps of the evolution of nanostructure excitations.

## Recent Progress

Our instrumental capability has improved during the past year through reduction of ground loop interference, with the best zero loss available now of 7.5 meV FWHM. This is an average over the AC mains frequency, and appears to be limited by low frequency mechanical or electrical instabilities, while we believe that our electron optical limit is around 5 meV.

Late last year, we made detailed mapping measurements of phonon modes in MgO nanometer-sized cubes, finding three main *bulk* peaks at 87, 51 and 35 meV, Figure 2. On the surfaces we find Fuchs-Kliewer (F-K) surface phonons in the 60-80 meV range depending on the measurement position and cube size. We believe the 35-51 meV peaks are combinations of TO and acoustic modes, but do not yet have a full theoretical understanding. We observe energy gain peaks corresponding to lower energy EELS peaks. We also see strong, unexpected broadening of the zero loss peak that we speculate is Rutherford scattering into the forward direction, which is expected to peak in the 5-10 meV range. Simple comparisons of the bulk scattering with Im(-1/ε) fail to reproduce the lower lying peaks, and so we are collaborating with U. Hohenester (Graz), to aid in understanding. Currently, comparisons are encouraging, but not yet complete. KeV electron EELS promises to create surprises here, because it couples to specimen excitations very differently from other probes: neutron, Raman, IR, HREELS, or inelastic x-ray scattering. Thus we expect, also, new information, complimentary to existing techniques. In Fig. 3, we show mapping of various spectral peaks:

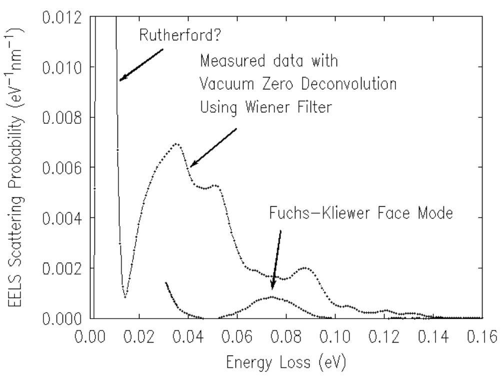

Fig. 2. MgO bulk spectrum with peaks at 35, 51, and 87 meV. Fuchs-Kliewer Face mode near 78 meV. (deconvoluted to suppress resolution tails)

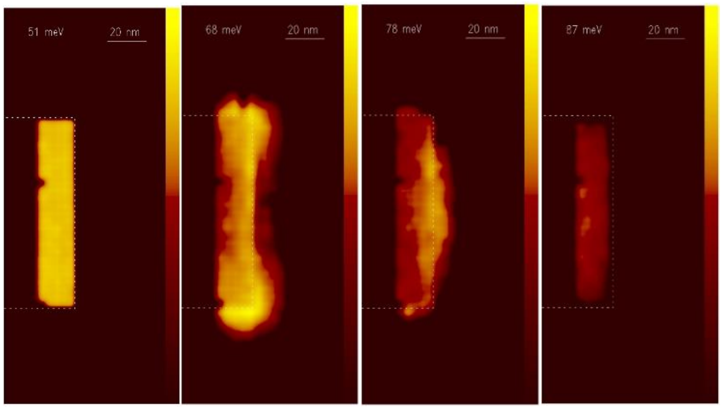

Fig.3 Energy filtered maps for 51, 68, 78, and 87 meV for the end of a 100nm MgO cube. F-K face and corner modes are visible, together with bulk modes. (Dashed lines define edge of MgO cube, Intensity of F-K mode enhanced relative to bulk for visibility.)

the 51 meV bulk, 68 meV F-K corner, 78 meV F-K face and 87 meV bulk LO modes. This data has been assembled into an mp4 format for display.

To begin with time domain work, we have modeled the optical behavior of MgO from meV to keV energies, using dielectric data from Palik [2]. This data includes phonons (a single Lorentz oscillator in the optical case), valence excitations, and the 532 eV oxygen core loss. Fig 4. shows the resulting time dependent FFT of that optical data. Our next step in this process will be to replace the Palik data with EELS data piecewise, using the optical data for guidance, and finally produce an EELS based time varying dielectric response. This result will be compared with the theoretical work of Hohenester using insight gained with J. Aizpurua (San Sebastian) about the interpretation of the general time-resolved results.

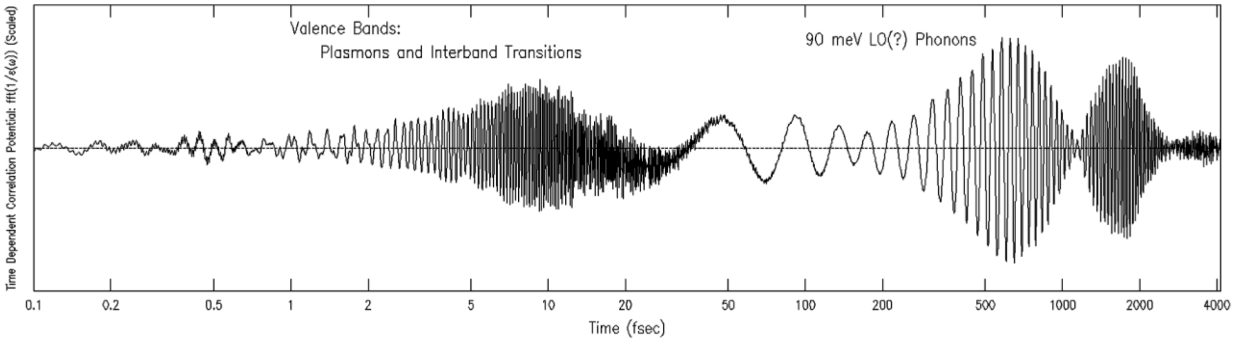

Fig 4. FFT (1/ε) showing valence and phonon time dependent behavior.

## Future Plans

During late May to early August, Andrea Konecna, a PhD student from the Aizpurua group in San Sebastian, Spain, visited Rutgers to begin working on time-dependent aspects of this project. Questions include, for instance, does a simple Fourier analysis of complex spectral amplitude provide time dependent information about the specimen response to an impulse probe? How might the spatial and time dependence of such a Fourier analysis relate to the movement of energy within a nanoscale object? How does the Kramers-Kronig analysis apply to heterogeneous structures; or how might it need modification to aid in obtaining time and spatially dependent information? During the coming fall, we will begin creating time domain plots for bulk and surface phonon modes, and attempt to map them in space onto the MgO cube to create a time dependent mpg4 illustration. We will also map valence bulk and surface scattering in MgO to match with the phonon results, looking for evidence of transfer of energy from higher to lower energy modes as a function of time.

## References

[1] M. Barbry, P. Koval, F. Marchesin, R. Esteban, A.G. Borisov, J. Aizpurua and D. Sanchez-Portal, *Atomistic Near-Field Nanoplasmonics: Reaching Atomic-Scale Resolution in Nano-optics*, Nano Letters, **15** 3410-3419 (2015). doi:10.1021/acs.nanolett.5b00759.

[2] E. Palik, Academic Press, New York (1985).

## Publications during the past two years which acknowledge DOE support.

[1] O.L. Krivanek, T.C. Lovejoy, N. Dellby, T. Aoki, R.W. Carpenter, P. Rez, E. Soignard, J. Zhu, P.E. Batson, M.J. Lagos, R.F. Egerton and P.A. Crozier, *Vibrational spectroscopy in the electron microscope*, Nature, 514 209-212 (2014). doi:10.1038/nature13870.

[1] M.J. Lagos, A. Reyes-Coronado, A. Koneˇcná, P.M. Echenique, J. Aizpurua and P.E. Batson, *Attosecond and femtosecond forces exerted on gold nanoparticles induced by swift electrons*, Phys. Rev. B, 93 205440 (2016) doi:10.1103/PhysRevB.93.205440.

[2] D. Voiry, R. Fullon, J. Yang, C. Silva, Rajesh, Kappera, I. Bozkurt, D. Kaplan, M.J. Lagos, P.E. Batson, G. Gupta, A.D. Mohite, L. Dong, D. Er, V.B. Shenoy, T. Asefa and M. Chhowalla, *The Role of Electronic Coupling between Substrate and 2D MoS*2 *Nanosheets on Electro-Catalytic Production of Hydrogen*, Nature Materials, 15 1003-1009 (2016) doi:10.1038/nmat4660.

## Extended Abstracts during the past two years that acknowledge DOE support.

[1] M.J. Lagos, A. Reyes-Coronado, P.M. Echenique, J. Aizpurua and P.E. Batson, *Attosecond Forces Imposed by Swift Electrons on Nanometer-Sized Metal Particles*, Microscopy and Microanalysis, 20 576–577 (2014) doi:10.1017/S1431927614004607.

[2] O. Krivanek, N. Dellby, T. Lovejoy, N. Bacon, G. Corbin, P. Hrncirik, Z. Szilagyi, T. Aoki, R. Carpenter, P. Crozier, J. Zhu, P. Rez, R. Egerton and P. Batson, *Exploring Phonon Signals by High Energy / High Spatial Resolution EELS*, Microscopy and Microanalysis, 20 66–67 (2014) doi:10.1017/S1431927614002050.

[3] M.J. Lagos, A. Reyes-Coronado, A. Koneˇcná, P.M. Echenique, J. Aizpurua and P.E. Batson, *Ultrafast Plasmonic Forces Imposed by Fast Electrons on Metal Particles*, Microscopy and Microanalysis, 21 1417–1418 (2015) doi:10.1017/S1431927615007862.

[4] M.J. Lagos and P.E. Batson, *Mapping EELS Vibrational Modes in MgO Nanocubes*, Microscopy and Microanalysis, (in press, 2016).

## Mapping interactions between individual coherent spins and dynamically driven ferromagnetic vortices

**PI: Jesse Berezovsky, Dept. of Physics, Case Western Reserve University, Cleveland OH 44106**

### Research Scope

This project aims to study and map interactions between components of hybrid nanodevices using a novel scanning probe approach. We have focused on hybrid devices in which single coherent electron spins are coupled to micron-scale ferromagnetic elements, which may prove useful for addressing single spins, enhanced sensing, or spin-wave-mediated coupling of spins for quantum information applications. A recent breakthrough was the realization that it is not necessary to fabricate a magnetic structure on a scanning probe – instead a ferromagnetic vortex core can act as an integrated, solid state, scanning probe. The vortex core of the vortex produces a very strong, localized fringe field which can be used analogously to an MFM tip. Unlike a traditional MFM tip, however, the vortex core is scanned within an integrated device (eliminating drift), and can be moved on vastly faster timescales. This approach allows the detailed investigation of interactions between single spins and complex driven ferromagnetic dynamics.

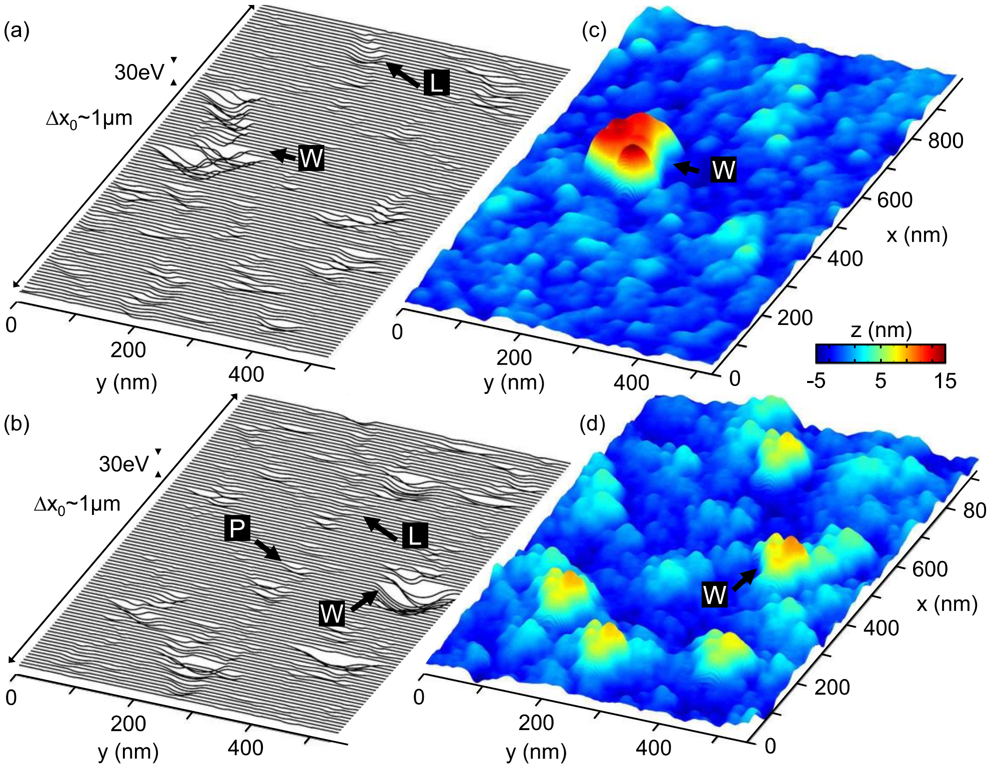

Figure 1. Mapping vortex pinning potential. (a) and (b) Maps of the effective pinning potential for a ferromagnetic vortex as it is raster scanned through a Permalloy disk. Three types of features are highlighted: "wide" features (W), "point-like" features (P), and "line-like" features (L). (c) and (d) Topographic AFM scans of the disks in the same area as the pinning maps. The largest features in the topographic scans correlate well with the W features in the pinning maps.

## Recent Progress

To exploit the motion of a vortex through a ferromagnetic film and to control that motion on nanosecond timescales and with nanometer scale precision, we first must characterize the effective pinning potential for a ferromagnetic vortex core (Fig. 1a and b) [1,2]. We also perform AFM scans (Fig. 1c and d) over the same regions of the sample, allowing us to correlate structural features of the film with the observed pinning. Once the pinning map is obtained, then the vortex can be controllably scanned across the disk. Further, the vortex core can be intentionally placed in a particular pinning site, for increased localization of the vortex position or for bistable switching of spin resonance in a nearby spin (see below).

With the vortex pinning potential mapped, we can then study coupling of the scanned ferromagnetic vortex to individual NV spins in diamond. In order to take full advantage of the nanoscale size of NVs for sensing applications, or to couple two NV spins via their dipole-dipole interaction, we need to be able to address and control NV spins separated by distances ~10 nm. The coupled NV/vortex system appears to be a promising avenue to achieve this, in a room temperature, integrated platform. Our results so far indicate that this hybrid system presents new intriguing physics, as the individual spin interacts with the mesoscopic, dynamic spin texture of the vortex.

Fig. 2a shows the concept of the coupled NV/vortex platform. The grayscale image shows a simulation of the out-of-plane magnetization of the vortex core. The arrows indicate the resulting simulated fringe field 20 nm above the surface of the magnetic disk (on a logarithmic scale). We then place a diamond nanoparticle, which contains several NVs within the particle's ~25 nm diameter, atop the disk. Using small magnetic fields, we then scan the vortex core across the disk. When the vortex core approaches the NVs, they experience a strong interaction with the vortex. Figure 2b shows the experimental realization of this platform, with the permalloy disk visible as the outlined blue circle, and the fluorescence from the NVs in the nanoparticle showing up as the bright red spot. We then perform optically-detected magnetic resonance (ODMR) and magneto-optical

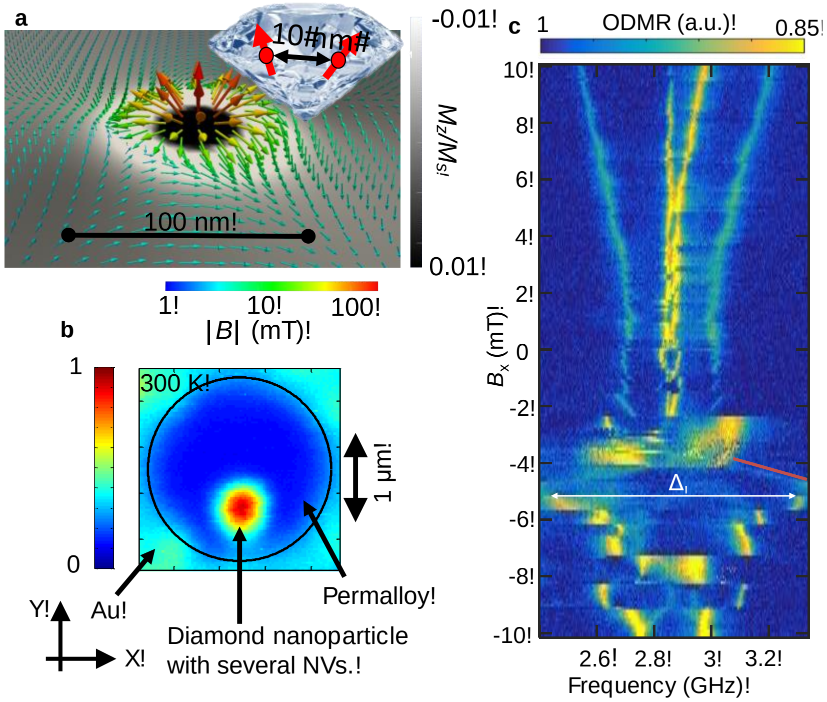

Figure 2. Coupling NV spins to a ferromagnetic vortex. (a) Simulation of vortex core out-of-plane magnetization (grayscale), and magnetic field 20 nm above surface (arrows). A diamond nanoparticle is then placed atop this structure. (b) Photoluminescence scan showing a Permalloy disk in a vortex state, with a diamond nanoparticle containing several NVs on top. (c) NV spin resonances vs. applied field. As the applied field drives the vortex near the NVs, large splitting Δ is observed, and large magnetic field gradient (red line).

microscopy measurements to map both the NV spin resonances and the vortex behavior.

Fig. 2c shows the rich interaction between the vortex and the NV spin transitions (revealed by the yellow lines in this ODMR data). At zero applied field, the vortex sits at the center of the disk. As the field is increased in the positive direction, the vortex moves away from the NVs and the spin splitting increases with field, as is typically observed. On the other hand, when the field is increased in the negative direction, the vortex core approaches the NVs, and more complex behavior in the spin transitions is seen resulting in large splitting, and large magnetic field gradients when the vortex makes its closest approach past the NVs (around $B_x = -5$ mT).

We have found that the coupling of the vortex to NV spins uncovers interesting physics beyond the large, local fringe field from the vortex core. A particularly rich facet of this system arises because the vortex as well as the NV spin can be driven dynamically by a microwave field, and the two then have a dynamic interaction with each other. In the confined geometry of the permalloy disk, spin wave excitations have a discrete spectrum of modes. When a microwave field is applied, these spin wave modes can be excited. These modes then emit some pattern of microwaves, which can drive transitions in a nearby NV. We have measured this effect, by studying coherent Rabi oscillations between spin levels in a single NV, as a function of the relative position of the vortex core. Rabi data for the two spin transitions in a single NV are shown in Fig. 3a. All conditions other than the microwave frequency are the same, yet the two traces show dramatically different Rabi frequency. Further, both Rabi frequencies are higher than would be expected from the applied microwave field alone. We conclude that the interaction with the vortex is amplifying the coherent spin rotations. We have mapped out this amplification as a function of vortex core position (Fig. 3b) and find that when the NV-vortex distance is small, we see more than an order of magnitude enhancement. These results suggest that a vortex can be used as an amplifier to increase the sensitivity of NV-based sensors. Another intriguing avenue opened by this effect is to explore spin waves as an intermediary to couple distant NVs.

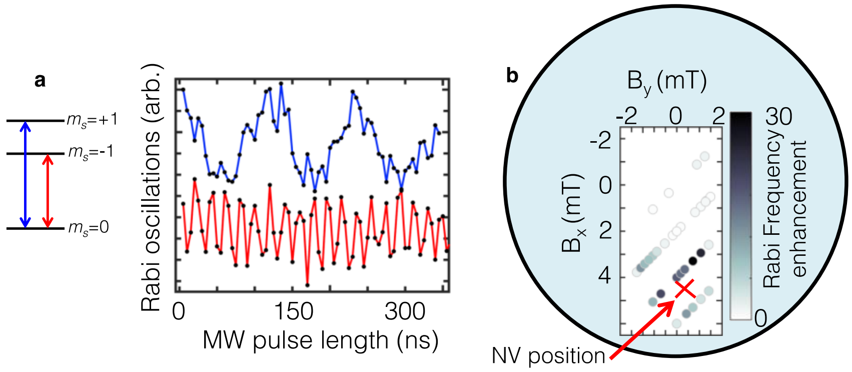

Figure 3. Vortex-induced amplification of spin resonance. (a) Rabi oscillations from $m_s$ = 0 to $m_s$ = +1 and $m_s$ = -1 states of an NV near the vortex core, showing significantly different Rabi frequency. (b) Map of Rabi frequency enhancement as a function of vortex core position. Enhancement is largest when the vortex core approaches the NVs.

Mapping the vortex pinning landscape using the technique described above allows us to exploit that effective potential to manipulate the NV spins coupled to the vortex. In particular, we can find places within the pinning map where two (or more) stable minima exist, providing for fast, low power switching of the

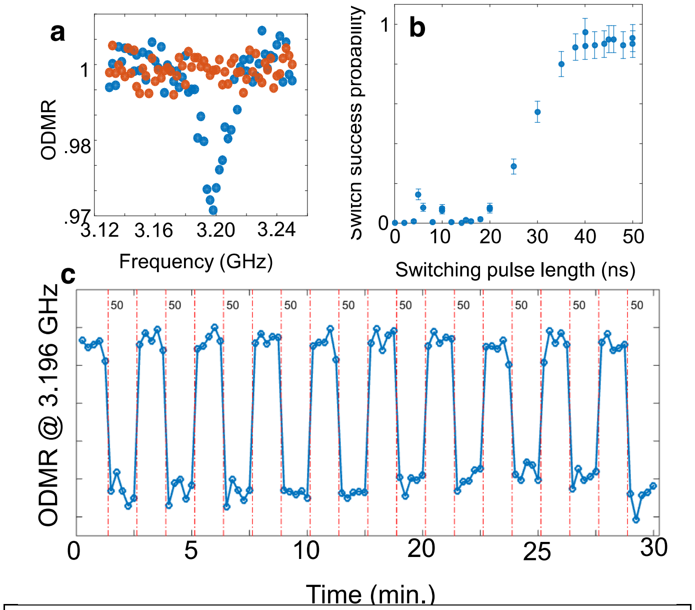

Figure 4. Bistable switching of NV resonances. (a) An NV resonance that is switched on resonance (blue) and off resonance (red) by moving the vortex between bistable positions. (b) Success of NV resonance switching vs. pulse length. (c) Demonstration of reliable, stable switching of an NV resonance over long timescales using single 50 ns pulses.

NV resonances. Switching between one stable point and another can be accomplished with magnetic field pulses of just a few Oersted, with duration ~tens of ns. The displacement of the vortex from one point to the other shifts the NV spins resonances, causing them to switch in and out of resonance with an applied microwave field. Fig. 4a shows two ODMR traces under the same experimental conditions, but with the vortex residing at two different stable points. At one point, a dip indicates the presence of a spin resonance, which is not present at the other point. The switching between these points can be carried out with a pulse of several Oersted – Fig. 4b shows the switching success vs. pulse time, with reliable switching requiring pulses with several tens of ns duration. Finally, Fig. 4c shows the long-term stability of this switching with a series of switches carried out with individual 50 ns pulses at each red dashed line.

## Future Plans

Our recent progress in coupling NV spins to a driven ferromagnetic vortex has opened up a number of interesting avenues to follow. One major area we plan to focus on is the dynamic behavior of this coupled system. First, we will characterize how the coupling to the vortex affects the spin coherence properties of a proximal NV. Furthermore, initial results suggest that the dynamic modes of the vortex have a non-trivial (repeatable) effect on the evolution of the spin state. We plan to characterize these modes using time-resolved magneto-optical microscopy, and to explore how they may be used for spin manipulation and mediating spin-spin interaction.

## References (supported by BES)

[1] Badea, R., J. A. Frey, and J. Berezovsky. "Magneto-optical imaging of vortex domain deformation in pinning sites." *J. Mag. Mag. Mat.* 381 (2015): 463-469.

[2] Badea, R., and J. Berezovsky. "Mapping the Landscape of Domain-Wall Pinning in Ferromagnetic Films Using Differential Magneto-Optical Microscopy." *Phys. Rev. Appl.* 5.6 (2016): 064003.

[3] Wolf, M. S. *et al.* Fast nanoscale addressability of nitrogen-vacancy spins via coupling to a dynamic ferromagnetic vortex. *Nat. Commun.* 7:11584 doi: 10.1038/ncomms11584 (2016).

[4] Badea, R., Wolf, M.S., Berezovsky, J., "Exploiting bistable pinning of a ferromagnetic vortex for nitrogen-vacancy spin control" *Under review* (Applied Physics Letters)

# Nanoscale Imaging of Optical-Frequency Plasmonic Energy Transfer in Hybrid Metal-Semiconductor Systems and Magnetic Metamolecule Assemblies

**Jon P. Camden[1] and David J. Masiello[2]**
**[1]Department of Chemistry and Biochemistry, University of Notre Dame, Notre Dame, IN 46556, [2]Department of Chemistry, University of Washington, Seattle, WA 98195**

**Research Scope:** Plasmons may enhance the efficiency of energy harvesting through one or more of the following mechanisms (Figure 1): (1) Photon-plasmon scattering, increasing the likelihood of absorption by a nearby semiconductor or molecule;[1] (2) Plasmonic resonance energy transfer (PRET), which occurs between an excited plasmon and the electronic transition dipole moment of a nearby semiconductor or molecule;[2] (3) Hot carrier transfer (HCT) from the nanoparticle to a nearby semiconductor or molecule, in which a localized surface plasmon (LSP) decays, through Landau damping, into an hot carriers that may then scatter into the neighboring material if it has sufficient energy.[3, 4] Despite significant progress achieved via optical spectroscopies and device geometries, understanding the differing and competing energy transfer pathways still presents a major challenge due to the lack of insights into the nanoscale. At the most basic level, directing energy flow at the nanoscale requires that we investigate the coupling between the plasmonic nanostructure and its environment with nanoscale precision, as such work will provide a guide for rational design of working nanosystems. Taking an example from plasmon-enhanced solar devices, it is still not known how to differentiate between competing energy transfer pathways in experimental observations, or how they are affected by the nanostructure's electronic properties, geometry, hybridization with other nearby nanoparticles, and dielectric environment. These insights are hidden under the aforementioned traditional techniques due to diffraction-limit. In contrast, electron energy loss spectroscopy (EELS) performed in a scanning transmission electron microscope (STEM) combines sub-nanometer resolving power with the

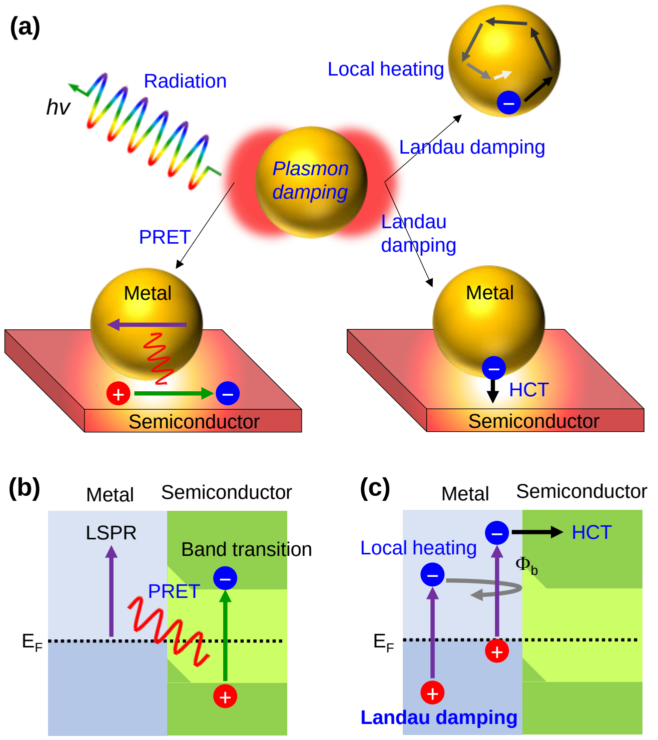

**Figure 1**. (a) A localized surface plasmon (LSP) can decay either radiatively via emitting photons to the far-field or non-radiatively via near-field dipole-dipole interaction with a neighboring semiconductor (PRET) or Landau damping. The hot carriers generated via Landau damping will either remain inside the metal and cause local heating, or overcome the Schottky barrier and enter the neighboring semiconductor (HCT). (b, c) Band diagrams illustrating PRET and HCT.

capability to interact with the full range of plasmon modes supported by a nanoparticle and therefore has become the leading technique in plasmon characterization.

**Recent Progress :** *Mapping plasmonic energy transfer via STEM/EELS:* While previous applications of STEM/EELS have focused on imaging surface plasmons in nanoparticles supported by an insulator, we have carefully tailored the dielectric environment by placing it on resonant semiconducting substrates instead.[5] This work shows that it is possible to not only direct the flow of plasmonic energy but also to isolate competing energy transfer pathways. To accomplish this, we performed 3D STEM/EELS experiments on both plasmon-insulator and plasmon-semiconductor systems, comparing the results to reveal both the spatial and spectral signatures of energy transfer. For the spatial signature (Figure 2(a)), we monitor the EELS map of the substrate-localized dipole mode (D-mode) of the Ag nanocube sitting with two different substrates: one insulating, silicon dioxide ($SiO_2$) which does not support energy transfer, and one semiconducting, amorphous silicon (a-Si) which allows both PRET and HCT to occur. We find that in the cube@a-Si system, the substrate-localization character of the D-mode disappears, suggesting the spatial character of energy transfer. In contrast, for the spectral signature of energy transfer (Figure 2(b)), we compare the EELS spectra of the D-mode of the nanocube sitting on two types of substrates: one exhibits a sharp absorption at 3.2 eV, crystalline silicon (c-Si), and the other exhibits a broadband absorption, a-Si. It turns out that the D-mode in the cube@a-Si system, which overlaps more with the broadband absorption of a-Si, is strongly broadened compared to that in the cube@c-Si system where the dipole mode and c-Si absorption is detuned. We recently extended the STEM/EELS method developed above to a Pt-decorated Au nanoprism system, and found that the Au plasmon is damped by the Pt nanoparticle, suggesting energy transfer between the plasmonic metal and the catalytic metal. Since plasmonic energy transfer is often associated with charge density increase in the neighboring material, the observed plasmon damping in Au implies that the catalytic property of the Pt nanoparticle should be enhanced due to charge density increase. Overall, our work indicates that energy transfer can be mapped via STEM/EELS and it is highly

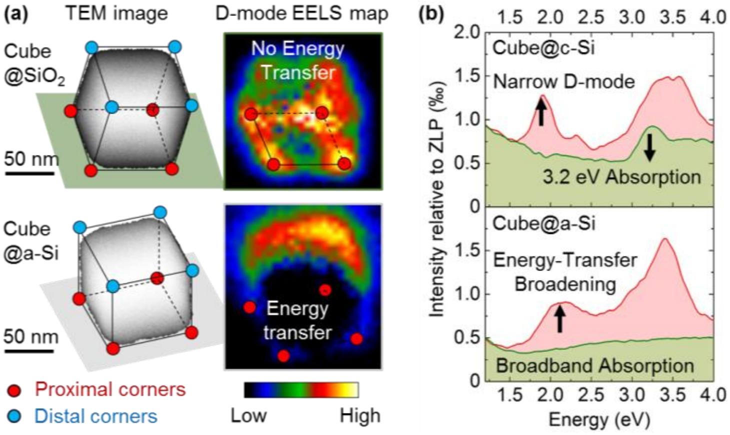

**Figure 2**. (a) Signature of energy transfer in EELS map. The EELS map of the dipole (D) mode in the cube@$SiO_2$system shows strong substrate-localization, indicating that no energy transfer occurs at the interface. In contrast, the near-zero EELS signal at the cube@amorphous silicon (a-Si) interface is the signature of energy transfer. (b) Signature of energy transfer in EELS spectra. Red traces are obtained via proximal beam positions while green traces are pure substrate signals. The D-mode, compared to that in the cube@c-Si system is spectrally broadened due to the PRET in a-Si. Here the efficiencies of HCT are assumed to be similar in both systems as c-Si and a-Si have similar Schottky barrier when

dependent on the relative energetics between the plasmon and semiconductor. The methods developed by our team have given researchers the first clear nanoscopic image of where in space energy is coming from, thereby greatly enhancing the usefulness of STEM/EELS in the study of plasmon-enhanced energy harvesting. We intend to continue down this line of thought, developing new methods aimed at unraveling the details of how energy is traded among the individual constituents of a nanosystem.

2. *Tracking the evolution of full plasmonic spectrum as a function of particle size, composition and dielectric environment with STEM/EELS:* Although it is well-known that the plasmonic property of a metal nanoparticle is sensitive to particle size, geometry, composition and dielectric environment, previous work has focused on theoretical predictions and far-field characterizations, leaving the near-field counterpart veiled. Such knowledge is important because it completes our understanding on how the surface plasmon modes respond, in both far-field and near-field, to a change in particle size, geometry, composition and dielectric environment. Moreover, the information in question contains the full map of plasmon energetics and can provide researchers with an ultimate guide in the design of energy-transfer systems described above. To address this objective, we performed a systematic STEM/EELS characterization of the plasmonic spectrum evolution in truncated nanospheres. The truncated nanospheres are synthesized via pulsed laser-induced dewetting (PLiD) which yields identical geometries with ultrasmooth surfaces, and more importantly, it allows a high tunability in particle size, composition and substrate species. Results are displayed in Figure 3. Figure 3(a) displays the size-dependent results for Ag nanoparticles on 30 SiN$_x$ substrates. The strong peak located at ~ 3.6 eV is due to the collective high-order plasmon modes. In contrast, the dipole (D) mode progressively redshift as particle size increases. Figure 3(b) displays the composition-dependent results for 100 nm sized particles sitting on 30 nm SiN$_x$ substrates. Here we show five compositions ranging from pure Au to pure Ag. Interestingly, the

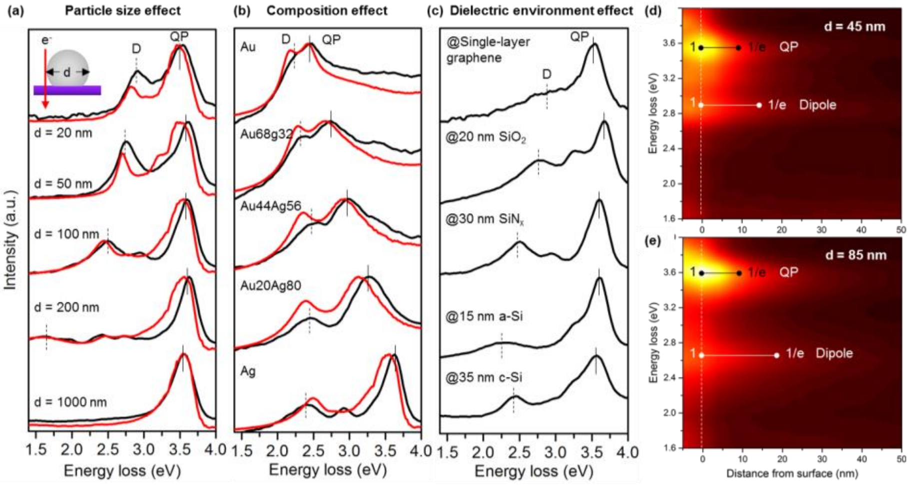

**Figure 3**. (a) Particle size effect. All Ag silver particles sit on a 30 nm SiN$_x$ substrate. The black traces are the experimental results and the red traces are simulation results. The QP mode and D mode are labelled with solid and dashed straight lines, respectively. (b) Particle composition effect. All sit on a 30 nm SiN$_x$ substrate and have a diameter of 100 nm. (c) Dielectric environment effect. Five different substrates: Single-layer graphene, SiO$_2$, SiN$_x$, a-Si and c-Si substrates are used. All Ag particles have diameter of 100 nm. (d, e) Spectrally-dispersed EELS line scan for a 45 nm and 85 nm diametered Ag nanoparticle. The straight lines represent the distances needed for the intensities of the particular plasmon modes to

QP mode shows more sensitivity to the composition compared to the D mode, as the QP mode is tightly bound to the particle surface and only the dielectric function of the particle affects its energy. In contrast, the D mode is not only affected by the dielectric function of the material but also the particle-substrate coupling. The combined effects make the D mode less sensitive to the particle composition compared to the QP mode. Figure 3(c) are the substrate-dependent results for 100 nm sized Ag nanoparticles. The single-layer graphene is used to mimic the "particle in vacuum" scenario where we observe an extremely-strong D mode. The 0.3 nm thick graphene does not introduce strong plasmon hybridization, leaving the D mode to strongly radiate. As the substrate refractive increases, the dipole mode continuously redshift and tapers while the QP mode stays almost unaffected. The redshift of the D mode is due to the increasing screening effect from the substrate while the narrowing phenomenon is due to stronger plasmon hybridization mediated by high-refractive index substrate. Figure 3(d, e) demonstrates the comparison of the near-field decay plots of a 45 nm and an 85 nm sized nanoparticle. Although in both cases the QP mode is much stronger, it decays faster in space. These two plots directly visualizes spatial localizations of the two modes. Overall, these results demonstrate the unique capability of the STEM/EELS in characterizing the full plasmon energetics as a function of commonly-used tuning knobs.

## Future Plans

(1) Individual particle size-dependent study of PIRET and DET for improved fundamental understanding and optimized energy transfer. Future experiments will involve replacing the insulating substrate with carefully-selected semiconducting substrates for more insights in the effect of energy transfer on the plasmon modes. (2) Exploit the electronic structure of alloy systems to boost hot-carrier generation for photocatalysis and photovoltaic applications. To experimentally address this objective, we propose to exploit alloy systems with STEM/EELS, aiming to optimize LSPR-interband overlap for a boost in hot-carrier generation.

## References

1. Atwater, H. A.; Polman, A. *Nat. Mater.* **2010,** 9, (3), 205-213.
2. Li, J.; Cushing, S. K.; Meng, F.; Senty, T. R.; Bristow, A. D.; Wu, N. *Nat Photon* **2015,** 9, (9), 601-607.
3. Brongersma, M. L.; Halas, N. J.; Nordlander, P. *Nat. Nanotechnol.* **2015,** 10, (1), 25-34.
4. Clavero, C. *Nat. Photonics* **2014,** 8, (2), 95-103.
5. Li, G.; Cherqui, C.; Bigelow, N. W.; Duscher, G.; Straney, P. J.; Millstone, J. E.; Masiello, D. J.; Camden, J. P. *Nano Lett.* **2015,** 15, (5), 3465-3471.

**Publications from BES support (2014-2016)**

1. Iberi, V.; Bigelow, N. W.; Mirsaleh-Kohan, N.; Griffin, S.; Simmons, P. D., Jr.; Guiton, B. S.; Masiello, D. J.; Camden, J. P. "Resonance-Rayleigh Scattering and Electron Energy-Loss Spectroscopy of Silver Nanocubes" *J. Phys. Chem. C* **2014,** 118, (19), 10254-10262.
2. Li, G.; Cherqui, C.; Bigelow, N. W.; Duscher, G.; Straney, P. J.; Millstone, J. E.; Masiello, D. J.; Camden, "Spatially Mapping Energy Transfer from Single Plasmonic Particles to Semiconductor Substrates via STEM/EELS" J. P. *Nano Lett.* **2015,** 15, (5), 3465-3471.
3. Li, G.; Cherqui, C.; Wu, Y.; Bigelow, N. W.; Simmons, P. D.; Rack, P. D.; Masiello, D. J.; Camden, J. P. "Examining Substrate-Induced Plasmon Mode Splitting and Localization in Truncated Silver Nanospheres with Electron Energy Loss Spectroscopy" *J. Phys. Chem. Lett.* **2015**, (6), 2569-2576.
4. Wu, Y.; Li, G.; Cherqui, C.; Bigelow, N. W.; Thakkar, N.; Masiello, D. J.; Camden, J. P.; Rack, P. D. "Electron Energy Loss Spectroscopy Study of the Full Plasmonic Spectrum of Self-Assembled Au-Ag Alloy Nanoparticles: Unraveling Size, Composition, and Substrate Effects" *ACS Photonics* **2016,** 3, (1), 130-138.
5. Cherqui, C.; Thakkar, N.; Li, G.; Camden, J. P.; Masiello, D. J. "Characterizing Localized Surface Plasmons Using Electron Energy-Loss Spectroscopy" *Annu. Rev. Phys. Chem.* **2016,** 67, (1), 331-357.
6. Quillin, S. C.; Cherqui, C.; Montoni, N. P.; Li, G.; Camden, J. P.; Masiello, D. J., "Imaging Plasmon Hybridization in Metal Nanoparticle Aggregates with Electron Energy-Loss Spectroscopy" *J. Phys. Chem. C* **2016**, Article ASAP.
7. Griffin, S, Montoni, N., Li, G., Straney, P., Millstone, J., Masiello, D. J., Camden, J.P., "Imaging Energy Transfer in Pt-Decorated Au Nanoprisms via Electron Energy-Loss Spectroscopy", *J. Phys. Chem. Lett.*, **2016**, ASAP.
8. Cherqui, C., Wu, Y., Li, G., Quillin, S. C., Brsche, J. A., Montoni, N.P., Thakkar, N., West, C. A., Rack, P.D., Camden, J. P.; Masiello, D. J. "STEM/EELS Imaging of Magnetic Hybridization in Symmetric and Symmetry-Broken Plasmon Oligomer Dimers and All-Magnetic Fano Interference" **2016**, submitted.

# Tunable Anisotropy at the (111) $LaAlO_3/SrTiO_3$ Interface

**Venkat Chandrasekhar, Department of Physics, Northwestern University**

## Research Scope

The primary focus of this project is to investigate the properties of novel electronic systems using a combination of electrical transport and low temperature scanning probe techniques. The current focus is on the two-dimensional (2D) conducting gas that forms at the interface between the band insulators $LaAlO_3$ (LAO) and $SrTiO_3$ (STO), and in particular on understanding the rich variety of physical phenomena that occur in this system.

## Recent Progress

### *(111) oriented LAO/STO interfaces*

Most of the work on LAO/STO interface devices to date has been on structures grown on (001) oriented STO substrates [1]. In the past two years, we have focused on studying LAO devices grown on (111) oriented STO substrates. Unlike the (001) devices, where the Ti orbitals in the STO at the interface have a square symmetry, the Ti orbitals at the (111) interface have hexagonal symmetry (Fig. 1a), and have been predicted to have novel band structure and potential topological properties. Thus it is of interest to study the properties of (111) oriented LAO/STO interfaces.

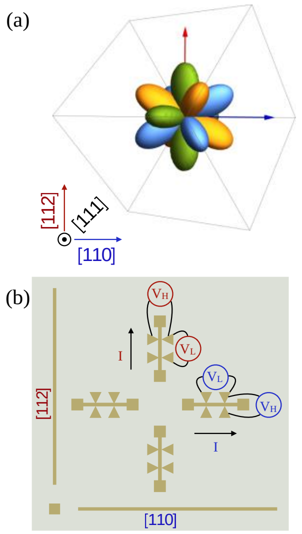

Figure 1 Ti $d_{xy}$, $d_{yz}$ and $d_{xz}$ orbitals in a cubic crystal viewed along the [111] direction. (b) Schematic representation of the surface of the (111) LAO/STO sample chip, showing the four Hall bars. The electrical connections for longitudinal and Hall resistance are marked.

To do this, we fabricated Hall bars from 20 monolayer (ML) (111) LAO/STO grown by pulsed laser deposition (PLD) in T. Venkatesan's group at the National University of Singapore. The Hall bars were patterned such that their long axes were oriented either along the $[1\bar{1}0]$ crystal direction, or the $[\bar{1}\bar{1}2]$ crystal orientation, as shown in Fig. 1b. The transport properties of these devices were measured down to millikelvin temperatures in a dilution refrigerator, although here we will discuss only their properties down to liquid helium temperatures (4.4 K).

Figure 2 shows the longitudinal sheet resistance of the two Hall bars with contacts marked in Fig. 1b as a function of the back gate voltage $V_g$ applied to the substrate at 4.4 K. Both curves are hysteretic, which is a characteristic generally seen in LAO/STO devices when the gate voltage is applied through the STO substrate [2]. We have found that this hysteresis is due to slow relaxation processes in the system, and that the long-term behavior is given by the average of the up and down gate voltage sweeps, as shown in the figure. Aside from the hysteresis, the most notable fact about these data is that the resistance is strongly anisotropic: while the resistance of the Hall bars aligned along the two mutually perpendicular directions is approximately the same at large positive $V_g$, the resistances start to diverge as $V_g$ falls below 20 V, and by $V_g$~-60 V, the resistance along the $[1\bar{1}0]$ direction is more than a factor of 7 larger than along the $[\bar{1}\bar{1}2]$ direction. In addition, unlike the (001) oriented samples measured previously, the resistance in the "high-resistance" $[1\bar{1}0]$ direction changes by orders of magnitude over this limited $V_g$ range, and continues to increase as $V_g$ is reduced.

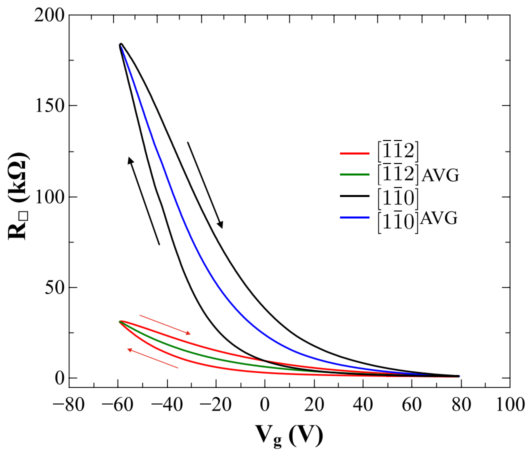

Figure 2 Sheet resistance of (111) LAO/STO interface Hall bars measured along the two mutually orthogonal directions shown in Fig. 1b, at 4.4K. Arrows denote the sweep direction of $V_g$; the averaged curves are averages of the up and down sweeps for each direction.

The anisotropy in the electrical characteristics of the (111) LAO/STO interface structures can also be seen in other measurements. Figure 3 shows the Hall coefficient $R_H$ measured on Hall bars aligned along the two crystal directions. The overall sign of $R_H$ is electron-like; however, the dependence on $V_g$, with $|R_H|$ decreasing with decreasing $V_g$, indicates that both electrons and holes contribute to charge transport. As with the sheet resistance, $R_H$ is anisotropic: above $V_g$~20 V, $R_H$ along both directions is roughly the same, and shows only a weak dependence on $V_g$. For $V_g \leq 20$ V, the Hall coefficient in the $[1\bar{1}0]$ direction shows a sharp drop, while $R_H$ along the $[\bar{1}\bar{1}2]$ direction starts decreasing rapidly for $V_g \leq 0$ V. It should be noted that $|R_H|$ approaches 0 as $V_g$ is decreased, a sign of a compensated system, and another indication that holes contribute to charge transport in this system. This anomalous behavior of $R_H$ with $V_g$ implies that $R_H$ cannot simply be used to determine the electron density using a single-band model of transport, as has been the common practice in the field.

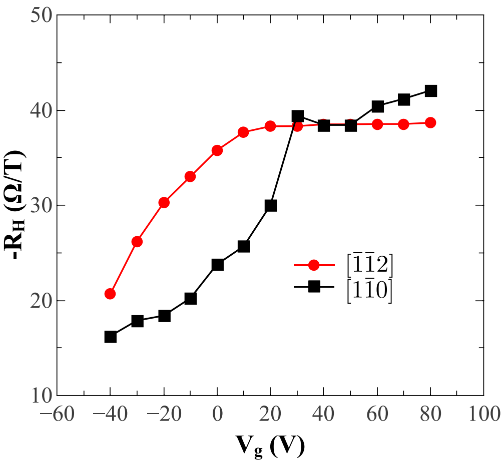

Figure 3 Hall coefficient at 4.4 K for Hall bars measured along the two different crystal directions shown in Fig. 1b.

In addition to charge transport, the anisotropy can also be observed in the capacitance of the devices. The total capacitance $C_T$ between the back gate and the 2D gas at the interface is the series combination the usual geometric capacitance ($C_g$) and the quantum capacitance ($C_q$), which is related to the density-of-states $dn/dE$ of charge carriers at the interface. Measurements confirm that $C_g$ is essentially independent of $V_g$, so any variation of $C_T$ with $V_g$ is determined by the variation of $C_q$ with $V_g$. We note that $dn/dE$ by definition is an average over the Fermi surface, and hence should be isotropic. Experimentally, however, we find that $C_T$ vs. $V_g$ is anisotropic. Figure 4 shows $C_T$ of Hall bars aligned along the $[1\bar{1}0]$ and $[\bar{1}\bar{1}2]$ directions. As the effective area of each capacitor is different (due to wire bond contacts, etc.), the quantitative value of $C_T$ is not comparable, so we compare the qualitative behavior by scaling the data so that the curves match for $V_g \geqq 20$ V. The overall trend for both crystal directions is that $C_T$ (and hence the density of states $dn/dE$) decreases with decreasing $V_g$, saturating for large negative $V_g$, and even showing hints of an increase for the most negative values. The scaled curves match for $V_g \geqq 20$ V, but $C_T$ for the $[1\bar{1}0]$ direction shows a sharp drop in comparison to the $[\bar{1}\bar{1}2]$ direction below this voltage. This matches the differences observed for $V_g \leq 20$ V between the two directions in the longitudinal sheet resistance (Fig. 2) as well as the Hall coefficient (Fig. 3).

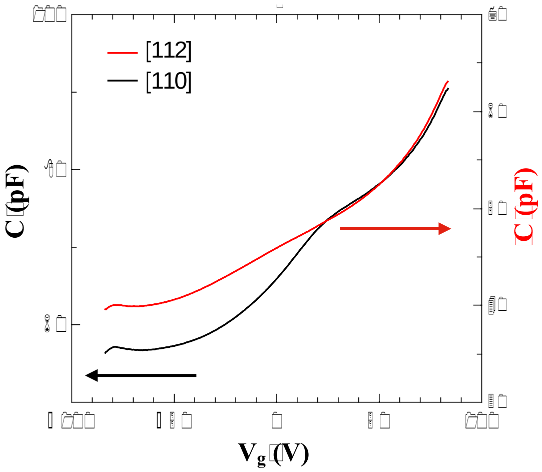

Figure 4. Capacitance $C_T$ as a function of $V_g$ for Hall bars along the two crystal directions, at 4.4 K. As the absolute values of $C_T$ differ due to different capacitor areas, the data are scaled to match at $V_g \geqq 20$ V.

STO at room temperature has a cubic perovskite crystal structure, and in crystals with cubic symmetry, the conductivity is isotropic. However, it is well known that STO undergoes a structural transformation to a lower symmetry phase at around ~105 K [3], but we do not observe strong anisotropy at liquid nitrogen temperatures (77 K), so the structural transition may not be the source of the anisotropy. In addition, the LAO/STO interface systems are highly disordered in general, and disorder might be expected to make things more isotropic. Indeed, we have recently discovered that we can tune the anisotropy by post-growth treatment of the devices, annealing in an $O_2$ environment, an $Ar/H_2$ environment, or by irradiation by an ultraviolet (UV) source. The origin of the anisotropy and the source of the hole conduction are not clear at the moment.

## Future Plans

### *Anisotropy in (111) oriented LAO/STO interface structures*

The (111) LAO/STO interface devices shows hints of superconducting correlations at millikelvin temperatures. Unlike the (001) interface samples, and the (110) interface samples measured by other groups, these devices do not go completely superconducting, but show a sharp drop in resistance at temperatures in the range 25-100 mK. As with the three properties discussed above (longitudinal resistance, Hall coefficient and quantum capacitance), the superconducting characteristics are also anisotropic, *i.e.*, they are different when measured on Hall bars oriented along the $[1\bar{1}0]$ and $[\bar{1}\bar{1}2]$ directions. Since superconductivity in STO and LAO/STO structures is supposed to be of a conventional *s*-wave type, we do not understand these observations at present. Our goal in the coming year is to try and understand the origin of the anisotropy in the superconducting properties.

Preliminary measurements of the magnetoresistance (MR) of the (111) LAO/STO devices show that it is hysteretic, a signature that these structures, like the (001) LAO/STO structures, are also magnetic. As with all the other properties, the MR is also anisotropic. In the coming year, we plan to study the MR in order to get a better understanding of the origin of magnetism in this system.

*Time-dependent phenomena at low temperatures*

One of the unusual characteristics of the LAO/STO system is a slow relaxation of its properties on changing the voltage applied to the STO substrate. At low temperatures and in gate voltage regimes where the resistance of the sample is very large, this relaxation can take place over many hours and even days. A signature of this long time-scale behavior is the hysteresis observed in gate voltage sweeps, as shown in Fig. 2. Similar long time-scale behavior has been observed in other systems called Coulomb glasses, where its origin is related to transport through localized states with strong Coulomb interactions. This topic is an active area of research in other systems (e.g., doped semiconductors), but has not been explored in LAO/STO devices. Interestingly, the hysteresis is not observed when using a metallic top gate (see below), indicating that it is associated with the STO substrate.

*Improvements in low-temperature scanning probe microscope*

We plan to continue to improve our low temperature scanning probe microscope. In order to extend our scanning range, we recently purchased a new Ti coarse approach/scanner from Attocube, and we have modified our high voltage amplifiers to work with this scanner. We are now working on implementing the control electronics completely in the digital domain using a Xilinx Zybo FPGA board. Our initial goal is to implement the phase locked loop for our tuning fork transducer digitally to improve our phase and frequency resolution. Later this year, we will also start developing the lithography protocol to start making our own piezoelectric cantilevers, enabling us to achieve the force sensitivity of commercial SPM cantilevers while retaining the advantage of the tuning fork transducers of all electrical cantilever excitation and detection.

## References

[1] A. Ohtomo, A. and H. Y. Hwang, *Nature* **2004** 427, 423.

[2] M.M. Mehta, D.A. Dikin, C.W. Bark, S. Ryu, C.M. Folkman, C.B. Eom, and V. Chandrasekhar, *Nat.Commun.* **2012** 3, 1959.

[3] R. Loetzsch, A. Lübcke, I. Uschmann, E. Forster, V. Grosse, M. Thuerk, T. Koettig, F.

Schmidl, and P. Seidel, Appl. Phys. Lett. **96**, 071901 (2010).

**Publications**

"Magnetic field tuned superconductor-to-insulator transition at the $LaAlO_3$/SrTiO interface," M. Mehta, D.A. Dikin, C.W. Bark, C.M. Folkman, C.B. Eom, and V. Chandrasekhar, Phys. Rev. B **90**, 100506(R) (2014).

"Gate-tunable superconducting weak link behavior in top-gated $LaAlO_3$-$SrTiO_3$," V.V. Bal, M.M. Mehta, S. Ryu, H. Lee, C.M. Folkman, C.B. Eom and V. Chandrasekhar, Appl. Phys. Lett. **106**, 212601 (2015).

"Anisotropic, multi-carrier transport at the (111) $LaAlO_3$/$SrTiO_3$ interface," S. Davis, V. Chandrasekhar, Z. Huang, K. Han, Ariando and T. Venkatesan, arXiv:1603.04538 [cond-mat.str-el] (*submitted for publication*).

"Electrical transport anisotropy controlled by growth conditions in (111) $LaAlO_3$/$SrTiO_3$ interface structures," S.K Davis, Z. Huang, K. Han, Ariando, T. Venkatesan and V. Chandrasekhar**,** *submitted for publication.*

# Domain Wall Stability and Domain Switching: Role of Oxygen Octahedral Tilt

Long-Qing Chen, Department of Materials Science and Engineering, The Pennsylvania State
University, University Park, PA 16802; lqc3@psu.edu, www.ems.psu.edu/~chen

## Research Scope

Domain pattern formation is one of the most common phenomena in nature and is a topic of immense interest in many fields ranging from materials science, physics, chemistry, to biology. The main objective of this research program is to explore the basic science concerning the thermodynamic stability of mesoscale polarization domain patterns and their temporal evolution mechanisms during formation and subsequent switching in ferroelectric nanostructures and heterostructures. We employ the phase-field method in combination of microelasticity and electrostatic theories. The research is being carried out in close collaboration with a number of experimental groups who use High Resolution Transmission Electron Microscopy (HRTEM), *in situ* TEM with Scanning Probe Microscopy (SPM), or Piezoresponse Force Microscopy (PFM) to characterize the domain structures and dynamics in high-quality ferroelectric and multiferroic thin films. Specifically, the project will be focused on the basic understanding of (1) the role of oxygen octahedral tilt in domain wall stability; (2) the emergence of charged domain walls during domain switching; and (3) the spatial length scales, temperature ranges, and electromechanical conditions leading to the emergence of both transient and stable novel polarization states containing vortex lattices in ferroelectric superlattices. The research is expected to not only advance the basic science on the stability of mesoscale polar states and pattern evolution but also improve our ability to control and engineer properties of ferroelectric thin films and heterostructures for applications in nanoscale electronic devices.

## Recent Progress

Our research efforts for the last two years have been primarily focused on *1*) extending our phase-field model to incorporate the contributions from the oxygen octahedral tilt order parameter for studying its influence on the stability of polar domain states and mechanism of polar domain switching; *2*) understanding the role of oxygen octahedral tilt order parameter in the domain wall energy and structures, and thus domain configurations under different electromechanical conditions; and 3) the emergence of charged domain walls during ferroelastic domain mediated polarization switching. These efforts have led to a basic understanding of the role of oxygen octahedral tilt in the variation of the domain wall energy and thickness among different domain walls in perovskites in general and in $BiFeO_3$ in particular [1, 2] and prediction of charged domain walls during ferroelectric switching in the presence of ferroelastic domains [3, 4]. We also formulated a new oxygen octahedral tilt compatibility condition for predicting domain wall orientations [1], and we study the role of oxygen octahedral tilt in the formation of polarization vortex and switching of a vortex by an irrotational electric field [5].

### *Incorporated the oxygen octahedral tilt order into the phase-field model*

Oxygen octahedral tilt or rotation is a common structural instability in complex oxides. One of our major accomplishments is the incorporation of the oxygen octahedral tilt into the phase-field model [1], which allows us to model and predict how oxygen octahedral tilt influences polar domain states and stable domain wall configurations. This is in addition to the capabilities of our existing phase-field model that we developed for arbitrary film crystallographic orientations, e.g. films on a miscut substrate, the strain relaxation due to the thickness effect, anisotropic misfit strains, the presence of inhomogeneous stress-field arising from an arbitrary distribution of dislocations, mixed electric boundary conditions, and ferroelectric islands attached onto a substrate. We also extended our model to simulate applied inhomogeneous stresses, e.g., from a probe, by modifying the mechanical boundary conditions to allow non-zero stress boundary conditions at the free surface of a film. We have exploited the scalability of phase-field solvers and parallelized the execution of the phase-field code, permitting us to simulate more realistic, larger systems and accelerate the pace of research.

### *A new domain wall compatibility condition with oxygen octohedral tilt*

A characteristic of the perovskite structure ($ABO_3$) is the corner-sharing network of the rigid $BO_6$ oxygen octahedra which can rotate or tilt as a whole with almost no distortion of the O-B bonds. It is found that the oxygen octahedral tilts are strongly correlated with the electronic, magnetic, and optical properties. The orientations of permissible (low-energy) domain walls are conventionally determined using two conditions: one is the mechanical compatibility condition which requires matching of the atomic displacements of the two adjacent domains to minimize the strain energy; the other is the electrical neutrality condition to minimize the electrostatic energy, e.g. at ferroelectric domain walls arising from the bound charges. We proposed an additional condition, namely "rotational compatibility condition", to determine the orientations of the low-energy octahedral tilt walls in perovskites [1]:

$$(\theta_i - \theta_i')n_j = 0 (j \neq i), \ with \ \theta_i = -\theta_i' \neq 0,$$

where $\theta_i$ *and* $\theta_i'$ are axial vectors which denote the octahedral tilt components in the two neighboring domains, and ***n*** is the domain wall normal. It is demonstrated that there exist universal low-energy domain walls, the orientations of which can be determined by the proposed rotational compatibility condition. For example, based on the polarization order parameter alone, one would expect the domain wall energy sequence, $\gamma_{71^o} < \gamma_{109^o} < \gamma_{180^o}$, where $\gamma$ is the polar domain wall energy. However, the oxygen octahedral tilt order coexists with polar order, and $109^o$ polar domain walls satisfy the rotational compatibility condition, and thus show the lowest domain wall energy in $BiFeO_3$. The $71^o$ walls, however, does not satisfy the rotational compatibility condition since the wall normal is not along any pseudocubic axes. Thus the energy and width of the $71^o$ wall are much larger than those of the $109^o$ wall. Therefore, the unusual wall energy sequence in $BiFeO_3$ can be well explained based on the rotational compatibility condition. The proposed new condition can serve as guidance to domain wall engineering in perovskites, and predict the low-energy oxygen octahedral tilt domain walls and consequently polarization domain walls in other systems such as hybrid improper ferroelectrics.

### *Influence of oxygen octahedral tilt on vortex wall orientations and switching the curl of polarization vectors by an irrotational electric field*

Ferroelectric vortex domains are of significant interest due to their rich physics and potential applications. We formulated the crystallographic, strain, and electric conditions for spontaneous vortex domains and study the influence of oxygen octahedral tilt on vortex wall orientations [5]. Using 109° domain walls in $BiFeO_3$ films as an example, it is demonstrated that vortex domains result from bound charge density waves, i.e., from alternating positive and negative bound charges. The vortex domains lead to a net curl of the polarization vectors that can be switched by an irrotational electric field.

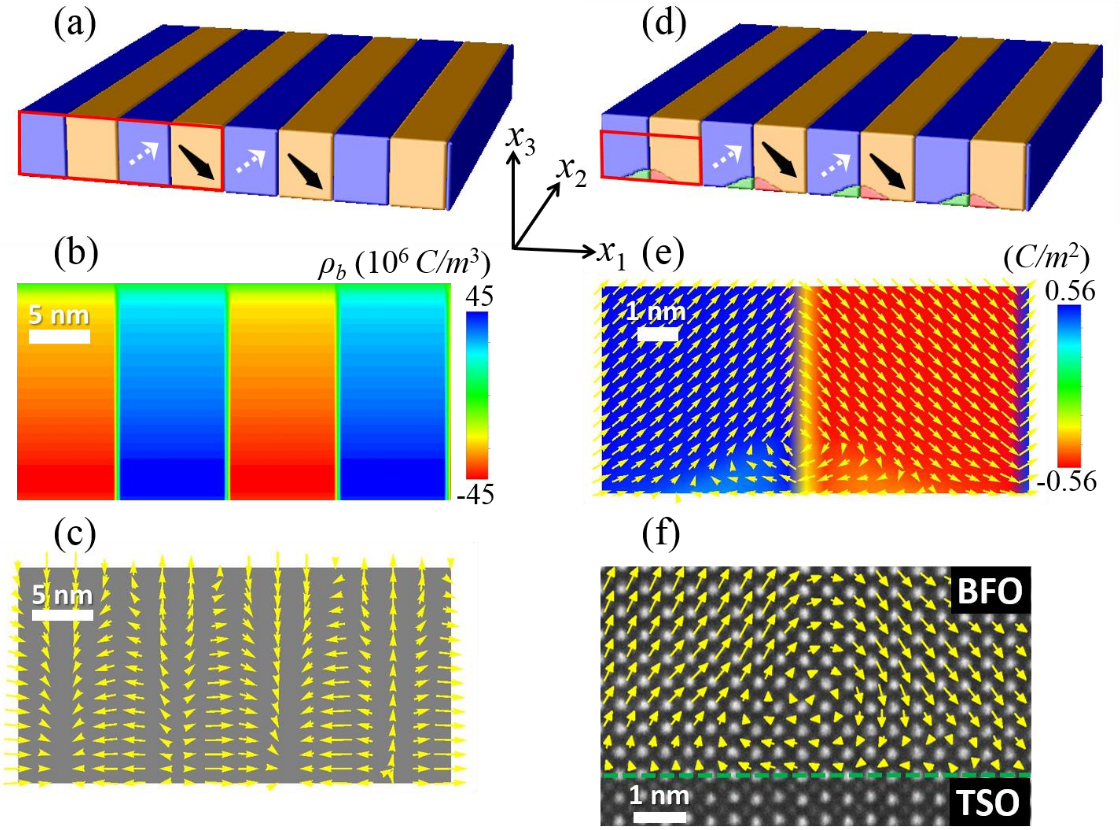

FIG. 1. The origin of vortex domains in BFO films. (a) 109° domain walls without vortex domains. (b) The distribution of bound charges within the rectangular region in (a). (c) The distribution of electric fields induced by the bound charges in (b). (d) 109/71 vortex domains from a phase-field simulation. (e) Polarization vectors within the region noted by the rectangle in (d). The color in (e) represents the polarization component out of the plane of the page. (f) Experimental HAADF STEM image (from X. Q. Pan's group) of a 5 nm think BFO film (from D. G. Schlom's group) grown on a (110) $TbScO_3$ substrate. The overlaid yellow vectors show the polarization distributions calculated from the atomic displacements between the Fe and Bi atoms. (a), (b), and (c) represent unstable structures, and are plotted to explain the origin of the vortex domains in (d) and (e).

## Future Plans

Our existing DOE efforts for the last two years mainly focused on understanding the role of oxygen octahedral tilt in the stability of domain states and domain walls, and elucidating the ferroelectric switching mechanisms in the presence of ferroelastic domains under non-uniform electric or mechanical field from a surface probe. Following the general direction of the original project to address the basic questions concerning the thermodynamic stability of ferroelectric domain states and their temporal/spatial evolution mechanisms under external stimuli, planned tasks will focus on discovering new mesoscale ferroelectric domain states and their switching mechanisms. Specifically, we propose to focus our research efforts for the next two years on the following two tasks:

- *To investigate the spatial length scales, temperature ranges, and electromechanical conditions leading to the emergence of both transient and stable mesoscale polarization vortex lattices; and*
- *To model and predict the switching mechanisms of polarization vortices under electrical and mechanical stimuli and understand the impact of polarization vortex formation and switching on magnetic spin configurations.*

Both tasks will be carried out by working closely with our experimental collaborators. We will take advantage of the fact that we have the full three-dimensional fields of stress, electric field, polarization, as well as electrostatic, strain, polarization gradient and magnetic energy density distributions, which are critical to the understanding of relative stabilities of various mesoscale domain states. Furthermore, we could readily explore a wide range of stable/metastable polar domain states artificially created by starting with different initial polarization distributions and electromechanical conditions. Therefore, while in some cases we will perform phase-field modeling to interpret the experimentally observed, often fascinating, polar domain patterns; in other cases, our modeling results and predictions will in turn provide guidance for our experimental collaborators to synthesize/grow a set of model heterostructures using advanced growth methods and to detect emergent mesoscale domain states to validate our predictions.

**References**

1. F. Xue, Y.J. Gu, L.Y. Liang, Y. Wang, and L.Q. Chen, *Orientations of low-energy domain walls in perovskites with oxygen octahedral tilts.* Physical Review B, 2014. **90**(22):220101
2. Y. Wang, C. Nelson, A. Melville, B. Winchester, S.L. Shang, Z.K. Liu, D.G. Schlom, X.Q. Pan, and L.Q. Chen, *$BiFeO_3$ Domain Wall Energies and Structures: A Combined Experimental and Density Functional Theory plus U Study.* Physical Review Letters, 2013. **110**(26):Unsp 267601
3. J. Britson, P. Gao, X.Q. Pan, and L.Q. Chen, *Phase field simulation of charged interface formation during ferroelectric switching.* Acta Materialia, 2016. **112**: p. 285-294
4. P. Gao, J. Britson, C.T. Nelson, J.R. Jokisaari, C. Duan, M. Trassin, S.H. Baek, H. Guo, L.Z. Li, Y.R. Wang, Y.H. Chu, A.M. Minor, C.B. Eom, R. Ramesh, L.Q. Chen, and X.Q. Pan, *Ferroelastic domain switching dynamics under electrical and mechanical excitations.* Nature Communications, 2014. **5**:3801
5. F. Xue, L.Z. Li, J. Britson, C. Adamo, Z.J. Hong, D.G. Schlom, X.Q. Pan, and L.Q. Chen, *Switching the curl of polarization vectors by an irrotational electric field.* Physical Review B Rapid Communications, 2016. **Under review**

**Publications**

1. C.S. Wang, X.X. Ke, J.J. Wang, R.R. Liang, Z.L. Luo, Y. Tian, D. Yi, Q.T. Zhang, J. Wang, X.F. Han, G. Van Tendeloo, L.Q. Chen, C.W. Nan, R. Ramesh, and J.X. Zhang, Ferroelastic switching in a layered-perovskite thin film. Nature Communications, 2016. 7:10636
2. R.K. Vasudevan, H. Khassaf, Y. Cao, S.J. Zhang, A. Tselev, B. Carmichael, M.B. Okatan, S. Jesse, L.Q. Chen, S.P. Alpay, S.V. Kalinin, and N. Bassiri-Gharb, Acoustic Detection of Phase Transitions at the Nanoscale. Advanced Functional Materials, 2016. 26(4): p. 478-486

3. J.M. Hu, T.N. Yang, K. Momeni, X.X. Cheng, L. Chen, S.M. Lei, S.J. Zhang, S. Trolier-McKinstry, V. Gopalan, G.P. Carman, C.W. Nan, and L.Q. Chen, Fast Magnetic Domain-Wall Motion in a Ring-Shaped Nanowire Driven by a Voltage. Nano Letters, 2016. 16(4): p. 2341-2348
4. H.Z. Guo, X.M. Liu, F. Xue, L.Q. Chen, W. Hong, and X.L. Tan, Disrupting long-range polar order with an electric field. Physical Review B, 2016. 93(17):174114
5. D. Edwards, S. Brewer, Y. Cao, S. Jesse, L.Q. Chen, S.V. Kalinin, A. Kumar, and N. Bassiri-Gharb, Local Probing of Ferroelectric and Ferroelastic Switching through Stress-Mediated Piezoelectric Spectroscopy. Advanced Materials Interfaces, 2016. 3(7):1500470
6. G.P. Cao, Y. Cao, H.B. Huang, L.Q. Chen, and X.Q. Ma, Analysis of multi-domain ferroelectric switching in BiFeO$_3$ thin film using phase-field method. Computational Materials Science, 2016. 115: p. 208-213
7. J. Britson, P. Gao, X.Q. Pan, and L.Q. Chen, Phase field simulation of charged interface formation during ferroelectric switching. Acta Materialia, 2016. 112: p. 285-294
8. F. Xue, L.Y. Liang, Y.J. Gu, I. Takeuchi, S.V. Kalinin, and L.Q. Chen, Composition- and pressure-induced ferroelectric to antiferroelectric phase transitions in Sm-doped BiFeO$_3$ system. Applied Physics Letters, 2015. 106(1):012903
9. B. Winchester, N. Balke, X.X. Cheng, A.N. Morozovska, S. Kalinin, and L.Q. Chen, Electroelastic fields in artificially created vortex cores in epitaxial BiFeO$_3$ thin films. Applied Physics Letters, 2015. 107(5):052903
10. Y. Wang, W.Y. Wang, L.Q. Chen, and Z.K. Liu, Bonding Charge Density from Atomic Perturbations. Journal of Computational Chemistry, 2015. 36(13): p. 1008-1014
11. K. Song, C.T. Koch, J.K. Lee, D.Y. Kim, J.K. Kim, A. Parvizi, W.Y. Jung, C.G. Park, H.J. Jeong, H.S. Kim, Y. Cao, T.N. Yang, L.Q. Chen, and S.H. Oh, Correlative High-Resolution Mapping of Strain and Charge Density in a Strained Piezoelectric Multilayer. Advanced Materials Interfaces, 2015. 2(1):1400281
12. D.M. Marincel, H.R. Zhang, J. Britson, A. Belianinov, S. Jesse, S.V. Kalinin, L.Q. Chen, W.M. Rainforth, I.M. Reaney, C.A. Randall, and S. Trolier-McKinstry, Domain pinning near a single-grain boundary in tetragonal and rhombohedral lead zirconate titanate films. Physical Review B, 2015. 91(13):134113
13. X.H. Liu, Y. Wang, J.O. Sofo, T.J. Zhu, L.Q. Chen, and X.B. Zhao, First-principles studies of lattice dynamics and thermal properties of Mg$_2$Si$_{1-x}$Sn$_x$. Journal of Materials Research, 2015. 30(17): p. 2578-2584
14. Y.J. Li, J.J. Wang, J.C. Ye, X.X. Ke, G.Y. Gou, Y. Wei, F. Xue, J. Wang, C.S. Wang, R.C. Peng, X.L. Deng, Y. Yang, X.B. Ren, L.Q. Chen, C.W. Nan, and J.X. Zhang, Mechanical Switching of Nanoscale Multiferroic Phase Boundaries. Advanced Functional Materials, 2015. 25(22): p. 3405-3413
15. Q. Li, Y. Cao, P. Yu, R.K. Vasudevan, N. Laanait, A. Tselev, F. Xue, L.Q. Chen, P. Maksymovych, S.V. Kalinin, and N. Balke, Giant elastic tunability in strained BiFeO$_3$ near an electrically induced phase transition. Nature Communications, 2015. 6:8985

16. Y.J. Gu, Z.J. Hong, J. Britson, and L.Q. Chen, Nanoscale mechanical switching of ferroelectric polarization via flexoelectricity. Applied Physics Letters, 2015. 106(2):022904
17. Y. Cao, Q. Li, L.Q. Chen, and S.V. Kalinin, Coupling of electrical and mechanical switching in nanoscale ferroelectrics. Applied Physics Letters, 2015. 107(20):202905
18. Y. Cao, A.V. Ievlev, A.N. Morozovska, L.Q. Chen, S.V. Kalinin, and P. Maksymovych, Intrinsic space charge layers and field enhancement in ferroelectric nanojunctions. Applied Physics Letters, 2015. 107(2):022903
19. F. Xue, Y.J. Gu, L.Y. Liang, Y. Wang, and L.Q. Chen, Orientations of low-energy domain walls in perovskites with oxygen octahedral tilts. Physical Review B, 2014. 90(22):220101
20. Y. Wang, L.Q. Chen, and Z.K. Liu, YPHON: A package for calculating phonons of polar materials. Computer Physics Communications, 2014. 185(11): p. 2950-2968
21. Y.B. Wang, L.M. Peng, Y.Z. Ji, X.X. Cheng, N. Wang, Y. Zhao, Y.A. Fu, L.Q. Chen, and W.J. Ding, The effect of low cooling rates on dendrite morphology during directional solidification in Mg-Gd alloys: In situ X-ray radiographic observation. Materials Letters, 2016. 163: p. 218-221
22. Yi Wang, Shun-Li Shang, Huazhi Fang, Zi-Kui Liu, and Long-Qing Chen, First-principles calculations of lattice dynamics and thermal properties of polar solids. npj Computational Materials (2016) 2, 16006; doi:10.1038/npjcompumats.2016.6
23. L. Li, J.R. Britson, J.R. Jokisarri, Y. Zhang, C. Adamo, A. Melville, D.G. Schlom, L.Q. Chen, and X.Q. Pan, Giant resistive switching via control of ferroelectric charged domain walls. Advanced Materials, 2016, in press.
24. F. Xue, Y.J. Li, Y.J. Gu, J.X. Zhang, and L.Q. Chen, Strain-induced Mixed Phases in a Ferroelastic Film – Phase De-strain. Physical Review Letters, 2016. Under review
25. F. Xue, L.Z. Li, J. Britson, C. Adamo, Z.J. Hong, D.G. Schlom, X.Q. Pan, and L.Q. Chen, Switching the curl of polarization vectors by an irrotational electric field. Physical Review, Rapid Communications, 2016, Submitted.
26. Y.L. Tang, Y.L. Zhu, Z.J. Hong, L.Q. Chen, E.A. Eliseev, A.N. Morozovska, Y.J. Wang, Y. Liu, Y.B. Xu, S.J. Pennycook, and X.L. Ma, 3D polarization texture of a flux-closure quadrant in strained ferroelectric $PbTiO_3$ films. Journal of Materials Research, accepted
27. Z.J. Hong, A.R. Damodaran, F. Xue, J. Britson, A. Yadav, C.T. Nelson, J.J. Wang, L.W. Martin, R. Ramesh, and L.Q. Chen, Stability of Polar Vortex Lattice in Ferroelectric Superlattices,. Physical Review Letters, 2016, submitted.
28. Z.B. Chen, L. Hong, F.F. Wang, X.H. An, X.L. Wang, S.P. Ringer, L.Q. Chen, and X.Z. Liao, Ferroelastic domain switching by mechanical and electrical stimulation for non-volatile memories. Nature Communications, 2016. Under review.
29. J. Britson, *Phase Field Simulation of domain Switching Dynamics in Multi-Axial Lead Zirconate Titanate Thin Films*, in *Materials Science and Engineering*. 2015, The Pennsylvania State University.

# Combined microscopy studies of complex electronic materials

**David H. Cobden - Department of Physics, University of Washington, Seattle, WA 98195**

## Research Scope

The aim of this project is to determine and understand the electronic properties of correlated electronic materials which are only available as micron-scale samples or which contain microscopic inhomogeneity. They are metallic above room temperature and exhibit phenomena such as charge-density waves, superconductivity, magnetism, topological protection, metal-insulator transitions, excitonic insulation, and structural transitions at lower temperatures. Examples of current interest are $VO_2$, with its still mysterious metal-insulator and structural phase transitions; $WTe_{2-x}S_x$, combining superconductivity and nontrivial topology; $W_{1-x}Re_xTe_2$, a doped topological/Weyl semimetal; $NbSe_2$, in which density waves compete with superconductivity; and $FeSe_{1-x}Te_x$, which hosts superconductivity, antiferromagnetism and nematicity. We employ control of temperature, magnetic field, and mechanical strain, allied to multiple submicron scanning microscopies including photocurrent microscopy (SPCM), STEM, AFM, and μ-ARPES.

## Recent Progress

*1. Scanning photocurrent microscopy (SPCM).* Photocurrent provides many ways to study the spatially resolved optoelectronic and electrical properties of a material or device. Photocurrent generation may occur by separation of photo-generated electrons and holes in the presence of an electric field (in semiconductors); by momentum-asymmetric relaxation of the electron distribution function (in acentric materials); or by thermoelectric current driven by the light-induced temperature gradient (in inhomogeneous systems). As a focused laser spot, or a tip scattering light, is scanned the spatial variation of the photocurrent gives insights into the electronic processes, on a submicron scale, and this can be done on small samples or domains with a moderate amount of preparation involving attachment of just two contacts. SPCM can readily be performed at low temperatures, high magnetic fields, and on a stage which allows strain application.

In developing this technique we worked with simple and convenient graphene samples such as the one shown in Fig. 1A. It is known that at zero magnetic field photocurrent is of a photoelectric nature, the electrons rapidly reaching local thermal equilibrium under the laser spot leading to a temperature gradient within the sample. We found that in a perpendicular magnetic field B additional photocurrent is generated when the laser spot is near a free edge, with opposite sign at opposite edges and antisymmetric in B, as shown in Fig. 1C. We explained this as resulting from the Nernst effect, combined with the Shockley-Ramo nature of long-range photocurrent generation in a gapless material as discussed by Song and Levitov[1].

The temperature gradient $\nabla T$ near the laser spot produces a thermoelectric current density $\boldsymbol{j}_{\mathrm{th}} = -\overleftrightarrow{\alpha}\nabla T$ ($\overleftrightarrow{\alpha}$ is the thermoelectric tensor) whose transverse component $\boldsymbol{j}_N$ tends to circulate around the spot, as indicated in Fig. 1D. With the spot in the sample center there is no net current in the contacts by symmetry. With the spot near the edge the circulation is truncated and a net current is generated, as shown in Fig. 1E. A theorem by Song and Levitov, based on the Shockley-Ramo theorem, allows one to calculate $I_{ph}$ given the extrinsically generated current density $\boldsymbol{j}_{th}$ and the geometry of a conducting (not semiconducting) sample: $I_{ph} = \iint \boldsymbol{j}_{\mathrm{th}}.\nabla\psi\, dxdy$, where $\psi$ is an auxiliary scalar field such that $-(\overleftrightarrow{\rho}^{T})^{-1}\nabla\psi$ is the current distribution created when a unit bias is applied between the contacts at $\boldsymbol{j}_{\mathrm{th}} = 0$, and $\overleftrightarrow{\rho}$ is the 2D resistivity tensor. In a model with a simple rectangular sample the result reduces to $I_{ph} = \beta NB\rho_{xx}^{-1}\Delta T_{av}$ where $N$ is the Nernst coefficient, $\beta$ is a numerical factor, and $\Delta T_{av}$ is the average temperature difference between the two free edges. We used this to calculate the B-antisymmetric photocurrent as a function of laser position, plotted in Fig. 1F. The excellent agreement with the data in Fig. 1C constitutes the first quantitative application of the Song-Levitov result.

The “photo-Nernst” signal shows a peak as a function of gate voltage $V_g$ at the neutrality point, flanked by wings of opposite sign at low fields, and quantum oscillations at higher fields (not shown), all of which can be explained by the dependence of $N$ on Fermi energy $E_F$ and $B$ for graphene calculated from $\overleftrightarrow{\rho}$ using the Mott relation. This demonstrates how the photo-Nernst effect can be used to probe the electronics properties of a 2D material.

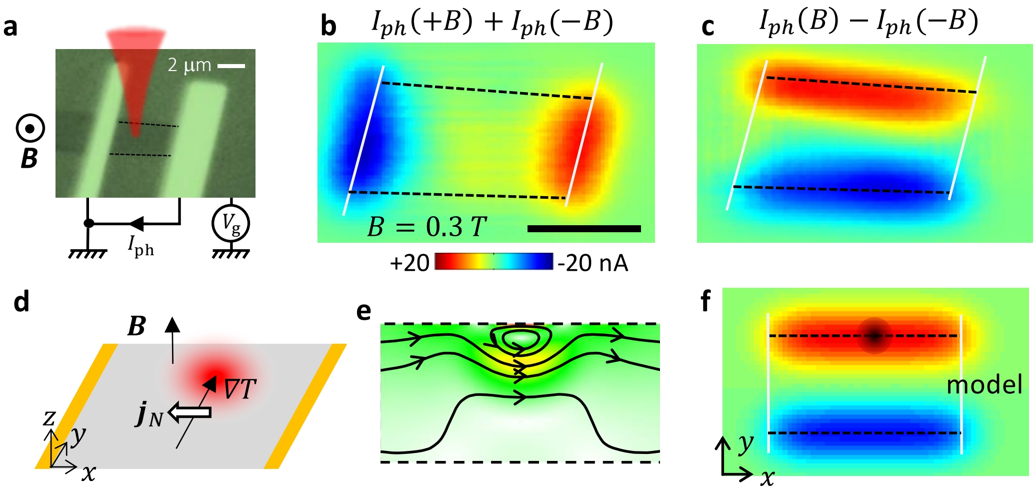

**Figure 1. a**, Optical image of a monolayer graphene device, with two gold contacts evaporated on top, on 290 nm SiO$_2$ with a conducting Si substrate at gate voltage $V_g$. The normal magnetic field B and application of a scanned laser spot ($\lambda$ = 632 nm, 40 µW) are indicated. **b** and **c**, color maps of the generated photocurrent $I_{ph}$ as a function of laser spot position at $B$ = 0.3 T, $V_g$ = +5 V. The B-symmetric component (**b**) is localized to the contacts edges (white lines), the B-antisymmetric component (**c**) to the free edges (dashed black lines). **d**, Picture for understanding the antisymmtric component in terms of a Nernst current density $j_N$. **e**, simulated current density in the sample with the (hot) laser spot near the upper edge. **f**, simulated map of the total photo-Nernst current as a function of laser position, for comparison with c, also indicating the position of the laser in e.

*2. Scanning angle-resolved photoemision (µ-ARPES).* In principle ARPES is ideal for determining the full band structures of layered and 2D materials, and it has been used successfully on 2D films that can be grown as a single crystal over a large area. However, the X-ray spot size is typically much larger than the few-micron sizes of typical exfoliated sheets, grains in vapor-deposition grown layers, or the interesting regions of more complex heterostructures. Recently some beamlines have been equipped with micro- or nano-ARPES capability but until now the spectral resolution in these systems was no better than ~0.5 eV. To determine the detailed electronic properties of layered materials by ARPES an order of magnitude better spectral resolution is needed. We have demonstrated this resolution for the first time using the Nanospectroscopy beamline at Elettra, Trieste by focusing on sample design and preparation. The key requirements are (a) dry transfer onto an exfoliated graphite flake to act as an ultra-flat conducting substrate, and (b) use of a monolayer graphene or hBN cap to allow annealing at up to 400 °C in the ARPES chamber to remove surface contaminants and to prevent oxidation and decomposition during preparation and annealing of these air-sensitive materials. The cap moderately attenuates the signal but does not distort the spectrum because its bands are far in k-space from the those of the sandwiched material. In the chamber we can easily locate the sample and obtain spectra with ~50 meV resolution from any point localized to less than a micron.

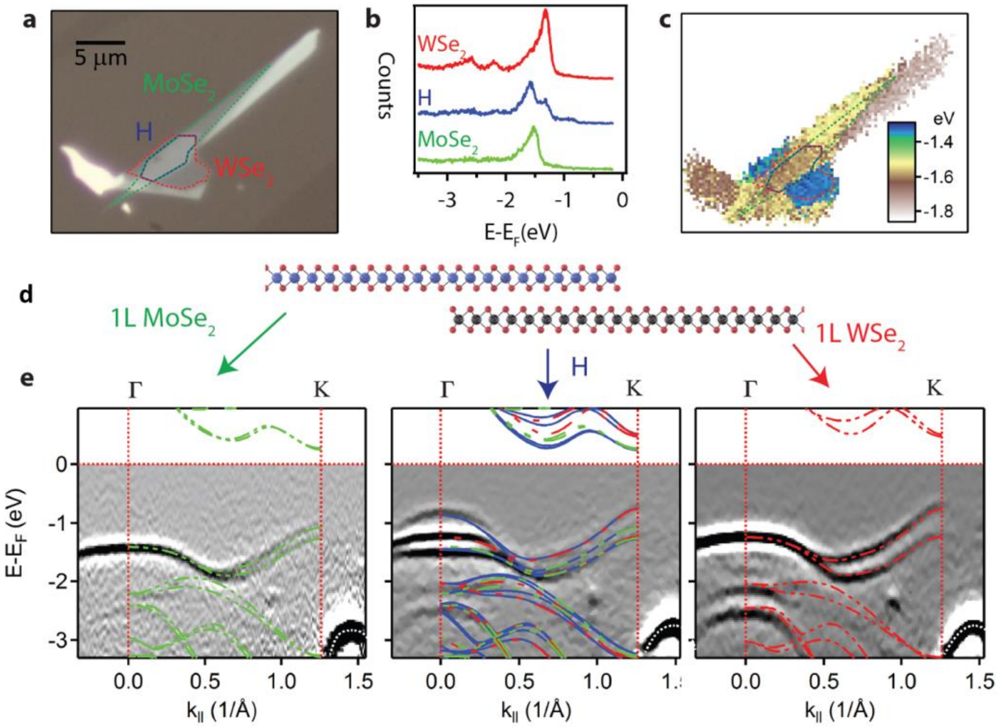

**Figure 2. a**, Optical image showing monolayer (1L) MoSe$_2$ and WSe$_2$ sheets which overlap (MoSe$_2$ on top), in an heterobilayer region (H) with a twist angle of a few degrees. Their boundaries are indicated with color-coded dotted lines. The substrate is a graphite flake and a graphene sheet caps the entire structure. **b**, Angle-integrated spectra in each of the three regions. **c**, Map of the energy of maximum emission, which is different for each of H, 1L MoSe$_2$ and 1L WSe$_2$. **d,** Schematic side view of heterobilayer. **e**, Momentum slices along $\Gamma - \mathrm{K}$ in the three regions (plotted is the intensity differentiated twice with respect to energy). Superposed dashed lines are DFT calculations for 1L MoSe$_2$ (green), 1L WSe$_2$ (red), and commensurate H (blue). The valence band of the graphene cap is indicated by a white dotted line in the bottom right of each plot.

The usefulness of μ-ARPES is seen for the case of WSe$_2$/MoSe$_2$ heterobilayers illustrated in Fig. 2. These 2D semiconductor heterostructures are of interest for optoelectronics, hosting long-lived interlayer valley excitons. Fig. 2b compares the momentum-integrated spectra at points in monolayer and heterobilayer regions. One can also obtain scanning photoemission (SPEM) images and obtain spatial maps with large contrast, for example by plotting the energy of peak emission (Fig. 2c). The valence band offset, not known before, is read off to be 300±30 meV. The different spin-orbit splittings at K in the two semiconductors are easily resolved (Fig 2e), and we observe hybridization at Γ but not at K, consistent with DFT predictions. An additional fainter third band can be seen near Γ in the heterobilayer region only. This is due to the existence of commensurate domains, where hybridization is stronger, mixed with incommensurate domains in the bilayer due to the misalignment and different lattice constants.

### Future Plans

We will apply photocurrent microscopy, μ-ARPES, and scanning-probe microscopy to layered correlated materials. We will need to fabricate suitable hBN-encapsulated van der Waals heterostructures from air-unstable FeSe, $NbSe_2$, $WTe_2$ and their cousins by dry transfer in a glove box. Building on our experience with $VO_2$ nanobeams we will also continue to develop apparatus for applying strain to small crystals at low temperatures, combined with microscopy-compatible sample geometry and stages. The goal remains to control and study electronic phase transitions.

### Acknowledgements

The 2D materials and photocurrent work is in collaboration with Xiaodong Xu (University of Washington). The μ-ARPES work is in collaboration with Neil Wilson (University of Warwick).

### References

1 J.C.W. Song and L.S. Levitov, "Shockley-Ramo theorem and long-range photocurrent response in gapless materials", Physical Review B **90**, 6, 075415 (2014).

### Publications with DoE ESPM support

"Band parameters and hybridization in 2D semiconductor heterostructures from photoemission spectroscopy", Neil R. Wilson, Paul V. Nguyen, Kyle Seyler, Pasqual Rivera, Alexander J. Marsden, Zachary P.L. Laker, Gabriel C. Constantinescu, Viktor Kandyba, Alexei Barinov, Nicholas D.M. Hine, Xiaodong Xu, and David H Cobden, submitted, http://arxiv.org/abs/1601.05865.

"Interlayer Exciton Optoelectronics in a 2D Heterostructure p-n Junction", Jason Ross, Pasqual Rivera, John Schaibley, Eric Wong, Hongyi Yu, Takashi Taniguchi, Kenji Watanabe, Jiaqiang Yan, David Mandrus, David Cobden, Wang Yao, Xiaodong Xu, submitted.

“Visualization of one-dimensional diffusion and spontaneous segregation of hydrogen in single crystals of $VO_2$" by T. Serkan Kasirga, Jim Coy, Jae H. Park, and David H. Cobden, Nanotechnology, to appear (2016), http://arxiv.org/abs/1606.08311.

“Ultrafast Nanoimaging of the Photoinduced Phase Transition Dynamics in $VO_2$”, S.A. Donges, O. Khatib, B.T. O'Callahan, J.M. Atkin, J.H. Park, D.H. Cobden, M.B. Raschke, Nano Lett 16 5 3029-3035.

"Photo-Nernst current in graphene", Helin Cao, Grant Aivazian, Jason Ross, Zaiyao Fei, David Cobden, and Xiaodong Xu, Nature Physics 12, 236 (2016); arXiv: cond-matt 1510.00765.

"Inhomogeneity in the ultrafast insulator-to-metal transition in $VO_2$", B.T. O'Callahan, A.C. Jones, J.H. Park, D.H. Cobden, J.M. Atkin, and M.B. Raschke, Nature Communications 6, 6849 (2015).

"Magnetic Control of Valley Pseudospin in Monolayer $WSe_2$", Grant Aivazian, Zhirui Gong, Aaron M Jones, Rui-Lin Chu, Jiaqiang Yan, David G Mandrus, Chuanwei Zhang, David Cobden, Wang Yao, Xiaodong Xu, Nature Physics 11, 148 (2015). doi:10.1038/nphys3201. arXiv:cond-matt 1407.2645.

# Probing Vibrational and Electronic Excitations on Photocatalytic Nanoparticles for Solar Fuel Generation

**Principle Investigator: Peter A. Crozier**
**School for Engineering of Matter, Transport and Energy, Arizona State University, Tempe, AZ 85287-6106**
**Email: crozier@asu.edu**

## Program Scope

We are investigating the structure and evolution of heterostructured semiconductor-based materials for $H_2$ generation via photocatalytic water splitting. Our catalysts are composite materials consisting of light harvesting semiconductors supporting catalytic nanoparticles that facilitate the transfer of excited electrons/holes for water reduction/oxidation. Light harvesting oxides and nitrides which may be functionalized with metal and metal oxide nanoparticles yielding model systems which are active under ultraviolet or visible light are the primary focus of this project. The local electronic surface structure of these materials is explored using vibrational and valence excitations with electron energy-loss spectroscopy (EELS). *In situ* approaches for performing spectroscopic analysis under photoreaction conditions are also under development.

## Recent Progress

***Probing Nanoparticle Surfaces with Localized Vibrational Spectroscopy:*** Recent advances in monochromated EELS (the Nion UltraSTEM) allowed us to probe vibrational excitations for the first time in the scanning transmission electron microscope (STEM) [1]. We are now applying this new technique to investigate water adsorbates on the surfaces of nanoparticles. Our recent work has demonstrated that we can detect and differentiate between the vibrational fingerprints from hydroxides and hydrates [7]. ***Figure 1a*** compares the vibrational energy-loss spectrum recorder from a hydrate with the IR spectrum from the same materials. The broad peak at 3500 $cm^{-1}$ (430 meV) is similar in both spectra and is the classic finger print for $H_2O$. Hydrate and hydroxide species are damaged rapidly by the electron beam. However, the vibrational EELS signal is delocalized over 10s of nanometers (for the conditions of our experiment) allowing the so-call *aloof beam* form of

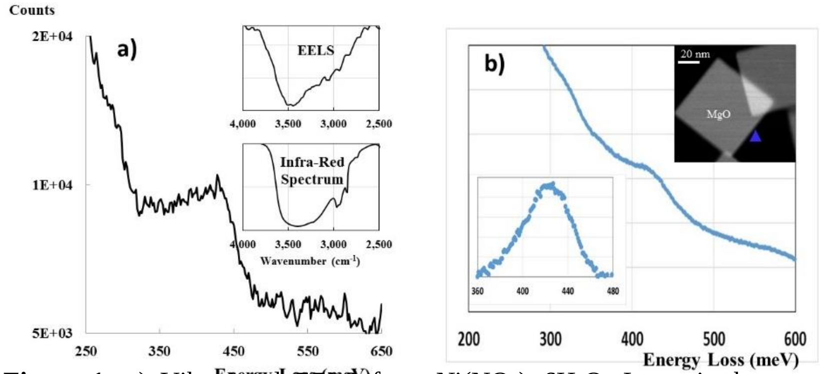

***Figure 1*****:** **a**) Vibrational EELS from $Ni(NO_3)_2.6H_2O$. Insert is the same plotted against wavenumber and the comparison with IR. **b**) MgO image and aloof beam vibrational spectrum showing peak at 430 meV indicating thin hydrate layer on (100) facet.

spectroscopy to be employed. In aloof-beam EELS, the focused electron beam is positioned 2 – 10 nm outside the sample surface. This greatly reduces radiation damage while still allowing the surface to be probe via vibrational excitations. ***Figure 1b*** shows an example of using aloof beam EELS to probe the surface chemistry of a 60 nm particle of MgO. In this case, the MgO was briefly exposed to water vapor before insertion into the TEM. The aloof beam spectrum from a particular (100) facet shows at peak at 430 meV demonstrating that the water is present on the surface of the MgO in the form of a thin layer of magnesium hydrate [7].

***Vibrational Spectroscopy Fingerprinting of Carbon Nitride Materials:*** Graphitic carbon nitrides, which are based on heptazine ($C_6N_7$) building blocks, and poly(traizine imides) with intercalated Li and Cl ions (or PTI/LiCl) are recently discovered non-metal visible-light photocatalytic materials active for solar-hydrogen production. We have demonstrated that by using monochromated EELS, we can differentiate between heptazine-based and triazine-based carbon nitrides solely on their vibrational spectra. Moreover, using the aloof-beam geometry reduces specimen damage while maintaining signal. ***Figure 2*** shows vibrational EELS from a commercial graphitic carbon nitride and a PTI/LiCl material that we synthesized at ASU. To better interpret this novel data, we have also collected infrared absorbance spectra and simulated the reduced energy resolution with a simple Gaussian convolution. By convoluting the FTIR absorbance with a Gaussian of 16 meV full-width at half-max (consistent with experimental energy resolution), there is agreement in the peak positions and shape, which corroborates the similarity of these different techniques.

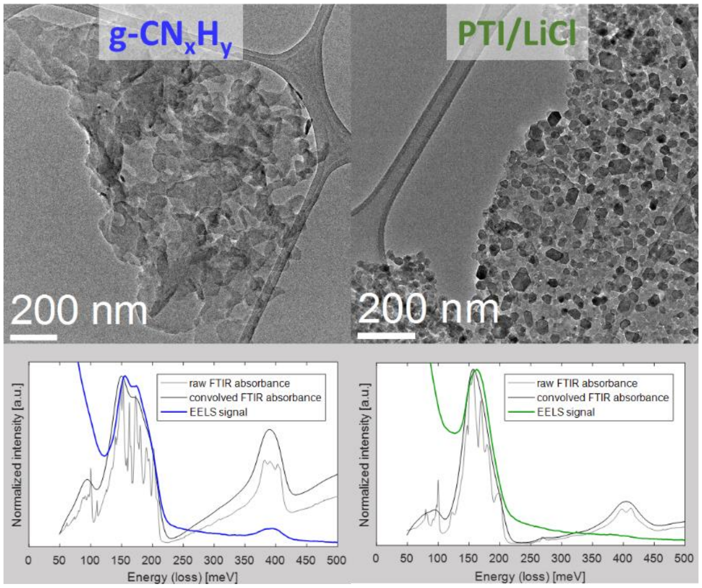

***Figure 2***: Vibrational EELS spectra for heptazine-based graphitic carbon nitride (blue curve, left) and triazine-based crystalline carbon nitride (green curve, right) with ZLP-convolved infrared absorbance spectra. Low-mag TEM images for each sample are shown above.

***Probing Electronic Structure on Oxide Nanoparticles:*** Charge transfer processes play a central role in many energy conversion processes. In catalytic materials, charge transfer between the particle surface and adsorbate species drives chemical conversion processes. On oxide surfaces, defects can give rise to surface states within the bandgap which may serve as electron or hole traps. These states may play a critical role in controlling both the thermodynamics and kinetics of charge transfer processes. Developing approaches to probe these states under *in situ* and *operando* conditions will provide insights for tailoring the surface properties of nanoparticles for photocatalytic functionality. We have been using aloof beam valence-loss EELS to investigate

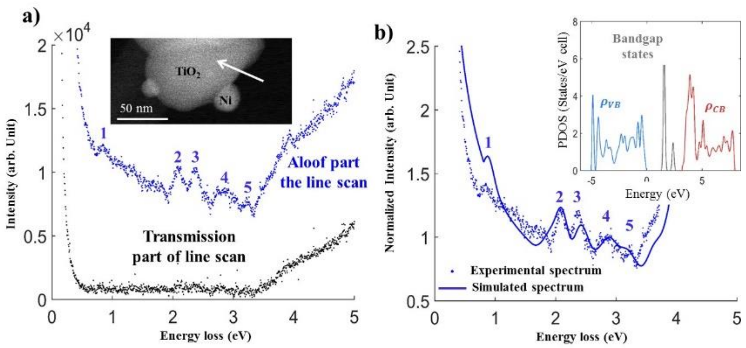

***Figure 3***: a) Transmission and aloof beam spectrum from anatase nanoparticle of Ni/$TiO_2$ photocatalyst show peaks (numbered) in bandgap region. b) Simulated spectrum (solid line) to aloof beam EELS. The insert shows the density of states which matches the experimental spectrum.

states within the bandgap on nanoparticle oxide surfaces [8]. Dielectric theory and density of states calculations are employed to interpret the spectra in terms of surface layers and bandgap states. ***Figure 3*** shows transmission and aloof beam spectra from a titania based catalyst employed in water splitting. The transmission spectrum shows the usual 3.2 eV bandgap but the aloof beam spectrum shows a series of peaks in the visible region below the conduction band edge. The peaks arise in part from electronic states within the bandgap. The energy-loss spectrum can be interpreted using a joint density of states approach in which the width and position of the surface states can be determine by optimizing the fit between the simulation and experiment. In this case, the peaks labeled 1–5 can be fitted by inserting bandgap states at 1.8 and 2.5eV above the valence band edge [8]. Other phenomena such as excitons, Cerenkov and transition radiation are also under investigation since they can also contribute to the intensity below the bandgap.

***In Situ Probing of Electronic Structure under Photoreaction Conditions:*** To investigate changes in surface electronic structure with photoreaction conditions it is necessary to install a light source in our FEI Titan environmental TEM. We have designed and build an *in situ* illumination system based on an optical fiber system (see ***Figure 4a***). We are able to illuminate the sample with a variety of different wavelengths and intensities to simulate solar and concentrated solar conditions. The structural changes taking place on the surface of anatase nanoparticles during exposure to UV light and water are shown in ***Figure 4b***. The disordered layer is associated with hydroxylation of the oxide surface triggered by the presence of light induced oxygen vacancies on the surface.

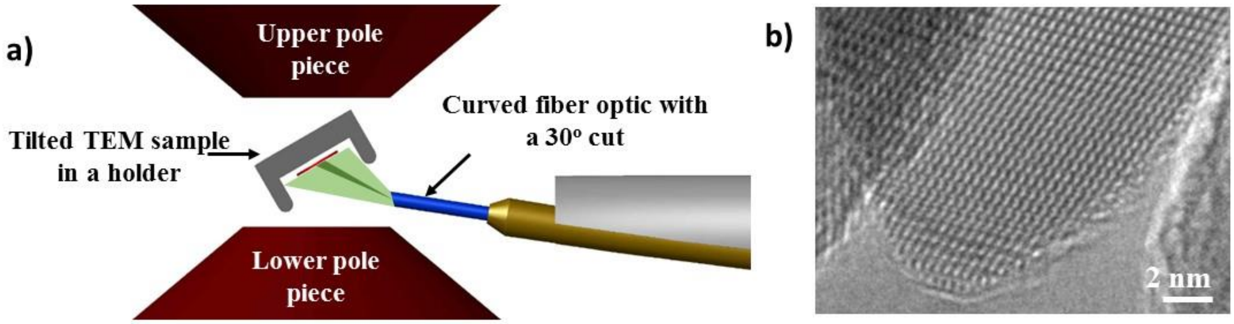

***Figure 4***: a) Schematic diagram of light source installed in FEI Titan ETEM b) High resolution image of surface of anatase particle after exposure to water and UV light. The disordered layer is associated with hydroxylation.

## Future Plans

*Ultra-high Energy Resolution EELS*: We will apply aloof beam EELS to locally probe the surfaces the oxide and nitride photocatalysts. With vibrational EELS will provide information on local hydrate and hydroxide species on nanoparticles surface facets. Valence loss EELS will provide information on defect states within in the bandgap. To correctly interpret the EELS data, we will perform relativistic calculations of the aloof beam spectra which take both Cerenkov and transition radiation effects into account. *In Situ Observations:* The surfaces of oxide nanoparticles will be strongly modified under photoreaction conditions. Under photon excitation, hole migration to the surface will give rise to oxygen vacancy formation which may react with water leading to surface hydroxylation. *In situ* aloof beam valence loss EELS will be performed to follow the evolution of the oxide surfaces under changing reaction conditions. The long-term goal if this work is to correlated catalyst structure with reactivity. The *in situ* spectroscopy and imaging observations will be correlated with *ex situ* reactor work on water splitting. Finite element simulations will be carried out to explore the feasibility of *operando* TEM for photocatalytic measurement.

## Publications Supported by BES (2014- 2016)

1) O.L. Krivanek, T.C. Lovejoy, N. Dellby, T. Aoki, R. W. Carpenter, P. Rez, E. Soignard, J. Zhu, P.E. Batson, M.J. Lagos, R. F. Egerton, and P.A., Crozier (2014). "*Vibrational spectroscopy in the electron microscope*". Nature 514, 209-212.
2) P.A. Crozier and T.W. Hansen (2015). "*In situ and operando transmission electron microscopy of catalytic materials*", MRS Bulletin, 40, 38-45.
3) Q. Liu, L. Zhang, and P.A. Crozier (2015). "*Structure-reactivity relationships of Ni-NiO core-shell co-catalysts on* $Ta_2O_5$ *for solar hydrogen production*", Applied Catalysis B: Environmental, 172, 58-64.
4) L. Zhang, Q. Liu, T. Aoki, and P.A. Crozier (2015). "*Photocorrosion of Ni/NiO Core/Shell Structures on* $TiO_2$ *for Water Splitting*", J. Phys. Chem. C, 119: 7207-7214.
5) P. A. Crozier and B. K. Miller, (2015), "*Spectroscopy of Solids, Gases and Liquids in the ETEM*" in Controlled Atmosphere Transmission Electron Microscopy (Eds. T. W. Hansen and J. B. Wagner), New York, Springer.
6) Candace K. Chan, Tuysuz Harun, Artur Braun, Chinmoy Ranjan, Fabio La Mantia, Benjamin K. Miller, Liuxian Zhang, Peter A. Crozier, Joel A. Haber, John M. Gregoire, Hyun S. Park, Adam S. Batchellor, Lena Trotochaud, and Shannon W. Boettcher, (2015). "*Advanced and In Situ Analytical Methods for Solar Fuel Materials*", in Topics in Current Chemistry: Solar Energy for Fuels. Switzerland, Springer International Publishing
7) P. A., Crozier, T. Aoki and Q. Liu (2016). "Nanoscale Detection of Water and Its Derivatives on Surfaces using Subnanometer Focused Electron Beams" Ultramicroscopy, 169: 30-36.
8) Q. Liu, K. March, and P.A. Crozier (2016). "Nanoscale Probing of Bandgap States on Oxide Particles Using Electron Energy-Loss Spectroscopy", Ultramicroscopy (in press).
9) F. Tao and P. A. Crozier (2016). "Atomic-Scale Observations of Catalyst Structures under Reaction Conditions and during Catalysis." Chemical Reviews (Impact Factor 46), 116(6): 3487-3539.

# Development of flexible in situ electrochemical cell for surface sensitive techniques; XPS, AES, SEM, and AFM

**Shen J. Dillon, University of Illinois at Urbana-Champaign**

## Research Scope

In our earlier work on this project, we developed in situ liquid cell TEM testing for Li-ion batteries in order to characterize changes in structure and chemistry with high spatial and temporal resolution. These capabilities are critical for both providing fundamental insights into reaction mechanisms and the nature of electrode degradation necessary to guide design of next generation high energy density batteries. While our group and others have reported results of such liquid cell experiments, the sensitivity of the electrolyte to the electron beam imposes significant barriers to acquiring the desired quality of imaging and spectroscopy. Open cell experiments have provided much more insights into electrochemical reactions and associated changes in structure and chemistry. However, they have not been implemented in a manner that provides good electrochemical I-V response useful for relating the in situ data to the function of real cells. Our recent efforts have focused on re-designing open cell experiments to provide high quality electrochemical data along with access to high-resolution imaging and spectroscopy. In the process, we developed a flexible approach that can be utilized for in situ and operando across multiple characterization platforms. To date, we have applied the approach to characterizing reaction and degradation mechanisms in high capacity anode materials and hope to extend the approach to characterizing high capacity cathodes.

## Recent Progress

We have applied the new open cell design to understanding the contribution of deformation creep to the fracture of high capacity Sn electrodes, understanding the mechanism for Li dendrite growth, and characterizing the chemistry of conversion reactions in CuO. The cell has been demonstrated in the SEM, TEM, AES, and XPS. This work includes the first application of in situ XPS and AES to study particle based electrodes during Li-ion cycling. These techniques are very powerful for understanding oxidation state, bonding, and compositional changes during Li-ion cycling that provide fundamental insights into reaction and degradation mechanisms.

Here we highlight recent progress associated with in situ testing of CuO conversion reaction anode materials. Some of the text here is reproduced from reference 1. The insertion of Li into Cu oxide should proceed via at least a two-step process;

$$2Li + 2CuO \Rightarrow Li_2O + Cu_2O \qquad (1)$$

$$2Li + Cu_2O \Rightarrow Li_2O + 2Cu \qquad (2)$$

providing a theoretical capacity of 674 mAh $g^{-1}$. Cyclic voltammetry (CV) measured *in situ* is shown in Figure 1. Distinct peaks associated with each step prompted us to study Li insertion at 1.2 V and 0.1V, and Li extraction at 4.5 V. To demonstrate the function of this electrochemical cell, we first cycled it in a SEM (figure 2). The volumetric strain (≈88% volume or 23% linear theoretical) associated with Li insertion into CuO and the conversion reaction at 0.1 V versus Li clearly occurs amongst the nanoparticle agglomerates.

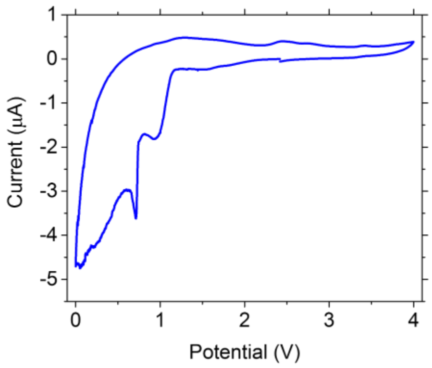

Figure 1. Cyclic voltammetry of high concentration CuO electrode measured in situ at a scan rate of 0.1mV/s.

We focus primarily on the Cu peak since the signal results only from the particles and provides useful bonding information. Figure 3 provides XPS spectra for the electrode equilibrated at different potentials. The data for Cu are in agreement with prior reports where Cu $2p_{3/2}$ occurs at 933.7 eV and Cu $2p_{1/2}$ at 953.7 eV. The satellite peaks at 940.7 eV and 943.7 eV indicate $Cu^{2+}$. After constant voltage lithiation at 1.2 V for 1.5 h, the heights of the satellite peaks reduce and the ratio of the Cu $2p_{3/2}$ to its $Cu^{2+}$ satellite increases by a factor of 2 signifying a reaction from $Cu^{2+}$ to $Cu^{+}$. The Cu $2p_{3/2}$ also shifts from 933.7 eV to 933.1 eV, which is also evidence of $Cu_2O$ formation. The O peak originates from both the particles and adsorption on the carbon (see figure S4). The O 1s peak initially at 529.6 eV corresponds to the oxygen in the CuO lattice, while the peak at 533.6 eV is consistent with C-O. The O 1s peak at 532.2 eV suggests the presence of $OH^{-}$. Lithiation at 1.2 V does not significantly affect the oxygen peak intensity or energy, but the C-O peak was no longer observable. The C-O peak indicates the presences of absorbed oxygen and water.

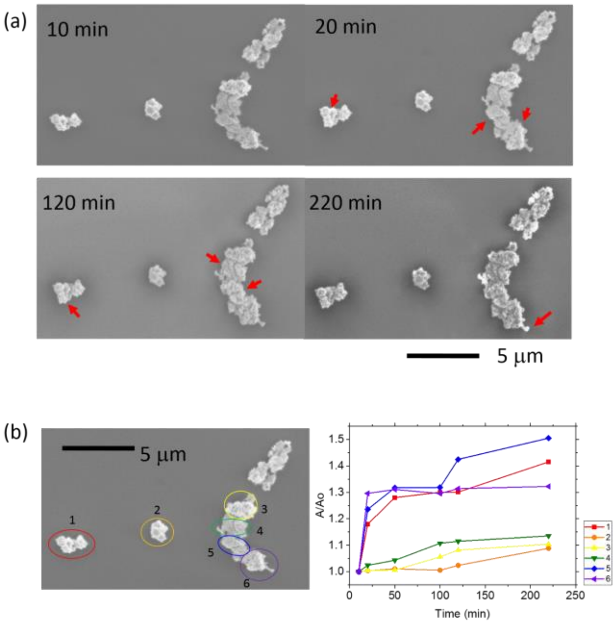

Figure 2. (a) Sequential SEM images of CuO nanoparticle agglomerates under galvanic charging at 0.1 V. The red arrows indicate the expansion. (b) Areal strain of six selected areas vs. charging time.

After lithiation at 0.1 V for 1 hr the Cu peak intensities are further reduced and the $Cu^{2+}$ satellite peaks are not observable. The reduction in Cu peak intensity should correlate with the formation of $Li_2O$ rich material at the surface. The Cu $2p_{3/2}$ now falls at 931.4 eV, consistent with $Cu^{o}$. The O 1s peak in the initial CuO lattice has disappeared, indicating CuO has reduced

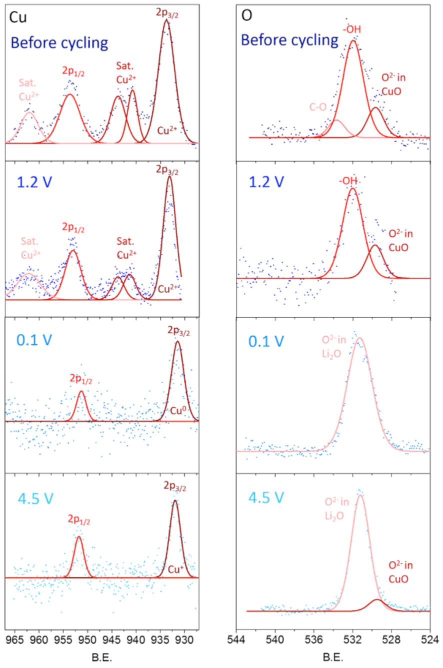

Figure 3. In-situ XPS analyses of the Cu 2p and O 1s core peaks performed onto CuO electrode at different stages.

to other Cu species, which agrees with the Cu 2p analysis. The new O 1s peak shown at 531.2 eV indicates $Li_2O$ formation. All of the O initially present in CuO, as OH, and as C-O reacts to form $Li_2O$.

The presence of O in the carbon impedes compositional analysis, motivating our use of *in situ* AES to characterize the composition of individual particle agglomerates. Figure 4 provides the raw spectra and Table I summarizes the results. The initial lithiation at 1.2 V only slightly reduces the surface O concentration, likely due to the initial reduction reaction. The results correlate well with the XPS data where the intensity and signal to noise during the 1.2 V lithiation step remain comparable to the pristine material. The Li signal is not yet detectable at 1.2 V, due to the limited sensitivity of AES to Li. However, after lithiation at 0.1 V, the Cu concentration reduces to 26%, while the Li and O concentrations are 24% and 50% consistent with $Li_2O$ formation.

Delithiation at 4.5 V for 8 h indicates that the reaction is partially reversible. The Cu does not fully return to $Cu^{2+}$, where $Cu^{+}$ instead dominates the chemistry. We verified this using the modified Auger parameter which is the sum of the kinetic energy of the Cu $L_3M_{45}M_{45}$ Auger transition and the binding energy of the Cu $2p_{3/2}$ photoelectron line, 916.07 + 931.91 = 1847.99 eV, the result of which denotes $Cu^{+}$ bonding, 1848 eV. The CuO peak also re-emerges at 529.5 eV. AES also indicated remnant Li at the surface of the particles after delithiation. This may correspond with disorder $Li_2O$ containing surficial films observed on conversion electrodes *via* transmission electron microscopy.

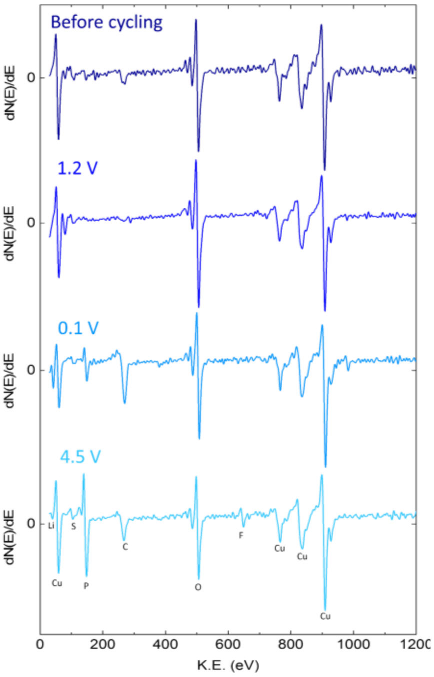

Figure 4. In-situ AES analyses performed on the CuO electrode at different stages.

## Future Plans

We have preliminarily applied our in situ open cell approach to TEM, but some issues still remain to optimize the geometry for ideal imaging conditions. We are also in the process of demonstrating the platform for in situ AFM testing. We are excited about the possibility of having a single in situ test platform that can be utilized across a range of characterization techniques that provide complementary information.

We also intend to apply the techniques developed in this program to study anionic redox in next-generation high capacity cathode materials. Specifically, we are interested in understanding the competition between oxygen evolution reactions and oxygen reduction reactions at high potentials. The combination of in situ liquid cell tests and in situ open cell tests enables us to access new information about chemical bonding, composition, and structure. Better fundamental understanding of these phenomena will enable the development of new high energy density batteries.

## Publications

(1) Tang, C.-Y., R. Haash, and S.J. dillon, *Operando X-ray Photoelectron Spectroscopy Study of the Conversion Reaction in CuO upon Lithiation.* In preparation.

(2) Tang, C.-Y. and S.J. Dillon, *In Situ Scanning Electron Microscopy Characterization of the Mechanism for Li Dendrite Growth.* Journal of The Electrochemical Society, 2016. **163**: p. A1660-A1665.

(3) Noh, K.W., K. Tai, S. Mao, and S.J. Dillon, *Grain Boundary Parting Limit during Dealloying.* Adv. Eng. Mater., 2015. **17**: p. 157-161.

(4) Huang, B., K. Tai, and S.J. Dillon, *Structural evolution of α-Fe2O3 nanowires during lithiation and delithiation.* J. Power Sources, 2014. **245**: p. 308-314.

(5) Huang, B., K. Tai, M. Zhang, Y. Xiao, and S.J. Dillon, *Comparative Study of Li and Na Electrochemical Reactions with Iron Oxide Nanowires.* Electrochim. Acta, 2014. **118**: p. 143-149.

(6) Barai, P., B. Huang, S.J. Dillon, and P.P. Mukherjee, *Mechano-electrochemical Interaction and Strain Relaxation in Sn Electrodes.* Submitted.

# Spin Polarized STM and STS of hybrid interface states at organic semiconductor interfaces

**Daniel B. Dougherty, Department of Physics, North Carolina State University**

## Research Scope

The project applies spin polarized scanning tunneling microscopy to the problem of interactions between organic semiconductors and substrates of interest for spintronic devices. The goal is to identify spin dependent interfacial interactions that can control spin injection.

## Recent Progress

### 1) Tuning Interfacial Spin Filter from Metallic to Resistive

In the past year, we have obtained the first SPSTM data on the "fruitfly" of the organic spintronics world: the Alq3 molecule (tris-(8-hydroxyquinolate)-aluminum, Figure 1). This was the first organic to hint at "giant" magnetoresistive effects in 2004 [1] and a steady stream of remarkable but poorly understood effects has continued for years [2]. Consensus has certainly been reached that interfaces are the deciding factor in the operation of these devices, but careful model experiments are needed to help understand the microscopic details of interfacial properties. To this end, we applied to spin polarized scanning tunneling microscopy with single molecule resolution to the Alq3 molecule and its variants.

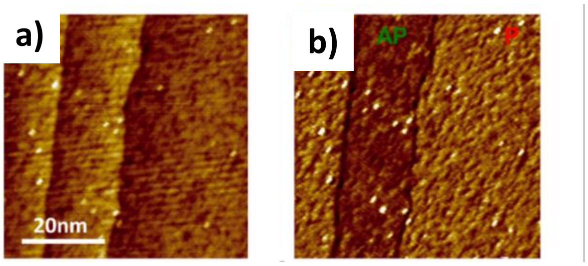

**Figure 1.** a) SPSTM topographic image showing bright protrusions that are individual Alq3 molecules; b) Conductance map corresponding to a) where spin contrast is seen across adjacent substrate terraces.

We have observed a stunning sensitivity of spin polarized interface state properties to the details of molecular orbitals. In the case of Alq3 adsorbed on a Cr(001) surface (Figure 2b) we find an indirect interaction with the low energy magnetic surface state similar to that identified in an earlier experiments in this project [3]. However, now we have added spin resolution to the tunneling spectroscopy measurement and find that the indirect interaction imprints a spin imbalance in the molecular orbital-modified states at the interface. In addition, the proximity of this state overlaps with the Fermi level and the Cr surface state leading to an enhancement of spin polarization at the Fermi level. Such an interfacial electronic structure is the canonical "metallic" spin filter.

Next, we made a subtle change to the adsorbate by replacing the $Al^{3+}$ in Alq3 by $Cr^{3+}$ to make Crq3 (with the synthetic help of local Chemistry collaborator Professor Phil Castellano). This paramagnetic variant of the Alq3 fruitfly is very similar in structure and remarkably even its lowest energy orbitals are quite similar. In particular, they are dominantly localized on the quinolate ligands and contain in addition just a small contribution from d-orbitals on the $Cr^{3+}$ center that is not present in Alq3 (insets of Figure 2b and 2c). Surprisingly, this small difference is enough to change the nature of the interface states qualitatively. Rather than an indirect interaction leaving the Cr(001) surface state present and un-shifted in energy, the Crq3 molecule participates in direct orbital overlap with the surface state. The result is a gap at the Fermi level and symmetrically located interface states centered around the original bare surface state, analogous to bonding and antibonding molecular orbitals. Rather than a metallic interface state (at the Fermi level), only a small change to the molecular adsorbate has resulted in a "resistive" spin polarized interface.

The observation of these new spin-dependent interaction mechanisms have been enabled by the development of very robust bulk Cr SPSTM probe trips in our lab. These allow magnetic sensitivity to be regained after numerous required in-situ tip processing steps that eventually result in probes that are stable to spectroscopic measurements such as shown in Figure 2. With magnetic film coatings, such processing rapidly degrades the probe's spin polarization and measurements such as

Collaborators in the Materials Science and Engineering department at the University of Utah have carried out ab initio density functional theory calculations to clarify the microscopic nature of the new interfacial effects seen in our SPSTM studies. They find that the Crq3 variant interacts more strongly with the surface than the more common Alq3 and that it directly mixes with the surface. Moreover, we find that the molecules are antiferromagnetically aligned with the local surface magnetization.

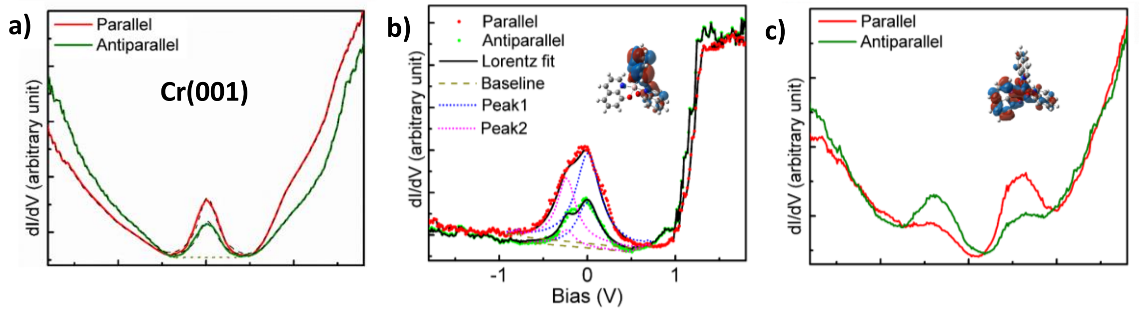

**Figure 2.** a) Spin asymmetric local tunneling spectra measured on different terraces of the clean Cr(001) surface; b) Local spectra measured on single Alq3 molecules showing enhanced spin asymmetry near the Fermi level; c) Local spectra measured on single Crq3 molecules showing a gap opening near the Fermi level with spin dependent peak intensities above and below. Insets show schematics of the lowest unoccupied molecular orbital for each molecule.

### 2) Hybrid Molecule-Substrate Interface States at Topological Insulator Surfaces

In related experiments, we have searched for spin polarized interface states when magnetic molecules are adsorbed on topological insulator surfaces. The goal is to identify spin-dependent interactions between the molecules and the spin textured topological surface state. The consequences of such interactions have been predicted to be only observable by SPSSTM measurements [4].

Our attention for most of this project has focused on the paramagnetic molecule manganese phthalocyanine (MnPc, with a high spin moment of S=3/2). Other groups have also searched for interfacial coupling effects and found unusually complicated behavior where molecules form a disordered first layer [5]. Despite relatively strong adsorption interactions in these studies, no evidence was found for direct interactions with the spin textured topological surface states.

Our project proceeded initially independently of other groups around the world. We identified new interface states (not discussed by other groups) with both spin-averaged STM and STS as well as complementary photoelectron spectroscopy studies (Figure 3). These non-dispersive states arise with increasing molecular coverage on the surface and are correlated with the onset of local molecular ordering (STM in Figure 3f) that was not observed in previous reports. This is an interesting and complex interfacial electronic structure that adds to the growing list of interface states at molecule-topological insulator surfaces [6]. Unfortunately, magnetic information about these states has not been accessible due to the relative instability of the molecule to local tunneling spectroscopy measurements. In fact, we hypothesize that the new state is not magnetic since it is far in energy from the topological surface states that might imprint a magnetic character. For this reason, despite interesting side observations, we consider molecule –TI interfaces non-ideal for SPSTM characterization within the scope of our project and have abandoned this research direction for future planning described below.

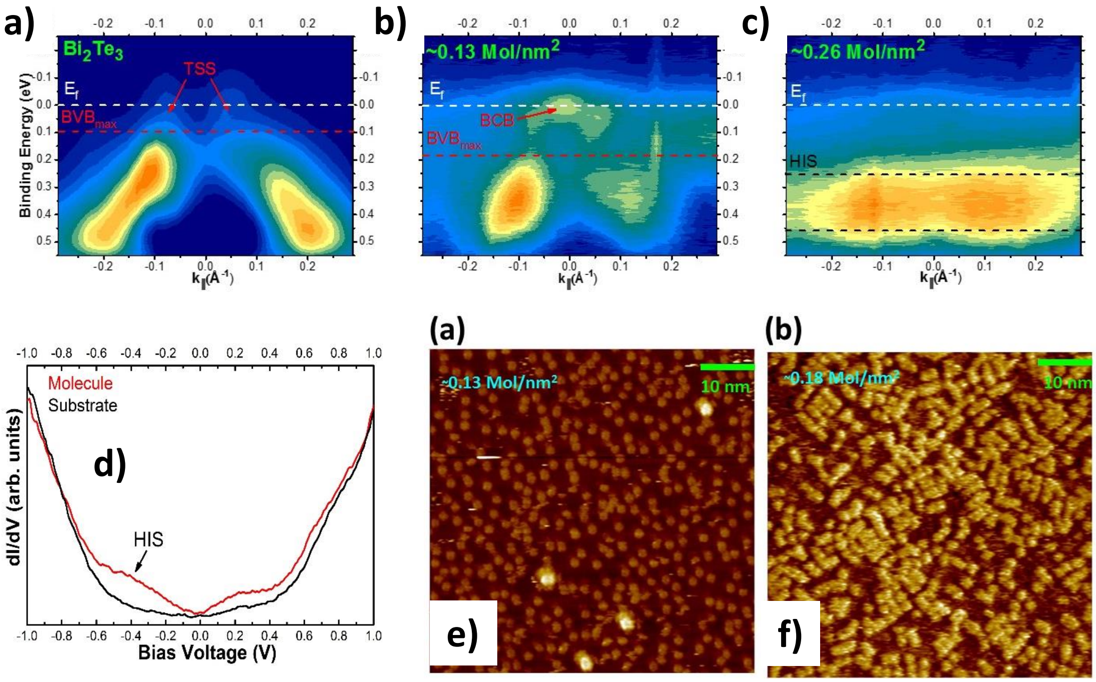

**Figure 3.** a) Angle resolved UPS spectrum of a Bi2Te3 surface; b) Spectrum modified by a submonolayer coverage of MnPc; c) Spectrum showing a new nondispersive feature (yellow band) assigned as a hybrid interface state; d) Local tunneling spectrum measured at a coverage near that of part c) also showing the HIS; e),f) STM images corresponding to approximate coverages in b) and c) respectively.

## Future Plans

There are two key objectives to future work on this project: 1) Extending SPSTM to the several layer organic film thickness regime; and 2) Extending SPSTM to magnetic complex oxide electrodes. The first goal is a natural extension of the new results described in the previous section on Crq3 and Alq3 that addresses how interfacial magnetism is transmitted through a growing organic active layer. Our plan is to consider both single species films in the 2-4 layer regime and also to create mixed-molecule “heterostructures” e.g. of Crq3/Alq3 to see how the metallic versus interfacial effects are transmitted between different species.

Extension to complex oxide surfaces is an important goal of this project in terms of connecting with ongoing device experiments. These almost always use LaSrMnO3 electrodes (which are half-metallic ferromagnets) as one of the spin injectors. The molecular-level details of interfacial interactions with such a surface are not known and will be characterized with our SPSTM instrument.

## References

[1] Xiong et al., Nature 427, 821 (2004).
[2] Barraud et al., Nat. Physics 6, 615 (2010).
[3] Wang and Dougherty, Phys. Rev. B 92, 161401R (2015).
[4] Guo and Franz, Phys. Rev. B 81, 041102R (2010).
[5] Sessi et al., Nano Letters 14, 5092 (2014).
[6] Jakobs et al., Nano Letters 15, 6022 (2015).

## Publications

Wang and Dougherty, Phys. Rev. B 92, 161401R (2015).

## Chiral magnetic excitations in FeGe thin films

**Gregory D. Fuchs, Cornell University Applied and Engineering Physics, Ithaca, NY**

### Research Scope

The overarching aim of this research is to investigate the interplay between charge, spin, heat, and light on the *dynamics* of nanoscale chiral, and topological spin textures. The prime example of a topological spin texture is a magnetic skyrmion, which is a “vortex-like” magnetic texture where the local magnetization vector can be topologically mapped to an outward facing vector on the surface of a sphere [1,2]. The topological nature of these magnetic textures makes them “particle-like” with extremely low critical current density for motion under spin-transfer torques [3,4]. These properties have formed the basis for proposals of ultra-low power information storage devices [5,6].

This project uses a wide range of experimental approaches: electrical, optical, thermal, and magnetic experimental probes to study chiral and topological magnetism, with a particular focus on the behavior of these materials in nanostructured environments. We have focused on chiral magnetic materials with broken inversion crystal symmetry, particularly the B20 monosilicides and monogermanides of transition magnetic elements, e.g. MnSi, FeCoSi, and FeGe [7]. The magnetism of these materials have chiral, noncollinear spin texture due to a competition between their exchange, anisotropy, and the Dzyaloshinskii-Moriya interaction (DMI) that arises from their broken inversion symmetry [8,9].

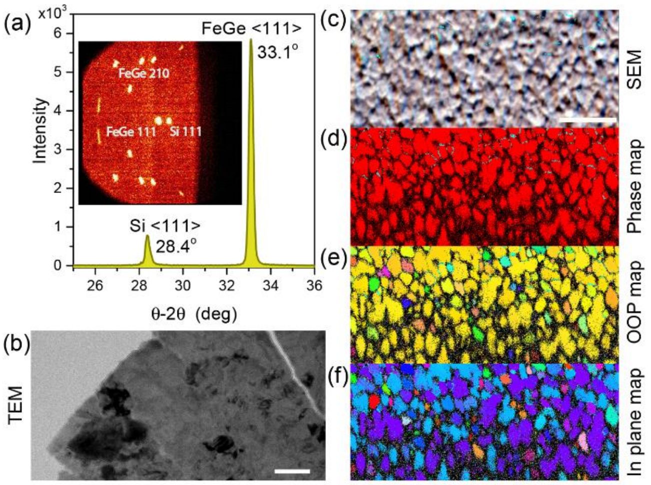

Figure 1. X-ray and electron diffraction characterizations and transmission electron micrograph of FeGe thin film. (a) shows θ-2θ scan of X-ray diffraction with an additional χ angle profile in the inset. Having sharp peaks instead of rings suggests good alignment of FeGe film. (b) is transmission electron micrograph of plain-view of the film (scale bar is 100nm). (c) is scanning electron micrograph, (d) is the crystalline phase map of the same region indicating >99% B20 phase. (e) is the out-of-plane alignment and f) is the in-plane alignment of the grain. The scale bar is 2 μm through (c)–(f). Figure from Ref. [21]

### Recent Progress

Understanding and measuring chiral magnetic excitations enables physical insight into the magnetic states of these materials and it offers quantitative characterization of dynamical properties that are relevant to future magnetic technologies. In the context of potential applications, it is important to characterize physical and dynamical properties of thin-film chiral magnetic materials that are scalably grown on a substrate, as opposed to grown as bulk crystals.

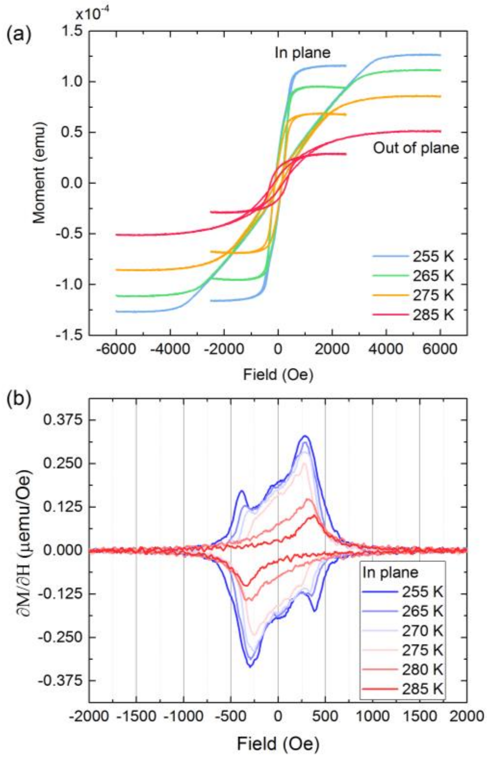

Figure 2. Magnetometry measurements of our thin film FeGe. (a) shows M-H curves for both the in-plane and out-of-plane fields, and (b) shows the derivative of the in-plane magnetization with respect to the applied magnetic field to better reveal unwinding of the helical phase. Figure from Ref. [21]

Among B20 compounds, FeGe has the highest critical temperature, 278 K, for ordered chiral spin textures [7,10]. FeGe also has -0.6% lattice mismatch with the Si [111] surface, enabling scalable thin film growth [11,12]. However, although B20 FeGe thin films have been the subject of intense theoretical and computational studies, experimental studies have been limited to reports of the topological Hall effect and polarized neutron scattering measurements [11–17]. Furthermore, recent Lorentz transmission electron microscopy and transport studies of FeGe and MnSi thin films have brought into question the common interpretation of the topological Hall effect as arising solely from a skyrmion lattice phase [11,13,18,19]. These studies point out that transport measurements of B20 films are hard to interpret unambiguously because electron skew scattering by complex helical spin structures also contributes a Hall effect signal [11,20]. This realization motivates alternative characterization methods to help identify chiral magnetic states and quantify magnetic behavior in thin film materials.

Recently, we have reported on our experimental, theoretical, and micromagnetic studies of chiral magnetic excitations in FeGe thin films [21]. We grew FeGe by co-sputtering Fe and Ge onto the surface of Si [111] and subsequently annealing to obtain the B20 crystal structure. Figure 1 shows physical characterization including x-ray diffraction, transmission electron microscopy, and electron back-scattering diffraction. We find that these films are polycrystalline, with grain size between 200

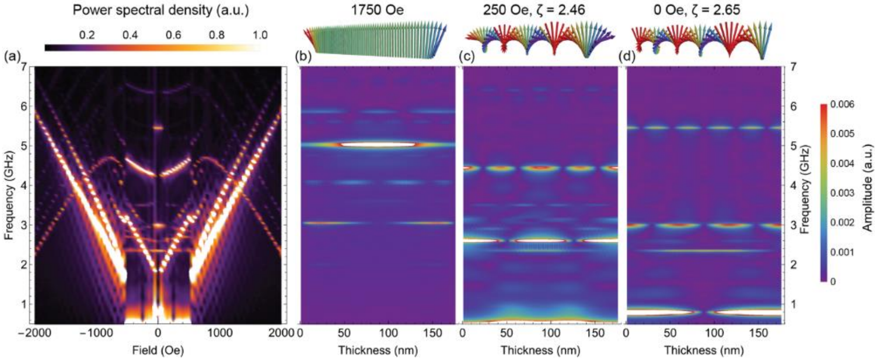

Figure 3. Power spectral density (PSD) and natural oscillation modes of spin waves. (a) shows the PSD of spatially summed Fourier coefficients as a function of in-plane magnetic field. The helical spin configuration presents between -500 Oe and 500 Oe, and the field-polarized state presents for the rest. (b) at $B_x$ = 1750 Oe field, the field-polarized state has a Kittel-type uniform mode. (c) at $B_x$ = 250 Oe field, the wrapping number $\zeta$ is 2.46, which allows only even nodes (0, 2, and 4.) (d) at $B_x$ = 0 Oe field, the wrapping number $\zeta$ is 2.65, which allows only odd nodes (1, 3, and 5.) Figure from Ref. [21]

nm – 400 nn.  Additionally, 99% of the grains in the B20 phase, with 95% of the grains aligned to underlying the Si [111] crystal.

Magnetic characterization (Figure 2) reveals that the films have a critical temperature of 273 K, at which point they enter a chiral magnetic phase with an overall easy-plane magnetic anisotropy.  The low-field magnetic ground-state is helical, with a feature in the in-plan magnetic susceptibility at 400 Oe marking the transition between the helical phase with an out-of-plane q-axis and a field-polarized phase magnetic state, in agreement with previous polarized neutron scattering studies in FeGe and MnSi thin films [13,15].

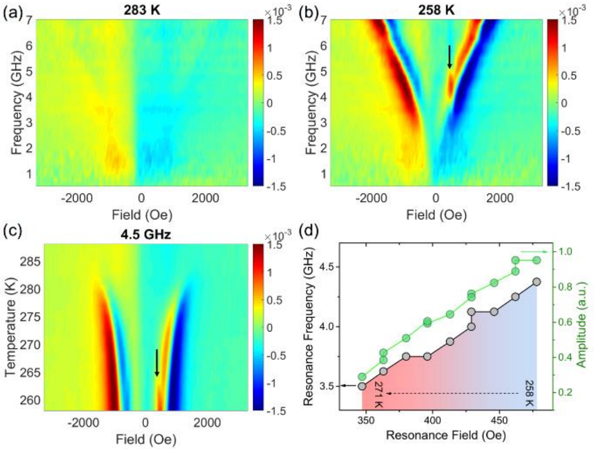

Figure 4. Experimental measurements of microwave absorption spectroscopy (MAS) of FeGe film at different temperature, in-plane magnetic field, and microwave frequency. (a) shows the MAS above the critical temperature with no clear absorption feature. (b) shows the MAS below the critical temperature, which has the helical (arrow) and field-polarized state resonances. (c) the MAS at 4.5 GHz as the field and the temperature vary. (d) shows trend of the frequency, field, and amplitude of the helical resonance for each temperature. Figure from Ref.  [21]

Drawing simulation parameters from physical and magnetic characterization, we use micromagnetic modeling to understand the dynamic excitations of FeGe (Figure 3).  We identified conventional ferromagnetic resonance modes in the field polarized states.  We also identified resonant spin wave modes that are sensitive to the helical wrapping number, $\zeta$.

To confirm this understanding, we perform microwave absorption spectroscopy, shown in Figure 4.  From the field-polarized magnetic resonance, we measure that the Gilbert damping coefficient of our FeGe films is $\alpha = 0.038 \pm 0.005$ at 258 K. This $\alpha$ is substantially lower than the recently reported value of 0.28 in thinner FeGe films  [22].  We observe the predicted helical resonance, marked in Fig. 4 (b)-(c) with an arrow and shown in micromagnetic simulations in Fig. 3 (c).  Its frequency and field behavior match well to the helical spin-wave resonance shown at 4.5 GHz in Fig. 3c, in which the spin-wave vector matches the out-of-plane helical vector.

## Future Plans

Preliminary magnetic resonance measurements of nanopatterned FeGe thin films suggest that skyrmions form in patterned micro-/nano-disks at temperature above 250 K.  Currently, we are confirming this with Lorentz STEM using a pixel array detector [23], before studying how their dynamical behavior can be controlled and modified using spin currents.

## References

[1] S. Mühlbauer, B. Binz, F. Jonietz, C. Pfleiderer, A. Rosch, A. Neubauer, R. Georgii, and

P. Böni, Science **323**, 915 (2009).

[2] X. Z. Yu, Y. Onose, N. Kanazawa, J. H. Park, J. H. Han, Y. Matsui, N. Nagaosa, and Y. Tokura, Nature **465**, 901 (2010).

[3] F. Jonietz, S. Mühlbauer, C. Pfleiderer, A. Neubauer, W. Münzer, A. Bauer, T. Adams, R. Georgii, P. Böni, R. A. Duine, K. Everschor, M. Garst, and A. Rosch, Science (80-. ). **330**, 1648 (2010).

[4] X. Z. Yu, N. Kanazawa, W. Z. Zhang, T. Nagai, T. Hara, K. Kimoto, Y. Matsui, Y. Onose, and Y. Tokura, Nat. Commun. **3**, 988 (2012).

[5] J. Iwasaki, M. Mochizuki, and N. Nagaosa, Nat. Nanotechnol. **8**, 742 (2013).

[6] A. Fert, V. Cros, and J. Sampaio, Nat. Nanotechnol. **8**, 152 (2013).

[7] N. Nagaosa and Y. Tokura, Nat. Nanotechnol. **8**, 899 (2013).

[8] I. Dzyaloshinsky, J. Phys. Chem. Solids **4**, 241 (1958).

[9] U. K. Rössler, A. N. Bogdanov, and C. Pfleiderer, Nature **442**, 797 (2006).

[10] H. Wilhelm, M. Baenitz, M. Schmidt, U. K. Rößler, A. A. Leonov, and A. N. Bogdanov, Phys. Rev. Lett. **107**, 127203 (2011).

[11] N. A. Porter, J. C. Gartside, and C. H. Marrows, Phys. Rev. B **90**, 024403 (2014).

[12] S. X. Huang and C. L. Chien, Phys. Rev. Lett. **108**, 267201 (2012).

[13] N. A. Porter, C. S. Spencer, R. C. Temple, C. J. Kinane, T. R. Charlton, S. Langridge, and C. H. Marrows, Phys. Rev. B **92**, 144402 (2015).

[14] N. Kanazawa, M. Kubota, A. Tsukazaki, Y. Kozuka, K. S. Takahashi, M. Kawasaki, M. Ichikawa, F. Kagawa, and Y. Tokura, Phys. Rev. B **91**, 041122 (2015).

[15] M. N. Wilson, E. A. Karhu, D. P. Lake, A. S. Quigley, S. Meynell, A. N. Bogdanov, H. Fritzsche, U. K. Rößler, and T. L. Monchesky, Phys. Rev. B **88**, 214420 (2013).

[16] M. Kugler, G. Brandl, J. Waizner, M. Janoschek, R. Georgii, A. Bauer, K. Seemann, A. Rosch, C. Pfleiderer, P. Boni, and M. Garst, Phys. Rev. Lett. **115**, 097203 (2015).

[17] J. C. Gallagher, K. Y. Meng, J. T. Brangham, H. L. Wang, B. D. Esser, D. W. McComb, and F. Y. Yang, arXiv: 1604.06684 (2016).

[18] M. N. Wilson, A. B. Butenko, A. N. Bogdanov, and T. L. Monchesky, Phys. Rev. B **89**, 094411 (2014).

[19] T. L. Monchesky, J. C. Loudon, M. D. Robertson, and A. N. Bogdanov, Phys. Rev. Lett. **112**, 059701 (2014).

[20] S. A. Meynell, M. N. Wilson, J. C. Loudon, A. Spitzig, F. N. Rybakov, M. B. Johnson, and T. L. Monchesky, Phys. Rev. B **90**, 224419 (2014).

[21] E. Turgut, A. Park, K. Nguyen, A. Moehle, D. A. Muller, and G. D. Fuchs, arXiv: 1608.03582 (2016).

[22] M. Beg, M. Albert, M.-A. Bisotti, D. Cortés-Ortuño, W. Wang, R. Carey, M. Vousden, O. Hovorka, C. Ciccarelli, C. S. Spencer, C. H. Marrows, and H. Fangohr, arXiv: 1604.08347 (2016).

[23] M. W. Tate, P. Purohit, D. Chamberlain, K. X. Nguyen, R. Hovden, C. S. Chang, P. Deb, E. Turgut, J. T. Heron, D. G. Schlom, D. C. Ralph, G. D. Fuchs, K. S. Shanks, H. T. Philipp, D. A. Muller, and S. M. Gruner, Microsc. Microanal. **22**, 237 (2016).

## Publications

E. Turgut, A. Park, K. Nguyen, A. Moehle, D. A. Muller, and G. D. Fuchs, “Chiral magnetic excitations in FeGe films” arXiv: 1608.03582 (2016).

# Multimodal In Situ Scanning Probes for Understanding Hybrid Perovskite Solar Cells

**PI: David S. Ginger, University of Washington Department of Chemistry, Box 351700**

## Research Scope

This project aims to elucidate the microstructural factors underpinning the remarkable photovoltaic properties of hybrid organic-inorganic halide perovskite semiconductors through unique combinations of scanning probe microscopy with optical and electrical excitation. Specifically, we seek to elucidate the local structure/function relationships[1] responsible for properties -- such as the unusually long carrier lifetimes and high open circuit voltages observed in seemingly defective polycrystalline films – that would help improve the long-term prospects for successful technologies to emerge from this class of materials. To this end, we are performing scanning probe imaging, including topography, piezoresponse force microscopy (PFM), electrostatic force microscopy (EFM), and time-resolved electrostatic force microscopy (trEFM), with correlated confocal optical microscopy including fluorescence lifetime imaging (FLIM) on perovskite films grown under different conditions. This information could lead to advances in new thin film semiconductors for applications in photovoltaics and beyond.

## Recent Progress

In the first year of the project, we have focused on investigating the effects of chemical passivation treatments that reduce defect densities and increase carrier lifetimes.[2] We have highlighted the role that defects and surface states play on carrier recombination losses,[3] and obtained the first direct evidence for halide migration following illumination of methylammonium lead triiodide perovskite films.[4] We have also begun a series of piezoresponsive force microscopy (PFM) experiments on halide perovskites with varying cations.

**Processing Additive Hypophosphorous Acid (HPA) Improves Solar Cell Performance and Microscopic Carrier Lifetimes** The processing additive hypophosphorous acid (HPA) improves the optoelectronic quality of perovskite thin films, resulting in an increase in performance of methylammonium lead triiodide solar cells.[2] We performed local confocal imaging and lifetime microscopy on samples prepared by the Oxford group to show that using hypophosphosphorous acid as a processing additive results in a significant increase in carrier lifetime, as well as a distinct clustering of long- and short-lifetime domains in

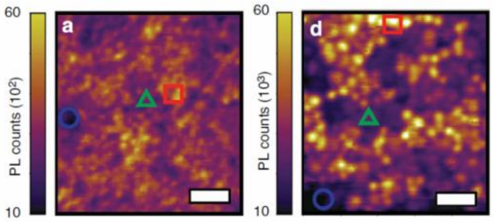

**Fig. 1** Photoluminescence images of perovskite films before (left) and after (right) treatment with HPA showing significant increase in overall brightness accompanying increased solar cell performance, but also increasing heterogeneity. Scale bar = 2 microns.[2]

methylammonium lead triiodide films perovskite thin films (Fig 1). These experiments set the stage for our studies of how chemical processing also affect local ferroelectric order (see below).

**Illumination Causes Perovskite Photocleaning Accompanied by Halide Ion Migration** Using correlated SEM, confocal photoluminescence, scanning kelvin probe microscopy, and time-of-flight secondary ion mass spectrometry (TOF-SIMS) we have provided the first direct chemical evidence that photoinduced cleaning in hybrid perovskite films is accompanied by iodide diffusion.[4] We demonstrated that exposure to simulated solar illumination results in a steady increase in the photoluminescence intensity and lifetime for methylammonium lead triiodide methylammonium lead triiodide films films. We showed that after light soaking, the intensity maps appear to redistribute (Fig. 2) with the dark domains gaining in brightness and the bright domains losing intensity. Importantly, by correlating our images with imaging time-of-flight secondary ion mass spectrometry we were able to show that the illuminated areas of the samples showed a decrease in local iodine concentration. Scanning probe experiments have verified that the direction of ion motion depends on the sign of the surface-induced band bending.

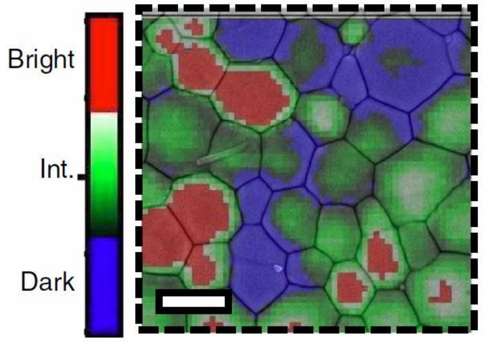

**Fig. 2** SEM map with correlated PL changes overlaid. Red regions were initially brighter, but moved towards the average after photocleaning. Blue regions were initially darker but showed significant improvements towards the average after

**Chemical Surface Passivation can Produce Produce Perovskite Thin Films With Single-Crystal Like Carrier Lifetimes** We studied the effects of a series of post-deposition ligand treatments on the photoluminescence (PL) of polycrystalline methylammonium lead triiodide perovskite thin films. We showed that a variety of Lewis bases can improve the bulk PL quantum efficiency (PLQE) and extend the average PL lifetime <τ>, with correlated microscopy revealing the greatest enhancements concentrated at grain boundaries. Notably, we demonstrated thin film PLQE as high as 36% and <τ> as long as 8.88 µs, at solar equivalent carrier densities using tri-n-octylphosphine oxide (TOPO) treated films.[3] These values are the best reported to date for thin films at solar equivalent intensity. Using glow discharge optical emission spectroscopy (GDOES) and nuclear magnetic resonance (NMR) spectroscopy, we showed that the ligands are incorporated primarily at the film surface and are acting as electron donors. These results

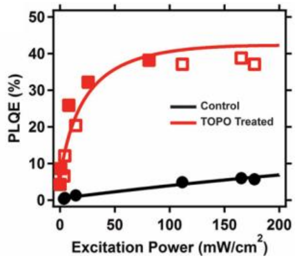

**Fig. 3** Photoluminescence quantum yield after treatment with tri-n-octylphosphine oxide (red) compared to control sample (black). The solid lines are fits to a sum of first, second, and third (Auger) recombination terms. Imaging confirms the enhancement occurs preferentially at grain boundaries.[3]

indicate it is possible to obtain thin film PL lifetime and PLQE values that are comparable to those from single crystals by control over surface chemistry and provide a model system for imaging local carrier dynamics.

**Ferroelectric Ordering in Hybrid Perovskite Films** The existence and importance of ferroelectric order within hybrid perovskite thin films has been an intriguing and controversial topic virtually since the beginning.[5] It now appears that some hybrid perovskite films may exhibit some ferroelectric response,[6, 7] but the relevance for device operation remains an open question. Interestingly, we have found that the HPA treatment discussed above not only improves the carrier lifetimes of MAPI perovskite films, but also appears to change the PFM signal from out-of-plane to in-plane. (Fig. 4)

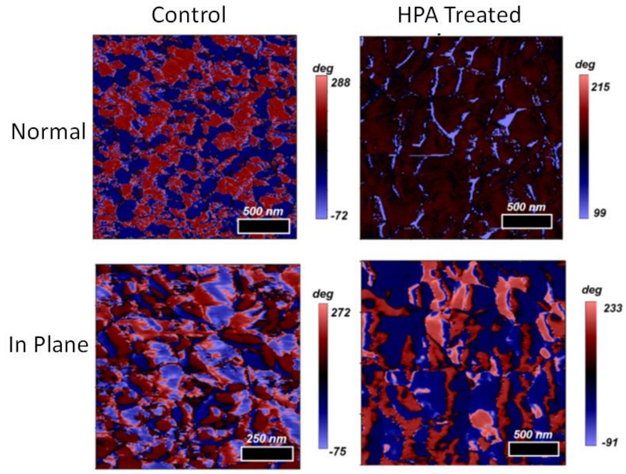

**Fig. 4** AFM topography and piezoresponsive force microscopy images of MAPI films with (top row) and without (bottom row) HPA treatment. The HPA treatment not only improves device performance but appears to switch the PFM signal from out-of-plane to in-plane orientation. (Ginger Lab – unpublished data)

## Future Plans

**Processing Additives and Post-Deposition Treatments** We plan to continue to explore the effects of a number of new processing additives and post-growth treatments on the local heterogeneity in carrier lifetimes in the perovskite thin films. Our first year results above indicate that these treatments are improve carrier lifetimes, and also altering local properties like PFM response. The next step is to correlate these changes with changes in local transport and cell performance.

**Map Ion Motion with Dynamic Scanning Probe Methods** To following up our published work on local halide ion motion, we plan to use both SKPM and time-resolved electrostatic force microscopy (trEFM) to map local ion transport rates and test the hypothesis that the ions move faster through grain boundaries and defects. We will also screen different surface chemistry treatments to see if they can surface ion transport by passivating specific defect states.

**Understand Role (or lack thereof) of Ferroelectric Domain Orientation** We plan to continue our piezoelectric force microscopy measurements to correlate local ferroelectric order with local photocurrent collection. We plan to try to use electroluminescence instead of photoluminescence to look at radiative recombination as the ferroelectric domains are smaller than the optical diffraction limit and are not resolvable with PL.

**Correlating PL with Local Electronic Properties** We plan to perform simultaneous electroluminescence, PL, cAFM, and SKPM on bromide perovskite samples, and to upgrade our instrument to improve performance in the near IR so that we can also study films of the lower bandgap methylammonium lead triiodide. Our goal is to identify the source of the heterogeneous non-radiative recombination centers.

**Measuring Sub-Diffraction Carrier Lifetimes** We plan to explore both time-resolved EFM (time domain) and intensity-modulated SKPM (frequency domain) for direct electrical measurements of carrier recombination (at sub-microsecond times) and ion motion (at ms and longer times).

## References

1. D. W. deQuilettes, S. M. Vorpahl, S. D. Stranks, H. Nagaoka, G. E. Eperon, M. E. Ziffer, H. J. Snaith, D. S. Ginger, Impact of microstructure on local carrier lifetime in perovskite solar cells. *Science*. 348, 683-686 (2015)
2. W. Zhang *et al.*, Enhanced optoelectronic quality of perovskite thin films with hypophosphorous acid for planar heterojunction solar cells. *Nature Communications*. 6, (2015)
3. D. W. deQuilettes, S. Koch, S. Burke, R. K. Paranji, A. J. Shropshire, M. E. Ziffer, D. S. Ginger, Photoluminescence Lifetimes Exceeding 8 μs and Quantum Yields Exceeding 30% in Hybrid Perovskite Thin Films by Ligand Passivation. 438-444 (2016)
4. D. W. Dequilettes *et al.*, Photo-induced halide redistribution in organic-inorganic perovskite films. *Nature Communications*. 7, DOI: 10.1038/ncomms11683 (2016)
5. J. M. Frost, K. T. Butler, F. Brivio, C. H. Hendon, M. van Schilfgaarde, A. Walsh, Atomistic Origins of High-Performance in Hybrid Halide Perovskite Solar Cells. *Nano Letters*. 14, 2584-2590 (2014)
6. Y. Kutes, L. H. Ye, Y. Y. Zhou, S. P. Pang, B. D. Huey, N. P. Padture, Direct Observation of Ferroelectric Domains in Solution-Processed CH3NH3PbI3 Perovskite Thin Films. *Journal of Physical Chemistry Letters*. 5, 3335-3339 (2014)
7. M. Coll, A. Gomez, E. Mas-Marza, O. Almora, G. Garcia-Belmonte, M. Campoy-Quiles, J. Bisquert, Polarization Switching and Light-Enhanced Piezoelectricity in Lead Halide Perovskites. *Journal of Physical Chemistry Letters*. 6, 1408-1413 (2015)

## Publications from 2015-2016

1. W. Zhang et al., Enhanced optoelectronic quality of perovskite thin films with hypophosphorous acid for planar heterojunction solar cells. Nature Communications. 6, (2015)

2. D. W. Dequilettes et al., Photo-induced halide redistribution in organic-inorganic perovskite films. Nature Communications. 7, DOI: 10.1038/ncomms11683 (2016)

3. D. W. deQuilettes, S. Koch, S. Burke, R. K. Paranji, A. J. Shropshire, M. E. Ziffer, D. S. Ginger, Photoluminescence Lifetimes Exceeding 8 μs and Quantum Yields Exceeding 30% in Hybrid Perovskite Thin Films by Ligand Passivation. 438-444 (2016)

## Collaborative Research: Atomistic studies of individual impurities and impurity complexes in III-V semiconductors

Jay A. Gupta, *Department of Physics, Ohio State University*

Michael Flatté, *Department of Physics, University of Iowa*

### Research Scope

The miniaturization of electronic components such as transistors to nanoscale dimensions is nearing fundamental limits imposed by the discrete atomic nature of the impurities in semiconductor materials. This motivates a rapidly emerging field of 'solotronics' in nanoscience, namely the characterization and control of individual dopants in semiconductors for next-generation information technologies [1].

We have begun an integrated experimental and theoretical program aimed at understanding individual impurities and complexes in two III-V semiconductors, GaAs and InSb. The central hypothesis to be tested is that *reduced symmetries* significantly influence the properties of individual impurities and impurity complexes in semiconductors. We will employ STM-based substitution [2, 3, 4, 5, 6] to prepare impurities and complexes with atomic precision in a controlled environment. STM images and tunneling spectra will be compared to calculated wavefunctions and local density of states using theoretical techniques pioneered for impurities in GaAs by the co-PI. [7, 8] Our specific objectives during the three year program are:

1. **Explore impurity hybridization in reduced symmetry environments:** Here we address the question of how the hybridization of individual impurities with the host semiconductor depends on reduced symmetries due to proximity to a surface and/or other impurities or defects. We will study how *p-d* hybridization of a series of transition metal dopants (Cr, Mn, Fe, Co, Ni, Zn) is influenced by symmetry-breaking of the $t_2$ and *e d*-levels, and if the more isolated intra 4*f*-shell transitions of a series of rare earth impurities (Eu, Gd, Er) are influenced at all compared to the bulk. Experimentally-measured shifts and splitting of impurity states will be interpreted within a theoretical framework using real-space Green's function methods and density functional theory.
2. **Discover novel properties in impurity complexes:** Chemical molecules offer a range of properties well beyond the scope of their constituent atoms in the periodic table. In analogy, we will explore how impurity complexes in a semiconductor host can provide access to energetic and spatial arrangements of discrete electronic states that cannot be achieved with single impurities. We will use atomic manipulation to form impurity complexes with a controlled separation and local electrostatic environment to directly correlate the unique properties of the complexes with their atomic structure. For example, heterogeneous exchange interactions will be studied by forming complexes with varying composition (e.g., Fe-Co, Fe-Ni, Er-Fe and permutations thereof). Variation of separation and orientation with respect to the GaAs surface will probe the spatial extent and anisotropy of the interaction, including when the interaction is mediated by a nonmagnetic

atom such as subsurface Zn (a form of superexchange). Measured impurity state splittings will be compared with theoretical density of state calculations. The hybridization in these complexes will be further tuned by positioning charged defects at particular symmetry points identified by STM mapping of the complex' bonding and anti-bonding orbitals.

3. **Develop spin-polarized STM to directly probe static and dynamic magnetic properties of dopants:** SPSTM offers the capability to directly measure magnetic anisotropy barriers and determine ferro- or anti-ferromagnetic ordering of dopant complexes. We will extend these methods for the first time to magnetic dopants in GaAs. Inelastic electron tunneling spectroscopy with spin-polarized currents will be performed to probe anisotropy energies of single magnetic dopants as well as dopant complexes. We will also probe the spin-dependent density of states in single dopants and dopant complexes by SPSTM imaging and spin-resolved tunneling spectroscopy as a function of magnetic field. These measurements will be directly compared with theoretical calculations of density of states, exchange interaction strengths and anisotropy energies.

## Recent Progress

In GaAs, we have begun exploring how the exchange interaction between pairs of Mn acceptors can be tuned by positioning charged impurities nearby. Tunneling spectroscopy reveals a series of six distinct states associated with the dimer that systematically shift with proximity to charged Ga or Mn adatoms. These data are currently being compared with theoretical calculations to understand the connection to the Mn exchange interaction. We have also begun imaging InSb(110) surfaces, and have found intriguing ionization behavior associated with individual adatoms on the surface.

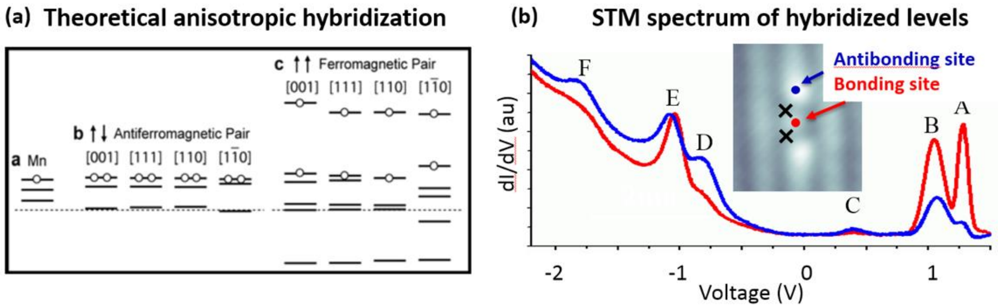

**Figure 1.** (a) Predictions by the co-PI for energy levels of Mn-Mn dimers with different orientation with respect to the GaAs lattice. The dotted line indicates the valence band edge, and circles represent the hole states. [9] Changes in the total energy stabilize ferro- or antiferromagnetic ordering for different orientations. (b) STS on the (1-10) Mn dimer, resolving bonding and antibonding hybridized states, consistent with the predictions. 'x' marks the atomic positions of the two Mn atoms, substituted for Ga in the surface layer. Blue and Red circles indicate the position of the tip to probe bonding and antibonding states.

## Future Plans

Initial studies in GaAs that build on our prior work will extend to InSb towards the end of the project. We will develop implantation methods for forming dopants in the InSb surface layer, and use tunneling spectroscopy to probe how donor/acceptor levels align with the conduction and valence bands. These measurements will be contrasted with bulk results in the literature to contrast impurity properties at/near the surface. The narrow gap of InSb is also favorable for inelastic electron tunneling spectroscopy, and so we will begin looking for spin polarized signatures in STM studies of magnetic impurities in InSb.

## References

1. Koenraad, P. M. and Flatté, M. E. "**Single Dopants in Semiconductors.**" *Nature materials* 10, no. 2 (2011): 91–100. doi:10.1038/nmat2940

2. Lee, D. H. and Gupta, J. a. "**Tunable Field Control over the Binding Energy of Single Dopants by a Charged Vacancy in GaAs.**" *Science (New York, N.Y.)* 330, no. 6012 (2010): 1807–10. doi:10.1126/science.1197434

3. Lee, D. and Gupta, J. A. "**Tunable Control over the Ionization State of Single Mn Acceptors in GaAs with Defect-Induced Band Bending.**" *Nano letters* 11, no. 5 (2011): 2004–7. doi:10.1021/nl2003686

4. Lee, D. H., Santagata, N. M., and Gupta, J. a. "**Influence of the Local Environment on Zn Acceptors in the GaAs(110) Surface**" *Applied Physics Letters* 99, no. 5 (2011): 053124. doi:10.1063/1.3624535

5. Gohlke, D., Mishra, R., Restrepo, O. D., Lee, D., Windl, W., and Gupta, J. "**Atomic-Scale Engineering of the Electrostatic Landscape of Semiconductor Surfaces.**" *Nano letters* 13, no. 6 (2013): 2418–22. doi:10.1021/nl400305q

6. Benjamin, A. L., Lee, D., and Gupta, J. A. "**Tuning the Electronic States of Individual Co Acceptors in GaAs**" *Journal of Vacuum Science & Technology B: Microelectronics and Nanometer Structures* 31, no. 4 (2013): 04D102. doi:10.1116/1.4803841

7. Tang, J.-M., Flatté, M., and Flatte, M. E. "**Multiband Tight-Binding Model of Local Magnetism in Ga1-xMnxas**" *Physical Review Letters* 92, no. 4 (2004): 047201. doi:10.1103/PhysRevLett.92.047201

8. Tang, J.-M. and Flatté, M. "**Spin-Orientation-Dependent Spatial Structure of a Magnetic Acceptor State in a Zinc-Blende Semiconductor**" *Physical Review B* 72, no. 16 (2005): 161315. doi:10.1103/PhysRevB.72.161315

9. Kitchen, D., Richardella, A., Yazdani, A., Tang, J.-M., and Flatté, M. E. "**Atom-by-Atom Substitution of Mn in GaAs and Visualization of Their Hole-Mediated Interactions.**" *Nature* 442, no. 7101 (2006): 436–9. doi:10.1038/nature04971

## Understanding and Control of Spin Currents in Diverse Materials and Settings

**P. Chris Hammel, Department of Physics, Ohio State University**

### Research Scope

The generation, control and detection of pure spin currents is a topic of intense study as a consequence of its fundamental richness and the range of technological opportunities it presents. Precessing magnetization emits spin currents (a phenomenon known as spin pumping); conversely applied spin currents can reduce magnetization damping, even to the point that they drive magnetization precession and inversion. These phenomena have applications to high frequency signal generation and detection. Most studies involve spin currents transmitted across a material interface separating a ferromagnet (FM) and a normal material (NM), thus making the efficiency of the current transmission, described by an interfacial spin conductance, sensitive to complex and often ill-characterized interface features. Under recent DOE funding we have studied these phenomena and developed new tools and approaches to studying this important problem (DOE BES publications 1-15), and we have leveraged our expertise to enable studies of spin dynamics and spin transport in other settings and materials (DOE BES publications 16-20). Spin pumping experiments in FM/NM bilayer systems measure spin current traversing the material interface. Modeling of inhomogeneous samples with strongly varying anisotropy fields has shown the importance of understanding FMR on the nanoscale [1]. We demonstrated FMR spectroscopic imaging using localized modes to probe nanoscale properties of FM films [2, 3]. This technique has been extended to other FMs [4]. We recently extended this approach to measure magnetization dynamics and demonstrate spin pumping from nanoscale localized modes in a uniform material where the only interface is defined by the confined dipolar field of a nearby magnetic particle [5, 6]. This approach complements studies of intralayer spin pumping in lithographically defined dots [7], by allowing lithographic edge damage to be avoided. We find that the damping of the confined mode scales like the surface-to-volume ratio of the mode, indicating an interfacial damping due to the transfer of angular momentum from the confined mode to the spin sink provided by the surrounding FM film. The intralayer spin-mixing conductance $g_{\uparrow\downarrow} = 5.3 \times 10^{19}\ m^{-2}$ that we measure demonstrates efficient intralayer angular momentum transfer [5, 6]. Intralayer spin pumping has been described for metallic systems as being mediated by conduction electrons moving through the spatially varying magnetization [8] in a Py nanodot where the damping depended on the magnetization gradient [9]. Our studies in magnetic insulators provide an opportunity to understand the mechanisms that mediate the transfer of spin angular momentum from localized modes.

## Recent Progress

Magnetoelectronic devices operating on pure spin currents without accompanying charge current promise new functionalities and significant energy savings. Generation of pure spin currents from ferromagnets to nonmagnetic materials (NM) has been actively investigated by ferromagnetic resonance (FMR) or thermally driven spin pumping. $Y_3Fe_5O_{12}$ (YIG) is highly attractive for this purpose due to its low magnetic damping and insulating nature. Since many magnetoelectronic applications, such as magnetic tunnel junctions, spin valves, spin torque oscillators, and spin transistors, rely on spin transport in heterostructures comprising multiple FM components, it will be highly desirable to achieve and understand spin currents in diverse materials including insulators, FMs and antiferromagnets (AF). We have extensively studied spin pumping from Yttrium Iron Garnet ($Y_3Fe_5O_{12}$; YIG) films under a variety of circumstances. We find a rich variety of behavior that points to the availability of strategies for optimizing performance and revealing new phenomena. A particular focus of our work is the study of spin transport across magnetic-field defined interfaces, which, in particular, avoid the necessity of material interfaces that can be complex and difficult to characterize. We accomplish this by locally exciting magnetostatic modes in an extended, pristine FM, and measuring the spin currents out of these localized modes.

### Spin Transport through Antiferromagnetic Insulators

Spin current carried by mobile charges in metallic and semiconducting ferromagnetic (FM) and nonmagnetic (NM) materials has been the central focus of spintronics for the past two decades; while spin transport in insulators is largely unexplored. We observe highly efficient dynamic spin current injection from $Y_3Fe_5O_{12}$ (YIG) into NiO, an antiferromagnetic (AF) insulator, via strong coupling between YIG and NiO, and robust antiferromagnon-mediated spin propagation in NiO up to 100-nm thickness. Strikingly, the insertion of a thin NiO layer between YIG and Pt significantly enhances the spin currents driven into Pt, suggesting exceptionally high spin transfer efficiency at both YIG/NiO and NiO/Pt interfaces. This offers a powerful platform for studying antiferromagnetic spin pumping and antiferromagnonic dynamics as well as for exploration of spin manipulation in tailored structures comprising metallic and insulating ferromagnets, antiferromagnets and nonmagnetic materials. Recent developments in ferromagnetic resonance (FMR) and thermally driven spin pumping have attracted intense interest in magnon-mediated spin current, which can propagate in both conducting and insulating FMs and antiferromagnets (AF). We systematically studied spin transport in six series of Pt/Insulator/ YIG trilayers, where the insulator includes diamagnetic $SrTiO_3$, paramagnetic (PM) GGG, and antiferromagnetic $Cr_2O_3$, amorphous YIG, amorphous $NiFe_2O_4$, and NiO. We observe surprisingly robust spin transport in the AF insulators, even in AF layers with low ordering temperatures. The spin transfer efficiency and spin current decay lengths appear related to the strength of magnetic correlation in these insulators. This result provides insights into the role of magnetic correlation for spin transport in magnetic insulators and opens a new venue for exploration of spin manipulation in tailored structures comprising metallic and insulating FM, AF and NM materials.

### Spin Pumping into Ferromagnetic Metals

We have used YIG based spin pumping to study the spin current and inverse spin Hall effect in ferromagnetic metals [10]. Spin currents can be injected and detected in Py by spin-thermal and spin pumping measurements. We have investigated FMR spin pumping from YIG epitaxial films into Py, Fe, Co, and Ni, either in direct contacts or through a Cu spacer. We observe injection of spin currents from YIG films to FM metals, including Py, Fe, Co, and Ni, and detection of spin currents by inverse spin Hall effect (ISHE) in the FM metals. We obtain a high effective spin mixing conductance of 6.3 x $10^{18}$ $m^{-2}$ in a YIG/Cu/Py trilayer and a spin Hall angle of 0.020 for Py.

### Spin Pumping Across Field-Defined Interfaces

Understanding the mechanism that couples precessing magnetization to spin transport is an important step in utilizing this phenomenon. Studies at these sub-micron lengthscales become difficult due to the confounding effects arising from interfaces in multilayer materials. We have measured size-dependent angular momentum transport in an extended, pristine sample in which spin currents need not traverse growth-defined interfaces nor encounter lithography-induced edge damage. This is achieved by confining the magnetization precession to a mode within an area defined by the controllable dipolar field from a nearby micron-sized magnetic particle. This enables a unique investigation of changes in relaxation due to angular momentum transfer across the field-defined interface between precessing magnetization within a mode to the spin sink of the surrounding quiescent material. We observe angular momentum transport in this insulating system with an efficiency larger than that measured in YIG-metal systems. The energy and angular momentum from the precessing confined mode can be absorbed by the surrounding ferromagnetic material of the unpatterned film, as depicted in Figure 1. We observe robust intralayer spin pumping within an insulating ferromagnet, which manifests as enhanced damping as the mode radius approaches micron size.

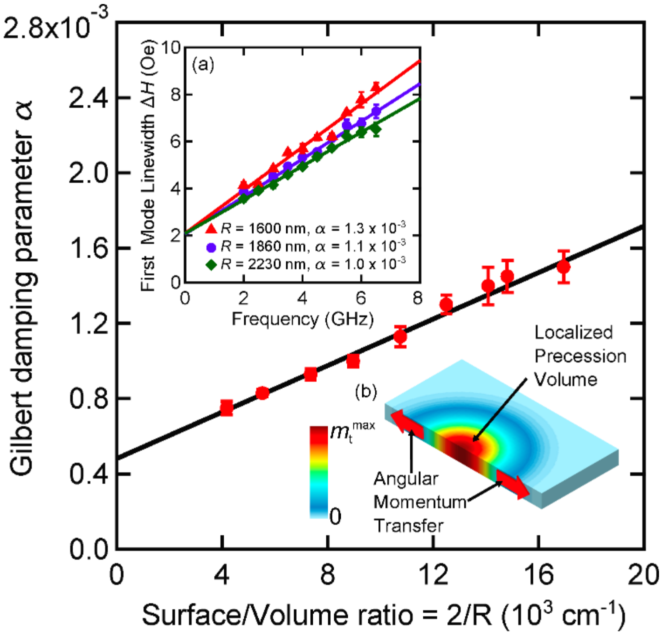

Figure 1. Dependence of the Gilbert damping of a magnetic field localized mode on mode radius. Inset shows the frequency dependence of the linewidth for several mode radii.

### **Future Plans**

In summary epitaxial YIG thin films provide a material platform for high-sensitivity investigation of dynamic spin transport in a broad range of materials including nonmagnetic, ferromagnetic, and antiferromagnetic materials, be they conducting or insulating. The phenomena uncovered in these materials and structures provide guidelines for potential spintronics applications and enable deeper understanding of fundamental interactions such as spin-orbit coupling and magnetic excitations. Locally excitation spin transport studies without the uncertainty added by materials interfaces. It further points to the ability to used scanned micromagnets to tune the character of the mode by modifying its size and energy structure through tip height, and its location by lateral scanning. We will study the interaction of spin waves generated by spin pumping or spin Hall induced spin torques with field localized modes.

## References

1. R.D. Mcmichael, D.J. Twisselmann and A. Kunz, "Localized Ferromagnetic Resonance in Inhomogeneous Thin Films," *Physical Review Letters*, **90**(22): p. 227601 (2003).
2. I. Lee, Y. Obukhov, G. Xiang, A. Hauser, F. Yang, P. Banerjee, D.V. Pelekhov and P.C. Hammel, "Nanoscale scanning probe ferromagnetic resonance imaging using localized modes," *Nature*, **466**(7308): p. 845 (2010).
3. Y. Obukhov, D.V. Pelekhov, J. Kim, P. Banerjee, I. Martin, E. Nazaretski, R. Movshovich, S. An, T.J. Gramila, S. Batra and P.C. Hammel, "Local Ferromagnetic Resonance Imaging with Magnetic Resonance Force Microscopy," *Physical Review Letters*, **100**(19): p. 197601 (2008).
4. H.-J. Chia, F. Guo, L.M. Belova and R.D. Mcmichael, "Nanoscale Spin Wave Localization Using Ferromagnetic Resonance Force Microscopy," *Physical Review Letters*, **108**(8): p. 087206 (2012).
5. R. Adur, C.H. Du, J. Cardellino, N. Scozzaro, C.S. Wolfe, H.L. Wang, M. Herman, V.P. Bhallamudi, D.V. Pelekhov, F.Y. Yang and P.C. Hammel, "Microscopic studies of nonlocal spin dynamics and spin transport," *Journal of Applied Physics*, **117**(17): p. 172604 (2015).
6. R. Adur, C.H. Du, H.L. Wang, S.A. Manuilov, V.P. Bhallamudi, C. Zhang, D.V. Pelekhov, F.Y. Yang and P.C. Hammel, "Damping of Confined Modes in a Ferromagnetic Thin Insulating Film: Angular Momentum Transfer across a Nanoscale Field-Defined Interface," *Physical Review Letters*, **113**(17): p. 176601 (2014).
7. H.T. Nembach, J.M. Shaw, T.J. Silva, W.L. Johnson, S.A. Kim, R.D. Mcmichael and P. Kabos, "Effects of shape distortions and imperfections on mode frequencies and collective linewidths in nanomagnets," *Physical Review B*, **83**(9): p. 094427 (2011).
8. C.H. Wong and Y. Tserkovnyak, "Hydrodynamic theory of coupled current and magnetization dynamics in spin-textured ferromagnets," *Physical Review B*, **80**(18): p. 184411 (2009).
9. H.T. Nembach, J.M. Shaw, C.T. Boone and T.J. Silva, "Mode- and Size-Dependent Landau-Lifshitz Damping in Magnetic Nanostructures: Evidence for Nonlocal Damping," *Physical Review Letters*, **110**(11): p. 117201 (2013).
10. H.L. Wang, C.H. Du, P.C. Hammel and F.Y. Yang, "Spin current and inverse spin Hall effect in ferromagnetic metals probed by Y3Fe5O12-based spin pumping," *Applied Physics Letters*, **104**(20): p. 202405 (2014).

**Publications under DOE BES funding**

1. R. Adur, C.H. Du, H.L. Wang, S.A. Manuilov, V.P. Bhallamudi, C. Zhang, D.V. Pelekhov, F.Y. Yang and P.C. Hammel, "Damping of Confined Modes in a Ferromagnetic Thin Insulating Film: Angular Momentum Transfer across a Nanoscale Field-Defined Interface," *Physical Review Letters*, **113**(17): p. 176601 (2014).
2. R. Adur, C.H. Du, J. Cardellino, N. Scozzaro, C.S. Wolfe, H.L. Wang, M. Herman, V.P. Bhallamudi, D.V. Pelekhov, F.Y. Yang and P.C. Hammel, "Microscopic studies of nonlocal spin dynamics and spin transport," *Journal of Applied Physics*, **117**(17): p. 172604 (2015).
3. R. Adur, C.H. Du, S.A. Manuilov, H.L. Wang, F.Y. Yang, D.V. Pelekhov and P.C. Hammel, "The magnetic particle in a box: Analytic and micromagnetic analysis of probe-localized spin wave modes," *Journal of Applied Physics*, **117**(17): p. 17e108 (2015).
4. C.H. Du, R. Adur, H.L. Wang, S.A. Manuilov, F.Y. Yang, D.V. Pelekhov and P.C. Hammel, "Experimental and numerical understanding of localized spin wave mode behavior in broadly tunable spatially complex magnetic configurations," *Physical Review B*, **90**(21): p. 214428 (2014).
5. C.H. Du, I. Lee, R. Adur, Y. Obukhov, C. Hamann, B. Buchner, J. Mccord, D.V. Pelekhov and P.C. Hammel, "Imaging interfaces defined by abruptly varying internal magnetic fields by means of scanned nanoscale spin wave modes," *Physical Review B*, **92**(21): p. 214413 (2015).
6. C.H. Du, H.L. Wang, P.C. Hammel and F.Y. Yang, "Y3Fe5O12 spin pumping for quantitative understanding of pure spin transport and spin Hall effect in a broad range of materials," *Journal of Applied Physics*, **117**(17): p. 172603 (2015).
7. C.H. Du, H.L. Wang, F.Y. Yang and P.C. Hammel, "Systematic variation of spin-orbit coupling with d-orbital filling: Large inverse spin Hall effect in 3d transition metals," *Physical Review B*, **90**(14): p. 140407 (2014).
8. C.H. Du, H.L. Wang, F.Y. Yang and P.C. Hammel, "Enhancement of Pure Spin Currents in Spin Pumping Y3Fe5O12/Cu/Metal Trilayers through Spin Conductance Matching," *Physical Review Applied*, **1**(4): p. 044004 (2014).
9. S.A. Manuilov, C.H. Du, R. Adur, H.L. Wang, V.P. Bhallamudi, F.Y. Yang and P.C. Hammel, "Spin pumping from spinwaves in thin film YIG," *Applied Physics Letters*, **107**(4): p. 042405 (2015).
10. H.L. Wang, C.H. Du, P.C. Hammel and F.Y. Yang, "Antiferromagnonic Spin Transport from Y3Fe5O12 into NiO," *Physical Review Letters*, **113**(9): p. 097202 (2014).
11. H.L. Wang, C.H. Du, P.C. Hammel and F.Y. Yang, "Spin current and inverse spin Hall effect in ferromagnetic metals probed by Y3Fe5O12-based spin pumping," *Applied Physics Letters*, **104**(20): p. 202405 (2014).
12. H.L. Wang, C.H. Du, P.C. Hammel and F.Y. Yang, "Strain-tunable magnetocrystalline anisotropy in epitaxial Y3Fe5O12 thin films," *Physical Review B*, **89**(13): p. 134404 (2014).
13. H.L. Wang, C.H. Du, P.C. Hammel and F.Y. Yang, "Spin transport in antiferromagnetic insulators mediated by magnetic correlations," *Physical Review B*, **91**(22): p. 220410 (2015).
14. H.L. Wang, C.H. Du, Y. Pu, R. Adur, P.C. Hammel and F.Y. Yang, "Scaling of Spin Hall Angle in 3d, 4d, and 5d Metals from Y3Fe5O12/Metal Spin Pumping," *Physical Review Letters*, **112**(19): p. 197201 (2014).

15. A.J. Berger, W. Amamou, S.P. White, R. Adur, Y. Pu, R.K. Kawakami and P.C. Hammel, "Magnetization dynamics of cobalt grown on graphene," *Journal of Applied Physics*, **115**(17): p. 17c510 (2014).
16. M. Harberts, Y. Lu, H. Yu, A.J. Epstein and E. Johnston-Halperin, "Chemical Vapor Deposition of an Organic Magnet, Vanadium Tetracyanoethylene," *Jove-Journal of Visualized Experiments*.e52891.(101): p. e52891 (2015).
17. Y.S. Ou, Y.H. Chia, N.J. Harmon, P. Odenthal, M. Sheffield, M. Chilcote, R.K. Kawakami, M.E. Flatte and E. Johnston-Halperin, "Exchange-Driven Spin Relaxation in Ferromagnet-Oxide-Semiconductor Heterostructures," *Physical Review Letters*, **116**(10): p. 107201 (2016).
18. Y. Pu, P.M. Odenthal, R. Adur, J. Beardsley, A.G. Swartz, D.V. Pelekhov, M.E. Flatte, R.K. Kawakami, J. Pelz, P.C. Hammel and E. Johnston-Halperin, "Ferromagnetic Resonance Spin Pumping and Electrical Spin Injection in Silicon-Based Metal-Oxide-Semiconductor Heterostructures," *Physical Review Letters*, **115**(24): p. 246602 (2015).
19. C.S. Wolfe, V.P. Bhallamudi, H.L. Wang, C.H. Du, S. Manuilov, R.M. Teeling-Smith, A.J. Berger, R. Adur, F.Y. Yang and P.C. Hammel, "Off-resonant manipulation of spins in diamond via precessing magnetization of a proximal ferromagnet," *Physical Review B*, **89**(18): p. 180406 (2014).
20. H. Yu, M. Harberts, R. Adur, Y. Lu, P.C. Hammel, E. Johnston-Halperin and A.J. Epstein, "Ultra-narrow ferromagnetic resonance in organic-based thin films grown via low temperature chemical vapor deposition," *Applied Physics Letters*, **105**(1): p. 012407 (2014).

# Transport and Optoelectronic Studies of van der Waals Material-Based Homojunctions and Heterojunctions

**Xia Hong, Department of Physics and Astronomy, University of Nebraska-Lincoln**

## Research Scope

The scope of the research is to achieve functional design of various van der Waals material-based homo- and hetero-junctions and nanostructures, examine their electrical transport and optoelectronic properties, and leverage the gained knowledge to impose band structure modification and induce new electronic states in layered two-dimensional (2D) crystals, including graphene and transition metal dichalcogenides (TMDCs). Our current research focuses on combining ferroelectric field effect with nanoscale ferroelectric domain patterning to induce local potential tuning in a layered 2D channel (Fig. 1(a)), which can lead to a Schottky- or pn-junction type interface underneath the ferroelectric domain wall (DW). By studying the electrical and optical responses of the 2D channel in the presence of different domain structures of the ferroelectric gate, we expect to gain fundamental understanding of 1) the dominant mobility limiting mechanisms in the ferroelectric-gated 2D systems, in particular the role of the ferroelectric polarization field, 2) the effects of DW roughness and electronic screening on the length scale of the induced junction, 3) the key parameters that control the induced potential profile.

## Recent Progress

We have examined the effect of ferroelectric polarization on the mobility of monolayer (ML) $MoS_2$ field effect transistor (FET) devices sandwiched between a $SiO_2$ bottom-gate and a ferroelectric copolymer poly(vinylidene fluoride-trifluoroethylene) (PVDF-TrFE) top-gate. Employing the conductive probe atomic force microscopy approach to control the polarization in P(VDF-TrFE), we have induced reversible modulation of the conduction and transfer characteristics of the $MoS_2$ FET. Based on the measured transfer curves, we modeled the back-gate voltage $V_{bg}$ dependence of the total carrier density $n_{total}$ and free carrier density $n_{free}$ in the channel when the ferroelectric top-gate is uniformly written into the polarization up ($P_{up}$) and

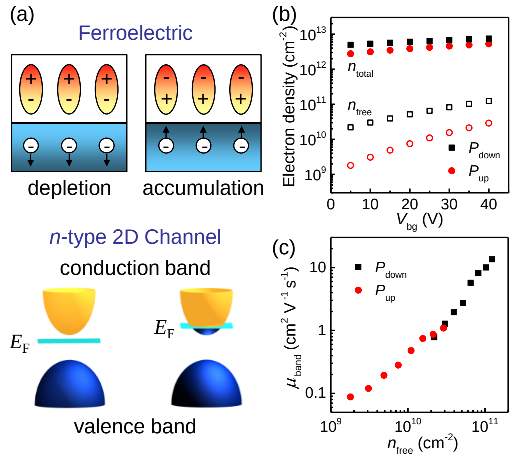

**Fig. 1: (a)** Schematic views of (a) ferroelectric field effect in an *n*-type 2D channel. **(b)** Extracted $n_{total}$ (solid symbols) and $n_{free}$ (open symbols) for a ML $MoS_2$ as a function of $SiO_2$ back-gate voltage for both polarization states of the P(VDF-TrFE) top-gate, and **(c)** the corresponding band mobility as function of $n_{free}$.

down ($P_{\mathrm{down}}$) domains (Fig. 1(b)). Here we adopted a model reported in Ref. [1] to describe the midgap impurity states due to intrinsic atomic defects such as S vacancies. Fitting to this model, we extracted the corresponding band mobility $\mu_{\mathrm{band}}$ as a function of $n_{\mathrm{free}}$ for both polarization states (Fig. 1(c)), which suggests charged impurity scattering rather than phonon scattering as the dominant mobility limiting mechanism [2]. In addition, at the same $n_{\mathrm{free}}$, the sample mobility is independent of the polarization direction, indicating that the polarization switching does not introduce additional scatterers. Another direction of ongoing research is to study the Schottky-junction states in $MoS_2$ induced by patterning a ferroelectric DW in the top-gate. We found that the barrier height of the junction can be tuned continuously by $V_{\mathrm{bg}}$, while the gate voltage window for the junction state depends sensitively on the impurity states at the $MoS_2$ conduction band tail.

In collaboration with Prof. Yongfeng Lu's group at UNL, we have also carried out scanning probe microscopy, transport, and optoelectronic studies on a range of van der Waals material-based homojunctions and heterojunctions. Figure 2(a) shows the Raman mapping of a $MoS_2$ ribbon grown via the solid-state sulfurization approach, where a natural junction has formed across the ribbon. Kelvin probe force microscopy (KPFM) studies reveal a potential step of about 400 meV (Fig. 2(b)-(c)), which is consistent with the value extracted from the junction $I_{\mathrm{DS}}$-$V_{\mathrm{DS}}$ characterizations (Fig. 2(d)). We also obtained pronounced optical response on this device, with the photo-current peaking right at the junction location (Fig. 2(e)). Next, we will apply the same techniques to study the ferroelectric-controlled junction devices.

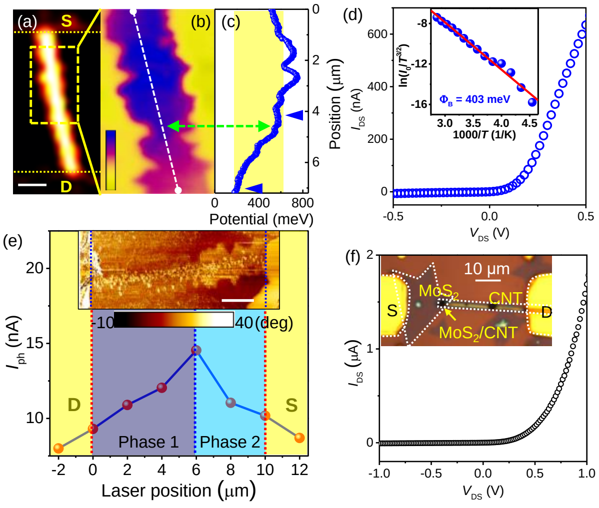

**Fig. 2 (a)** Raman mapping of $A_{1g}$ peak taken on a two-terminal $MoS_2$ ribbon device. **(b)** KPFM mapping of the surface potential of the device, with **(c)** a line-cut yielding a potential barrier $\Phi_B$ of ~400 meV. **(d)** Room temperature $I_{\mathrm{DS}}$ vs. $V_{\mathrm{DS}}$. Inset: Temperature dependence of $I_0$ reveals a $\Phi_B = 403$ meV. **(e)** Photocurrent ($I_{\mathrm{ph}} = I_{\mathrm{light}}-I_{\mathrm{dark}}$) as a function of laser position, and (inset) the AFM tapping mode phase image of the device. **(f)** $I_{\mathrm{DS}}$ - $V_{\mathrm{DS}}$ of a $MoS_2$ - CNT bundle junction device. Inset: optical image of the device.

## Future Plans

Based on our current progress, we plan to carry out research in the following directions.

1) Search for suitable contact materials for *p*-type TMDCs, and utilize the ferroelectric field effect to define programmable p-n junctions in 2D TMDs.

2) Use the junction devices as a model system to gain fundamental understanding of the interactions between the ferroelectric and 2D layers, including various mobility limiting

mechanisms in the hybrid systems, and the effect of the 2D material on ferroelectric polarization asymmetry, domain instability and switching dynamics, etc.

3) Use the gained knowledge to create nano-constrictions in TMDC and graphene, and examine the emergent phenomena.

4) Carry out transport and optical studies on various van der Waals heterojunctions, including graphene/TMDC and carbon nanotube (CNT)/TMDC (Fig. 2(f)) hybrid systems. We will obtain samples from the Lu group.

## References

[1] W. J. Zhu, T. Low, Y. H. Lee, H. Wang, D. B. Farmer, J. Kong, F. N. Xia, and P. Avouris, Electronic transport and device prospects of monolayer molybdenum disulphide grown by chemical vapour deposition, Nature Communications 5, 3087 (2014).

[2] N. Ma, and D. Jena, Charge Scattering and Mobility in Atomically Thin Semiconductors, Physical Review X 4, 011043 (2014).

## Vortex Matter in Superconductor/Ferromagnet Heterostructures

**Maria Iavarone, Physics Department, Temple University, Philadelphia PA 19122**

**e-mail: iavarone@temple.edu**

### Research Scope

The primary emphasis of this project is on the physics of vortices in confined superconductors and hybrid heterostructures such as superconductor-ferromagnet (S/F) systems. The goal is to understand how the physics of vortex matter changes in order to be able to predict and control the electronic properties of new hybrid systems. Low temperature scanning tunneling microscopy and spectroscopy can be used to probe the vortex configuration as well as the electronic states within the vortex core directly.

The understanding of the local changes in the electronic density of states is crucial as it also affects all the thermodynamic properties of the material. This effort will be combined with searching novel guiding principles to enhance materials and devices functionalities by combining specific properties of ferromagnets and superconductors.

In proximity coupled structures the interplay between magnetism and superconductivity will lead to new physical phenomena with superconductivity coexisting with ferromagnetism at the interface. In magnetically coupled structures the inhomogeneous stray field of the ferromagnet leads to an inhomogeneous superconducting state where superconductivity and vortices can be confined in channels determined by the underlying magnetic template and make these structures attractive model systems that offer the possibility to control the strength and the location of the superconducting nucleus by applying an external magnetic field.

### Recent Progress

In the concurrence time we have focused on different S/F heterostructructures magnetically coupled and we started working on the S/F systems in the regime of proximity coupling. We had already shown the criteria for the existence of vortex-antivortex pairs in planar S/F, we had visualized domain wall superconductivity and reverse domain wall superconductivity, during the last two years we have shown that STM applied to these structures can be used to visualize the screening currents and the vortex supercurrents (Doppler effect). We also have shown, by combining MFM and STM measurements, that vortex clusters can be stabilized.

### Doppler STM

Mapping the distribution of currents inside a superconductor is usually performed indirectly through imaging of the stray magnetic fields above the surface. We have showed that by direct imaging of the Doppler shift contribution to the quasiparticle excitation spectrum in the superconductor using low temperature scanning tunneling microscopy, we obtain directly the distribution of supercurrents inside the superconductor. We demonstrated the technique at the example of superconductor/ferromagnet hybrid structure that produces intricate current pattern consisting of combination Meissner shielding currents and Abrikosov vortex currents.

The superfluid velocity is directly proportional to the gradient of the phase of the order parameter, Δφ. It modifies the quasiparticle excitation spectra in the superconductor to [1] :

$$E_k = \left(\varepsilon_k^2 + \Delta^2\right)^{1/2} + m\vec{v}_F \cdot \vec{v}_s \quad (1)$$

where Δ is the superconducting pair potential, $v_F$ is the Fermi velocity and $v_s$ is the superfluid velocity. The second term in the equation is the Doppler energy. The Doppler term shifts the energy of the quasiparticles up or down depending on the relative directions between the velocities $v_F$ and $v_s$. Scanning tunneling spectroscopy measures the spatial distribution of quasiparticle DOS and thus could be used to map the supercurrents in the superconductors with high spatial resolution, being limited by the superconducting coherence length [2].

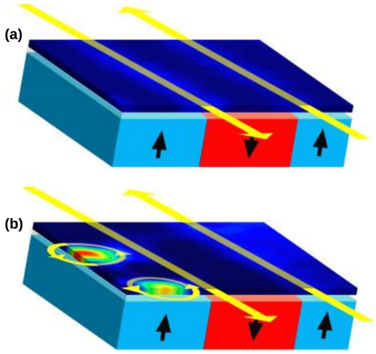

**Figure 1** Schematic of currents in the superconducting film in absence of vortices (a), and in the presence of vortices (b). The top layer in each schematic is the zero bias conductance map acquired in presence of zero applied magnetic field (a) and in the presence of a magnetic field H= +200Oe applied perpendicular to the film surface (b). The bottom layer shows the magnetic domains of the underlaying ferromagnetic layer.

In Figure 1 (a) the low-temperature zero bias conductance map acquired in the absence of any externally applied magnetic field reveals a clear spatial modulation on the length scale congruent with that of the underlying ferromagnet domain structure having stripe periodicity of (*w*~150-200nm), that persists to temperatures close to the superconducting critical temperature. We can attribute this spatial modulation to the pair-breaking effect of the Meissner currents, i.e. the Doppler term in Equation 1, partially shielding the field emanating from the magnetic stripe domains in the ferromagnetic layer (Co-Pd film). In the presence of an applied magnetic field vortices nucleate in the system and in this case the Doppler term in Equation 1 is a superposition of supercurrents due to Meissner shielding (above the domain walls) and paramagnetic vortex fux. Since they circulate in opposite directions, as shown schematically in Figure 1(b), the appearance of vortices will significantly reduce the Doppler term in the regions when these two contributions meet, i.e. above the domain walls (Figures 1(b)). This method could prove invaluable for mapping the supercurrents in applications where maximization of the supercurrent is desired.

## Observation of superconducting vortex clusters in S/F hybrids

While Abrikosov vortices usually repel each other in bulk superconductors, strong confinement potential, either geometric in mesoscopic superconductors or magnetic in superconductor/ferromagnet (S/F) hybrids, profoundly affects the superconducting vortex distribution and can lead to vortex clusters formation. We studied the vortex confinement in S/F thin film heterostructures by direct observation of vortex clusters pinned at the dislocations of stripe-like magnetic domains by using magnetic force microscopy and scanning tunneling microscopy and spectroscopy. Magnetic force microscopy allows the imaging of such dislocations as well as of the superconducting vortex distribution. Scanning tunneling microscopy and spectroscopy give detailed information of the local electronic density of states outside and inside the vortex cluster.

We demonstrate that superconducting vortex clusters can appear as a consequence of peculiar micromagnetic configurations and topology as a result of a competition between vortex-vortex interaction, enhanced local stray field and Lorentz force.

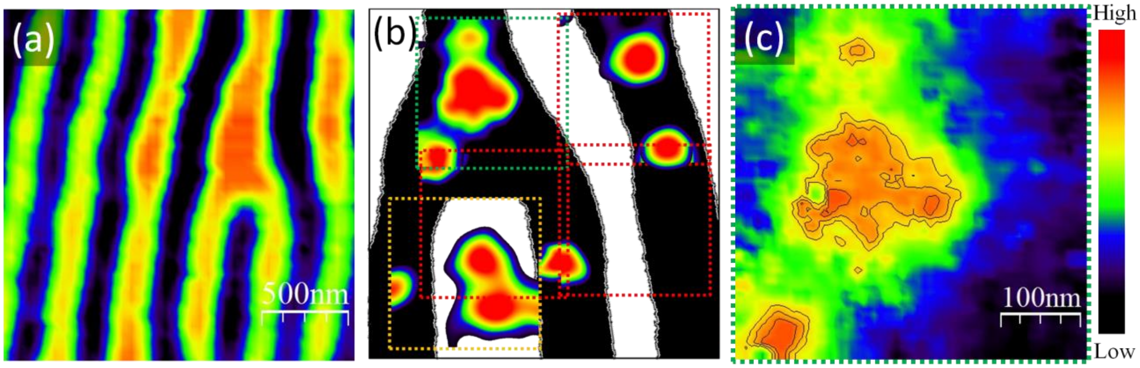

**Figure 2: (a) STM observation of vortex clusters at the bifurcation.** Room temperature MFM of Co(2nm)/Pd(2nm)$_{200\text{-bilayers}}$. (b) Spontaneous superconducting vortices in Pb(30nm)/[Co(2nm)/Pd(2nm)$_{200\text{-bilayers}}$] superimposed to a cartoon of the magnetic domains. The vortices have been mapped by acquiring five conductance maps, each of them 438nm×438nm in size, at the Fermi energy and at T=1.5 K after a zero field cooling. (c) Conductance map at the dislocation (the location is the green dotted square in (b)), acquired at the Fermi energy and at T=1.5K in zero field cooling.

## Future Plans

We will continue to explore the physics of mesoscopic and S/F structures with an emphasis on the vortex matter. In particular we will focus on both magnetically coupled and proximity coupled S/F structures.

The possibility of tuning the ferromagnetic state by changing size and shape of the ferromagnet offers an additional degree of freedom. Specifically, in a dot of ferromagnetic material of micrometer or submicrometer size, a curling spin configuration— that is, a magnetization vortex will occur in place of domains. This magnetic vortex is expected to affect the vortex distribution in a superconductor magnetically coupled to the ferromagnet. Moreover, it was proposed theoretically [3,4] that proximity-induced long-range triplet components are generated by the ferromagnetic vortex coupled to a singlet superconductor. This configuration allows controllable switching between long- and short-range proximity effects by employing the peculiar properties of ferromagnetic vortex.

## References

[1] P. Fulde, *Tunneling phenomena in solids: lectures,* edited by E. Burstein and S. Lundqvist (Plenum Press, New York, 1967), p. 427

[2] P. De Gennes, *Superconductivity of metals and alloys* (Addison-Wesley, Redwood City, Calif, 1989)

[3] M. S. Kalenkov, A. D. Zaikin, and V. T. Petrashov "Triplet Superconductivity in a Ferromagnetic Vortex" *Phys. Rev. Lett*. **107,** 087003 (2011)

[4] A. A. Golubov, M. Yu Kupriyanov, Ya V. Fominov "Critical current in SFIFS junctions" *Pis'ma Zh. Eksp. Teor. Fiz.* **75,** 223–7 (2002)

## Publications (DOE sponsored 2014-2016)

[1] "Observation of superconducting vortex cluster in S/F hybrids", C. Di Giorgio, F. Bobba, A.M. Cucolo, A. Scarfato, S.A. Moore, G. Karapetrov, D. D'Agostino, V. Novosad, V. Yefremenko, and M. Iavarone, Under Review (2016)

[2]"Doppler-STM Current Imaging in Superconductor-Ferromagnet Hybrids", S. A. Moore, G. Plummer, J. Fedor, J. Pearson, V. Novosad, G. Karapetrov, and M. Iavarone, Featured Article in Appl. Phys. Lett. 108, 042601 (2016)

[3] ]"Anisotropic Superconducting Gaps and Boson Mode in FeSe1-xSx single crystals", C. Di Giorgio, A.V. Putilov, D.J. Trainer, O.S. Volkova, A.N. Vasiliev, D. Chareev, G. Karapetrov, J.F. Zasadzinski, M. Iavarone, in press Journal of Superconductivity and Novel Magnetism (2016) DOI: 10.1007/s10948-016-3644-6

[4] "Evolution of the superconducting properties in $FeSe_{1-x}S_x$"S. A. Moore, J.L. Curtis, C. Di Giorgio, E. Lechner, M. Abdel-Hafiez, O.S. Volkova, A.N. Vasiliev, D.A. Charrev, G. Karapetrov, and M. Iavarone *Phys. Rev. B* **92**, 235113 (2015)

[5] "Low-temperature scanning tunneling microscopy and spectroscopy measurements of ultrathin Pb films", S. A. Moore, J. Fedor and M. Iavarone, *Superconductor, Science and Technology* **28(4)**, 045003 (2015)

[6] "Magnetic pinning in a superconducting film by a ferromagnetic layer with stripe domains", D. Mancusi, C. Di Giorgio, F. Bobba, A. Scarfato, A.M. Cucolo, M. Iavarone, S.A. Moore, G. Karapetrov, V. Novosad, V. Yefremenko, S. pace and M. Polichetti, *Superconductor, Science and Technology* **27(12)**, 125002 (2014)

[7] "Influence of Domain Width on Vortex Nucleation in Superconductor/Ferromagnet Hybrid Structures", M. Iavarone, S.A. Moore, J. Fedor, V. Novosad, J. A. Pearson, G. Karapetrov, *J. Supercond. Nov. Magn*. 28(3), 1107-1110 (2015) DOI: 10.1007/s10948-014-2650-9

[8]"Anisotropic Superconducting Gaps and Boson Mode in FeSe1-xSx single crystals", C. Di Giorgio, A.V. Putilov, D.J. Trainer, O.S. Volkova, A.N. Vasiliev, D. Chareev, G. Karapetrov, J.F. Zasadzinski, M. Iavarone, in press Journal of Superconductivity and Novel Magnetism (2016) DOI: 10.1007/s10948-016-3644-6

[9] Book Chapter:"Mesoscopic Effects in Superconductor-Ferromagnet Hybrids", Goran Karapetrov, Steven A. Moore and Maria Iavarone, in the book "The Oxford Handbook of Small Superconductors" edited by V. Narlikar, Oxford University Press ISBN: 9780198738169 (2016)

[10] Book Chapter""Low Temperature Magnetic Force Microscopy Studies of Static and Dynamic Vortex-Antivortex Configurations in Magnetically-coupled Superconductor-Ferromagnet Hybrids" C. Di Giorgio, F. Bobba, A. Scarfato, D. D'Agostino, M. Iavarone, G. Karapetrov, S.A. Moore, M. Polichetti, D. Mancusi, V. Novosad, V. Yefremenko, and A.M. Cucolo in the book: Vortex Dynamics which will be published by InTech - Open Access Publisher (Under Review 2016).

# Spatial Evolution of Electric-field-driven Metal-insulator Transitions

**PI: Keji Lai (kejilai@physics.utexas.edu)**

**Department of Physics, University of Texas at Austin, Austin, TX 78712**

## Program Scope

The goal of this DOE supported Early Career program is to explore the microscopic details of metal-insulator transitions when charge carriers in advanced quantum materials are electrostatically modulated in field-effect transistor (FET) structures. In particular, we utilize the microwave impedance microscope (MIM)[1], a novel technique capable of resolving nanoscale dielectric and conductivity information, to image the local conductance at the buried transistor interface. The visualization of conductance fluctuations is scientifically significant for the understanding of electronic phase transitions induced by density modulation. The results are also of technological relevance to address the microscopic origin of sub-threshold behaviors in novel FETs for nanoelectronic applications.

## Recent Progress

Two types of FET structures, as shown in Fig. 1, have been studied by our MIM work. The conventional back-gated MOSFET is the most straightforward structure to modulate the density up to ~ $10^{13}$ $cm^{-2}$. Electric-double-layer transistors (EDLTs)[2] using a spin-coated ion gel thin film as the gate dielectric, on the other hand, have demonstrated a remarkable density modulation as high as $10^{14}$ ~ $10^{15}$ $cm^{-2}$.

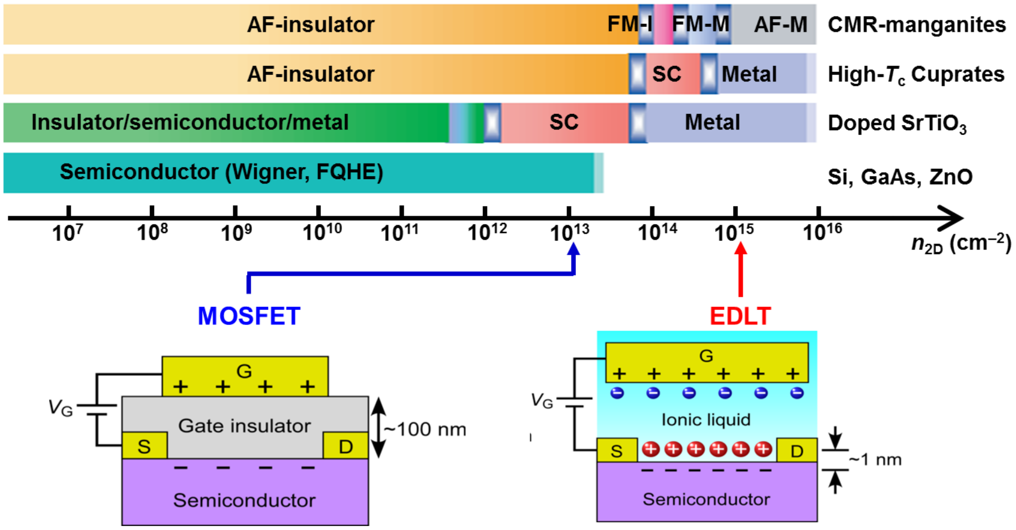

Figure 1. Zero-temperature behavior of various correlated systems as a function of sheet charge density. AF, antiferromagnetic; FM, ferromagnetic; I, insulator; M, metal; SC, superconductor; CO, charge order; FQHE, fractional quantum Hall effect; Wigner, Wigner crystal. The maximum density modulations in MOSFETs and EDLTs (schematics of the device structures included here) are indicated in the plot.

## Electrical inhomogeneity and edge states in $MoS_2$ MOSFETs

Devices in the FET configuration have played an essential role in the blooming field of semiconducting transition metal dichalcogenides (TMDs)[3] such as $MoS_2$ and $WSe_2$. Due to the intrinsic defects and the inevitable charged states in the substrates, electrical inhomogeneity is not uncommon in TMDs, leading to hopping transport and percolation transition in the devices. For van der Waals materials, another feature takes place at the sample edges, where the broken crystalline symmetry and the presence of dangling bonds introduce additional electronic states to the bulk band structure. Spatially resolved conductance maps are therefore highly desirable for the understanding of electrical inhomogeneity and edge channels in TMD FETs.

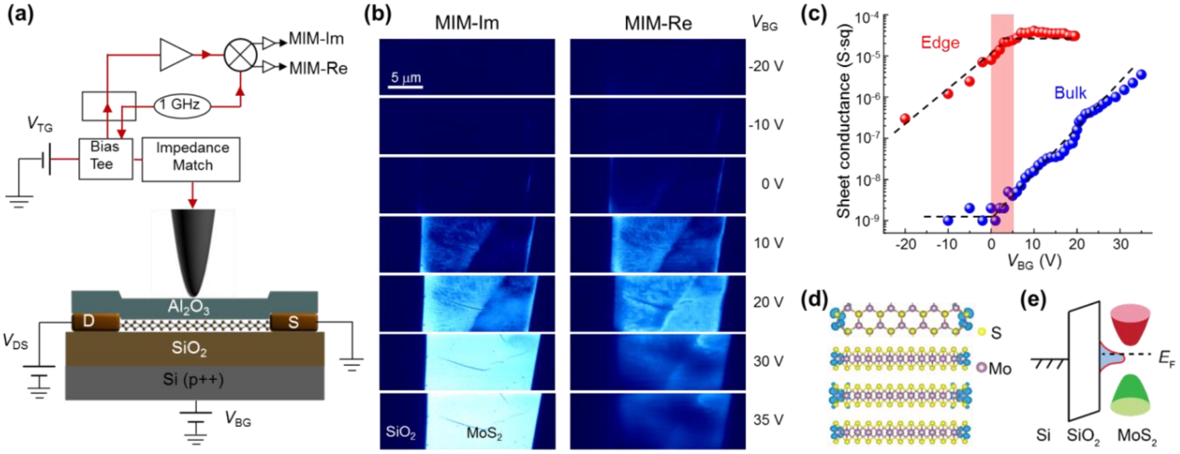

Figure 2. (a) Schematic diagram of the device and the MIM setup. (b) Selected MIM images of an exfoliated $MoS_2$ device at different $V_{BG}$'s. Note that the MIM-Im signals increase monotonically as the local conductance, while the MIM-Re signals peak around $g_{bulk} \sim 10^{-7}$ S·sq. (c) Effective edge and bulk conductance as a function of $V_{BG}$. The shaded column marks the onset of bulk conduction and the saturation of edge conduction. (d) DFT calculations of the electron wave functions for selected orbitals, showing the localized edge states at the boundary atoms. (e) Cartoon of the edge and bulk bands of $MoS_2$ and the $SiO_2$/Si substrate. [Wu2016]

Fig. 2a illustrates the experimental setup for MIM measurements [Wu2016]. The conductance evolution in Fig. 2b vividly demonstrates the insulator-to-metal transition as a function of $V_{BG}$. When the flake is insulating ($V_{BG} = -20$ V), there is no electrical contrast between $MoS_2$ and the substrate. As $V_{BG}$ gradually goes up to 0 V, the contrast first emerges at the edges and then in the interior of the sample. Around $V_{BG} = 20$ V, strong inhomogeneity is observed, whereas the conductive edges gradually merge into the bulk. For even higher $V_{BG}$, the sample appears uniformly bright in MIM-Im and dim in MIM-Re. Using finite-element analysis (FEA)[4], we can quantify the local conductance at the sample bulk and edges, as shown in Fig. 2c. As $V_{BG}$ increases, the edge conductance increases initially and levels off beyond $V_{BG} = 0$ V, where the bulk conductance starts to increase above the noise floor. The scenario is consistent with our density functional theory (DFT) calculations (Fig. 2d), which shows the additional electronic states localized at boundary atoms. As illustrated in Fig. 2e, electrons first populate the edges before the in-gap states are completely filled. The further increase of $V_{BG}$ will then raise the Fermi level into the bulk conduction band, resulting in the upturn of $g_{bulk}$.

### Insulator-to-metal transition in ion-gel-gated EDLTs

The unprecedented tunability of electron concentration using EDLTs represents a paradigm shift in condensed matter physics research since many carrier-mediated processes, previously only accessible through chemical substitution, can now be studied in the FET configuration with better controllability and less disorder effect. In conventional EDLTs[2], however, the electrolyte-semiconductor interface is usually buried underneath a large droplet of ionic liquid and thus cannot be directly studied by surface-sensitive probes. As a result, a major challenge here is to microscopically study the conductance evolution in the devices.

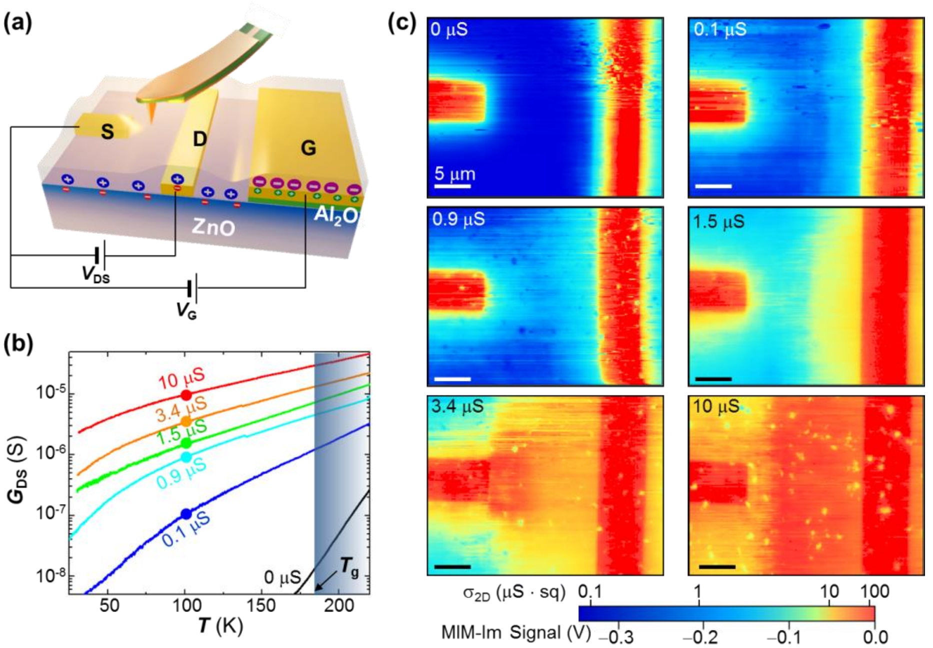

Figure 3. (a) Schematic diagram of the ion-gel-gated EDLT with source-drain and gate voltages and the MIM tip. (b) Temperature dependence of the channel conductance $G_{DS}$ as the device is gradually turned on. The $G_{DS}$'s at 100 K are labeled on each curve. (c) MIM-Im images with different $G_{DS}$'s at 100 K. The false-color scale shows both the MIM signals and $\sigma_{2D}$ simulated from FEA. All scale bars are 5μm. [Ren2015]

Our innovation is to spin coat a 50nm-thick layer of ionic gel on the device that maintains the gate tunability, as schematically shown in Fig. 3a [Ren2015]. The gel freezes below its glass transition temperature of ~ 200 K so that we can perform contact-mode imaging at low temperatures. The insulator-to-metal transition is clearly observed from the $T$-dependent measurements in Fig. 3b. For each transport curve, we acquire the MIM images in Fig. 3c near the source/drain electrodes at $T$ = 100 K. For a quantitative understanding, we again convert the MIM signals to the 2D sheet conductance $\sigma_{2D}$ by FEA[4], as indicated by the false-color scale in Fig. 3c. When a gate bias above the threshold voltage is applied, electrons in ZnO are first induced by fringing fields from the cations accumulated on the electrodes, which is vividly manifested by the MIM data as $G_{DS}$ increases from 0 to 1.5 μS. For $G_{DS}$ = 3.4 μS, the highly conductive areas originated from the two electrodes start to merge. At the highest $G_{DS}$ of 10 μS, the ZnO became highly conductive with $\sigma_{2D}$ > 10 μS · sq everywhere inside the channel. We emphasize that, while the process is ubiquitous in FETs, it is a rare occasion that the evolution can be imaged by scanning probes, which provide not only strong support on the effectiveness of ion-gel gating but also the real-space information of insulator-to-metal transitions.

## Future Plans

With the substantial progress made in the past two years, we are well positioned to proceed with this DOE program to make further scientific discoveries on various FETs. We will perform MIM studies on vertical and lateral heterostructures of TMD materials in the back-gated MOSFET configuration. The local conductance at the hetero-interfaces is of particular interest for the application of these devices. The TMD samples will also be coated with an ion-gel layer for the EDLT research. The goal is to apply a large source-drain voltage ($V_{DS} > V_{GS}$), which will set up a p-n junction in the material, and image the resultant spatial distribution inside the channel. In addition, we have obtained thin-film manganite and nickelate samples from our collaborators and have started to fabricate EDLT devices on them. We aim to investigate the local inhomogeneity in these materials and compare the microscopic evolution of metal-insulator phase transitions induced by magnetic field and electric field. We expect to enter an exciting and uncharted regime through the unique MIM measurements.

## References

1. K. Lai, W. Kundhikanjana, M. A. Kelly and Z.-X. Shen, "Nanoscale microwave microscopy using shielded cantilever probes", *Appl. Nanoscience* **1**, 13 (2011).
2. R. Misra, M. McCarthy, and A. F. Hebard, "Electric field gating with ionic liquids", *Appl. Phys. Lett.* **90**, 052905 (2007).
3. Q. H. Wang, K. Kalantar-Zadeh, A. Kis, J. N. Coleman, and M. S. Strano, "Electronics and optoelectronics of two-dimensional transition metal dichalcogenides. *Nature Nanotechnol.* **7**, 699-712 (2012).
4. K. Lai, W. Kundhikanjana, M. Kelly, and Z. X. Shen, "Modeling and characterization of a cantilever-based near-field scanning microwave impedance microscope", *Rev. Sci. Instrum.* **79**, 063703 (2008).

## Publications

1. [Ponath2015] P. Ponath, K. Fredrickson, A. B. Posadas, Y. Ren, X. Wu, R. K. Vasudevan, M. B. Okatan, S. Jesse, T. Aoki, M. R. McCartney, D. J. Smith, S. V. Kalinin, **K. Lai**, and A. A. Demkov, "Carrier density modulation in a germanium heterostructure by ferroelectric switching", *Nature Commun*. **6**, 6067 (2015).

2. [Ren2015] Y. Ren, H. Yuan, X. Wu, Z. Chen, Y. Iwasa, Y. Cui, H. Y. Hwang, and **K. Lai**, "Direct Imaging of Nanoscale Conductance Evolution in Ion-Gel-Gated Oxide Transistors", *Nano Lett*. **15**, 4730 (2015).

3. [Wu2016] D. Wu, X. Li, L. Luan, X. Wu, W. Li, M. N. Yogeesh, R. Ghosh, Z. Chu, D. Akinwande, Q. Niu, **K. Lai**, "Uncovering Edge States and Electrical Inhomogeneity in $MoS_2$ Field Effect Transistors", *Proc. Natl. Acad. Sci*. **31**, 8583 (2016).

# The SQCRAMscope:  A Scanning Quantum Cryogenic Atom Microscope

**Prof. Benjamin Lev**
**Departments of Physics and Applied Physics and Ginzton Laboratory**
**Stanford University**
**benlev@stanford.edu**

**Research Scope:** Microscopic imaging of local magnetic fields provides a window into the organizing principles of complex and technologically relevant condensed matter materials. However, a wide variety of intriguing strongly correlated and topologically nontrivial materials exhibit poorly understood phenomena outside the detection capability of state-of-the-art high-sensitivity, high-resolution scanning probe magnetometers. Here we introduce a quantum-noise-limited scanning probe magnetometer that can operate from room to cryogenic temperatures with unprecedented DC-field sensitivity and micron-scale resolution. The Scanning Quantum Cryogenic Atom Microscope (SQCRAMscope) [1] employs a magnetically levitated atomic Bose-Einstein condensate (BEC), thereby providing immunity to conductive and blackbody radiative heating. The SQCRAMscope has a noise floor of 300 pT and provides a 100x improvement in magnetic flux sensitivity over previous atomic scanning probe magnetometers [2]. These capabilities are carefully benchmarked by imaging magnetic fields arising from microfabricated wire patterns. We anticipate the SQCRAMscope will provide charge transport images at temperatures from room-to-4 K in unconventional superconductors and topologically nontrivial materials.

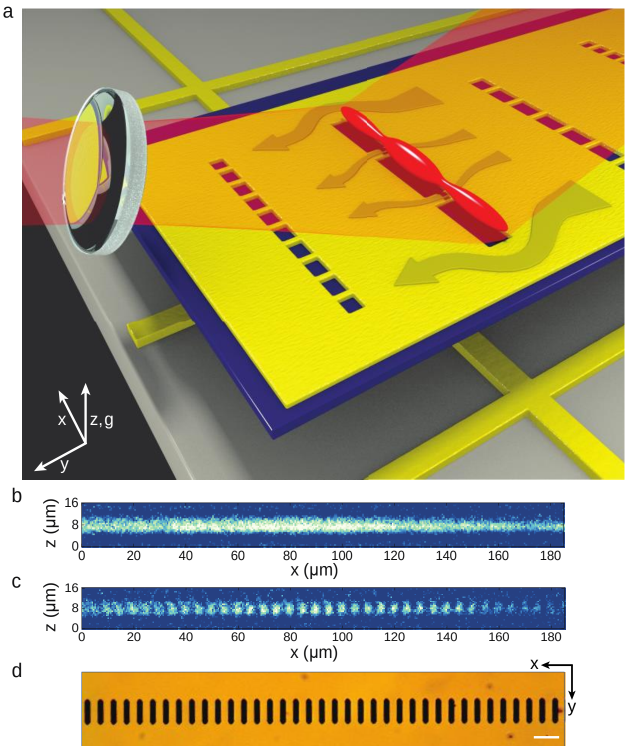

**Figure 1. SQCRAMscope operation**. **a**, A quasi-1D BEC (red) is magnetically confined using an atom chip trap (light grey with gold wires). Suspended between the atom chip and the BEC is the silicon sample substrate (blue) onto which the gold calibration pattern is fabricated. Current (yellow arrows) flowing through gaps in the gold, defining microwires, fragments the BEC; contact leads not shown. Atomic density is imaged with a high-NA lens by reflecting a resonant laser (transparent red) off the gold. BEC position is fixed while the sample substrate, not connected to the atom chip, may be scanned and cryogenically cooled. **b**, Absorption image of an unfragmented quasi-1D BEC. **c**, Absorption image of fragmented BEC. Current flows through periodic array of 2.5-μm wide wires spaced 2.5-μm apart. **d**, Image of the microwire array used in panels b and c. White scale bar is 10 μm.

**Recent Progress:** Quantum sensors comprised of nitrogen-vacancy (NV) color centers in diamond have joined scanning Superconducting Quantum Interference Devices (SQUIDs) in advancing high-sensitivity magnetometry into the nanoscale regime [3,4]. We add to this quantum metrology toolbox a carefully calibrated cryogenic scanning magnetometer that exploits the extreme sensitivity of quantum gases to external fields. The SQCRAMscope operating principle is sketched in Fig. 1. Inhomogeneous magnetic fields from a nearby source exert a Zeeman force on atoms Bose-condensed in a smoothly varying harmonic trap. The atoms move in response, distorting the otherwise smooth wavefunction of the BEC. The BEC density is then imaged by recording the absorption of resonant light using a CCD camera. The local density may be related to field through the BEC equation of state. A 2D-field map is created by raster-scanning the relative position of the BEC and the source with a duty cycle limited by the time needed to recreate the BEC after the destructive absorption imaging process. Assuming no z-dependence of the source, application of the Biot-Savart law, conservation of current, and a measurement of the distance d between BEC and sample allows one to convert an x-y map of the x field component into a 2D map of the current flow (or magnetic domains) in the source.

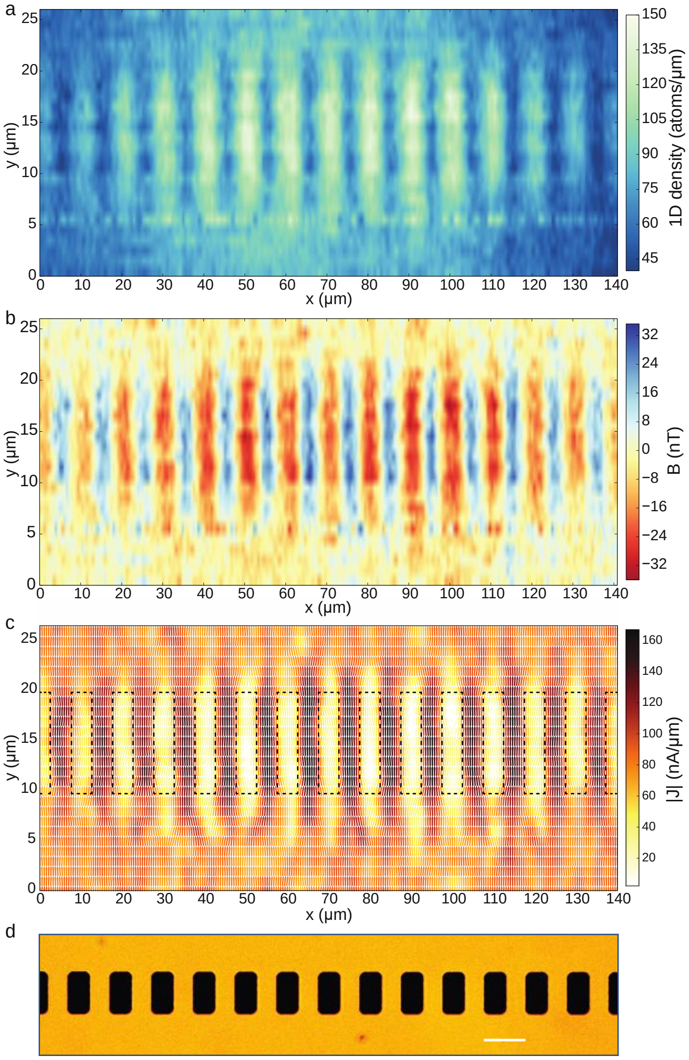

**Figure 2**. **Wide-area image of current density in microwire array.** Current flows through room-temperature array of 5-µm-wide gold wires spaced 5-um apart. Sample is scanned in 1-µm steps along y. The BEC is confined 1.4(1)-µm below. **a**, Line density of BEC. **b**, Magnetic field along x derived from density data using equation of state. **c**, Current density obtained from magnetic field and measurement of d through use of Biot-Savart equation. Arrows indicate current direction; black dashed rectangles demarcate the gaps between microwires. **d**, Image of the microwire array. White scale bar is 10 µm.

The BEC is confined in a high-aspect-ratio, cigar-shaped trap formed using an atom chip-based magnetic microtrap. This quasi-1D Bose gas lies within the quasicondensate regime because the transverse trap frequency is 157x larger than the longitudinal trap frequency, the chemical potential is similar in magnitude to the transverse trap frequency, and the gas temperature is 2.6x lower than this frequency. As such, density fluctuations are suppressed below the quantum shot-noise limit, enhancing field sensitivity. The equation of state in the quasicondensate regime relates the potential to the atomic density. This potential is the sum of the well-characterized trapping potential and the magnetic potential to be measured. For the employed atomic state and at the small fields that are measured, the magnetic potential is linearly proportional to field. Small inhomogeneous fields only perturb the trap potential along the weakly trapped axis; imaging the BEC density therefore provides a measurement of a vector component of the magnetic potential.

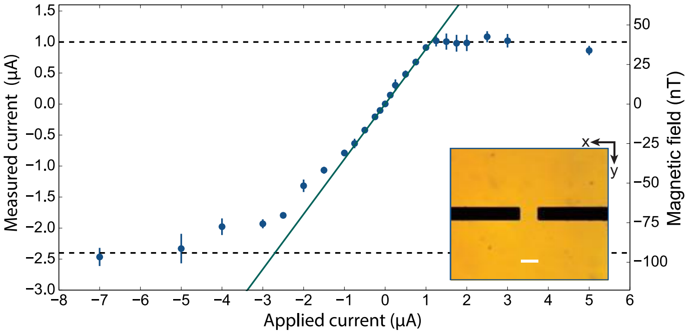

**Figure 3. Accuracy, repeatability, linearity, and dynamic range.** Measurement of current in the 12-μm wide calibration wire shown in inset. White scale bar is 12 μm. BEC is positioned 1.7(1)-μm below wire center, and the current is varied to create either a density dimple or peak in the atomic density. The green line is a fit to the linear region.

Figure 2 shows a typical magnetic field scan above a room-temperature microwire array, and the resulting image of the current density flowing through the wires. The FWHM point-spread resolution of the atomic density and magnetic field is 2.2(1) μm. The lower resolution of the current density map is due to the convolution of the typical single-shot distance d = 1.4(1) μm of the atoms from the sample. Distances as short as 0.8(1) μm, shown in Fig. 1c, provide a source resolution of 2.3(1) μm. Current flow through the microwires is clearly visible in Fig. 2c, as is the fanning out of current into the bulk. Patches of lower current density may result from higher-resistance grains in the polycrystalline film, as measured in Ref. 2.

The accuracy, repeatability, linearity, and dynamic range of the magnetometer are shown in Fig. 3. The green line is a fit to the linear region of the measured versus applied current data and has a slope of 0.88(2). This implies an accuracy of 11(2)% and a responsivity only 11(2)% lower than that predicted, 1.97(3) nT/(atom/μm). The fields and current densities reported in Fig. 3 correspond to those calculated with a finite-element solver for the employed gold microwire dimensions to within 10%.

The linear part of the dynamic range is between approximately ±1.0 μA (±40 nT). The upper limit arises due to lack of atoms in the high-field regions, while the lower limit arises due to all the atoms pooling into the low-field regions. An extended-dynamic-range trap provided a 3x-larger linear dynamic range, though with a responsivity 3x worse. We have employed a thermal gas to increase the dynamic range by 50x, though at worse resolution and with 100-fold-worse responsivity.

The repeatability, or average standard deviation in the data about the linear fit, is 2.3(3) nT, and the stability of the field measurement, measured as Allan deviation, is 1.1(1) nT after 30 experimental runs. With no current applied to sample, we measure a minimum detectable field of 2.8(5) nT. The magnetometer simultaneously provides many independent pixels of information because the quasi-1D BEC may be several hundred microns in length while the imaging resolution is on the micron scale. Given our 16-s duty cycle and the 140-μm usable BEC length, the field sensitivity for wide-area imaging is 0.9(2) nT/Hz$^{1/2}$ with a noise floor of 300 pT after 100 runs. Future improvements can both decrease this duty cycle and elongate the usable BEC length.

This noise floor is consistent with two independently measured quantum-noise-limited sources: photon shot noise accounts for 2.5(4) nT, while atom density noise is 1.7(7) nT. Due to the quasicondensate nature of the gas, this noise is a factor of ~2 below that expected for shot noise in the higher density regions of the BEC. These field measurements translate into a 2-nA minimum detectable current from an infinitely thin wire or 80 horizontally oriented 1-$\mu_B$ dipoles, if the BEC is located d = 0.8 μm from these sources.

We now highlight other demonstrated features of the SQCRAMscope. Because the samples are physically detached from the chip, we can rapidly replace the sample without disturbing the BEC production apparatus in less than a week's time. This is up to several months faster than current systems whose samples are attached directly to the atom chip. Secondly, the sample temperature may be independently controlled and stabilized; for attached samples, trapping wire currents can heat and cool the sample, or fix the sample temperature to be the same as the superconducting atom chip [5]. The SQCRAMscope allows any ~1-cm$^2$ area, ~150-μm-thin sample made of UHV-compatible material to be imaged from room-to-cryogenic temperatures. We have demonstrated here the functionality of the SQCRAMscope at room temperature and 35 K and believe operation down to ~4 K will soon be possible with the addition of a heat shield [6].

**Future plans:** The SQCRAMscope will enable the high-sensitivity study of strongly correlated and topologically nontrivial materials in unexplored regimes of high temperature and low frequency. For example, domain structure and transport near twin boundary interfaces in underdoped Fe-arsinide superconductors can be explored as the $T_N$ ~ 50-150 K nematic transition is crossed [7]. Imaging transport near 1/8 doping in the cuprate superconductor LBCO may reveal spontaneous currents due to the possible emergence of pair-density-wave superfluidity below ~30 K [8]. Other unconventional superconductors and complex oxide interfaces (LAO/STO) may be explored at high temperatures, as well as the metal-to-insulator transition in $VO_2$. Both transport and static magnetization at the ~100-K ferromagnetic-metallic and antiferromagnetic-insulating transition in colossal magnetoresistive systems may be imaged. Investigations of topologically protected transport should be possible, as should the electronic hydrodynamic flow in graphene above $LN_2$ temperatures [9]. Lastly, the SQCRAMscope will also find use in engineering hybrid quantum systems, in coupling BECs to photonic topological metamaterials, and in studying the Casimir-Polder force.

**References:**

2) S. Aigner *et al.*, *Long-range order in electronic transport through disordered metal films,* Science **319** 319 (2008).

3) I. Lovchinsky *et al., Nuclear magnetic resonance detection and spectroscopy of single proteins using quantum logic*, Science **351**, 836 (2016).

4) J. R. Kirtley, *et. al., Scanning SQUID susceptometers with sub-micron spatial resolution* arXiv:1605.09483 (2016).

5) J. Reichel, V. Vuletic, *Atom chips*, Wiley, 2011.

6) M. A. Naides, R. W. Turner, R. A. Lai, J. M. DiSciacca, and B. L. Lev, *Trapping ultracold gases near cryogenic materials with rapid reconfigurability*, Appl. Phys. Lett. **103**, 251112 (2013).

7) J.-H. Chu, J. Analytis, K. De Greve, P. Mcmahon, A. Islam, Y. Yamamoto, and I. Fisher, *In-Plane Resistivity Anisotropy in an Underdoped Iron Arsenide Superconductor,* Science **329**, 824 (2010).

8) E. Berg, E. Fradkin, E. A. Kim, S. A. Kivelson, V. Oganesyan, J. M. Tranquada, and S. C. Zhang, *Dynamical Layer Decoupling in a Stripe-Ordered High-$T_c$ Superconductor, Phys*. Rev. Lett. **99**, 127003 (2007).

9) J. Zaanen, *Electrons go with the flow in exotic material systems,* Science **351**, 1026 (2016).

**Publications:**

1) F. Yang, A. J. Kollár, S. F. Taylor, R. W. Turner, and B. L. Lev, *A Scanning Quantum Cryogenic Atom Microscope*, arXiv:1608.06922 (2016).

# Heterostructures of Dirac materials

**PI: Lian Li**

**Department of Physics and Astronomy, West Virginia University, Morgantown, WV**

## Program Scope

Exploration of heterostructures of Dirac materials through an integrated approach of molecular beam epitaxial growth, scanning tunneling microscopy/spectroscopy (STM/S), and density functional theory (DFT) calculations.

## Recent Progress

### 1. *Unveiling novel indirect interlayer bonding mechanism in graphene / topological insulator van der Waals heterostructures*

Van der Waals (vdW) heterostructures of two-dimensional materials exhibit properties and functionalities well beyond those of each individual constituent layers. Without direct covalent bonding at the interface, these properties likely arise from mechanisms of unconventional nature. Here, we explore several intrinsic characteristics that underline the emergent properties of vdW heterostructures.

We synthesize a prototypical vdW heterojunction by transferring CVD graphene onto topological insulator (TI) $Bi_2Se_3$ grown by MBE. Using STM/S, we demonstrate a giant spin-orbit splitting of the graphene Dirac states up to 80 meV (compared to intrinsic values of 24-50 μeV), with a spatial variation of ±20 meV. Density functional calculations show that this splitting is a result of the proximity to $Bi_2Se_3$, which breaks the inversion and horizontal mirror symmetries of the graphene, thus lifting the four-fold degeneracy of its bands at the Dirac point ($E_D$). Furthermore, the transfer of the spin-orbit coupling is found to be through Bi character introduced into the graphene Dirac states due to orthogonalization to the $Bi_2Se_3$ states. Moreover, we find that the strong spatial fluctuation in the transferred spin orbit coupling (SOC) in graphene is due to the inherent non-epitaxial relation at the graphene / $Bi_2Se_3$ interface.

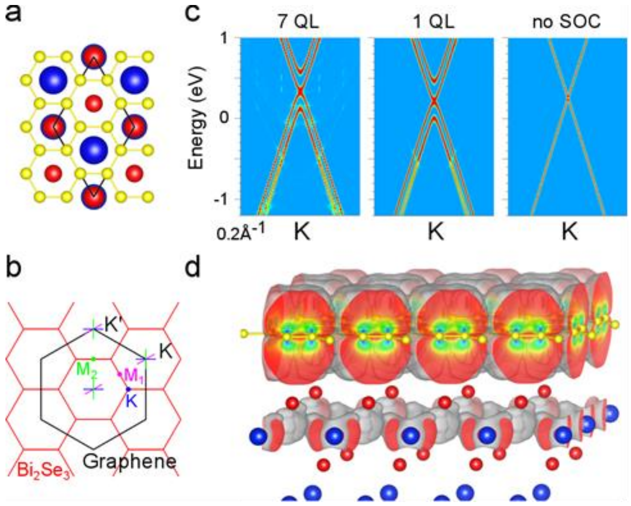

Fig. 1 (a) Ball-and-stick model of graphene/$Bi_2Se_3$ with an $\sqrt{3} \times \sqrt{3}$ epitaxial relationship. Yellow: C; blue: Bi; red: Se. (b) $Bi_2Se_3$ and graphene BZ with high symmetry points marked. The colored lines show different cuts along high symmetry directions around Γ and the K (K'). (c) The *k*-projected bands for graphene on 7 and 1 QL $Bi_2Se_3$, and on the 7 QL without SOC, respectively. (d) Density corresponding to the graphene Dirac states at the graphene/$Bi_2Se_3$ junction, showing that graphene π orbitals also have weight on the Bi atoms, which accounts for the transferred SOC. (Isosurface: $10^{-4}\ e^-/a_B^3$; maximum of the R-G-B color is $0.125\ e^-/a_B^3$.)

Our results not only demonstrate an enhancement of several orders of magnitude of the spin splitting of the graphene Dirac bands in a vdW heterostructure, but further reveal two intrinsic characteristics – the symmetry breaking and orthogonalization of the wave functions at the interface – that are key to the properties in vdW heterostructures. A manuscript reporting these results is under review at ACS Nano.

### 2. *Observation of topological phase transition in Sb/$Sb_2Te_3$ heterostructures*

Topological insulators are distinguished by a bulk topological $Z_2$ index and metallic boundary states populated by massless Dirac fermions. These boundary states are protected by time-reversal symmetry, and can only be tuned through topological phase transition induced by external variables such as strain, electrical field, and composition. Here we demonstrate a thickness driven topological phase transition in heterostructures of Sb/$Sb_2Te_3$ ($Bi_2Te_3$) grown by MBE.

At 300K, the growth of Sb initially follows a step-flow mode with a thickness of 3 bilayers (BLs), which is about the thickness of one $Sb_2Te_3$ quintuple layer. Interestingly, before completely covering the surface of $Sb_2Te_3$, the 4th Sb BL begins to grow on top of the existing 3 BL Sb islands (Fig. 2(a)). Atomic resolution imaging indicates that most of the step edges of the Sb islands are zigzag without any reconstructions (Fig. 2(b)), providing an ideal platform to verify the existence of one-dimensional (1D) edge mode that is the hallmark of 2D topological insulators.

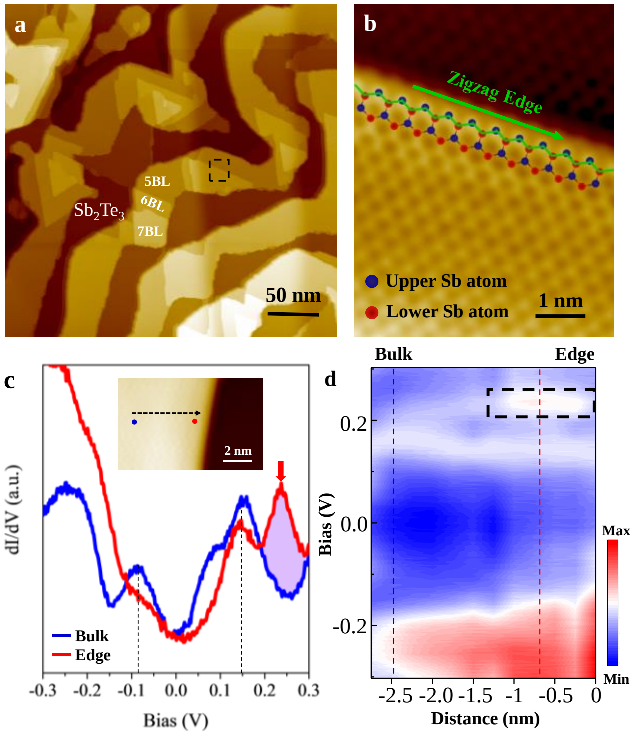

Fig. 2 (a) STM image of Sb/$Sb_2Te_3$ (-3V, 100pA). (b) Close-up view of the boxed region in (a) showing the Sb zigzag edge (-0.4V, 100pA). (c) dI/dV spectra taken in the bulk (blue) and edge (red) of a 7BL Sb film, respectively. (d) A 2D plot of the dI/dV measured along the dotted arrow marked (c), showing the presence of edge states with 3 nm of the zigzag edge.

Figure 2(c) shows dI/dV tunneling spectra taken along the direction perpendicular to the step edge of a 7 BL film. Far away from the edge, the dI/dV spectra exhibit features mainly related to Sb(111) surface states. Approaching the step edges, a prominent peak around 0.2 V appears within 1.5-2.0 nm from the step edge, which is further confirmed by spatially resolved spectra taken perpendicular to the edge (Fig. 2(d)), suggesting that the peak at ~0.2V can be attributed to the edge state of Sb(111) films.

Measurements were also carried out for 5, 6, and 8 BL films, where similar edge states are observed. On the other hand, no such edge states are observed for films below 3 and above 10 BL. These findings indicate that Sb(111) films undergo a series of topological phase transition induced by the competition between quantum confinement and surface effect. A manuscript is under preparation to report these findings.

### 3. *Electrical detection of spin-momentum locking in Dirac and Rashba states*

A hallmark of the 3D TIs is that their Dirac surface states are occupied by a single spin and exhibit helical spin-momentum locking. On the other hand in a two-dimensional electron gas (2DEG) with a parabolic energy dispersion, the Rashba form of SOC also leads to a pair of Fermi surfaces that exhibit counter-rotating chiral spin texture, locking spin to the linear momentum (Fig. 3(a)). As such, an unpolarized bias current is expected to create a net spin polarization due to spin-momentum locking in both systems (Fig. 3(b)), however with signs that are predicted to be opposite. In collaborations with Naval Research Lab, spin potentiometric measurements of bias current-generated spin polarization were carried out on $Bi_2Se_3(111)$ films where Dirac surface states coexist with normal 2DEG states, and on InAs(001) samples where only normal 2DEG states are present. Spin polarization arising from spin-momentum locking are observed in both cases, with opposite signs of the spin voltage (Fig. 3(c&d). A model based on spin dependent electrochemical potentials is also developed to directly derive the signs expected for the TI surface states, and unambiguously show that the dominant contribution to the current-generated spin polarization measured in the TI is from the Dirac surface states.

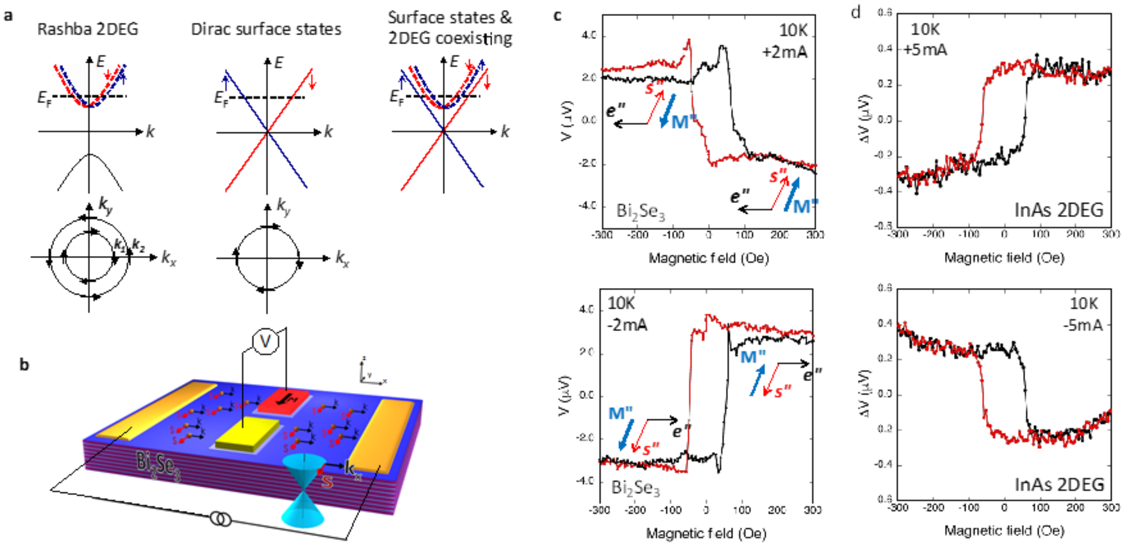

Fig. 3 (a) Schematic diagram of the spin-momentum locking of the Rashba 2DEG, TI Dirac surface states, and coexistence of both, respectively. (b) Experimental concept of the potentiometric measurement. (c) Magnetic field dependence of the voltage measured at the ferromagnetic detector contact with the magnetization collinear with the induced TI spin in $Bi_2Se_3$ (c) and InAs (d).

This work provides the first direct comparison of the helical spin texture of Dirac and Rashba 2DEG states through electrical transport measurements. This direct electrical access of the helical spin texture of Dirac and Rashba 2DEG states is an enabling step toward the development of TI and SOC-based spintronics for energy efficient computation and information storage. A manuscript reporting these results is under review at Nature Communications.

### 4. *Calculation of gapped Dirac states in silicene and germanene on $Al_2O_3(0001)$*

Silicene and germanene, the silicon and germanium 2-D analogues of graphene, are predicted to have linearly dispersing Dirac states at the Fermi level. In contrast to carbon in graphene, however, both silicon and germanium favor $sp^3$ bonding rather than $sp^2$. Thus, while free standing graphene is stable and can be transferred rather easily, substrates appear to be required to stabilize silicene. Our calculations show that wide band gap materials are promising candidates to minimize the effect of the substrate on their electronic properties, as shown here for silicene (and germanene) on $Al_2O_3$(0001).

The calculated low energy structure of $\sqrt{13}$x$\sqrt{13}$ silicene on a 3x3 $Al_2O_3$(0001) is reconstructed, consisting of both high- and low-buckled Si atoms. The binding energy is reduced compared to silicene on Ag(111), but is still sizable (~0.52 eV/Si), indicating that the interaction is not simply van der Waals. The band alignment for Al-terminated $Al_2O_3$(0001) and silicene (Fig. 4(a)) places the Dirac point of isolated silicene in the middle of the gap, and suggests no charge transfer or direct interaction between substrate states and the silicene Dirac states. (For oxygen-terminated surface, the silicene Dirac point is also in the gap, but closer to the top.)

Next, we calculated the electronic states for both an isolated silicene layer with the same reconstructed structure and the interacting system (Fig. 4(b&c)). For the isolated silicene, while the calculated bands are very similar to that of the ideal silicene, particularly for the valence bands, the reconstruction breaks symmetry, leading to the opening of a small gap (~0.1 eV) at the Dirac point. The changes are more significant for the interacting case: (i) the $\sigma$ bands below -5 eV are heavily modified, indicating interactions with the substrate; (ii) both the valence and conduction $\pi$ bands are broken up by minigaps; (iii) the gap at K is increased to 0.44 eV; and (iv) the dispersion around the Dirac point is no longer a cone, but rather consists of sections of almost flat bands. These modifications in the electronic bands occur in absence of substrate states in the same energy region (c.f., Fig. 4(b&c), and are a result of indirect interactions via deeper lying states.

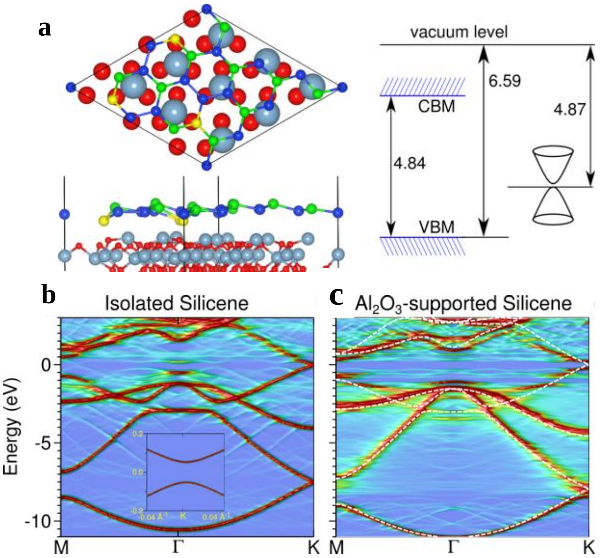

Fig. 4 (a) Top and side view of the lowest energy relaxed structure of silicene/Al-terminated $Al_2O_3$(0001), and band alignments for these systems. Electronic k-projected bands to the 1x1 silicene zone for (b) the relaxed isolated silicene layer, and (c) the corresponding bands for the interacting system. The inset to (b) shows the bands around the Dirac point. The white dashed lines in (c) are the bands for an ideal (unreconstructed) silicene layer.

For germanene/Au(111) with an almost flat honeycomb lattice, the electronic interactions with the substrate are so strong that the isolated germanene features become indistinguishable. For $Al_2O_3$ substrate, on the other hand, germanene effectively maintains the ideal low-buckled structure, along with approximately linear dispersion of the Dirac states and a small gap.

These results demonstrate the sensitivity of the electronic states of silicene and germanene to substrate interactions, and suggest pathways to tune their electronic properties. These findings have been published in Physical Review B.

## Future Plans

We will continue the systematic studies already underway to investigate 1) edge states in graphene/TI heterostructures; 2) epitaxial growth of 2D TIs on conventional semiconductors (e.g, Sb on SiC(0001)); 3) chiral-based topological insulators (e.g, strained Te).

**Publications resulting from work supported by the DOE grant over the previous two years**

1. "Indirect interlayer bonding in graphene-topological insulator van der Waals heterostructure: giant spin-orbit splitting of the graphene Dirac states", S. Rajput, Y. Y. Li, M. Weinert, and L. Li, ACS Nano (revised manuscript submitted).
2. "Direct comparison of current-induced spin polarization in topological insulator $Bi_2Se_3$ Dirac states and InAs Rashba states", C. H. Li, O. M. J. van 't Erve, S. Rajput, L. Li, and B. T. Jonker, Nat. Commun. (revised manuscript submitted).
3. "Designing substrates for silicene and germanene: First-principles calculations", M. X. Chen, M. Weinert, and Z. Zhong, Phys. Rev. B **94**, 075409 (2016).
4. "Half-metallic Dirac cone in zigzag graphene nanoribbons on graphene", M. X. Chen and M. Weinert, Phys. Rev. B **94**, 035433 (2016).
5. "Determining charge state of graphene vacancy by noncontact atomic force microscopy and first-principles calculations", Y. Liu, M. Weinert, and L. Li, Nanotechnol. **26**, 035702 (2015).
6. "Carrier transport in reverse-biased graphene/semiconductor Schottky junctions", D. Tomer, S. Rajput, L. J. Hudy, C. H. Li, and L. Li, Appl. Phys. **106**, 173510 (2015).
7. "Inhomogeneity in barrier height at graphene/Si (GaAs) Schottky junctions", D. Tomer, S. Rajput, L. J. Hudy, C. H. Li and L. Li, Nanotechnol. **26**, 215702 (2015).
8. "Transport and photoconduction characteristics of metal-graphene-4H-SiC(0001) heterojunction devices", T. Hosseini, D. Tomer, S. Rajput, L. Li, and N. Kouklin, Appl. Phys. Lett. **105**, 223107 (2014).

## Quasiparticle Interference and Strong Electron-Mode Coupling in the Quasi-One-Dimensional Bands of $Sr_2RuO_4$

**Vidya Madhavan**
**Department of Physics. University of Illinois, Urbana-Champaign**

### Research Scope

Our goal is to realize topological superconductivity, proximity induced superconductivity, and Majorana bound states (MBS) in bulk and thin films and measure them using advanced STM spectroscopic techniques of Fourier transform scanning tunneling spectroscopy (FT-STS) and Landau level spectroscopy (LLS). The ability to directly measure the properties of Dirac systems in both real- and momentum space makes scanning tunneling microscopy (STM) one of the most powerful tools for probing novel topological phases. Furthermore, combining STM spectroscopy with thin film growth provides a tunable, versatile platform for both realizing and measuring novel phases. The materials we propose to study include 3D-TIs, TCIs and 2D topological insulators. We will particularly concentrate on thin films of these materials which are susceptible to being tuned by doping, strain or gating, allowing us to explore their physical properties in the most interesting regimes and set the stage for future technological applications.

### Recent Progress

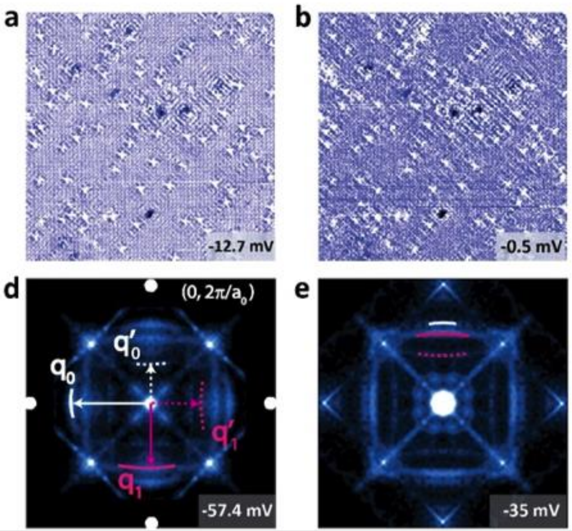

**Fig. 1 Quasiparticle interference (QPI) of $Sr_2RuO_4$. a, b**, Spatially resolved dI/dV conductance maps at -12.7meV and -0.5meV. **d,** e, Drift-corrected and symmetrized Fourier transforms of dI/dV conductance maps.

One of the goals of the project is to study the single-layered ruthenate $Sr_2RuO_4$. $Sr_2RuO_4$ has attracted a great deal of interest as a spin-triple superconductor with an order parameter that ma potentially break time reversal invariance and hos half-quantized vortices with Majorana zero modes While the actual nature of the superconducting state is still a matter of controversy, it has long been believed that it condenses from a metalli state that is well described by a conventional Ferm liquid. In this work we used a combination o Fourier transform scanning tunneling spectroscop (FT-STS) and momentum resolved electron energy loss spectroscopy (M-EELS) to probe interaction effects in the normal state of $Sr_2RuO_4$[1]. Our high-resolution FT-STS data show signatures of the β-band with a distinctly quasi-one-dimensional (1D) character (Fig. 1). The band dispersion reveals surprisingly strong interaction effects that dramatically renormalize the Fermi velocity, suggesting that the normal state of $Sr_2RuO_4$ is that of a `correlated metal' where correlations are strengthened by the quasi 1D nature of the bands. In addition, kinks at energies of approximately 10meV, 38meV and 70meV are observed. By comparison with M-EELS data we show that the two higher energy features arise from coupling with collective modes. The strong correlation effects and the kinks in the quasi 1D bands have important implications for the superconducting state. This work opens up a unique approach to reveal the superconducting order parameter in this compound, where the superconducting instability may be dominant on the quasi-1D bands.

We continue to perfect our thin film growth techniques. In a previous study we had measured the effect of spatially varying strain on the band structure of topological crystalline insulator thin films using quasiparticle interference spectroscopy[2]. Expanding on this, we have recently studied the influence of the orbital nature of bands on their stain response. Orbital degrees of freedom have strong effects on the fundamental properties of electrons in solids. In addition to influencing bandwidths, gaps, correlation strength, and dispersion, orbital effects have also been implicated in generating novel electronic and structural phases such as Jahn-Teller effect and colossal magneto resistance. Here we show for the first time how the orbital nature of bands can create non-trivial strain effects. We use scanning tunneling microscopy (STM) to study the influence of strain on the electronic structure of a heteroepitaxial thin film of

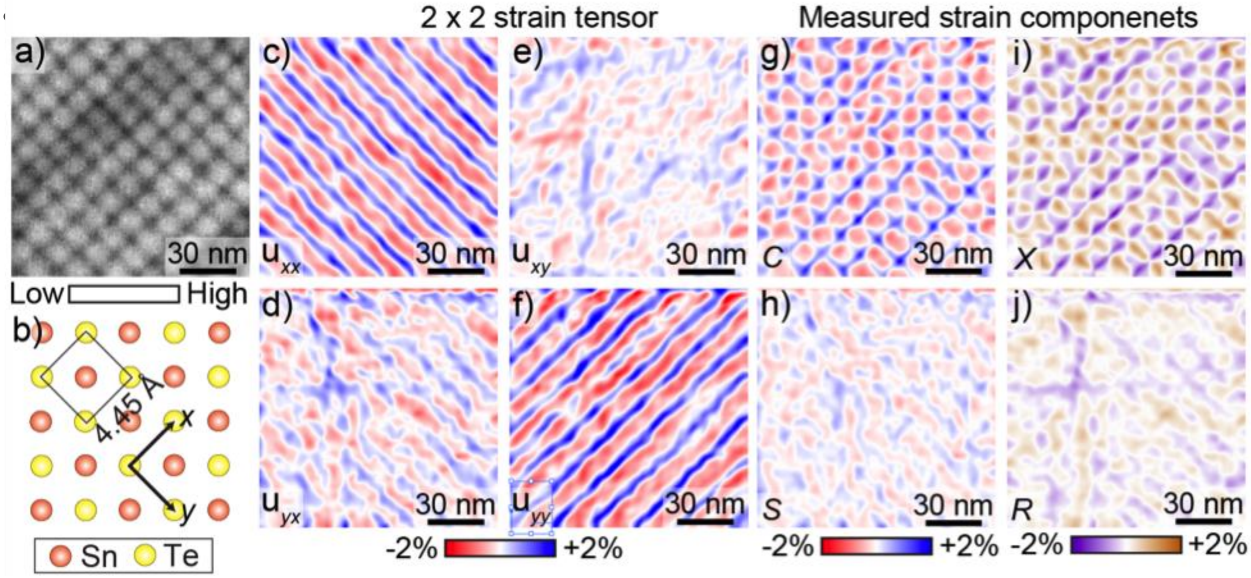

**Fig. 2 Spatial distribution of different types of strain. (a)** STM topograph of ~130 nm square region of the sample ($V_{set}$ = -50 mV, $I_{set}$ = 200 pA) **(b)** Schematic of the (001) surface of SnTe. Arrows in (b) denote the x- and y-axes. **(c)-(f)** The components of the 2 x 2 strain tensor extracted from topograph in **(a)**. $u_{ij}$ denotes . **(g)-(j)** Physically significant linear combinations of the tensor elements in **(c)-(f)**: **(g)** The isotropic compression ; **(i)** the uniaxial strain ; **(h)** the shear strain ; **(j)** the local rotation angle . **Fig. 1 Quasiparticle interference (QPI) of $Sr_2RuO_4$. a, b**, Spatially resolved dI/dV conductance maps at -12.7meV and -0.5meV. **d, e**, Drift-corrected and symmetrized Fourier transforms of dI/dV conductance maps.

insulator, SnTe. First we demonstrate how the complete strain tensor can be directly measured on the local scale with nanometer precision using STM. This allows us to create two-dimensional maps of biaxial, uniaxial and sheer strain components (Fig. 2), which can then be correlated with the local electronic structure using local Fourier-transform scanning tunneling spectroscopy. Applying these techniques to SnTe thin films, we find a surprising effect where uniaxial strain in one direction affects the band structure in the perpendicular direction. Theoretical calculations indicate that this arises from the effects of strain on hopping matrix elements, which depend on the orbital quantum number of the bands. Our results imply that a microscopic model capturing strain effects on band structure must include a consideration of the orbital nature of the bands.

We continue to expand the toolset available to us in the powerful probe of scanning tunneling microscopy. Quantifying the interaction between phonons and electrons is of immense importance for a complete understanding of many materials systems. Nearly all information about electron-phonon coupling (EPC) is contained in the Eliashberg function of the material, but its precise extraction has in part been limited due to the lack of local experimental probes. By utilizing Landau level spectroscopy, we have constructed a method to directly extract the Eliashberg function, and demonstrate its applicability to lightly doped thermoelectric bulk insulator PbSe[3]. In addition to its high energy resolution only limited by thermal broadening, as well as access to both occupied and unoccupied electronic states, this novel experimental method could be used to detect variations in mass enhancement factor ($\lambda$) on microscopic length scales, which opens up a unique pathway for investigating the effects of chemical defects, surface doping and strain on $\lambda$.

## Future Plans

We plan to continue our studies of $Sr_2RuO_4$ and extend the study to temperatures below $T_c$ where we can probe the order parameter and search for signatures of Majorana fermions.

We will measure bulk materials like Cu and Sr intercalated $Bi_2Se_3$ to study topological superconductivity

We will continue to perfect our growth superconducting/TI heterostructures to realize and measure topological superconductivity and Majorana modes.

## Publications

1. Zhenyu Wang, Daniel Walkup, Philip Derry, Thomas Scaffidi, Melinda Rak, Sean Vig, Anshul Kogar, Ilija Zeljkovic, Ali Husain, Luiz H. Santos, Yuxuan Wang, Andrea Damascelli, Yoshiteru Maeno, Peter Abbamonte, Eduardo Fradkin, and Vidya Madhavan, Quasiparticle Interference and Strong Electron-Mode Coupling in the Quasi-One-Dimensional Bands of $Sr_2RuO_4$, under review ***Nature Physics*** (2016)

2. Ilija Zeljkovic, Daniel Walkup, Badih Assaf, Kane L Scipioni, R. Sankar, Fangcheng Chou, **Vidya Madhavan,** Strain engineering Dirac surface states in heteroepitaxial topological crystalline insulator thin films, ***Nature Nanotechnology*** 10, 849–853 (2015)

3. Ilija Zeljkovic, Kane L Scipioni, Daniel Walkup, Yoshinori Okada, Wenwen Zhou, R. Sankar, Guoqing Chang, Yung Jui Wang, Hsin Lin, Arun Bansil, Fangcheng Chou, Ziqiang Wang and **Vidya Madhavan**, Nanoscale Determination of the Mass Enhancement Factor in the Lightly-Doped Bulk Insulator Lead Selenide, ***Nature Communications*** 6, 6559 (2015)

4. Ilija Zeljkovic, Yoshinori Okada, Maksym Serbyn, R. Sankar, Daniel Walkup, Wenwen Zhou, Junwei Liu, G.Chang, Yung Jui Wang, M. Zahid Hasan, Fangcheng Chou, Hsin Lin, A. Bansil, Liang Fu and **V. Madhavan**, Dirac mass generation from crystal symmetry breaking on the surfaces of topological crystalline insulators, ***Nature Materials*** 14, 318–324 (2015)

5. Ilija Zeljkovic, Yoshinori Okada, Cheng-Yi Huang, R. Sankar, Daniel Walkup, Wenwen Zhou, Maksym Serbyn, Fangcheng Chou, Wei-Feng Tsai, Hsin Lin, A. Bansil, Liang Fu, M. Zahid Hasan and **V. Madhavan,** Mapping the unconventional orbital texture in topological crystalline insulators, ***Nature Physics*** 10, 572–577 (2014)

## Oxides Surfaces and Novel Electromechanical Phenomena

**Laurence D. Marks**
**Department of Materials Science and Engineering, Northwestern University**
**Evanston, IL 60208 USA**

### Research Scope

Oxides surfaces are ubiquitous and show promise in a wide array of applications including growth, electronics, and catalysis, extending the scope of this work across many disciplines. In spite of their wide use, our understanding of oxides surfaces is still incomplete. For example, most of the literature where oxides are used as substrates for growth ignores the surface structure beyond a simple bulk truncation. There is an expanding body of literature that has demonstrated that many, perhaps most oxides have surface reconstructions that often make those know for semiconductor and other surfaces look simple. The PIs group has been studying oxides surfaces for almost two decades and has solved approximately 20 different complex surface reconstructions on various oxides (*1*, *2*). These reconstructions not only influence growth, but also alter surface chemistry and properties that give rise to interesting electronic phenomena at the interface as seen in the case of $LaAlO_3/SrTiO_3$ (*3*). Further, they are present not just on bulk surfaces but also on nanoscale oxides (*5*).

Our recent work has been in two directions. The first, the prior grant, was to develop new methods for imaging oxide surfaces, exploiting aberration-corrected microscopies as well as furthering our understanding of oxide surface structure. The second was the discovery of a completely unexpected large flexoelectric response on in lanthanide scandates which is the basis of new research.

### Recent Progress: Oxide Surfaces and Techniques

Significant progress has been made in the last two years in understanding oxides surfaces including those of $SrTiO_3$, $LaAlO_3$, and $DyScO_3$. The process of solving these reconstructions has been aided by the development of new tools. A question we asked was how useful will aberration-corrected electron microscopes be for surfaces? Are the gains going to just be from improved signal-to-noise or more?

One target was to understand atomic resolution secondary electron imaging (ARSEM) in detail, using the c(6×2) surface reconstruction on $SrTiO_3$ (001) surface (*4*). This was a complex problem, involving a relatively large collaboration by five institutions and techniques ranging from accurate scattering modelling to DFT to name only two. One key aspect was to incorporate dielectric screening from the valence states in addition to the core states to match experimental data, and also include via a statistically accurate model surface disorder. To illustrate this the correlation of fit between the simulated and experimental images as a function of the different states incorporated in damping is given in Figure 1. The agreement between experiment and calculation is excellent, and we can now claim that the key physics of ARSEM are understood, although fine details of, for instance, the dielectric screening can still be improved upon.

A second target was understanding inversion of high resolution plan view images of the surfaces with aberration-corrected instruments. While aberration-correction certainly helps, it does not correct for dynamical diffraction and we found that the method is limited by the thickness of the sample and symmetry of the surface structure. Surfaces with inversion symmetry solve better since inversion symmetry limits the phase of reflections to be either 0 or $\pi$. The results have been published in detail (*6*).

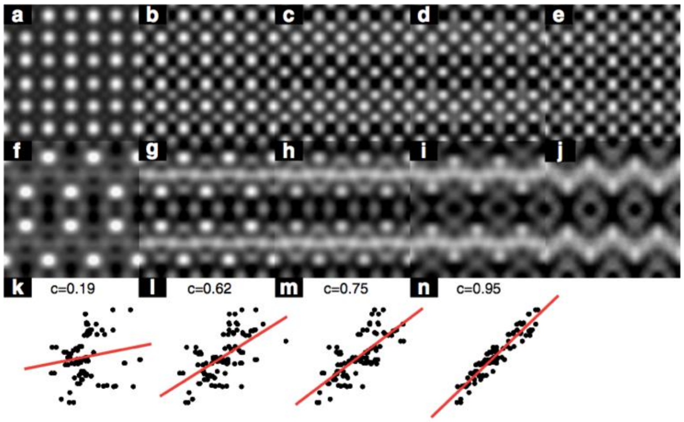

**Figure 1**. Comparison of HRSEM experimental and simulated images. (**a** – **c**) HRSEM simulations of the Sr7 structure including damping due to dielectric screening: (**a**) Using only core states (up to and including the 3d state in Sr, the 2p in Ti and 1s in O). (**b**) Adding the 4s and 4p for S4, the 3s and 3p for Ti and 2s for O, (**c**) Adding the contribution for the filled 2p orbital in O, (**d**) Shows the HRSEM simulations including all orbitals for the Sr7-effective structure. (**e**) Shows the experimental result with translational 6×2 unit cell averaging and c2mm symmetry applied. In (**f** – **j**), we show the corresponding bulk-subtracted results from **a** through **e**. In (**k** – **n**), we show the Pearson product-moment correlation of image intensities corresponding to **f** through **j**. (Adapted

The reconstructions on the SrTiO$_3$ (110) surface were studied using a combination of scanning tunneling microscopy, transmission electron diffraction, and X-ray absorption spectroscopy, and analyzed with density functional theory (DFT) calculations. The (110) surface is invariably terminated with an overlayer of titania and with increasing density of titania switches from n×1 to 2×n. The (4×1) and (2×5) structures can be reversibly switched with the deposition of Ti/Sr followed by annealing (*7*). Stress and packing density driven transitions from a reconstruction with tetrahedral networks of TiO$_5$[] to a thin film with octahedral coordination of TiO$_6$ were observed. At low surface excess of Ti, the structure is driven by local chemistry and coordination of Ti.

The $n\times n$ ($2\leq n\leq 4$) reconstructions on the (111) surface of SrTiO$_3$ were solved using a combination of transmission electron diffraction, DFT modeling, and scanning tunneling microscopy. The surfaces contain a mixture of the tetrahedral TiO$_4$ units sitting on top of octahedral TiO$_5$[] and TiO$_6$ units in the second layer. In addition, at high temperatures a transition from enthalpy-dominated 3×3 and 4×4 reconstructions to configurational entropy-dominated 2×2 reconstructions occurs (*2*).

In addition to SrTiO$_3$, the (5×2) and (2×1) reconstructions on the (001) and (110) surface of LaAlO$_3$ respectively, are also being studied. Angle resolved X-ray photoelectron spectroscopy shows that both of these reconstructions are Al rich. Similar to reconstructions found in SrTiO$_3$ which are Ti terminated, these reconstructions are also B site terminated. Feasible sets of solutions are currently being investigated.

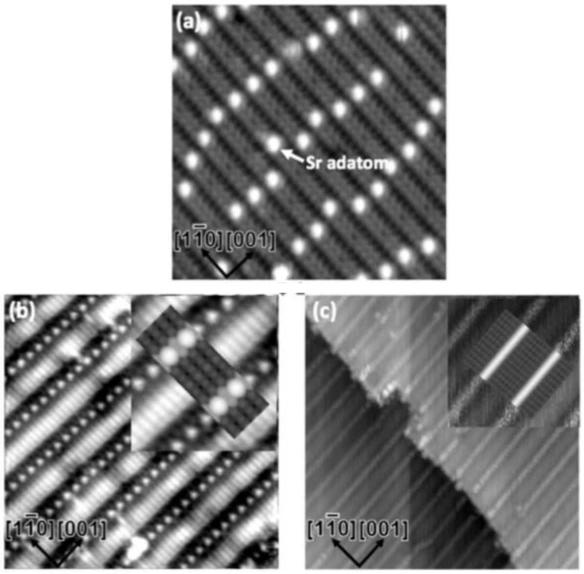

**Figure 2**. STM images of the 4×1 (**a**) and two kinds of (2×5) surfaces (**b**,**c**). (Simulated images of the two kinds of (2×5) are inset in (**b**) and (**c**)).

## Recent Progress: Unexpected Flexoelectric Bending

The $SrTiO_3$ perovskite is part of the family of “242” perovskites where all the elements have even valence. With even valence many of the main surfaces are valence neutral automatically. Other perovskites such as the lanthanide scandates are “332” are almost unexplored, despite their growing use as substrate materials for oxide MBE. They also have strongly-correlated 4f electrons for which spin-orbit effects are significant, an incompletely understood issue where conventional DFT can break down catastrophically. Exploratory surface studies on three such materials, $LnScO_3$ (Ln=Gd, Tb, Dy) were conducted by a graduate student. He noticed something “odd”, and was smart enough to realize that it was worth pursuing. Very large bending of samples *in-situ* occurred, which radii of curvature of the order of a micron which corresponds to strains of 2-6%, well beyond the expected yield strain of a brittle ceramic.

We argue that this is due to the polarization created by charging, i.e. the flexoelectric effect (*8*). This is the first direct observation of such large bending of a ceramic material due to the flexoelectric effect. The observed bending was proportional to the electron flux and reversible. The illustration in Figure 3 summarizes the results of the observed bending. These results were corroborated with ex-situ measurements of the flexoelectric coefficient (Figure 4). Although the measured flexoelectric coefficients of $DyScO_3$ is comparable to previously studied materials(*9*), the flexocoupling voltage (ratio of flexoelectric coefficient to dielectric constant) is ~40 V, which is larger than predicted by any current theory. This makes $DyScO_3$ the material with the second largest known flexocoupling voltage ($BaTiO_3$ is larger), a strong candidate for applications ranging from energy harvesting to nanoscale actuators.

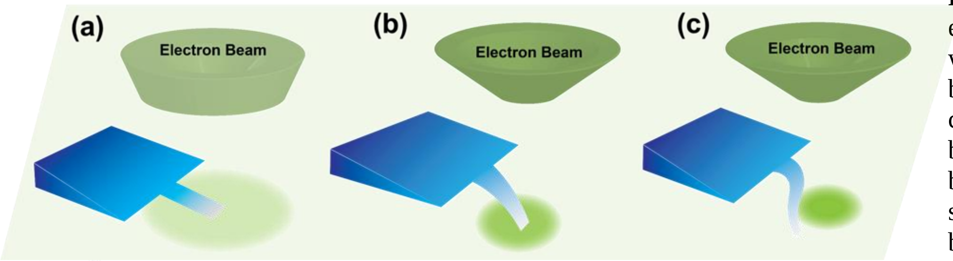

**Figure 3**. Bending in the electron beam where: (a) the sample is not bending due to low beam current, (b) the sample is bends down with a focused beam centered on the sample and (c) the sample bends down and sideways with the focused beam centered to one side of the sample

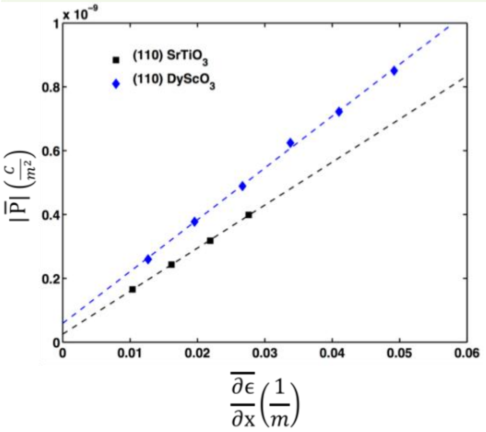

**Figure 4.** Ex-situ measurements of strain gradient induced polarization in (110) $SrTiO_3$ and (110) $DyScO_3$. The flexoelectric coefficient (slope of polarization vs strain gradient) was found to be ~$10^{-8}$ C/m in both materials.

These results are only the tip of the iceberg. For instance, we have definitive XPS evidence for temperature-dependent band bending and the formation of a metallic-like state at the surface above about 90C for both $DyScO_3$ and $TbScO_3$ (but not $GdScO_3$); evidence for complex spin and orbital ordering with multiple near degenerate 4f states from relatively accurate DFT as well as preliminary data from DFT about the source of the large flexoelectric effect in this compounds.

The lanthanide scandates show every indication of being a source of a large amount of new science with many potential energy applications, although it is still early days.

## Future Plans

The flexoelectric effect is in its early stages and there is much work to be done, and a reasonably high probability of unexpected results. We are developing a loose network of collaborators (at DOE national labs and elsewhere) since we recognize that we cannot do everything. A few directions are:

1. The flexoelectric effect as a function of temperature both macroscopically and in-situ. Preliminary in-situ data suggests a suppression, which may be due to surface metallization.
2. DFT based calculations will be employed to calculate flexoelectric coefficients. In most publications to date theoretical values are orders of magnitude off from the experimental data.
3. Calibration of the DFT calculations with experimental data on the electronic structure. Hard X-ray photoelectron spectra of the electronic structure of lanthanide scandates will be obtained, and we are also investigating the possibility of using resonant photoelectron spectra (RPES) with the O1s edge since normal XPS of the valence edge isdominated by the 4f states.
4. Analysis of EELS spectra. We have preliminary low-loss data for clean, charging samples which needs further analysis.
5. Holographic measurements, if possible, of the degree of charging (with collaborators).

In addition to these we will continue with, as relevant, analysis of the surface structure of oxides. In some cases this will be dual purpose; for instance flexoelectric measurements of $CaTiO_3$ will test the role of octahedral tilts in the absence of 4f electrons, as well as being in its own right an interesting material to test the role of octahedral tilts on surface reconstructions.

## References:

1. J. A. Enterkin *et al.*, A homologous series of structures on the surface of SrTiO3(110). *Nat Mater* **9**, 245 (2010).
2. L. D. Marks, A. N. Chiaramonti, S. U. Rahman, M. R. Castell, Transition from Order to Configurational Disorder for Surface Reconstructions on SrTiO3 (111). *Phys Rev Lett* **114**, 226101 (2015).
3. A. Ohtomo, H. Y. Hwang, A high-mobility electron gas at the LaAlO3/SrTiO3 heterointerface. *Nature* **427**, 423 (2004).
4. J. Ciston *et al.*, Surface determination through atomically resolved secondary-electron imaging. *Nat Commun* **6**, 7358 (2015).
5. Y. Lin *et al.*, Synthesis-dependent atomic surface structures of oxide nanoparticles. *Phys Rev Lett* **111**, 156101 (2013).
6. P. Koirala, Y. Lin, J. Ciston, L. D. Marks, When does atomic resolution plan view imaging of surfaces work? *Ultramicroscopy* **170**, 35 (2016).
7. Z. Wang *et al.*, Transition from Reconstruction toward Thin Film on the (110) Surface of Strontium Titanate. *Nano Lett* **16**, 2407 (2016).
8. P. Koirala, L. D. Marks, Direct Observatio of Large Flexoelectric Bending at the Nanoscale in Lanthanide Scandates. *arXiv*, (2016).
9. P. Zubko, G. Catalan, A. K. Tagantsev, Flexoelectric Effect in Solids. *Annual Review of Materials Research* **43**, 387 (2013).

## Publications

1. J. Ciston et al., Surface determination through atomically resolved secondary-electron imaging. Nat Comm. 6, 7358 (2015).

2. L. D. Marks, A. N. Chiaramonti, S. U. Rahman, M. R. Castell, Transition from Order to Configurational Disorder for Surface Reconstructions on $SrTiO_3$ (111). Phys Rev Lett 114, 226101 (2015).
3. D. Kienzle, P. Koirala, L. D. Marks, Lanthanum aluminate (110) 3 x 1 surface reconstruction. *Surf. Sci.* **633**, 60 (2015).
4. M. J. Marshall, A. Becerra-Toledo, L. Marks, M. Castell, in *Defects at Oxide Surfaces*, J. Jupille, G. Thornton, Eds. (Springer International Publishing, 2015), vol. 58, pp. 327-349.
5. R. Xu *et al.*, Three-dimensional coordinates of individual atoms in materials revealed by electron tomography. *Nat Mater* **14**, 1099 (2015).
6. P. Koirala, Y. Lin, J. Ciston, L. D. Marks, When does atomic resolution plan view imaging of surfaces work? Ultramicroscopy 170, 35-42 (2016).
7. Z. Wang et al., Transition from Reconstruction toward Thin Film on the (110) Surface of Strontium Titanate. Nano Lett 16, 2407-2412 (2016).
8. P. Koirala, L. D. Marks, Direct Observation of Large Flexoelectric Bending at the Nanoscale in Lanthanide Scandates. arXiv (2016).

# Structured Electron Beams for Electron Microscopy

**Benjamin J. McMorran, Department of Physics, University of Oregon**

## Research Scope

The goal of this project is to develop new electron microscopy capabilities using structured electrons, such electron vortex beams[1–3]. Electron microscopy is one of the most widely used tools for studying energy-related materials at atomic lengthscales, yet the performance and utility of these tools is determined by the precision with which electrons in free space can be manipulated. There are both physical and economic limits to what can realistically be achieved using conventional electron optics. However, new types of electron optics developed under this project – for example, nanofabricated diffractive optical elements (DOEs) – offer a new way to sculpt and utilize electrons inside electron microscopes[4–6]. This project uses these devices to produce structured electrons and apply them to enhance the spatial resolution and contrast in electron microscopes. For example, the project investigates methods for using electrons with helical wavefront structure to directly probe magnetization and electronic orbital structure within materials. Such electron vortex beams are remarkable for their quantized orbital angular momentum (OAM) and spiral phase.

## Recent Progress

### *1. Demonstration of chiral interactions using STEM-EELS with vortex beams*

We excited chiral surface plasmon modes in nanoparticle systems by transferring OAM from an electron vortex beam[7]. Several optical studies have induced plasmon vortices using optical vortices and circularly polarized light [8,9]. It is hoped that measurement of OAM transfer from electron vortices allows for unique identification of the OAM associated with localized plasmons and excitons.

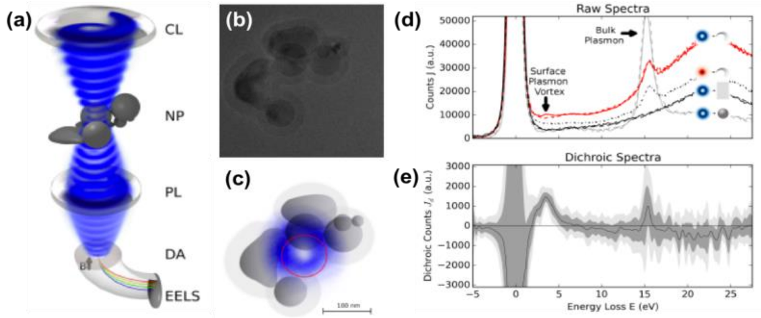

Figure 1 – Example of electron chiral dichroism using electron vortex beams. (a) Schematic of electron vortex beam illuminating a chiral nanoparticle (NP) cluster. (b) A TEM image of the cluster. (c) A schematic of the chiral cluster with an overlaid image of the vortex probe. The red circle indicates the effective entrance aperture for the EEL spectrometer. (d) Comparison of EEL spectra for several incident wavefunction and specimen permutations. (e) Differences in spectra between right-handed and left-handed vortex beams appears at 3.5 eV only when illuminating the chiral cluster (not when illuminating symmetric particles or the substrate.

Electron vortex beams were produced in an FEI Titan TEM at 300 kV. A forked grating DOE was located in the condenser lens aperture of the microscope. The +1 and -1 diffracted probe beams each carry one unit ($\hbar$) of OAM per electron, with opposite handedness in the two beams[11]. They are alternately focused in the plane of the sample to be analyzed.

We observed a clear OAM dependence in low-loss EELS in a chiral distribution of $Al/Al_2O_3$ core-shell nanoparticles (Fig. 1). The cluster was illuminated by +1, 0, and -1 OAM vortex beams, as well as a “fake” vortex probe having a donut-shaped intensity distribution but no OAM. EEL spectra were acquired using electrons in the optical axis of each beam. It was found that illumination of a -1 OAM beam generated an additional plasmon peak at approximately 3.5 eV, whereas illumination by a +1 OAM beam or a fake vortex beam *with identical intensity distribution* did not produce the plasmon. This dichroism signal was robust against relative beam-cluster alignments, but the experiment was quite challenging.

Similar dichroism signals have now been observed in chiral cobalt nanoparticles made by the group of Nicholas Kotov at University of Michigan. The same chiral nanoparticles show asymmetric absorption of circularly polarized light (optical circular dichroism). Although this signal is much cleaner, we must wait for further characterization of these NPs from our collaborators before submitting these results to a journal.

In the past two years, we have found that a crucial overlooked necessity for electron vortex dichroism is the post-specimen measurement of the OAM distribution of scattered electrons. This finding has a strong impact on the initial plan for the project.

### *2. Holographic Aberration-Correction and Apodization of Electron Beams*

Working with Martin Linck at CEOS GmbH and Peter Ercius and Colin Ophus at NCEM-Molecular Foundry, we designed and produced a nanofabricated DOE that holographically imprints reverse spherical aberration onto an electron beam[10]. As shown in Fig 2, the DOE holographically encodes a spatial phase that mimics the spherical aberration imparted by the objective lens of the TEM. These gratings were installed in the C2 aperture of two different FEI Titans – the UO TEM and the Titan-X instrument at NCEM. In STEM mode, multiple probes were diffracted by these DOEs and focused down on the specimen plane. We recorded Ronchigrams and several atomic resolution STEM images to demonstrate that in one of the diffracted probes, spherical aberration imprinted by the objective lens had effectively been removed.

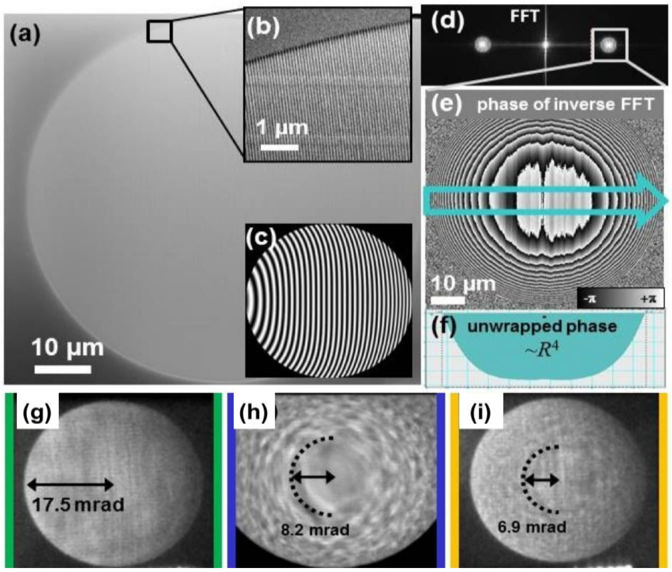

Figure 2 - (a) An SEM image of a diffraction hologram for $C_S$-correction. The magnified subarea (b) exhibits the bending of the grating lines similar to the exaggerated model (c). Fourier analysis (d) allows reconstructing the geometric phase of the grating (e). The unwrapped phase profile (f) confirms the power-of-four behavior of the grating’s phase shift. Ronchigrams taken with the +1 aberration-corrected diffraction order (g), the uncorrected 0 diffraction order (h), and the doubly-aberrated +1 diffraction order (i) demonstrate the effectiveness of the hologram.

*3. Electron interferometry with structured electron probes*

We have produced several methods for measuring phase shifts of structured electrons, and are applying this to enhance the contrast of electron-transparent specimens. We have been designing and fabricating phase plates for use in matched illumination and detector interferometry in a STEM (MIDI-STEM)[11]. Development of this technique is headed by our close colleague at NCEM, Colin Ophus. Under this project, we design, optimize, and fabricate the multizone phase plates. As show in Fig. 3, MIDI-STEM provides a way to dramatically enhance the contrast of electron-transparent specimens while preserving high resolution. In MIDI-STEM, phase plates having two sets of equal-area zones, one of which imprints a π/2 phase with respect to the other, are installed in the condenser system of a STEM. The probe-forming optics of the instrument focuses and scans a resulting structured probe on the specimen. A fast imaging detector such as the Gatan K2 on TEAM I is used to image the phaseplate at each probe position. The difference in signal within the two zones (shown in red in Feg. 3b) is calculated, and this is used to provide a linear contrast transfer function. An interferometric image of an electron-transparent carbon membrane (Fig. 3c) shows enhanced contrast compared to a standard STEM-ADF image (Fig. 3d).

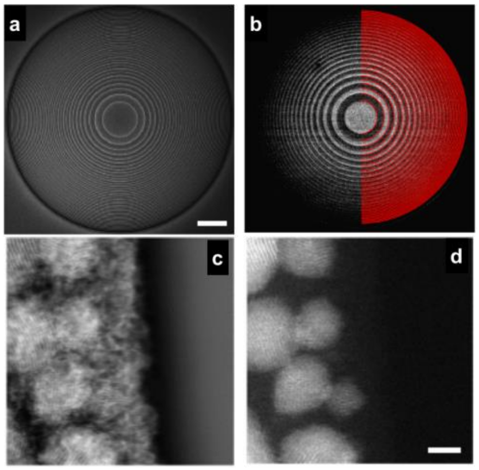

Figure 3 - (a) SEM image of the patterned MIDI-STEM phase plate with 20 ring pairs (5 μm scale bar). (b) Image of the phase plate after the electron probe has passed through a specimen, with locations of virtual detectors shown in red overlay. (c) Images of Au nanoparticles on amorphous carbon are formed by subtracting the intensity in one set of zones from that of the other set for each probe position on the specimen. The resulting image has phase contrast. (d) A conventional STEM images using the ADF detector only shows the Au nanoparticles.

## Future Plans

*Mechanical manipulation of nanoparticles using electron vortex beams* – We are investigating the use of electron vortex beams to manipulate nanoparticles. The UO currently has a liquid flow cell holder, and we have been using this to image gold nanoparticles in the TEM. Initial experiments illuminating these nanoparticles with vortex beams seem to indicate that the beams have a rotary effect, but further experiments are necessary. For these experiments we will produce some grating that maximize the OAM current in the beam, defined as the produce of the topological charge of the electron beam and the beam current.

*Atomic resolution orbital interactions of vortex STEM probes* – We are currently fabricating gratings and planning experiments for a concerted effort to demonstrate magnetic dichroism at atomic spatial resolution using aberration-corrected electron vortex probes. One major limit to this work has been that UO researchers can only visit TEAM I for a few days at a time. However, a senior PhD student, Tyler Harvey, was recently awarded a DOE SCGSR to support concentrated research at NCEM-Molecular Foundry in 2017. With this award, we will be able to spend months at NCEM, and make more efficient use of off-hours access to TEAM I and TEAM 0.5. We will use a higher-OAM beam to align and stigmate the diffracted probe, then switch to another grating that produces the desired probe with one unit of OAM for dichroism experiments. Our intermediate goal is to verify the presence of a clean vortex mode in the focused, aberration corrected probe by demonstrating STEM images with hollow spots at atomic column positions. In addition to thinned single crystal iron, we have acquired cobalt oxide nanoparticles with antiferromagnetic ordering in the shell structure that we believe will provide a suitable test specimen. We are also investigating the suitability of molybdenum disulfide for these experiments, as it is a 2D material without channeling effects.

*Phase microscopy* – In collaboration with Dr. Colin Ophus, Dr. Peter Ercius, and Dr. Hao Yang at NCEM, we plan to further develop interferometric techniques such as MIDI-STEM and STEM-holography. We need to optimize the design and construction of the nanofabricated phase plates used for this work. We also plan to incorporate some of our other technologies into the design of the structured electrons used for this work, such as holographic aberration correction, and electron vortices. to study magnetic materials.

## References

1. Uchida, M. & Tonomura, A. Generation of electron beams carrying orbital angular momentum. *Nature* **464,** 737 (2010).
2. Verbeeck, J., Tian, H. & Schattschneider, P. Production and application of electron vortex beams. *Nature* **467,** 301 (2010).
3. McMorran, B. J. *et al.* Electron Vortex Beams with High Quanta of Orbital Angular Momentum. *Science* **331,** 192 –195 (2011).
4. Harvey, T. R. *et al.* Efficient diffractive phase optics for electrons. *New J. Phys.* **16,** 093039 (2014).
5. McMorran, B. United States Patent: 8,680,488 - System and method for producing and using multiple electron beams with quantized orbital angular momentum in an electron microscope. (2014).
6. McMorran, B., Linck, M. & Moeck, P. United States Patent: 9,240,255 - Device and method for creating Gaussian aberration-corrected electron beams. (2014).
7. Harvey, T. R., Pierce, J. S., Chess, J. J. & McMorran, B. J. Demonstration of electron helical dichroism as a local probe of chirality. *Phys. Rev. Lett.* **(under review)** (2015).
8. Tan, P. S. *et al.* Phase singularity of surface plasmon polaritons generated by optical vortices. *Opt. Lett.* **36,** 3287–3289 (2011).
9. Gorodetski, Y., Niv, A., Kleiner, V. & Hasman, E. Observation of the Spin-Based Plasmonic Effect in Nanoscale Structures. *Phys. Rev. Lett.* **101,** 043903 (2008).
10. Linck, M., Ophus, C., Ercius, P. A. & McMorran, B. J. Holographic Aberration Correction in an Electron Microscope. *Ultramicroscopy* **(under review),** (2016).
11. Ophus, C. *et al.* Efficient linear phase contrast in scanning transmission electron microscopy with matched illumination and detector interferometry. *Nat. Commun.* **7,** 10719 (2016).

**Publications (2015 – 2016)**

J. J. Chess, S. A. Montoya, T. R. Harvey, C. Ophus, S. Couture, V. Lomakin, E. E. Fullerton, and B. J. McMorran, "A streamlined approach to mapping the magnetic induction of skyrmionic materials," arXiv:1608.06000 (2016); *Phys. Rev. B*, **under review** (submitted 08/2016)

S. A. Montoya, S. Couture, J. J. Chess, J. C. T. Lee, N. Kent, D. Henze, S. K. Sinha, M.-Y. Im, S. D. Kevan, P. Fischer, B. J. McMorran, V. Lomakin, S. Roy, and E. E. Fullerton, "Tailoring magnetic energies to stabilize dipole skyrmions and skyrmion lattices," arXiv:1608.01368 (2016); *Phys. Rev. X*, **under review** (submitted 08/2016)

M. Linck, C. Ophus, P. Ercius, B. J. McMorran, "Holographic Aberration Correction in an Electron Microscope", *Ultramicroscopy*, **under review** (submitted)

T. R. Harvey, B. J. McMorran, "A Stern-Gerlach-like approach to electron orbital angular momentum measurement," arXiv:1606.03631 (2016); *Phys. Rev. Lett.*, **under review** (submitted 06/2016)

**Invited article:** B. J. McMorran, "Structured Electron Matter Wave", *Journal of Optics* special issue: 'Roadmap on structured light', **accepted with revisions** (submitted 06/2016)

J. C. T. Lee, J. J. Chess, S. A. Montoya, X. Shi, N. Tamura, S. K. Mishra, P. Fischer, B. J. McMorran, S. K. Sinha, E. E. Fullerton, S. D. Kevan, S. Roy, "Synthesizing skyrmion bound pairs in Fe-Gd thin films," *Applied Physics Letters* **109**, 022402 (2016)

C. Ophus, J. Ciston, J. Pierce, T. R. Harvey, J. Chess, B. J. McMorran, C. Czarnik, H. H. Rose, and P. Ercius, "Efficient linear phase contrast in scanning transmission electron microscopy with matched illumination and detector interferometry," *Nature Communications* **7**, 10719 (2016)

T. R. Harvey, J. S. Pierce, J. J. Chess, B. J. McMorran, "Demonstration of electron helical dichroism as a local probe of chirality", arXiv:1507.01810 (2015); *Phys. Rev. Lett.* **under review** (submitted 06/2015)

# Advancing *In situ* Analytical Electron Microscopy for Probing Dynamic Nano-Scale Solid State Electrochemistry

**Ying Shirley Meng, Department of NanoEngineering, University of California San Diego**

## Research Scope

The current project focuses on the advancement of our newly developed *in situ* analytical electron microscopy and the development of additional high-end capabilities to quantitatively elucidate the dynamic changes in the bulk and interfaces of electrodes and electrolytes in various forms of solid state energy storage and conversion devices. The main goal is to characterize and elucidate the mechanisms by which dynamic structural and electrochemical transformations occur in various electrode/electrolyte solid-solid interfaces in order to *build guiding principles for functional solid state batteries*. We also utilize additional advanced techniques such as coherent x-ray diffraction imaging (CXDI) and quantum mechanical computation in order to identify the underlying fundamental science of phase transformations, roles of defect formation and dynamics in the solid state electrochemical systems at the nanometer scale.

## Recent Progress

*In situ* analytical electron microscopy (AEM) is a fast-growing and fascinating area of research that has drawn tremendous attention from various fields ranging from materials science to chemistry and biology. In fundamental studies of energy storage system, particularly electrochemical energy storage (EES), *ex situ* experiments often have limited time-scale resolution due to sample preparation and transfer, preventing the determination of the time constant of a reaction/transformation. More importantly, electrochemical systems often operate at states far from equilibrium. On the other hand, the EES systems' macroscopic properties such as the energy and power density are often governed the electrode/electrolyte interfaces that by nature are of atomic and nano scales. Therefore, *in situ* AEM provides great opportunities to characterize dynamic changes in morphology, electronic bonding state, and chemical composition in materials at and below the nanoscale. *In situ* electrochemical operation in the ultra-high vacuum column of a TEM has been pursued by three major strategies (**Fig. 1**). Our team has focused on the solid state approach (2 in

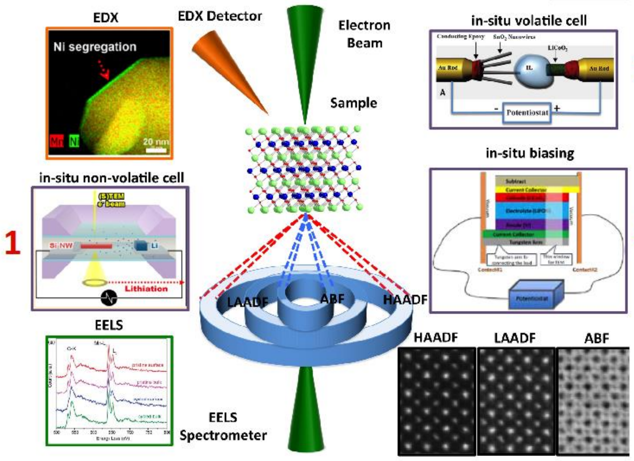

**Figure 1.** State-of-the-art (S)TEM techniques and their applications in battery research. (Publication 1)

Fig.1), where a full cell “nanobattery” can be fabricated from an all-solid-state thin film battery using a set of fully optimized focused ion beam (FIB) fabrication procedure.

Our methodology is at the forefront of this particular strategy by fully enabling galvanostatic cycling of FIB processed cross-sections in the TEM [Publication 2]. Galvanostatic biasing, as opposed to using potentiostatic biasing commonly seen in the literature [1-3], provides a powerful and precise control over the state of charge (e.g. Lithium content) at which we can characterize the electrochemical system as a function of states of charge. We established our *in situ* TEM methodology using a model system of lithium cobalt oxide (LCO) cathode, lithium phosphorus oxynitride (LiPON) electrolyte, and amorphous silicon (a-Si) anode all-solid-state battery [Publication 3]. The current work extends this technique to other battery chemistries to (1) understand how novel bulk materials function, we have focused on high energy high voltage systems where a large amount of lithium can be extracted (2) identify dynamic mechanisms limiting the ion transport, electron transport and phase transformations (if any), and (3) facilitate the design and optimization of better solid state battery materials. For layered compounds, work has focused on fully or partially substituting the Co ions with other transition metals. One compound is $LiCo_xNi_yMn_{1-x-y}O_2$ (NMC), which could extend the operation voltage window to 4.7 V [4]. Another possibility is the introduction of excess Li ions to improve material capacity. Li-rich $Li[Li_{1/3-2x/3}Ni_xMn_{2/3x/3}]O_2$ ($0 < x < 1/2$) can exceed 300 mAh/g, however there is a large irreversible capacity loss in the first cycle of 40-100 mAh/g and poor rate capability [5]. Alternatively, $Li(NiMn)_2O_4$ spinel structures are promising because they allow for three-dimensional Li diffusion. For phase pure $LiNi_{0.5}Mn_{0.5}O_4$ the redox couple switches from $Mn^{3+}$-$Mn^{4+}$ to $Ni^{2+}$-$Ni^{4+}$ raising the voltage up to 4.7 V [6]. However, these new materials development has been dominated mostly by liquid electrolytes such as carbonate based electrolytes, whose thermal stability and electrochemical stability are poor at high voltages more than 4.5V. Our approach of exploring the compatibility of these high voltage materials with solid electrolytes will open up a new venue for exploring strategies to enable ultra-high energy density EES (doubling or tripling the energy density).

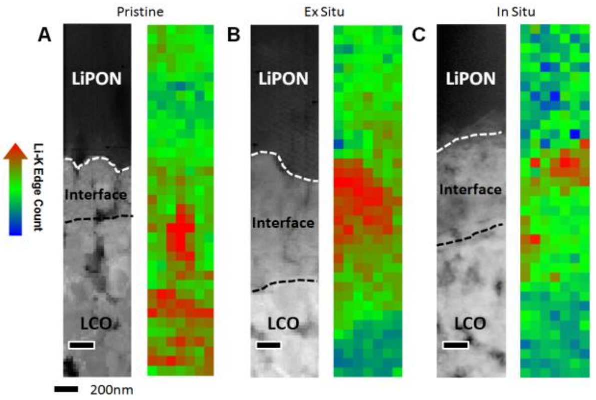

**Figure 2.** High angle annular dark field (HAADF) and Li-K edge concentration mapping of (a) pristine, (b) *ex situ*, (c) *in situ* thin film battery charged samples between the LCO and LiPON interface.

Building off of the *in situ* TEM analysis of the model LCO/LiPON/a-Si battery, we moved forward to analyze the LNMO/LiPON/a-Si system. We have successfully fabricated an electrochemically active LNMO/LiPON/a-Si micro-battery through close collaboration between UCSD and ORNL. Preliminary results indicate that the LNMO/LiPON interface is more stable than that of LCO/LiPON (**Fig 2**. From Publication 4), however the exact atomistic level understanding is still lacking.

We are currently investigating and comparing the layered and spinel systems when charged to high voltages. The primary goal of high-end characterization techniques on lithium ion battery materials has always been to apply the knowledge gain through these techniques in order to improve material synthesis and explore new regimes of material. We hope to use our *in situ* AEM methodology on additional interfaces between the novel cathodes and novel electrolytes that have been proposed in the previous section. As a preliminary study, we have looked at the Spinel-LNMO/LiPON interface and observe that there is no evidence of a disordered interfacial layer that forms (**Fig. 3**). Such a new interface is drastically different from what we previous seen. This is particularly interesting as Li et al [7] has shown over ten thousand cycles using a LNMO/LiPON/Li cell chemistry. Henceforth, it is of great scientific curiosity to understand what causes and prevents the formation of the disordered layer and not just its effects. Some recent computational papers have shown that there is a certain chemical instability between layered cathode material and solid state electrolytes [8]. There is a thermodynamic driving force for decomposition when the materials are in contact with each other. However if we can understand why certain interfaces do not form decomposition interfaces, we can use the knowledge learned in order to form guiding principles of interfacial engineering that produce distinct electrode-electrolyte interfaces with an additional protection layer. Such knowledge would be greatly useful in designing the next generation of all-solid-state thin film batteries and electrode coatings design for bulk systems.

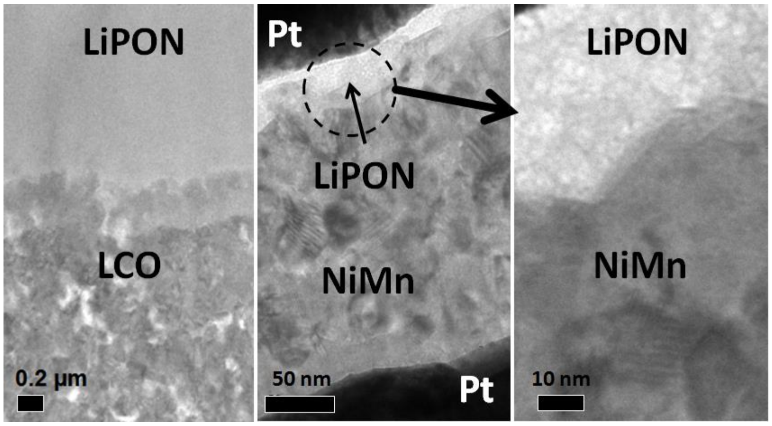

**Figure 3.** TEM image of the NiMn/LiPON interface showing no evidence of a disordered layer.[Manuscript in prep]

## Future Plans

Going forward, we will to do a full analysis of the electrode/electrolyte interfaces via *in situ* STEM/EELS at improved spatial, energy and temporal resolutions. This has and will continue to uncover fundamental mechanisms at solid interfaces that would otherwise elude bulk characterization techniques. However, there are merits to bulk-scale measurement techniques, and recent developments in coherent x-ray coherent diffraction imaging (CDXI) will greatly compliment our atomic-scale thin film research, potentially allowing dynamic observation of defects through the thickness of the thin film batteries. Further, computational methods will be applied, using fundamental quantum mechanical calculations to fully describe the observed mechanisms and validate our interpretations.

## References

1. Huang, J.Y., et al., *In Situ Observation of the Electrochemical Lithiation of a Single SnO2 Nanowire Electrode.* Science, 2010. 330(6010): p. 1515-1520.
2. Brazier, A., et al., *First Cross-Section Observation of an All Solid-State Lithium-Ion "Nanobattery" by Transmission Electron Microscopy.* Chemistry of Materials, 2008. 20(6): p. 2352-2359.
3. Yamamoto, K., et al., *Dynamic Visualization of the Electric Potential in an All-Solid-State Rechargeable Lithium Battery.* Angew. Chem. Int. Ed., 2010. 49: p. 4414-4417.
4. Ohzuku, T. and Y. Makimura, *Layered lithium insertion material of* $LiCo_{1/3}Ni_{1/3}Mn_{1/3}O_2$ *for lithium-ion batteries.* Chemistry Letters, 2001(7): p. 642-643.
5. Lu, Z.H. and J.R. Dahn, *Understanding the anomalous capacity of Li/Li[NixLi(1/3-2x/3)Mn(2/3-x/3]O-2 cells using in situ X-ray diffraction and electrochemical studies.* Journal of the Electrochemical Society, 2002**.** 149(7): p. A815-A822.
6. Xiao, J., et al., *High-Performance LiNi0.5Mn1.5O4 Spinel Controlled by Mn3+Concentration and Site Disorder.* Advanced Materials, 2012. **24**(16): p. 2109-2116.
7. Li, J., et al., *Solid Electrolyte: the Key for High-Voltage Lithium Batteries.* Advanced Energy Materials, 2014: p. 1401408.
8. Richards, W.D., et al., *Interface stability in solid-state batteries.* Chemistry of Materials, 2015.

## Publications

1. D. Qian, C. Ma, K. L More, Y. S. Meng and M. Chi, "Advanced analytical electron microscopy for lithium-ion batteries", NPG Asia Materials, 2015, 7, e193
2. Wang, Z. and Y.S. Meng, *Analytical Electron Microscopy Study of All Solid-State Batteries*, in *Handbook of Solid State Batteries*. 2015, p. 109-131.
3. H. Zheng, Y. S. Meng and Y. Zhu, "Frontiers of in situ electron microscopy", MRS Bulletin., 2015, 40, 12
4. Z. Wang, D. Santhanagopalan, W. Zhang, F. Wang, H. L. Xin, K. He, J. Li, N. Dudney, and Y. S. Meng,"In Situ STEM-EELS Observation of Nanoscale Interfacial Phenomena in All-Solid-State Batteries", Nano Letters, 2016, 16 (6), 3760
5. Z. Wang, J. Z. Lee, H. L. Xin, L. Han, N. Grillon, D. Guy-Bouyssou, E. Bouyssou, M. Proust, Y. S. Meng, "Effects of cathode electrolyte interfacial (CEI) layer on long term cycling of all-solid-state thin-film batteries" Journal of Power Sources, 2016, 324, 342
6. M. G. Verde, L. Baggetto, N. Balke, G. M. Veith, J. K. Seo, Z. Wang, and Y. S. Meng, "Elucidating the Phase Transformation of Li4Ti5O12 Lithiation at the Nanoscale", ACS Nano, 2016, 10 (4), 4312
7. A. Ulvestad, A. Singer, J. N. Clark, H. M. Cho, J. W. Kim, R. Harder, J. Maser, Y. S. Meng and O. G. Shpyrko, "Topological defect dynamics in operando battery nanoparticles", Science, 2015, 348(6241), 1344

# ATOMIC ELECTRON TOMOGRAPHY: 3D STRUCTURE WITHOUT CRYSTALS

**Jianwei (John) Miao**
**Department of Physics & Astronomy and California NanoSystems Institute, University of California, Los Angeles, CA 90095-1547. Tel: 310 206 2645, Email: miao@physics.ucla.edu.**

## Program Scope

To understand material properties and functionality at the most fundamental level, one must know the 3D positions of atoms with high precision. For crystalline materials, x-ray crystallography has provided this information since the pioneering work of Max von Laue and the Braggs around 100 years ago. But perfect crystals are rare in nature. Real materials often contain defects, surface reconstructions, nanoscale heterogeneities and disorders, which strongly influence material properties and performance. Completely different approaches from crystallography are needed to determine the 3D atomic arrangement of crystal defects and non-crystalline systems. In recent years, dramatic developments in aberration-corrected electron microscopes, advanced detectors, data acquisition methods, powerful 3D image reconstruction and atom tracing algorithms have placed one method on the cusp of this breakthrough: atomic electron tomography (AET) (1). AET has been used to image the 3D structure of grain boundaries, stacking faults, and the core structure of edge and screw dislocations at atomic resolution (2). It has also revealed the existence of atomic steps at 3D twin boundaries that are hidden in conventional 2D projections. Furthermore, the combination of AET and atom tracing algorithms has enabled the determination of the coordinates of individual atoms and point defects in materials with a 3D precision of 19 pm, allowing direct measurements of 3D atomic displacements and the full strain tensor (3). More recently, the 3D atomic arrangement of chemical order/disorder in a material was determined with 22 pm precision. The measured atomic positions and chemical species were used as direct input to quantum mechanical calculations to correlate crystal defects and chemical order/disorder with material properties at the single-atom level.

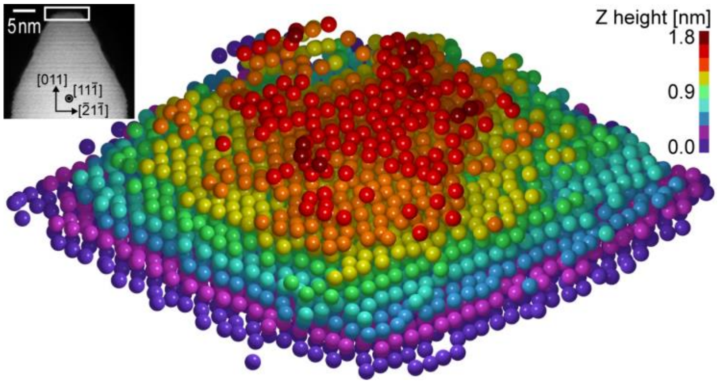

**Fig. 1.** 3D determination of the positions of individual atoms in a material with 19 pm precision. The experiment was conducted using an aberration-corrected ADF-STEM. A tilt series of 62 projections was acquired from a tungsten needle sample by rotating it around the [011] axis. The inset shows a representative projection at 0˚. After post-processing, the apex of the sample (labelled with a rectangle in the inset) was reconstructed by the EST method. The 3D positions of individual atoms were then traced from the reconstructions and refined using the 62 experimental projections. The 3D atomic model of the sample consists of 9 atomic layers along the [011] direction, labelled with crimson (dark red), red, orange, yellow, green, cyan, blue, magenta and purple from layers 1 to 9, respectively. [Ref. 3]

Building upon these developments, the scope of this project is:

- To resolve the 3D distribution of dipole moments of ferroelectric nanoparticles at the single-atom level, which will enable us to understand the underlying physics behind the ferroelectrics.
- To determine the full 3D atomic arrangement, including point defects, dislocations and grain boundaries, of 2D materials such as $Bi_2Se_3$. The atomic coordinates as well as the defect structure will be used to obtain the defect-induced electronic properties with DFT calculations.
- To identify the positions of all atoms in Ru@Pt core-shell electrocatalysts with emphasis on the strained Pt lattice and the Ru/Pt heterometallic interface. The experimentally determined atomic positions will be used for DFT calculations to correlate the crystal defects and lattice strain with the physical and chemical properties of Ru@Pt nanoparticles.

**Recent Progress**

*3D coordinates of individual atoms in materials revealed by AET.* In 1959, Richard Feynman challenged the electron microscopy community to locate the positions of individual atoms in substances (4). Over the last fifty-five years, significant advances have been made in electron microscopy. With the development of aberration-corrected electron optics (5,6), TEM imaging has reached sub-0.5Å resolution in 2D (7). Using STEM and 3D image reconstruction method known as equal slope tomography (EST) (8), AET has achieved 2.4Å resolution (9) and was applied to image the 3D core structure of edge and screw dislocations at atomic resolution (2). Notwithstanding these important developments, however, Feynman's 1959 challenge − 3D localization of the positions of atoms in a substance without using averaging or a priori knowledge of sample crystallinity − remains elusive. Here, we report the determination of the 3D positions of 3,769 individual atoms in a tungsten needle sample with a precision of ~19 pm and the identification of a point defect inside the sample in three dimensions (3). Our method consists of acquisition of a tilt series with an aberration-corrected STEM, 3D EST reconstructions of the tilt series, tracing individual atoms from the reconstructions, and 3D atomic model refinement, in which the crystallinity of the sample is not assumed.

*3D measurements of the atomic displacement and strain tensor in materials*. The structural, mechanical, electronic and optical properties of many materials are directly related to the strain in the materials (10). However, conventional methods to measure local strain at the nanoscale based on TEM, electron diffraction and holography are limited to 2D (10). Although coherent diffractive imaging (CDI) can measure the strain tensor in 3D (11), they offer limited spatial resolution. Very recently, we have applied AET to precisely determine the 3D positions of individual atoms in a tungsten needle sample. From the coordinates of these individual atoms, we measure the atomic displacement field and the full strain tensor with a 3D resolution of ~1 $nm^3$ and a precision of ~$10^{-3}$, which are further verified by density functional theory calculations and molecular dynamics simulations (3). As conventional methods for strain measurements are primarily based on geometric phase analysis of crystalline samples in Fourier space (10), the ability to precisely determine the 3D positions of individual atoms opens the door towards directly measuring the strain tensor in materials at the atomic scale.

## Future Plans

*Resolve the 3D distribution of dipole moments of ferroelectric nanoparticles at the single-atom level*. To truly understand the underlying physics behind the zero-dimensional ferroelectrics, one must obtain accurate 3D information of the polarization distribution inside the system. This can only be achieved by precise determination of individual atom positions and species. Using AET, we propose to accurately measure the polarization distribution of $Pb(Zr_{0.5}Ti_{0.5})O_3$ (PZT) nanoparticles in 3D. Current synthesis techniques can make PZT nanoparticles in the range of 5-10 nm (12), which is ideally suitable for electron tomography studies. The large Z contrast among the cations in PZT (Pb: 82, Zr: 40, Ti: 22) provides the best chance of successfully determining the atom species. Finally, ferroelectric polarizations can be inferred from relative displacements between cations within the perovskite unit cell. The cation displacement is expected to be about 30 pm for PZT (13), whereas our atomic resolution electron tomography approach has achieved a 3D precision of ~19 pm (3). We can further increase the precision by using kernel averaging, which improves the accuracy of the map with slightly sacrificing the spatial resolution, as shown in our previous study on strain tensor measurements of a W tip (3).

*Determine the full 3D atomic arrangement, including point defects, dislocations and grain boundaries, of 2D materials*. The discovery of graphene has ignited a "2D material rush" across several disciplines, and diverse functional systems have since been found to hold stable 2D forms (14,15). Several important 2D functional materials consist of multiple atomic layers (e.g. the Se-Bi-Se-Bi-Se quintuple layer of $Bi_2Se_3$), and a full structural characterization of these systems requires localizing the 3D coordinates of individual atoms in these materials. We propose to determine the 3D positions of individual atoms as well as crystal defects, such as point defects, grain boundaries and dislocations, of 2D nanoplate materials. We will first focus on focus on $Bi_2Se_3$ materials. Individual Bi and Se atoms will be traced from the 3D reconstruction based on the Z-contrast of the atomic species. From the 3D coordinates of the Bi and Se atoms of the $Bi_2Se_3$ materials, we will locate point defects, dislocations and grain boundaries at the single-atom level. The atomic coordinates as well as the defect structure will be used to obtain the defect-induced electronic properties with DFT calculations. This will allow us to correlate point defects, dislocations and grain boundaries with conductive surface states of $Bi_2Se_3$ topological insulators. Finally, while we will initially focus on $Bi_2Se_3$ nanoplates, our 3D atomic resolution electron tomography can be broadly applied to investigate the 3D crystal defects in 2D materials, such as $Bi_2Te_3$, $Sb_2Te_3$, $MoS_2$ and $WS_2$, and to probe the relationship between the defects and physical/chemical properties using DFT calculations

## References

1. J. Miao, P. Ercius, S. J. L. Billinge and U. Dahmen, "Atomic resolution electron tomography: 3D structures without crystals", *Science*, in press (2016).
2. Chen, C.-C. *et al.* Three-dimensional imaging of dislocations in a nanoparticle at atomic resolution. *Nature* **496**, 74–77 (2013).
3. Xu, R. *et al.* Three-dimensional coordinates of individual atoms in materials revealed by electron tomography. *Nature Mater.* **14**, 1099–1103 (2015).
4. Feynman, R. P. *Feynman and Computation*, pages63–76 (Perseus Press, Cambridge, Massachusetts, 1999).
5. Haider, M. *et al.* Electron microscopy image enhanced. *Nature* **392**, 768–769 (1998).
6. Batson, P. E., Dellby, N. & Krivanek, O. L. Sub-ångstrom resolution using aberration corrected electron optics. *Nature* **418**, 617–620 (2002).

7. Erni, R., Rossell, M. D., Kisielowski, C. & Dahmen, U. Atomic-resolution imaging with a sub-50-pm electron probe. *Phys. Rev. Lett.* **102**, 096101 (2009).
8. Miao, J., Förster, F. & Levi, O. Equally sloped tomography with oversampling reconstruction. *Phys. Rev. B* **72**, 052103 (2005).
9. Scott, M. C. *et al.* Electron tomography at 2.4-angstrom resolution. *Nature* **483**, 444–447 (2012).
10. Hÿtch, M. J. & Minor, A. M. Observing and measuring strain in nanostructures and devices with transmission electron microscopy. *MRS Bull.* **39**, 138–146 (2014).
11. Miao, J. et al. Beyond crystallography: Diffractive imaging using coherent x-ray light sources. *Science* **348**, 530–535 (2015).
12. Xu, G. *et al.* Hydrothermal synthesis of lead zirconate titanate nearly free-standing nanoparticles in the size regime of about 4 nm. *Cryst. Growth Des.* **9**, 13–16 (2009).
13. Jia, C.-L. *et al.* Atomic-scale study of electric dipoles near charged and uncharged domain walls in ferroelectric films. *Nature Mater.* **7**, 57–61 (2008).
14. Geim, A. K. & Grigorieva, I. V. Van der Waals heterostructures. *Nature* **499**, 419–425 (2013).
15. Butler, S. Z. *et al.* Progress, challenges, and opportunities in two-dimensional materials beyond graphene. *ACS Nano* **7**, 2898–2926 (2013).

## Recent two-year publications supported by BES

1. J. Miao, P. Ercius, S. J. L. Billinge and U. Dahmen, "Atomic resolution electron tomography: 3D structures without crystals", *Science*, in press (2016).
2. R. Xu, C.-C. Chen, L. Wu, M. C. Scott, W. Theis, C. Ophus, M. Bartels, Y. Yang, H. Ramezani-Dakhel, M. R. Sawaya, H. Heinz, L. D. Marks, P. Ercius and J. Miao, "Three-Dimensional Coordinates of Individual Atoms in Materials Revealed by Electron Tomography", *Nature Mater*. **14**, 1099-1103 (2015).
3. Z. Huang, M. Bartels, R. Xu, M. Osterhoff, S. Kalbfleisch, M. Sprung, A. Suzuki, Y. Takahashi, T. N. Blanton, T. Salditt and J. Miao, "Grain rotation and lattice deformation during photoinduced chemical reactions revealed by in-situ X-ray nanodiffraction", *Nature Mater*. **14**, 691–695 (2015).
4. B. Leshem, Y. Dallal, R. Xu, J. Miao, B. Nadler, D. Oron, N. Dudovich and O. Raz, "Direct single-shot phase retrieval from the diffraction pattern of separated objects", *Nature Commun*. 7, 10820 (2016).
5. B. D.A. Levin, E. Padgett, C.-C. Chen, M. C. Scott, Rui Xu, W. Theis, Y. Jiang, Y. Yang, C. Ophus, H. Zhang, D.-H. Ha, D. Wang, Y.,Yu, H. D. Abruña, R. D. Robinson, P. Ercius, L. F. Kourkoutis, J. Miao, D. A. Muller and R. Hovden, "Nanomaterial datasets to advance tomography in scanning transmission electron microscopy", *Sci. Data* **3**, 160041 (2016).
6. J. Miao, C.-C. Chen, M. C. Scott, P. Ercius, C. Zhu, M. Mecklenburg, E. R. White, C.-Y. Chiu, B. C. Regan, Y. Huang, L. D. Marks and U. Dahmen, "Three-Dimensional Imaging of Dislocations and Defects in Materials at Atomic Resolution Using Electron Tomography", *Microsc. Microanal.* **20**, 1062-1063 (2014).
7. M. C. Scott, W. Theis, Rui Xu, Li Wu, C.-C. Chen, C. Ophus, P. Ercius and J. Miao, "Implementation of Atomic Resolution Electron Tomography of a Needle Sample", *Microsc. Microanal* **21**, 1523-1524 (2015).
8. Y. Yang, C.-C. Chen, M. C. Scott, C. Ophus, R. Xu, A. Pryor Jr, L. Wu, F. Sun, W. Theis, J. Zhou, M. Eisenbach, P. R. C. Kent, R. F. Sabirianov, H. Zeng, P. Ercius and J. Miao, "Deciphering chemical order/disorder and material properties at the single-atom level", submitted.
9. Z. Huang , S. Jiang , F. S. Ochoa , T. W. B. Lo , Y. Chen , M. C. Scott , M. Mecklenburg, P. Hu , P. Ercius , Z. Amghouz , F. Xu , C. Tang , S. C. E. Tsang , M. Springborg , J. Miao and X. Tang, "Ohmic atomic wires", submitted.
10. Z. Zhao, M. Feng, J. Zhou, Z. Liu, M. Li, Z. Fan, O. Tsen, J. Miao, X. Duand and Y Huang, "Composition Tunable Ternary Pt-Ni-Co Octahedra for Optimized Oxygen Reduction Activity", submitted.

# Atomically Engineered Ferroic Layers Yield a Room-Temperature Magnetoelectric Multiferroic: Design, Realization, and Picometer-Precision Imaging of Polarization Switching

**David A. Muller[1], Craig J. Fennie[1], Darrell G. Schlom[1]**

**[1]Cornell University, Ithaca, NY 14853**

## Research Scope

Materials that exhibit simultaneous order in their electric and magnetic ground states hold tremendous promise for enabling the electrical control of magnetism. Such materials are, however, exceedingly rare due to competing requirements for ferroelectricity and magnetism. Single-phase multiferroics are currently limited to antiferromagnetic or weak ferromagnetic alignments, lack coupling between the order parameters or have properties that only emerge well below room-temperature, stymieing device applications.

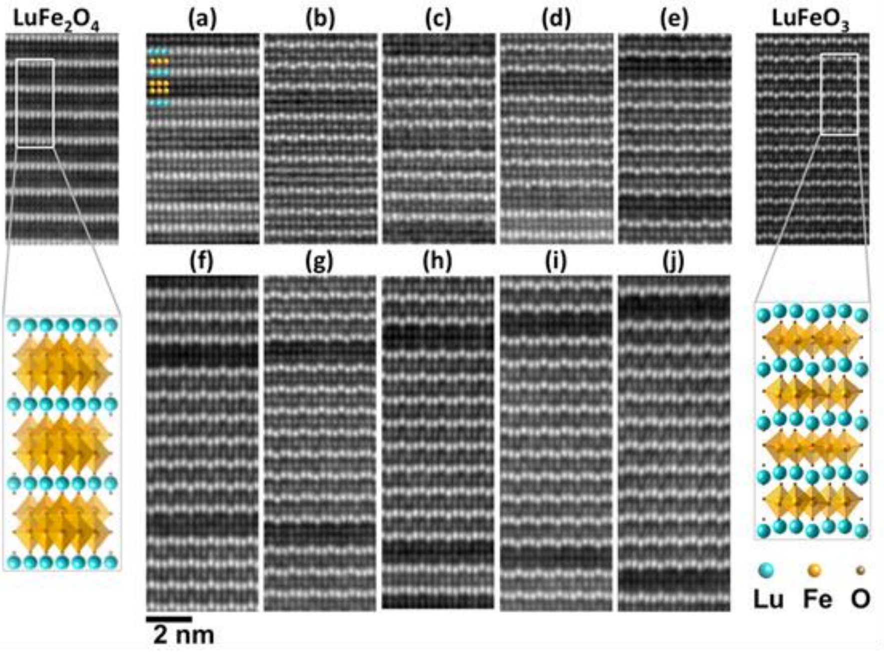

**Figure 1.** HAADF-STEM images of the $(LuFeO_3)_m/(LuFe_2O_4)_1$ superlattice series for $1 \le m \le 10$. Samples are imaged along the $LuFeO_3$ $P6_3cm$ [100] zone.

Advances in thin film deposition and characterization have enabled materials to be rationally designed at the atomic-scale where the local chemistry, bonding and electronic environment can be tailored to stabilize emergent phenomena.

Here we exploit such techniques to directly perturb the structural environment of the frustrated hexagonal ferrimagnet $LuFe_2O_4$ at the sub-Angstrom scale, tuning the magnetic order to construct a new magnetoelectric multiferroic where ferroelectricity and strong magnetic ordering are coupled near room-temperature (281K). We investigate the switching behavior across multiple lengthscales using PFM, XMCD PEEM and both new and established electron microscopy methods for imaging polarization, including our new electron microscope pixel-array detector (EMPAD). Our results demonstrate a design methodology for creating higher-temperature magnetoelectric multiferroics by exploiting a combination of geometric frustration, lattice distortions and epitaxial engineering.

## Recent Progress

Starting with hexagonal $LuFeO_3$, a geometric ferroelectric with the greatest known planar rumpling, we introduce individual extra monolayers of FeO during growth to construct formula-unit-thick syntactic layers of ferrimagnetic $LuFe_2O_4$ within the $LuFeO_3$ matrix, i.e., $(LuFeO_3)_m/(LuFe_2O_4)_1$ superlattices. The severe rumpling imposed by the neighbouring $LuFeO_3$ drives the ferrimagnetic $LuFe_2O_4$ into a simultaneously ferroelectric state, while also reducing the $LuFe_2O_4$ spin frustration.

Scanning transmission electron microscopy (STEM) images (Fig. 1) shows that the room-temperature improper ferroelectricity characteristic of $LuFeO_3$, manifest as a sub-Angstrom displacement of the lutetium atoms, propagates through the structure for $m \geq 2$. The polarization monotonically tracks the magnitude of this lutetium trimer distortion [1], allowing the ADF STEM to be used as a local probe of ferroelectricity (larger fields of view by EMPAD STEM). Increasing the number of $LuFeO_3$ layers in the superlattice enhances the ferroelectric distortions up to $m$~9. Density functional theory calculations indicate that these distortions reduce the $LuFe_2O_4$ spin frustration, which in turn boosts the magnetic transition temperature from ~240 K in the bulk compound to ~280 K for the $(LuFeO_3)_9(LuFe_2O_4)_1$ superlattice.

Coupling the ferroelectric distortion to the magnetic layer increases the magnetic transition temperature significantly (Figure 2) — from 240 K for $LuFe_2O_4$ to 281 K for $(LuFeO_3)_9/(LuFe_2O_4)_1$. Moreover, the ferroelectric order couples to the ferrimagnetism, enabling direct electric field control of magnetism at 200 K as shown by XMCD PEEM and PFM imaging of electrically poled structures. Such coupling is distinct from the better-studied Dzyaloshinskii-Moriya coupling previously observed between ferroelectricity and weakly canted antiferromagnetism at room temperature in $BiFeO_3$. Further understanding of this coupling mechanism could guide the design of higher temperature ferromagnetic ferroelectrics that can be deterministically switched between symmetry equivalent states using an electric field.

The structure and statistics of switched domains was studied with ex-situ and in-situ biasing (Figure 3). From atomic-resolution STEM heating experiments we construct a phase diagram for ferroelectricity. With increasing temperature, ferroelectricity disappears starting with lower $m$ first. Above $T$ =

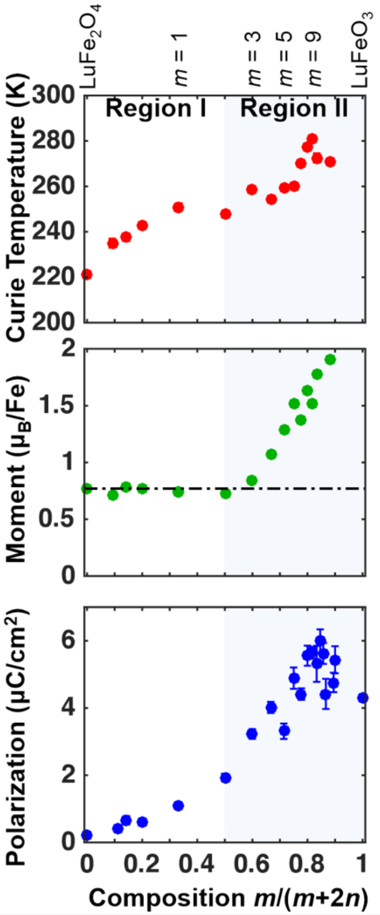

**Figure 2.** Magnetic and ferroelectric characterization of $(LuFeO_3)_m/(LuFe_2O_4)_n$ The ferromagnetic Curie temperature reaches a maximum of 281 K for the $(LuFeO_3)_9/(LuFe_2O_4)_1$ compound (top). The total moment per $LuFe_2O_4$ iron atom at 50 K assuming the moment of $LuFeO_3$ remains constant (middle). Average polarization from HAADF-STEM for superlattice layering plotted as a function of the composition for the $(LuFeO_3)_m/(LuFe_2O_4)_1$ and $(LuFeO_3)_1/(LuFe_2O_4)_n$ series (bottom). Ferroelectric distortions are observed for the $(LuFeO_3)_m/(LuFe_2O_4)_1$ superlattices with $m \geq 2$.

675 K, we see no ferroelectric distortions.

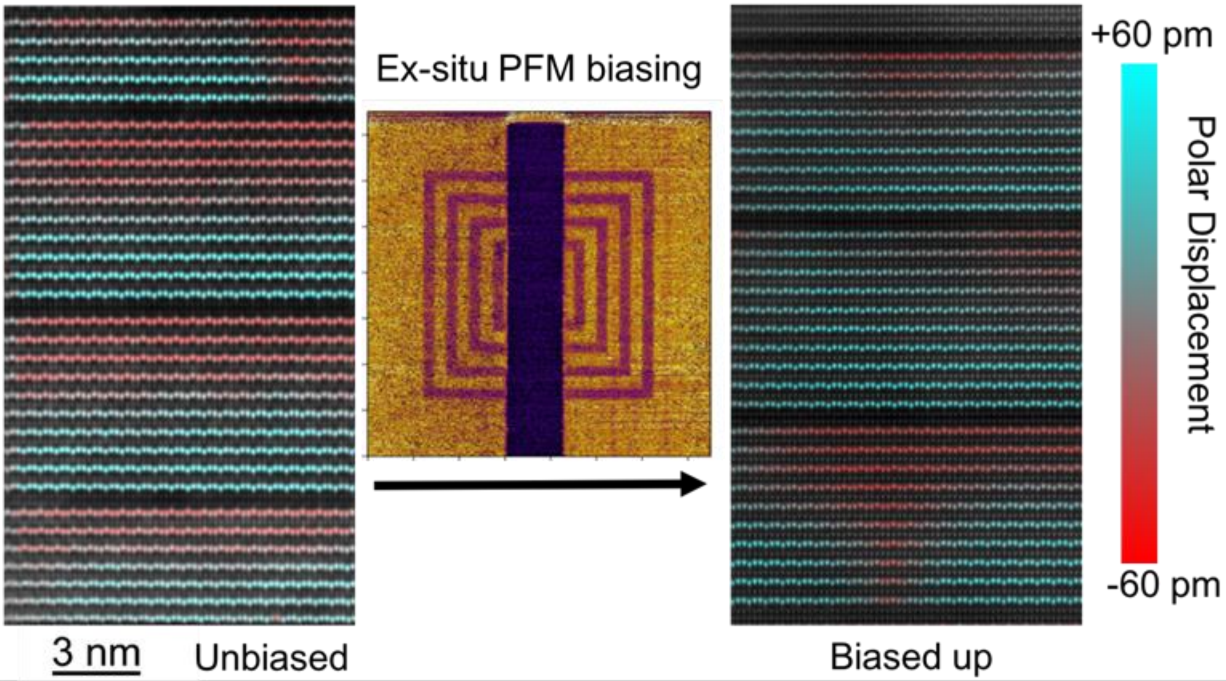

**Figure 3**. Domain wall motion after electrical poling, showing switching of the near-surface domains after electrical biasing with a sharp tip.

## Future Plans

Starting at the level of electrons and atoms our long-term goal is to rationally design complex oxide heterostructures and interface-materials with targeted emergent behaviors. This is not a matter of simply optimizing material parameters, but rather begins with understanding a mechanism to control the interplay between the diverse microscopic degrees of freedom prevalent in complex oxides in order to create targeted macroscopic phenomena, and ends with the design of new material realizations. These realizations are in turn created with atomic-layer precision, structurally assessed to see that they are the intended realization, and finally their relevant properties are measured. In this program we are developing the scientific ideas necessary to apply this design paradigm to the creation of relaxor ferroelectrics without disorder.

Our starting point is a new class of $A_{n+1}B_nO_{3n+1}$ Ruddlesden-Popper (RP) phases possessing a ferroic instability. Our first-principles calculations indicate that the ferroelectric vs. antiferroelectric alignment of neighboring polar slabs in $Sr_{n+1}Ti_nO_{3n+1}$ is nearly energetically degenerate,[2] The first research objective of our project is to **manipulate control parameters to create novel functionalities in a new family of ferroics**. The near degeneracy between ferroelectric vs. antiferroelectric alignment of neighboring polar slabs in $Sr_{n+1}Ti_nO_{3n+1}$**Error! Bookmark not defined.** begs the question of whether relaxor ferroelectricity can be created and systematically studied in this system without the chemical disorder[3,4] or free surfaces[5] that are present in all known relaxor ferroelectrics. Our studies will go beyond strained $Sr_{n+1}Ti_nO_{3n+1}$ by considering the site-specific incorporation of species that lead to ferroelectric instabilities without strain, e.g., the introduction of calcium, barium, and lead into this general family to form ordered $(Ca,Sr,Ba,Pb)_{n+1}Ti_nO_{3n+1}$ phases. These hypothetical phases containing calcium, barium, and lead are metastable. Figure 4 shows preliminary results from the n=5, m=1 $(SrTiO_3)_n(BaTiO_3)_mSrO$ RP phase from the n=1 to 5 homologous series grown on $DyScO_3$ (110) to minimize epitaxial strain. Octahedral rotations damp within 1 unit cell from the substrate. Intriguingly, our first-principles calculations reveal a nearly isotropic in-plane polarization of $Pb_2TiO_4$ under appropriate biaxial strain (about 0.7%).[6] This unusual energetic landscape is tantalizing in that it might give rise to an electrical analog of ferromagnetic resonance. Guided by theory, we will explore this and other unusual physical properties of these ordered $(Ca,Sr,Ba,Pb)_{n+1}Ti_nO_{3n+1}$ phases.

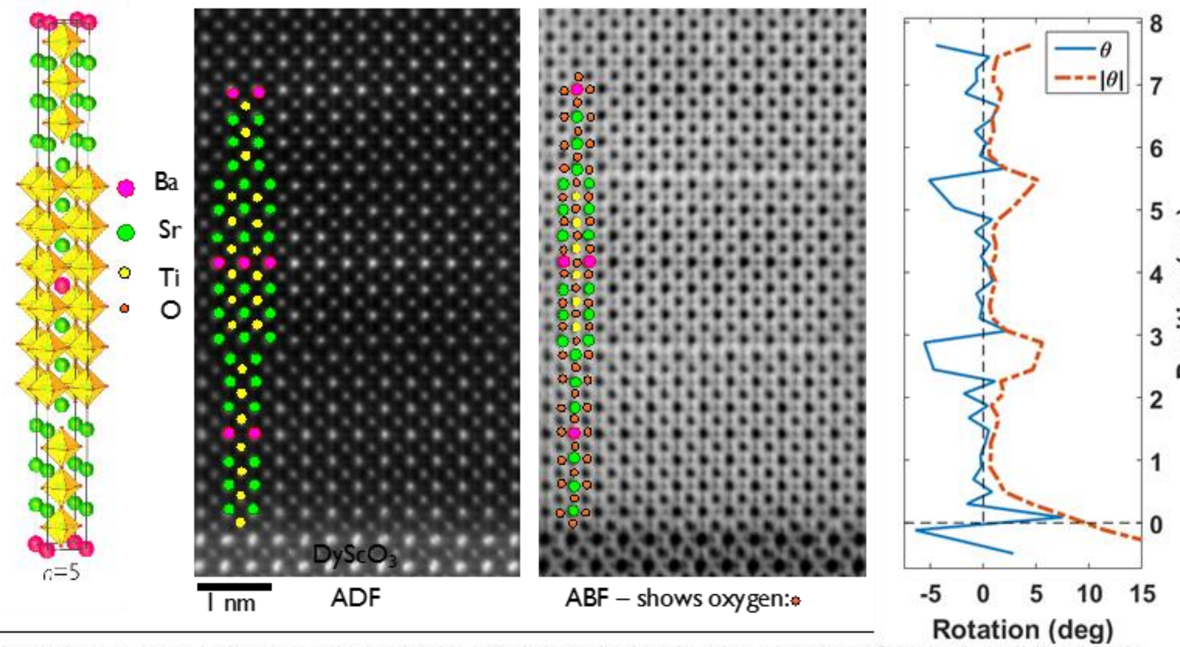

Figure 4. n=5, m=1 designer $(SrTiO_3)_n(BaTiO_3)_mSrO$ superlattice showing a cartoon of the basic building block (left), simultaneous annular dark field (ADF) and annular bright field images (ABF) along with the layer-by-layer averaged octahedral rotations measured from the ABF image.

## References

1. Das, H., Wysocki, A. L., Geng, Y., Wu, W. & Fennie, C. J. Bulk magnetoelectricity in the hexagonal manganites and ferrites. Nat. Commun. 5, 2998 (2014).
2. T. Birol, N.A. Benedek, and C.J. Fennie, “Interface Control of Emergent Ferroic Order in Ruddlesden-Popper $Sr_{n+1}Ti_nO_{3n+1}$,” *Phys. Rev. Lett.* **107** (2011) 257602.
3. L.E. Cross, “Relaxor Ferroelectrics,” *Ferroelectrics* **76** (1987) 241–267.
4. A.A. Bokov and Z.G. Ye, “Recent Progress in Relaxor Ferroelectrics with Perovskite Structure,” *J. Mater. Sci.* **41** (2006) 31–52.
5. B. Meyer and D. Vanderbilt, “*Ab Initio* Study of $BaTiO_3$ and $PbTiO_3$ Surfaces in External Electric Fields,” *Phys. Rev. B* **63** (2001) 205426.
6. C. Fennie and K. Rabe, “First-Principles Investigation of Ferroelectricity in Epitaxially Strained $Pb_2TiO_4$,” *Phys. Rev. B* **71** (2005) 100102.
7. In collaboration with Julia A. Mundy, Charles M. Brooks, Megan E. Holtz, Jarrett A. Moyer, Hena Das, Alejandro F. Rébola, John T. Heron, James D. Clarkson, Steven M. Disseler, Zhiqi Liu, Alan Farhan, Rainer Held, Robert Hovden, Elliot Padgett, Qingyun Mao, Hanjong Paik, Rajiv Misra, Lena

F. Kourkoutis, Elke Arenholz, Andreas Scholl, Julie A. Borchers, William D. Ratcliff, Ramamoorthy Ramesh, Peter Schiffer

## Publications

1. J.A. Mundy, Y. Hikita, T. Hidaka, T. Yajima, T. Higuchi, H.Y. Hwang, D.A. Muller, and L.F. Kourkoutis, “Visualizing the Interfacial Evolution from Charge Compensation to Metallic Screening Across the Manganite Metal–Insulator Transition,” *Nature Communications* **5** (2014) 3464.
2. J.A. Moyer, R. Misra, J.A. Mundy, C.M. Brooks, J.T. Heron, D.A. Muller, D.G. Schlom, and P. Schiffer, “Intrinsic Magnetic Properties of Hexagonal $LuFeO_3$ and the Effects of Nonstoichiometry,” *APL Materials* **2** (2014) 012106.
3. B.S. Holinsworth, D. Mazumdar, C.M. Brooks, J.A. Mundy, H. Das, J.G. Cherian, S.A. McGill, C.J. Fennie, D.G. Schlom, and J.L. Musfeldt, “Direct Band Gaps in Multiferroic *h*-$LuFeO_3$,” *Applied Physics Letters* **106** (2015) 082902.
4. T. Yajima, Y. Hikita, M. Minohara, C. Bell, J.A. Mundy, L.F. Kourkoutis, D.A. Muller, H. Kumigashira, M. Oshima, and H.Y. Hwang, “Controlling Band Alignments by Artificial Interface Dipoles at Perovskite Heterointerfaces,” *Nature Communications* **6** (2015) 6759.
5. S.M. Disseler, J.A. Borchers, C.M. Brooks, J.A. Mundy, J.A. Moyer, D.A. Hillsberry, E.L. Thies, D.A. Tenne, J. Heron, M.E. Holtz, J.D. Clarkson, G.M. Stiehl, P. Schiffer, D.A. Muller, D.G. Schlom, and W.D. Ratcliff, “Magnetic Structure and Ordering of Multiferroic Hexagonal $LuFeO_3$,” *Physical Review Letters* **114** (2015) 217602.
6. T. Mairoser, J.A. Mundy, A. Melville, D. Hodash, P. Cueva, R. Held, A. Glavic, J. Schubert, D.A. Muller, D.G. Schlom, and A. Schmehl, “High-Quality EuO Thin Films the Easy Way via Topotactic Transformation,” *Nature Communications* **6** (2015) 7716.
7. C.M. Brooks, R.B. Wilson, A. Schäfer, J.A. Mundy, M.E. Holtz, D.A. Muller, J. Schubert, D.G. Cahill, and D.G. Schlom, “Tuning Thermal Conductivity in Homoepitaxial $SrTiO_3$ Films via Defects,” *Applied Physics Letters* **107** (2015) 051902.
8. Julia A. Mundy, Charles M. Brooks, Megan E. Holtz, Jarrett A. Moyer, Hena Das, Alejandro F. Rébola, John T. Heron, James D. Clarkson, Steven M. Disseler, Zhiqi Liu, Alan Farhan, Rainer Held, Robert Hovden, Elliot Padgett, Qingyun Mao, Hanjong Paik, Rajiv Misra, Lena F. Kourkoutis, Elke Arenholz, Andreas Scholl, Julie A. Borchers, William D. Ratcliff, Ramamoorthy Ramesh, Craig J. Fennie, Peter Schiffer, David A. Muller & Darrell G. Schlom, “Atomically Engineered Ferroic Layers Yield a Room-Temperature Magnetoelectric Multiferroic”, Nature, (in press)

# Magnetic imaging of topological phases of matter

**Katja Nowack, LASSP, Department of Physics, Cornell University, Ithaca, NY**

## Research Scope

This project seeks to advance our understanding of electronic and magnetic phenomena emerging in topological phases of matter[1,2]. Topological phases of matter hold the promise to unlock a broad range of phenomena including the quantum anomalous Hall effect (QAHE), topological magnetoelectric effects, electric field-induced magnetic image monopoles, axionic-like electrodynamics, and even emergent supersymmetry in conjunction with superconductivity[3]. Of these the QAHE has recently been realized[4], opening the door to an exciting array of further experiments. However, many aspects of the QAHE remain unclear; progress towards the predicted phenomena hinges on our detailed understanding of the materials involved. In this project we will study relevant materials and devices through a combination of local magnetic and transport measurements with the ultimate goal to observe more of the anticipated phenomena. Our experimental approach consists of superconducting quantum interference devices (SQUIDs) and Hall probes as local and non-invasive magnetic scanning probes combined with low-noise transport and high-frequency excitations.

In this project we will focus on two major research thrusts. First, we will study the intricate interplay of magnetic order and the topologically non-trivial electronic system in the QAHE realized in magnetically doped topological insulators. We will image the structure and dynamics of the magnetic order and simultaneously determine how transport happens on the local scale in a network of chiral modes. We will contrast relevant materials with different magnetic characteristics, such as Cr-doped $(Bi,Sb)_2Te_3$ [4]18,19,21, V-doped $Sb_2Te_3$[5] , and Mn-doped HgTe quantum wells[6,7]. Second, we will broadly explore and characterize new materials predicted to realize topological phases of matter with the goal to provide guidance and feedback for material growth. In particular, we will investigate ternary half-Heusler compounds, a class of materials that promises to support topologically non-trivial band structure[8,9] and simultaneously displays intrinsic stochiometric magnetism and superconductivity.

This project will also push the frontiers of submicron magnetic microscopy through the implementation of high-sensitivity graphene Hall probes and through the combination of magnetic probes with microwave excitation. Hall probes will extend the accessible magnetic field and temperature range compared to magnetic imaging using SQUIDs. Microwave compatible probes will allow us to implement a novel imaging technique that is inspired by scanning gate microscopy[10] and recently developed magnetic scanning techniques[11]. We will use an on-chip coil to apply a local magnetic field while monitoring the transport characteristic of a device as a function of the position of the perturbation. Field amplitudes of several mT and excitation frequencies >10 GHz are feasible, making it possible to e.g. locally excited ferromagnetic resonance.

## Recent Progress

This program has been active for only two months, and thus we are in the early stages of the research. We are finalizing the construction of our mK scanning probe microscope and are calibrating our 4K microscope. We have developed new SQUID designs with impedance matched leads for the field coils which will allow us to apply local microwave magnetic fields while scanning. We have also started the fabrication of graphene Hall probes.

## Future Plans

We will start imaging Cr-doped $(Bi,Sb)_2Te_3$ and V-doped $Sb_2Te_3$ as soon as our mK scanning probe microscope is finalized. The new SQUIDs with microwave compatible field coil leads will allow us to perform first proof of principle measurements as described above in the near future. Scanning Hall probes will allow us to explore the QAHE in a wide range of magnetic fields.

## References

1. Hasan, M. Z. & Kane, C. L. Colloquium : Topological insulators. *Rev. Mod. Phys.* **82,** 3045–3067 (2010).
2. Qi, X.-L. & Zhang, S.-C. Topological insulators and superconductors. *Rev. Mod. Phys.* **83,** 1057–1110 (2011).
3. Grover, T., Sheng, D. N. & Vishwanath, A. Emergent Space-Time Supersymmetry at the Boundary of a Topological Phase. *Science* **344,** 280–283 (2014).
4. Chang, C. Z. *et al.* Experimental Observation of the Quantum Anomalous Hall Effect in a Magnetic Topological Insulator. *Science* **340,** 167–170 (2013).
5. Chang, C.-Z. *et al.* High-precision realization of robust quantum anomalous Hall state in a hard ferromagnetic topological insulator. *Nat. Mater.* **14,** 473 (2015).
6. Liu, C.-X., Qi, X.-L., Dai, X., Fang, Z. & Zhang, S.-C. Quantum Anomalous Hall Effect in $(Hg_{1-y},Mn_y)Te$ Quantum Wells. *Phys. Rev. Lett.* **101,** 146802 (2008).
7. Buhmann, H. Towards the quantum anomalous Hall effect in HgMnTe. *Bull. Am. Phys. Soc.* http://meetings.aps.org/link/BAPS.2012.MAR.P27.1 (2012).
8. Chadov, S. *et al.* Tunable multifunctional topological insulators in ternary Heusler compounds. *Nat. Mater.* **9,** 541–545 (2010).
9. Lin, H. *et al.* Half-Heusler ternary compounds as new multifunctional experimental platforms for topological quantum phenomena. *Nat. Mater.* **9,** 546–549 (2010).
10. Eriksson, M. a. *et al.* Cryogenic scanning probe characterization of semiconductor nanostructures. *Appl. Phys. Lett.* **69,** 671 (1996).
11. Bhallamudi, V. P. *et al.* Experimental Demonstration of Scanned Spin-Precession Microscopy. *Phys. Rev. Lett.* **111,** 117201 (2013).

# Structure and Dynamics of Domains in Ferroelectric Nanostructures – In-situ TEM Studies

**Xiaoqing Pan**

**Department of Chemical Engineering & Materials Science and Department of Physics and Astronomy, University of California, Irvine, CA 92697-2575**

## Research Scope

The main goal of the proposed research is to explore the structure and dynamic behaviors of ferroelectric domains in ferroelectric thin films and nanostructures by advanced transmission electron microscopy (TEM) techniques in close collaboration with phase field modeling. The experimental techniques used include aberration-corrected sub-Å resolution TEM and *in-situ* TEM using a novel scanning tunneling microscopy (STM) - TEM holder which allows the direct observation of nucleation and dynamic evolution of ferroelectric domains under applied electric field. Specifically, we propose (1) to study the roles of static electrical boundary conditions and electrical charge in controlling the equilibrium domain structures of $BiFeO_3$ thin films with controlled substrate constraints, (2) to explore the fundamental mechanisms of ferroelectric domain nucleation, growth, and switching under an applied electric field in both uniform thin films and nanofabricated nanostructures, and to understand the roles of crystal defects such as dislocations and interfaces in these processes, (3) to understand the physics of ferroelectric domain walls and the influence of defects on the electrical switching of ferroelectric domains. The nucleation and dynamic evolution of ferroelectric domains observed by *in-situ* TEM under applied external electric field are quantitatively analyzed and directly compared with phase field simulations in Professor Long-Qing Chen's group at Penn State University.

## Recent Progress

### *Switching of ferroelectric charged domain walls*

In our previous work under this project, we have identified a type of strongly charged domain walls (sCDWs) with a "head-to-head" polarization configuration in $BiFeO_3$ thin films [1]. Such sCDWs carrying net bound charge can have distinct properties from uncharged domain walls, such as a metallic conductivity. An understanding of the local response and underlying dynamic mechanism of sCDWs under external excitations is thus necessary to engineer reliable ferroelectric devices. Using *in situ* transmission electron microscopy (TEM), we studied the nanoscale behavior of individual sCDWs under applied electric fields in a 20 nm thick $BiFeO_3$ (BFO) film with 20 nm thick $La_{0.7}Sr_{0.3}MnO_3$ (LSMO) bottom electrode grown on (110) $TbScO_3$ (TSO) substrates (Fig. 1a) by reactive molecular-beam epitaxy (MBE) [2]. In Fig. 1b, a vertical 109° domain wall is intersected with an inclined 180° wall to form a triangular 109°/180° domain wall junction. The tip of the triangular junction is located above the BFO/LSMO interface, and thus a 71° sCDW with

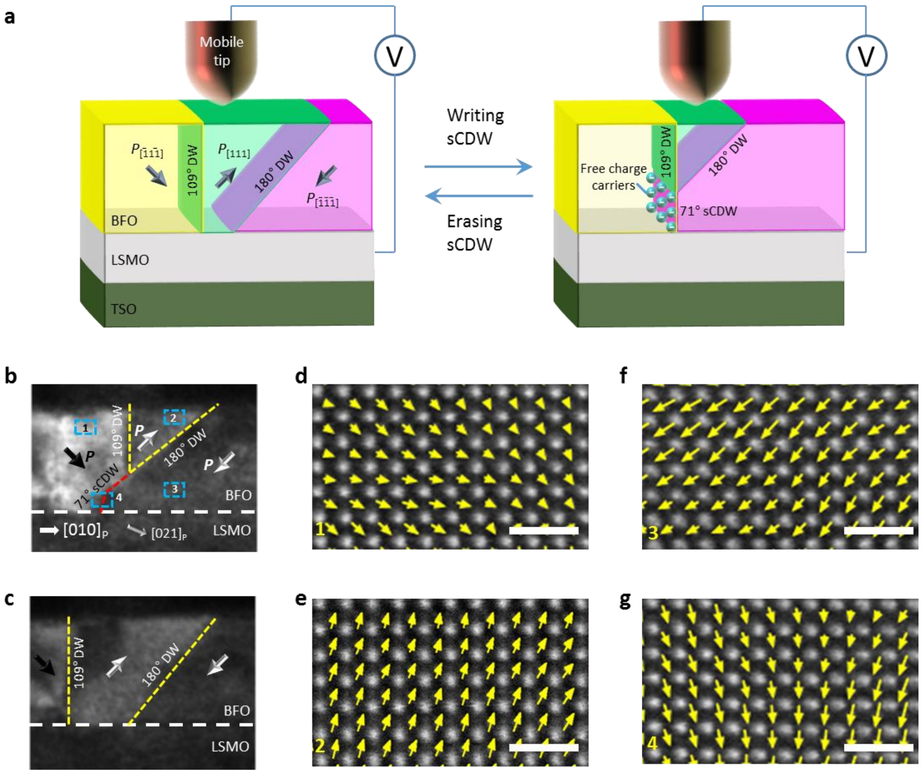

Fig. 1 | Bistability of the system associated with a sCDW in $BiFeO_3$ thin film. a, Schematic of experimental set-up: a BFO thin film was grown on LSMO/TSO, and a mobile tungsten tip acts as one electrode for electrical switching with the LSMO layer being grounded. b, Cross-sectional dark-field TEM image showing a triangular 109°/180° domain wall (DW) junction with a 71° sCDW in BFO film. c, TEM image showing domain configuration of separated 109° and 180° domain walls, without a sCDW. Note: *P*, polarizations. For scale, the $BiFeO_3$ film thickness in b and c is 20 nm. d-g, High-resolution HAADF STEM image of four different regions highlighted by the rectangular in b overlaid with vectors describing the polarizations. Scale bar, 1 nm.

"head-to-head" polarization is created below the triangular 109°/180° domain wall junction near the bottom interface. The polarization configuration was unambiguously determined through quantitative mapping of the displacements between the Fe and Bi atoms using atomic-scale high-angle annular dark-field (HAADF) scanning transmission electron microscopy (STEM) imaging, as shown in Fig. 1d-g. Compared to the $\langle 111\rangle_P$ polarized *R*-like structure of the bulk domains (Fig. 1d-f), the "head-to-head" sCDW possesses a *T*-like structure with a $[00\bar{1}]_P$ orientated ferroelectric polarization (Fig. 1g). Since the bound charge adjacent to the interface can be compensated by free carriers from the bottom electrode, the system favours formation of the sCDW to reduce the total domain wall area to minimize its electrostatic energy. On the other hand, the system can also be stable without a sCDW as shown in Fig. 1c. In this case the 109° and 180° domain walls are separated by sufficient distance so that their interaction is weak.

We observed that a sCDW can be created by applying a bias, as shown in the chronological series of images presented in Fig. 2. The bias was linearly increased from 0 to 6.0 V over 50 seconds. The initial stable structure (Fig. 2a) contained 109° and 180° domain walls separated by

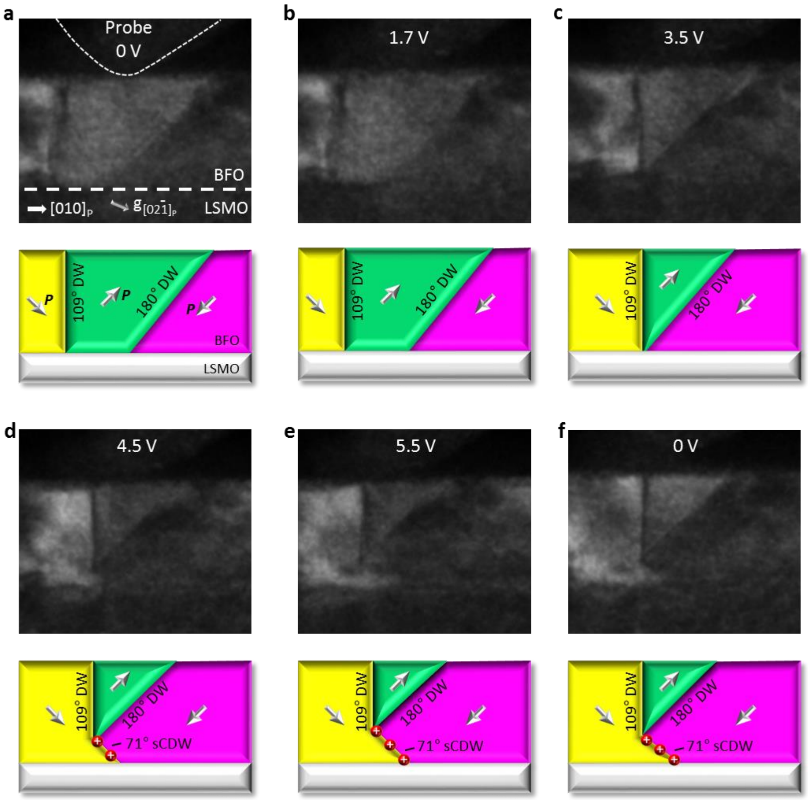

Fig. 2 | Creation of a sCDW caused by applying a positive ramp bias using *in situ* TEM. a, The original stable state without a sCDW in BFO film. b, At the critical bias, the domain wall (DW) started to move. c, The 109° and 180° domain walls intersect at the substrate interface as a result of domain wall motion. d,e, Formation and growth of a sCDW as a result of upward motion of the tip of the triangular 180°/109° domain wall junction. f, After removal of the bias, the sCDW relaxed to be shorter than that observed in e. For scale, the film thickness is

10 nm at the substrate interface. The onset of domain wall motion occurred at a critical applied bias of 1.7 V (Fig. 2b). As larger biases were applied, a two-stage switching process occurred. During the first stage, the two 109° and 180° domain walls moved toward each other until they intersected (Fig. 2c). During the second stage, further shrinkage of the triangular domain led to upward motion of the triangular domain tip and resulted in the formation and elongation of a sCDW (Fig. 2d,e). After the bias was removed, the system relaxed to a stable state and the length of the sCDW remained to be ~5 nm (Fig. 2f). The sCDW can also be erased by reversing the applied voltage (linearly decreasing from 0 to -6.0 V over 50 seconds), as shown in Fig. 3. The critical bias to induce domain wall motion in this case (-1.46 V, as shown in Fig. 3b) was similar in magnitude to that in the sCDW writing process. Switching occurred by growth of the triangular domain (Fig. 3c), exactly reversing the domain shrinkage in the creation process. Finally, the system was returned to the original stable domain structure without a sCDW (Fig. 3d). This state remained stable after removal of the bias (Fig. 3e).

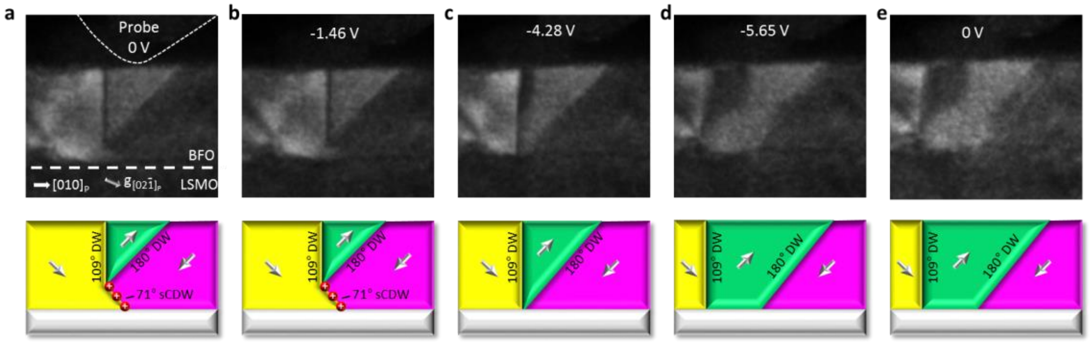

Fig. 3 | Erasure of a sCDW caused by a negative ramp bias. a, The original stable state with a sCDW. b, At the critical bias, the domain wall started to move. c, The sCDW was annihilated as a result of the expansion of the triangular domain. d, The system went back to the stable state without a sCDW. e, After removal of the bias, this state remained stable. For scale, the film thickness is 20 nm.

## Future Plans

In the next year, we will continue our experimental work on TEM studies of ferroelectric domain structures and dynamic behaviors under applied electric field or mechanical stress using in-situ TEM techniques. In particular, we want to obtain a fundamental understanding of the formation and switching mechanisms of charged domain walls and explore its potential for device applications. With access to the new TEM facilities available at UCI, we plan to image ferroelectric domain wall motion with atomic resolution in real-time. With the double-corrected JEOL Grand ARM at UCI, we will be able to map the polarization change around defects and at film surfaces, which will allow us to gain the insight into the polarization enhancement at the ferroelectric thin film surface and around charged defects.

We plan to further explore the effects of defects on the polarization configurations in ferroelectrics. One research topic we plan to work on is to study the effects of non-stoichiometric defects on the static polarization patterns by using our polarization mapping techniques based on atomic-scale STEM imaging. We plan to explore such interaction by studying samples with different defect configurations and employing phase-field or first principle simulations. The non-stoichiometric defects inserted into the ferroelectric matrix as nano-building-blocks can control local polarization configuration and domain structure, which can be useful for the development of novel ferroelectric-based nano-devices.

## References

[1] L. Z. Li, P. Gao, C. T. Nelson, J. R. Jokisaari, Y. Zhang, S. J. Kim, A. Melville, C. Adamo, D. G. Schlom, and X. Q. Pan, "Atomic Scale Structure Changes Induced by Charged Domain Walls", *Nano Letters* **13**, 5218-5223 (2013).

[2] L.Z. Li, J. Britson, J. R. Jokisaari, Y. Zhang, C. Adamo, A. Melville, D.G. Schlom, L.Q. Chen, and X.Q. Pan, "Giant Resistive Switching via Control of Ferroelectric Charged Domain Walls", Adv. Mater. **28**[31], 6574–6580 (2016). DOI: 10.1002/adma.201600160.

## Publications

1. Y. Zhang, L. Z. Li, L. Xie, P. Gao, J. R. Jokisaari, H. Li. Y. H. Chu, and X. Q. Pan, "Oxygen-vacancy engineered domain switching in ferroelectric-paraelectric multilayer system", in preparation.
2. L. Xie, L.Z. Li, P. Gao, C.T. Nelson, J.R. Jokisaari, C.A. Heikes, Z. Hong, X. Fei, E. Kioupakis, D.G. Schlom, L.-Q. Chen, P. Wang, and X.Q. Pan, "Surface induced giant ferroelectric polarization in ultrathin ferroelectric film," in preparation.
3. L.Z. Li, J. Britson, J. R. Jokisaari, Y. Zhang, C. Adamo, A. Melville, D.G. Schlom, L.Q. Chen, and X.Q. Pan, "Giant Resistive Switching via Control of Ferroelectric Charged Domain Walls", Adv. Mater. **28**[31], 6574–6580 (2016). DOI: 10.1002/adma.201600160.
4. L. Z. Li, J. Britson, P. Gao, J. R. Jokisaari, C. T. Nelson, C. Adamo, A. Melville, D. G. Schlom, L. Q. Chen, and X. Q. Pan, "Atomic-scale mechanisms of domain wall motion in ferroelectrics", under review at *Nature Physics*.
5. J. Britson, , P. Gaob, , X.Q. Panc, , and L.Q. Chen. Phase field simulation of charged interface formation during ferroelectric switching. *Acta Materialia* **112,** 285-294 (2016); doi:10.1016/j.actamat.2016.04.026
6. L. Z. Li, J. R. Jokisaari, and X. Q. Pan, "In situ electron microscopy of ferroelectric domains", *MRS Bulletin* 40[1], pp 53-61 (2015), DOI http://dx.doi.org/10.1557/mrs.2014.302
7. P. Gao, Y. Zhang, S. Y. Zhang, S. Lee, J. Weiss, J. R. Jokisaari, E. E. Hellstrom, D. C. Larbalestier, C. B. Eom, and X. Q. Pan, "Atomic and electronic structures of superconducting $BaFe_2As_2/SrTiO_3$ superlattices", *Phys. Rev.* B91, 104525 (2015). DOI:10.1103/PhysRevB.91.104525
8. K. Zhang, X. F. Du, M. B. Katz, B. H. Li, S. J. Kim, K. X. Song, G. W. Graham, and X. Q. Pan, "Creating high quality Ca:$TiO_2$-B ($CaTi_5O_{11}$) and $TiO_2$-B epitaxial thin films by pulsed laser deposition", *Chem. Commun.* DOI: 10.1039/c5cc01878a (2015).
9. J. Britson, C. T. Nelson, X. Pan, and L. Q. Chen "First-order morphological transition of ferroelastic domains in ferroelectric thin films." *Acta Mat*. 75. 188 (2014).
10. J. Seidel, M. Trassin, Y. Zhang, P. Maksymovych, T. Uhlig, P. Milde, D. Köhler, A. P Baddorf, S. V. Kalinin, L. M. Eng, X. Q. Pan, and R. Ramesh, "Electronic Properties of Isosymmetric Phase Boundaries in Highly Strained Ca-Doped $BiFeO_3$", *Advanced Materials,* DOI: 10.1002/adma.201400557 (2014).
11. P. Gao, J. Britson, C. T. Nelson, J. R. Jokisaari, C. Duan, M. Trassin, S. H. Baek, H. Guo, L. Li, Y. Wang, Y. H. Chu, A. M. Minor, C. B. Eom, R. Ramesh, L. Q. Chen, and X. Q. Pan, "Ferroelastic Domain Switching Dynamics under Electrical and Mechanical Excitations", *Nature Communications* **5**, 3801 (2014). DOI: 10.1038/ncomms4801**.**

## Physics of complex materials systems through theory and microscopy/EELS

Principal Investigator: Sokrates T. Pantelides
Department of Physics and Astronomy
and Department of Electrical Engineering and Computer Science
Vanderbilt University, Nashville, TN 37235

### Research Scope

The main objective is to combine density functional theory (DFT) with Z-contrast imaging and electron-energy-loss spectroscopy, obtained with scanning transmission electron microscopes (STEMs), or with other kinds of microscopy, such as scanning tunneling microscopy, to elucidate structure-property relations in complex materials structures and predict new functionalities. A key subtask has been the development of computer codes that combine DFT calculations of electron excitations in solids with dynamical scattering theory that tracks the STEM's finely focused electron beam as it undergoes diffraction in the sample, exits, and gets collected in the detector, including all interference effects. These simulations are aimed at the capabilities of aberration-corrected STEMs (AC-STEMs) and, more recently, monochromated AC-STEMs, which provide high-resolution two-dimensional maps of EELS spectral features, generated by collecting probe-position-dependent EELS, both core-loss and low-loss (this subtask is done in collaboration with Mark P. Oxley). We primarily collaborate with the STEM microscopists at Oak Ridge National Laboratory (ORNL).

Here we describe our recent progress in EELS maps and a few of the many case studies of combining theory and microscopy to investigate complex materials structures.

### Recent Progress

#### *1. Valence-electron-energy-loss-spectroscopy (VEELS) impurity signatures in graphene*

M. D. Kapetanakis, M. P. Oxley, W. Zhou, S. J. Pennycook, J.-C. Idrobo, and S. T. Pantelides, "Impurity signatures in atomic-resolution valence-electron-energy-loss spectroscopy – application to graphene", *Physical Review B* (under review).

At the prior two-year review, we reported simulations of VEELS maps of electronic excitations in pristine graphene together with experimental maps obtained by Wu Zhou, Juan Idrobo, *et al*. at ORNL. In the current period we extended the work to demonstrate that VEELS maps provide characteristic signatures of the two known distinct configurations of Si impurities in graphene (threefold- and fourfold-coordinated Si, occupying a single vacancy and divacancy, respectively). Figure 1 shows experimental and calculated VEELS spectra and VEELS maps. The agreement is excellent (the experimental maps are somewhat noisy). Figures 1e and 1f show the simulated VEELS maps for fourfold- and threefold-coordinated Si, demonstrating that such maps provide unique signatures for different impurity configurations. Detailed analysis of the maps provides information on the nature of the excitations. With the advent of new monochromators

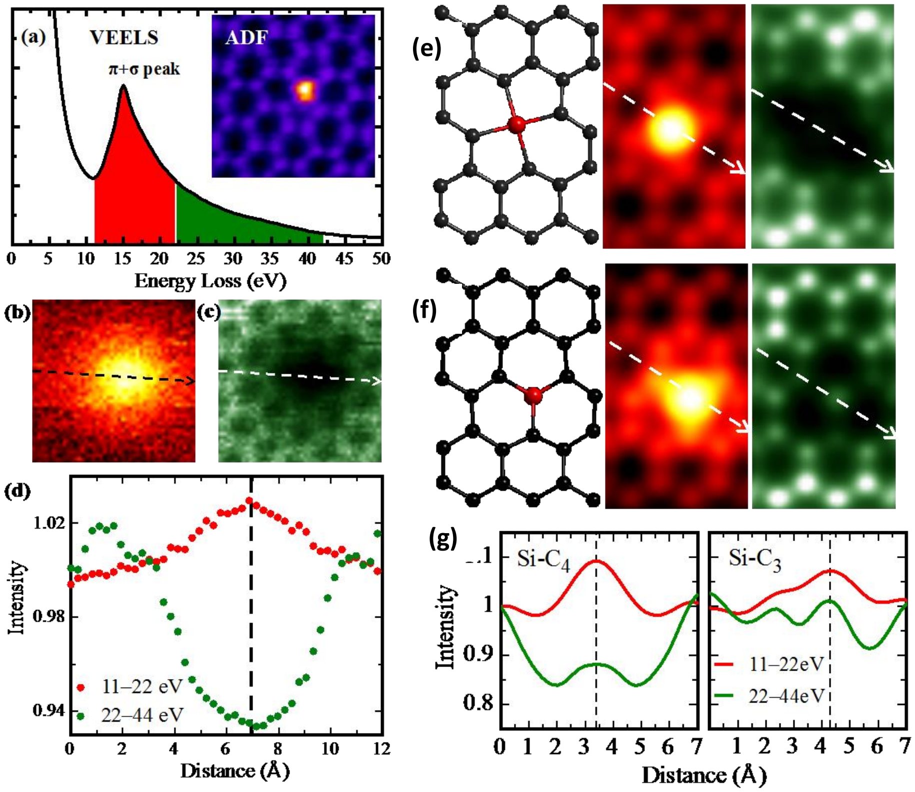

Fig. 2.1 Left panels: Experimental VEELS of a fourfold-coordinated Si impurity in graphene. (a) Average spectrum. Inset: Z-contrast image. (b) and (c) VEELS maps obtained by integrating the signal over the red and dark regions of the spectrum at each probe position. (d) Line profiles for the integrated images along the dashed lines in (b) and (c). Right panels: Calculated VEELS maps in the same energy regions for (e) fourfold-coordinated Si and (f) threefold-coordinated Si. (g) Line profiles along the dashed lines in the images in (e) and (f).

with high energy resolution and detectors with low signal-to-noise ratio, the present work ushers an atomically-resolved STEM-based spectroscopy of individual impurities as an alternative to conventional spectroscopies for probing impurities and defects, which obtain average signals from a large concentration of impurities and defects. Simulations of VEELS maps for impurities in bulk materials, in particular the so-called DX center in GaAs (substitutional Si impurities, which have two distinct configurations) are under way. Data are not currently available, but monochromated AC-STEMs promise the advent of such data in which case the method will provide a unique way to probe individual impurities in complex structures.

### 2. *Discovery of a new type of magnetoelectricity holds promise for novel device applications*

X. Shen, T. J. Pennycook, D. Hernandez-Martin, A. Perez, Y. S. Puzyrev, Y. Liu, S. G. E. te Velthuis, J. W. Freeland, P. Shafer, C. Zhu, M. Varela, C. Leon, Z. Sefrioui, J. Santamaria, and S. T. Pantelides, "High on/off ratio memristive switching of manganite/cuprate bilayer by interfacial magnetoelectricity", *Advanced Materials Interfaces* **2016**, 1600086 (May 27, 2016).

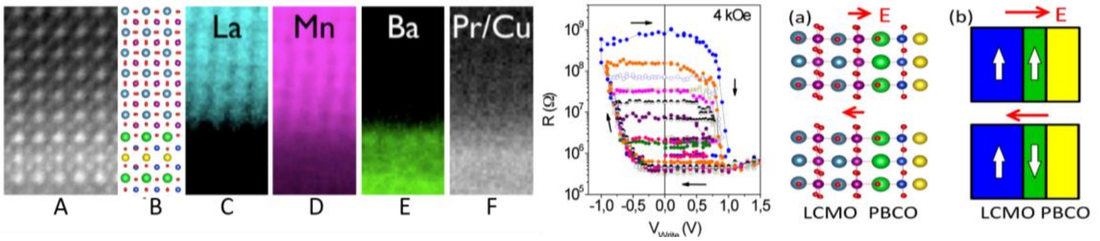

Fig. 2 Z-contrast image, atomic-scale schematic of the interface, and chemical maps of the constituent elements. Hysteresis loops in the resistance vs voltage and schematic diagrams of the switching mechanism based on switching on and off an interfacial magnetic dead layer by an external electric

Memristive materials exhibit high- and low-resistance states and are suitable for two-terminal memory devices. They are targeted to replace transistor-based memory devices and for use in neuromorphic computing. Typically, memristive switching is controlled by the motion of defects under electric fields. In this work we demonstrated memristive switching in a transition-metal heterojunction controlled by interfacial magnetoelectricity without defect motion (Fig. 2). $La_{0.7}Ca_{0.3}MnO_3/PrBa_2Cu_3O_7$ (LCMO/PBCO) junctions were fabricated and characterized by collaborators in Spain (Jacobo Santamaria's group). STEM Z-contrast images and EELS maps of the constituent elements were obtained by our former student Timothy Pennycook. Theory was carried out at Vanderbilt. The data show that switching does not occur above 180 K, which is roughly the Curie temperature of LCMO, suggesting that magnetic ordering is at the core of the mechanism. Combining DFT calculations and the data we proposed that the switching occurs when the external voltage induces tiny displacements of the interfacial Mn ions that are sufficient to induce or eliminate an interfacial magnetic dead layer. The conductive state occurs when the magnetic dead layer is eliminated, which enables polarized transport. When the magnetic dead layer is present, conductivity through the interface is impeded. We estimated the ON/OFF ratio to be 1000, in good agreement with the data and the fact that switching is a low-energy process. These characteristics are highly desirable for applications and may occur in other transition-metal-oxide interfaces.

### 3. ***Room-temperature, low-barrier boron doping of graphene***

L. Pan, Y. Que, H. Chen, D. Wang, J. Li, C. Shen, W. Xiao, S. Du, H. Gao, and S. T. Pantelides, "Room-temperature, low-barrier boron doping of graphene", *Nano Letters* **15**, 6464-6468 (September 8, 2015).

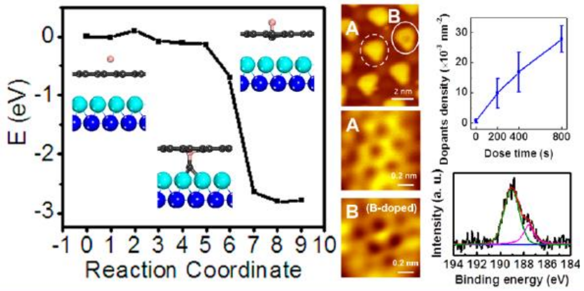

Fig. 3 Left: Calculated total energy of the system as a function of the boron position. The initial, an intermediate, and the final position are shown in the schematics. Middle: Scanning tunneling microscopy images; Site B is doped with a boron atom. Right: Concentration of doping B atoms scales with the dose of B on the surface; XPS peak corresponds to threefold-coordinated B.

The most desirable way to dope a material n-type or p-type is by substitutional impurities. For graphene, substitutional boron would yield a p-type material while substitutional nitrogen would yield an n-type material. Substitutional doping has been difficult, however, because of the strong C-C bonds. In this work we came up with a theoretical prediction that boron can be inserted substitutionally in graphene by a virtually athermal process when graphene is on a suitable substrate. The idea was motivated by our earlier calculations of the ability of atoms to penetrate a free-standing graphene lattice by pushing a carbon atom. We had found that a boron atom penetrates with a relatively small barrier (1.6 eV). We surmised that, when graphene is on a substrate, the barrier would be lower because the substrate might help pull the carbon atom. Indeed, DFT calculations found that a Ru (0001) substrate helps pull the carbon atom in an intercalated position with essentially zero barrier (Fig. 3). Additional calculations found that the intercalated C atom can migrate away with an energy barrier of only 0.8 eV. These results mean that the process should happen at room temperature. Indeed, our collaborators at the Institute of Physics of the Chinese Academy of Sciences in Beijing succeeded in obtained boron-doped graphene by simply exposing monolayer graphene on a Ru(0001) substrate to $B_2H_6$ at room temperature. STM images and XPS data, as well as verification that the number of dopant atoms increases linearly with the $B_2H_6$ dose, proved that B doping was indeed achieved (Fig. 3). In contrast, similar calculation for nitrogen found a significant barrier for the same process.

### Future Plans

The subtask of developing computer codes of EELS maps continues, as mentioned above, to cover impurities and defects in bulk materials. We are also exploring application of these codes to the detection of magnetic properties. We have work in progress in several complex materials structures for which experimental data are available in 2D materials, nanostructures, and transition-metal oxides. A new monochromated AC-STEM is expected to be installed in September 2016 at ORNL with an energy resolution of 10 meV or smaller. We anticipate new data from this microscope will enrich our portfolio for theoretical investigations.

### Publications in the last two years

1. R. Ishikawa, R. Mishra, A. R. Lupini, S. D. Findlay, T. Taniguchi, S. T. Pantelides, and S. J. Pennycook, “Direct observation of dopant atom diffusion in a bulk semiconductor crystal enhanced by a large size mismatch”, *Physical Review Letters* **113**, 155501 (October 6, 2014).

2. Y.-M. Kim, A. Morozovska, E. Eliseev, M. P. Oxley, R. Mishra, S. M. Selbach, T. Grande, S. T. Pantelides, S. V. Kalinin, and A. Y. Borisevich, "Direct observation of ferroelectric field effect and vacancy-controlled screening at the $BiFeO_3/La_xSr_{1-x}MnO_3$ interface", *Nature Materials* **13**, 1019-1025 (November 2014).
3. X. Shen, E. A. Hernandez-Pagan, W. Zhou, Y. S. Puzyrev, J.-C. Idrobo, J. E. Macdonald, S. J. Pennycook, and S. T. Pantelides, "Interlaced crystals having a perfect Bravais lattice and complex chemical order revealed by real-space crystallography", *Nature Communications* **5**, 5431 (November 2014).
4. J. J. Guo, J. Lee, C. I. Contescu, N. C. Gallego, S. T. Pantelides, S. J. Pennycook, B. A. Moyer, and M. F. Chisholm, "Crown ethers in graphene", *Nature Communications* **5**, 5389 (November 2014).
5. Y. Gong, J. Lin, X. Wang, G. Shi, S. Lei, Z. Lin, X. Zou, G. Ye, R. Vajtai, B. I. Yakobson, H. Terrones, M. Terrones, B. K. Tay, J. Lou, S. T. Pantelides, Z. Liu, W. Zhou, and P. M. Ajayan, "Vertical and in-plane heterostructures from $WS_2/MoS_2$ monolayers", *Nature Materials* **13**, 1135-1142 (December 2014).
6. J. Lin, S. T. Pantelides, and W. Zhou, "Vacancy-induced formation and growth of inversion domains in transition-metal dichalcogenide monolayer", *ACS Nano* **9**, 5189-5197 (May 2015).
7. X. Shen, K. Yin, Y. S. Puzyrev, Y. Liu, L. Sun, R.-W. Li, and S. T. Pantelides, "2D nanovaristors at grain boundaries account for memristive switching in polycrystalline $BiFeO_3$", *Advanced Electronic Materials* **1**, 1500019-1-6 (May 2015).
8. Y. Wang, L. Li, W. Yao, S. Song, J. T. Sun, J. Pan, X. Ren, C. Li, E. Okunishi, Y. Q. Wang, E. Wang, Y. Shao, Y. Y. Zhang, H. Yang, E. F. Schwier, J. Iwasawa, K. Shimada, M. Taniguchi, Z. Cheng, S. Zhou, S. Du, S. J. Pennycook, S. T. Pantelides, and H. Gao, "Monolayer $PtSe_2$, a new semiconducting transition-metal-dichalcogenide, epitaxially grown by direct selenization of Pt", *Nano Letters* **15**, 4013-4018 (May 21, 2015).
9. X. Lu, M. I. B. Utama, J. Lin, X. Luo, Y. Zhao, J. Zhang, S. T. Pantelides, W. Zhou, S. Y. Quek, and Q. Xiong, "Rapid and nondestructive identification of polytypism and stacking sequences in few-layer molybdenum diselenide by Raman spectroscopy", *Advanced Materials* **27**, 4502-4508 (July 2, 2015).
10. S. Yu, J. Hachtel, M. F. Chisholm, S. T. Pantelides, A. Laromaine, and A. Roig, "Magnetic gold nanotriangles by microwave-assisted polyol synthesis", *Nanoscale* **7**, 14039-14046 (July 21, 2015).
11. G. X. Duan, J. Hachtel, X. Shen, E. X. Zhang, C. X. Zhang, B. R. Tuttle, D. M. Fleetwood, R. D. Schrimpf, R. A. Reed, J. Franco, D. Linten, J. Mitard, L. Witters, N. Collaert, M. F. Chisholm, and S. T. Pantelides, "Activation energies for oxide- and interface-trap charge generation due to negative-bias temperature stress of Si-capped SiGe-pMOSFETs", *IEEE Transactions on Device and Materials* **15**, 352-358 (September

2015).

12. L. Pan, Y. Que, H. Chen, D. Wang, J. Li, C. Shen, W. Xiao, S. Du, H. Gao, and S. T. Pantelides, "Room-temperature, low-barrier boron doping of graphene", *Nano Letters* **15**, 6464-6468 (September 8, 2015).
13. S. J. Pennycook, W. Zhou, and S. T. Pantelides, "Watching atoms work: Nanocluster structure and dynamics", *ACS Nano* **9**, 9437-9440 (September 25, 2015).
14. M. D. Kapetanakis, W. Zhou, M. P. Oxley, J. Lee, M. P. Prange, S. J. Pennycook, J. C. Idrobo, and S. T. Pantelides, "Low-loss electron energy loss spectroscopy: An atomic-resolution complement to optical spectroscopies and application to graphene", *Physical Review B* **92**, 125147 (September 25, 2015).
15. R. J. T. Nicholl, H. J. Conley, N. V. Lavrik, I. Vlassiouk, Y. S. Puzyrev, V. P. Sreenivas, S. T. Pantelides, and K. I. Bolotin, "The effect of intrinsic crumpling on the mechanics of free-standing graphene", *Nature Communions* **6**, 8789 (November 6, 2015).
16. Q. Qiao, Y. Y. Zhang, R. Conteras-Guerrero, R. Droopad, S. T. Pantelides, S. J. Pennycook, S. Ogut, and R. F. Klie, "Direct observation of oxygen-vacancy-enhanced polarization in a SrTiO3-buffered ferroelectric $BaTiO_3$ film on GaAs", *Applied Physics Letters* **107**, 201604 (November 18, 2015).
17. Y. Y. Zhang, R. Mishra, T. J. Pennycook, A. Y. Borisevich, S. J. Pennycook, and S. T. Pantelides, "Oxygen disorder, a way to accommodate large epitaxial strains in oxides", *Advanced Materials Interfaces* **2**, 1500344 (December 14, 2015).
18. Y. S. Puzyrev, X. Shen, and S. T. Pantelides, "Prediction of giant thermoelectric efficiency in crystals with interlaced nanostructure", *Nano Letters* **16**, 121-125 (December 21, 2015).
19. W. Zhou, K. Yin, C. Wang, Y. Y. Zhang, T. Xu, A. Borisevich, L. Sun, J. C. Idrobo, M. F. Chisholm, S. T. Pantelides, R. F. Klie, and A. R. Lupini, "The observation of square ice in graphene questioned", *Nature* **528**, E1-E2 (December 24, 2015) [*No acknowledgement of funding was allowed in this paper*].
20. G. Ye, Y. Gong, J. Lin, B. Li, Y. He, S. T. Pantelides, W. Zhou, R. Vajtai, and P. M. Ajayan, "Defects engineered monolayer $MoS_2$ for improved hydrogen evolution reaction", *Nano Letters* **16**, 1097-1103 (January 13, 2016).
21. J. Lin, Y.Y. Zhang, W. Zhou, and S. T. Pantelides, "Structural flexibility and alloying in ultrathin transition-metal chalcogenide nanowires", *ACS Nano* **10**, 2782-2790 (January 18, 2016).
22. T. Kishida, M. D. Kapetanakis, J. Yan, B. C. Sales, S. T. Pantelides, S. J. Pennycook, and M. F. Chisholm, "Magnetic ordering in $Sr_3YCo_4O_{10+x}$", *Scientific Reports* **6**, 19762 (January 28, 2016).
23. Y. Gong, G. Ye, S. Lei, G. Shi, Y. He, J. Lin, X. Zhang, R. Vajtai, S. T. Pantelides, W. Zhou, B. Li, and P. M. Ajayan, "Synthesis of millimeter-scale transition metal

dichalcogenides single crystals“ *Advanced Functional Materials* **26**, 2009 (February 10, 2016).

24. J. Hachtel, S. Yu, A. R. Lupini, S. T. Pantelides, M. Gich, A. Laromaine, and A. Roig, “Gold nanotriangles decorated with superparamagnetic iron oxide nanoparticles: a compositional and microstructural study”, *Faraday Discussions* published online March 11, 2016.
25. J. Gazquez, R. Guzman, R. Mishra, E. Bartolome, J. Salafranca, C. Magen, M. Varela, M. Coll, A. Palau, S. Manuel Validares, P. Gargiani, E. Pellegrin, J. Herrero-Martin, S. J. Pennycook, S. T. Pantelides, T. Puig, and X. Obradors, “Emerging Diluted Ferromagnetism in High-$T_c$ Superconductors Driven by Point Defect Clusters”, *Advanced Science* **3**, 1500295 (March 15, 2016).
26. J. Hachtel, C. Marvinney, A. Mouti, D. May, R. Mu, S. J. Pennycook, A. R. Lupini, M. F. Chisholm, R. F. Haglund, and S. T. Pantelides, “Probing plasmons in three dimensions by combining complementary spectroscopies in a scanning transmission electron microscope”, *Nanotechnology* **27**, 155202 (April 15, 2016).
27. X. Li, M. W. Lin, J. Lin, B. Huang, A. A. Puretzky, C. Ma, K. Wang, W. Zhou, S. T. Pantelides, M. Chi, C. M. Rouleau, D. B. Geohegan, and K. Xiao, “Two-dimensional GaSe/MoSe$_2$ misfit bilayer heterojunctions by van der Waals epitaxy”, *Science Advances* 2, e1501882 (April 15, 2016).
28. J. Lin, S. T. Pantelides, and W. Zhou, “Vacancy-induced formation and growth of inversion domains in transition-metal dichalcogenide monolayer”, *ACS Nano* **9**, 5189-5197 (April 23, 2015).
29. X. Shen, T. J. Pennycook, D. Hernandez-Martin, A. Perez, Y. S. Puzyrev, Y. Liu, S. G. E. te Velthuis, J. W. Freeland, P. Shafer, C. Zhu, M. Varela, C. Leon, Z. Sefrioui, J. Santamaria, and S. T. Pantelides, “High on/off ratio memristive switching of manganite/cuprate bilayer by interfacial magnetoelectricity”, *Advanced Materials Interfaces* **2016**, 1600086 (May 27, 2016).
30. J. Chen, Y. Puzyrev, E. Zhang, D. Fleetwood, R. Schrimpf, A. Arehart, S. Ringel, S. Kaun, E. Kyle, J. Speck, P. Saunier, C. Lee, and S. T. Pantelides, “High-Field Stress, Low-Frequency Noise, and Long-term Reliability of AlGaN/GaN HEMTs”, *IEEE Transactions on Devices Materials* June 15, 2016 (early access).
31. W. Zheng, J. Lin, W. Feng, K. Xiao, Y. Qiu, S. T. Pantelides, W. Zhou, X. S. Chen, G. Liu, W. Cao, and P. A. Hu, “Patterned growth of p-type MoS$_2$ atomic layers using sol-gel as precursor”, *Advanced Functional Materials* (July 19, 2016).
32. R. Mishra, Y. Kim, Q. He, X. Huang, S. K. Kim, M. A. Susner, A. Bhattacharya, D. D. Fong, S. T. Pantelides, and A. Y. Borisevich, “Towards spin-polarized two-dimensional electron gas at a surface of an antiferromagnetic insulating oxide”, *Physical Review B* **94**, 045123 (July 18, 2016).

33. H. He, J. Lin, W. Fu, X. Wang, H. Wang, Q. Zeng, Q. Gu, Y.i Li, C. Yan, B. K. Tay, C. Xue, X. Hu, S. T. Pantelides, W. Zhou, and Z. Liu, “$MoS_2/TiO_2$ edge-on heterostructure for efficient photocatalytic hydrogen evolution” *Advanced Energy Materials* 1600464 (2016).
34. F. Liu, L. You, K. L. Seyler, J. Wang, P. Yu, J. Lin, X. Wang, J. Zhou, H. Wang, H. He, S. T. Pantelides, W. Zhou, X. Xu, P. M. Ajayan, and Z. Liu, “Room-temperature ferroelectricity in atomically thin $CuInP_2S_6$” *Nature Communications* (in press).
35. G.X. Duan, J.A. Hachtel, E.X. Zhang, C.X. Zhang, D.M. Fleetwood, R.A. Reed, D. Linten, J. Mitard, M.F. Chisholm, S.T. Pantelides. Effects of negative-bias-temperature-instability on low-frequency noise in SiGe *p*MOSFETs. *IEEE Transactions on Device and Materials Reliability* (in press).

**Under review**

36. J. A. Santana, R. Mishra, J. T. Krogel, A. Y. Borisevich, P. R. C. Kent, S. T. Pantelides, and F. A. Reboredo, “Quantum Monte Carlo comes of age: Unraveling the role of site-specific oxygen vacancies in a transition-metal-oxide superlattice”, *Physical Review Letters* (under review).
37. M. D. Kapetanakis, M. P. Oxley, W. Zhou, S. J. Pennycook, J.-C. Idrobo, and S. T. Pantelides, “Impurity signatures in atomic-resolution valence-electron-energy-loss spectroscopy – application to graphene”, *Physical Review B* (under review).
38. J. Zhou, F. Liu, J. Lin, X. Huang, J. Xia, B. Zhang, Q. Zeng, H. Wang, C. Zhu, L. Niu, X. Wang, W. Fu, P. Yu, T. Chang, C. Hsu, D. Wu, H. Jeng, Y. Huang, H. Lin, Z. Shen, C. Yang, L. Lu, K. Suenaga, W. Shou, S. T. Pantelides, G. Liu, and Z. Liu, “Large-area and high-quality 2D transition metal ditelluride”, *Advanced Materials* (under review).
39. L. Huang, Y. F. Zhang, Y. Y. Zhang, W. Xu, Y. Que, E. Li, J. Pan, Y. Wang, Y. Liu, S. Du, S. T. Pantelides, and H.-J. Gao, “Sequence of silicon monolayer structures grown on a Ru surface: from a herringbone structure to silicene” *Nature Communications* (under review).
40. H. D. Yoo, Y Li, J. Lin, X. Qian, Q. Ru, Y. Jing, Q. An, Y. Liang, S. T. Pantelides, W. Zhou, and Y. Yao, “In-situ electrochemical activation of two-dimensional materials for high performance rechargeable magnesium batteries”, *Nature Communications* (under review).
41. E.-X. Zhang, D. M. Fleetwood, J. Hachtel, C. Liang, R. A. Reed, M. L. Alles, R. D. Schrimpf, D. Linten, J. Mitard, M. F. Chisholm, and S. T. Pantelides, “Total ionizing dose effects on strained Ge pMOS FinFETs on bulk Si”, *IEEE Transactions on Nuclear Science* (under review).
42. C. Li, Y. Zhang, T. J. Pennycook, Y. Wu, A. R. Lupini, N. Paudel, S. T. Pantelides, Y. Yan, and S. J. Pennycook, “Column-by-column observation of dislocation motion in CdTe: dynamic scanning transmission electron microscopy”, *Applied Physics Letters* (under review).

## Emerging Functionality in Transition-Metal Compounds Driven by Spatial Confinement

### Ward Plummer, Department of Physics and Astronomy, Louisiana State University

**Research Scope:** The exotic properties displayed by correlated electronic materials (CEMs) such as the cuprates, manganites, ruthenates, Fe-based penictides, and heavy-fermion compounds are intimately related to the coexistence of competing nearly degenerate states which couple simultaneously active degrees of freedom—charge, lattice, orbital, and spin states. This project focuses on the exploration of novel behavior in heterojunctions and superlattices induced by spatial confinement, broken symmetry, strain, and chemical or physical modification of the surface or interface. The members of our team are shown in Fig. 1. Thin films will be grown and characterized *in situ* in an ultra-high vacuum environment at LSU, using a combination of techniques, such as STM and STS, LEED, XPS, ARPES, and HREELS. Hangwen Guo is a postdoctoral fellow, Lina Chen (just graduated) and Mohammad Saghayezhian are graduate students, and Weimei Xie is a visiting student from Nanjing University. High resolution scanning transmission electron microscopy, and spectroscopy are done in collaboration with Yimei Zhu and Jing Tao at BNL, Zhen Wang is a postdoctoral fellow at LSU but stationed at BNL. X-ray diffraction and electrical and magnetic transport measurements will be conducted *ex situ* at LSU or UTK. New nanofabrication capabilities at the Center for Nanophase Materials Sciences at ORNL will be utilized to push the size of spatial confinement into the nanometer range. The electronic and magnetic properties can be tuned in these spatially confined films by depositing electronic donors or acceptors or by patterning of magnetic nano-clusters. Zac Ward (ORNL) and Phillip Rack (UTK) lead the program in Tennessee. Tony Wong was supported by this project but received a prestigious Chancellors fellowship, so Michael Stafford is now supported by our grant.

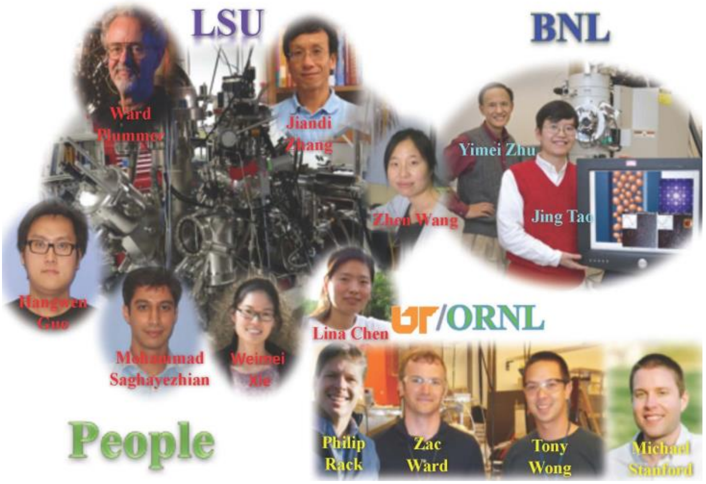

**Fig. 1:** People involved in the project.

### Recent Progress:

Totally unexpected quantum phases appear at interfaces of transition metal compounds, including two dimensional electron gases and superconductivity, or high-temperature superconductivity with $T_C$ around 77 K at the interface between a single layer (FeSe) of an iron-based low-temperature superconductor and an insulator ($SrTiO_3$). Additional richness is added by the fabrication of periodic arrays of heterojunctions in superlattices of two materials, as shown in Figure 2 (a). Not only are there interfacial phases, but the interfaces can couple, and there are new properties arising from the dimensional confinement of materials A and B. Using prototype $La_{2/3}Sr_{1/3}MnO_3$ (LSMO)/$BaTiO_3$ (BTO) magnetoelectric superlattices, we provide direct evidences of structural evolution in LSMO under reduced dimensionality via interfacial coupling with BTO. In this experiment the thickness of the BTO was fixed at 21 u.c. and the

LSMO thickness ranged from 32 to 2 u.c. Fig. 2(b) shows the HADDF-STEM image and the EELS elemental profile for a 4 u.c. LSMO film. There is very little intermixing at the interface, indicating our high quality growth control. Fig. 2(c) shows the inverse ABF-STEM image of a 4 u.c. LSMO layer on the left and a 32 u.c. layer on the right. These images clearly show thickness dependence in the LSMO structure. For a thick film you see the bulk tilt or rotation of the $MnO_6$ octahedra, while a thin film (4 u.c.) shows a polar distortion. This polar distortion in the LSMO drives a reemergence of ferromagnetism as seen in bottom center panel. The dashed line represents the common decrease in magnetism as a film becomes thin. This observation suggests that one can grow a robust ultrathin ferroelectric film with ferromagnetic order: a phase that rarely exists in nature.

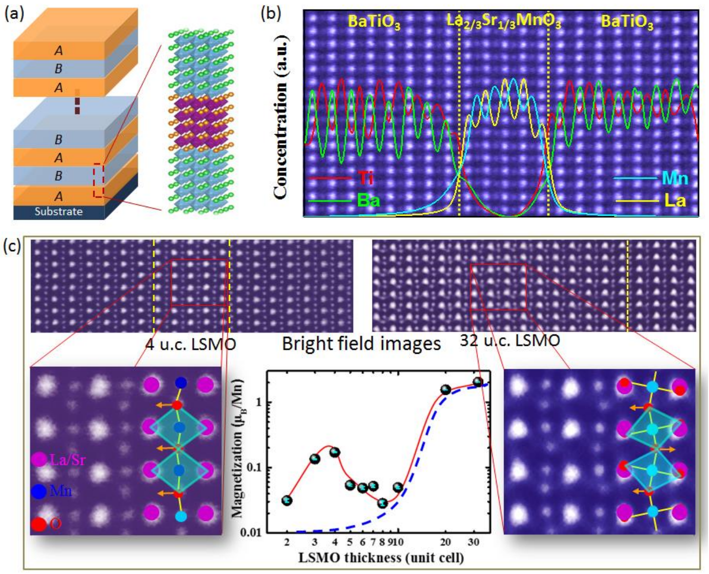

**Fig. 2:** (a) schematic drawing of superlattice. (b) HADDF-STEM image and EELS chemical identification for 4 u.c. LSMO. (c) ABF-STEM image and structure determination for 4 u.c. (left) and 32 u.c. (right) LSMO. Inset is the magnetization as a function of LSMO thickness.

When one grows films using a doped compound such as $La_{1-x}Sr_xMnO_3$ there is always the possibility that one of the components preferentially segregates to the interface or surface. If this happens the physical properties at the surface or interface could be significantly different from these in the bulk or the center of the film. We have carefully explored the segregation in $La_{2/3}Sr_{1/3}MnO_3$ films grown on (001) STO as a function of the film thickness. What one would expect from size arguments is that the Sr should segregate. The interface concentration was determined using electron microscopy and ELS as shown in Fig. 3(b). This technique can't be used for the free surface so we have used angle-dependent XPS measurements (Fig. 3(a)) to determine the chemical compositing near the surface. The short mean free path of the escaping electron means that large

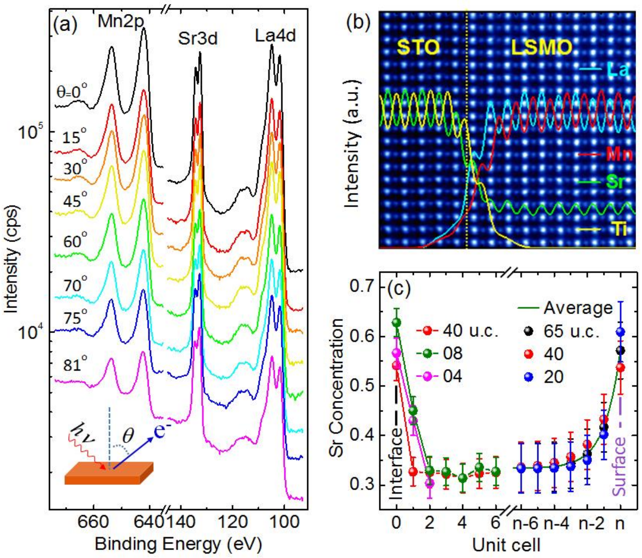

**Fig. 3:** ARXPS data for ARXPS spectra of a 65 u.c. LSMO film. (b) ) HADDF-STEM image and EELs chemical identification for 32 u.c. LSMO (c) Layer-by-layer dependence of Sr concentration of LSMO films near (*left*) the interface determined by STEM/EELS and (*right*) the surface determined by ARXPS.

angles of collection are more surface sensitive. The data in Fig. 3(a), when analyzed shows that the free surface in terminate with a SrO layer and that there is an enhancement is the Sr concentration at the surface. Fig. 3(c) shows the measured Sr concentration at the interface (0) and at the free surface (right) for many different film thicknesses. The Sr concentration at both the interface and surface is almost double that in the center of the film. In the bulk this concentration of Sr forms a charge ordered insulator. The segregation of Sr to the surface and interface could be the origin of the “dead” layers of LSMO.

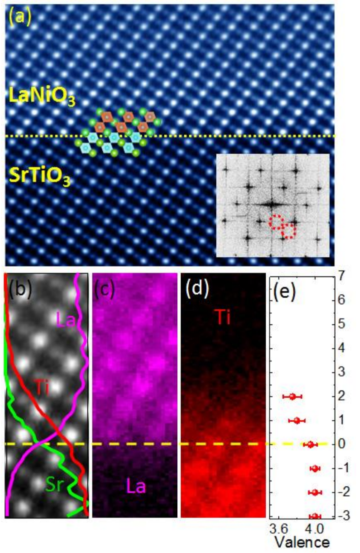

**Fig. 4:** (a-b) HADDF-STEM image and EELS elemental profiles of the LNO/STO(111) interface with the inset from ABF-STEM image showing no fractional order spots (red circles). EELS spectroscopic images of (c) La and (d) Ti near the interface and (e) the atomic layer-dependence of Ti valence.

The segregation profile at the surface is more gradual than at the interface, indicating that the chemical driving force for segregation is different. But it is surprising that the Sr concentration at the interface seems to be the same as at the surface. This study was the thesis project of Lina Chen.

The common STO substrate for growth is the (001) termination. The alternating planes are composed of $TiO_2$ or SrO, with our substrates terminated by $TiO_2$. For a STO(111) substrate the layer spacing $d_{111}$ =0.6$d_{100}$ with the alternate planes being Ti and $SrO_3$ creating a polar stacking sequence. In addition to polarity of (111) direction, the smaller layer spacing in this direction, makes it harder to avoid atomic inter-diffusion. To understand how to control the polarity at the interface, we investigated the processing of $SrTiO_3$ (111), finding that there is a narrow temperature window where the surface termination is Ti without any surface reconstruction (Phys. Rev. B **93** 125408). Our ability to control the polarity at the surface of $SrTiO_3$ (111) enabled us to grow $LaNiO_3/SrTiO_3$ (111) (LNO/STO (111)) with sharp interface as seen in the STEM image in Fig. 4(a). Previous reports indicate that LNO grows in the $La_2Ni_2O_5$ structure. The inset is the Fourier transform of the ABF-STEM image showing the fractional order spots associated with $La_2Ni_2O_5$ are missing.

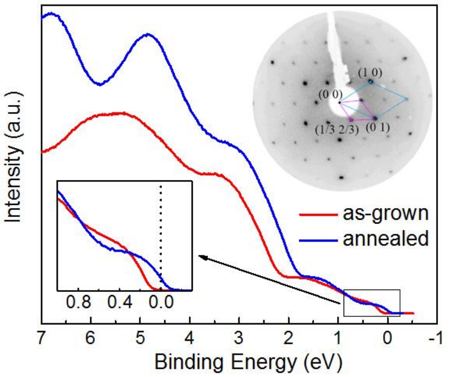

**Fig. 5:** Photoemission spectra of 8 uc SRO film on STO(111) with reconstructed (as-grown) and unreconstructed (annealed) surface, with photon energy of 21.2 eV. The inset is the zoom-in spectra near $E_F$ and the LEED image of the reconstructed surface.

It is worth noticing that the inter-diffusion of Ti into LNO film (Fig. 4 (b) and (d)) is about 2.5 unit cells (uc) which is about 5.5 Å which translates to 1.5 uc in (001) direction. Analysis of the Ti EELS data shows that the Ti valence which is +4 in STO drops to ~3.8 for the Ti in the LNO. At all thicknesses the surface maintains 1x1 structure. EELS elemental analysis shows that the polar mismatch is screened by electrons from oxygen vacancies.

Compared with LNO, $SrRuO_3$ (SRO) has smaller lattice mismatch with STO. Interestingly, the surface exhibits a $(\sqrt{3}\times\sqrt{3})R30^\circ$ reconstruction, regardless of the film thickness (see **Fig. 5**). This surface reconstruction can be removed by annealing in oxygen. Such reconstruction cannot be understood as the consequence of orthorhombic structure existing in the bulk SRO. The reconstruction likely originates from ordered oxygen vacancies. As should have been expected the valence UPS spectra changes dramatically as the reconstructed is removed. The inset shows the UPS spectra near the Fermi energy. The reconstructed surface is a semiconductor but the unreconstructed surface is a metal like the bulk.

Jian Shen was a co-PI on the original proposal funded by DOE when he was at ORNL. We have maintained collaboration after he moved to Fudan University. We have studied the manifestation of dimensional confinement of the electronic and magnetic properties of thin films of $La_{0.325}Pr_{0.3}Ca_{0.375}MnO_3$ (LPCMO) which in the bulk displays colossal magnetoresistance behavior due to electron phase separation (EPS). In the most recent study published in PNAS we looked at EPS as a function of the size of the LPCMO dot. The results illustrated in **Fig. 6** show that when the size is < ~700 nm, which is smaller than the characteristic length scale for EPS in the bulk the ground state is a single phase. The ground state of bulk LPCMO shows EPS.

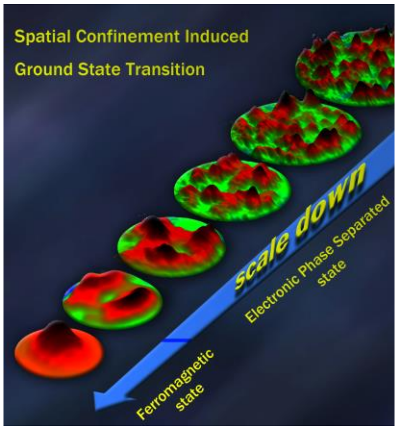

**Fig. 6:** MFM images of EPS in LPCMO nanodots. Red is the FM regions.

## Future Plans

- **Explore magnetic and magnetoelectric properties of superlattices with interface coupling.** We intend to focus on projects like described in Fig. 2, tuning the properties of superlattices to enhance magnetic response and to use electric field to control the magnetic properties through interfacial coupling. We are going to begin working on magnetic properties in superlattices with neutron scattering and X-ray magnetic circular dichroism techniques, correlated to structural properties determined by STEM.
- **Coupling of substrate and film properties.** We have done a lot of work on the electronic properties of thin films of LSMO on (001) STO. There is a critical thickness of the LSMO where the film undergoes a metal to insulator transition. We plan to explore the strain coupling to these films what the substrate STO goes through a structural transition at 105 K.
- **Explore the lattice and charge dynamics in heterojunctions and superlattices:** We are establishing collaboration with Dr. Jimin Zhao (IOP, China) and Professor Louis Haber (LSU) to use ultra-fast nonlinear optics to probe buried interfaces in heterostructures and superlattices.
- **Development of STEM for interface and thin film studies:** A technical development in our future plane is, through the close collaboration with BNL, to combine intra-unit-cell convergent-beam electron diffraction (CBED) and scanning technique to determine the structure symmetry at the interface and in the film. CBED is a technique with high sensitivity on the crystal symmetry, strain and charge density. We propose to image the quantitative results including the strain and charge density from CBED in real space. Together with the EEL spectrum imaging, we believe that such technical development will provide great insight into the physics at interfaces and in film materials.

## Publications: Primary Acknowledgement

- "*Designing Novel Superlattices via Coupled Interfaces*," Hangwen Guo, Zhen Wang, Shuai Dong, Mohammad Saghayezhian, Lina Chen, Yakui Weng, Rongyin Jin, Yimei Zhu, Jiandi Zhang & E.W. Plummer, *Submitted*
- "*Anomalously Deep Polarization in $SrTiO_3(001)$ Interfaced with an Epitaxial Ultrathin Manganite Film*," Zhen Wang, Jing Tao, Liping Yu, Hangwen Guo, Lina Chen, Myung-Geun Han, Lijun Wu, Huolin Xin, Kim Kisslinger, E. W. Plummer, Jiandi Zhang, and Yimei Zhu, *Phys. Rev.*
- "*Focused helium-ion beam irradiation effects on electrical transport properties of few-layer $WSe_2$: enabling nanoscale direct write homo-junctions,"* Michael G. Stanford, Pushpa Raj Pudasaini, Alex Belianinov, Nicholas, Cross, Joo-Hyon Noh, Michael R. Koehler, David G. Mandrus, Gerd Duscher, Adam J. Rondinone, Ilia N. Ivonov, T. Zac Ward, and Philip D. Rack, *Scientific Reports* **6**, 27276 (2016).
- "*Polar compensation at the surface of $SrTiO_3$ (111)*," M. Saghayezhian, Lina Chen, Gaomin Wang, Hangwen Guo, E.W. Plummer, and Jiandi Zhang, Phys. Rev B **93**, 125408 (2016).
- "*Epitaxial Growth of Complex Metal Oxides"*, Hangwen Guo and Jiandi Zhang, "Scanning tunneling microscopy of epitaxial oxide films" Book Chapter (Chap. 11), eds. Gertjan Koster and Guus Rijnders, Woodhead Publishing Series in Electronic and Optical Materials 2015.
- "*Origin of the Metal-Insulator Transition in Ultrathin Films of $La_{2/3}Sr_{1/3}MnO_3$*", Zhaoliang Liao, Fengmiao Li, Peng Gao, Jiandong Guo, Xiaoqing Pan, E. W. Plummer and Jiandi Zhang, Phys. Rev. B **92**, 125123 (2015).

### Secondary Acknowledgement

- "*$\delta$-Doping of Oxygen Vacancies in Epitaxial Oxide Films Dictated by Thermodynamics,*" Fengmiao Li, Shanming Li, Zhenzhong Yang, Yan Liang, Qinghua Zhang, Fang Yang, Wentao Li, Xuetao Zhu, Lin Gu, Jiandi Zhang, E. W. Plummer, and Jiandong Guo, submitted.
- "*The Role of $SrTiO_3$ Phonon Penetrating into FeSe Films in the Interfacial Superconductivity Enhancement*," Shuyuan Zhang, Jiaqi Guan, Xun Jia, Bing Liu, Weihua Wang, Fangsen Li, Lili Wang, Xucun Ma, Qikun Xue, Jiandi Zhang, E. W. Plummer, Xuetao Zhu, and Jiandong Guo, *Phys. Rev. B.*
- "Emerging single phase state in small manganite nanodisks," Jian Shao, Hao Liu, Kai Zhang, Yang Yu, Weichao Yu, Hanxuan Lana, Jiebin Niu, Kai Du, Yunfang Kour, Wengang Wei, Fanli Lan, Yinyan Zhu, Wenbin Wang, Jiang Xiao, Lifeng Yin, E. W. Plummer, Jian Shen, accepted *PNAS*
- "*Giant Magneto-Optical Raman Effect in a Layered Transition Metal Compound*," Jianting Ji, Anmin Zhang, Jiahe Fan, Yuesheng Li, Xiaoqun Wang, Jiandi Zhang, E. W. Plummer, and Qingming Zhang, "*Giant Magneto-Optical Raman Effect in a Layered Transition Metal Compound*," PNAS, **113**, 2349 (2016).
- *"Ionic Liquid Activation of Amorphous Metal-Oxide Semiconductors for Flexible Transparent Electronic Devices,"* Pushpa Raj Pudasaini , Joo Hyon Noh , Anthony T. Wong , Olga S. Ovchinnikova , Amanda V. Haglund , Sheng Dai , Thomas Zac Ward , David Mandrus , and Philip D. Rack, *Adv. Funct. Mater,* **26**, 2820 (2016).

- "*Multimodal Responses of Self-Organized Circuitry in Electronically Phase Separated Materials,"* Andreas Herklotz, Hangwen Guo, Anthony T. Wong, Ho Nyung Lee, Philip D. Rack, and Thomas Z. Ward, *Adv. Electron. Mater.* **2,** 1600189 (2016).
- "*Cr-doped $TiSe_2$ – a layered dichalcogenide spin glass*," H. Luo, Jason W. Krizan, E. M. Seibel, W. Xie, G. S. Sahasrabudhe, B. F. Phelan, J. Tao, Z. Wang, Jiandi Zhang, and R. J. Cava, Chem. Materials **27**, 6810 (2015).
- *"Controlling a reversible, single axis lattice expansion in complex oxide thin films via helium implantation*," H. Guo, S. Dong, P.D Rack, J. Budai, C. Beekman, Z.Gai, W. Siemons, C.M. Gonzalez, R. Timilsina, A.T. Wong, P. Snijders, E. Degotto, T.Z. Ward, *Phys. Rev. Lett.* **114**, 25 256801 (2015).
- *"Ferromagnetism and nonmetallic transport of a stabilized metastable material: $\alpha$-FeSi2 thin film"*, Guixin Cao, D. J. Singh, Xiaoguang Zhang, German Samolyuk, Liang Qiao, Chad Parish, Ke Jin, Yanwen Zhang, Hangwen Guo, Siwei Tang, Wenbin Wang, Jieyu Yi, Claudia Cantoni, Wolter Siemons, E. Andrew Payzant, Michael Biegalski, T. Z. Ward, David Mandrus, G.M. Stocks and Zheng Gai, *Phys. Rev. Lett.* **114**, 147202 (2015).

## Nano-imaging and -spectroscopy of complex and correlated materials

**Markus B. Raschke, Department of Physics, and JILA, University of Colorado, Boulder**

**Program Scope:** The combination of optical spectroscopy with scanning probe microscopy has emerged as a new frontier of optical ultra-microscopy providing few nanometer spatial resolution. We have generalized this approach of *scattering scanning near-field optical microscopy* (*s*-SNOM) to *any optical modality* including linear (mid-IR to vis), inelastic (Raman), nonlinear (SHG, F4M), and ultrafast nano-spectroscopy [AP12], and extended it to variable and cryogenic temperatures [RSI13]. On that basis we continue to demonstrate unique application potential for probing nanoscale behavior in correlated, complex, and 2D materials. We pursue the multi-modal and multi-spectral nano-imaging of electronic and vibrational (including Drude and polaritonic) resonances, structural symmetry, and ultrafast dynamics to gain insight into properties, mechanisms, and functions of complex materials.

**Recent Progress:** In our project we pursue method development, demonstration and application of *s*-SNOM in our lab, as well as in collaboration with EMSL/PNNL and ALS/LBL to disseminate the technique making it available as user facilities. In addition to the application to problems in complex materials our work ties into new fundamental questions of optical physics that enables, e.g., the combination of *s*-SNOM with femtosecond spectroscopy to access ultrafast dynamics, or taking advantage of the enhanced electromagnetic density of states of the thermal near-field or the coherence of mid-IR synchrotron radiation, for broadband spectroscopy within the only nanoscale sample volumes inherent with the increase in spatial resolution. Specific examples of our work over the past 2 years include:

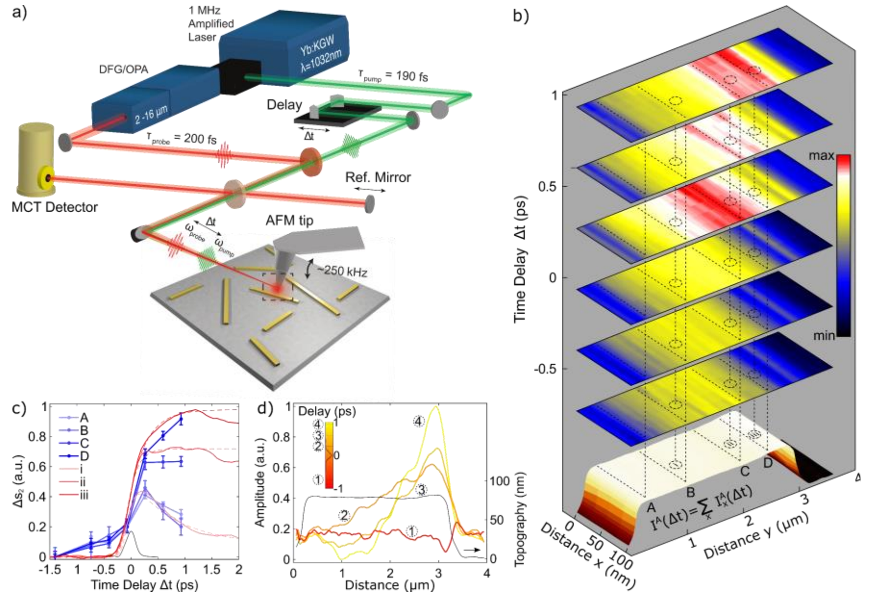

Figure 1. (a) Near-field femtosecond pump-probe nano-imaging of the photoinduced insulator-to-metal transition dynamics in $VO_2$. Femtosecond-nanometer spatial and temporal variations in IMT dynamics of a single $VO_2$ micro-crystal (b). Spatially varying photoinduced IMT dynamics (c). Averaged line profiles across the images in b) (d).

*Inhomogeneity in the ultrafast insulator-to-metal transition dynamics of $VO_2$:* Vanadium dioxide ($VO_2$) is a prototypical correlated electron material (CEM), exhibiting an insulator-to-metal phase transition (IMT) with concurrent structural and electronic transitions. Despite extensive research the coupling between the structural and electronic degrees of freedom is yet to be fully understood. In our previous work we both studied the thermally induced IMT in $VO_2$ micro-crystals on the nanoscale, and discovered heterogeneities of the photoinduced ultrafast transition dynamics on the microscale

[NC15]. We extend this work by combining the two approaches to perform spatio-temporal nanoimaging of the photoinduced IMT dynamics in $VO_2$ single micro-crystals. As shown in Fig. 1 with our far from equilibrium laser excitation, we discover the presence of three different dynamical regimes on the same micro-crystal within just a few 100 nm spatial separation. The observed nano-pump-probe characteristics indicate a high degree of spatial inhomogeneity in the transition dynamics. The results of the transient spatial inhomogeneities in the electronic structure are caused by slight variations in the oxygen or vanadium concentration and associated defects during the growth process. This study highlights the importance and difficulties in accessing the intrinsic material properties of $VO_2$ or CEMs in general. The combination of *s*-SNOM with pump-probe spectroscopy with high fluence excitation opens a new regime of spatiotemporal nano-imaging of dynamic processes in complex matter [NL16-2].

*Hybrid tip-enhanced nano-spectroscopy and -imaging of monolayer $WSe_2$ with local strain control:* Opto-electronic properties of monolayer (ML) transition metal dichalcogenides (TMDs) are highly inhomogeneous and sensitive to nanoscale defects associated with grain boundaries and edges. In this study, we demonstrate and apply a new hybrid nano-optomechanical tip-enhanced spectroscopy and imaging approach combining nano-Raman (tip-enhanced Raman scattering, TERS), nano-PL (tip-enhanced photoluminescence, TEPL), and atomic force local strain control to investigate the correlation of local structural heterogeneities with nanoscale optical properties of ML $WSe_2$ (Fig. 2a). We developed a novel tilted tip approach, where the resulting localized surface plasmon excitation in the axial direction of the tip leads to effective excitation of the in-plane Raman and exciton modes as characteristic for layered 2D materials with ~15 nm spatial resolution (Fig. 2b).

We study the excited state PL response in twinned $WSe_2$ ML physical vapor deposition (PVD) grown microcrystals. A combination of PL quenching and selective spectral changes at nanoscale defects is resolved on tens of nanometers length scales. Specifically, local PL quenching and a spectral blueshift are observed at crystal edges and nucleation sites (NS). On the

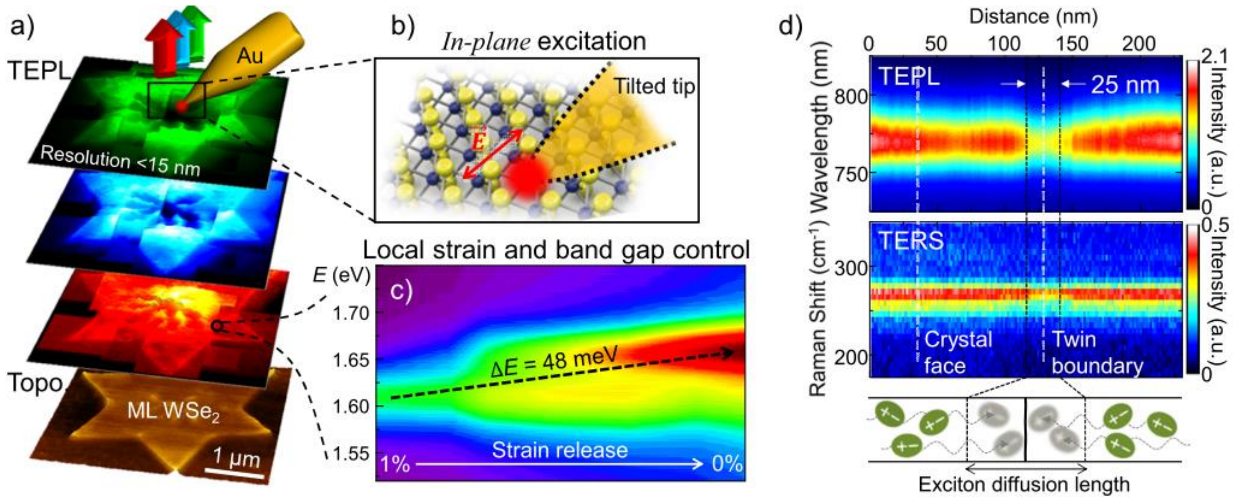

Figure 2: a) 15 nm spatial resolution multispectral TEPL images of a ML $WSe_2$ crystal and corresponding AFM topography. b) Illustration of a novel tilted tip approach for efficient excitation and detection of Raman and exciton modes of 2D materials. c) Evolution of TEPL spectra of the as-grown ML $WSe_2$ with increasing compressive force induced by the tip, giving rise to an irreversible release of the tensile strain of the crystal. d) Spectral TEPL and TERS trace across twin boundary (TB) and illustration of exciton diffusion length at TB.

other hand, only PL quenching is observed without change in energy at twin boundaries (TBs) over ~30 nm length scales correlated with exciton diffusion into nonradiative recombination centers (Fig. 2d). In addition to the nano-spectroscopy and -imaging, we can control local strain and bandgap of TMDs via nano-mechanical tip force interaction that gives rise to both reversible and irreversible strain release and bandgap shifts (Fig. 2c).

The combined results clarify many of the apparent inconsistencies of earlier studies, i.e., these results allow for the separation of the effect of strain from controlling the PL modification at edges, NS, and TBs and suggest defects and stoichiometry as the primary factors modifying the PL at the structural heterogeneities but in distinctly different ways [NL16-1].

*Broadband infrared near-field nano-spectroscopy* For IR vibrational, phonon, and low-energy electronic excitation spectroscopy and imaging using IR *s*-SNOM many bottlenecks persist in terms of available IR sources. Lasers provide high spectral irradiance, although over limited bandwidths. Synchrotrons provide lower irradiance, although over much larger bandwidth.

In order to improve the ultimate sensitivity of synchrotron IR near-field nano-spectroscopy (SINS) as developed by our group previously [PNAS14], using a symmetric Michelson configuration, we demonstrate a type of self-homodyne interferometry capable of registering molecular and phonon resonances, with sensitivity to the spectral phase, and significantly enhanced signal-to-noise [NL16]. Further, we explore new optimized detector parameters for extending the spectral range of SINS down to far-infrared wavelengths (Fig 3a), opening up a new realm of accessible electronic phenomena in condensed matter physics. Combining laser *s*-SNOM and SINS and selective probing of in- and out-of plane vibrational modes we were able to for the first time demonstrate IR vibrational nano-crystallography [SA16].

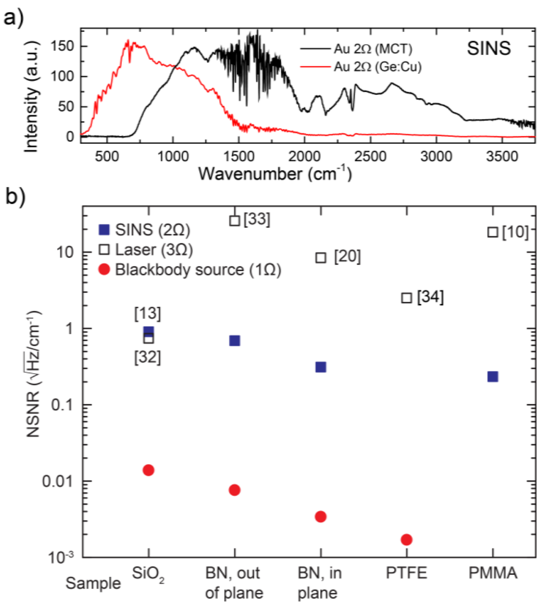

Figure 3: a) Extension of synchrotron infrared near-field spectroscopy (SINS) into the far-IR spectral region. b) Comparison of broadband coherent and incoherent IR sources for IR *s*-SNOM.

Blackbody sources, routinely used in commercial FTIR systems, provide a table-top source for broadband IR spectroscopy at low cost, however with unfavorably low irradiance. We extend the application range of broadband nano-spectroscopy using blackbody radiation and provide a signal-to-noise analysis and comparison across a range of samples and sources as a benchmark for irradiance and noise requirements for sources for broadband *s*-SNOM (Fig. 3b) [OE15].

Lastly, we investigate the possibility of broadband near-field IR nano-spectroscopy without the use of an external light source at all, instead generating the near-fields locally by laser heating of the AFM tip or sample itself to study thermally excited vibrational modes. Using laser irradiation for photothermal heating of tips allowed us to reach high temperatures with off-the-shelf tips, where we observe TINS spectra of PTFE, hBN, and SiC [APL16].

**Future Plans:** We will continue our nano-optical investigations of correlated and complex materials with an emphasis on new materials with emergent properties:

*Near-field pump-probe:* Building on our recent near-field pump-probe results on $VO_2$ [NL16-2] we plan to extend to phase resolved broadband ultrafast near-field pump-probe *s*-SNOM to be applied to $VO_2$ metamaterials with specifically designed antenna patterns, as well other CEM and superlattice materials. This will allow us to investigate the heterogeneity of the phase transition dynamics and discern potential ways of accessing the true intrinsic response of strongly correlated electron materials.

*Transition metal dichalcogenides* We will extend our hybrid TERS/TEPL experiments to the broader range of ML TMDs to investigate nanoscale heterogeneities of multi-excitons, interlayer excitons and Raman modes of TMD heterostructures, and exciton diffusion in *in-plane* heterostructures. We have begun to study novel phase change phenomena in $MoTe_2$, which undergoes a semiconductor-to-semimetal transition that can be induced both with strain and laser irradiation.

*Nonlinear and ultrafast graphene dynamics* The interband excitation of carriers in graphene directly influences its electrical and optical properties, affecting potential applications in photovoltaic devices and saturable absorbers. Plasmons coupled to infrared light also lead to free carrier absorption and may result in variations in the plasmonic response, as detectable by plasmon interferometry experiments. We study this response in the form of intensity dependent nonlinear plasmon interferometry measurements. In addition, we plan to investigate fs spatially-resolved nonequilibrium carrier dynamics and other inhomogeneous phenomena.

## References

[AP12] J. M. Atkin, S. Berweger, A. C. Jones, and M. B. Raschke, "Nano-optical imaging and spectroscopy of order, phases, and domains in complex solids", *Adv. Phys.* **61**, 745 (2012)

[RSI13] H. U. Yang, E. Hebestreit, E. E. Josberger, and M. B. Raschke, "A cryogenic scattering-type scanning near-field optical microscope", *Rev. Sci. Instrum.* **84**, 023701 (2013).

[PNAS14] H. A. Bechtel, E. A. Muller, R. L. Olmon, M. C. Martin, and M. B. Raschke, "Ultrabroadband infrared nanospectroscopic imaging", *PNAS* **111**, 7191 (2014).

## Publications (supported by BES, past 2 years)

[NC15] B. T. O'Callahan, J. M. Atkin, A. C. Jones, J. H. Park, D. Cobden, and M. B. Raschke, "Inhomogeneity in the ultrafast insulator-to-metal transition dynamics of $VO_2$", *Nature Commun.* 6, 6849, (2015).

[OE15] Brian T. O'Callahan, William E. Lewis, Eric A. Muller, Silke Moebius, Jared C. Stanley, and Markus B. Raschke, Optics Express 23, 32063 (2015)

[NL16-1] K. D. Park, O. Khatib, V. Kravtsov, G. Clark, X. Xu, and M. B. Raschke, "Hybrid Tip-Enhanced Nanospectroscopy and Nanoimaging of Monolayer $WSe_2$ with Local Strain Control", *Nano Lett.* 16, 2621 (2016).

[NL16-2] S. A. Dönges, O. Khatib, B. T. O'Callahan, J. M. Atkin, J. H. Park, D. Cobden, M. B. Raschke, "Ultrafast Nanoimaging of the Photoinduced Phase Transition Dynamics in $VO_2$", *Nano Lett.* 16, 3029, (2016).

[NL16] Pollard, B., Maia, F. C. B., Raschke, M. B. & Freitas, R. O., Nano Lett. 16, 55 (2016).

[SA16] Muller, E. A., Bechtel, H. A., Blerkom, P. van, Martin, M. C., and Raschke, M. B. Nanoscale Molecular Crystallography with Near-Field Infrared Spectroscopy, Science Advances (*in press*) (2016).

[APL16] O'Callahan, B. T. and Raschke, M. B., Applied Physics Letters, (*in prep*) (2016).

# Radiative Heat Transfer at the Nanoscale

**Pramod Reddy, Department of Mechanical Engineering, Department of Materials Science, University of Michigan, Ann Arbor, 48109**

## Research Scope

The goal of this research is to experimentally investigate radiative thermal transport in nanoscale gaps. In macroscale devices, heat transport via radiation is well described by the Stefan-Boltzmann law[1]. However, recent studies have highlighted that the Stefan-Boltzmann law fails to adequately describe heat transport at the nanoscale. For example, recent computational studies of radiative heat transport in nanoscale gaps, employed using the framework of fluctuational electrodynamics[2], have suggested that the radiative heat flux in a one-nanometer sized gap between suitably chosen planar dielectric surfaces could be five orders of magnitude larger than what is predicted by the Stefan-Boltzmann law. This large deviation arises primarily due to contributions from evanescent waves that decay exponentially on a length scale comparable to their wavelength. Such enhancements are expected at the nanoscale because contributions from the evanescent modes increase dramatically as the gap-size decreases. In spite of the great potential of nanoscale thermal radiation for several technologies it has remained largely unexplored due to experimental challenges. Below, we explain in some detail some of our recent progress in understanding nanoscale thermal radiation.

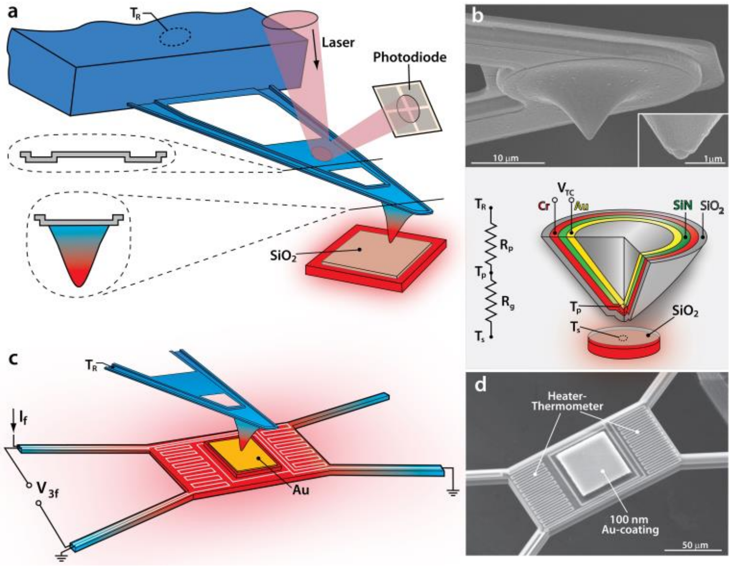

***Figure 1: Experimental setup and images of SThM probes and suspended microdevices. a,*** *Schematic of the experimental setup where a SThM probe is in close proximity to a heated substrate.* ***b,*** *SEM image (top panel) of a SThM probe. The inset shows a SEM image of the hemispherical probe tip, which features an embedded Au-Cr thermocouple. The bottom panel shows a schematic cross-section for a* $SiO_2$*-coated probe employed in* $SiO_2$ *measurements.* ***c,*** *Schematic showing the measurement scheme employed for high resolution eNFRHT measurements of Au-Au..* ***d,*** *SEM image of the suspended microdevice featuring the central region coated with Au.*

## Recent Progress

Our recent work (***Kim et al., Nature, 2015***)[3], performed using novel scanning thermal probes (see Fig. 1), has led to important insights into nanoscale radiative heat transfer. Past experiments[4, 5] of extreme near-field radiative heat transfer (eNFRHT), i.e. heat transfer in single-digit nanometer gap sizes, have questioned the validity of current theories of nanoscale radiative heat transfer and have suggested that processes, even of non-radiative origin such as phonon tunneling, could dominate the heat transfer in this regime. The resulting controversy is of great concern because understanding eNFRHT is critical for the development of a range of novel technologies.

Experimental elucidation of eNFRHT is exceedingly difficult due to numerous technical challenges in creating and stably maintaining such gaps while simultaneously measuring minute (pW) heat currents across them. One key innovation used by us in our recent work to overcome the technical challenges was to leverage highly sensitive, custom-fabricated probes with embedded Au-Cr thermocouples (Fig. 1), called scanning thermal microscopy (SThM) probes. The basic strategy employed by us for quantifying eNFRHT is to record the tip temperature, via the embedded nanoscale thermocouple, which rises in proportion to the radiative heat flow when the tip is displaced towards a heated substrate. In performing the measurements the substrate is heated while the SThM probe was maintained at ambient temperature. The spatial separation between the probe and the substrate is reduced from a gap size of 50 nm until probe-substrate contact. During this process the temperature difference between the tip ($T_P$) and the reservoir ($T_R$), $\Delta T_P = T_P - T_R$, was monitored via the embedded thermocouple while the deflection of the cantilever is concurrently measured optically via an incident laser. This temperature difference was used to estimate the radiative thermal conductance.

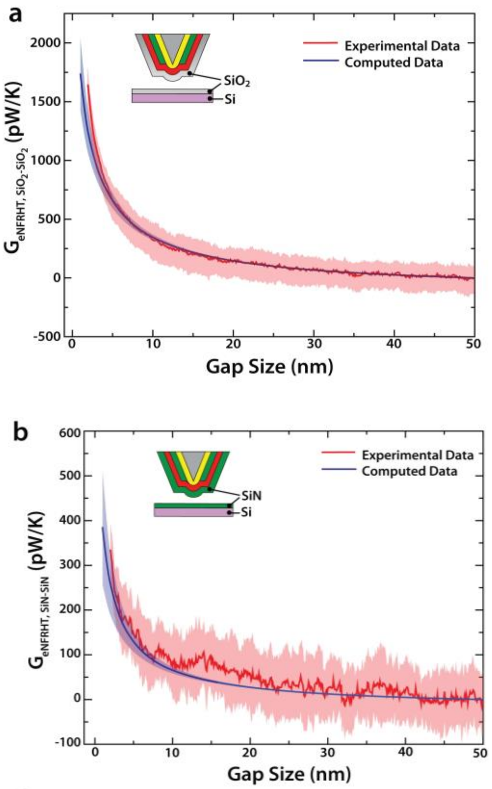

***Figure 2: Measured extreme near-field thermal conductances for dielectric and metal surfaces. a,*** *Measured radiative conductance between a $SiO_2$-coated probe (310 K) and a $SiO_2$ substrate at 425 K. The blue solid line shows the average of the computed radiative conductance for 15 different tips with stochastically chosen roughness profiles (RMS roughness ~10 nm) and a tip diameter (450 nm) obtained from SEM images of the probe.* ***b*** *same as (a), but for SiN-SiN.*

The measured conductance of the gaps for $SiO_2$ and SiN surfaces is shown in Fig. 2a and b, respectively. It can be seen that $G_{eNFRHT}$ increases monotonically until the probe snaps into contact at a gap size of ~2 nm. These measurements represent the first observation of eNFRHT in single-digit nanometer-sized gaps between dielectric surfaces. We compared these results to our computational predictions based on fluctuational electrodynamics and found very good agreement (solid lines in Fig. 2a & b). These results along with others described in our work [3] provided first conclusive evidence supporting the validity of fluctuational electrodynamics in modeling nanoscale thermal radiation.

In addition to the work described above, we also performed studies[6] where we demonstrated for the first time that it is possible to achieve radiative thermal conductances that exceed the limits posed by the blackbody limit by several orders of magnitude (***Song et al., Nature Nanotechnology, 2016***). In performing these measurements, we used microfabricated devices such as those shown Figs. 3a & 3b. The receiver device (Fig. 3b) features a 3 μm thick $SiO_2$ layer deposited in the central region. Subsequently this device was placed in close proximity to an emitter device (Fig. 3b) that features a plateau coated with a 3 μm thick $SiO_2$ layer. The plateau region and the suspended $SiO_2$ coated region of the receiver are placed such that they face each other (inset Fig. 3c). Subsequently, the two surfaces are parallelized using a enables achieving excellent parallelism such that any two corresponding points on the emitter and receiver devices deviate by ~5 nm or less from their desired positions. The resulting radiative heat currents from the emitter to the receiver were quantified by measuring the temperature oscillations of the receiver ($\Delta T_{rec}$) using the integrated resistance thermometer and from knowledge of the thermal conductance of the beams of the receiver (2 μW/K). To measure the gap dependence of NFRHT we step the emitter towards the receiver with a piezoelectric actuator until contact is detected.

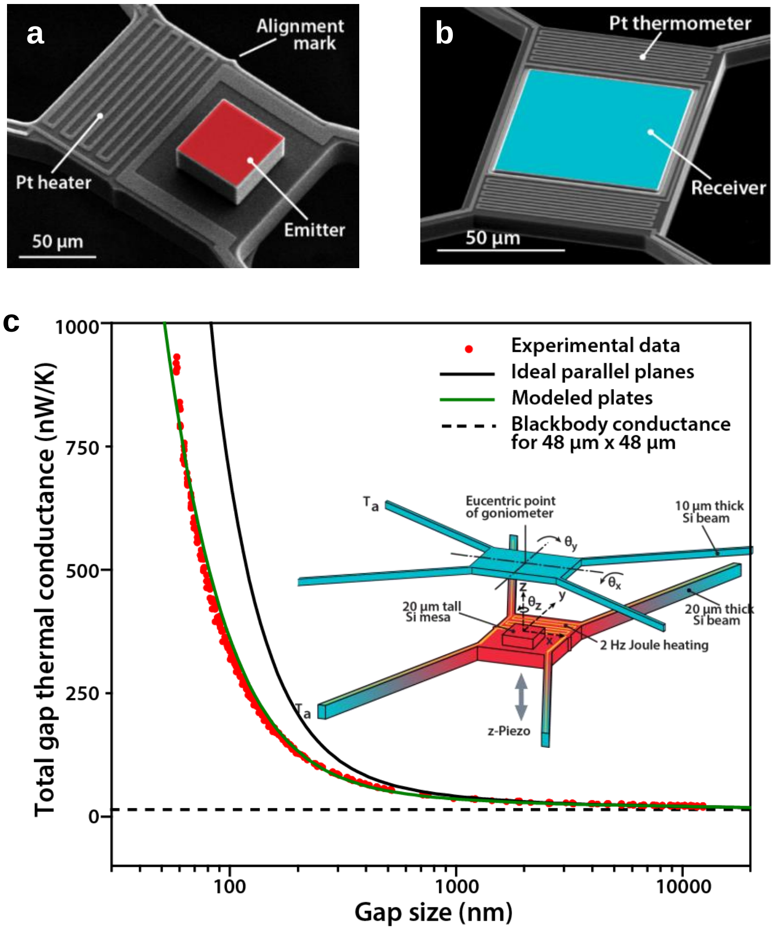

***Figure 3: Experimental platform for measurements of radiative conductance in nanoscale gaps and representative experimental data. a,*** *SEM image of microfabricated emitter device.* ***b,*** *SEM image of the receiver device..* ***c,*** *The measured conductance vs. gap-size for the micro-device. The measured conductance is found to agree well with computational predictions and is several orders of magnitude larger than that predicted by the blackbody limit.*

The measured gap-dependent thermal conductance (dots) is shown in Fig. 3c along with the estimated thermal conductance between the two surfaces (solid line, obtained using fluctuational electrodynamics). It is clear from the agreement between the experimental and computational results that our measurements are consistent with theory. Further, it can be seen that at the smallest gaps (~50 nm) the measured radiative conductance is at least two orders of magnitude larger than that predicted by the blackbody limit (solid-dashed line). These results represent the first successful demonstration of dramatic enhancement in radiative thermal conductances in nanoscale gaps.

## Future Plans

Near-field thermal radiation has significant potential for power generation (heat to electricity) and solid-state refrigeration (electro luminescent cooling). However, the principles of such energy conversion processes have not yet been experimentally established. In the near future we will both leverage our recent technical advances and develop novel scanning probe based approaches to provide first insights into near-field based energy conversion.

## References

1. M. Planck and M. Masius, The theory of heat radiation. (P. Blakiston's son & co., 1914).
2. "Theory of Radiative Heat Transfer between Closely Spaced Bodies". D. Polder and M. Vanhove. Physical Review B, **4**(10): p. 3303(1971).
3. "Radiative heat transfer in the extreme near field". K. Kim, B. Song, V. Fernandez-Hurtado, W. Lee, W.H. Jeong, L.J. Cui, D. Thompson, J. Feist, M.T.H. Reid, F.J. Garcia-Vidal, J.C. Cuevas, E. Meyhofer, and P. Reddy. Nature, **528**(7582): p. 387-391(2015).
4. "Near-field heat transfer in a scanning thermal microscope". A. Kittel, W. Muller-Hirsch, J. Parisi, S.A. Biehs, D. Reddig and M. Holthaus. Physical Review Letters, **95**(22): p. 224301(2005).
5. "Enhanced near-field heat flow of a monolayer dielectric island". L. Worbes, D. Hellmann and A. Kittel. Physical Review Letters, **110**(13): p. 13402(2013).
6. "Radiative heat conductances between dielectric and metallic parallel plates with nanoscale gaps". B. Song, D. Thompson, A. Fiorino, Y. Ganjeh, P. Reddy and E. Meyhofer. Nature Nanotechnology, **11**(6): p. 509-514(2016)
7. "A platform to parallelize planar surfaces and control their spatial separation with nanometer resolution". Y. Ganjeh, B. Song, K. Pagadala, K. Kim, S. Sadat, W. Jeong, K. Kurabayashi, E. Meyhofer and P. Reddy. Review of Scientific Instruments, **83**(10): p. 105101(2012)

## Publications

1. Y. Kim, A. Lenert, E. Meyhofer, P. Reddy, “Temperature dependence of thermopower in molecular junctions” **Applied Physics Letters** (2016)
2. B. Song, D. Thompson, A. Fiorino, Y. Ganjeh, P. Reddy, E. Meyhofer, “Radiative heat conductances between dielectric and metallic parallel plates with nanoscale gaps” **Nature Nanotechnology** (2016).
3. K. Kim, B. Song, V. Fernandez, W. Lee, W. Jeong, L. Cui, D. Thompson, J. Fiest, M. T. H. Reid, F. G. Vidal, J. C. Cuevas, E. Meyhofer, P. Reddy, “Radiative Heat Transfer in the Extreme Near Field” **Nature** (2015)
4. W. Jeong, S. Hur, E. Meyhofer, P. Reddy, “Scanning probe microscopy for thermal transport measurements” **Nanoscale and Microscale Thermophysical Engineering** (2015)
5. Y. Kim, W. Jeong, K. Kim, W. Lee, P. Reddy, “Electrostatic Control of Thermoelectricity in Molecular Junctions” **Nature Nanotechnology** (2014)
6. K. Kim, W. Jeong, W. Lee, S. Sadat, D. Thompson, E. Meyhofer, P. Reddy, “Quantification of Thermal and Contact Resistances of Scanning Thermal Probes” **Applied Physics Letters** (2014)
7. W. Jeong, Y. Kim, K. Kim, W. Lee, P. Reddy, “Characterization of Nanoscale Temperature Fields during Electromigration of Nanowires” **Scientific Reports** (2014)
8. L. A. Zotti, F. Pauly, M. Bürkle, F. Pauly, W. Lee, K. Kim, W. Jeong, Y. Asai, P. Reddy, and J. C. Cuevas, “Heat Dissipation and its Relation to Thermopower in Single-Molecule Junctions”, **New Journal of Physics** (2014)

# Deformation process in multi-layered Ag-Cu system

**Ian M. Robertson, Department of Materials Science and Engineering, University of Wisconsin-Madison, Madison, Wisconsin 53711**

## Research Scope

The scope of this program is to first develop the technique of electron tomography of defect structures in metallic systems and to couple it with in-situ TEM deformation capabilities. Successful combination of the two will permit four-dimensional (time and three spatial dimensions) characterization of the microstructure evolution processes. Critical to the success is the ability to include the real space coordinate system in the tomogram, resolving the defect invisibility issue and drastically reducing the number of images acquired to produce a useful tomogram. The second component is to apply this method to determine the evolution pathway of the deformation microstructure and to discovery how this is transmitted across interfaces and influenced by precipitates.

## Recent Progress

The AgCu eutectic system has been used as a model material system to determine the dependence of the deformation mode and the transfer of strain across FCC/FCC interfaces with either a cube-on-cube orientation relationship or an incoherent twin interface [1,2]. In directionally solidified AuCu eutectic alloy, the percentage of cube-on-cube versus incoherent twin interfaces decreases with decreasing bilayer thickness and this can be controlled by processing conditions. It has been found that the cube-on-cube interface permits transmission of deformation twins across it whereas the incoherent and coherent twin interfaces do not [3,4]. In the 500 nm bilayer thick AgCu eutectic, which has a preponderance of incoherent twin interfaces, following loading parallel to the interfaces plastic strain recovery occurs [5]. This plastic strain recovery was only observed in samples loaded in compression at a strain rate of $10^3$ $s^{-1}$. Through the combination of transmission electron microscopy analysis of the deformed microstructure and molecular dynamics computer simulations of the deformation processes, the mechanisms of plastic strain recovery have been revealed. The character of the incoherent twin interfaces was found to rotate following dynamic compressive loading and this change drove the recovery. This rotation, as determined experimentally and in the simulations is shown in Fig. 1. After 10% compressive loading the interface rotation measured experimentally and in the simulations to be on average 6 and 3.4 degrees, respectively. This rotation can be seen by the dashed lines in

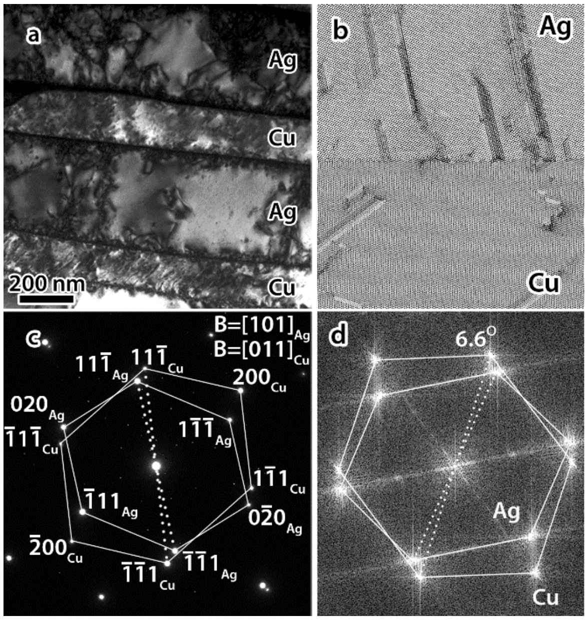

Figure 1. a. Microstructure following compressive loading to 10% experimentally; b. simulated microstructure after 10% compressive loading; c. experimental diffraction pattern and d. Fourier transform of the simulated structure.

the diffraction patterns. The recovery was shown to be due to dislocation retraction and rearrangement of the interfaces. The experimental observation that the magnitude of the recovery decreased with increasing strain was shown to be due to the formation of dislocation tangles and dislocation cell structures in both layers. No change in the orientation relationship was found at cube-on-cube interfaces and these exhibited a lesser amount of plastic strain recovery in the simulations and none experimentally.  This study highlights the importance to understand the role interfaces play in determining the deformation response of a material

## Future Plans

Publish the remaining papers associated with this project.

## References

[1] S.J. Zheng, J. Wang, J.S. Carpenter, W.M. Mook, P.O. Dickerson, N.A. Mara, I.J. Beyerlein. Acta Materialia 2014, 79  282-291.
[2] Y.Z. Tian, Z.F. Zhang. Bulk eutectic Cu-Ag alloys with abundant twin boundaries, Scripta Materialia 2012, 66 65-68.
[3] O.T. Kingstedt, B. Eftink, J. Lambros, I.M. Robertson. Materials Science and Engineering: A 2014, 595 54-63.
[4] J. Kacher, B.P. Eftink, B. Cui, I.M. Robertson. Curr. Opin. Solid State Mat. Sci. 2014, 18 227-243.
[5] O.T. Kingstedt, B.P. Eftink, I.M. Robertson, J. Lambros. Acta Materialia 2016, 113, 293 -300

## Publications

[1] Kacher J, Hattar K, Robertson IM. Mater. Sci. and Engin. A 2016;675:110.
[2] Kacher J, Robertson IM. Phil. Mag. 2016;96:1437.
[3] Eftink BP, Li A, Szlufarska I, Robertson IM. Acta Mater. 2016;117:111.
[4] Liu GS, House SD, Kacher J, Tanaka M, Higashida K, Robertson IM. Mater Charact 2014;87:1.
[5] Kacher J, Robertson IM. Phil. Mag. 2014;94:814.
[6] Kacher J, Eftink B, Cui B, Robertson IM. Current Opin. Solid State and Mater. Sci. 2014;18 227.

# Femtosecond imaging of dynamical texture (re)formation in charge-density wave systems with coherent electron beams

Chong-Yu Ruan
Michigan State University, East Lansing, MI 48824. E-mail: ruan@pa.msu.edu

## (i) Program Scope

Our project will leverage on emerging high-brightness electron beam technology for high-throughput femtosecond electron diffraction and imaging, designed to study the emergence and interplay between different orderings, such as density wave formation and structurally ordered states near insulator-metal (or superconductivity) transitions in the nonequilibrium regime. The experiments will also build on our recently established femtosecond optical doping approach for control and studies of the electronically driven energy landscape and resulted phase diagrams, and the cooperative dynamics of different order parameters that are entangled under nonequilibrium driving.

The project includes: (i) addressing the open questions on the symmetry breaking mechanism for the formation of stripe and checkerboard phases, (ii) disentangling the complex interplay between temperature, strain, disorder, chemical and external optical tuning of charge carriers in correlated metal-insulator transitions, and (iii) imaging the formation and transformation of highly debated the intertwined phase in the pseudo-gap region of transition-metal superconducting compounds.

## (ii) Recent Progress

This presentation will discuss the latest development of ultrafast electron imaging and microdiffraction technologies and their first applications in imaging large scale textured states evolution and microstructures in correlated systems near metal-insulator transitions. The new femtosecond imaging and spectroscopy technologies utilize the inherent high brightness in the controlled femtosecond photoemission processes. Through a series flexible electron optical deployments that optimize the longitudinal (energy-time) and transverse (coherent length-dose) ultrashort electron pulse characteristics, new capabilities that incorporate spatial, temporal, and energy resolution are emerging. We first report that with dynamical pulse compression and magnetic focusing adjustments can now produce highly coherent electron beams (> 20 nm) while maintain relative high electron dose ($D>1$ e/$\mu m^2$) and high temporal resolution (~ 100 fs). For our DOE project, these new capabilities provide new opportunities of studying large periodic domain formations in a charge density waves system ($1T$-$TaS_2$) and the ultrahigh speed restructuring of $VO_2$ microstructures near metal-insulator switching. The notably higher electron dose and coherent length provide the flexibilities in dealing with complex transformations through efficiently generating large datasets covering extended dynamical ranges where the diffusive and dynamical scaling behavior can be differentiated. On the other hand, different electron-optical arrangements also produce highly concentrated beams into a subdominant structure of microstructures, allowing microstructure responses to be differentiated with respect to the averaged responses in ensembles. These examples exemplify the range of problems that can be tackled successfully even in the sub-relativistic energy scale more common to traditional electron TEM system.

Secondly, we will report on the ultrafast studies of 2D samples, traditionally prepared for steady-state transport measurements using Scotch-tape exfoliation. Such preparation is essential to produce very clean samples and to control the strain. Importantly, in ultrafast investigation of correlated systems there is a growing recognition that the strain may develope dynamically as part of photoinduced phase transition that may influence the microscopic phase evolution, similar to the steady state conditions(*1*-*3*). Capabilities for imaging of long-range interactions in these very clean systems under nearly stress-free environment permit a means to decouple the complex behaviors which may otherwise be obscured due to long-range elastic interactions smoothing out the sharp nature of the transitions.

On addressing the mechanism for the formation of different textured states, we applied the ultrafast coherent electron beams to obtain diffraction patterns resulted from high-order interactions of charge density waves in tantalum disulfide (1T-$TaS_2$). These high-harmonic interactions carry crucial information of the formation of long-range charge-ordered domains(*4*-*6*). Specifically, in $TaS_2$ the near-commensurate (NC) phase exists in distinctively textured state with sharp domains walls separating the locally insulating commensurate hexagonal domains, while being overall metallic. Raising the temperature to Tc ~ 350K, the domain state reconstructs into an incommensurate (IC) state with triply degenerate charge density waves(CDW) where no distinct domain walls can be identified. Prior studies using the scanning tunneling microscopy technique showed that this phase transition proceeds via gradually reducing the commensurate domain region while increasing the size of domain walls within which the new incommensurate phase emerges(*7*, *8*). Meanwhile, photo-emission(*9*) and X-ray scattering(*10*) techniques showed the phase transitions induced by applying pressure within the bulk of $TaS_2$ samples to proceed without expanding the domain walls. Instead, the reduction of commensurate domain occurs via forming new domain walls that gradually subdivide the domains. Whereas these steady-state studies characterized the initial trends of transformation, but due to the strongly first order nature of the transition, the pathways of the domain state transformation are hidden in the abrupt transformations when the critical temperature or pressure are crossed. Recently, the discoveries of new or hidden domain states under photoexcitation(*11*, *12*) or electrostatic gating(*13*) have fueled the debates over the subtle nature of phase transitions and their relationship to superconductivity.

Through controlled photo-doping and ultrafast imaging with coherent electron beams, we are able to delineate the underlying processes and uncover the dynamical scaling behavior close to metal-insulator switching where CDW texture development plays a role. By differentiate the dynamical responses in the long range and over different timescales, the diffusive and cooperate regimes of phase transition are isolated. The surprising physics of the scaling behavior against thermal fluctuations is examined with clear threshold onset, which is distinctly different from the behavior driven by thermal quasiparticle excitations. In the dynamically scaling regime, high-fidelity cooperative switching can be established whereas in the quasiparticle-excitation-dictated regime, the responses are more akin to conventional semiconductors. These time-domain characterizations together with imaging of macroscopic texture developments provide a microscopic picture of how different phase transitions may occur under heating and photo-doping.

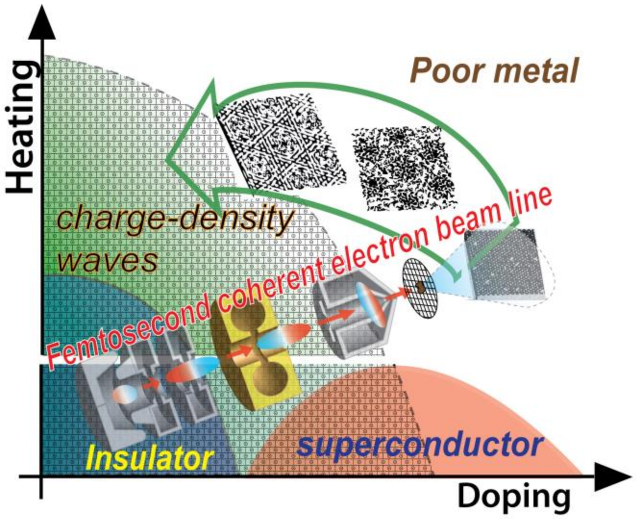

**Fig.** *Ultrafast imaging of long-range textured density-wave evolutions using femtosecond coherent electron beams in* $TaS_2$. *The phase diagram of* $1T$-$TaS_2$ *under thermal heating and chemical doping (or applying pressure) encompasses textured charge-density wave states near insulator-metal transitions. The origins of these large-scale charge ordering textures and their relationship to the formation of superconductivity and coupling to structural transitions are open issues. Ultrafast imaging with coherent electron beam provides essential features that underlie the organizing principle of collective state transformation that spans from atomic scale to very long range (>10 nm).*

On disentangling the interplay between different tuning physical parameters that drive the metal-insulator switching in correlated electron crystals, we studied phase transitions in $VO_2$ nanocrystalline films. Unlike what has been perceived previouslyas monolithic transformation(*14-16*), we observed that the photoinduced phase transitions between the monoclinic insulator ($M_1$) and the rutile metal (R) phase involves two separate transformations that take place via distinctly different mechanisms and over different timescales. We establish a new monoclinic metastable phase that locally takes on reduced lattice distortions while macroscopically possessing a different ordering motif, mediating the two different transformations. In the first transition where photoexcitation dives the system from $M_1$ to the metastable phase, the lattice dynamics proceed cooperatively but differently along the two separate sublattices, manifesting the strong interaction-driven character. While the new crystalline motif emerges in the femtosecond timescale, the overall lattice continues to evolve along the monoclinic motif for tens of ps during which the second transition is incubated by lattice fluctuations. Intriguingly, the second transformation also follows a threshold behavior with clearly onset in the time domain that leads to an incipient coherent acoustic wave generation as the system evolves to the quasi-equilibrium rutile state with changes in lattice rigidity. The dual transformation and the distinct role of lattice fluctuations in driving the electronic phase transition separate $VO_2$ from conventional electron crystals, and the results report here may help elucidate the complexities that have been the sources of recent debates(*17-20*).

### (iii) Future Plans

Building on the success of the first year and new technical advances, we will move to the next stage of the three thrust directions, including more in-depth studies of charge-density wave materials with regard to morphological evolutions and layer-dependence, and further investigation of the effects of doping and strain using nanoscopic single-crystal $VO_2$ samples. Additionally, an attempt will be made to conduct electron imaging of fluctuating charge ordering in the pseudo-gap region of the superconducting materials.

### (iv) References

1. J. Cao *et al.*, Strain engineering and one-dimensional organization of metal-insulator domains in single-crystal vanadium dioxide beams. *Nature Nanotechnology* **4**, 732 (2009).
2. J. Wei, Z. H. Wang, W. Chen, D. H. Cobden, New aspects of the metal-insulator transition in single-domain vanadium dioxide nanobeams. *Nature Nanotechnology* **4**, 420 (2009).
3. Z. S. Tao *et al.*, Decoupling of structural and electronic phase transitions in $VO_2$. *Physical Review Letters* **109**, 166406 (2012).
4. K. T. Nakanishi, Y.Yamada, H. Shiba, The near commensurate phase and effect of Harmonics on the successive phase transition in 1T-$TaS_2$. *J. Phys. Soc. Jap.* **43**, 1509 (1977).
5. R. E. Thomson *et al.*, Local charge-density-wave structure in 1T-$TaS_2$ determined by scanning tunneling microscopy. *Physical Review B* **38**, 10734 (1988).
6. A. Spijkerman, J. L. de Boer, A. Meetsma, G. A. Wiegers, S. van Smaalen, X-ray crystal-structure refinement of the nearly commensurate phase of 1T-TaS2 in (3+2)-dimensional superspace. *Physical Review B* **56**, 13757 (1997).
7. X. L. Wu, C. M. Lieber, Direct observation of growth and melting of the hexagonal-domain charge-density-wave phase in 1T-$TaS_2$ by scanning tunneling microscopy. *Physical Review Letters* **64**, 1150 (1990).
8. B. Sipos *et al.*, From Mott state to superconductivity in 1T-$TaS_2$. *Nature Materials* **7**, 960 (2008).
9. R. Ang *et al.*, Real-space coexistence of the melted Mott state and superconductivity in Fe-substituted 1T-$TaS_2$. *Physical Review Letters* **109**, 176403 (2012).
10. T. Ritschel *et al.*, Pressure dependence of the charge density wave in 1T-$TaS_2$ and its relation to superconductivity. *Physical Review B* **87**, 125135 (2013).
11. L. Stojchevska *et al.*, Ultrafast switching to a stable hidden quantum state in an electronic crystal. *Science* **344**, 177 (2014).
12. T.-R. T. Han *et al.*, Exploration of meta-stability and hidden phases in correlated electron crystals visualized by femtosecond optical doping and electron crystallography. *Science Advances* **1**, e1400173 (2015).
13. Y. Yu *et al.*, Gate-tunable phase transitions in thin flakes of 1T-$TaS_2$. *Nat Nano* **10**, 270 (2015).
14. J. B. Goodenough, The two components of the crystallographic transition in VO2. *Journal of Solid State Chemistry* **3**, 490 (1971).
15. A. Zylbersztejn, N. F. Mott, Metal-insulator transition in vanadium dioxide. *Physical Review B* **11**, 4383 (1975).
16. V. Eyert, The metal-insulator transitions of $VO_2$: a band theoretical approach. *Annalen Der Physik* **11**, 650 (2002).
17. V. R. Morrison *et al.*, A photoinduced metal-like phase of monoclinic VO2 revealed by ultrafast electron diffraction. *Science* **346**, 445 (2014).
18. J. Laverock *et al.*, Direct Observation of Decoupled Structural and Electronic Transitions and an Ambient Pressure Monocliniclike Metallic Phase of $VO_2$. *Physical Review Letters* **113**, 216402 (2014).
19. D. Wegkamp, J. Stahler, Ultrafast dynamics during the photoinduced phase transition in $VO_2$. *Progress in Surface Science* **90**, 464 (2015).
20. B. T. O'Callahan *et al.*, Inhomogeneity of the ultrafast insulator-to-metal transition dynamics of $VO_2$. *Nat Commun* **6**, 6849 (2015).

## (v) 2-Year Publications (DOE sponsored)

1. T.-R. T. Han, F. Zhou, C. Malliakas, S.D. Mahanti, P.M. Duxbury, M. Kanatzidis, C.-Y. Ruan, **Exploration of meta-stability and hidden phases in correlated electron crystals visualized by femtosecond optical doping and electron crystallography**. Science Advances, 1, e1400173 (2015).
2. M. Berz, P. M. Duxbury, Kyoko Makino, and C. Y. Ruan, **Femtosecond electron imaging and spectroscopy**,_ Adv. Imag. Elect. Phys., 191, 1 (2015).
3. C.-Y. Ruan, P. M. Duxbury, M. Berz, **The perspectives of femtosecond imaging and spectroscopy of complex materials using electrons**. Z. Liu, I. C. Khoo, Eds., Ultrafast Nonlinear Imaging and Spectroscopy II, Proc. of SPIE, vol. 9198 (2014).
4. K. Chang, R.A. Murdick, T.-R.T. Han, F. Yuan, C.-Y. Ruan, Book Chapter: **Light-induced charge carrier dynamics at nanostructured interfaces investigated by ultrafast electron diffractive photovoltammetry**, Eds. J. Wu and Z.M. Wang, Springer Book Series on Quantum Dot Solar Cell (2014).
5. Z. Tao, F. Zhou, T.-R. T. Han, D. Torres, T. Wang, N. Sepulveda, K. Chang, M. Young, R. R. Lunt, C.-Y. Ruan, **The nature of the photoinduced phase transition and metastable states in vanadium dioxide**, (under review).

## Atomic-scale Surface Studies of Bulk Metallic Glasses

**Udo Schwarz, Department of Mechanical Engineering and Materials Science, Yale University**

### Research Scope

Bulk metallic glasses (BMGs) are of both scientific and technological interest because the absence of periodic atomic arrangements provides them with unique physical, chemical, and mechanical properties. Their high strength, superior elasticity, and an ability to be easily formed into virtually unlimited shapes with feature sizes from centimeters to Angstroms by blow molding and thermoplastic forming makes them an attractive choice for more and more practical applications and products. Due to their complex internal structure, however, experiments that yield insight into their exact atomic arrangements have been scarce.

The main reason for the slow progress is the lack of experimental tools that enable access to atomic-scale structural and behavioral information for disordered materials. The aim of the research, to be executed during the next three years (this project is started only very recently on 8/15/2016), is to enable significant progress in our understanding of BMGs by introducing a novel sample preparation scheme that results in high-quality samples ideally suited for inspection using an array of surface characterization methods. The radically new step is that we are performing nanoimprinting by thermoplastic forming (TPF) in ultrahigh vacuum with well ordered, in-situ cleaned oxide crystals as templates to produce atomically flat, uncontaminated surfaces that are yet fully amorphous. Alternately, atomically flat, uncontaminated surfaces will be produced using a novel vacuum-based growth approach. Through a combination of innovative scanning probe studies complemented by more standard surface science experiments, we will then obtain unprecedented insight into the nature of the glassy state.

### Recent Progress

Nanoimprinting has attracted significant attention in recent years due to its promise of low-cost fabrication of nanostructured devices. Usually performed using polymers, BMGs have been identified as a material class that might be even better suited for nanoimprinting due to a combination of mechanical properties and processing ability. As a particular advantage, their featureless atomic structure suggests that there may not be an intrinsic size limit to the material's ability to replicate a mold. We recently demonstrated that atomic step edges of a $SrTiO_3$ (STO) single crystal used as mold could be successfully imprinted into amorphous $Pt_{57.5}Cu_{14.7}Ni_{5.3}P_{22.5}$ with high fidelity. Terraces on the BMG replicas possess atomic smoothness with sub-Angstrom roughness that is identical to the one measured on the STO mold.

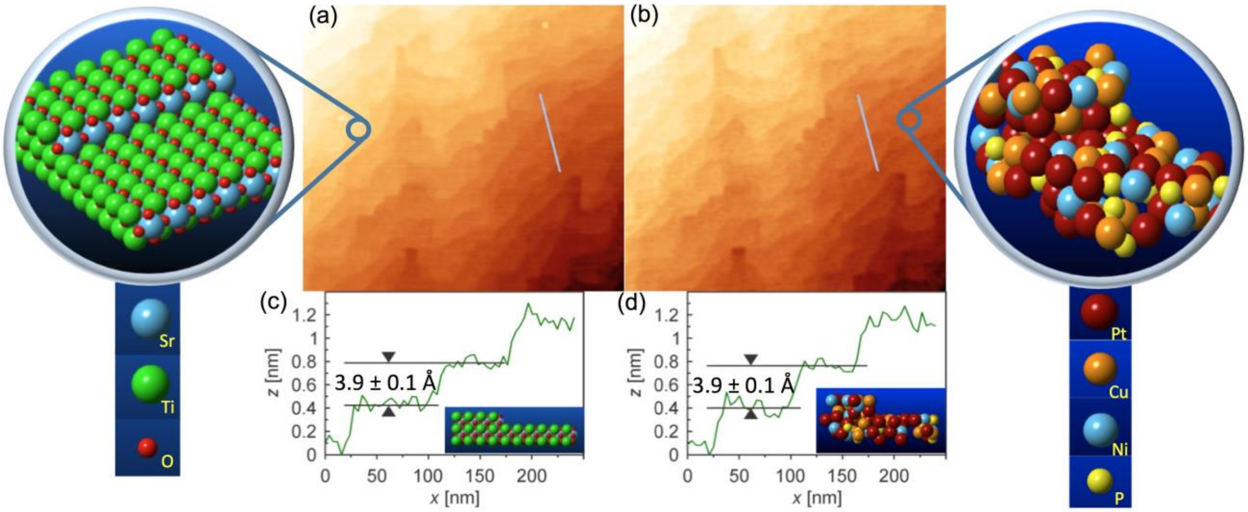

Atomically precise imprinting of $Pt_{57.5}Cu_{14.7}Ni_{5.3}P_{22.5}$ by thermoplastic forming at 270 °C. **(a)** Ambient-air AFM image of a $SrTiO_3$(100) crystal after annealing at 1000 °C; atomic steps of excellent quality are visible. The cross section shown in panel (c) demonstrates that the individual steps are of unit cell height (3.9 ± 0.1 Å). **(b)** Corresponding area in the pressed BMG (image mirrored and inverted for easy comparison). Every detail of the atomic structure has been replicated; as illustrated in (d), even the step heights reproduce with an accuracy of better than 0.1 Å despite the fact that the atomic structure of the imprinted material remains amorphous (see insets). During the course of this work, samples prepared under clean conditions in ultrahigh vacuum will be investigated.

## Future Plans

Using the nanoimprinting method introduced above, we will produce samples from BMG alloys directly in ultrahigh vacuum whose surfaces feature large atomically flat terraces despite being entirely amorphous. Our approach starts with the in-situ preparation of oxide crystals that are terminated by large terraces, from which exact mirror images out of Pt- and Au-based BMG will be formed. Since the resulting BMG replicas display all features of the original crystal with sub-Angstrom fidelity, thereby mimicking the original crystal's termination by atomically flat terraces without being crystalline themselves, they are ideally suited for further investigation. The following experiments are then planned within this proposal: (1) Using Auger spectroscopy, x-ray photoelectron spectroscopy, low-energy ion scattering spectroscopy, and temperature-programmed desorption of CO molecules, the surface composition of the BMG samples will be clarified. (2) Using CO molecules as molecular markers for the locations of Pt and Ni surface atoms, the distribution of these species in the surface of Pt-BMG will be imaged at low temperatures by scanning tunneling microscopy (STM) and noncontact atomic force microscopy (NC-AFM). (3) Low-temperature STM and NC-AFM measurements on the atomically flat terraces will reveal details of the atomic structure of BMGs. (4) By repeating point 1-3 for samples with different preparation histories (e.g., after additional annealing, pressed with different flow speeds during TPF, etc.), variations in the atomic arrangements due to relaxation and energy minimization effects can be revealed.

# Characterization of Energy-Relevant Materials with Multifrequency and Conductive Atomic Force Microscopy, and Kelvin Probe Force Microscopy

**Santiago D. Solares, The George Washington University, Department of Mechanical and Aerospace Engineering, Washington, DC 20052**

## Research Scope

The overall scope of this project is the development of a trimodal atomic force microscopy (AFM) method for the multi-dimensional characterization of nanoscale surfaces. Here multidimensional refers to either mapping of multiple surface observables through a single 2-dimensional scan, or to mapping of a single observable as a function of the Cartesian position of the probe, with the possibility of including the probe velocity as a fourth dimension. The ability to visualize the subsurface with trimodal AFM has been previously reported [1] and a variety of nanomechanical mapping approaches with single- and multifrequency AFM methods have been previously develop or studied [2-6]. The project scope for the past (4th) and the final (5th) years consists of the application of these methods to elucidate scientific aspects of energy-relevant materials. The studies have focused on two systems, namely (i) Nafion® proton exchange membranes subjected to varying chemical environments, whereby a description of the corresponding mechanical properties as a function of environmental changes is sought, and (ii) PCDTBT:$PC_{70}BM$ bulk hetero-junction active layers in organic photovoltaics (OPVs) subjected to localized nanomechanical stresses, where the objective is to elucidate the physical origins of the evolution of localized defects in the electron/hole transport capability of the system.

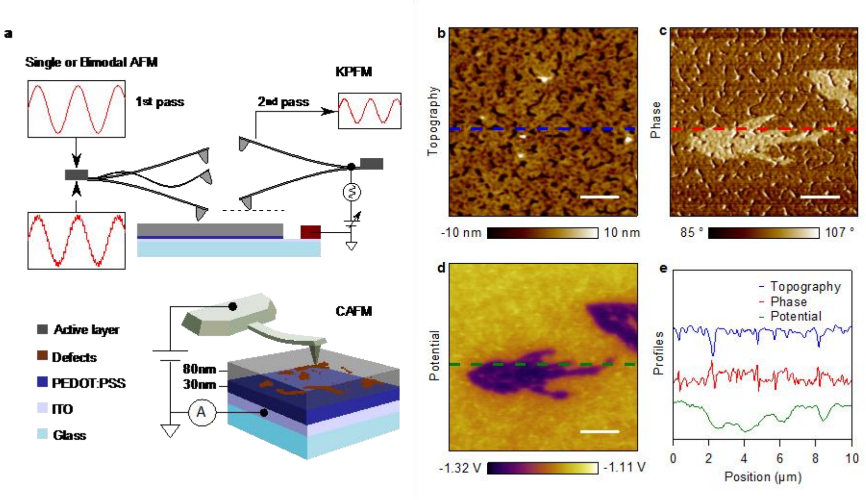

## Recent Progress

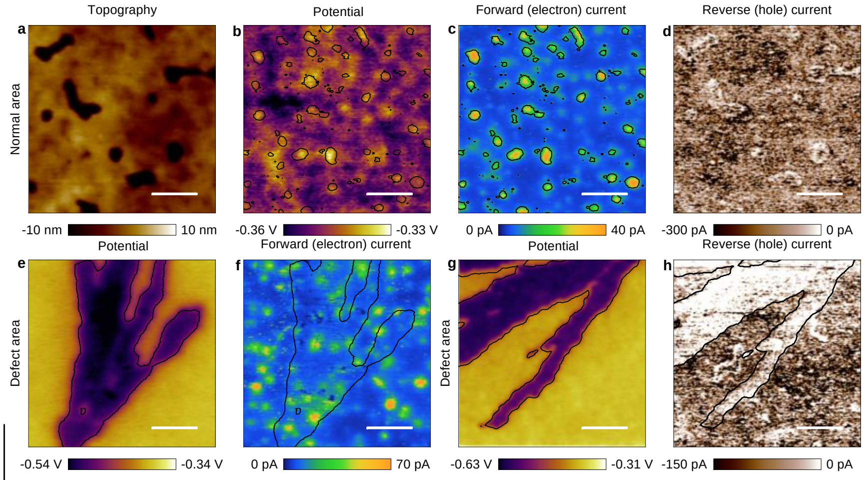

**Figure 2.** Correlation of potential with electron and hole currents for normal and defective areas of the device illustrated in Figure 1. (a) Topography of a normal area; (b) potential of the normal area; (c) electron current of the same area measured with forward (−5 V) tip bias; (d) hole current of the same area for reverse (+5 V) tip bias; (e) potential of an abnormal area containing defects; (f) corresponding electron current; (g) potential of second defective area; (h) corresponding hole current. Black contour lines highlight the correlation between potential and electron current in (b)-(c) and the defect boundaries in (e)-(h). Scale bars are 500 nm. The Multifrequency AFM healing process applied leads to the elimination of the defective (purple) areas in the above images and the recovery of the current.

*PCDTBT:$PC_{70}BM$ bulk hetero-junction active layers:* Organic photovoltaic (OPV) systems comprising donor polymers and acceptor fullerene derivatives are attractive for inexpensive energy harvesting, and extensive research on polymer solar cells offers insight on device-level efficiency and stability, but direct correlations between device-level performance and nanoscale component images are still challenging to obtain. Through recent experiments, the PI's group has demonstrated local recovery of defective areas, possibly caused by donor polymer clusters, by means of nanomechanical manipulation. The overall approach was as follows: defects in a PCDTBT-based solar cell device were characterized electrically by Kelvin probe force microscopy (KPFM) and conductive AFM (CAFM), whereby correlation between local electrical potential and current confirmed losses of hole percolation pathways at the defects. It was found that the defect population depends on the sample preparation process followed (e.g., on the type of solvents used), suggesting a possible relationship between polymer solubility and defect concentration. Afterwards, multifrequency (bimodal) AFM was used to applied controllable mechanical stresses using the *resonant* peak force modulation methods introduced in [1], followed by a second characterization with KPFM and CAFM, which confirmed healing of the defective areas. Since the healing process is mechanically-based, it offers the possibility of large-scale implementation in the commercial manufacturing of OPV systems, for example through the use of rolling processes. The key contributions so far have been the development of a correlation between device-level phenomena and nanoscale images by a systematic AFM characterization approach, and the implementation of a scanning probe procedure to recover the surface defects of the OPV devices studied.

*Nafion$^{\circledR}$ Proton Exchange Membranes:* Addition of a strong base to Nafion$^{\circledR}$ proton exchange membranes (PEM) is a common practice in industry to increase their overall performance in fuel cells by reducing membrane wrinkling and hydrolyzing the functional groups. However, no

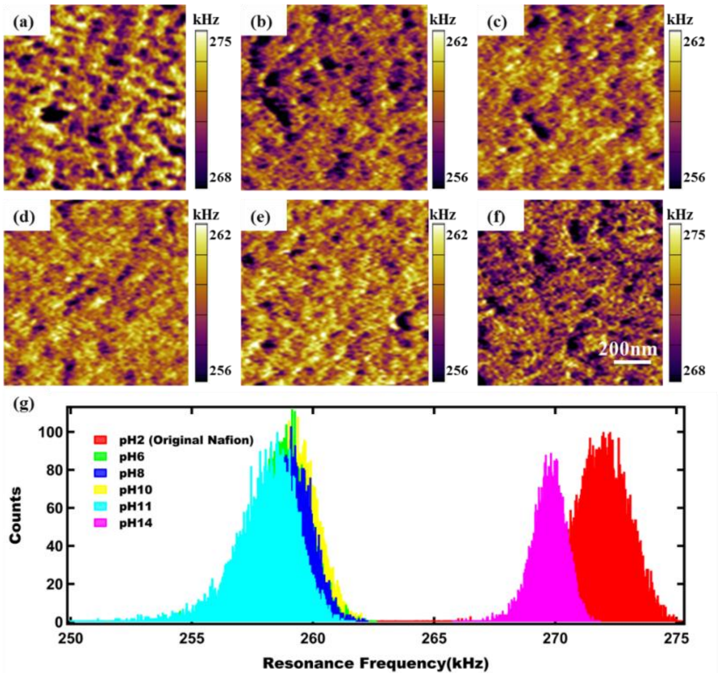

**Figure 3.** Example of the results obtained in the characterization of Nafion® thin films with dynamic AFM. The images show resonance frequency maps obtained with dual-amplitude-resonance-tracking (DART) AFM conducted on thin films prepared from: pH 2 solution (a regular Nafion® solution without base addition) (a), pH 6 solution (b), pH 8 solution (c), pH 10 solution (d), pH 11 solution (e) and pH 14 solution (f). The distribution histograms are shown in (g). The images illustrate the spatial material property variation of the films, whereby a high frequency indicates stiffer regions and vice-versa. As the histograms show, the films prepared at extreme pH values have similar mechanical properties, which differ from those prepared near neutral pH.

guidelines exist for carrying out this process rationally. The evolution of the rheological properties of Nafion® thin films was therefore studied as a function of the casting pH, via characterization with static and dynamic, contact and intermittent-contact AFM techniques. The addition of the strong base KOH caused non-monotonic changes in the viscoelastic properties of the films, which behaved as highly-dissipative, softer materials near neutral pH values, and as harder, more elastic materials at extreme pH values. This behavior was quantified through calculation of the temporal evolution of the compliance and the glassy compliance under static AFM measurements. These observations were further complemented with dynamic AFM metrics, including dissipated power and virial (for intermittent-contact-mode measurements), and contact resonance frequency and quality factor (for dynamic contact-mode measurements). Finally, the non-monotonic material property behavior was explained in terms of the degree of ionic crosslinking and moisture content of the films, which vary with the addition of KOH. This work focused on the special case study of the addition of strong bases, but the observed mechanical property changes are broadly related to water plasticizing effects and ionic cross-linking, which are also important in other types of films under varying chemical conditions. The above results can be extremely useful in the development of industrial guidelines for the conditioning of fuel cell membranes in order to reduce the occurrence of undue mechanical stresses and damage during operation. This work has been reported in [7].

## Future Plans

The final year (5th) of the project will be devoted to completing the investigations on the restoration of the percolation network in PCDTBT-based solar cells. Specifically, it is necessary to elucidate the source of the defects and the precise mechanism through which they are healed.

Additionally, work is currently in progress on the development of a nacre-mimetic polymer composite based on PEDOT:PSS and nano-clay additives, which offers the possibility of developing highly-conductive, transparent oxygen barriers for use in OPVs. Both initiatives are ideally suited for the multifrequency AFM techniques and equipment platform developed, due to the anisotropic, viscoelastic/plastic mechanical properties of the materials, as well as the interplay of these behaviors with electron transport properties..

## References

1. Ebeling, D.; Eslami, B.; Solares, S.D.; “Visualizing the subsurface of soft matter: simultaneous topographical imaging, depth modulation, and compositional mapping with triple frequency atomic force microscopy,” *ACS Nano* **2013,** *7,* 10387-10396.

2. Eslami, B.; López-Guerra, E.A.; Diaz, A.J.; Solares, S.D.; “Optimization of the excitation frequency for high probe sensitivity in single-eigenmode and bimodal tapping-mode AFM,” *Nanotechnology* **2015,** *26,* 165703.

3. Stan, G.; Solares, S.D.; Pittenger, B.; Erina, N.; Su, C.M.; “Nanoscale mechanics by tomographic contact resonance atomic force microscopy,” *Nanoscale* **2014,** *6,* 962-969.

4. Eslami, B.; Ebeling, D.; Solares, S.D.; “Trade-offs in sensitivity and sampling depth in bimodal atomic force microscopy and comparison to the trimodal case,” *Beilstein J. Nanotech.* **2014,** *5,* 1144–1151.

5. Solares, S.D; “Probing viscoelastic surfaces with bimodal tapping-mode atomic force microscopy: Underlying physics and observables for a standard linear solid model,” *Beilstein J. Nanotech.* **2014,** *5,* 1649-1663.

6. Diaz, A.J.; Eslami, B.; López-Guerra, E.A.; Solares, S.D.; “Selection of higher eigenmode amplitude Based on dissipated power and virial contrast in bimodal atomic force microscopy,” *J. Appl. Phys.* **2014,** 116, 104901.

7. Eslami, B.; Raftari, M.; López-Guerra E.A.; Solares, S.D.; “Evolution of nano-rheological properties of Nafion® thin films during pH modification by strong base treatment: A static and dynamic force spectroscopy study,” *J. Appl. Phys.* **2016,** *119,* 165301.

## Publications

1. Eslami, B.; Solares, S.D.; “Imaging of surface nanobubbles by atomic force microscopy in liquids: influence of the drive frequency on the characterization of ultra-soft matter,” *Microscopy Res. & Tech.* **2016,** online publication, DOI 10.1002/jemt.22711.

2. Eslami, B.; Raftari, M.; López-Guerra E.A.; Solares, S.D.; “Evolution of nano-rheological properties of Nafion® thin films during pH modification by strong base treatment: A static and dynamic force spectroscopy study,” *J. Appl. Phys.* **2016,** *119,* 165301.

3. Solares, S.D.; “Nanoscale effects in the characterization of viscoelastic materials with atomic force microscopy: coupling of a quasi 3-dimensional standard linear solid model with in-plane surface interactions,” *Beilstein J. Nanotech.* **2016,** *7,* 554-571.

4. Eslami, B.; Solares, S.D.; “Experimental approach for selecting the excitation frequency for maximum compositional contrast in viscous environments for piezo-driven bimodal atomic force microscopy,” *J. Appl. Phys.* **2016,** *119,* 084901.

5. Meier, T.; Eslami, B.; Solares, S.D.; “Multifrequency force microscopy using flexural and torsional modes in liquid: atomic resolution imaging of calcite (10-14),” *Nanotechnology* **2016,** *27,* 085702.

6. Solares, S.D.; “A simple and efficient quasi 3-dimensional viscoelastic model and software for simulation of tapping-mode atomic force microscopy,” *Beilstein J. Nanotech.* **2015,** *6,* 2233-2241.

7. Eslami, B.; López-Guerra, E.A.; Diaz, A.J.; Solares, S.D.; “Optimization of the excitation frequency for high probe sensitivity in single-eigenmode and bimodal tapping-mode AFM,” *Nanotechnology* **2015,** *26,* 165703.

8. López-Guerra, E.A.; Solares, S.D.; “Modeling viscoelasticity through spring-dashpot models in intermittent-contact atomic force microscopy,” *Beilstein J. Nanotech.* **2014,** *5,* 2149-2163.

9. An, S.; Solares, S.D.; Santos, S.; Ebeling, D.; “Energy transfer between eigenmodes in multimodal atomic force microscopy,” *Nanotechnology* **2014,** *25,* 475701

## Probing Correlated Phenomena in Oxide Structures with Quantitative STEM

**Susanne Stemmer, Materials Department, University of California, Santa Barbara**

### Research Scope

In this project, we combine advances in quantitative scanning transmission electron microscopy (STEM) and in oxide heterostructure engineering to establish the relationships between the atomic-scale structure and the electrical and magnetic properties of correlated oxides. The project makes use of advanced STEM-based diffraction and imaging techniques that allow for mapping of small lattice distortions and changes in the oxygen octahedral tilt patterns, with unit cell spatial resolution across interfaces and heterostructures. These are correlated with macroscopic properties that arise from strong electron correlations and coupling to the lattice, such as metal-insulator transitions and non-Fermi liquid behavior. The project also seeks to advance quantitative STEM for analysis of materials structure and defects by making use of variable angle imaging to improve contrast and interpretability, thereby contributing to the development of methods for atomic scale imaging of functional materials.

### Recent Progress

a) Development of variable-angle high-angle annular dark-field (HAADF) STEM [1]

In previous work in this project [2], we showed that quantitative HAADF-STEM can be used for complete 3D imaging of individual Gd dopant atoms in a thin foil of $SrTiO_3$ from a *single image*. In this approach, quantitative depth position information is extracted from a sufficiently thin sample using quantitative STEM, by comparing the experimental column intensities with calculations for all possible dopant configurations, and determining the most probable dopant position given an experimentally determined noise function. This method is limited by inherent experimental noise (detector noise, sample instability under the beam, sample contamination, surface amorphous layers, sample imperfections, etc.), in particular, when intensity differences between different configurations are small. One avenue of improving experimental identification of dopant atoms using quantitative STEM lies in reducing the experimental noise, for example, through the development of brighter sources or more stable environments that allow for longer exposures. However, such approaches face inherent limitations, such as beam damage.

In this project, we have developed an alternative method to improve contrast and interpretability, which we term *variable-angle HAADF-STEM* (VA-HAADF). A key feature of VA-HAADF it utilizes information provided by the angular dependence of the scattering in HAADF. This angular dependence depends on the dopant depth position. As the incident probe channels along a column, atoms deeper in the foil see a more focused probe, resulting in scattering to higher angles (more electrons travelling closer to the nucleus), relative to a dopant atom nearer to the entrance surface. Thus, by selecting certain angular ranges, different dopant atom configurations may be more easily distinguished (Fig. 1).

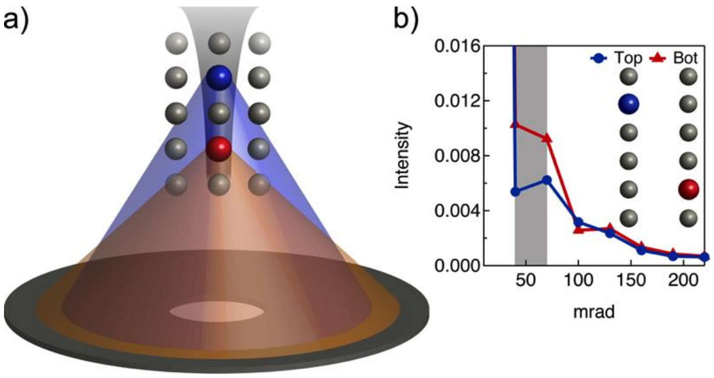

**Figure 1: Principle of VA-HAADF to accurately determine dopant depth positions.** (a) Schematic showing how beam channeling along an atomic column can result in angle-dependent scattering in STEM. Atoms further down a column "see" a more focused probe and consequently scatter more to higher angles. (b) Simulated multislice results showing scattered intensity as a function of annular detector angle (in 30 mrad segments, as exemplified by the gray box). From ref. [1].

We applied variable-angle high-angle annular dark-field (HAADF) imaging in scanning transmission electron microscopy to the precise and accurate determination of three-dimensional (3D) dopant atom configurations in Gd-doped $SrTiO_3$ films. We showed that one particular detector range is not unilaterally better than the other, but the acquisition of multiple variable angle data and use of compound probabilities significantly improved the accuracy and precision of both the number of dopants as well as the their position(s). Configurations that are ambiguous in one detector regime can be resolved in the other (Fig. 2).

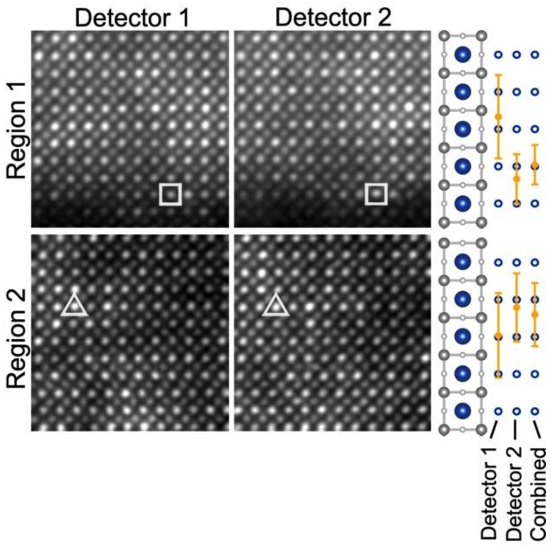

**Figure 2: Experimental analysis of Gd-doped $SrTiO_3$.** (a) HAADF STEM images of two regions containing dopant atoms in Gd-doped $SrTiO_3$ for detector 1 (left) and detector 2 (right). White squares/triangles indicate the doped column of interest. Selected dopant configurations are labeled for each detector. From ref. [1].

b) <u>Direct observation of vacancies by quantitative STEM [3]</u>

While methods to measure the global concentration of point defects exist, determining their spatial arrangement is significantly more challenging. Furthermore, most techniques cannot provide direct information about atom relaxations around a point defect even though they are crucial for the properties. As discussed above, quantitative HAADF-STEM has been used to determine the three-dimensional dopant atom configurations with unit-cell depth resolution for dopants that have a relatively large atomic number (*Z*) difference with the host crystal. Here we have combined recent advances in STEM, in particular variable angle HAADF-STEM and rigid registration methods to detect not just foreign atoms with large *Z*-contrast but also vacancies *and* their associated local atom relaxations. We demonstrate direct imaging of Sr vacancies in $SrTiO_3$ and determine the lattice relaxation around the vacancies with picometer precision. We show that rigid registration methods not only improve the precision in measurements of atom column positions but also the quantification of image intensities, as needed to detect point defects with low Z-contrast, such as vacancies. We show that the number of vacancies in each column can be quantified. Discrepancies between the measured lattice relaxations and predictions from DFT simulations underscore the need for atomic-scale experimental input in developing a microscopic understanding of how point defects control real materials properties.

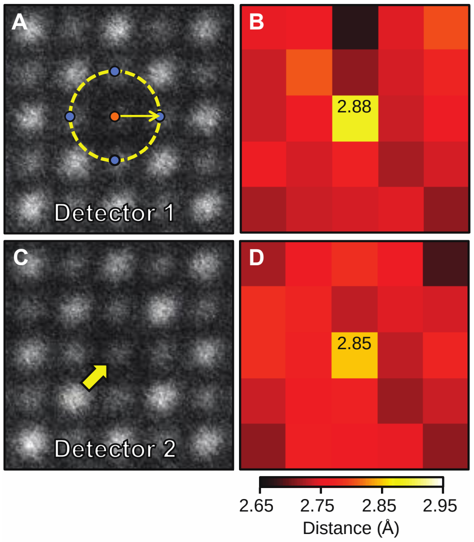

**Figure 3: Local structure relaxation around Sr vacancies.** (A, C) Magnified HAADF STEM images near a column that contains three Sr vacancies (circle and arrow). (B, D) Atomic distance maps, where each pixel value indicates the averaged distance from one cation to its four nearest neighbor unlike cations, showing Ti-O columns being displaced away from Sr vacancies. The overlay in (A) shows an example of a distance measurement from a Sr column (orange circle) to the Ti-O columns (blue circle). From ref. [1].

### c) Role of lattice symmetry in the metal-insulator transition of $NdNiO_3$ films [4]

Bulk $NdNiO_3$ exhibits a metal-to-insulator transition (MIT) as the temperature is lowered that is also seen in tensile strained films. In contrast, films that are under a large compressive strain typically remain metallic at all temperatures. To clarify the microscopic origins of this behavior, we have used PACBED in STEM to characterize strained $NdNiO_3$ films both above and below the MIT temperature. We show that a symmetry lowering structural change takes place in case of the tensile strained film, which undergoes an MIT, but is absent in the compressively strained film. Using space group symmetry arguments, we showed that these results support the bond length disproportionation model of the MIT in the rare-earth nickelates. Furthermore, the results provide insights into the non-Fermi liquid phase that is observed in films for which the MIT is absent.

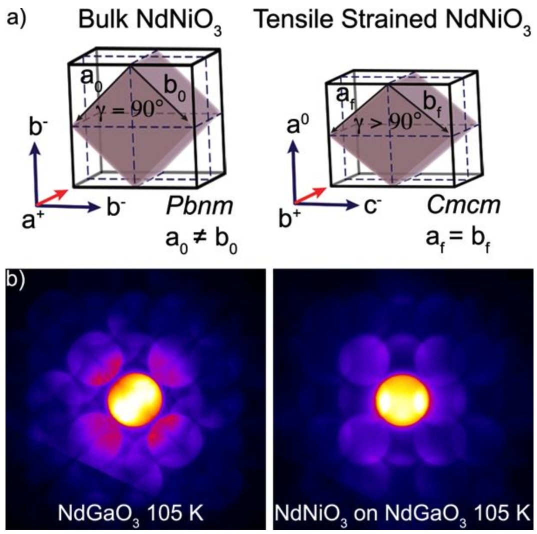

**Figure 4: PACBED can resolve small structural distortions at the metal-insulator transition of an ultra-thin film.** (a) Schematic of the expanded 2×2×2 pseudocubic unit cell for bulk $NdNiO_3$ and tensile strained $NdNiO_3$ films, showing relationships between key features in the orthorhombic lattice parameters and most probable Glazer octahedral tilts. (b) Low temperature LA-PACBED patterns from the $NdGaO_3$ substrate and $NdNiO_3$ film. While the substrate pattern is similar to its room temperature counterpart, the low temperature film displays a different symmetry from both the room temperature film and the substrate. From ref. [4].

## Future Plans

Our future plans include continuing to develop quantitative methods for 3D point defect imaging. We are particularly interested in understanding how the underlying microscopic structure determines whether a foreign atom or a vacancy acts as a dopant, which to date has only been achieved for very few point defects. We will also apply quantitative STEM techniques to understand metal-insulator transitions.

## References

[1] J. Y. Zhang, J. Hwang, B. J. Isaac, and S. Stemmer, *Variable-angle high-angle annular dark-field imaging: application to three-dimensional dopant atom profiling*, Sci. Rep. **5**, 12419 (2015).

[2] J. Hwang, J. Y. Zhang, A. J. D'Alfonso, L. J. Allen, and S. Stemmer, *Three-Dimensional Imaging of Individual Dopant Atoms in* $SrTiO_3$, Phys. Rev. Lett. 111, 266101 (2013).

[3] H. Kim, J. Y. Zhang, S. Raghavan, and S. Stemmer, *Direct observation of vacancies by quantitative scanning transmission electron microscopy***,** submitted.

[4] J. Y. Zhang, H. Kim, E. Mikheev, A. J. Hauser, and S. Stemmer, *Key role of lattice symmetry in the metal-insulator transition of* $NdNiO_3$ *films*, Sci. Rep. **6**, 23652 (2016).

**DOE Sponsored Journal Publications (2014 – 2016)**

- J. Y. Zhang, C. A. Jackson, R. Chen, S. Raghavan, P. Moetakef, L. Balents, and S. Stemmer, *Correlation between metal-insulator transitions and structural distortions in high-electron-density* $SrTiO_3$ *quantum wells*, Phys. Rev. B **89**, 075140 (2014).
- S. Stemmer and S. J. Allen, *Two-Dimensional Electron Gases at Complex Oxide Interfaces*, Ann. Rev. Mater. Res. **44**, 151-171 (2014).
- S. Raghavan, J. Y. Zhang, and S. Stemmer, *Two-dimensional electron liquid at the (111)* $SmTiO_3/SrTiO_3$ *interface*, Appl. Phys. Lett. **106**, 132104 (2015).
- J. Y. Zhang, J. Hwang, B. J. Isaac, and S. Stemmer, *Variable-angle high-angle annular dark-field imaging: application to three-dimensional dopant atom profiling*, Sci. Rep. **5**, 12419 (2015).
- S. Raghavan, T. Schumann, H. Kim, J. Y. Zhang, T. A. Cain, and S. Stemmer, *High-mobility* $BaSnO_3$ *grown by oxide molecular beam epitaxy*, APL Mater. **4**, 016106 (2016).
- E. Mikheev, S. Raghavan, J. Y. Zhang, P. B. Marshall, A. P. Kajdos, L. Balents, S. Stemmer, *Carrier density independent scattering rate in* $SrTiO_3$*-based electron liquids*, Sci. Rep. **6**, 20865 (2016).
- J. Y. Zhang, H. Kim, E. Mikheev, A. J. Hauser, and S. Stemmer, *Key role of lattice symmetry in the metal-insulator transition of* $NdNiO_3$ *films*, Sci. Rep. **6**, 23652 (2016).
- S. Raghavan, J. Y. Zhang, O. F. Shoron, and S. Stemmer, *Probing the metal-insulator transition in* $BaTiO_3$ *by electrostatic doping*, accepted, Phys. Rev. Lett. (2016).

# Exploring and Embracing Heterogeneity in Atomically Thin Energy Materials

**Peter Sutter, Dept. of Electrical & Computer Engineering, University of Nebraska-Lincoln, Lincoln, NE 68588 (psutter@unl.edu); Eli Sutter, Dept. of Mechanical & Materials Engineering, University of Nebraska-Lincoln, Lincoln, NE 68588 (esutter@unl.edu)**

## Research Scope

Atomically thin semiconductors offer extraordinary opportunities for the manipulation of charge carriers, many-body optical excitations, and non-charge based quantum numbers such as spin and valley degrees of freedom. Carrier confinement and reduced dielectric screening in these two-dimensional (2D) materials can give rise to characteristic energies large enough that many-body and quantum effects are dominant even at room temperature. Optical excitations in extended homogeneous areas of these materials have been investigated intensely. Much less understood are effects that arise in heterogeneous materials, either near naturally occurring defects, impurities, edges, and grain boundaries, or as a result of intentional alloying and interface formation.

Probing such systems experimentally involves significant challenges: *Understanding atomistic growth mechanisms* of 2D materials, so that systems with specific "imperfections" and controlled interfaces can be realized; and *detecting local excitations* at scales that match the relevant (nanometer) length scales in heterogeneous materials (Fig. 1). In this research program, we address these challenges by using novel platforms for quantitative *in-situ* microscopy of the growth of 2D materials and heterostructures, combined with local spectroscopic measurements of quasiparticles excited at the nanometer scale. Experiments are guided and analyzed *via* computations of the structure, chemistry, and excitation spectra of defects and interfaces. The program focuses on three distinct classes of materials: Graphene-hexagonal boron nitride alloys, interesting for realizing tunable bandgaps and novel excitonic effects; transition metal dichalcogenides and heterostructures, for which fundamental materials synthesis processes, the behavior of optically excited quasiparticles near defects, and their manipulation near interfaces are being investigated; and

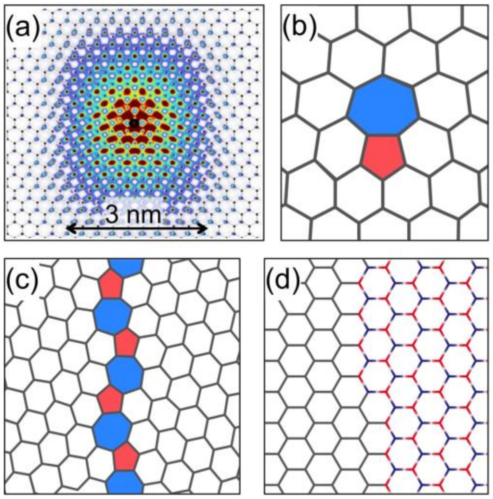

**Figure 1. Nanometer-scale heterogeneity affecting electronic excitations in 2D materials. (a)** Modulus squared of the real-space wave function of the A-exciton in single-layer $MoS_2$. After Qiu et al., Phys. Rev. Lett. 111, 216805 (2013). **(b)** Dislocation in a (projected) honeycomb lattice. **(c)** Grain boundary. **(d)** In-plane heterojunction.

group IV chalcogenides, a largely unexplored family of 2D materials promising for energy conversion processes.

The defining characteristics of the chosen technical approach are: (i) A *focus on powerful in-situ methods* to understand and direct the synthesis of 2D materials; and (ii) the *probing of optical excitations* near natural or engineered heterogeneities in 2D materials *at the nanometer scale*. The strategy for controlling growth, interface formation and associated properties (structure, composition, defects) in 2D materials involves an *in-situ* platform that integrates low-energy electron microscopy (LEEM) with UHV scanning tunneling microscopy (STM) to achieve real-time microscopy at the mesoscale combined with atomic-resolution imaging/ spectroscopy on the same samples transferred *in-situ*. To extend the real-time imaging capabilities of LEEM to the atomic level, e.g., for imaging edge-flow growth, defect generation, *etc.*, we are developing a novel *in-situ* platform that translates the functionality of widely used tube furnaces to a miniaturized setup suitable for high-resolution transmission electron microscopy (TEM). The optoelectronic properties of heterogeneous 2D materials are probed by scanning TEM-cathodoluminescence (STEM-CL), in which a tightly focused (~1 nm) electron beam replaces a laser as an excitation source (Fig. 2). The exciting beam can be positioned with nanometer precision for local spectroscopy or scanned to generate high-resolution luminescence maps. In this way, the optoelectronic properties of heterogeneous samples can be correlated with the local structure and composition determined by analytical (S)TEM.

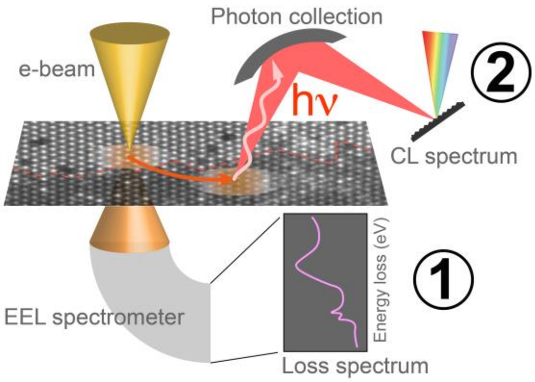

**Figure 2. Nanometer-scale optical spectroscopy in STEM. (1)** Absorption measurement by EEL spectroscopy in monochromated STEM. After Tizei et al., Phys. Rev. Lett. 114, 107601 (2015). **(2)** Locally excited cathodoluminescence (CL) spectroscopy, which is the focus of this program.

The fundamental research carried out within this program promises impact in several areas. Insight into the interaction of optical excitations with short-range atomic motifs in alloys and near defects has the potential to uncover novel many-body physics in atomically thin materials and can form the basis for creating robust technologies that harness the inherent imperfections of real-world materials. The manipulation of excited electronic states near interfaces addresses the Grand Challenge of controlling materials processes at the level of electrons, and can enable novel approaches to energy conversion and quantum information processing. And finally, the development of novel experimental methodologies, e.g., for atomistic observations of growth processes in complex environments, has the potential to cause a paradigm shift in research on synthesis and processing of 2D and nanoscale materials.

# High Precision STEM Imaging: Improved Data Quality, Imaging Vacancies

**Paul M. Voyles and Dane Morgan, Department of Materials Science and Engineering, University of Wisconsin-Madison**

## Research Scope

The goals of this project are to improve the quantitative reliability of STEM data and to use that data to characterize point defects in crystals. Our approach to improved data is to use adapt techniques from image science and data science specifically to STEM data and apply them to state-of-the-art quantitative experiments. The low-noise, low-distortion, quantitatively reliably data can then be compared rigorously to simulations from atomic structures derived from density functional theory. The focus of our experimental work has been on imaging La single vacancies is $LaMnO_3$.

## Recent Progress

### Limits to Precision at Coarse Pixel Sampling

Our previous high precision STEM imaging used high magnification and extremely high electron dose of 10-15 pm/pixel and 80,000-160,000 C/cm$^2$ [1]. These parameters are acceptable only for materials that are very robust under the electron beam. To reduce the dose, we can reduce the probe current or the dwell time per pixel, or we can increase the pixel size. The pixel size is the easiest parameter to change and has the added advantage of increasing the field of view. Figure 1 shows an image of a gold nanoparticle acquired with 64 pm pixels, so each atomic column is covered by just 4×4 pixels. However, the image still has precision of 2 pm in repeated measurements of interatomic spacings in the interior of the particle demonstrates precision. The image in Figure 1 was acquired at 100 times less dose that the initial high precision results.

### Non-local Denoising

Achieving high precision at even lower dose is likely to require denoising. Familiar denoising approaches in microscopy combine the intensity of pixels close to one another in the image to reduce noise, using, for example a convolution filter. However, we can take advantage of redundancy in the image by combining groups of pixels based on whether or not they contain similar patterns of intensity [2]. Such non-local denoising approaches first break an image up into small patches, then denoised them based on their similarity to one another.

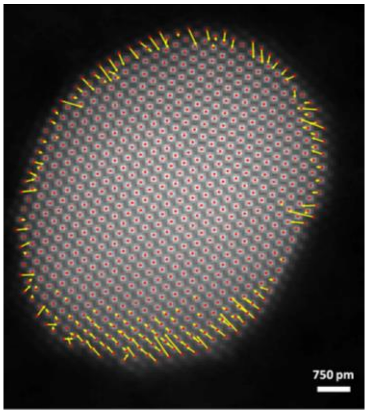

Figure 1: High precision STEM image of a gold nanoparticle with coarse pixel sampling

With Benjamin Berkels, we adapted one of the leading non-local denoising algorithms, the block-matching and 3D filtering

(BM3D) algorithm [3] to EM images [C] by implementing a similarity measure appropriate for data dominated by Poisson noise and by developing an adaptive periodic search for matching blocks within the image. Figure 2 shows the results of denoising simulated STEM data using BM3D. Figure 2(a) is a multislice simulated image of a dislocation core in Si [110]. Figures 2(b) and (c) are the same image, corrupted by Poisson noise. Figure 2(d) is the denoised image of (b) and (e) is the denoised version of (c). For the moderate noise level of (b), the denoised version is virtually indistinguishable from the original. For the high-noise version of (c), the denoised version still recovers all of the Si dumbbells, including the near the aperiodic dislocation. Working with simulated data for which all the true pixels values are known enabled quantitative determination of the optimal parameters for our adapted BM3D, tracking of precision in denoised images, and demonstration that our BM3D outperforms competing algorithms [C].

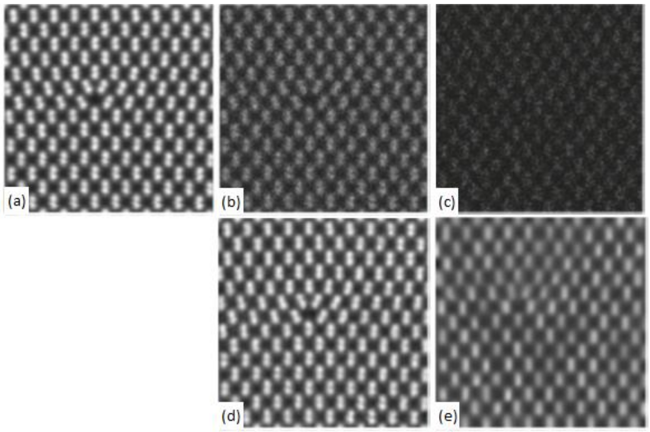

Figure 2: Denoising of simulated Z-contrast images using adapted BM3D. (a) a noiseless simulated STEM image. (b) moderate Poisson noise added to (a). (c) High noise added to (a). (d) and (e), images (b) and (c) respectively, denoised using Poisson BM3D.

STEM spectrum images, especially STEM EDS at atomic resolution, have even lower signal than Z-contrast STEM images, so we have combined non-rigid registration and non-local denoising to significant improve the data quality [B]. We acquired a series of 100 STEM EDS spectrum images of Ca-doped $NdTiO_3$ with simultaneous Z-contrast images. Then we registered the Z-contrast images and applied the shifts to every energy channel of the spectra. The result was significantly better in terms of peak signal and contrast in elemental maps than conventional drift correction using a reference area. Then, we applied non-local principle component analysis (NLPCA) denoising in collaboration with the method developer Rebecca Willett [4]. NLPCA produced higher signal to noise ratio with fewer artifacts than conventional weighted PCA and BM3D applied to the same data [B].

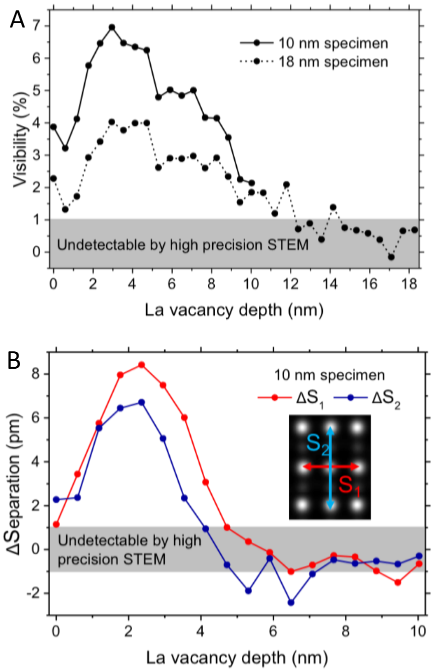

Figure 3: Simulated visibility and surrounding atomic column distortions for a La vacancy in $LaMnO_3$ as a function of the vacancy depth in the STEM

## Imaging Single Vacancies with High-Precision STEM

We have combined high precision STEM imaging and simulations to image single La vacancies in $LaMnO_3$.

Figure 3(a) shows the visibility of a single La vacancy as a function of depth derived from multislice simulations from a DFT-relaxed vacancy structure. The low noise of high-precision STEM images makes changes in intensity of just a few percent detectable, so a single vacancy is visible at any depth in a 10 nm thick sample. Figure 3(b) shows the distortion of the neighboring La atomic columns in the simulated image, which is detectable for high-precision STEM if the vacancy is near the entrance surface of the sample. The 3D motion of the nearest La atoms to the vacancy is much larger, up to 20 pm, but only a fraction of that displacement survives in the 2D projection of the STEM image. The ability to identify a vacancy from both the visibility and the lattice distortion enables us to distinguish surface vacancies from vacancies in the bulk.

Figure 4 shows examples taken from experimental high-precision STEM images of a $LaMnO_3$ thin film, with the measured column visibility and the distortions of the surrounding columns. For each example, the experimental values are compared to simulations from a sample with the same thickness. Figure 4(a) has a visibility consistent with a vacancy between 1 and 5 nm deep. The distortions, however, are consistent only with the entrance surface and a depth of 3 to 4.5 nm. By combining all the measurements and simulations, with estimates of their uncertainties, in a Bayesian statistical model, we derive the probability that the column contains a single vacancy as a function of depth. For Figure 4(a), the probability is strongly peaked at a depth 3.5 nm, localizing the vacancy to one or two atomic sites. Figure 4(b) and (c) show similar data for a surface vacancy and a column containing no vacancy.

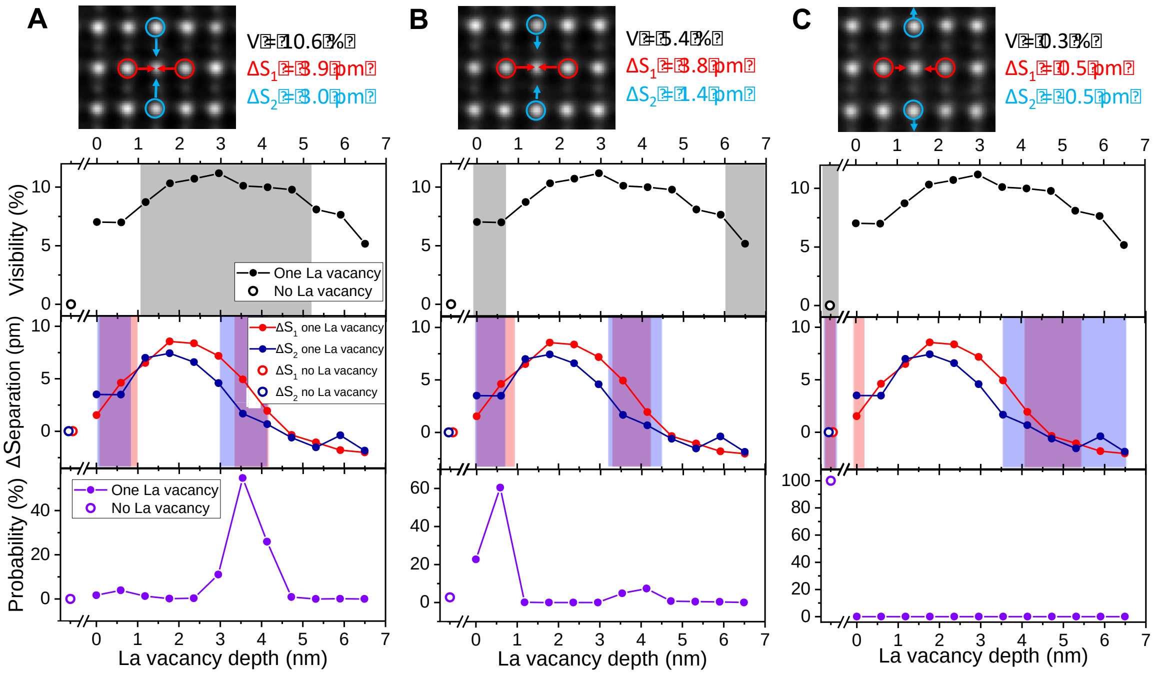

Figure 4: Experimental images of $LaMnO_3$ showing (a) a vacancy inside the sample, (b) a vacancy on the sample surface, and (c) a region containing no vacancy. For each image, the measured visibility and displacements are compared to simulations for the same sample thickness, then combined to obtain the probability that a vacancy exists at a particular depth.

Analysis of 358 La columns in several images found 35 isolated La vacancies randomly distributed in the film. A 0.78% concentration of vacancies in a thin film is difficult to independently confirm, but it is consistent with the expected composition control during the thin film growth. These results represent the first atomic-resolution imaging of a vacancy in a bulk crystal.

## Future Plans

We will complete work La vacancies in $LaMnO_3$, then extend similar methods to study cation-anion vacancy clusters in $LaMnO_3$ and $(La,Sr)MnO_3$ that may be involved in limiting oxygen transport. Then, we will extend our approach to other cation vacancies in other perovskites and begin exploring approaches to image single oxygen vacancies.

We will seek further improvements in STEM data at lower dose by combining denoising, registration, and atom finding in a single step, rather than our current sequential. The combined approach makes use of the maximum amount of information directly, which may yield better results and better scaling behavior with the number of images at low dose.

## References

[1] A. B. Yankovich, B. Berkels, W. Dahmen, P. Binev, S. I. Sanchez, S. a. Bradley, A. Li, I. Szlufarska, and P. M. Voyles, Nat. Commun. **5**, 4155 (2014).
[2] A. Buades, B. Coll, and J.-M. Morel, 2005 IEEE Comput. Soc. Conf. Comput. Vis. Pattern Recognit. **2**, 60 (2005).
[3] K. Dabov, A. Foi, V. Katkovnik, and K. Egiazarian, in *Image Process. Algorithms Syst. Neural Networks, Mach. Learn.*, edited by E. R. Dougherty, J. T. Astola, K. O. Egiazarian, N. M. Nasrabadi, and S. A. Rizvi (Proc. of SPIE-IS&T Electronic Imaging, SPIE Vol. 6064, 2006), p. 606414.
[4] J. Salmon, Z. Harmany, C.-A. Deledalle, and R. Willett, (2012).

## Publications

A. “Informatics and Data Science in Materials Microscopy”, Paul M. Voyles (submitted)
B. “Non-rigid registration and non-local principal component analysis to improve electron microscopy spectrum images” Andrew B. Yankovich, Chenyu Zhang, Albert Oh, Thomas J. A. Slater, Feridoon Azough, Robert Freer, Sarah J. Haigh, Rebecca Willet, and Paul M Voyles Nanotechnology **27**, 364001 (2016).
C. “Poisson Denoising High-Resolution Electron Micrographs based on periodic Block-matching” Niklas Mevenkamp, Peter Binev, Wolfgang Dahmen, Paul M. Voyles, Andrew B. Yankovich and Benjamin Berkels, Advanced Structural and Chemical Imaging **1**, 3 (2015). DOI: 10.1186/s40679-015-0004-8
D. “High-precision scanning transmission electron microscopy at coarse pixel sampling” Andrew B. Yankovich, Benjamin Berkels, W. Dahmen, P. Binev, and Paul M. Voyles Advanced Chemical and Structural Imaging **1**, 2 (2015). DOI: 10.1186/s40679-015-0003-9

# Visualizing emergent phenomena in topological and quantum materials

Weida Wu
*Department of Physics and Astronomy, Rutgers University, Piscataway, NJ, 08854*

## Research Scope

The objective of this project is to explore the emergent topological phenomena and to understand the unconventional properties of topological and correlated materials such as quantum anomalous Hall (QAHE) systems and multiferroics. The giant magnetoelectric effect due to coupled ferroic orders in multiferroics is of both fundamental and technological interest, and is promising for energy-efficient multifunctional applications. The presence of domains and domain walls is a distinguishing feature of any ferroic order; their responses to external stimuli determine the macroscopic properties and the functionalities of ferroic materials, including magnetic topological insulators, where quantum Hall transition is coupled to magnetization reversal. To address the challenges and to directly visualize the cross-coupled phenomena and their responses to the applied electric and magnetic fields, the PI proposed and developed unique SPM techniques, e.g. magnetoelectric force microscopy (MeFM). The real space imaging of domains and domain walls shed new light on fundamental understanding of the nature of cross-coupling in multiferroic and topological materials.

## Recent Progress

- **Instrumentation development**
  - *Development of ultra-low temperature MFM with Akiyama probe*

The PI's variable temperature magnetic force microscopy (VT-MFM) system was a power magnetic imaging tool that produced many high impact results in the last few years. However, many interesting phenomena such as topological superconductivity, quantum anomalous Hall effect, quantum critical phenomena, etc., cannot be studied by the PI's MFM due to base temperature limit (~2.8 K), which is due to the Joule heating of the integrated piezo-resistive element for sensing cantilever deflection. To address this issue, a graduate student in the PI's group is investigating a new type self-sensing cantilever, called Akiyama probe (A-probe), where a silicon cantilever is glued to the end of a Quartz tuning fork to form coupled harmonic oscillators[1]. Both cantilever actuation and deflection detection are accomplished via the Quartz sensor, thus it further simplifies the mechanical structure of AFM head. More importantly, the power consumption of Quartz tuning fork sensor is of the order of nW, much less than that of piezo-resistive sensors (~mW), which opens up possibility of ultra-

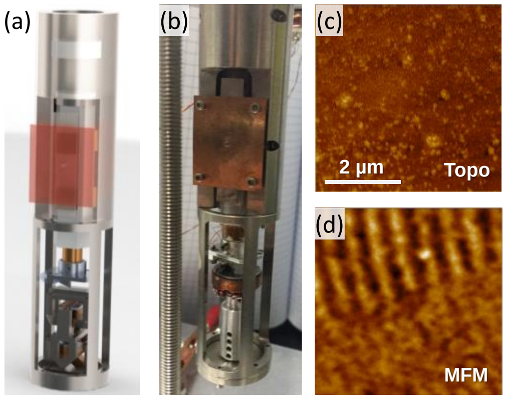

**Figure 1** | (a) A 3D rendering of ULT-MFM scanner head with both z-walker (top) and xy-walker (bottom). (b) A photo of a homemade AFM (without xy-walker) for testing the performance of A-probe at ambient condition. (c)/(d) Preliminary AFM/MFM image of the same location taken with an A-probe on a magnetic tape sample.

low temperature (mK) operation. A homemade amplifier circuit was developed for driving and sensing the Akiyama probes. New AFM head for ultra-T application has been designed, as shown in Fig.1(a). A simplified version (without xy-walker) has been constructed for testing the AFM and MFM performance of A-probe. A photo of the test AFM head is shown in Fig. 1(b). Preliminary results of at room temperature are very promising. As shown in Fig.1(c) and (d), decent topographic and magnetic images of the same location on a magnetic tape test sample (Bruker) are obtained with an A-probe coated with Co films. The stripes in MFM image are the recorded bits of the tape sample. These results demonstrate that it is feasible to use A-probe for MFM measurements. The next step will be to test the AFM and MFM operation of A-probe in cryogenic environment. It is straightforward to perform such tests because the design of test scanner head is compatible with the PI's cryogenic MFM probe. With further optimization and testing, the PI expects to achieve high quality MFM imaging with A-probe in cryogenic environment, and ultimately, in ultra-low temperature.

- *Quantitative lateral Piezo-response Force Microscopy (L-PFM)*

The PI's previous work on using background-free PFM setup allows quantitative vertical PFM measurements with high sensitivity[2]. The PI's group continues to develop new approach to improve the functionality of PFM. Our recent effort is to calibrate lateral piezoelectric response in PFM setup. The key point is to simultaneously detect both torsional and buckling motions of atomic force microscopy (AFM) cantilevers induced by the lateral piezoelectric response of the sample. This requires the quantitative calibration of torsional and buckling response of AFM. This method is validated by measuring the angular dependence of the in-plane piezoelectric response of a piece of piezoelectric a-quartz. The accurate determination of the amplitude and orientation of the in-plane piezoelectric response, without rotation, would greatly enhance the efficiency of lateral piezoelectric force microscopy. This result was published in APL early this year[i].

- **Scientific accomplishments**

  - Magnetoelectric response in hexagonal manganites and ferrites

As planned, the PI's group continued MeFM studies of local magnetoelectric (ME) response in hexagonal manganites. Giant ME response was observed on hexagonal $YbMnO_3$. Comparing with the PI's previous work on $ErMnO_3$ (published in Nature Mater. 2014)[3], the ME response in $YbMnO_3$ show qualitatively similar temperature dependence, but different field dependence, which helps to separate the ME contributions from Mn spins and RE moments. A manuscript on the new results and a deeper understanding of ME effect is being prepared in collaboration with M. Mostovoy at Groningen.

In collaboration with D. Schlom (Cornell), the PI's group is investigating magnetic and ME properties of MBE thin films of hexagonal $LuFeO_3$, a system related to hexagaonl mangnites. Recent theory predicts that $LuFeO_3$ might host strong ME coupling without applied magnetic field. The PI's group has obtained beautiful magnetic images of weak-ferromagnetic domains in $LuFeO_3$ thin films. Preliminary MFM results are in good agreement with transport measurements in literature[4]. A manuscript that summarizes these results is in preparation.

- Magnetic imaging of ferromagnetic domains in quantum anomalous Hall systems

Topological insulators (TI) are a new quantum state of matter where an insulating bulk state is surrounded by conducting surface states because of topological properties of twisted electronic band structure. The topological twist originates from strong spin-orbit coupling combined with time reversal symmetry. Breaking time reversal symmetry would result in quantum anomalous hall effect (QAHE), which was observed in ferromagnetic Cr doped $(Bi,Sb)_2Te_3$ (BST) thin films[5]. However, there is no report of magnetic domain structure of magnetic TIs despite of many follow-up studies. The PI's group has performed MFM studies of both single crystals and MBE thin films of Cr doped TIs. A manuscript on this work has been published in APL materials (2015)[ii]. The typical domain size in single crystals is order of microns, while in thin films the domain size is order of few hundreds of nm.

The QAH state is very fragile in the Cr doped BST thin films, where quantized Hall conductance was observed at mK temperature. Recently the PI is collaborating with Prof. Moodera's group at MIT on V doped BST thin films where robust QAHE effect was discovered[6]. A systematic MFM study of domain behavior in thin films of the magnetic topological insulator V doped $Sb_2Te_3$ revealed that in the virgin domain state, after zero-field cooling, an equal population of up and down domains occurs. Interestingly, the cooling field dependence of MFM images (shown in Fig. 2) demonstrates that small cooling magnetic field (~5-10 Oe) is sufficient to significantly polarize the film despite the coercive field ($H_C$) for these films being on the order of a tesla at low temperature. By visualizing the magnetization reversal process around $H_C$ of V-doped $Sb_2Te_3$, we observed a typical domain behavior of a ferromagnet, i.e. domain nucleation and domain wall propagation. Our results provide direct evidence of ferromagnetic behavior of the magnetic topological insulator, a necessary condition for robust quantum anomalous Hall effect. The manuscript is in 2nd round of review (minor revision) in NPJ Quantum Materials[iii].

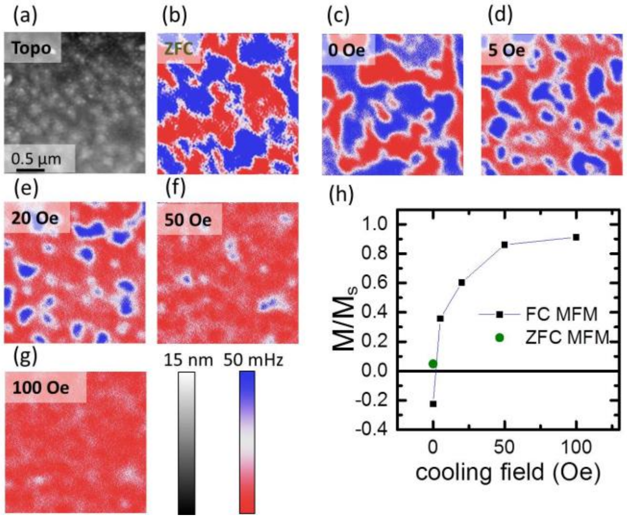

**Figure 2 |** Topographic (a) and MFM image (b) measured at 5 K after ZFC. The equal population of up (red) and down (blue) domains indicates a zero-magnetization virgin domain state. (c)-(g) MFM images (5 K) of FC domain states with cooling fields ranging from 0 Oe to 100 Oe. The cooling field values are labeled at the upper-left corner of each MFM image. The color scale is 15 nm (50 mHz) for topographic (MFM) image(s), and 20 mHz for the ZFC MFM image (b). (h) Cooling field dependence of net magnetization of various domain states inferred from MFM images using a histogram analysis of MFM images. The trapped flux in the superconducting magnet is estimated to be ~3Oe.

## Future Plans

MeFM studies of hexagonal manganites and ferrites and heterostructures

The PI will continue to improve the sensitivity our unique MeFM technique for visualizing mesoscopic magnetoelectric coupling of domains or domain walls in either single-phase mulitferroics (e.g. *hex-RE*$MnO_3$, *hex-RE*$FeO_3$) and magnetoelectrics (e.g. $DyFeO_3$), or heterostructural thin films where interfacial strain or exchange bias provide the cross-coupling.

Systematic studies of magnetoelectric effect in hexagonal manganites would shed new light on the fundamental mechanism of magnetoelectric response in hexagonal systems. In collaboration with D. Schlom at Cornell, the PI's group is investigating weak-ferromagnetic domain structure and magnetoelectric effect in hexagonal ferrite (e.g. $LuFeO_3$) MBE thin films.

Magnetic imaging of QAH systems and chiral edge states

The PI will investigate ferromagnetic domain behaviors in magnetic TIs, using VT-MFM with *in situ* high magnetic/electric field capabilities. The ultimate goal is to visualize one-way conduction of chiral edge states in these fascinating systems.

Background-Free PFM on new piezoelectric materials

The PI will continue to optimize background-free PFM setup for quantitative piezoelectric responses, both out-of-plane and in-plane PFM measurements. A used multi-mode AFM was acquired for dedicate PFM measurements and general surface characterization. Background-free PFM will be applied to other novel ferroelectric or piezoelectric materials to study their domain structure and piezoelectric properties.

Design and development of ULT-AFM based on Akiyama probe

The PI will design new LT-AFM head with Akiyama probe for ultra-low temperature operation. Once the new LT-AFM is constructed, it will be combined with the advanced SPECS SPM controller for multimodal operations at extreme conditions.

## References

1 Akiyama, T. *et al.* Implementation and characterization of a quartz tuning fork based probe consisted of discrete resonators for dynamic mode atomic force microscopy. *Rev Sci Instrum* **81**, 063706, (2010).

2 Wang, W., Geng, Y. & Wu, W. Background-free Piezoresponse Force Microscopy for quantitative measurements. *Appl. Phys. Lett.* **104**, 072905, (2014).

3 Geng, Y. *et al.* Direct visualization of magnetoelectric domains. *Nat. Mater.* **13**, 163-167, (2014).

4 Moyer, J. A. *et al.* Intrinsic magnetic properties of hexagonal $LuFeO_3$ and the effects of nonstoichiometry. *APL Materials* **2**, 012106, (2014).

5 Chang, C.-Z. *et al.* Experimental Observation of the Quantum Anomalous Hall Effect in a Magnetic Topological Insulator. *Science* **340**, 167-170, (2013).

6 Chang, C. Z. *et al.* High-precision realization of robust quantum anomalous Hall state in a hard ferromagnetic topological insulator. *Nat Mater* **14**, 473-477, (2015).

## Publications supported by BES

[i] Wenbo Wang, Ying Sun, Yonggang Zhao and Weida Wu, "Quantitative measurements of shear displacement using atomic force microscopy", Appl. Phys. Lett., **108**, 122901 (2016).

[ii] Wenbo Wang, Fang Yang, Chunlei Gao, Jinfeng Jia, G. D. Gu, and Weida Wu, "Visualizing ferromagnetic domains in magnetic topological insulators", APL Materials, **3**, 083301 (2015).

[iii] Wenbo Wang, Cui-Zu Chang, Jagadeesh S. Moodera, and Weida Wu, "Visualizing ferromagnetic domain behaviors of V-doped $Sb_2Te_3$ thin films", under review in NPJ Quantum Materials, (2016).

## Transport and Imaging of Mesoscopic Phenomena in Novel Low-Dimensional Materials

**Yacoby, Amir - Harvard University, yacoby@physics.harvard.edu**
**Jarillo-Herrero, Pablo – MIT, pjarillo@mit.edu**

### Project Scope

The recent invention of simple techniques to produce highly ordered macroscopic films of graphene—a two-dimensional sheet of carbon atoms arranged in a honeycomb lattice—and the remarkable series of discoveries that followed, from anomalous quantum Hall effect to proximity-induced superconductivity, marks the advent of a new era of carbon-based electronics. Moreover, graphene just constitutes the first example of a large family of two-dimensional materials that can be mechanically assembled to form van der Waals heterostructures, the most famous example being those formed by graphene and hexagonal boron nitride (hBN).

Several features make graphene of interest for exploring new physical effects. Its electronic spectrum for example is best described by ultra-relativistic dynamics. Unlike photons or neutrinos however, the electrons in graphene are charged and posses not only spin, but also pseudospin and valley degrees of freedom that lead to novel new physics that remains largely unexplored. This includes the fractional quantum Hall effect, chiral spin currents at the boundaries and more. Furthermore, the tunability of carrier density in graphene and the ease by which it may be contacted opens up new possibilities for exploring phenomena that rely on the coexistence of electrons and holes as well as controlling superconductivity, quantum Hall physics, magnetism, and the interface between all them. In addition, by controllably stacking different 2D materials, such as graphene, hBN, or transition metal dichalcogenides (TMDs), novel heterostructures and devices which exhibit equally remarkable electronic structures can be nanofabricated, where all these phenomena can be further explored.

Our focus in this proposal is to use innovative methods to fabricate ultra-low disorder graphene and other novel 2D materials devices, in conjunction with ultra sensitive scan probe, local tunneling, and capacitance methods, as well as low-temperature electronic transport techniques in order to explore new and spatially varying mesoscopic phenomena in graphene and TMD devices and heterostructures. Our research focuses on transport and current flow imaging of ultra-high mobility graphene; induced superconductivity and Andreev tunneling spectroscopy in graphene; proximity effect between superconductivity and quantum Hall physics; transport and imaging of graphene in inhomogeneous electric and magnetic fields; compressibility in TMD and graphene using capacitance and gateable scanning SET's; and imaging the electronic and spin transport properties of graphene using scanning diamond NV centers.

### Recent Progress

#### Spatially resolved edge currents and guided-wave electronic states in graphene

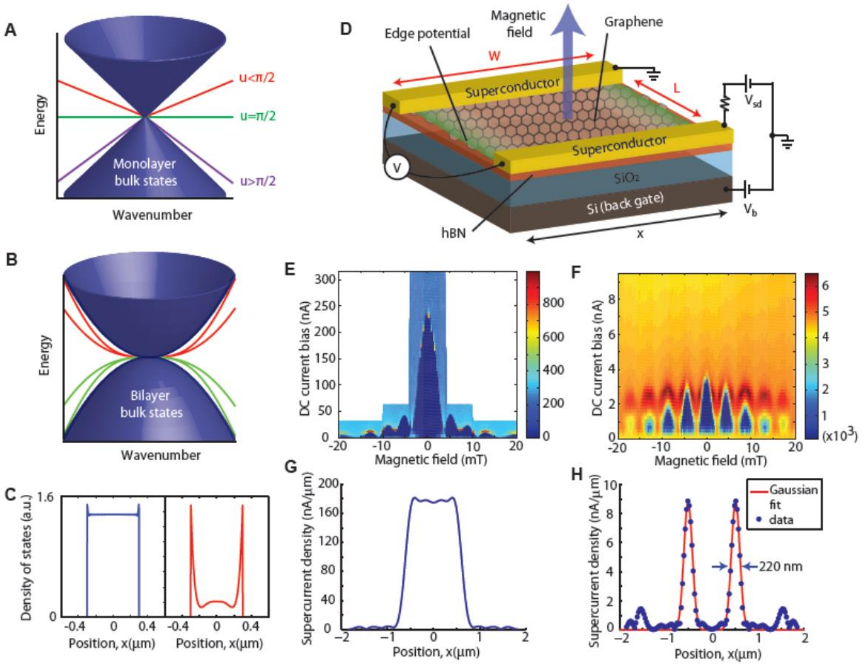

Fig. 1. ‘Fiber-optic’ modes and spatially resolved current imaging in a graphene Josephson junction. (A, B) Guided edge modes induced by an intrinsic band bending near crystal boundary, for single-layer and bilayer graphene (schematic). Guided modes exist for any edge potential no matter how weak. (C) The guided modes are manifested through peaks in the density of current-carrying states at the crystal boundaries, prominent near charge neutrality (red: $n = 0.05 \times 10^{11}$cm−2 ; blue: $n = 2.5 \times 10^{11}$cm−2 ). (D) Schematics of superconducting interferometry in a graphene Josephson junction, which is used to image the spatial structure of current-carrying states. (E, F) The recorded interference pattern is of a single-slit Fraunhofer type at high carrier density, turning into a SQUID-like interference near neutrality (colorscale is dV/dI (Ω)). (G, H) Current flow, extracted from the interference data using Fourier techniques, is uniform at high carrier density and peaks at the crystal edges for carrier density close to neutrality.

A far-reaching goal of graphene research is exploiting the unique properties of carriers to realize extreme nonclassical electronic transport. Of particular interest is harnessing wavelike carriers to guide and direct them on submicron scales, similar to light in optical fibers. Such modes, while long anticipated, have never been demonstrated experimentally. In order to explore this behavior, we employ superconducting interferometry in a graphene Josephson junction to reconstruct the real-space supercurrent density using Fourier methods. Our measurements reveal charge flow guided along crystal boundaries close to charge neutrality. We interpret the observed edge currents in terms of guided-wave states, confined to the edge by band bending and transmitted as plane waves. As a direct analog of refraction based confinement of light in optical fibers, such non-classical states afford new means for information transduction and processing at the nanoscale.

## Visualization of phase-coherent electron interference in a ballistic graphene Josephson junction

Interference of standing waves in electromagnetic resonators forms the basis of many technologies, from telecommunications and spectroscopy to detection of gravitational waves. However, unlike the confinement of light waves in vacuum, the interference of electronic waves in solids is complicated by boundary properties of the crystal, notably leading to electron guiding by atomic-scale potentials at the edges [1-4]. Understanding the microscopic role of boundaries on coherent wave interference is an unresolved question due to the challenge of detecting charge flow with submicron resolution. Here we employ Fraunhofer interferometry to achieve real-space imaging of cavity modes in a graphene Fabry-Perot (FP) resonator, embedded between two superconductors to form a Josephson junction [5]. By directly visualizing current flow using Fourier methods [6], our measurements reveal surprising redistribution of current on and off resonance. These findings provide direct evidence of separate interference conditions for edge and bulk currents and reveal the ballistic nature of guided edge states. Beyond equilibrium, our measurements show strong modulation of the multiple Andreev reflection amplitude on an off resonance, a direct measure of the gate-tunable change of cavity transparency. These results demonstrate that, contrary to the common belief, electron interactions with realistic disordered edges facilitate electron wave interference and ballistic transport.

### Tunneling spectroscopy of Andreev states in graphene

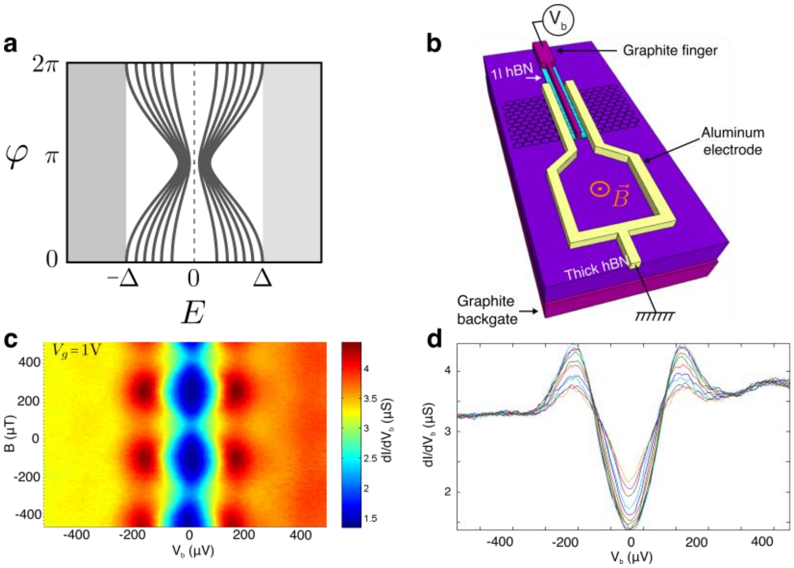

Figure 3. Andreev spectroscopy of graphene-hBN heterostructure. a. Graphical illustration (not simulation) of Andreev bound states in a short junction with multiple conductance channels. At zero phase ($\varphi = 0$), lower energy ABS detach from the gap edge due to imperfect coupling to superconductor. b. Schematic of a Van der Waals heterostructure fabricated for ABS spectroscopy. c. Color plot of differential conductance ($dI/dV$) with respect to bias voltage ($V_b$) and magnetic field ($B$) at constant gate voltage. The soft-BCS gap in graphene oscillates at a periodicity corresponding to threading one magnetic flux through the SQUID. d. $dI/dV$ traces taken at different magnetic fields spanning over half of a period. Each trace exhibits a soft BCS gap, of which $dI/dV$ oscillates out of phase between at the center and at two peaks. Measurements depicted in c and d suggest that the gap is populated with a number of ABS that couple differently to superconductors.

A normal conductor placed in good contact with a superconductor can inherit its electronic properties. This proximity effect originates from the formation in the conductor of entangled electron-hole states, called Andreev states. Spectroscopic studies of Andreev states have been performed in just a handful of systems. With its large mobility, ease of access and electrostatically tunable carrier density, graphene provides a novel platform for studying Andreev physics in two dimensions. Using a full van der Waals heterostructure, we have performed a direct tunnelling spectroscopy of proximitized graphene. The measured energy spectra, which depend on the phase difference between the superconductors and on graphene carrier density, evidence a continuum of Andreev bound states with energies smaller than the superconducting gap. Notably, out of gap modulations are also observed and could be related to the long-predicted Andreev scattering states [7,8,9,10]. This work opens up new avenues for probing exotic phase of matter in hybrid superconducting Dirac materials.

## Future Plans

Our research effort for the next years will focus on the following topics:
1. Transport and imaging of ultra-high mobility in hBN encapsulated single and few layer graphene.
2. Induced superconductivity and Andreev bound states spectroscopy in single layer, bilayer and twisted

few layer graphene van der Waals heterostructures.
3. Proximity effect between superconductivity and quantum Hall, quantum spin Hall and fractional quantum Hall physics.
4. Engineering topological phases in graphene by tuning electron-electron interactions. Such phases include quantum spin Hall and non-Abelian fractional quantum Hall states.
5. Study superconductivity in the ultra-thin limit in novel transition metal dichalcogenides van der Waals heterostructures.

## References

1. Pereira, J. M., Mlinar, V., Peeters, F. M. & Vasilopoulos, P. Confined states and direction-dependent transmission in graphene quantum wells. *Phys. Rev. B* **74**, 045424 (2006).
2. Zhang, F.-M., He, Y. & Chen, X. Guided modes in graphene waveguides. Applied Physics Letters **94** (2009).
3. Hartmann, R. R., Robinson, N. J. & Portnoi, M. E. Smooth electron waveguides in graphene. *Phys. Rev. B* **81**, 245431 (2010).
4. Williams, J. R., Low, T., Lundstrom, M. S. & Marcus, C. M. Gate-controlled guiding of electrons in graphene. *Nat. Nanotech*. **6**, 222–225 (2011).
5. Heersche, H. B., Jarillo-Herrero, P., Oostinga, J. B., Vandersypen, L. M. K. & Morpurgo, A. F. Bipolar supercurrent in graphene. *Nature* **446**, 56–59 (2007).
6. Dynes, R. C. & Fulton, T. A. Supercurrent density distribution in Josephson junctions. *Phys. Rev. B* **3**, 3015 (1971).
7. Kulik, I. O. Macroscopic quantization and the proximity effect in S-N-S junctions. *Sov. Phys. JETP* **30,** 944–950 (1970).
8. Bagwell, P. F. Suppression of the Josephson current through a narrow, mesoscopic, semiconductor channel by a single impurity. *Phys. Rev. B* **46,** 12573 (1992).
9. Bardeen, J. & Johnson, J. L. Josephson Current Flow in Pure Superconducting-Normal-Superconducting Junctions. *Phys. Rev. B* **5,** 72–78 (1972).
10. Samuelsson, P., Lantz, J., Shumeiko, V. S. & Wendin, G. Nonequilibrium Josephson current in ballistic multiterminal SNS junctions. *Phys. Rev. B* **62,** 1319–1337 (2001).

## Publications from DOE supported research

1. M. T. Allen, O. Shtanko, I. C. Fulga, A. Akhmerov, K. Watanabe, T. Taniguchi, P. Jarillo-Herrero, L. S. Levitov, and A. Yacoby, “Spatially resolved edge currents and guided-wave electronic states in graphene”, *Nature Physics* **2**, 128 (2016).
2. M. T. Allen, O. Shtanko, I. C. Fulga, J. I.-J. Wang, D. Nurgaliev, K. Watanabe, T. Taniguchi, A. R. Akhmerov, P. Jarillo-Herrero, L. S. Levitov, and A. Yacoby, “Visualization of phase-coherent electron interference in a ballistic graphene Josephson junction”, arXiv 1506.06734.
3. Joel I-J. Wang, L. Bretheau, R. Pisoni, K. Watanabe, T. Taniguchi, A. Yacoby, P. Jarillo-Herrero, “Tunnelling Spectroscopy of Andreev States in Graphene”, (in preparation, 2016).

# Probing Correlated Superconductors and their Phase Transitions on the Nanometer Scale

**Ali Yazdani**
**Department of Physics**
**Princeton University, Princeton, NJ 08544**
**Grant #: DE-FG02-07ER46419**
**Program Monitors: Dr. Jane Zhu**
**Reporting Period: May 2015-May 2016**

## Research Scope:

Our experimental program provides an atomic scale perspective of unconventional superconductivity—how it evolves from an unconventional conducting state and how it competes with other forms of order in correlated electronic systems. Such phenomena are at the heart of some of the most debated issues in condensed matter physics, and understanding these phenomena is an intellectual driver for many of the DOE-BES projects for the development of novel materials, including the search for higher temperature superconductivity. Our aim is to provide a microscopic view of these exotic materials and their phase transitions into the superconducting state using some of the most sophisticated scanning tunneling microscopy (STM) and spectroscopy techniques.

Our experimental program builds upon our previous advances in the study of heavy fermion systems to examine such systems in new ways—not only to understand the connections between unconventional superconductivity and other exotic electronic orders—but to also examine the role of materials' dimensionality in both the normal and superconducting properties. The layered heavy fermion compound $CeCoIn_5$ offers an electronically rich system for such studies. Moving beyond unconventional superconductivity emerging from strong electronic interactions, we are working to examine the emergence of exotic superconductivity in the presence of ferromagnetism in proximity-type heterostructures as well as in materials with strong spin-orbit interactions. Our work in this area is motivated by the recent theoretical proposals and experimental efforts that topological superconductivity can be engineered into hybrid materials by proximity-induced pairing on their spin texture bands. This is an effort to create $p+ip$ superconducting states in two-dimensional structures, which can host Majorana quasiparticles at their edges or cores of magnetic field-induced vortices. Finally, the proposed program will advance the techniques of Josephson STM that we have been developing under DOE support. As we have established that the Josephson effect between a superconducting tip and sample can be mapped on the atomic scale, we now propose ways in which the Josephson effect in such ultra-small junctions can be better understood and apply this method to study exotic superconducting phases with modulated pairing amplitudes.

## Highlights of breakthroughs under the DOE grant in this funding cycle:

- Detection of quasiparticle interference using resonant x-ray scattering (Science Advances, to appear 2016)
- Development of Josephson STM with atomic resolution (Rapid Communication **93**, 2016)
- Quasiparticle interference of the Fermi arcs and surface-bulk connectivity of Weyl semimetals (Science **351**, 1184 2016)

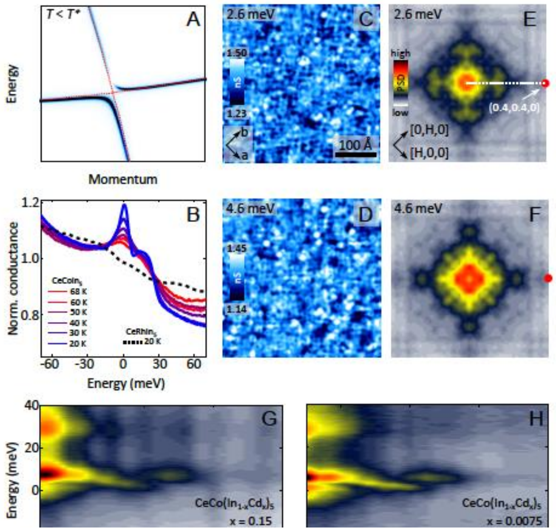

**Figure 1. STM studies on heavy fermion CeCoIn$_5$.** (**A**) Illustration of heavy fermion band formation as a result of hybridization below the $T^*$ (**B**) Temperature dependence of the averaged tunneling spectra on the Co terminated surface of pure CeCoIn$_5$ and CeRhIn$_5$ (dashed line). (**C** and **D**) Conductance map near the Fermi energy on the Co terminated surface of CeCo(In$_{1-x}$Cd$_x$)$_5$ at $x = 0.15$ doping level, which show clear heavy-quasiparticle interference waves. (**E** and **F**) Fourier transforms of the real space conductance maps at the corresponding energies display dispersing peaks in the [H, H, 0] direction. Red dot indicates the (0.4, 0.4, 0) point in the reciprocal space. (**G** and **H**) Energy-momentum cuts of the Fourier transforms in the [H, H, 0] direction (dashed line on E) for $x = 0.15$ and $x = 0.0075$. The heavy fermion band formation and quasiparticle interference is unaffected by the Cd doping.

## Recent Progress:

### Quasiparticle interference of heavy fermions in resonant elastic x-ray scattering

The quest to understand strongly correlated electronic states has pushed the frontiers of experimental measurements of solids leading to the development of new experimental techniques and methodologies. Resonant x-ray scattering (RXS) has recently become an increasingly important tool for the study of ordering phenomena in correlated electron systems. Yet, the interpretation of the RXS experiments remains theoretically challenging due to the complexity of the RXS cross-section. Central to this debate is the recent proposal that impurity-induced Friedel oscillations, akin to quasiparticle interference signals observed by scanning tunneling microscopy (STM), can lead to scattering peaks in the RXS experiments. The possibility that quasiparticle properties can be probed in RXS measurements opens up a new avenue to study the bulk band structure of materials with orbital and element selectivity provided by RXS. During the last year, we have tested these ideas by combining RXS and STM measurements of the heavy fermion compound CeMIn$_5$ (M = Co, Rh). Previously, we had made detailed STM measurements of how the emergence of heavy quasiparticles leave distinct signatures in the

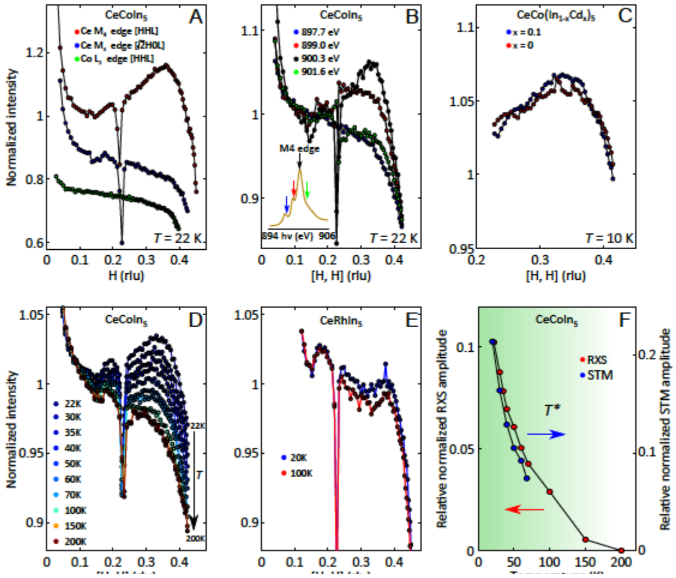

**Figure 2. Quasiparticle interference and RXS.** (**A**) Energy-momentum structure of the quasiparticle band in the [H, H] direction on the Co terminated surface with red dashed lines indicating the boundary of the integral (Eq. 1) used to calculate the RXS intensity. (**B**) Calculated RXS intensity which exhibits a broad kink starting around H = 0.2. (**C**) Experimentally measured RXS intensity on CeCoIn$_5$ at T = 22 K, which shows a broad peak around $0.2 < H < 0.4$.

quasiparticle interference (QPI) as a function of temperature in $CeCoIn_5$, while with $CeRhIn_5$ in the same temperature window (100K-10K) there is no signature of a heavy hand formation. This turns out to be an ideal material system to correlate STM observation of QPI with RXS measurements as the QPI has both a characterized temperature and doping dependence (Figure 1).

Temperature and doping dependent RXS measurements at the Ce-$M_4$ edge show a broad scattering enhancement that correlates with the appearance of heavy *f*-electron bands in these compounds (figure 2). The scattering enhancement is consistent with the measured quasiparticle interference signal in the STM measurements, indicating that quasiparticle interference can be probed through the momentum distribution of RXS signals. Overall, our experiments demonstrate new opportunities for studies of correlated electronic system using RXS techniques.

## Josephson spectroscopy on the atomic scale with the STM

During the last year, we have had a major breakthrough in the development of spatially resolved Josephson tunneling measurements with the STM. The Josephson effect, and its associated critical supercurrent, is directly related to the strength of the superconducting condensate and can provide a powerful method to study unconventional superconductivity and its spatial variations on the atomic scale. A key challenge in establishing a Josephson coupling between a superconducting tip and a superconducting sample is the high junction impedance usually required for STM imaging. At such high junction resistances, the Josephson energy is very small compared to thermal energy, hence requiring the use of instruments with ultra-low temperature capability to observe a critical Josephson current. Last year, we succeeded in establishing such an STM Josephson junction in our millikelvin STM instrument that was developed with partial DOE support. Figure 3 shows conductance measured at different junction resistances between a Pb tip and a Pb single crystal sample plotted as a function of tip-sample bias. At closer tip-sample separation, we see indication of a Josephson supercurrent at zero bias as well as other features associated with Andreev reflection between the tip and sample. Measurements of the current versus voltage show a peak in the current near zero energy, as shown in Figure 3, which is an indication of a fluctuating Josephson current that appears at a small but finite bias. The fluctuating nature of the Josephson effect in our STM setup stems from the ultra-small size of our junction. With a small tip-sample capacitance, the charging energy across the junction is larger than both the thermal and Josephson energy, making the charge a good quantum number and the phase of the junction is fluctuating. A theory that takes into account the electromagnetic environment of our junction can be used to capture the shape of the current-voltage characteristics and extract the values of the critical current for our junctions (Figure 3, lower panel). The extracted values of the critical current from such a theory agrees well with the Ambegaokar-Baratoff relation, $I_c=(\pi/2e)\ \Delta/R_N$ using appropriate parameters for our junctions.

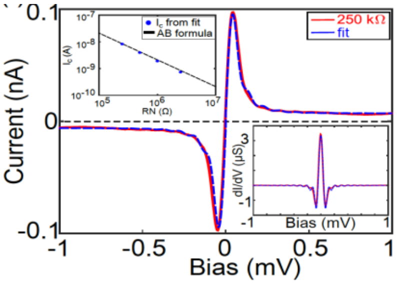

**Figure 3**. Tunneling conductance between Pb tip and Pb(110) sample as a function of tip sample junction resistance. The center peak shows signature of fluctuating Josephson current in conductance. The lower panel shows the IV characteristics that is fitted with the P(E) theory. The inset shows the extract critical current and that expected from Ambegaokar-Baratoff model and a fit to the conductance curve.

Having accomplished this local observation of a Josephson current with atomic size STM junctions, we have succeeded in mapping its amplitude as a function of position near single magnetic impurities deposited on the surface of Pb, as shown in Figure 4. Magnetic impurities are known to suppress superconductivity and this measurement demonstrates their effect on local pairing amplitude as detected through the suppression of the strength of the Josephson critical current locally. This is the first atomic scale examination of the Josephson effect and probing of spatial variations near single atomic impurities.

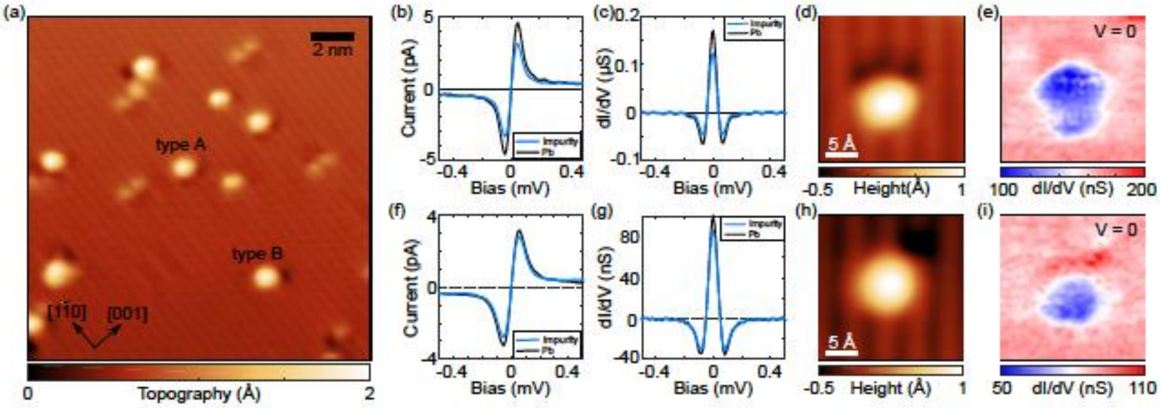

**Figure 4.** (a) Topography of Pb after evaporating a submonolayer of Fe. Individual Fe adatoms tend to be centered on a trench (type A) or row (type B) of the Pb(110) surface as marked. Suppression of pair current [(b),(f)] and dI/dV [(c),(g)] on the Fe adatom (blue) compared to on Pb (black) at 1 MΩ junction impedance for type A [(b)-(e)] and type B [(f)-(i)] adatoms. Simultaneous topographies [(d),(h)] and differential conductance maps [(e),(i)] at V = 0 for $R_N = 1$ MΩ demonstrate the spatial suppression of the Josephson effect over the Fe adataoms. Parking conditions V = −5 mV and I = 5 nA for data in (b)-(i), ensuring that RN is the same over both the adatom and bare Pb. Different superconducting tips were used for the point spectra and the conductance maps, but the Ic suppression is consistent across measurements.

## Future Plans:

Our plans moving forward will focus on the following key ideas:

1. Exploring the layer dependence and the composite nature of heavy quasiparticles in $CeCoIn_5$
2. Spatially resolved studies of the vortex phase, Q-phase, and Pauli-limiting, upper critical field in $CeCoIn_5$
3. Probing ferromagnetic-superconducting heterostructures that have been fabricated with MBE (recent new capability) to examine the possibility of triplet and topological superconductivity in these systems

## Publications supported by the DOE-BES (2014-2016):

In addition to publications directly related to DOE-BES projects, the DOE funding that supports the instrumentation in our lab have assisted other projects. The publications from these projects benefiting from DOE support are also included in the list below (marked as partially supported by DOE).

1. M. T. Randeria, B. E. Feldman, I. K. Drozdov, and A. Yazdani, “Scanning Josephson spectroscopy on the atomic scale,” Physical Review B Rapid Communication **93**, 161115R (2016). Selected as an Editors choice.

2. A. Yazdani, E. H. da Silva Neto, and P. Aynajian, "Spectroscopic imaging of strongly correlated electronic states," Annual Review of Condensed Matter Physics **7**, 11 (2016).
3. H. Inoue, A. Gyenis, Z. Wang, J. Li, S. W. Oh, S. Jiang, N. Ni, B. A. Bernevig and A. Yazdani, "Quasiparticle interference of the Fermi arcs and surface-bulk connectivity of Weyl semimetals," Science **351**, 1184 (2016). Partial support by DOE.
4. A. Yazdani, "Visualizing Majorana fermions in a chain of magnetic atoms on a superconductor," Proceeding of Nobel symposium on Topological Phases of Matter, Physica Scripta **T164**, 014012 (2015). Partial support by DOE.
5. S. K. Kushwaha, J. W. Krizan, B. E. Feldman, A. Gyenis, M. T. Randeria, J. Xiong, S-Y. Xu, N. Alidoust, I. Belopolski, T. Liang, M. Z. Hasan, N. P. Ong, A. Yazdani, and R. J. Cava, "Bulk crystal growth and electronic characterization of the 3D Dirac semimetal $Na_3Bi$," Applied Physics Letters Materials **3**, 041504 (2015). Partial support by DOE.
6. H. Luo, W. Xie, J. Tao, H. Inoue, A. Gyenis, J. W. Krizan, A. Yazdani, Y. Zhu, and R. J. Cava, "Polytypism, polymorphism, and superconductivity in TaSe2−x Tex," Proceeding of National Academy of Sciences, AOP, vol. **112** no. 11 (2015).
7. E. H. da Silva Neto, P. Aynajian, A. Frano, R. Comin, E. Schierle, E. Weschke, A. Gyenis, J. Wen, J. Schneeloch, Z. Xu, S. Ono, G. Gu, M. Le Tacon, and A. Yazdani, "Ubiquitous interplay between charge ordering and high-temperature superconductivity in cuprates," Science, **343**, 393 (2014). (Covered in Perspective) Fully supported by DOE.
8. P. Aynajian, E. H. da Silva Neto, B. B. Zhou, S. Misra, R. E. Baumbach, Z. Fisk, J. Mydosh, J. D. Thompson, E. D. Bauer, and A. Yazdani, "Visualizing heavy fermion formation and their unconventional superconductivity in f-electron materials," Journal of the Physical Society of Japan **83**, 061008 (2014) (Invited review). Fully supported by DOE.
9. S. Nadj-Perge, I. K. Drozdov, J. Li, H. Chen, S. Jeon, J. Seo, A. H. MacDonald, B. A. Bernevig, A. Yazdani, "Observation of Majorana fermions in ferromangetic atomic chains on a superconductor," Science **346**, 6209 (2014). Partially supported by DOE.
10. S. Jeon, B. B. Zhou, A. Gyenis, B. E. Feldman, I. Kimchi, A. C. Potter, Q. D. Gibson, R. J. Cava, A. Vishwanath, A. Yazdani, "Landau quantization and quasiparticle interference in the three-dimensional Dirac semimetal $Cd_3As_2$," Nature Materials **13,** 851-856 (2014). Partially supported by DOE
11. I. K. Drozdov, A. Alexandradinata, S. Jeon, S. Nadj-Perge, H. Ji, R. J. Cava, B. A. Bernevig, A. Yazdani, "One-dimensional topological edge states of bismuth bilayers," Nature Physics **10,** 663-669 (2014). Partially supported by DOE.

# Fundamental Symmetry of Ferroelectric Crystals

**Jian-Min Zuo**
**Dept. of Materials Science and Engineering and Materials Research Laboratory, University of Illinois, Urbana-Champaign, IL 61801**

## Program Scope

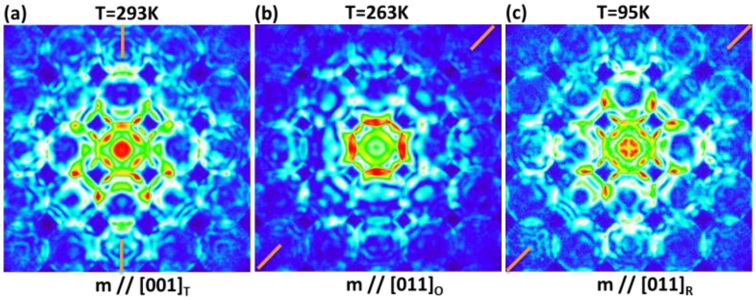

*Fig. 1 Highest symmetry recorded in energy-filtered CBED patterns from BaTiO3 single crystal at T=293, 263 and 95 K. The highest symmetry was determined using the scanning CBED technique developed under the support of this program.*

A major unresolved question in the study of ferroelectrics is the microscopic origin of polarization, and the related transformation mechanism. Knowing the nature of polarization is a prerequisite for providing an accurate description of domains and interface, and thus the microstructure. In $BaTiO_3$, phase transition is popularly explained by the displacive model ([1]; [2]), in which each Ti atom is positioned in the middle of the oxygen octahedron at equilibrium in the cubic phase, the equilibrium position moves toward the $\langle 111\rangle$, $\langle 011\rangle$, or $\langle 001\rangle$ directions for the R, O, and T ferroelectric phases, respectively. Experimentally, the x-ray absorption fine structure (XAFS) experiments ([3]) show that the Ti atoms are displaced along various of the eight possible $\langle 111\rangle$ directions in all phases. In X-ray diffraction, anomalous and strong diffuse scattering was reported in all but the rhombohedral phase ([4]). These and other results suggest a spontaneous symmetry breaking. It has been hypothesized that all Ti atoms are microscopically located in one of eight potential minima along the $\langle 111\rangle$ directions for all crystal phases and phase transition occurs through an order-disorder transformation. Zhang et al. suggested that the stable rhombohedral phase has all distortions in phase, whereas higher temperature phases have antiferroelectric coupling in one, two, or three dimensions corresponding to orthorhombic, tetragonal, cubic phases respectively ([5]). However, the observed entropy changes (≤0.52 J/mol) for each transition in $BaTiO_3$ is far smaller than the entropy change in an order-disorder transition (5.76 J/mol, see [6] and [7]. To explain this, a short correlation length between 5 to 10 nm has been postulated.

The direction and magnitude of spontaneous polarization can be determined by convergent beam electron diffraction (CBED). The principle is based on crystal symmetry and symmetry breaking induced by polarization. Under the DOE BES support, we have developed a quantitative method for quantifying and mapping crystal symmetry using scanning CBED. The experiment is carried out using the scanning electron nanodiffraction (SEND) technique by recording electron diffraction patterns at every probe positions. Electron diffraction patterns are energy-filtered and recorded on a CCD camera. To map out symmetry variations across a region of interest, symmetry in the recorded CBED patterns is quantified using the normalized cross-correlation coefficient ($\gamma$) of intensities between pairs of CBED discs.

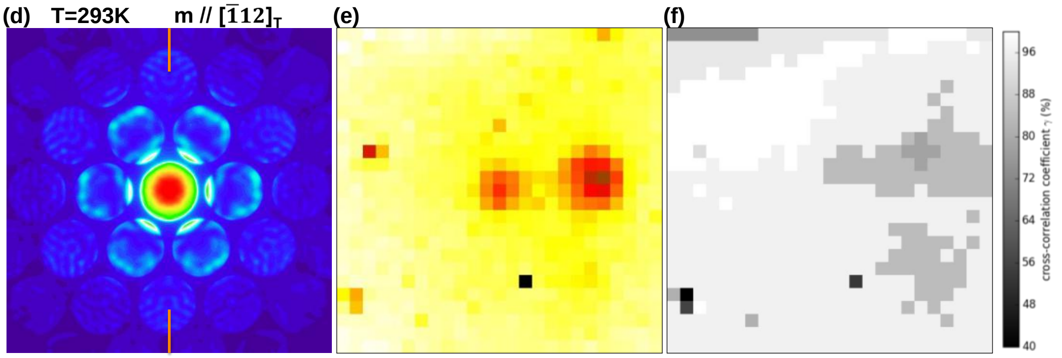

*Figure 1, continued. (d) a CBED pattern of T phase taken along pseudocubic incidence $[111]_c$ with mirror plane $m//[1\bar{1}2]$. Figure (e) shows the reconstructed bright-field image and (f) maps the symmetry variations in the same region.*

## Recent Progress

*Background:* $BaTiO_3$ successively transforms from a high-temperature paraelectric cubic phase to three low-temperature ferroelectric phases with tetragonal (T), orthorhombic (O), and rhombohedral (R) symmetries. The transformation is often considered as a classic example of displacive phase transition. The atomic displacements change the symmetry at the transition as well as polarization. However, [8] observed nanoscale rhombohedral symmetry (a single diagonal mirror observed along the cubic axes) in the orthorhombic and tetragonal phases of $BaTiO_3$ using CBED.

*Results:* To determine the fundamental symmetry of $BaTiO_3$, we recorded multiple datasets of scanning CBED patterns. Each of these dataset consists of 625 CBED patterns over an area of 25nm x 25nm. We identified regions of highest symmetry from these dataset. Figure 1 shows examples of patterns with the highest symmetry, taken along pseudocubic incidence $[100]_{pc}$ at different temperatures. In the T (*P4mm*), O (*Amm2*), and R (*R3m*) phases, the spontaneous polarization $P_s$ lies in one of the $<100>_T$, $<110>_O$, and $<111>_R$ directions, respectively. Thus for CBED patterns taken along the [100]pc incidence, we should expect mirror planes normal to $[010]_T$, $[001]_T$, $[011]_O$, $[0\bar{1}1]_O$, $[011]_R$, and $[0\bar{1}1]_R$ directions. Figure 1(a) shows the CBED pattern of T phase with mirror plane $m//[001]_T$ and correlation between symmetry related discs, $\gamma = 98.5\%$, which is consistent with the space group *P4mm*. At T=263K (O phase) and 95K (R phase), the mirror plane is observed with $m//[011]_O$ and $\gamma = 95.8\%$, $m//[011]_R$ and $\gamma = 94.6\%$, respectively (Fig. 1 (b) and (c)). To further confirm the symmetry, Figure (d) shows the CBED pattern of T phase taken along $m//[\bar{1}12]_O$ pseudocubic incidence $[111]_c$ with mirror plane and $\gamma$=95.4%.

The highest symmetry is measured only in parts of the crystal. Figure 1(f) maps the symmetry variations, where H marks the highest symmetry and L for the lowest symmetry. The low symmetry is observed where the reconstructed bright-field image (Fig. 1(e)) shows defect-like contrast.

## Future Plans

The above results clearly shows that the recorded highest symmetry of BaTiO$_3$ at nanoscale is consistent with the symmetry detected at the macroscopic scale. However, the symmetry in the single crystal is not uniform. Significant variations in the symmetry are observed in regions that show defects like image contrast. Questions remain about the nature of crystal defects and their impact on phase transition. Nonetheless, the new CBED results show the coexistence of different symmetry regions.

Further study is also planned for ferroelectric domain walls (DWs), which are topological defects that involve changes in the polarization direction accompanied by small lattice distortions. Having a large density of mobile DWs in general facilitates domain switching and therefore dramatically enhances the susceptibility of ferroelectrics and piezoelectric coupling coefficients [1]. DWs also exhibit emergent physical properties. For example, charged DWs of BiFeO$_3$ [2] and Pb(Zr,Ti)O$_3$ [3] exhibit a significant conductivity increase compared to bulk materials, which can be advantageous for device applications [4]. The structural determination of DWs will be carried out by 1) identifying two neighboring polarization domains, 2) determining the transition structure between the domains, and 3) identifying the nature of the polarization in the transition region, using the scanning CBED approached we have developed.

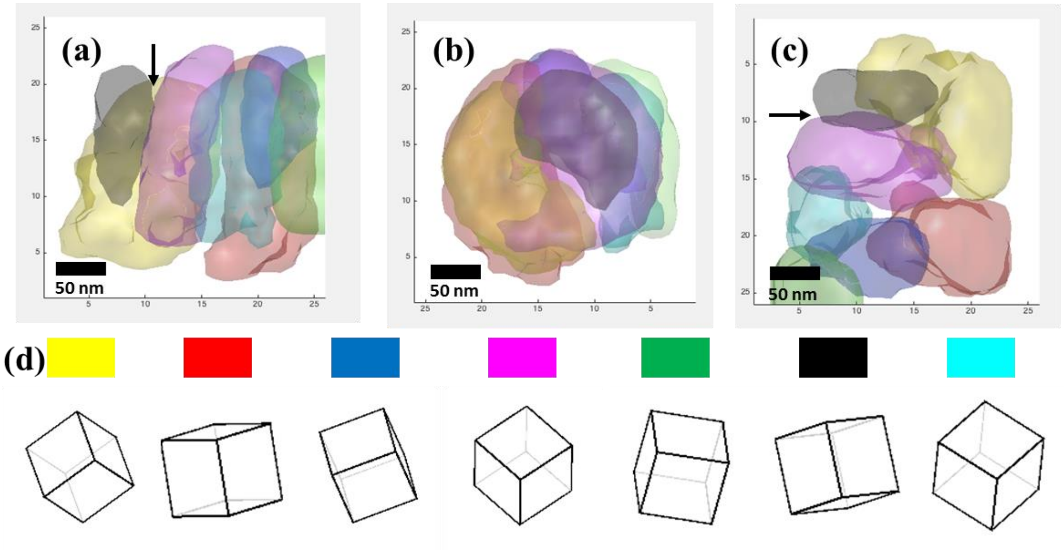

*Figure 2. Reconstructed grains and their orientations using 3D-SEND. Side (a), front (b) and top view (c) of the 3D morphologies of reconstructed grains. (A $\Sigma 9$ grain is indicated by the arrows) (d) Orientations of the seven grains. Each cube is labelled by the colour used to represent the grain.*

Another research direction is the development of 3D-SEND (scanning electron nanodiffraction) for 3D nanostructure determination. Recently, we have reported this technique for the determination of the 3D morphologies and orientations of TiN nanograins (Fig. 2). 3D-SEND is a diffraction based technique, taking advantage of the non-destructive, high resolution, sensitive nature of TED. Compared to regular electron tomography, this technique determines both the 3D morphology and the orientation of nanograins without relying on composition/thickness contrast. It uses high resolution electron diffraction that is adaptive to various nanocrystalline samples. With further improvement, this technique can be easily coupled with other characterization techniques such as atom-probe tomography and nanoindentation. Future applications of this technique are anticipated for studying single-phase and multi-phase grain boundaries at nanoscale.

## References

[1] C. Kittel, Introduction to solid state physics, Wiley, New York, 1976.
[2] W. Cochran, Crystal stability and the theory of ferroelectricity, Advances in Physics, 9 (1960) 387-423.
[3] B. Ravel, E.A. Stern, R.I. Vedrinskii, V. Kraizman, Local structure and the phase transitions of BaTiO3, Ferroelectrics, 206 (1998) 407-430.
[4] R. Comes, M. Lambert, A. Guinier, Desordre lineaire dans les cristaux (cas du silicium, du quartz, et des perovskites ferroelectriques), Acta Crystallographica Section A, 26 (1970) 244-254.
[5] Q. Zhang, T. Cagin, W.A. Goddard, The ferroelectric and cubic phases in BaTiO3 ferroelectrics are also antiferroelectric, Proceedings of the National Academy of Sciences, 103 (2006) 14695-14700.
[6] R. Comes, M. Lambert, A. Guinier, Chain structure of $BaTiO_3$ and $KNbO_3$, Solid State Commun., 6 (1968) 715.
[7] A.S. Chaves, F.C.S. Barreto, R.A. Nogueira, B. Zẽks, Thermodynamics of an eight-site order-disorder model for ferroelectrics, Physical Review B, 13 (1976) 207-212.
[8] K. Tsuda, R. Sano, M. Tanaka, Nanoscale local structures of rhombohedral symmetry in the orthorhombic and tetragonal phases of $BaTiO_3$ studied by convergent-beam electron diffraction, Physical Review B, 86 (2012) 214106.

## DOE Sponsored Publications in 2014-2016

### *Publications in refereed journals:*

1. Kim, K. H. & Zuo, J. M. Convergent-beam electron-diffraction-pattern symmetry of nanodomains in complex lead-based perovskite crystals. *Acta Crystallogr. Sect. A* 70, 583-590, doi:10.1107/s2053273314013643 (2014).
2. Kang, S. J., Kim, Y. W., Kim, M. & Zuo, J. M. Determination of interfacial atomic structure, misfits and energetics of Omega phase in Al-Cu-Mg-Ag alloy. *Acta Materialia* 81, 501-511, doi:10.1016/j.actamat.2014.07.074 (2014).
3. Kyou-Hyun Kim, Hui Xing, Jian-Min Zuo, Peng Zhang, and Haifeng Wang, TEM based high resolution and low-dose scanning electron nanodiffraction technique for nanostructure imaging and analysis, Micron 71 (0), 39 (2015)
4. Xiangwen Lu, Wenpei Gao, Jian-Min Zuo, and Jiabin Yuan, Atomic resolution tomography reconstruction of tilt series based on a GPU accelerated hybrid input-output algorithm using polar Fourier transform, Ultramicroscopy 149, 64 (2015).
5. Jianbo Wu, Wenpei Gao, Jianguo Wen, Dean J. Miller, Ping Lu, Jian-Min Zuo, and Hong Yang, Growth of Au on Pt Icosahedral Nanoparticles Revealed by Low-Dose In Situ TEM, Nano Letters 15 (4), 2711 (2015).

6. J. M. Zuo and J. L. Rouviere, Solving difficult structures with electron diffraction, IUCrJ 2 (Pt 1), 7 (2015).
7. Kim, K.-H., D. A. Payne and J.-M. Zuo. "Determination of 60 degrees polarization nanodomains in a relaxor-based ferroelectric single crystal." *Applied Physics Letters* 107(16) 162902 (2015).
8. Meng, Y.F. and J.M. Zuo, "Three-dimensional nanostructure determination from a large diffraction data set recorded using scanning electron nanodiffraction", IUCRj 3, doi:10.1107/S205225251600943X, (2106)

***Publications in conference proceedings:***

1. Jianbo Wu, Wenpei Gao, Hong Yang, and Jian-Min Zuo, "Imaging Shape-Dependent Corrosion Behavior of Pt Nanoparticles in HAuCl4 solution Over Extended Time using a Liquid Flow Cell and TEM", Microcopy and Microanalysis, 2014, proceedings, accepted.
2. Aram Yoon, Xiaofeng Zhang, Wenpei Gao, Jianbo Wu, Yung-Tin Pan, Hong Yang and Jian-Min Zuo, "Oxidation of Fe whiskers and surface diffusion observed by environmental TEM, Microcopy and Microanalysis", 2014, proceedings, accepted.
3. Wenpei Gao, Jianbo Wu, Aram Yoon, J. Mabon, W. Swiech, W.L. Wilson, H. Yang and Jian-Min Zuo, "Surface atomic diffusion processes observed at milliseconds time resolution using environmental TEM", Microcopy and Microanalysis, 2014, proceedings, accepted.
4. Yu-Tsun Shao, Kyou-Hyun Kim and Jian-Min Zuo, "Principles and Applications of Scanning CBED for Ferroelectric Domain Imaging and Symmetry Determination", Microcopy and Microanalysis, 21, suppl. 3, 1245 (2015).
5. Yu-Tsun Shao and Jian-Min Zuo, "Fundamental Symmetry of Barium Titanate Single Crystal Determined Using Energy-Filtered Scanning Convergent Beam Electron Diffraction", Microcopy and Microanalysis, 22, suppl. 3, 516 (2016).

**Book**

J.M. Zuo, J.C.H. Spence, Advanced Transmission Electron Microscopy, Imaging and Diffraction in Nanoscience, Springer, 2017, in print

# *INVITED TALKS*

# Quantum materials: insights from infrared nano-optics

D.N. Basov
Department of Physics, Columbia University
db3056@columbia.edu

Light trapped at the nanoscale, deep below the optical wavelength, exhibits an increase in the associated electric-field strength, which results in enhanced light-matter interaction. This leads to strong nonlinearities, large photonic forces, and enhanced emission/absorption probabilities. Thus, compact nano-scale light offers outsized opportunities for exploring, controlling and creating novel physical phenomena. Various nano-scale optical methods are becoming increasingly adept at inquiry into previously unattainable effects in quantum materials. I will overview recent development in infrared nano-optics of two classes of quantum materials: transition metal oxides undergoing the insulator-to-metal transition and van der Waals systems.

Several groups utilized infrared nano-optics to investigate the interplay between electronic, structural, and magnetic phase separation in correlated quantum materials in the vicinity of phase transitions. Static and time-resolved probes were able to interrogate nano-scale transformations of electronic, structural and magnetic origin[1,2,3]. Scanning probe local measurements of the conductivity have identified elusive electronic phases that only exist at the nano-scale[4,5].

Van Der Waals (vdW) crystals represent yet another interesting class of quantum material. vdW systems support a variety of light-matter modes referred to as polaritons including: Dirac plasmon polaritons in graphene, hyperbolic phonon polaritons in hexagonal boron nitride, exciton polaritons in dichalcogenides, Cooper pair plasmon polaritons in high-Tc cuprates and many others. Real space images of polaritonic standing and traveling waves contain rich insights into quantum phenomena occurring in the host material supporting polaritons[6]. The analysis of polaritonic images allows on one reconstruct local variations of the electronic response occurring at the atomic scale[7,8,9]. This line of inquiry into fundamental physics through polaritonic observations constitutes an entirely novel approach toward optics-based materials research.

---

[1] M. K. Liu, M. Wagner, E. Abreu, S. Kittiwatanakul, A. McLeod, Z. Fei, M. Goldflam, S. Dai, M. M. Fogler, J. Lu, S. A. Wolf, R. D. Averitt, and D. N. Basov Phys. Rev. Lett. 111, 096602 (2013).

[2] Sven A. Doenges, Omar Khatib, Brian T. O'Callahan, Joanna M. Atkin, Jae Hyung Park, David Cobden, and Markus B. Raschke Nano Letters 2016.

[3] M. A. Huber, M. Plankl, M. Eisele, R. E. Marvel, F. Sandner, T. Korn, C. Schüller, R. F. Haglund, R. Huber, and T. L. Cocker Nano Letters 16, 1421-1427 (2016)

[4] Eric Yue Ma, Yong-Tao Cui, Kentaro Ueda, Shujie Tang, Kai Chen, Nobumichi Tamura, Phillip M. Wu, Jun Fujioka, Yoshinori Tokura, Zhi-Xun Shen Science 350 538 (2015).

[5] A. S. McLeod, E. van Heumen, J. G. Ramirez, S. Wang, T. Saerbeck, S. Guenon, M.Goldflam, L. Anderegg, P. Kelly, A. Mueller, M. Liu, Ivan K. Schuller, D. N. Basov "*Nanotextured phase coexistence in the correlated insulator* $V_2O_3$" Nature Physics 2016 (in press).

[6] D.N. Basov, M.M. Fogler and J. Garcia De Agajo, "Polaritons in van der Waals Materials", to appear in Science (2016).

[7] G. X. Ni, H. Wang, J. S. Wu, Z. Fei, M. D. Goldflam, F. Keilmann, B. Ozyilmaz, A. H. C. Neto, X. M. Xie, M. M. Fogler, and D. N. Basov, "*Plasmons in graphene moire superlattices*," Nature Materials 14, 1217 (2015).

[8] Z. Fei, A.Rodin, W.Gannett, S. Dai, W. Regan, M. Wagner, M. K. Liu, A. S. McLeod, M. Thiemens, A. H. Castro-Neto, F. Keilmann, A. Zettl, R. Hillenbrand, M. M. Fogler, D. N. Basov Nature Nanotechnology 8, 821 (2013).

[9] Lili Jiang, Zhiwen Shi1, Bo Zeng, ShengWang, Ji-Hun Kang, Trinity Joshi, Chenhao Jin, Long Ju, Jonghwan Kim, Tairu Lyu, Yuen-Ron Shen, Michael Crommie, Hong-Jun Gao and FengWang, "Soliton-dependent plasmon reflection at bilayer graphene domain walls" Nature Materials (2016) in press.

# AUTHOR INDEX

# *PARTICIPANT LIST*

| Name | Organization | Email |
|---|---|---|
| Balsara, Nitash | University of California, Berkeley | nbalsara@berkeley.edu |
| Basov, Dmitri | Columbia University | db3056@columbia.edu |
| Batson, Philip | Rutgers University | batson@physics.rutgers.edu |
| Berezovsky, Jesse | Case Western Reserve University | jab298@case.edu |
| Borisevich, Albina | Oak Ridge National Laboratory | albinab@ornl.gov |
| Camden, Jon | University of Notre Dame | jon.camden@nd.edu |
| Campbell, Geoffrey | Lawrence Livermore National Laboratory | ghcampbell@llnl.gov |
| Chandrasekhar, Venkat | Northwestern University | v-chandrasekhar@northwestern.edu |
| Chen, Long-Qing | Pennsylvania State University | lqc3@psu.edu |
| Chisholm, Matthew | Oak Ridge National Laboratory | chisholmmf@ornl.gov |
| Cobden, David | University of Washington | cobden@uw.edu |
| Crozier, Peter | Arizona State University | crozier@asu.edu |
| Dillon, Shen | University of Illinois | sdillon@illinois.edu |
| Dougherty, Daniel | North Carolina State University | dbdoughe@ncsu.edu |
| Flatté, Michael | University of Iowa | michael_flatte@mailaps.org |
| Fuchs, Gregory | Cornell University | gdf9@cornell.edu |
| Fujita, Kazuhiro | Brookhaven National Laboratory | kfujita@bnl.gov |
| Gersten, Bonnie | U.S. Department of Energy | bonnie.gersten@science.doe.gov |
| Ginger, David | University of Washington | dginger@uw.edu |
| Gupta, Jay | The Ohio State University | jgupta@physics.osu.edu |
| Hammel, P Chris | The Ohio State University | hammel@mps.ohio-state.edu |
| Han, Myung-Geun | Brookhaven National Laboratory | mghan@bnl.gov |
| Hong, Xia | University of Nebraska, Lincoln | xia.hong@unl.edu |
| Iavarone, Maria | Temple University | iavarone@temple.edu |
| Kalinin, Sergei | Oak Ridge National Laboratory | sergei2@ornl.gov |
| Lai, Keji | University of Texas, Austin | kejilai@physics.utexas.edu |
| Lev, Benjamin | Stanford University | benlev@stanford.edu |
| Li, Dongsheng | Pacific Northwest National Laboratory | dongsheng.li2@pnnl.gov |
| Li, Lian | West Virginia University | lian.li@mail.wvu.edu |
| Lupini, Andrew | Oak Ridge National Laboratory | andy_lupini@hotmail.com |
| Madhavan, Vidya | University of Illinois, Urbana-Champaign | vm1@illinois.edu |
| Maracas, George | U.S. Department of Energy | george.maracas@science.doe.gov |
| Marks, Laurence | Northwestern University | L-marks@northwestern.edu |
| Masiello, David | University of Washington | masiello@chem.washington.edu |
| McMorran, Benjamin | University of Oregon | mcmorran@uoregon.edu |
| Meng, Ying Shirley | University of California, San Diego | shirleymeng@ucsd.edu |
| Miao, Jianwei | University of California, Los Angeles | miao@physics.ucla.edu |
| Minor, Andrew | Lawrence Berkeley National Laboratory | aminor@lbl.gov |
| Muller, David | Cornell University | dm24@cornell.edu |
| Nowack, Katja | Cornell University | kcn34@cornell.edu |
| Orenstein, Joseph | Lawrence Berkeley National Laboratory | jworenstein@lbl.gov |
| Oxley, Mark | Oak Ridge National Laboratory | oxleymp@ornl.gov |
| Pan, Xiaoqing | University of California, Irvine | xiaoqing.pan@uci.edu |
| Pantelides, Sokrates | Vanderbilt University | pantelides@vanderbilt.edu |
| Pechan, Michael | U.S. Department of Energy | michael.pechan@science.doe.gov |
| Petford-Long, Amanda | Argonne National Laboratory | petford.long@anl.gov |
| Phatak, Charudatta | Argonne National Laboratory | cd@anl.gov |
| Plummer, Ward | Louisiana State University | wplummer@phys.lsu.edu |
| Raschke, Markus | University of Colorado | Markus.Raschke@Colorado.edu |
| Reddy, Pramod | University of Michigan | pramodr@umich.edu |

| | | |
|---|---|---|
| Roberston, Ian | University of Wisconsin, Madison | ian.robertson@wisc.edu |
| Ruan, Chong-Yu | Michigan State University | ruan@pa.msu.edu |
| Schwarz, Udo | Yale University | udo.schwarz@yale.edu |
| Solares, Santiago | The George Washington University | ssolares@gwu.edu |
| Stemmer, Susanne | University of California, Santa Barbara | stemmer@mrl.ucsb.edu |
| Sutter, Peter | University of Nebraska, Lincoln | psutter@unl.edu |
| Tao, Jing | Brookhaven National Laboratory | jtao@bnl.gov |
| Vasudevan, Rama | Oak Ridge National Laboratory | rama87@gmail.com |
| Voyles, Paul | University of Wisconsin, Madison | paul.voyles@wisc.edu |
| Wu, Lijun | Brookhaven National Laboratory | ljwu@bnl.gov |
| Wu, Weida | Rutgers University | wdwu@physics.rutgers.edu |
| Yacoby, Amir | Harvard University | Yacoby@physics.harvard.edu |
| Yazdani, Ali | Princeton University | yazdani@princeton.edu |
| Zheng, Haimei | Lawrence Berkeley National Laboratory | hmzheng@lbl.gov |
| Zhu, Yimei | Brookhaven National Laboratory | zhu@bnl.gov |
| Zhu, Jane | U.S. Department of Energy | jane.zhu@science.doe.gov |
| Zuo, Jian-Min | University of Illinois | jianzuo@illinois.edu |